NASA/CR–2017-219668

Hybrid Wing Body Multi-Bay Test Article Analysis and Assembly Final Report

Alexander Velicki, Krishna Hoffman, Kim A. Linton, Jaime Baraja,
Hsi-Yung T. Wu and Patrick Thrash
The Boeing Company, Huntington Beach, California

September 2017

NASA STI Program . . . in Profile

Since its founding, NASA has been dedicated to the advancement of aeronautics and space science. The NASA scientific and technical information (STI) program plays a key part in helping NASA maintain this important role.

The NASA STI program operates under the auspices of the Agency Chief Information Officer. It collects, organizes, provides for archiving, and disseminates NASA's STI. The NASA STI program provides access to the NASA Aeronautics and Space Database and its public interface, the NASA Technical Report Server, thus providing one of the largest collections of aeronautical and space science STI in the world. Results are published in both non-NASA channels and by NASA in the NASA STI Report Series, which includes the following report types:

- TECHNICAL PUBLICATION. Reports of completed research or a major significant phase of research that present the results of NASA Programs and include extensive data or theoretical analysis. Includes compilations of significant scientific and technical data and information deemed to be of continuing reference value. NASA counterpart of peer-reviewed formal professional papers, but having less stringent limitations on manuscript length and extent of graphic presentations.

- TECHNICAL MEMORANDUM. Scientific and technical findings that are preliminary or of specialized interest, e.g., quick release reports, working papers, and bibliographies that contain minimal annotation. Does not contain extensive analysis.

- CONTRACTOR REPORT. Scientific and technical findings by NASA-sponsored contractors and grantees.

- CONFERENCE PUBLICATION. Collected papers from scientific and technical conferences, symposia, seminars, or other meetings sponsored or co-sponsored by NASA.

- SPECIAL PUBLICATION. Scientific, technical, or historical information from NASA programs, projects, and missions, often concerned with subjects having substantial public interest.

- TECHNICAL TRANSLATION. English-language translations of foreign scientific and technical material pertinent to NASA's mission.

Specialized services also include organizing and publishing research results, distributing specialized research announcements and feeds, providing information desk and personal search support, and enabling data exchange services.

For more information about the NASA STI program, see the following:

- Access the NASA STI program home page at *http://www.sti.nasa.gov*

- E-mail your question to help@sti.nasa.gov

- Fax your question to the NASA STI Information Desk at 443-757-5803

- Phone the NASA STI Information Desk at 443-757-5802

- Write to:
  STI Information Desk
  NASA Center for AeroSpace Information
  7115 Standard Drive
  Hanover, MD 21076-1320

NASA/CR–2017-219668

Hybrid Wing Body Multi-Bay Test Article Analysis and Assembly Final Report

Alexander Velicki, Krishna Hoffman, Kim A. Linton, Jaime Baraja,
Hsi-Yung T. Wu and Patrick Thrash
The Boeing Company, Huntington Beach, California

National Aeronautics and
Space Administration

Langley Research Center
Hampton, Virginia 23681-2199

Prepared for Langley Research Center
under Contract NNL1OAA05B/NNL11AA68T

September 2017

Available from:

NASA STI Program / Mail Stop 148
NASA Langley Research Center
Hampton, VA 23681-2199
Fax: 757-864-6500

FOREWORD

This report summarizes work performed by The Boeing Company, through its Boeing Research & Technology organization located in Huntington Beach, California, under the Environmentally Responsible Aviation (ERA) project. The report documents work performed to structurally analyze and assemble a large-scale Multi-bay Box (MBB) Test Article capable of withstanding bending and internal pressure loadings representative of a Hybrid Wing Body (HWB) aircraft. The work included fabrication of tooling elements for use in the fabrication and assembly of the test article. The report also documents the fabrication of several large integrated stitched panels and associated hardware, which were assembled into the MBB.

The NASA technical monitor was Dawn Jegley of the Structural Mechanics and Concepts Branch, NASA Langley Research Center.

This document was written by the following Boeing personnel:

Mr. Alex Velicki	Principal Investigator
Mr. Krishna Hoffman	Program Manager
Mr. Kim Linton	Lead Design Engineer
Mr. Jaime Baraja	Design Engineering
Dr. Tom Wu	Lead Stress Engineer
Mr. Patrick Thrash	Lead Manufacturing Engineer

Technical content was created by the following Boeing personnel:

Mr. Cris Garcia	Design Engineering
Dr. Peter Shaw	Stress Engineering
Mr. Bob Pickell	Manufacturing Engineering
Mr. Rob Turley	Manufacturing Engineering
Mr. John Jimenez	Lead Tool Design Engineer
Mr. Steve Morgan	Tool Design Engineering

Acknowledgment is also made to the following individuals at the NASA Langley Research Center for their technical support, Ms. Dawn Jegley, Mr. Marshall Rouse, Mr. Andrew Lovejoy, Mr. James Gaspar, and Dr. Adam Przekop.

TABLE OF CONTENTS

LIST OF FIGURES

284067

284067

LIST OF ACRONYMS

Acronym	Definitions
1P	Aircraft Cabin Nominal Pressure (9.2 psi)
2P	Design Ultimate Pressure (Overpressure) at Two Times Nominal Pressure (18.4 psi)
3D	Three Dimensional
A/C	Air-Conditioning
ABAQUS	Finite Element Modeling Software Program
ACT	Advanced Composites Technology
AFB	Air Force Base
AHS	American Helicopter Society
AIAA	American Institute of Aeronautics and Astronautics
AJ1	Assembly Jig 1
APT	Advanced Process Technology, Inc.
ASC	American Society for Composites
ASCE	American Society of Civil Engineers
ASME	American Society of Mechanical Engineers
Assy	Assembly
AST	Advanced Subsonic Technology
BC	Boundary Condition
BHD	Bulkhead
Bldg	Building
BMS	Boeing Material Specification
BVID	Barely Visible Impact Damage
BWB	Blended Wing Body
CA	California
CAD	Computer-Aided Design
CAI	Compression After Impact
CAPRI	Controlled Atmospheric Pressure Resin Infusion
CD	Cold Dry
CDR	Critical Design Review
CG	Center of Gravity
CL	Center Line
CLIN	Contract Line Item Number
CLT	Classical Laminated Theory
CNC	Computer Numerically Controlled
COLTS	Combined Loads Test System
CR	Contractor Report
D&DT	Durability and Damage Tolerance
DA	Determinate Assembly
deg	Degree
DIM	Dimension
DLL	Design Limit Load
DMS	Douglas Material Specification
DRT	Drill-Ream Template
DUL	Design Ultimate Load

Acronym	Definitions
DWG	Drawing
ELM	Element
ε_{by}	Bypass Strain Axis in Bearing/Bypass Interaction Chart
ε_{byt}	Extrapolated Bypass Strain Value from Bearing/Bypass Interaction Curve
ε_{pt}	Bypass Strain Calculated from FEA
ε_{uhc}	Net-Section Strength Value for Compression Strain
ε_{uht}	Net-Section Strength Value for Tension Strain
ERA	Environmentally Responsible Aviation
FAA	Federal Aviation Administration
FAR	Federal Aviation Regulation
f_{br}	Bearing Stress Calculated from FEA
f_{BR}	Bearing Stress Axis in Bearing/Bypass Interaction Chart
F_{brl}	Net-Section Strength Value for Bearing Stress
F_{brt}	Extrapolated Bearing Stress Value from Bearing/Bypass Interaction Curve
F_{bru}	Allowable Bearing Ultimate Stress
F_{bry}	Allowable Bearing Yielding Stress
FE	Finite Element
FEA	Finite Element Analysis
FEM	Finite Element Model
FS	Factor of Safety
ft	Foot
ft^2	Square Foot
ft^3	Cubic Foot
ft-lb	Foot -Pound
FWD	Forward
g, G	Acceleration of Gravity
gal	Gallon
gsm	Grams per Square Meter
H/W	Hot/Wet
HB	Huntington Beach, California
hr	Hour
HWB	Hybrid Wing Body
ICD	Interface Control Drawing
ID	Identification
σ_{ILT}	Inter-Laminar Tensile Stress
IML	Inner Moldline
in.	Inch
$in.^2$	Square Inch
$in.^3$	Cubic Inch
IRAD	Independent Research and Development
JSC	Johnson Space Center
KEAS	Knots Equivalent Airspeed
KIPS	Thousand Pounds
ksi	Thousand Pounds Force per Square Inch
LaRC	Langley Research Center

Acronym	Definitions
LB	Long Beach, California
lb	Pound
lbf	Pound-Force
LC	Load Case
LHS	Left-Hand Side
LVDT	Linear Variable Displacement Transducer
m	Meter
M&PE	Material and Process Engineering
Max.	Maximum
MBB	Multi-bay Box
MD	Multi-Discipline
με	Micro Strain
MIL-HDBK	Military Handbook
MIL-S	Military Specification
MLG	Main Landing Gear
Min.	Minimum
min	Minute
mm	Millimeter
MRL	Manufacturing Readiness Level
MS	Margin of Safety
Msi	Megapounds per Square Inch
MTOGW	Maximum Takeoff Gross Weight
MWAR	Mitigate, Watch, Accept, Research
Myy	Rocking Moment on T-cap
MZFW	Maximum Zero Fuel Weight
N/A	Not Applicable
NASA	National Aeronautics and Space Administration
NASTRAN	NASA Structural Analysis (Finite Element Analysis Software)
NC	Numerical Control
NCF	Non-Crimp Fabric
Nd	Node
NDE	Nondestructive Evaluation
NDI	Nondestructive Inspection
NFS	NASA FAR Supplement
no.	Number
NRA	NASA Research Announcement
Nx	Axial Load in x-direction
Nxy	Shear Load in xy-plane
Ny	Axial Load in y-direction, or Pull-off Load on T-cap
OB	Outboard
OEW	Operating Empty Weight
OHC	Open Hole Compression
OML	Outer Moldline
OWNG	Outboard Wing
Patran	Patch Translator (Pre/Post-Processing Software for Finite Element Analysis)

Acronym	Definitions
pcf	Pounds per Cubic Foot
PCOMP	Layered Composite Element Property in NASTRAN
PRSEUS	Pultruded Rod Stitched Efficient Unitized Structure
psi	Pounds per Square Inch
PTP	Protect The Part
R&D	Research and Development
RAMP	Risk Assessment and Mitigation Plan
Rev.	Revision
RHS	Right-Hand Side
SC1	Subcase 1
SMAAART	Structures, Materials, Aerodynamics, Aerothermodynamics, and Acoustics Research and Technology
SOA	State of the Art
SQ-IN	Square Inches
SRD	Servo Rotary Dispensing
T1C72	Type 1, Class 72
TAI	Tension After Impact
TCP	Tool Center Point
TM	Technical Memorandum
TO	Task Order
TRL	Technology Readiness Level
Typ	Typical
ULT	Ultimate
UP-BKHD	Upper Bulkhead
VARTM	Vacuum-Assisted Resin Transfer Molding
VIC-3D	Video Image Correlation in Three Dimensions
WBS	Work Breakdown Structure

1.0 INTRODUCTION

NASA created the Environmentally Responsible Aviation (ERA) project to explore and document the feasibility, benefits, and technical risks of advanced vehicle configurations and enabling technologies that will reduce the effects of aviation on the environment. A critical aspect of this pursuit is the development of a lighter, more robust airframe that will enable the introduction of unconventional aircraft configurations that have higher lift-to-drag ratios, reduced drag, and lower community noise. The primary structural concept being developed under the ERA project in the Airframe Technology element is Pultruded Rod Stitched Efficient Unitized Structure (PRSEUS).

1.1 Task Order Relationships

The work statement described in this report is a blend of the larger multi-year effort to design, fabricate, and test the Hybrid Wing Body Multi-bay Box (MBB) Test Article (Figure 1-1). Initial concept development was followed by a risk reduction effort involving fabrication and testing of a pressure cube. The cube was built at The Boeing Company's Huntington Beach, California, facility and tested at NASA's Combined Loads Test System (COLTS) facility. The PRSEUS panels for the MBB were also fabricated at the Boeing Huntington Beach facility. The MBB was assembled at the Boeing Long Beach, California, facility and delivered to NASA in December 2014 for testing in the COLTS facility during 2015.

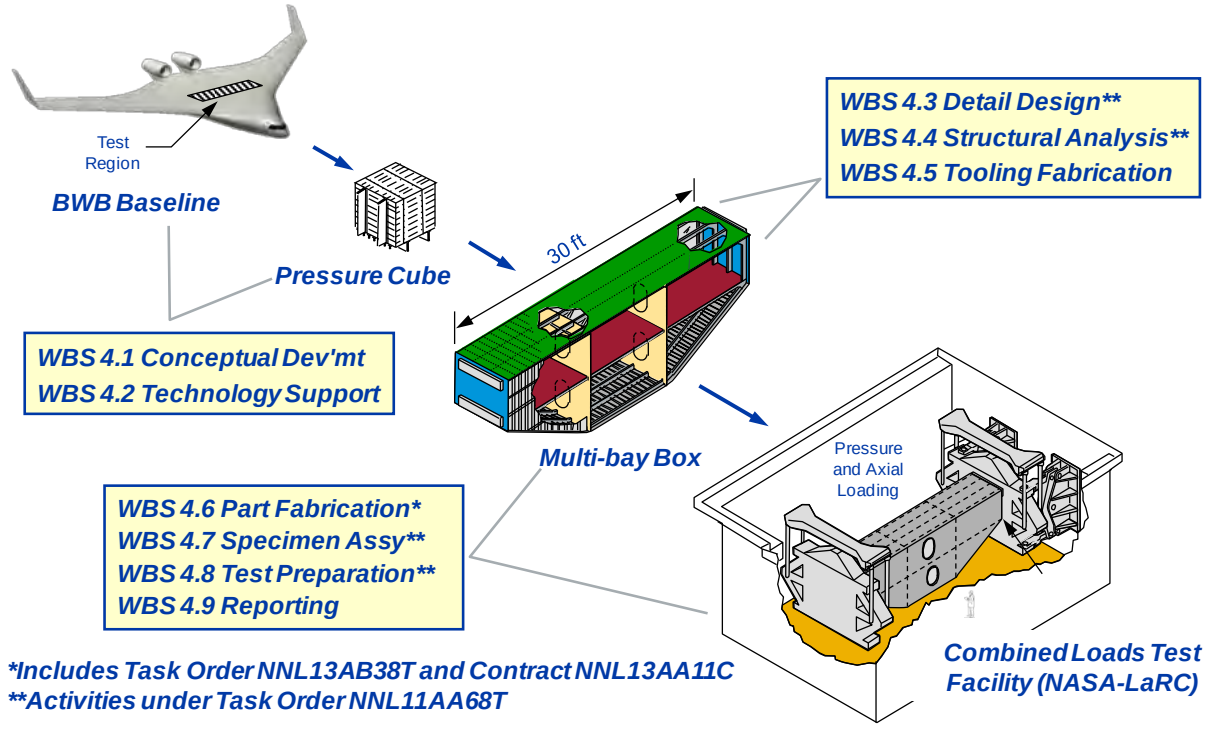

Figure 1-1. Task Order NNL11AA68T Was a Subset of the Overall Multi-bay Box Development

The MBB buildup was completed using several different task order contracts to expedite the work and recover schedule delays that were experienced during the detail design and tool fabrication phases of the project. The detail design, analysis, and tool design tasks for the MBB were completed under contract NNL04AA11B, Task Order (TO) NNL10AB00T in 2011. Tooling was procured under contract NNL04AA11B, TO NNL10AB00T and contract

NNL10AA05B, TO NNL11AA68T, which also included a portion of the overall panel fabrication, acceptance, and nonconformance reporting tasks. Several PRSEUS panels and associated hardware were provided by contract NNL13AA11C. The remaining panel fabrication work was performed under TO NNL13AB38T. The panels from TO NNL13AB38T were completed and then delivered in the 2013 to 2014 timeframe (Figure 1-2).

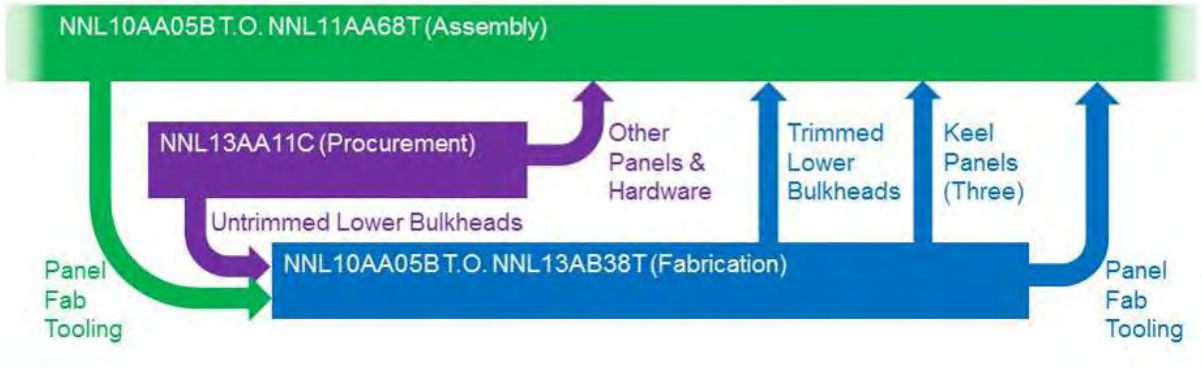

Figure 1-2. Contract and Task Order Relationships Used to Fabricate the MBB

1.2 Development Schedule

The Boeing concept for a large-scale test article to validate the structural response of the flat-sided pressure cabin under combined pressure and bending loads was first proposed in the American Institute of Aeronautics and Astronautics (AIAA) technical paper, “Airframe Development for the Hybrid Wing Body Aircraft” (Ref. 1-1), in 2009. The technical rationale and specimen description in that paper were used to develop a joint NASA-Boeing work statement whereby the majority of the initial design, linear analyses, and fabrication work would be performed by Boeing, and the activities related to nonlinear analysis and testing would be completed by NASA at the Langley Research Center. Although initially envisioned to be a 3- to 4-year program, it soon grew into a 6-year effort as problems in tool design were discovered and corrected before starting panel fabrication.

A schedule for the overall effort, including the multiple contracts involved, is shown in Figure 1-3.

The panel fabrication and pressure box assembly tasks were critical to the schedule for delivering the MBB to NASA in time for testing. In Figure 1-3, the milestone markers for these tasks show when specific panels were infused and when they were delivered to the assembly site. Particular attention was given to these milestones during program execution to maintain schedule and to reduce remaining program risk.

The final task of testing the MBB in the COLTS facility was performed by NASA, with Boeing providing support under Boeing funding and not under NASA contract.

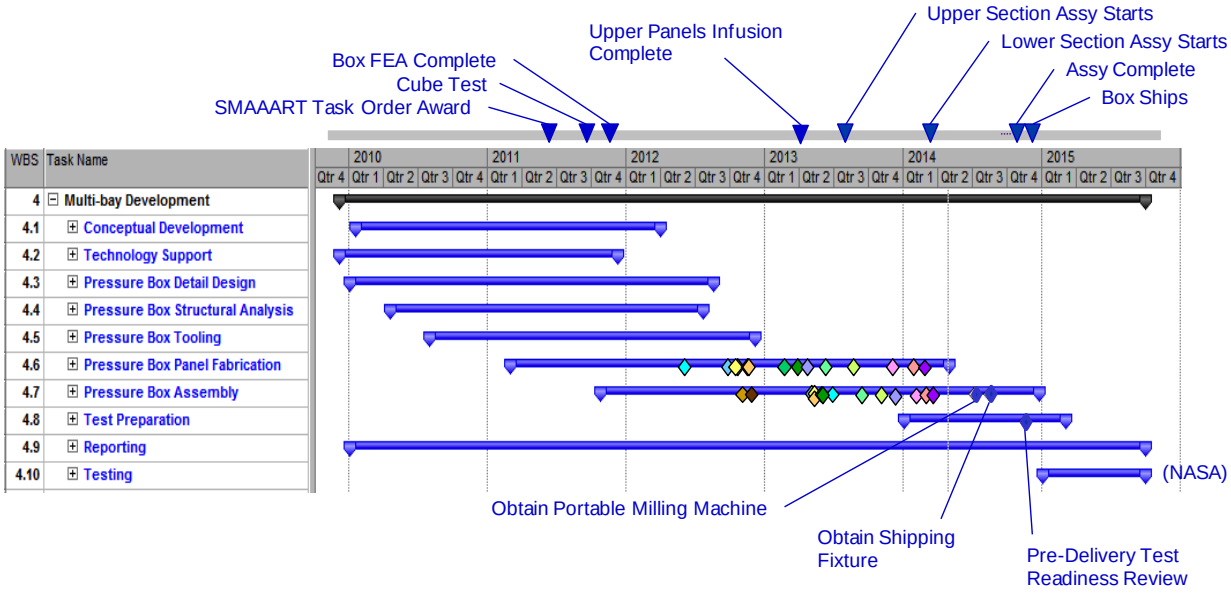

Figure 1-3. MBB Development Schedule

2.0 TEST ARTICLE DEVELOPMENT

The Hybrid Wing Body Multi-bay Box (MBB) Test Article was the final test specimen in a building-block development program that was conceived to investigate the unique design and loading aspects of the noncircular HWB pressure cabin. Each test article was carefully coupled with an analytical component that could be used to quantify test results in terms of added airframe weight. From the initial single-element structural specimens to the larger and more complicated subcomponent tests, increasing levels of structural complexity and loading scenarios were confronted until the final nonlinear combined pressure-and-axial loading conditions were replicated in the NASA LaRC COLTS facility for the HWB MBB Test Article work described in this report.

2.1 Configuration Development

The center section of the HWB represents a profound design challenge—even the most highly efficient composite primary structures used on today's state-of-the art aircraft would not be capable of overcoming the weight and cost penalties induced by the highly contoured pressurized airframe. Principally, in the pressure cabin regions that are primarily driven by out-of-plane loading considerations, using traditional layered material systems would require thousands of additional mechanical attachments to suppress interlaminar failures and to join structural elements, which would render the aerodynamically efficient HWB configuration uncompetitive due to the increase in structural weight. The other argument against adopting a conventional composite approach is the high manufacturing costs associated with building highly contoured shapes. Not only would complex outer moldline (OML) tooling be needed, but all interior stringers and frame members would also require individual toolsets for fabrication and joining elements, which would adversely affect affordability. The essential characteristics of a more capable HWB structural solution is one that operates effectively in out-of-plane loading scenarios while simultaneously meeting the demanding producibility requirements inherent in building a highly contoured airframe.

Beyond the obvious secondary bending stresses experienced during pressurization, another essential design difference for the HWB fuselage is the unique bi-axial loading pattern that occurs during maneuver loading conditions (Figure 2-1). For the lifting-body shape, load magnitudes are more nearly equal in each in-plane direction (Nx and Ny) than what is typically found on conventional tube-and-wing fuselage arrangements, wherein the cantilevered fuselage is more highly loaded longitudinally in the Nx direction (along the stringer) than in the Ny direction (along the frame).

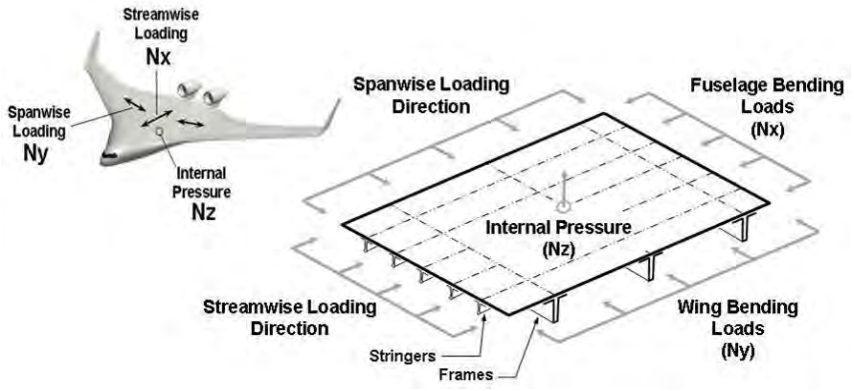

Figure 2-1. Combined Loading Condition for Fuselage Upper Crown

This single difference has a profound effect on the structural concept selection because it dictates that optimum panel geometry should have continuous load paths in both directions (Nx and Ny), in addition to efficiently transmitting internal pressure loads (Nz) for the near-flat panel geometry. The prevalence of these high compression loads in the Ny direction is unique to the HWB design. For a conventional skin-stringer-frame built-up panel, the frame shear clip member is typically discontinuous, allowing the stringer to pass through uninterrupted in the primary longitudinal loading direction. If such an arrangement were used for the HWB, the frame member (attached by a discontinuous shear clip to the skin) would be less effective in bending and/or axial-compression loading than a continuous frame design that is attached directly to the skin to effectively create a taller frame member. For the HWB configuration, this loading condition dominates the upper crown panel across the wing carry-through region. Here, the wing bending loads move across the fuselage during positive flight maneuver conditions, generating beam-column loading on the frame members in addition to internal pressurization loads that bow them outward. This challenging combined-axial-plus-bending design condition is then further exacerbated by the relatively large unsupported span length that occurs between the internal rib members that define the panel end conditions.

Within this difficult design space, the most challenging region occurs in the crown panel along the aft pressure bulkhead (which also acts as the rear wing spar member). In this region, the adjacent frame members that run parallel to the bulkhead undergo the highest compression loads, in addition to internal pressurization. As the cabin pressure deflects the crown panel outward (bowing the frame members), the maneuver loading simultaneously induces compression loads that buckle the skin between the stringers before transferring those internal loads into the frame members. It is this unique “combined” loading scenario that generates the distinctive nonlinear beam-column panel loading phenomena in the shell that makes the HWB fuselage design so demanding. Replicating this complex loading condition was the primary objective of the large-scale MBB test because the test would demonstrate the feasibility of meeting airframe weight targets established by the system-level airplane analysis during the ERA trade studies. This initial concept proposed at the outset of the program (Figure 2-2) closely resembles the final design of the final MBB.

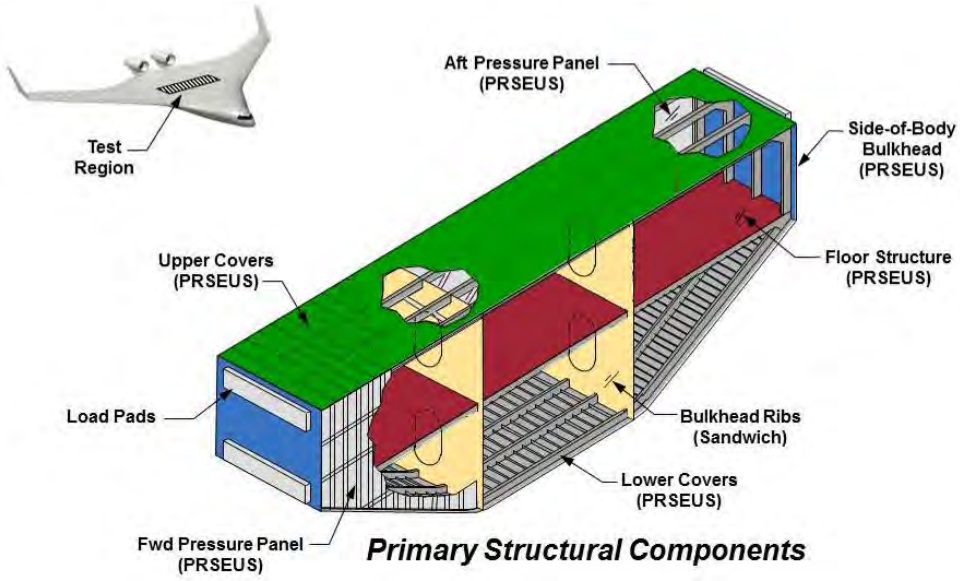

Figure 2-2. Initial Concept Sketch for the Multi-bay Test Article

2.2 Specimen Design Considerations

When it became evident that the sandwich panel concepts initially proposed for the HWB shell structure would not meet the minimum damage-tolerance and fail-safe design requirements established for primary airframe structures, a more focused effort was undertaken to identify a multi-load path structural concept with adequate structural redundancy. As is typical for highly loaded transport aircraft primary structures, this search led to an examination of discretely stiffened panel designs that would be capable of not only sustaining damage, but also of maintaining residual load-carrying capability over a wide range of damage scenarios. In addition to these fundamental design requirements, the unique configuration challenges of the HWB also had to be accommodated in the structural concept selection.

To overcome these challenges, an improved fuselage concept was designed as a bi-directionally stiffened panel, wherein the spanwise wing bending loads would be carried by the frame members and the longitudinal fuselage bending loads would be carried by the stringers. Additionally, the panel would be designed to include continuous loads paths in both directions, using stringer and frame members attached directly to the skin and made from highly tailored laminates, with thin skins designed to operate well into the post-buckled design regime, and with crack-stopping features designed to minimize damage propagation. Capturing such improvements would be necessary to offset the inherent weight penalties of the noncircular pressure cabin.

The design effort identified a Pultruded Rod Stitched Efficient Unitized Structure (PRSEUS) panel concept, as shown in Figure 2-3. PRSEUS represents a combination of dry carbon warp-knit fabric, pultruded rods, foam core, and stitching threads that are brought together in a unique manner to create a stiffened panel geometry that utilizes resin infusion and out-of-autoclave curing. This approach reduces recurring fabrication costs below what would be possible using traditional composite manufacturing practices for the compound curvatures of the HWB. The resulting panels are one-piece unitized assemblies with seamless cocured interfaces, which are reinforced with through-thickness stitching to preserve the orthotropic nature and continuity of the carbon-fiber tows.

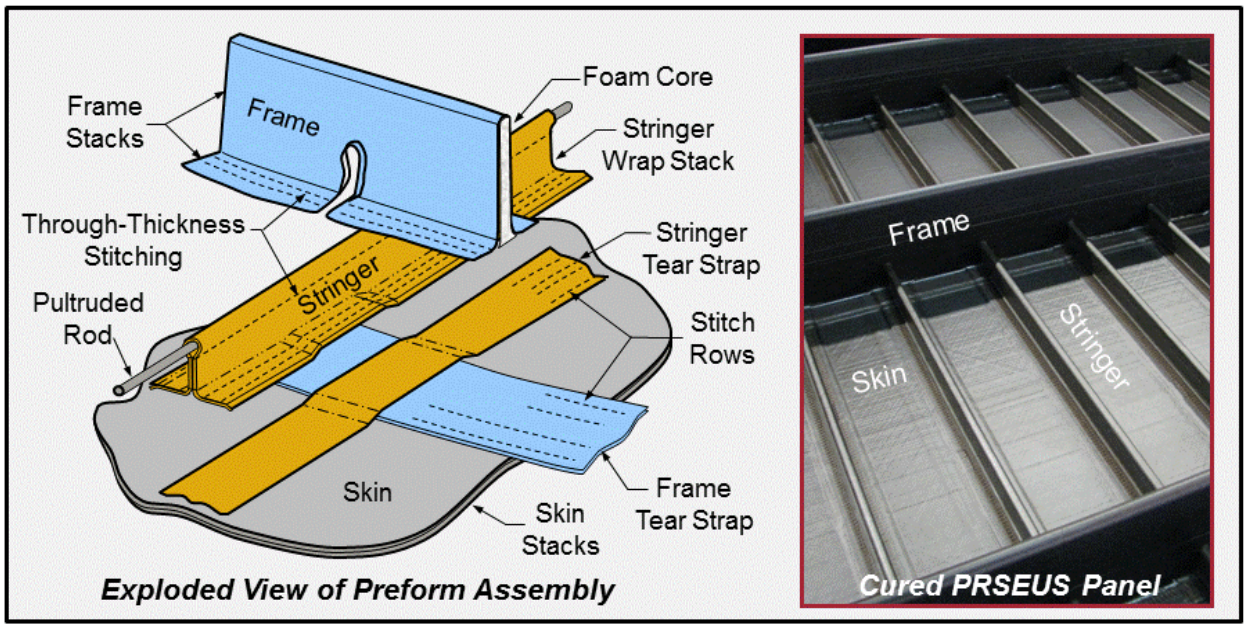

Figure 2-3. Pultruded Rod Stitched Efficient Unitized Structure (PRSEUS) Panel Concept

Structural continuity is maintained by eliminating mechanical attachments, gaps, and "mouse holes," providing uninterrupted load paths between the skin, stringer, and frame elements. These features are shown in the photograph of a PRSEUS panel in Figure 2-4. Load paths at the stringer-to-frame intersection are maintained in both directions by passing the rod-stiffened stringer through a small keyhole in the frame web while keeping both frame caps continuous. The high-modulus rod embedded in the stringer cap increases the local strength and stability of the stringer section, while simultaneously shifting the neutral axis away from the concentrated material near the skin. Frame members are stitched directly onto the skin to eliminate shear tie details, and they are designed to take advantage of carbon-fiber tailoring by placing bending and shear-conducive layups where they are the most effective. Because all interfaces are stitched together to provide through-thickness strength, a higher degree of fiber tailoring is possible, even with composite material systems that are known to be brittle, layered, and prone to delamination.

This unprecedented level of panel integration is enabled by the use of dry material forms, single-sided stitching, and a unique self-supporting preform design that eliminates inner moldline (IML) cure tooling. Using these technologies, complicated stitched preforms can be fabricated without the exacting tolerances normally needed to accurately fit and assemble rigid details together. One of the principal goals in developing the PRSEUS fabrication technology was to demonstrate that stitched dry fabric panels can be infused and cured in an oven to consistently produce high-quality parts with lower recurring fabrication costs than possible using conventional composite processes. Because all materials in the stitched assembly are dry, there are no out-time limitations as with prepreg systems, and the oven-cure removes the size restrictions of fitting the assembly into an autoclave.

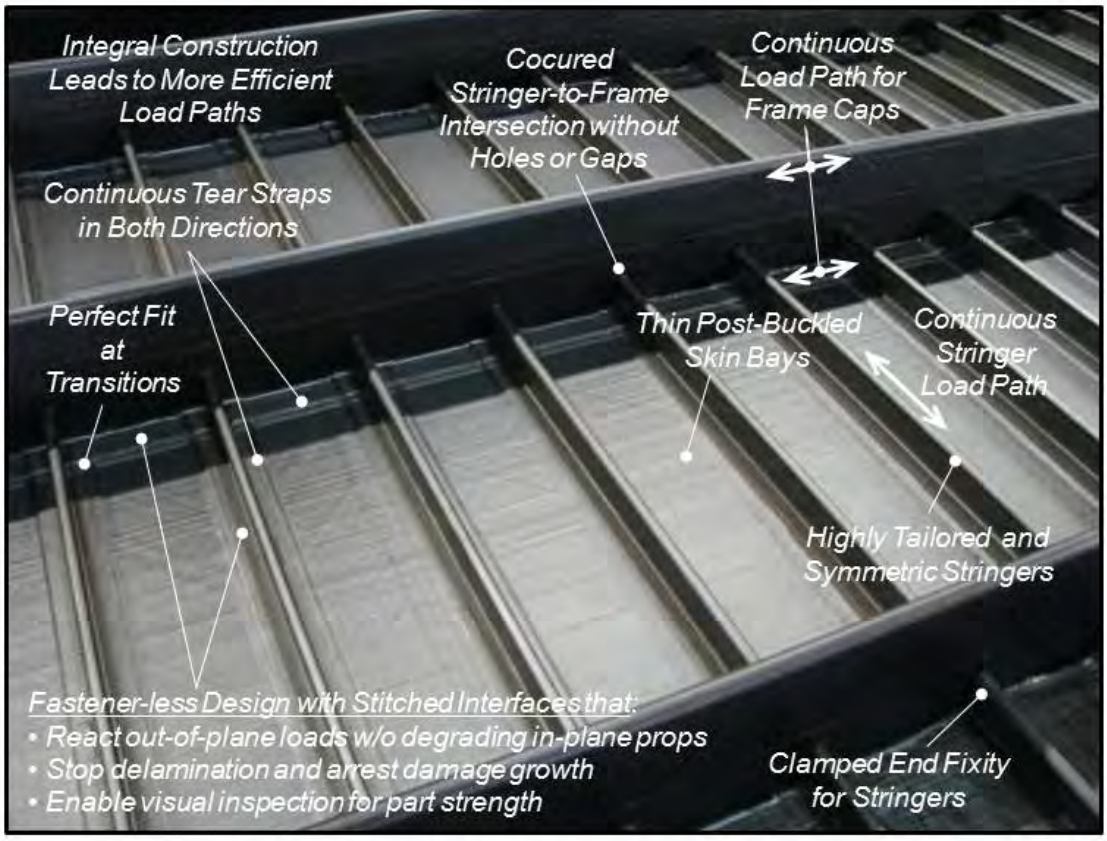

Figure 2-4. Summary of PRSEUS Structural Performance Advantages

The PRSEUS fabrication sequence, as depicted in Figure 2-5, starts with cutting individual pieces of warp-knit fabric, which are then organized into kits. Pre-cured rods and foam core details are also prepared and, in some cases, assembled into pre-stitched assemblies. These details are then positioned in the preform assembly fixture and stitched in place to create a self-supporting dry carbon preform. Resin infusion is accomplished using a soft-tooled fabrication scheme wherein the bagging film conforms to the IML surface of the preform geometry and seals against a rigid OML tool, thus eliminating costly internal tooling that would normally be required to shape the interior details. The preform is then infused with resin and cured using an out-of-autoclave process. The initial cure takes place at 250°F, followed by vacuum bag and resin line removal, and then a 350°F freestanding post-cure. The PRSEUS process results in cocured, stitched flange-to-skin interfaces, integral tear straps-to-skin interfaces, and stitched transitions wherever there are thickness changes in the skin. There are no exposed machined carbon-fiber edges within the panel because all elements are infused and cured in a single operation.

Manufacturing multiple PRSEUS panels during this program demonstrated that the self-supporting preform that eliminates interior mold tooling is feasible for the HWB-representative geometries that have been fabricated to date. The processing parameters developed in the laboratory have also been shown to be scalable to even larger and more complex panel geometries. Increasing levels of panel integration, beyond just the stringers and frames, were also demonstrated. For example, solid integral cap features were incorporated into the panel assemblies to facilitate joining of the large panels that were used to construct the MBB.

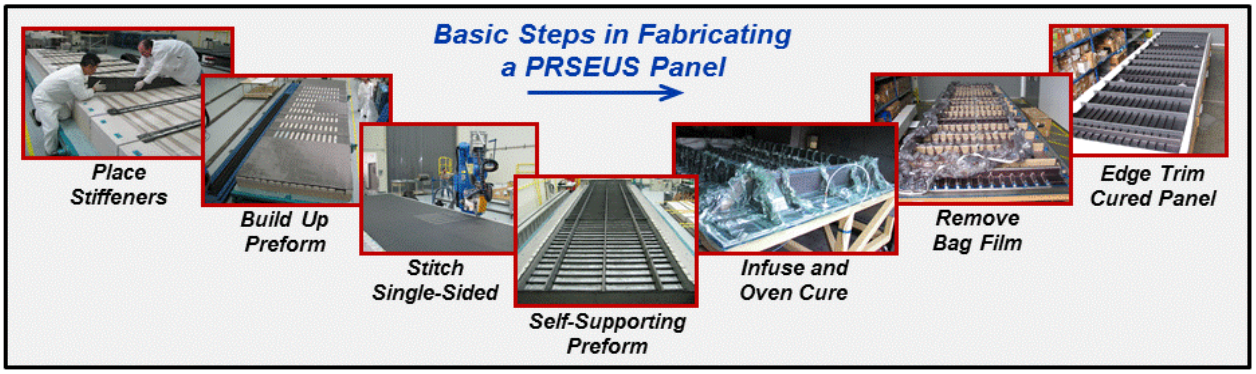

Figure 2-5. Summary of PRSEUS Panel Fabrication Sequence

Once the basic panel architecture was established, an initial set of structural sizing studies was performed to determine the minimum gage part dimensions that would be needed to satisfy the ultimate Two Times Maximum Internal Pressure (2P) static proof load design condition (internal pressurization of 18.4 psi). This term is derived from the nominal cabin pressure differential, which for the baseline aircraft and cruise altitude selected was determined to be 1P = 9.2 psi. Prior trade studies (Ref. 2-1) had shown that (1) about 80% of the pressurized cabin is relatively unaffected by the maneuver loads due to its large cross-sectional height, and (2) the critical design condition for the near-flat panels generally defaults to the internal pressurization design condition. As such, a detailed panel-level analysis was suitable to determine the minimum gage part dimensions to achieve acceptable operating strains and deflections for the HWB shell structure. The resulting minimum gage panel geometries are summarized in Figure 2-6. These general dimensions were then used to design a series of uniaxial-loaded test specimens that would be taken through the building-block development test program (Figure 2-7). The goal was to validate the load-carrying capability of the PRSEUS panel construction under the most critical HWB pressure, maneuver, and combined loading conditions under relevant damage scenarios.

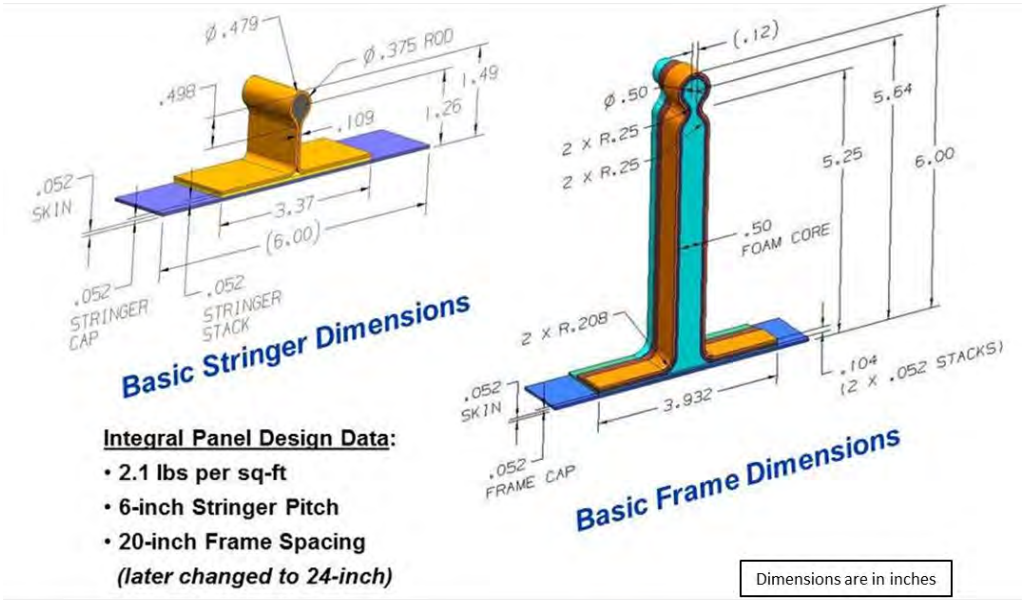

Figure 2-6. Starting Minimum Gage Design to Meet 2P Loading Conditions

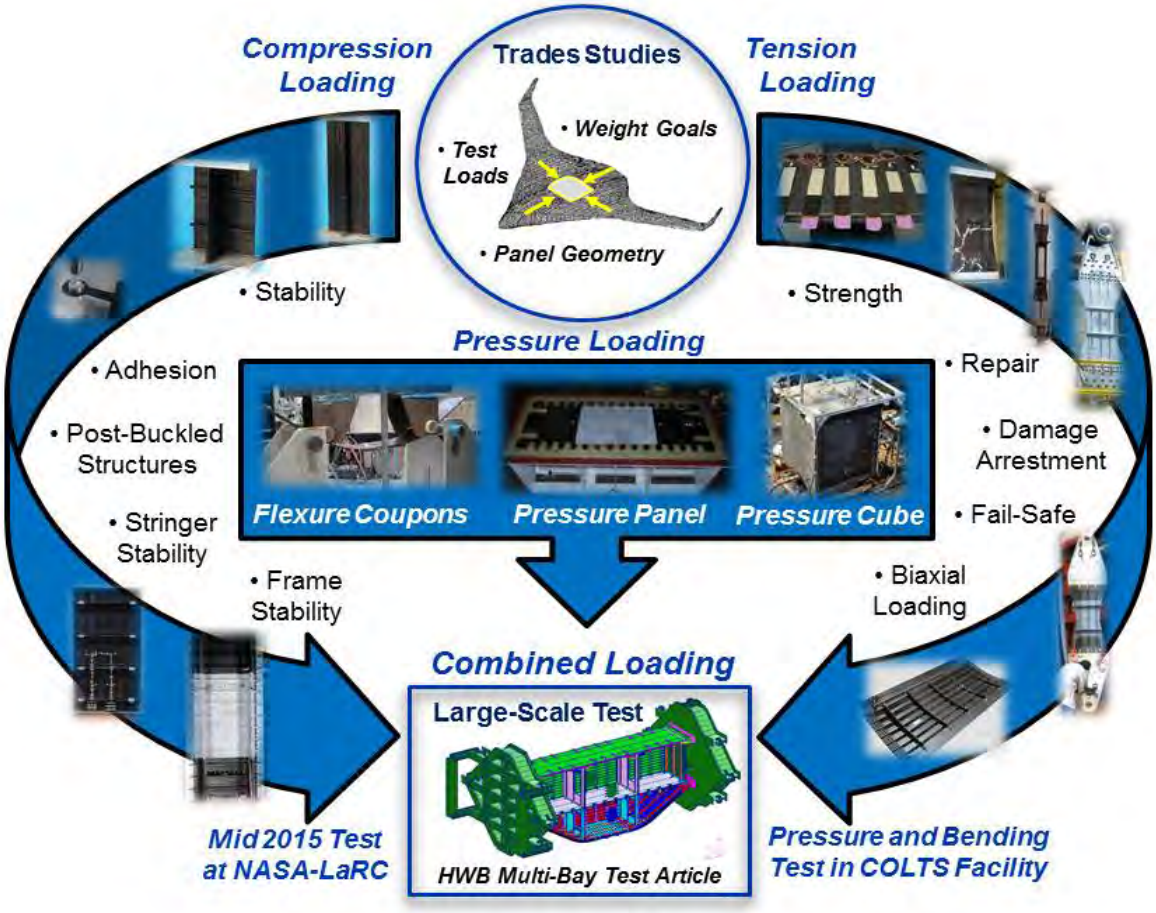

Figure 2-7. HWB Building-Block Test Program Leading up to the Multi-bay Box Test

Element and subcomponent development testing primarily focused on evaluating the PRSEUS panel construction under each of the three fundamental loading directions (compression, tension, and pressure) that would be representative of the HWB airframe design. Multiple compression tests were run to determine the local stability constraints of the individual structural details, in addition to testing to assess the stability of the built-up panels in both the stringer and frame directions. A rigorous batch of tension tests was completed to demonstrate both the large-notch damage-arrestment capability of the stitched interfaces and how damage propagation could be controlled to permit panel designs with superior residual strength capabilities. Pressure panels were also successfully tested to validate the basic features of the minimum-gage panel design as determined by the panel-level structural analyses conducted at the outset of the program. When the fundamental characteristics of the PRSEUS panel design had been validated, the three large subcomponent panels shown in Figure 2-8 were then designed and tested to isolate the key loading conditions that would eventually be tested in the combined-loads environment in the MBB test at the COLTS facility (Ref. 2-2). The resulting load levels and failure modes achieved in those tests not only provided the basis for the MBB structural analysis, they also indicated the expected load levels derived from the vehicle-level trade studies (Ref. 2-1) that would be imparted by the actuators in the COLTS test cell (as summarized in Figure 7-21).

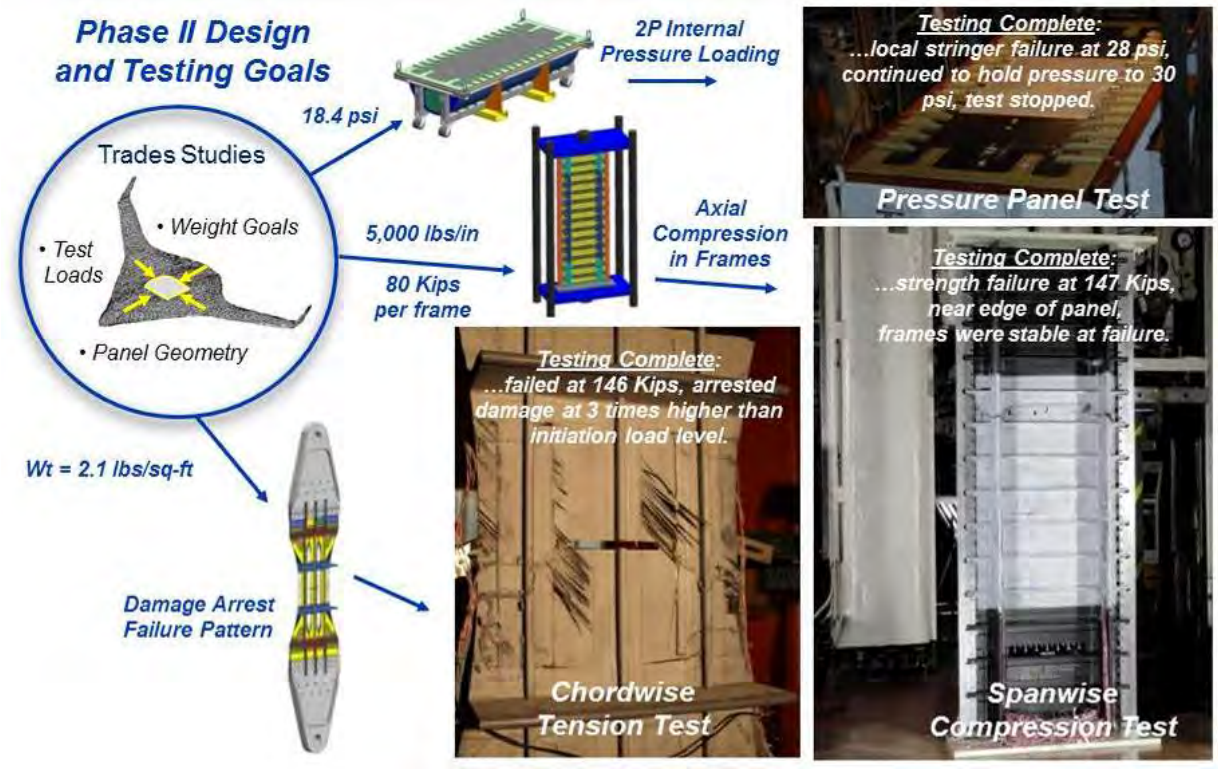

Figure 2-8. Principal Subcomponent Tests to Assess Critical Loading Conditions

As the fundamental design aspects of the panel were coalescing, the focus of research shifted to another high-risk area of the HWB cabin design, the square corners along the edges of the pressure vessel. To better understand how the large integral PRSEUS panels could be efficiently joined in the corners to avoid adding excessive weight to the design, the cube risk-reduction test specimen pictured in Figure 2-9 was tested. The pressure-tight test article was to be tested to destruction in the COLTS facility to validate the edge and corner joint designs that would ultimately be used to design the larger MBB. Cube specimen buildup and completion are shown in Figure 2-9 (prior to testing).

Figure 2-9. Cube Test Article Used to Validate MBB Design Approach

To generate representative loading in the corners of the small test article, an over-pressure condition was created until the bending moments in the corners were equal in magnitude to those that would be experienced in the larger MBB. These values were exceeded as the final failure load of 48 psi was achieved, when the frame metallic splice fittings failed in the corners. (Figure 2-10).

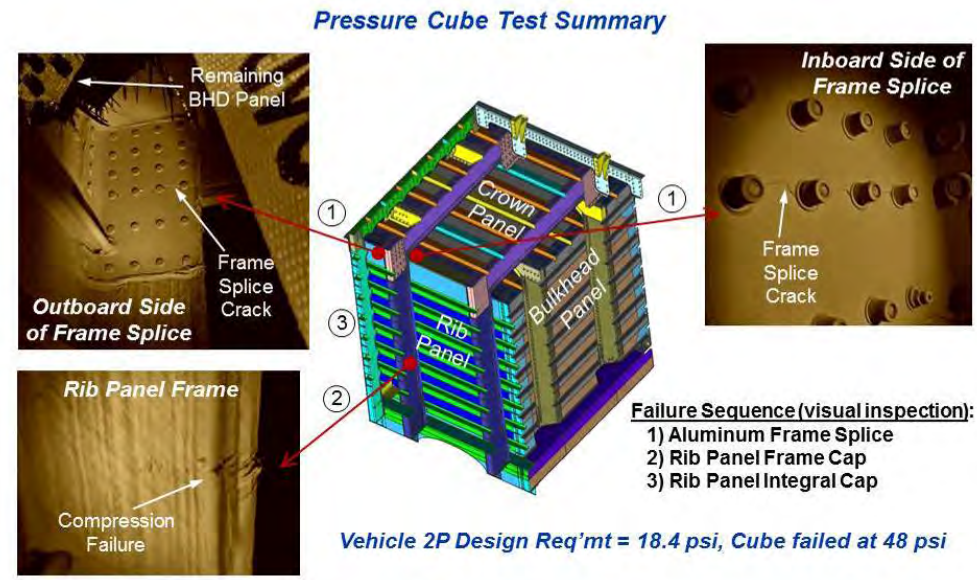

Figure 2-10. Cube Test Article Exceeded Design Requirements

The loss of bending moment continuity in the corners led to the subsequent overloading of the bulkhead panel, which caused it to fail catastrophically, but not before validating the structural integrity of the joining methods and the design approach of the cube. With the basic panel design parameters and joining techniques validated by test, the detail design and analysis work on the MBB was confidently moved forward.

2.3 Design Loads

In conjunction with the detail design for the MBB, results of the vehicle-level trade studies (Figure 2-11) (Ref. 2-1) were used to establish the critical load cases as well as calculate the running loads that would be imparted on the MBB Finite Element Model (FEM). It was important to preserve the analytical linkage between the vehicle and MBB FEMs so that the eventual test results could be correlated back to an airframe weight or sizing assumption that would quantify the relative success of the testing.

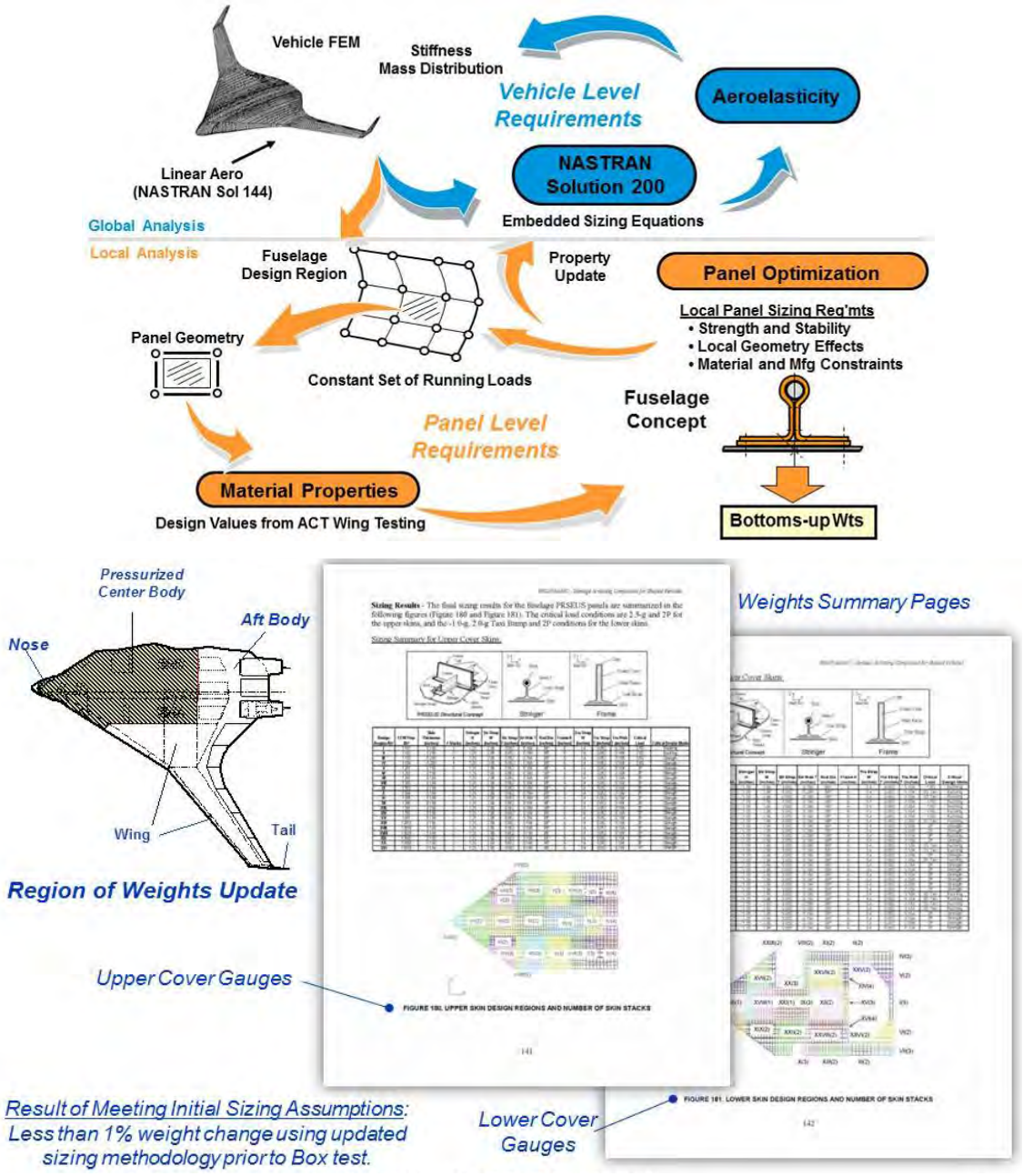

Figure 2-11. Summary of FEM-based Trade Study Structural Weights

A high-fidelity NASTRAN FEM was constructed for the MBB that included the proper boundary conditions and loading inputs for the COLTS facility. The point load actuator inputs that drove the rigid end platens were adjusted until the running loads in the crown and keel panels closely matched the magnitudes generated by the vehicle-level analyses (Figure 2-12).

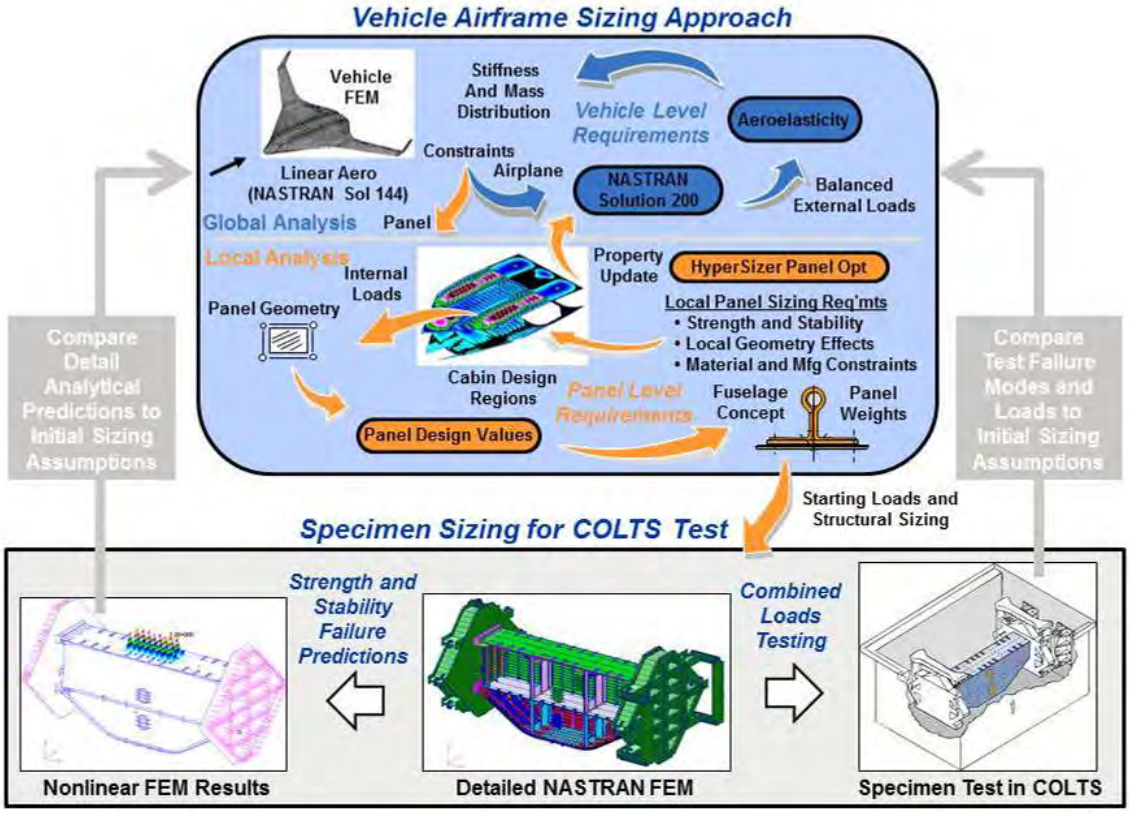

Figure 2-12. MBB Loads/Gages Were Derived from Vehicle-Level Sizing Results

Due to the limited size of the MBB (relative to an entire airplane), the 14 predominant sizing load cases used in the vehicle-level trades could be further reduced to five basic loading conditions: 2.5-g with and without pressure, -1.0-g with and without pressure, and the 2P pressure-only load case (Figure 2-13).

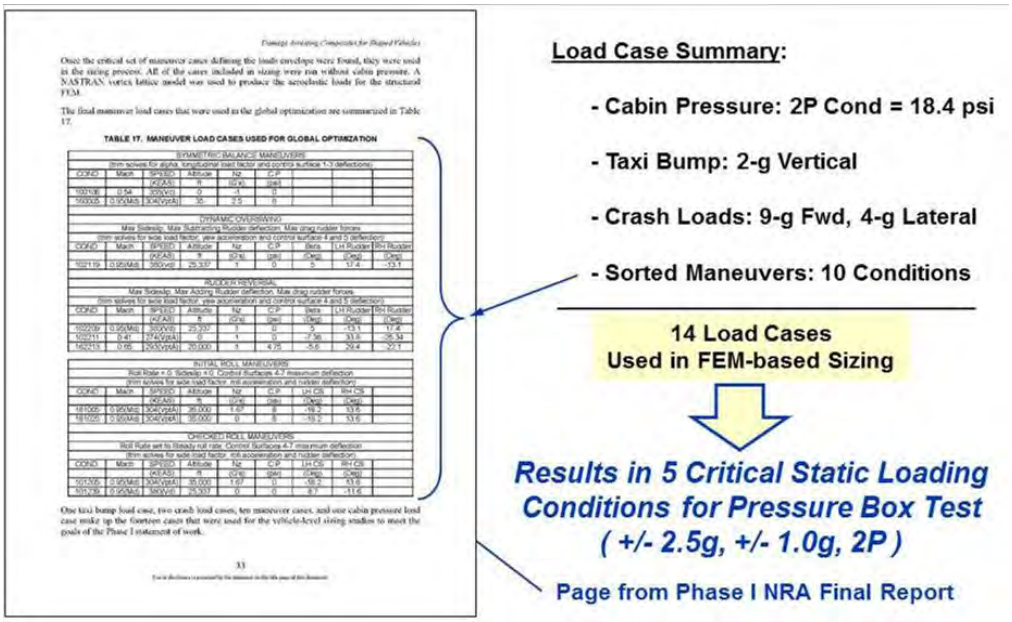

Figure 2-13. Critical Fuselage Sizing Loads From Vehicle-Level Loads Sort

Inasmuch as the primary objective of the MBB testing was to enable assessment of the panel stability of the upper crown, the critical load case was identified as the 2.5-g maneuver condition. This was because this case would produce the maximum compressive running loads across the wide unsupported center region of the fuselage. Using the baseline vehicle-level sizing data (Ref. 2-1), the average crown panel running loads across this region were determined to be in the 5,000-lb/in. range Design Ultimate Load (DUL). This value was used, together with the vehicle 16-in. frame spacing in the methodology outlined in Figure 2-14, to calculate an average frame loading of 80,000-lb per frame (metric M2D).

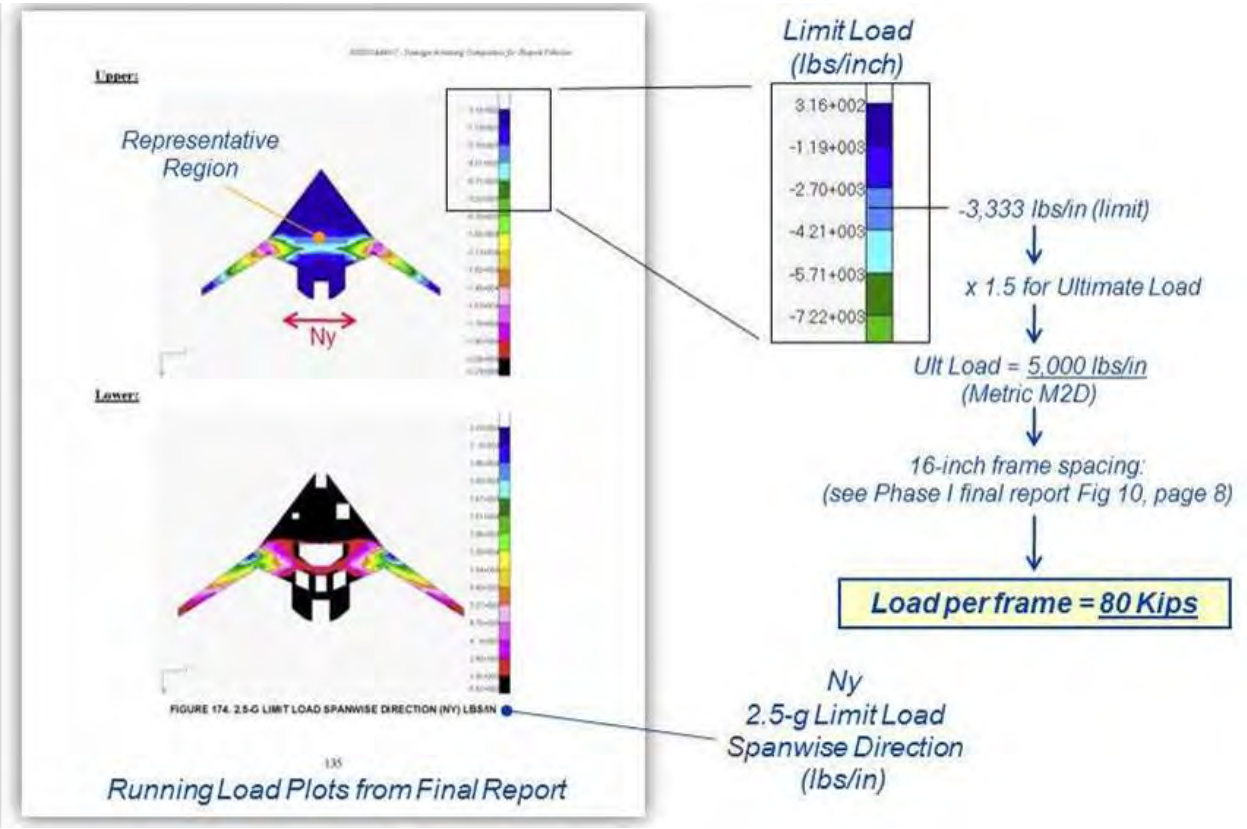

Figure 2-14. Critical Compression Frame Running Loads Would Occur Under 2.5-g Loading

This load case produces the maximum spanwise compressive running loads in the crown panel. However, the 2.5-g case with internal pressure (along with its corresponding lower compressive loading) must also be considered in assessing both the overall panel and local frame stability failure modes due to the out-of-plane curvature caused by the internal pressure in the combined loading scenario.

Because either condition could produce minimum crown panel stability margins, both conditions were thoroughly analyzed in the final failure predictions, as well as carefully tracked by the two metrics, M1A and M2D, shown in Section 2.4 (Figure 2-17). This methodology ensured that not only would the relevant load magnitudes be achieved, but also that the proper testing sequence would occur to gather all critical data points. The resulting actuator loads needed in the COLTS test cell to create the 80-kips frame loading (metric M2D) for the 2.5-g maneuver condition are shown in the free-body diagram in Figure 2-15, as well as the corresponding condition for the 2.5-g+1P combined loading condition that will satisfy metric M1A in Figure 2-16. Once both of these design conditions were satisfied during testing, it would verify that the minimum gage crown panel design geometry is capable of bearing the highest spanwise compression running loads encountered in the baseline airplane configuration with and without internal pressure.

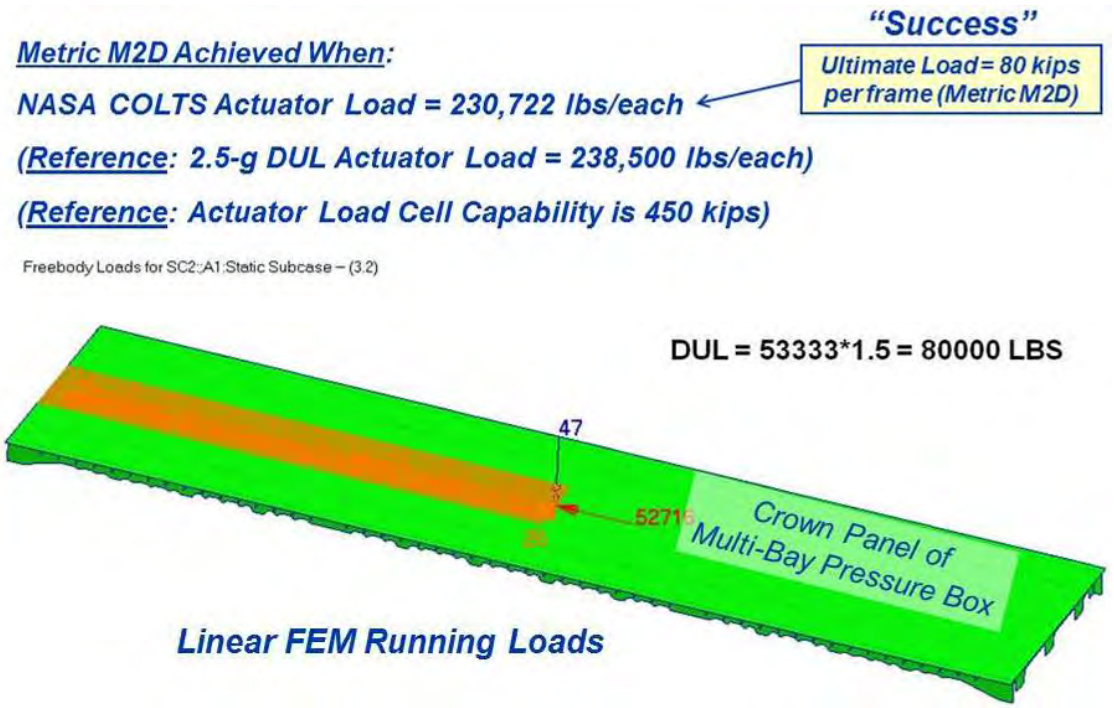

Figure 2-15. 2.5-g Load Case Produces Compression Loading in Upper Crown Panel

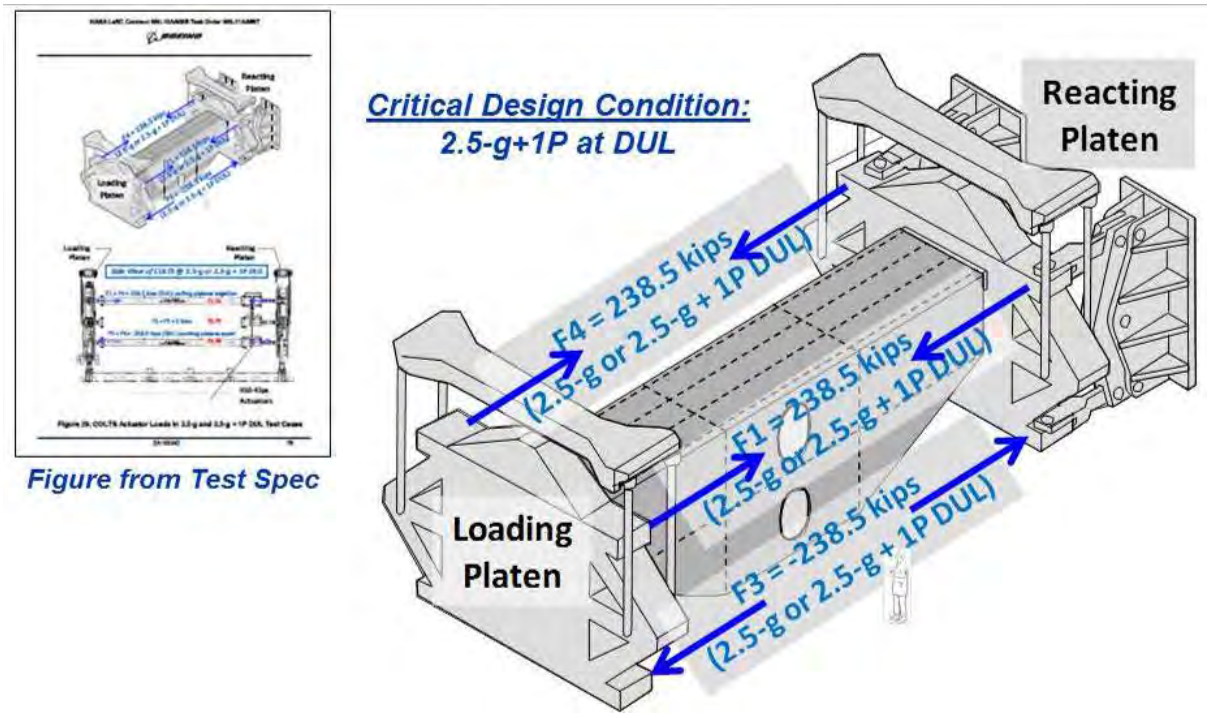

Figure 2-16. COLTS Loads Needed to Generate Critical Compression Loading in the Crown Panel

2.4 Design Metrics

The design metrics for quantifying the success of testing were derived directly from the vehicle-level trade study results (Ref. 2-1), as well as the subcomponent tests (Ref. 2-2) that were completed at previous stages of the development program. This cumulative building-block approach was completed to ensure that the weight targets, specimen geometries, and load levels selected for specimen testing would be relevant and, ultimately, be used to quantify the airframe weight values generated during the HWB baseline configuration (BWB-5-200G) trade studies (Ref. 2-1).

Knowledge gained during element testing was used as the basis for developing increasing levels of specimen complexity, which served to isolate and validate the three primary loading directions found on the HWB pressure cabin (Nx, Ny, and Nz). In each case, the magnitude and direction of the loading was intended to correspond with a specific load case and location on the airframe, which, in turn, could be used to validate the analytical results and assumptions generated during the trade studies. The relationship between the test results and the metrics established at the outset of the program was consistently maintained up to and through the final MBB test, as depicted in Figure 2-17.

All test components exceeded their metric goals, except for the two-frame spanwise compression panel, which was about 7% below the stated target value of 80 kips per frame (M2D). Although this particular test result was below the target value, the final evaluation of the specimen failure determined that a strength failure emanated at the panel free edge before achieving a high enough load level to buckle the frame elements. Because the integral frame design remained stable without any indications of column instability throughout the entire loading regime of the specimen, and the FEM-based buckling analysis prediction was also higher, the possibility of not achieving the frame stability metric in the MBB test would represent only a minor concern going into the final test.

In all other tests, metric values were readily exceeded. The large magnitude of these positive results indicated that as each component of loading (Nx, Ny, and Nz) was brought together into the more complex combined-loading environment, ample margin still existed within the PRSEUS structural concept to accommodate the interaction that was expected between the in-plane and out-of-plane components of loading. The complexity of this interaction formed the basis of the development activities going into the final test. Although increasing levels of loading complexity have been used in the ensuing test program, the basic metric values established at the outset have continued to form the basis for quantitatively measuring the success in each phase of testing throughout the building-block program.

With the successful completion of each test and metric evaluation, the structural feasibility evaluation of the HWB pressure cabin continued to progress. For the first time, large subcomponent-level tests were undertaken with a structural concept that was capable of meeting both the producibility and performance challenges of the noncircular HWB airframe. Throughout the course of this effort, the fundamental enabling aspects of the HWB pressure cabin design were analytically characterized by FEM-based trade studies and then validated by testing in representative loading conditions. Beyond exceeding the metric values described in the preceding section, these tests established the foundation for challenging the conservative sizing assumptions used in the initial trade studies. Once the final MBB test was successfully completed, satisfying all metrics, then airframe weights could be revisited and recalculated using the new higher load levels resulting from the testing.

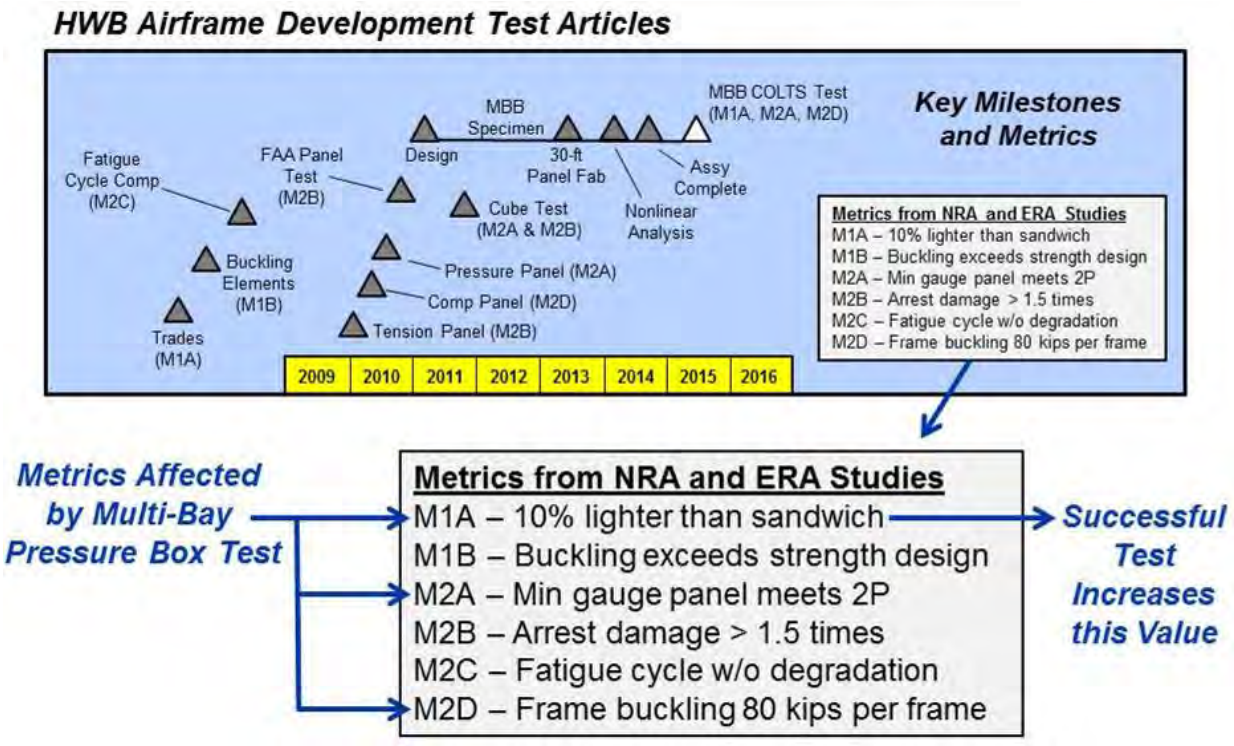

Figure 2-17. Summary of Metrics Established to Measure the Success of Testing

The expectation was that areas of the crown panel that were previously multi-stack skin configurations could be reduced to the minimum gage geometries of the one-stack skin gage (0.052-in. thick) with further reduced frame thicknesses, as demonstrated by the MBB. The effect of such changes within the given design region encompassed by the MBB is shown in Figure 2-18.

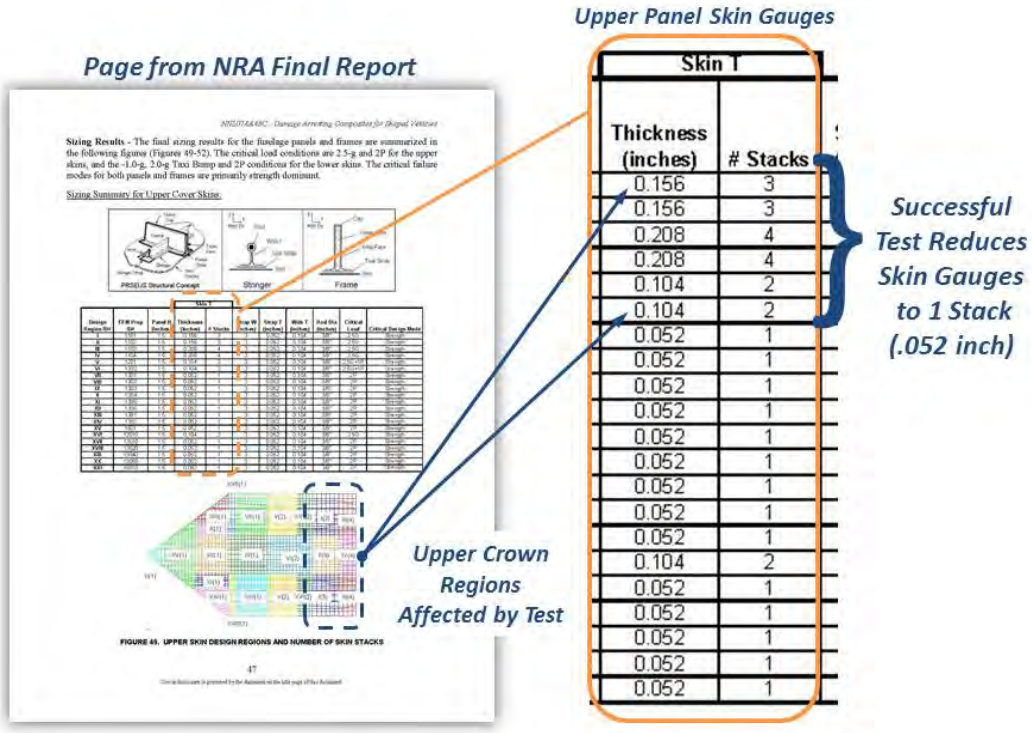

Figure 2-18. Upper Crown Panel Regions Affected by Successful MBB Test Results

Ultimately, weight savings achieved in the most highly loaded aft region of the shell can be implemented throughout the airframe to reduce the overall weight and further improve HWB operational performance. Such changes will also affect the weight savings value of 10.3% calculated in the initial studies to show the benefits of PRSEUS over the old baseline sandwich concept (Figure 2-19).

Beyond exceeding the metric values described in the preceding section, the building-block tests have also established the foundation for the evolution of HWB pressure cabin design. The tests have validated the possibility of designing large flat-sided composite structures that can be internally pressurized and yet remain light enough to retain the superior operating performance enabled by the lifting-body shape of the HWB pressure cabin.

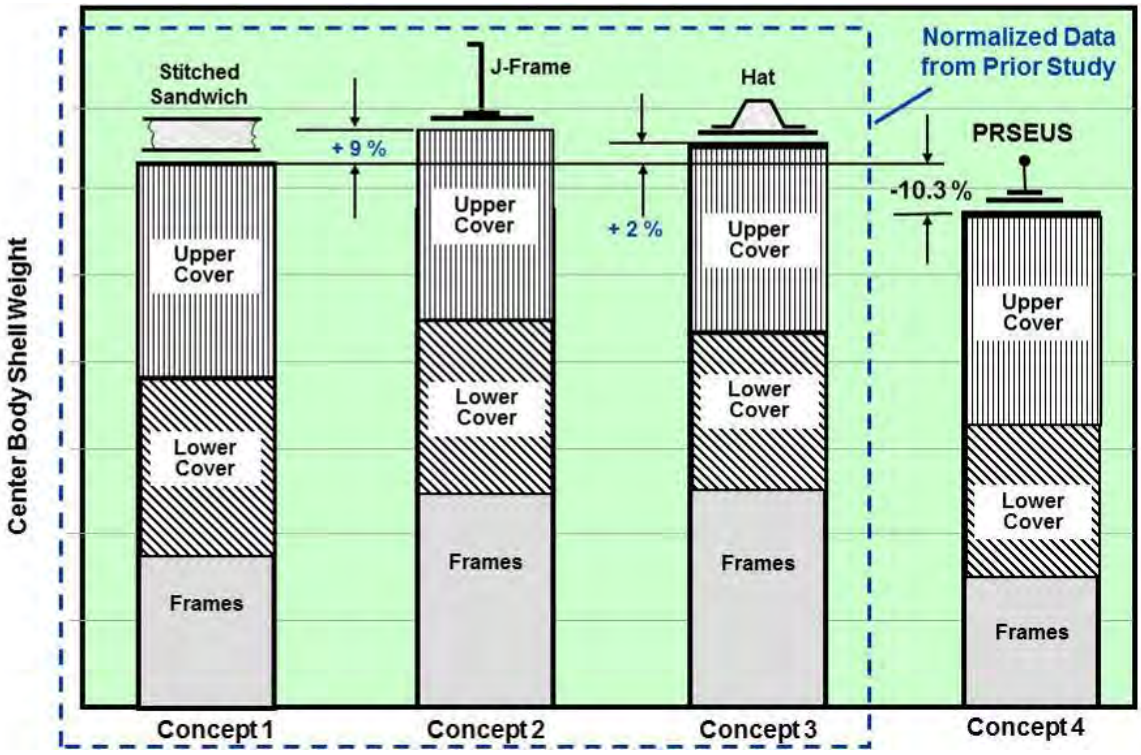

Figure 2-19. Overall Weight Savings Metric (M1A) Established for Fuselage Center Body

3.0 DETAIL DESIGN DEVELOPMENT

The primary goal of the MBB project was to replicate the combined bending-and-pressure loading environment found in the HWB pressure cabin. To accomplish this for the maneuver load cases (with nominal internal pressures), as well as for the 2P (18.4 psi) static proof load case, the MBB would have to be a closed vessel capable of maintaining internal pressurization. To introduce the representative wing-bending loads from the 2.5-g and -1.0-g load cases, axial loads would need to be applied at the upper and lower edges of the MBB structure where the wing joins the fuselage. These two fundamental requirements drove the basic MBB design, whereas the overall test article size was reduced to approximately 80%-scale of the baseline airplane configuration to help reduce fabrication and testing costs without adversely affecting data generated in the test.

3.1 MBB Layout

Relative to the baseline airplane configuration (BWB-5-200G) used to develop the load cases and structural sizing data, the overall MBB dimensions were photographically scaled down until the length of the aft pressure bulkhead (equal to the distance across the pressure cabin) on the baseline airplane matched one of the discrete loading stations in the COLTS test facility. The best match was the 30-ft station, which ultimately determined the 80%-scale value used to design the MBB, as shown in Figure 3-1.

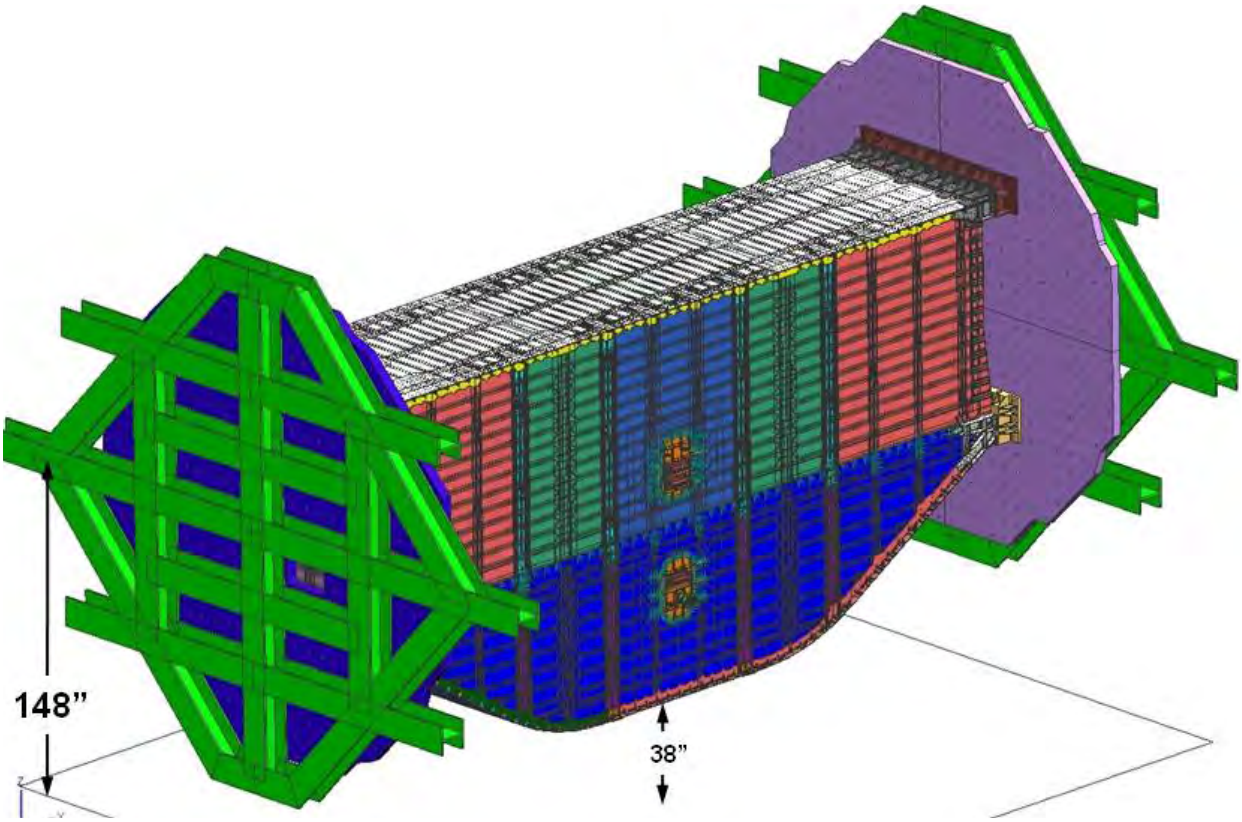

Figure 3-1. Multi-bay Box Located Between COLTS Platens

Once the overall scale and width (distance between the platens) was set, then MBB depth (distance between the forward and aft pressure bulkheads) was selected based on minimizing the fabrication cost while still achieving a representative loading condition within the middle region of the MBB. This resulted in a center frame spotted at the centerline with an open bay on either side to help wash out the edge effects created by the pressure bulkheads and free edges. As with any simplified test article, introduction of finite edges creates some unrepresentative effects, but these were not deemed to be sufficient to affect the basic loading patterns along the centerline.

The basic dimensions that defined the MBB design envelope are summarized in Figure 3-2 using a common airplane reference system (X axis = inboard/outboard). The neutral axis of the MBB was placed along the 148-in. "Z" plane to match the rotation axis of the platens. The resulting clearance from the lower keel panel to the floor then became 38 in. The overall distance between the platens was 30 ft, and once the adapter and load-introduction fitting envelopes were subtracted, the nominal composite panel width became about 28 ft. The center bay was maintained at 10 ft, making it slightly larger than the outer bays. The floor line was also pushed down slightly to make the upper module height and, ultimately, the crown panel compression loads more representative.

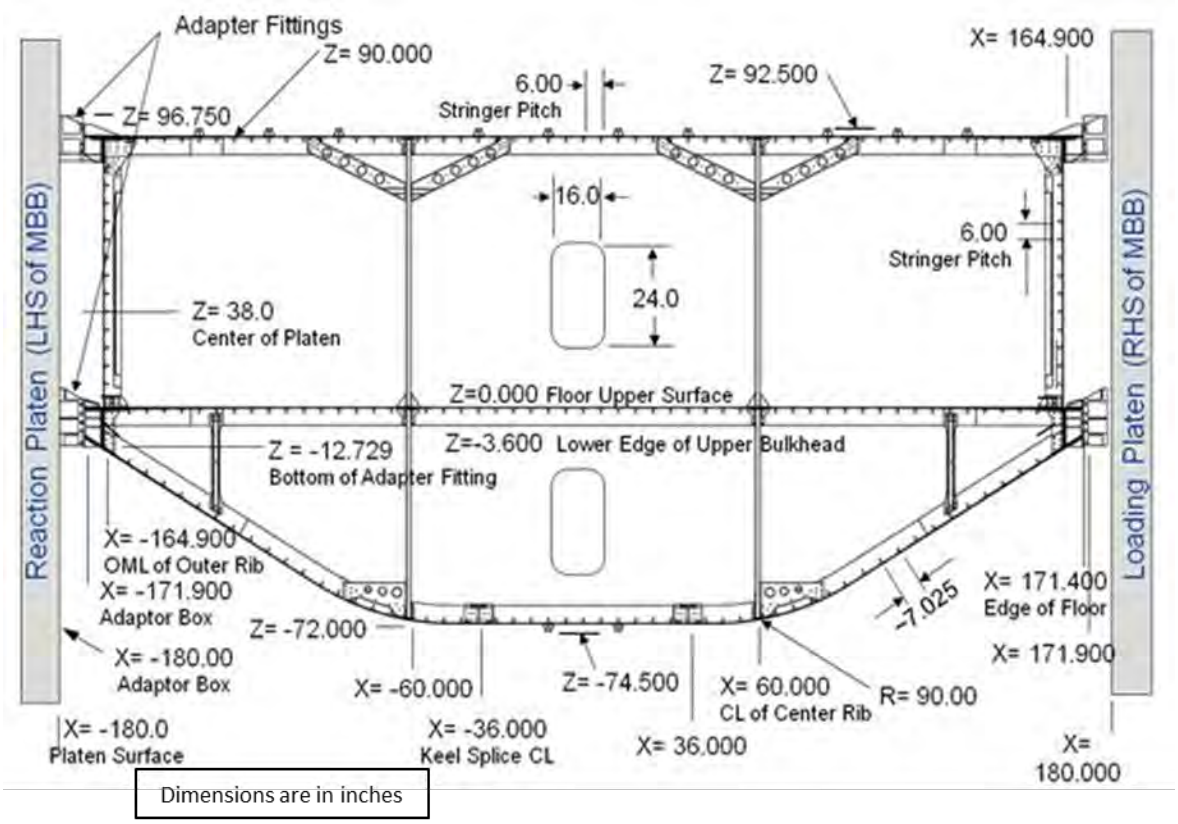

Figure 3-2. MBB Assembly and Facility layout Dimensions Used

Working within this design envelope, the MBB design was developed using a solid-model-based definition format in Unigraphics. The resulting solid-model geometries were then used both by the stress group to create the FEM and by manufacturing to design the tools. The geometries were eventually also used to help build and assemble the completed panels into the final MBB structure. A complete list of all drawings is contained in Table 3-1.

Table 3-1. Dataset and Drawing List

Part No.	Description
ZA153292-501	Rod, Pultruded
ZA151384-501-A	Fillets, Woven - .235R
ZA151384-503-D	Fillets, Woven - .15R
ZA151384-505-A	Fillets, Woven - .50R
ZJ153384	General Arrangement Layout – Pressure Box
ZJ153340	ICD – COLTs Test Facility to Pressure Box
ZJ153341	Test Installation – Pressure Box in COLTs
ZJ153342	Test Specification
ZJ153343-1	Upper Test Adapter Box
ZJ153344-1	Lower Test Adaptor Box
ZJ153345-1	Upper OML Load Introduction Fitting
ZJ153346-1	Upper IML Load Introduction Fitting
ZJ153346-2	
ZJ153346-501	
ZJ153346-502	
ZJ153346-503	
ZJ153346-504	
ZJ153346-505	
ZJ153346-506	
ZJ153347-1	Upper IML External Frame Load Intro Fitting
ZJ153348-1	Upper IML Internal Frame Load Intro Fitting (outside frames)
ZJ153348-2	
ZJ153348-501	Upper IML Internal Frame Load Intro Fitting (Center frame)
ZJ153348-502	
ZJ153349-1	Auxiliary Outer Rib Plate
ZJ153350-1	Pressure Box Assembly
ZJ153351-1	Crown Panel
ZJ153352-1	Floor Panel
ZJ153353-1	Upper Bulkhead Panel
ZJ153354-1	Lower Bulkhead Panel
ZJ153355-1	Side Keel Panel
ZJ153356-1	Center Keel Panel
ZJ153357-1	Outbd Rib Panel
ZJ153358-1	Upper Center Rib Panel
ZJ153359-1	Lower Center Rib Panel
ZJ153650-1	Lower OML Load Introduction Fitting
ZJ153651-1	Lower IML Load Introduction Fitting
ZJ153651-501	
ZJ153652-1	Lower IML External Frame Load Intro Fitting
ZJ153652-2	
ZJ153652-501	
ZJ153652-502	
ZJ153653-1	Lower IML Internal Frame Load Introduction Fitting (Keel & Floor)
ZJ153653-2	
ZJ153654-1	Lower External Side Load Introduction Fitting
ZJ153654-2	
ZJ153655-1	Mid Continuous Load Introduction Fitting
ZJ153656-1	Mid Discontinuous Load Introduction Fitting
ZJ153656-2	
ZJ153656-501	
ZJ153656-502	
ZJ153657-1	OML Skin Splice Plate
ZJ153658-1	Keel Splice/ Bulkhead Intercostal Fitting (frame to cap)
ZJ153658-501	Keel Splice/ Bulkhead Intercostal Fitting (frame to frame)
ZJ153658-503	Keel Cap Flange Splice Plate
ZJ153658-505	Keel Cap Splice Fitting
ZJ153659-1	Keel Splice Intercostal Fitting
ZJ153659-2	
ZJ153659-501	
ZJ153659-503	Keel Splice Strap
ZJ153660-1	Bulkhead Frame to Panel Stringer Fitting
ZJ153660-2	
ZJ153660-501	
ZJ153660-502	
ZJ153662-1	Bkhd Frame Splice Fitting
ZJ153662-2	
ZJ153662-501	
ZJ153662-502	
ZJ153662-503	
ZJ153662-504	
ZJ153662-505	
ZJ153662-506	
ZJ153663-1	Access Door, Lower Bulkhead
ZJ153663-501	Access Door, Upper Bulkhead
ZJ153663-503	Access Door, Lower Bulkhead w/ Instrumentation Holes
ZJ153663-505	Access Door, Upper Bulkhead w/ Instrumentation Holes
ZJ153664-1	Bkhd Frame to Canted Stringer #14 Fitting
ZJ153664-2	
ZJ153664-501	
ZJ153664-502	
ZJ153664-503	Bkhd Frame to Canted Stringer #18 Fitting
ZJ153664-504	
ZJ153664-505	
ZJ153664-506	
ZJ153664-507	Bkhd Frame to Canted Stringer #22 Fitting
ZJ153664-508	
ZJ153664-509	
ZJ153664-510	
ZJ153664-511	Bkhd Frame to Stringer #2 Fitting
ZJ153664-512	
ZJ153664-515	
ZJ153664-516	
ZJ153666-1	External Center Keel Stringer Support
ZJ153666-501	External Crown Stringer Support
ZJ153667-1	Keel Gusset
ZJ153667-2	
ZJ153668-1	Wire Clamp Fitting
ZJ153669-1	Crown Gusset
ZJ153669-2	
ZJ153669-501	
ZJ153669-502	
ZJ153900-1	Gang Channel for Access Door
ZJ153900-501	
ZJ153900-503	
ZJ153900-505	
ZJ153900-506	
ZJ153900-507	
ZJ153900-509	
ZJ153900-511	
ZJ153901-1	External Bulkhead Cap Load Introduction Fitting
ZJ153901-2	
ZJ153902-1	Internal Bulkhead Cap Crown Load Intro Fitting
ZJ153902-2	
ZJ153903-1	Bkhd Frame to Floor Cap Clip
ZJ153903-2	
ZJ153903-501	
ZJ153903-502	
ZJ153904-1	Lower Bkhd Skin Splice Strap
ZJ153904-501	Floor Skin Back-Up Plate
ZJ153905-1	Lower Center Rib Clip
ZJ153905-2	
ZJ153905-501	Upper Center Rib Clip
ZJ153905-502	
ZJ153905-503	
ZJ153905-504	
ZJ153905-505	
ZJ153905-506	
ZJ153906-1	Outer Rib Frame to Floor Fitting
ZJ153906-2	
ZJ153906-501	
ZJ153906-502	
ZJ153906-503	Radius Block
ZJ153906-504	
ZJ153907-1	Auxiliary Outer Rib Access Cover
ZJ153907-501	
ZJ153908-1	Floor Strut
ZJ153908-2	
ZJ153909-1	Floor Corner Fitting – Lower Center Rib
ZJ153909-2	
ZJ153910-1	Keel Corner Fitting – Lower Center Rib
ZJ153910-2	
ZJ153911-1	Mid Internal Side Load Introduction Fitting
ZJ153911-2	
ZJ153912-1	Lower Internal Side Load Introduction Fitting
ZJ153912-2	
ZJ153912-501	Stringer Shear Fitting (Lower Bkhd Panel)
ZJ153912-502	
ZJ153913-1	Corner Fitting – Upper Center Rib
ZJ153913-2	
ZJ153915-1	Lower Center Rib to Keel Center Fitting
ZJ153915-2	
ZJ153915-501	
ZJ153915-502	
ZJ153916-1	Center Rib to Bulkhead Fitting
ZJ153916-2	
ZJ153916-501	
ZJ153916-502	
ZJ153917-1	Center Rib to Crown/Floor Corner Fitting
ZJ153917-2	
ZJ153917-501	
ZJ153917-502	
ZJ153918-1	Center Rib to Floor Center Fitting
ZJ153918-2	
ZJ153918-501	Center Rib to Crown Center Fitting
ZJ153918-502	
ZJ153918-503	Center Rib to Crown Center Fitting
ZJ153918-504	
ZJ153918-505	Center Rib to Floor Center Fitting
ZJ153918-506	
ZJ153918-507	Center Rib to Floor Center Fitting
ZJ153918-508	
ZJ153919-1	Upper Center Rib to Floor Fitting (flat side)
ZJ153919-501	
ZJ153931-1	Crown Frame Foam Core
ZJ153931-2	
ZJ153931-501	
ZJ153931-502	
ZJ153931-503	
ZJ153931-504	
ZJ153931-505	
ZJ153931-506	
ZJ153931-507	
ZJ153931-509	
ZJ153931-511	
ZJ153931-513	
ZJ153932-1	Crown Frame Fiberglass Core
ZJ153932-501	
ZJ153932-503	
ZJ153932-505	
ZJ153932-507	
ZJ153933-1	Floor Frame Foam Core
ZJ153933-2	
ZJ153933-501	
ZJ153933-503	
ZJ153933-505	
ZJ153933-507	
ZJ153933-509	
ZJ153934-1	Floor Frame Fiberglass Core
ZJ153934-501	
ZJ153934-503	
ZJ153934-505	
ZJ153935-1	Upper Bulkhead Frame Foam Core
ZJ153935-501	
ZJ153935-503	
ZJ153935-505	
ZJ153936-1	Upper Bulkhead Frame Fiberglass Core
ZJ153936-501	
ZJ153936-503	
ZJ153936-505	
ZJ153936-507	
ZJ153936-509	
ZJ153936-511	
ZJ153937-1	Lower Bulkhead Frame Foam Core
ZJ153937-501	
ZJ153937-503	
ZJ153937-505	
ZJ153937-507	
ZJ153938-1	Lower Bulkhead Frame Fiberglass Core
ZJ153938-501	
ZJ153938-503	
ZJ153938-505	
ZJ153938-507	
ZJ153938-509	
ZJ153938-510	
ZJ153938-511	
ZJ153938-512	
ZJ153938-513	
ZJ153938-515	
ZJ153938-517	
ZJ153938-518	
ZJ153939-1	Side Keel Frame Foam Core
ZJ153940-1	Side Keel Frame Fiberglass Core
ZJ153940-501	
ZJ153940-503	
ZJ153941-1	Center Keel Frame Foam Core
ZJ153942-1	Center Keel Frame Fiberglass Core
ZJ153943-1	Side Rib Frame Foam Core
ZJ153944-1	Center Keel Frame Fiberglass Core
ZJ153944-501	
ZJ153945-1	Corner Strut Fitting
ZJ153945-2	
ZJ153945-501	Corner Strut Fitting
ZJ153945-502	
ZJ153956-1	Strut, Corner Brace
ZJ153957-1	Shim, Side Keel Tee to Center Rib
ZJ153957-501	
ZJ153957-503	Shim, used with 3910-1
ZJ153957-505	Shim, used with 3908-1 at Floor Struts
ZJ153957-507	Shim, used with 3658-1 Keel Splice
ZJ153957-509	Shim, used with 3653-1 at Outer Frame
ZJ153957-511	Shim, used with 3652-1 at outer Frame
ZJ153957-513	Shim, used with 3652-1 at Cap
ZJ153957-515	Shim, used with 3653-1 at Center Frame
ZJ153957-517	Shim, used with 3652-501 at Center Frame
ZJ153978	Locating Cleat Box to Platen (NASA)
ZJ153981	Crown Strain Gages
ZJ153982	Floor Strain Gages
ZJ153983	Upper Bulkhead Strain Gages
ZJ153984	Lower Bulkhead Strain Gages
ZJ153985	Side Keel Strain Gagaes
ZJ153986	Center Keel Strain Gages
ZJ153987	Outer Rib Strain Gages
ZJ153988	Upper Center Rib Strain Gages
ZJ153989	Lower Center Rib Strain gages

3.2 Panel Design Features

Although improvements in feature design and processing parameters continue to be incorporated into the basic PRSEUS design, the materials selection for this effort summarized in Figure 3-3 was identical to what was used in prior development efforts (Ref. 2-2). In spite of there being no conscious decision made to limit the introduction of improved material forms, the lack of progress in this area is indicative of the challenges facing materials suppliers when developing new products for next-generation composite designs—and especially so when those new product forms deviate substantially from their primary product lines.

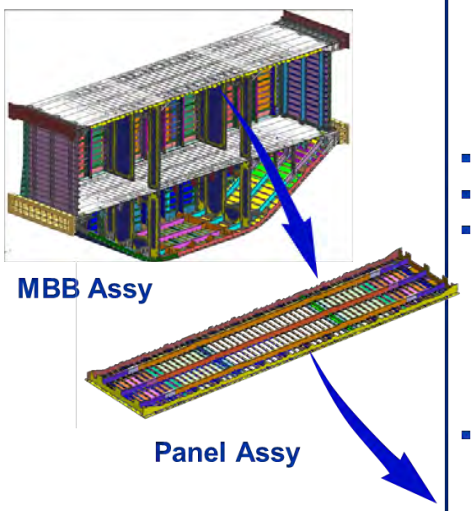

- **Carbon Warp Knit Fabric:**
  - DMS 2436 Type 1, Class 72, Grade A
    - Cured thickness = 0.052
    - Each stack has 7 plies in a +45, -45, 0, 90, 0, -45, +45 pattern
    - Percentage of fiber by area weight is (45/43/12) using a (0/45/90) nomenclature
  - DMS 2436 Type 1, Class 76/77, Grade A
    - Cured thickness = 0.0157
    - Each stack has 2 plies in a 0, 90 or, 90, 0 pattern
- **Fiberglass Fabric: DMS 2212**
- **Epoxy Resin: DMS 2479 Type 2, Class 1 (VRM-34)**
- **Stitching:**
  - One-Sided stitching is used on all stitching except stringer & cap webs
    - 1600 denier Vectran Thread DMS 2443
    - Stitch penetrations are 5 per inch
    - Uses Altin RN820 End Effector
  - Two-Sided stitching is used on stringer and cap webs
    - 1200 denier Vectran Thread DMS 2443
    - Stitch penetrations are 8 per inch
    - Bobbin: Vectran 1200 denier thread
- **Pultruded Carbon Rod**
  - Standard modulus carbon fiber with epoxy resin
  - Small tear drop shape 0.375” dia.
- **Frame Core Material:**
  - Rohacell 110WF foam
  - Thickness = 0.50”
  - Fiberglass/ Epoxy core at the joints
- **Fillet: Woven Standard Modulus Carbon Fibers**
  - Stringers 0.15” radius
  - Integral Tee: 0.345” radius
  - Integral Cap: 0.50” radius

Figure 3-3. PRSEUS Panel Materials Summary

From a structural performance perspective, the single most important improvement made relative to the previous studies was the decision to incorporate the near-edge-of-seam stitching change to the stringer and frame flanges. This change was made based on the results of compression panel testing at NASA LaRC. Under compression loading, high-speed video was used to capture the local delamination growth that occurred between the stringer flange and skin before the full effectiveness of the stitching was realized. To reduce these effects, the outer stitch seam was moved to within a 0.25-in. distance of the flange edge (as shown in Figure 3-4) as compared to the 0.625-in. distance on prior panels. This reduced distance enhanced the out-of-plane strength as the flange and skin pull away from one another. Although a small weight reduction was also realized, the overall flange and tear strap widths were reduced by about 1.25 in. as compared to previous panels, which required extra material to hold the flange in the stitching assembly jig. The primary motivation for this change was to arrest delaminations more effectively, which would, ultimately, increase the overall panel buckling load in the post-

impacted condition. It also increased the width of the open bay, which would allow the skin to deflect even more in post-buckling.

The original intent for the over-sized flange was to support the preform stacks from deflecting during the needle-insertion step in the stitching operation. However, by changing the method of supporting the preform to accommodate the new and narrower flange width, more efficient stringer geometry could now be used for the MBB.

Using a similar approach, frame detail was also improved to capture the near-edge-of-seam stitching method, but some minor differences were required to accommodate the extra stitch rows needed for the wider flanges. The width of the tear strap was increased to soften the transition between the four-stack region of the flange and the one-stack region of the basic skin. Most other detail dimensions remained common to the nominal two-stack frame design depicted in Figure 3-5. Stacks were added to this basic arrangement in regions where higher bending stiffness or increased fastener bearing area were needed. Overall frame spacing was increased to a 24-in. pitch so that the stringer and frame spacing would be multiples of one and other, which permitted the vertically oriented bulkheads to align with the horizontally oriented cover panels.

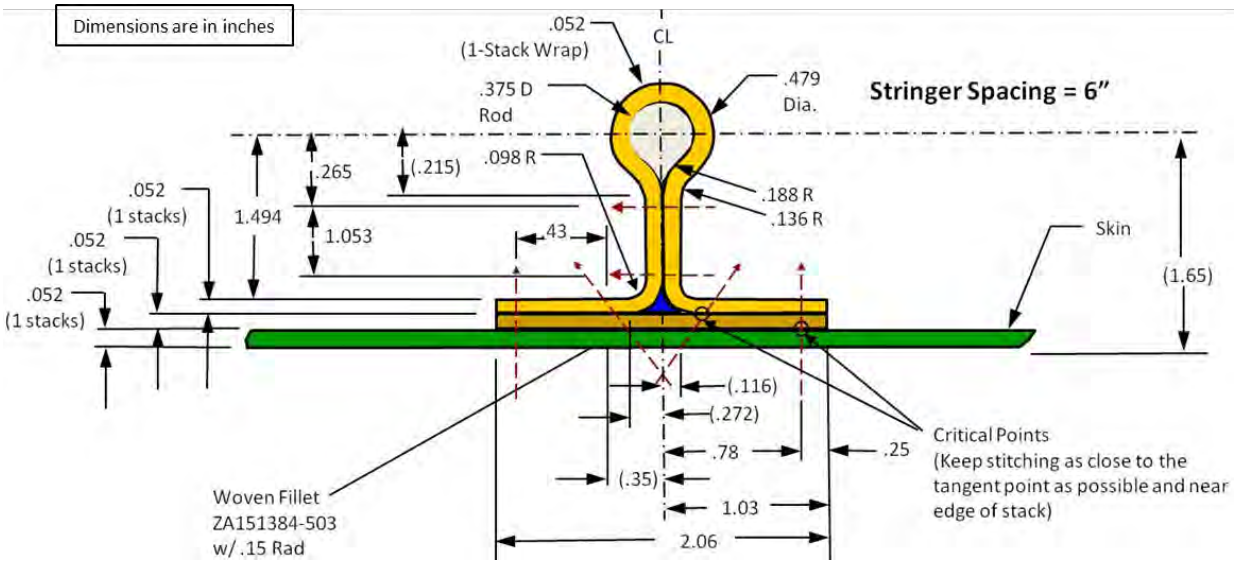

Figure 3-4. Stringer Dimensions

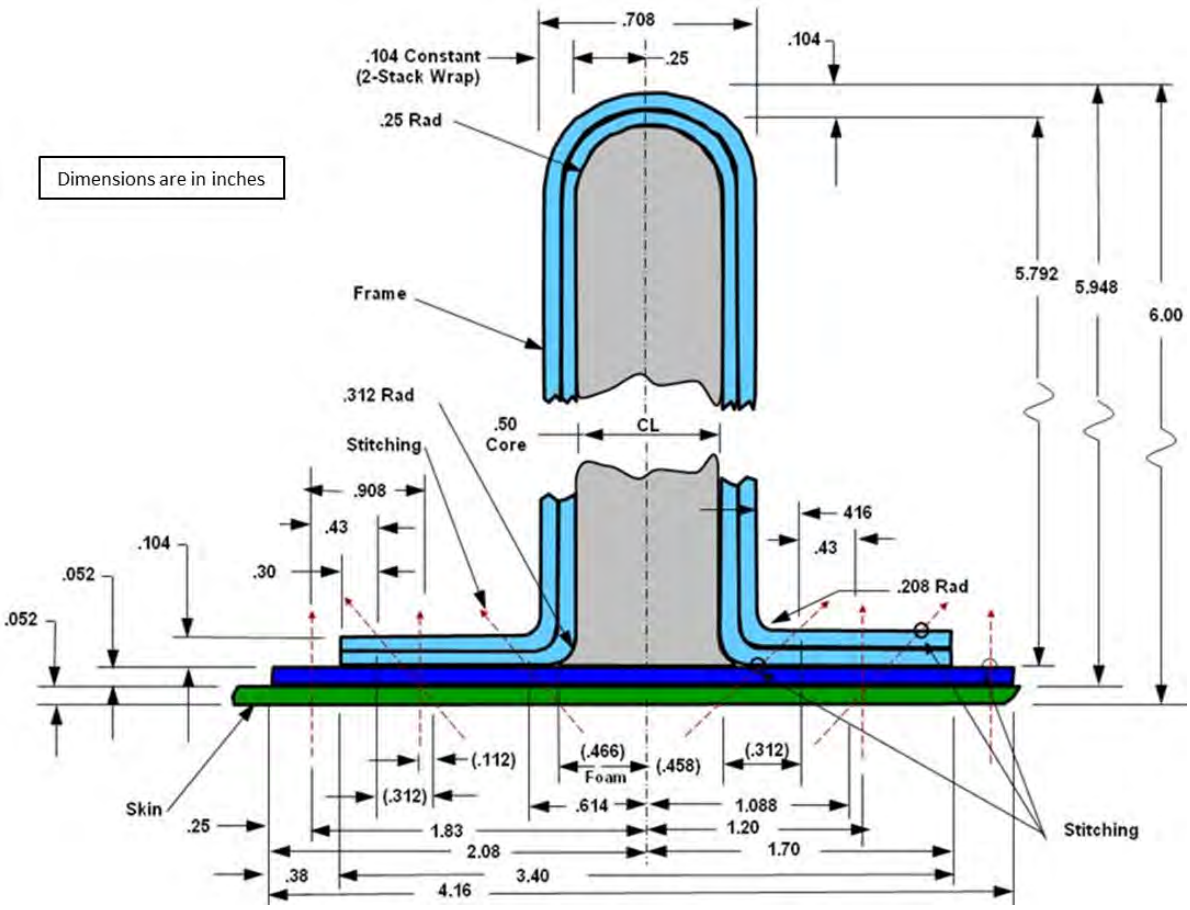

Figure 3-5. Frame Dimensions

The foam core elements of the frame were built up using multiple details. The Rohacell foam core was used in the nominally loaded regions, and solid fiberglass pieces were added at the fitting locations to react fastener clamp-up loads. The locking feature shown in Figure 3-6 was developed to join the separate details without the need for bond tools to hold the separate details in place.

Another important design feature developed under this contract was an integral cap member (with intersecting stringers) that was used to join the bulkhead panels to the cover panels, as shown in Figure 3-7. The advantage of this approach was that it eliminated the metallic fittings and fasteners (through the cover panels) that would otherwise have been needed to attach the panel assemblies.

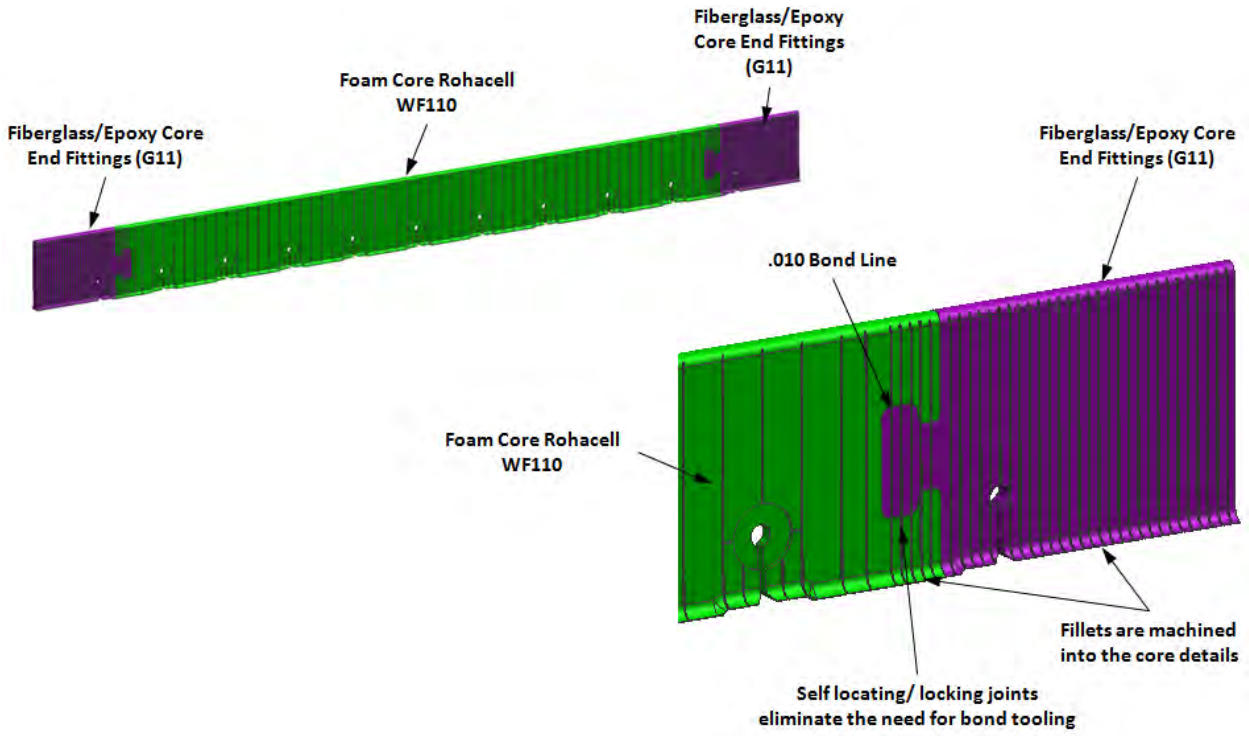

Figure 3-6. Frame Core Inserts

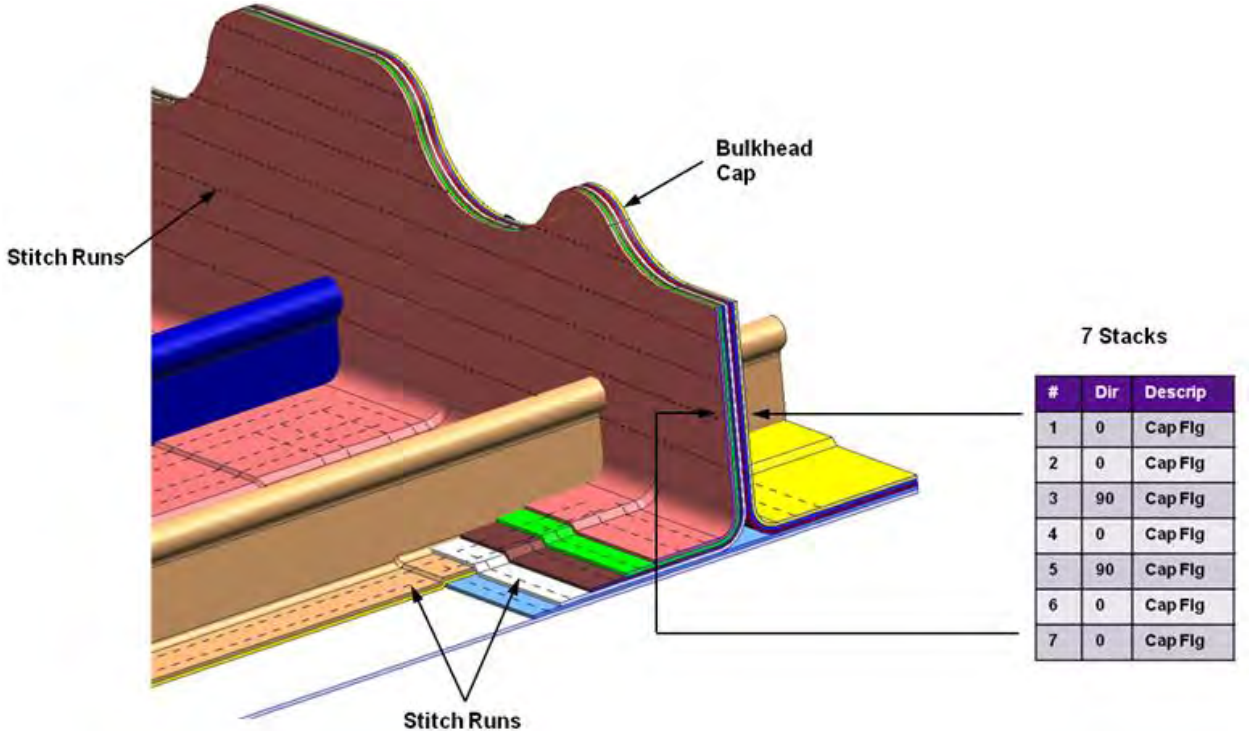

Figure 3-7. Integral Cap Detail

Additional increases in panel integration were accomplished by stitching (reacted out-of-loading) and using the self-support preform fabrication approach (simplified IML tooling). The integral cap feature was molded using a single backup tooling plate under the vacuum bag to create the smooth mating surface needed at the panel mating surfaces.

3.3 Panel Assembly Descriptions

Figure 3-8 shows the completed MBB assembly with the forward bulkhead omitted. Each of the major panel assemblies is described in more detail in the following sections.

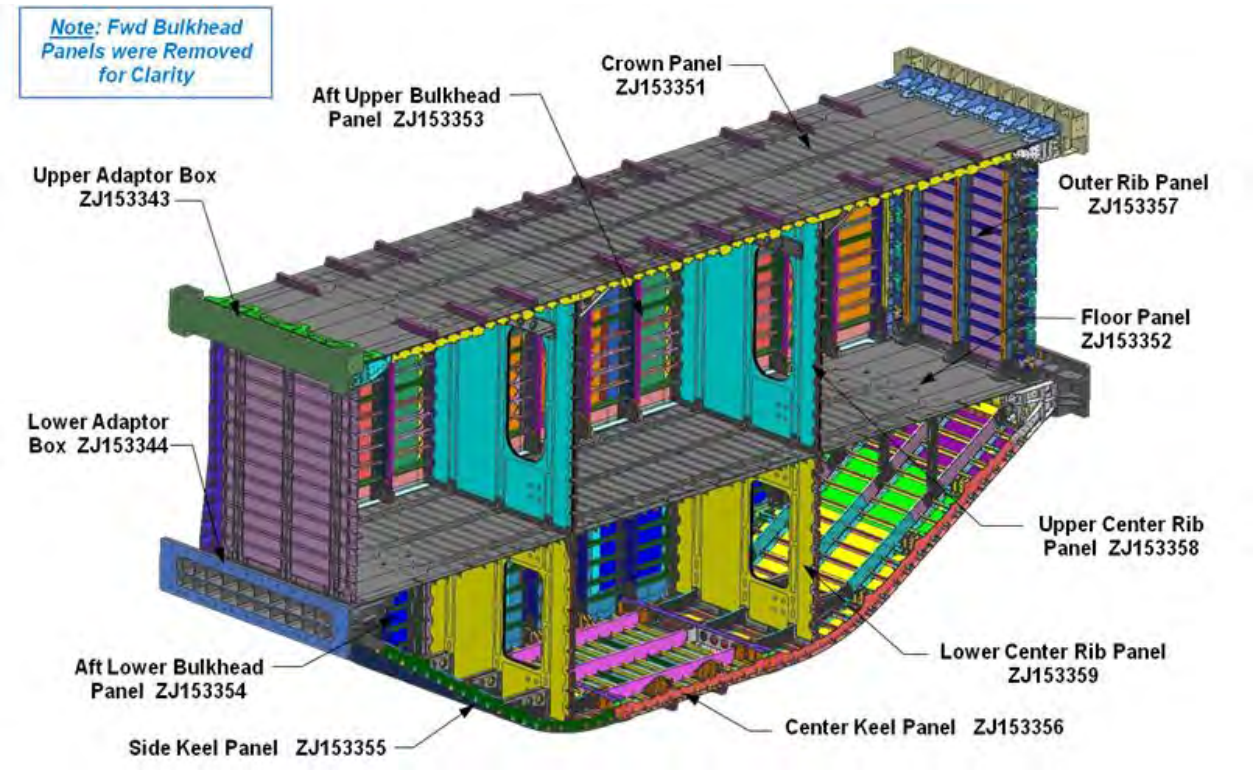

Figure 3-8. MBB Panel Assembly Nomenclature

3.3.1 Crown Panel Assembly (ZJ153351)

The center bay of the crown panel was the critical test region where the combined loading of internal-pressure plus axial-compression was evaluated on the nominal panel geometry. The results were compared with the data already gathered from the single-component loaded test panels (pressure panel [internal pressure only] and buckling panel [axial compression only]) to assess the nonlinear effects of the combined condition.

Because the center bay of the crown panel constituted the test section, all surrounding structure acted to introduce loading into the region of interest. The other panels were also nominally representative of generic fuselage panels in a BWB-type aircraft. Panel thicknesses and the fittings required to integrate them varied from what would be expected in an actual aircraft.

The crown panel comprised the central panel in the pressure box design as it included the test section shown in Figure 3-9. It was a rectangular and flat PRSEUS-type panel with integral rib and bulkhead T-caps at all four edges and two T-caps at locations corresponding to the center rib panels. Both the frame and skin stack buildups were relatively complex in order to drive load into the test section while sustaining the bearing loads at the interface to the COLTS facility.

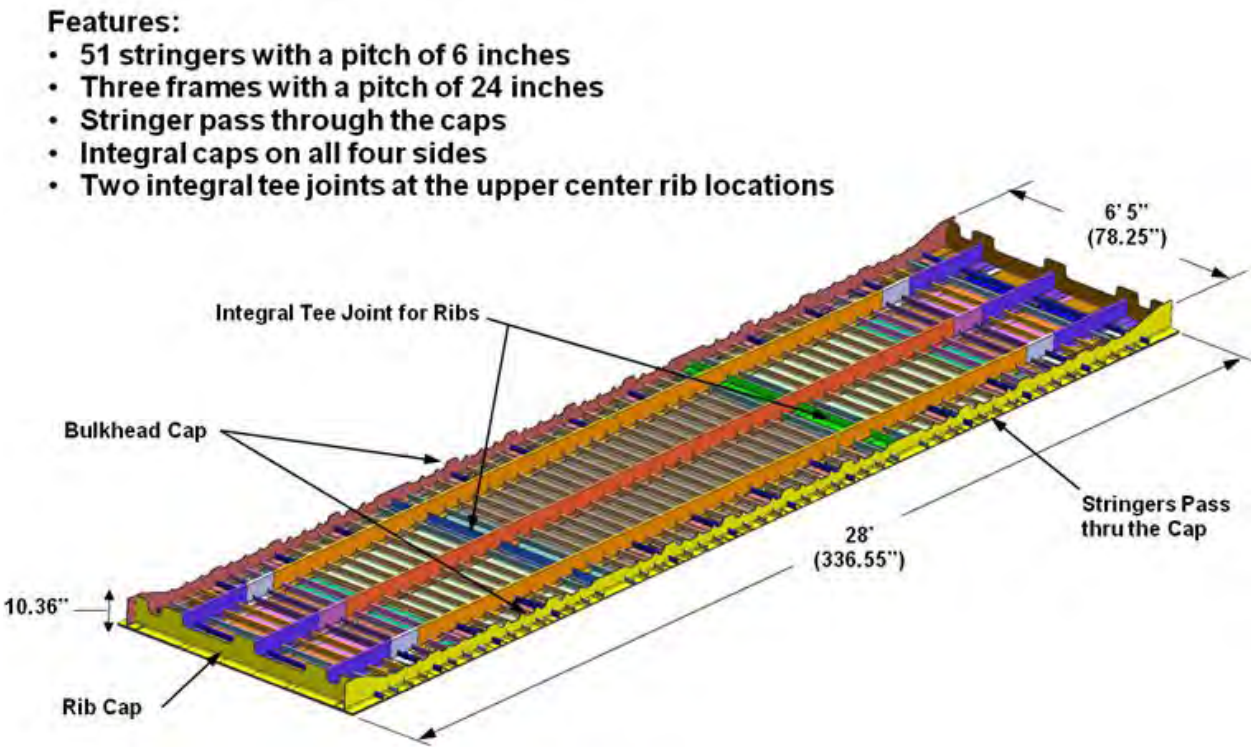

Figure 3-9. Crown Panel Assembly

As shown in Figure 3-10, the rib T-cap was eight stacks thick and was approximately 0.42-in. thick after curing. The integral bulkhead T-caps were seven stacks thick, whereas the T-caps at the center ribs were four stacks thick. Extensive doublers were used in the frame end regions, tapering from four stacks on the frames at the ends to two stacks over the 41-in. run indicated in Figure 3-10. Doubler stacks were also used on the skin, tapering from five additional stacks at the outer rib caps down to the basic one-stack skin at the center rib caps. The intent was to allow for a smooth transition of the load from the load-introduction fittings at the corners to the central test section in the center of the panel.

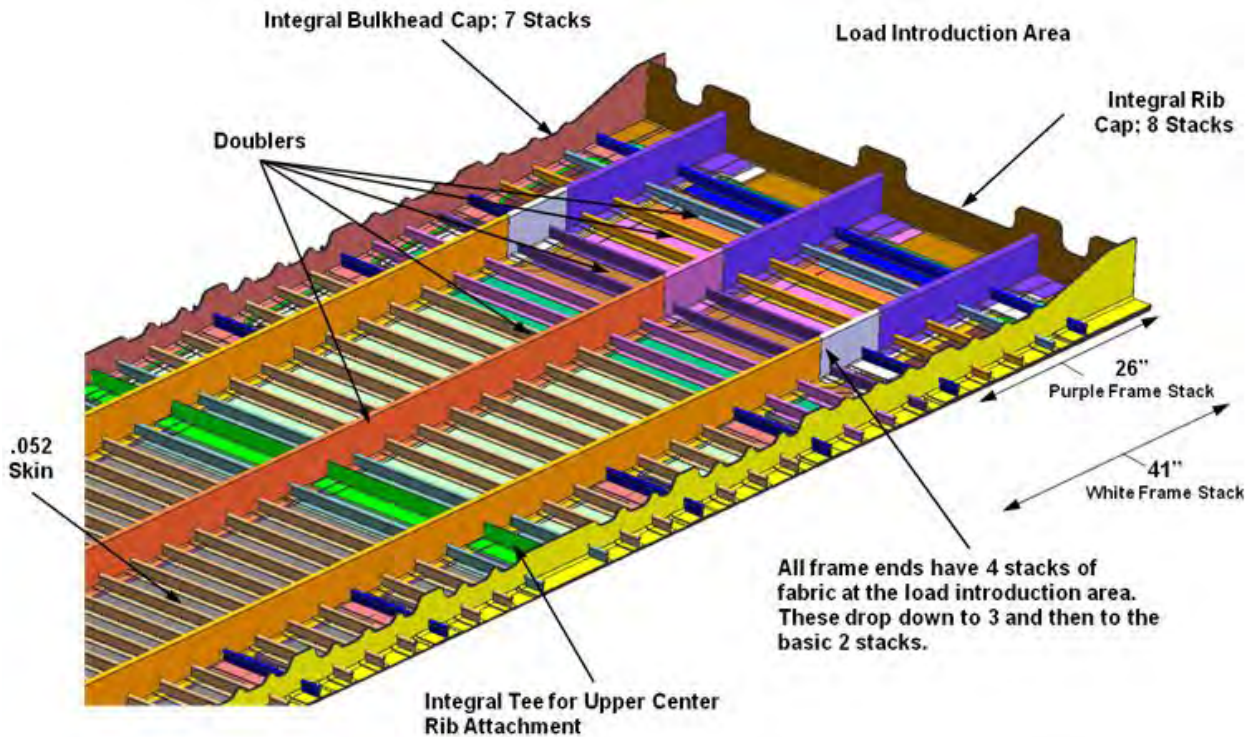

Figure 3-10. Crown Panel Features

Extensive double- and single-sided-type stitching was used throughout the crown panel for through-thickness reinforcement. Figure 3-11 shows the stitching present in the corner region of the crown panel as well as the butt joints at the intersections of the frame end/rib cap and rib cap/bulkhead T-caps. Because large load-introduction fittings were required in this area, these joints were designed as butt joints to reduce the complexity of fabricating the panel.

The stringer ends on the crown panel were also reinforced at locations that corresponded to the frames on the bulkhead panels. This created a flat bearing surface for the frame-to-stringer fittings that further tied the bulkheads to the crown panel, in addition to the integral joint provided by the bulkhead cap. As shown in Figure 3-12, the bulkhead cap and frame stacks were butted together and interleaved. This arrangement created a strong land area for fitting attachment, minimized some of the liquid shimming, and simplified the machining of the fitting by eliminating the joggled interface.

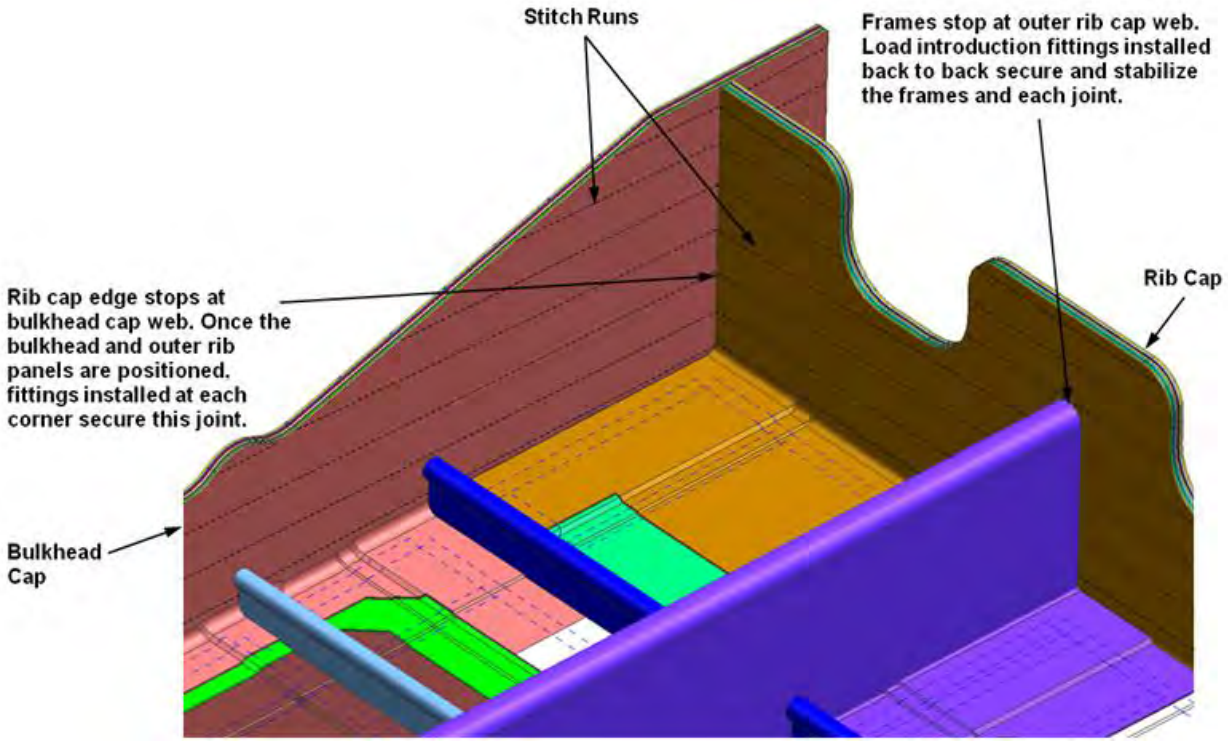

Figure 3-11. Crown Panel Corner Detail

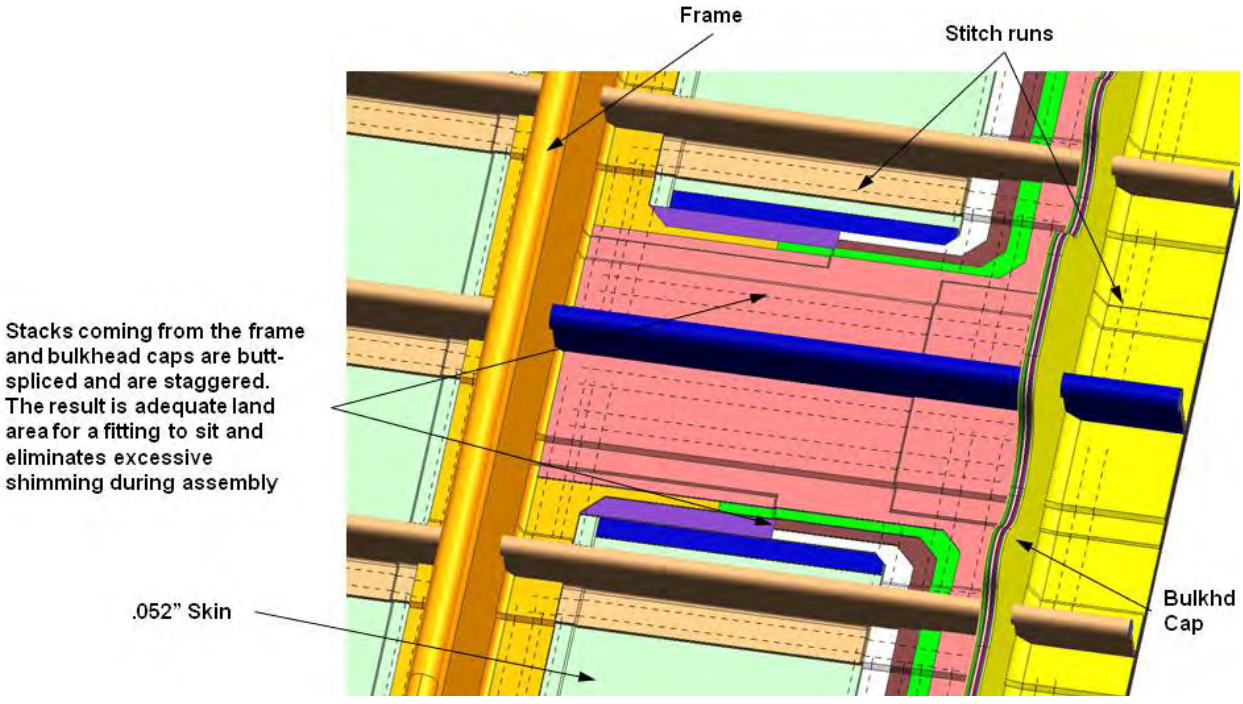

Figure 3-12. Crown Panel Edge Buildups

The bulkhead cap stacks that formed continuous tees along the long sides of the crown panel are shown in Figure 3-13. The cap stacking sequence was balanced and all free edges stitched down. Fillet radii were large (~0.5 in.) in the bulkhead cap to provide for a smooth transition and alleviate stress concentrations in the stacks over the 90-deg bend.

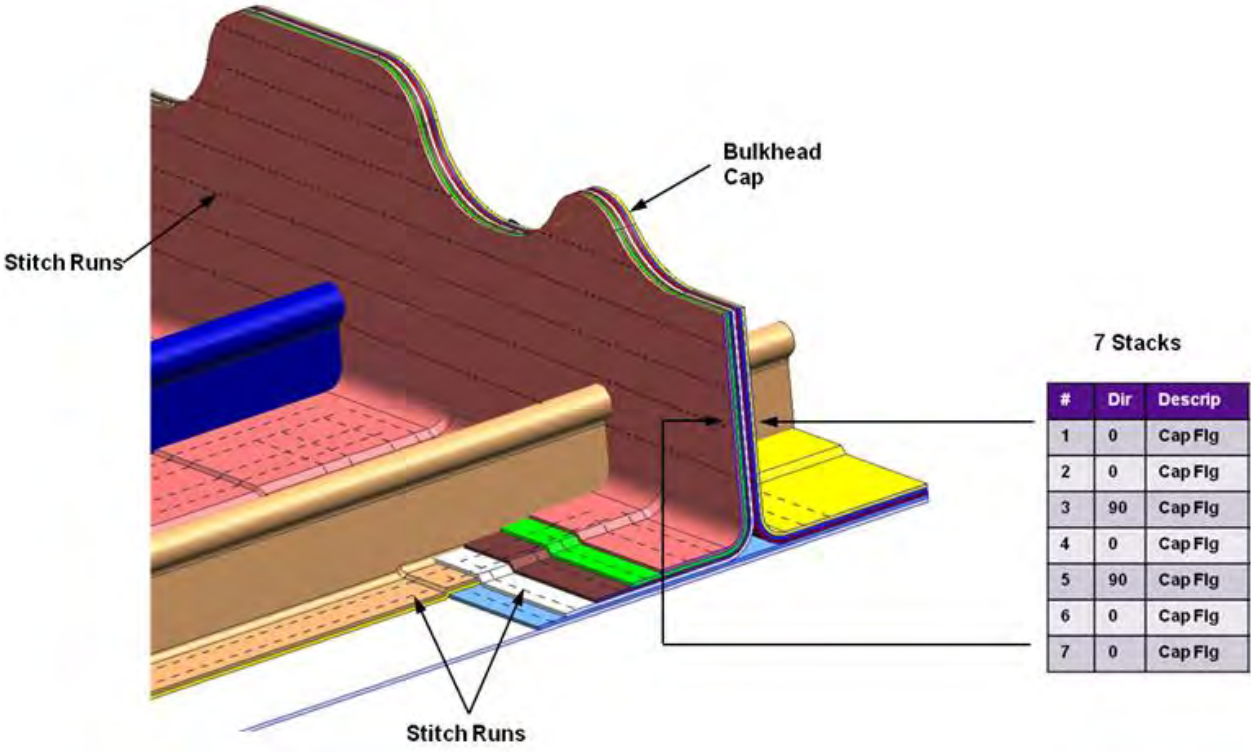

#	Dir	Descrip
1	0	Cap Flg
2	0	Cap Flg
3	90	Cap Flg
4	0	Cap Flg
5	90	Cap Flg
6	0	Cap Flg
7	0	Cap Flg

Figure 3-13. Crown Panel Bulkhead Cap Stacks

The integral rib T-cap shown in Figure 3-14 at the end of the crown panel created the joint at the upper edge of the outer rib panel. Forming panel interface features as part of the panels enabled fewer and lighter fittings to be used at the joints. The outer rib cap layup on the crown panel was constructed using stacks with a balanced orientation.

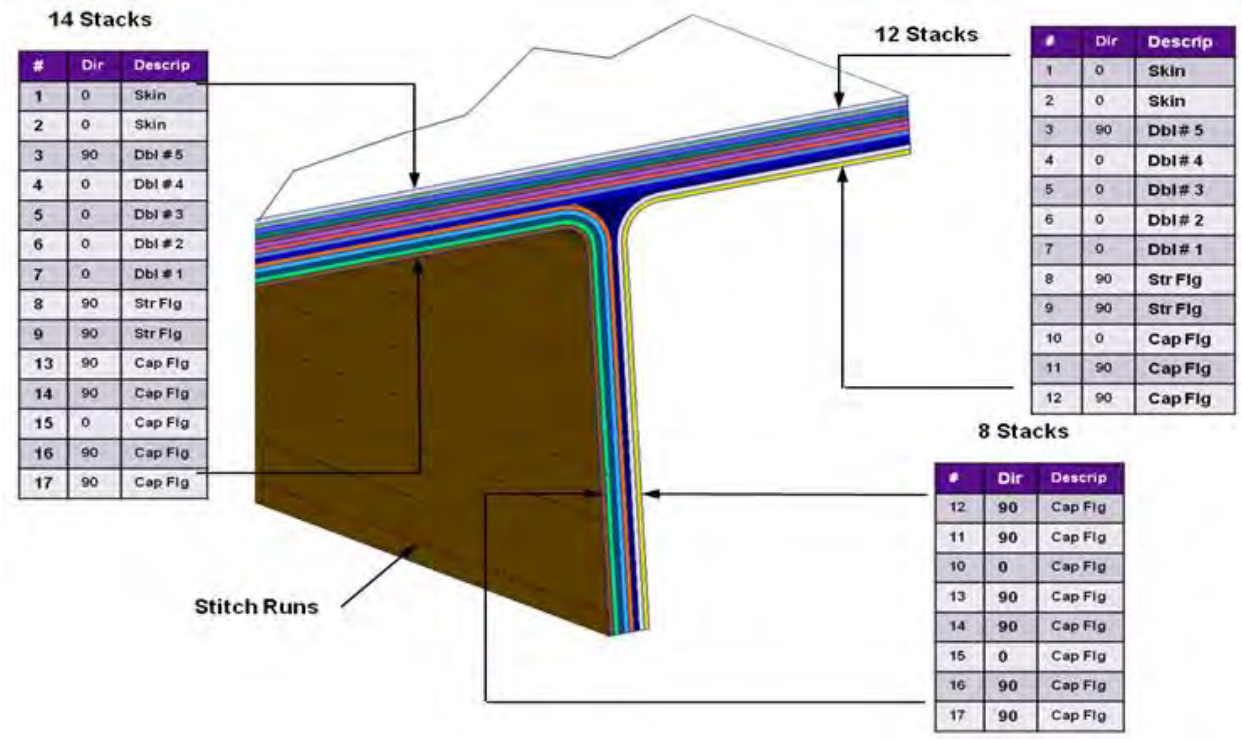

#	Dir	Descrip
1	0	Skin
2	0	Skin
3	90	Dbl # 5
4	0	Dbl # 4
5	0	Dbl # 3
6	0	Dbl # 2
7	0	Dbl # 1
8	90	Str Flg
9	90	Str Flg
13	90	Cap Flg
14	90	Cap Flg
15	0	Cap Flg
16	90	Cap Flg
17	90	Cap Flg

#	Dir	Descrip
1	0	Skin
2	0	Skin
3	90	Dbl # 5
4	0	Dbl # 4
5	0	Dbl # 3
6	0	Dbl # 2
7	0	Dbl # 1
8	90	Str Flg
9	90	Str Flg
10	0	Cap Flg
11	90	Cap Flg
12	90	Cap Flg

#	Dir	Descrip
12	90	Cap Flg
11	90	Cap Flg
10	0	Cap Flg
13	90	Cap Flg
14	90	Cap Flg
15	0	Cap Flg
16	90	Cap Flg
17	90	Cap Flg

Figure 3-14. Crown Panel Rib Cap Stacks

Figure 3-15 shows a detail view of a rib cap interface for a center rib panel. The rib T-cap formed a 90-deg T-cap that functioned as a tie to one side of the center rib sandwich panel. The center rib T-cap radii were smaller than those at the bulkhead and outer rib T-caps (approximately 0.3 in. as opposed to 0.5 in.), which corresponded to the lighter loading in these regions.

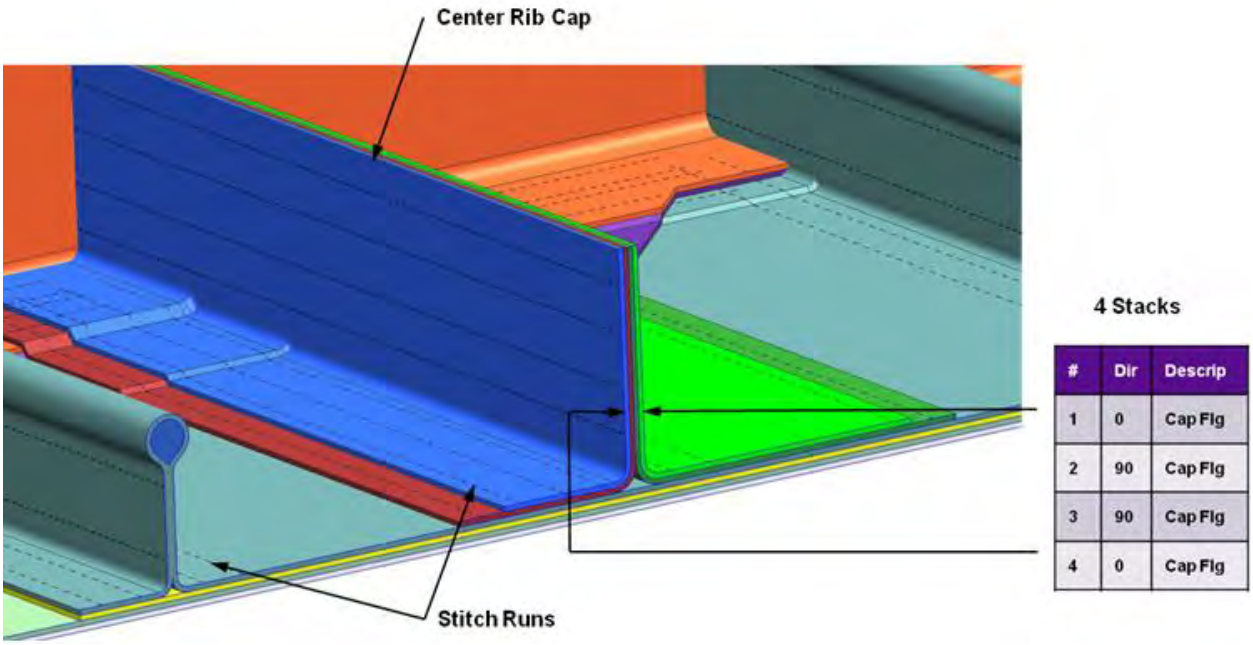

#	Dir	Descrip
1	0	Cap Flg
2	90	Cap Flg
3	90	Cap Flg
4	0	Cap Flg

Figure 3-15. Crown Panel Center Rib Cap Stacks

3.3.2 Floor Panel Assembly (ZJ153352)

As shown Figure 3-16, the floor panel was designed to use most of the same modular tooling as the crown panel, and it was comparable in footprint, although slightly longer. It was also a simpler panel design in that no bulkhead caps were required. This was because the floor panel was designed to fit between the forward and aft bulkhead panels that had integral T-caps.

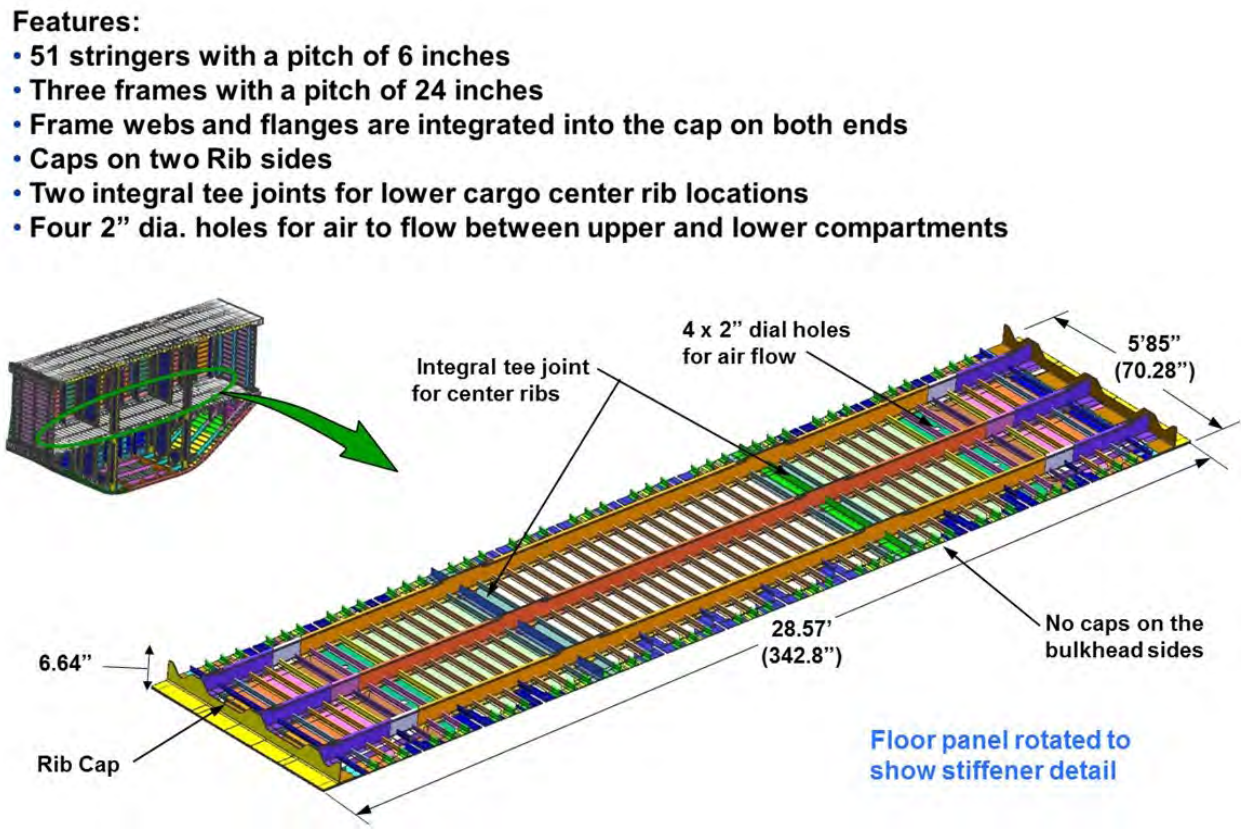

Figure 3-16. Floor Panel Assembly

The layup used for the floor panel was similar to that used for the crown panel, which was necessitated by the desire to use the same stitching and cure tools for both panels. Doublers on the frames and skin were identical to those on the crown panel; however, as shown in Figure 3-17, the bulkhead T-caps were not present. The integral caps followed the same design configuration as those on the crown panel and coincided with the center rib panel locations.

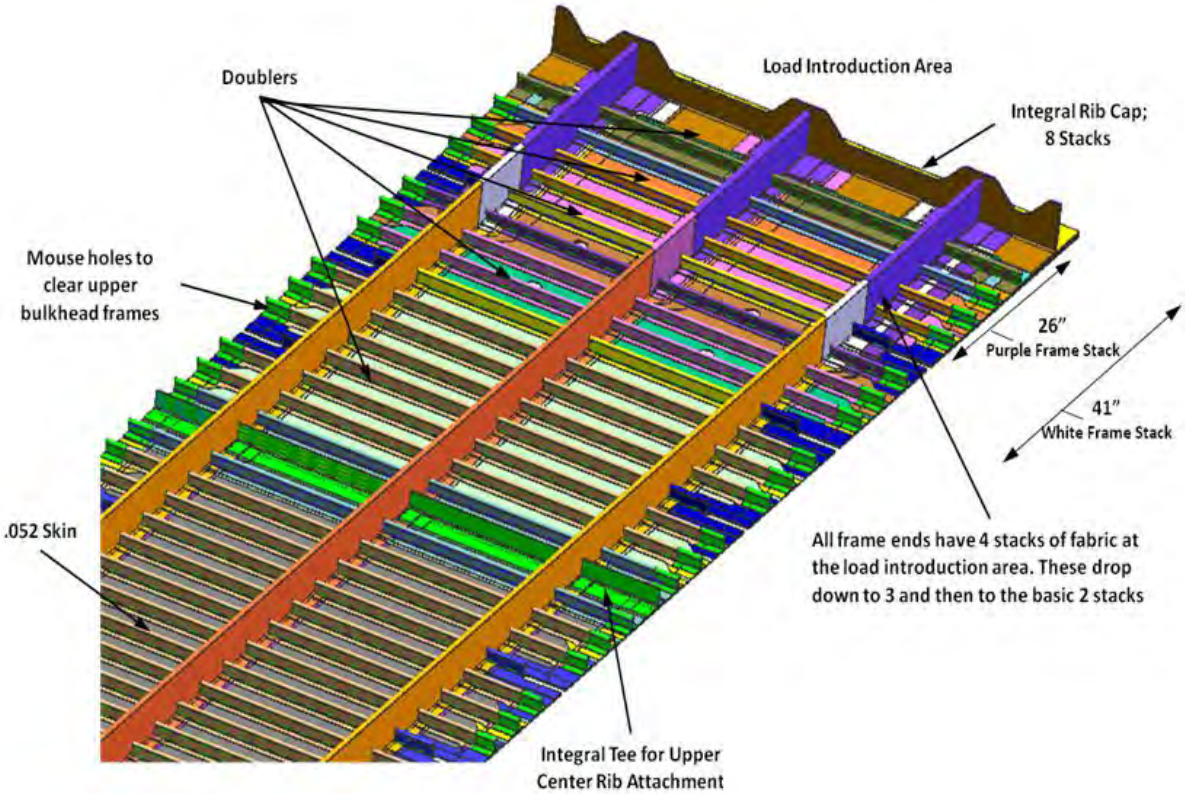

Figure 3-17. Floor Panel Features

Figure 3-18 shows the frame pad-ups on the floor panel that were similar to ones on the crown panel. However, a key difference here was in the stringer ends, as shown in the figure. Stringer end doubler overwraps were added to the ends of every stringer for the floor panel preform in place of the bulkhead caps on the crown panel.

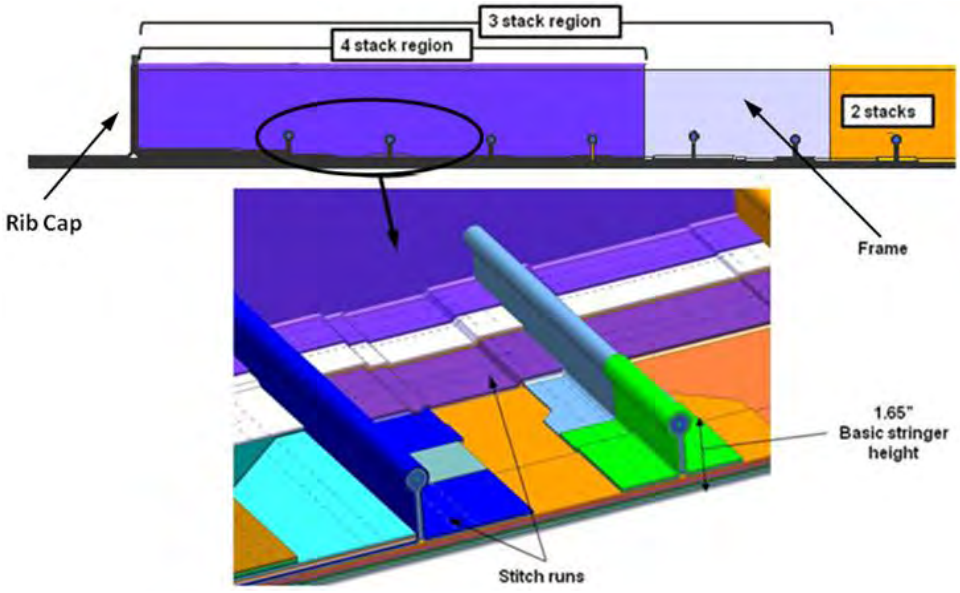

Figure 3-18. Floor Panel Beam Buildups

Auxiliary rib caps on the floor panel were similar to the outer rib caps on the crown panel. The frame flange stacks and cap stacks were overlapped, interleaved, and stitched as shown. Two-sided stitching was used through the thickness of the rib cap web, and single-sided stitching was used through the skin and frame/stringer flanges for reinforcement, as shown in Figure 3-19.

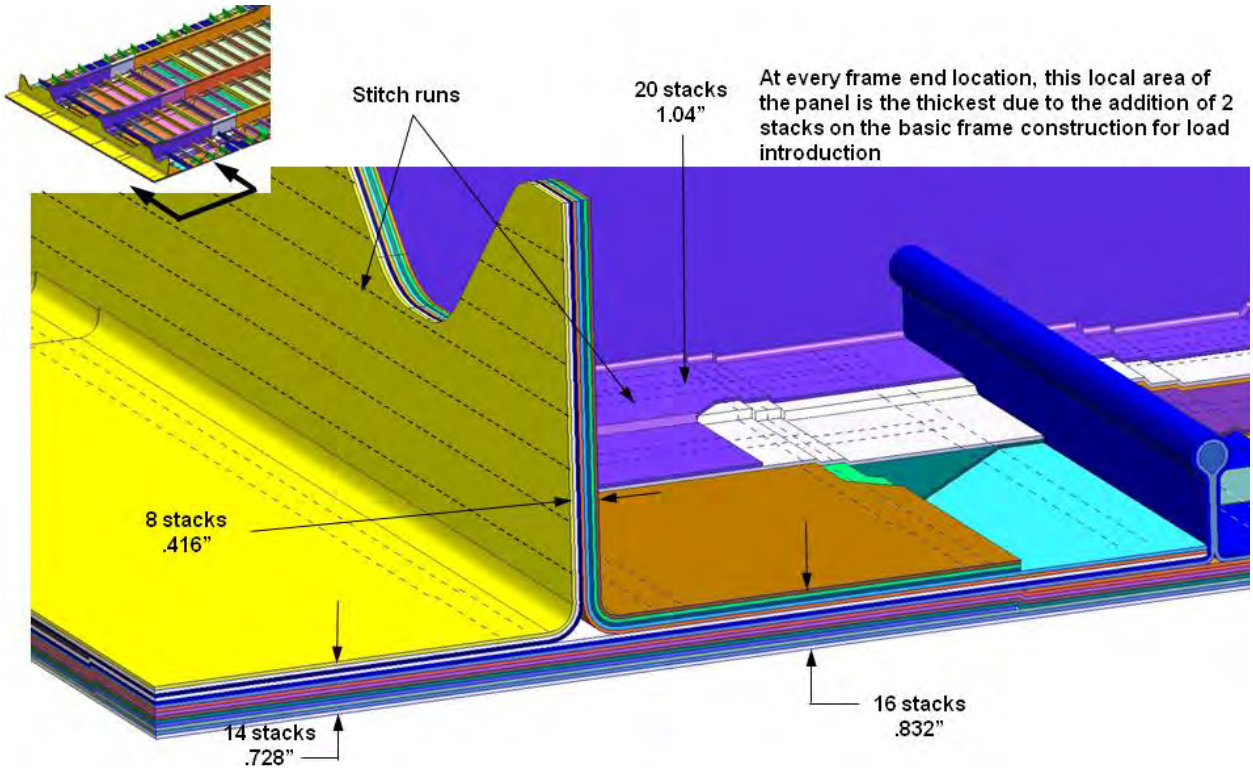

Figure 3-19. Floor Panel Rib Caps Buildups

3.3.3 Upper Bulkhead Panel Assembly (ZJ153353)

The upper bulkhead panel shown in Figure 3-20 was the largest PRSEUS panel incorporated into the MBB design. It was a flat PRSEUS panel with many stiffening features and added detail. Provisions for an access door cutout were central to both forward and aft bulkhead panels. The forward and aft panels were designed to be interchangeable, facilitating fabrication and assembly tasks.

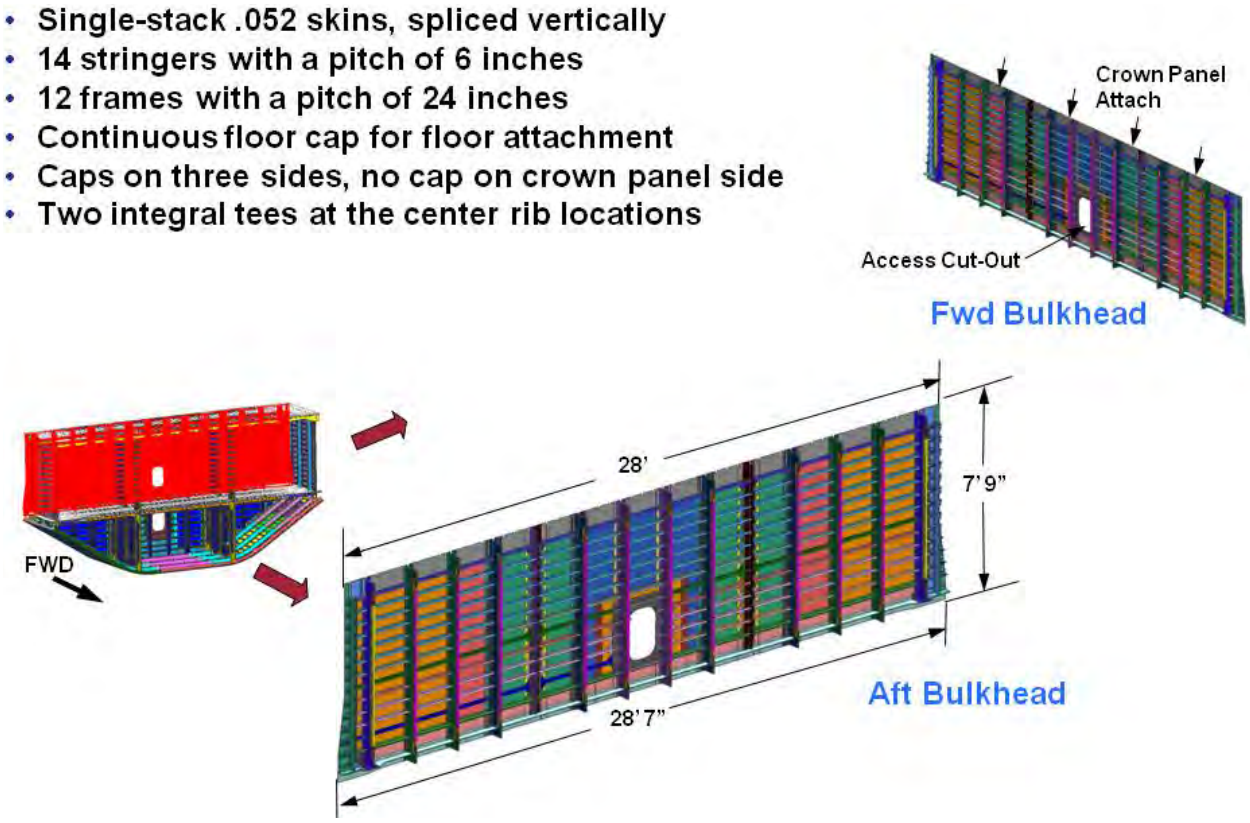

Figure 3-20. Upper Bulkhead Panel Assembly

The upper bulkhead panels in the MBB interfaced with the crown and floor panels as well as the upper center rib and side rib panels. T-caps were integral to the bulkhead at the floor, side, and center rib locations, with the crown panel attach area built up to mate with the crown panel bulkhead cap.

As shown in Figure 3-21, the upper bulkhead design incorporated many stiffening members of varied type. The design included 12 frames and four T-caps (one at each vertical rib location), which were oriented vertically, with 14 stringers and a continuous floor cap running horizontally. Stringer pitch was a constant 6 in., with the frames at the standard 24-in. spacing. The frames were in line with the frames on the crown panel and the lower bulkhead panel. The baseline PRSEUS frame, stringer, and skin design were built up with additional material at the periphery of the panel as well in the region of the cutout for the access door. Unique to the upper bulkhead were the doubler caps on each of the vertical frames.

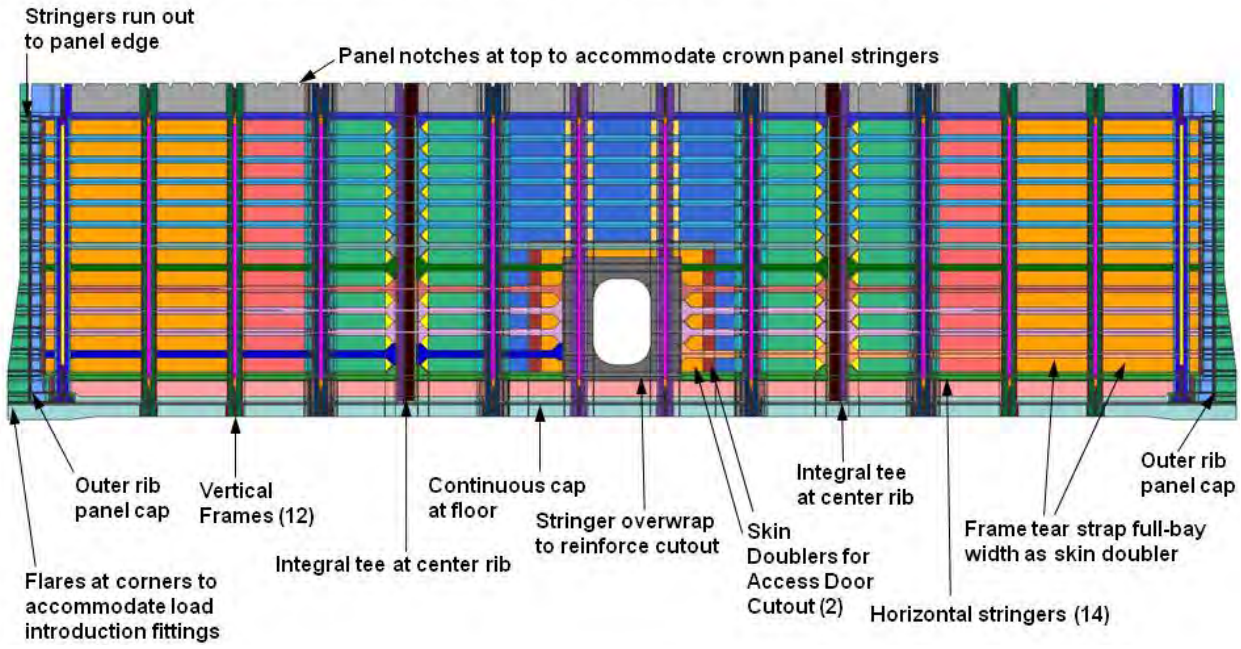

Figure 3-21. Upper Bulkhead Panel Features

The 0-deg direction of the skin fabric in the upper bulkhead panels corresponded with the vertical direction of the box. This meant that the roll of skin fabric was oriented perpendicular to the length of the panel when laying it out for fabrication. The maximum available width of carbon-fiber fabric necessitated a distinctive design feature—four large vertical skin splices. Positioned under frame stations for additional stiffness at the joint, these skin splices were present on the lower bulkhead panels as well. The splice locations were at corresponding frames in both the upper and lower bulkheads. This would aid with panel alignment during assembly of the MBB and simplified the fitting design at the floor cap.

As shown in Figure 3-22, the skin splices were butt joints reinforced with four overlapping straps of fabric, two on the IML and two on the OML at each splice location. The splice strap ties were Class 75/78 two-ply material, whereas the base skin was the standard Class 72 fabric. The splice straps were oriented in a 45/-45/0/90/(skin)/90/0/-45/45 deg fashion, moving from IML to OML, in order to mesh with the layup of the Class 72 material.

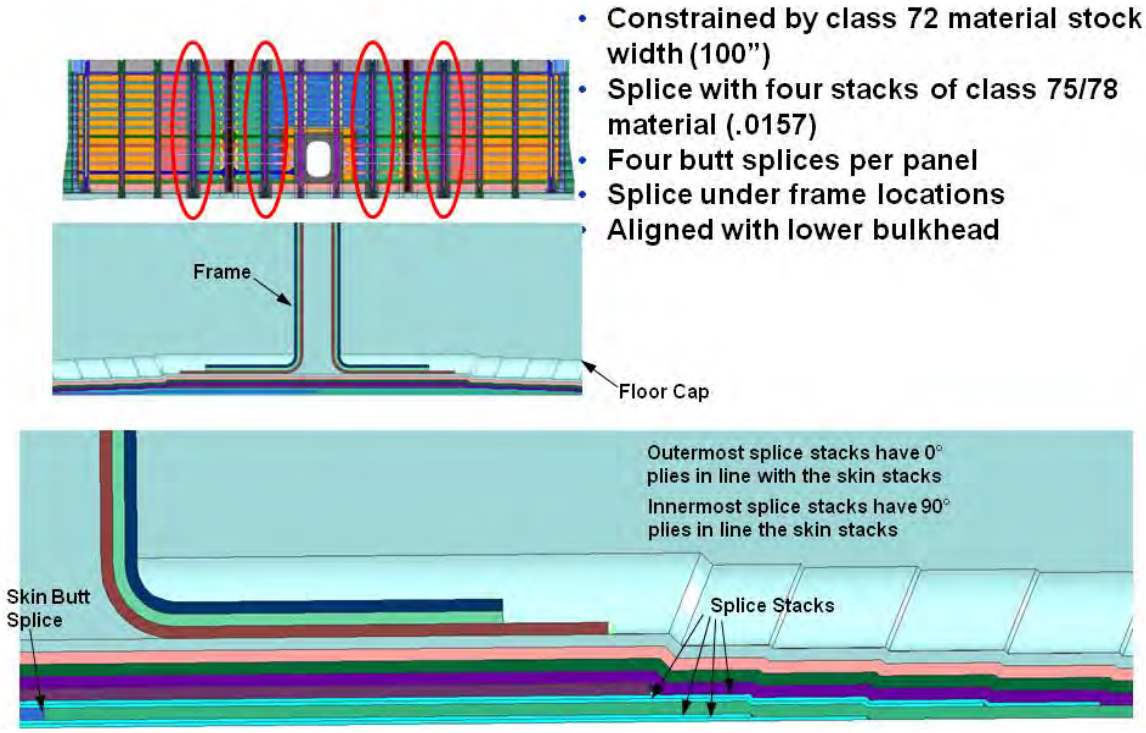

Figure 3-22. Upper Bulkhead Panel Skin Splices

The edges of the OML skin splice straps were the innermost two dropoffs, reducing the eccentricity in the skin stack as it stepped over the splice straps where the built-up region was the thickest. Figure 3-23 shows a close-up 3D view of the splice.

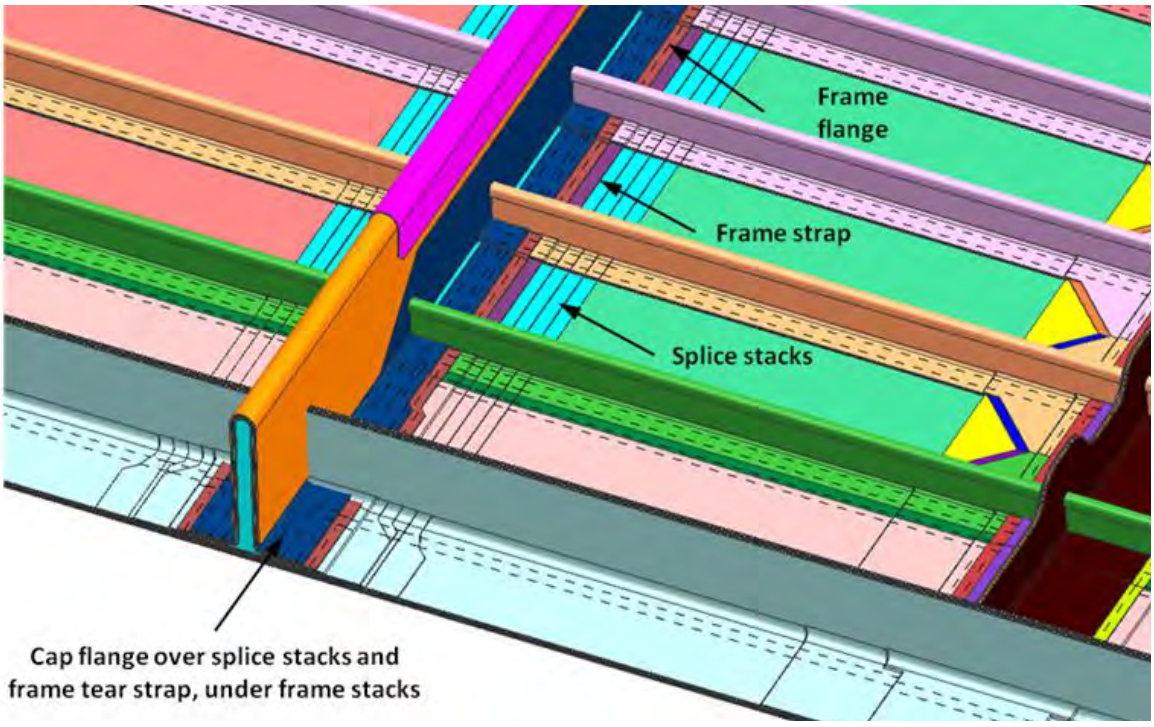

Figure 3-23. Upper Bulkhead Skin Splice Stitching

Figure 3-24 provides a view of the typical frame cap reinforcement, a feature present only on the upper bulkhead panels. These frame cap doubler stacks were added after the panel was stitched and prior to infusion. They functioned to further stiffen the panel in the vertical direction, countering some of the deflection resulting from pressure pillowing. Trade studies of potential frame designs of varying stiffness were conducted to determine a preferred solution. An advantage of the design finally selected was that it used foam cores that were the same height as the frame cores on all other panels in the MBB. It was determined that a taller frame would stiffen the panel in the vertical direction; however, buckling of the frame itself was also a concern. The addition of the two frame cap plies plus one additional frame stack to the baseline two-stack frame was an effective solution to the problem of bulkhead deflection.

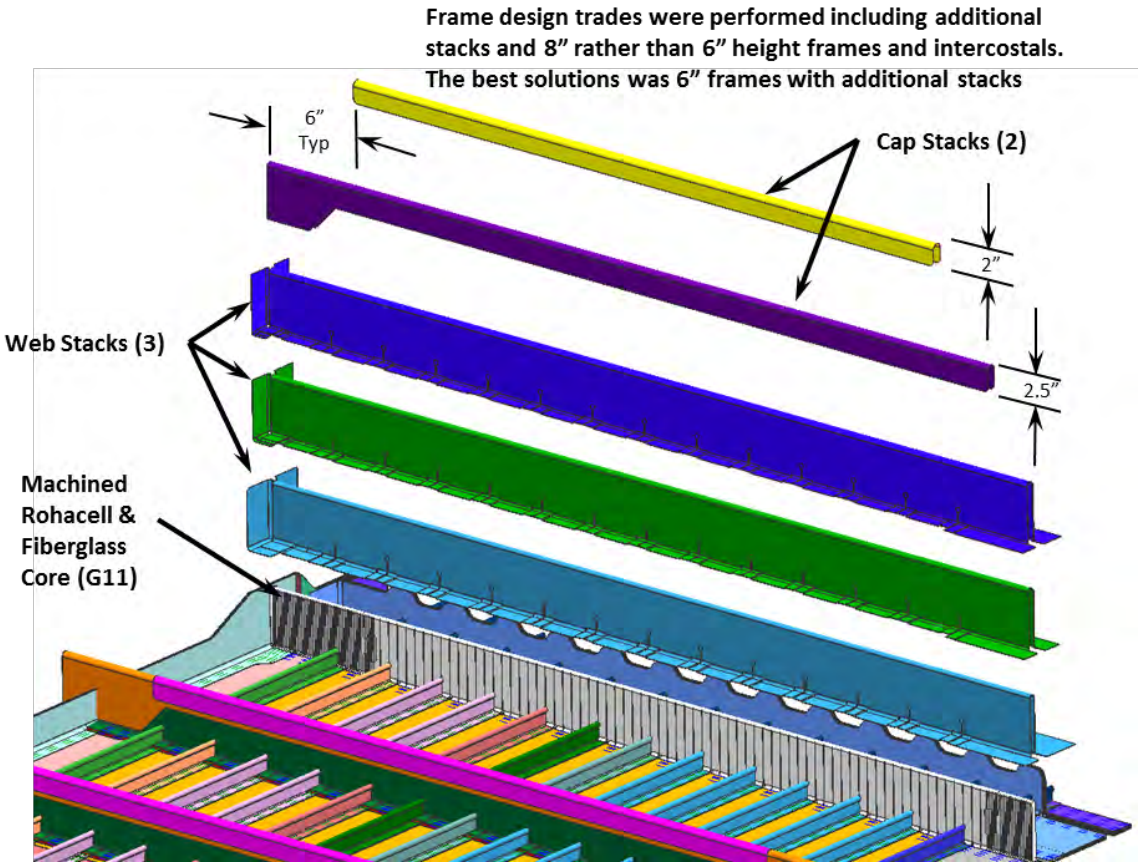

Figure 3-24. Upper Bulkhead Panel Frame Caps

The floor T-cap on the upper bulkhead was the largest single structural feature on the panel, running its entire length. It consisted of six Class 72 stacks formed into a 90-deg T-cap with a 0.5-in. fillet at the base of the T-cap. The floor T-cap was continuous and the frame ends were slotted (keyholed) to fit over the cap vertical web. These extended frame ends tied into the frames on the lower bulkhead panel. The upper bulkhead floor cap was designed as one piece to create a stiffened integral fitting to tie the floor into the MBB structure. The web of the floor T-cap was machined at the ends of the panel to clear the ends of the outermost frames that terminated at the floor cap, as shown in light blue in Figure 3-25. Fittings backed up the frame ends at these locations in the assembled MBB structure.

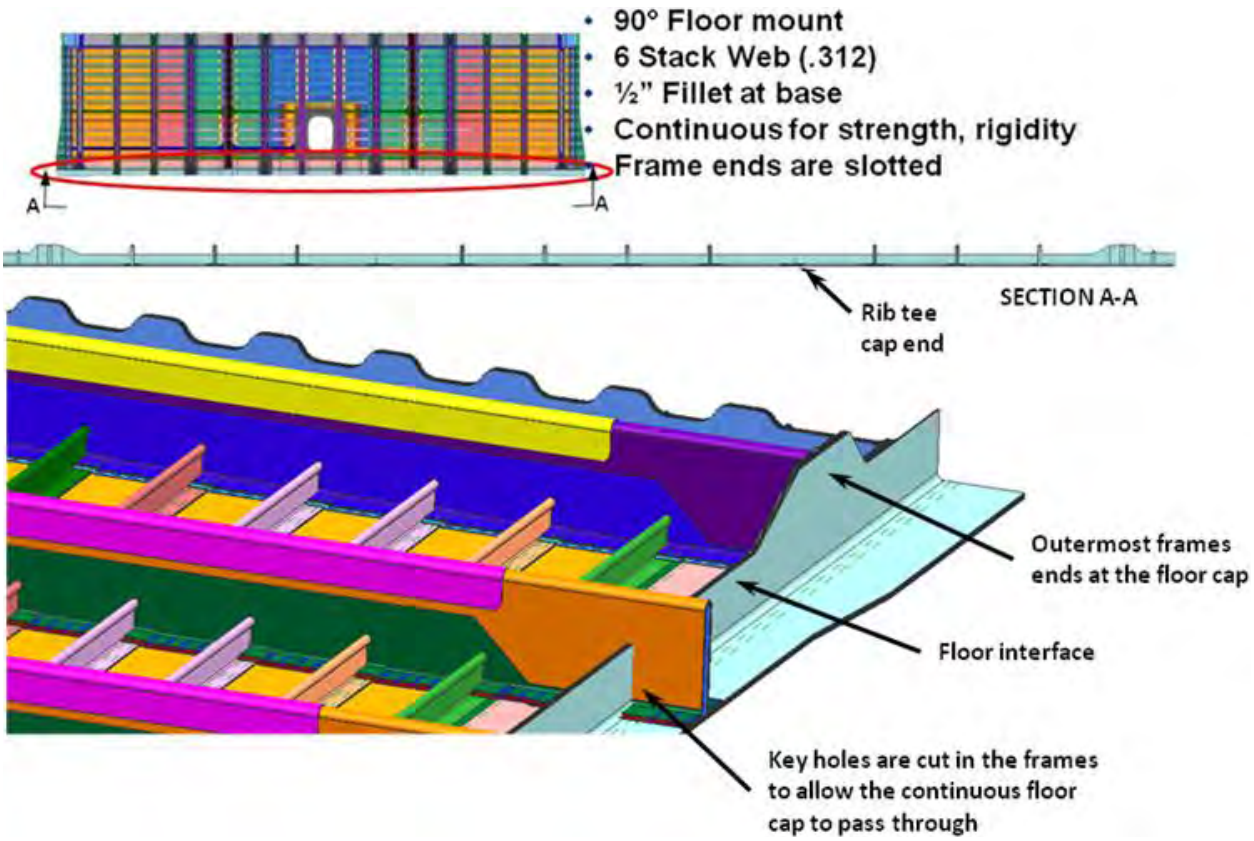

Figure 3-25. Upper Bulkhead Panel Corners

Figure 3-26 provides another view of the outermost frame end termination at the floor T-cap. (This is an IML view showing the frame stacks at the floor T-cap as well as the side rib cap stack termination.) Fillets (0.3-in.) were incorporated into the frame fiberglass core ends to facilitate the forming of the frame end flange interface with the floor T-cap. The interleaved region highlighted in Figure 3-26 comprised the frame end flange wrapping underneath the frame flange on top of the floor T-cap flange. This was designed to obviate the need for complicated fittings on the IML at the frame end. Fittings, as indicated above, were installed on the opposite side of the floor T-cap to provide end fixity. The lack of a corresponding frame to tie into on the lower bulkhead panel necessitated these fittings.

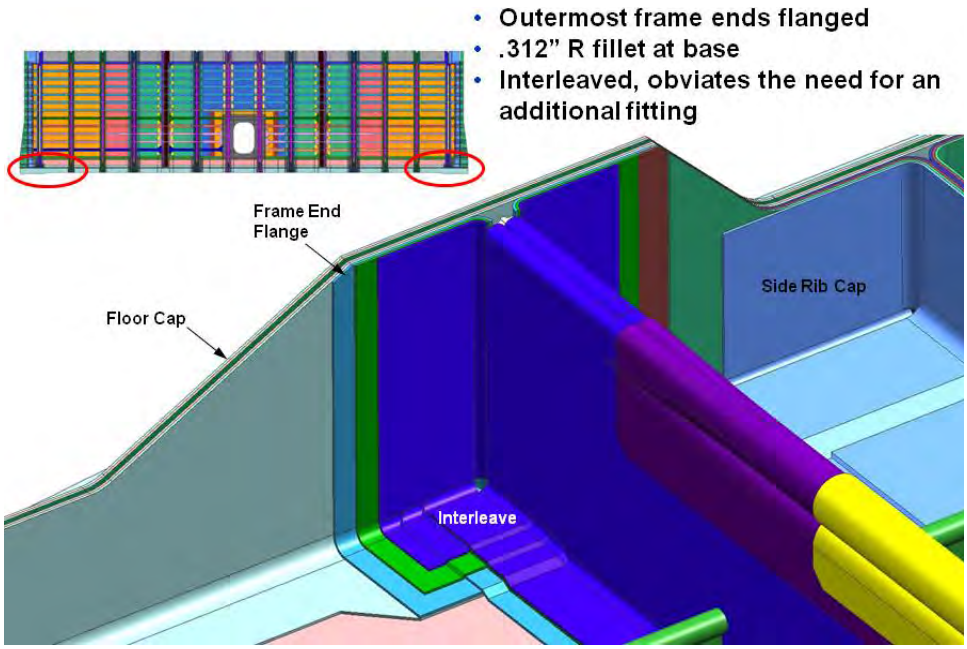

Figure 3-26. Upper Bulkhead Panel Frame Runout

The upper bulkhead was reinforced at all interface regions, including the area that would be trimmed out for the access door. This was a post-processing machining step in that the panel was cured without this hole and then cut out after the panel edges were trimmed. Each upper bulkhead had one cutout at the middle of the panel, as shown in Figure 3-27. Two skin doublers reinforced the skin, and the stringers had an overwrap doubler. These added stacks served to stiffen the panel in the door region and absorb bearing loads from door attachment fasteners.

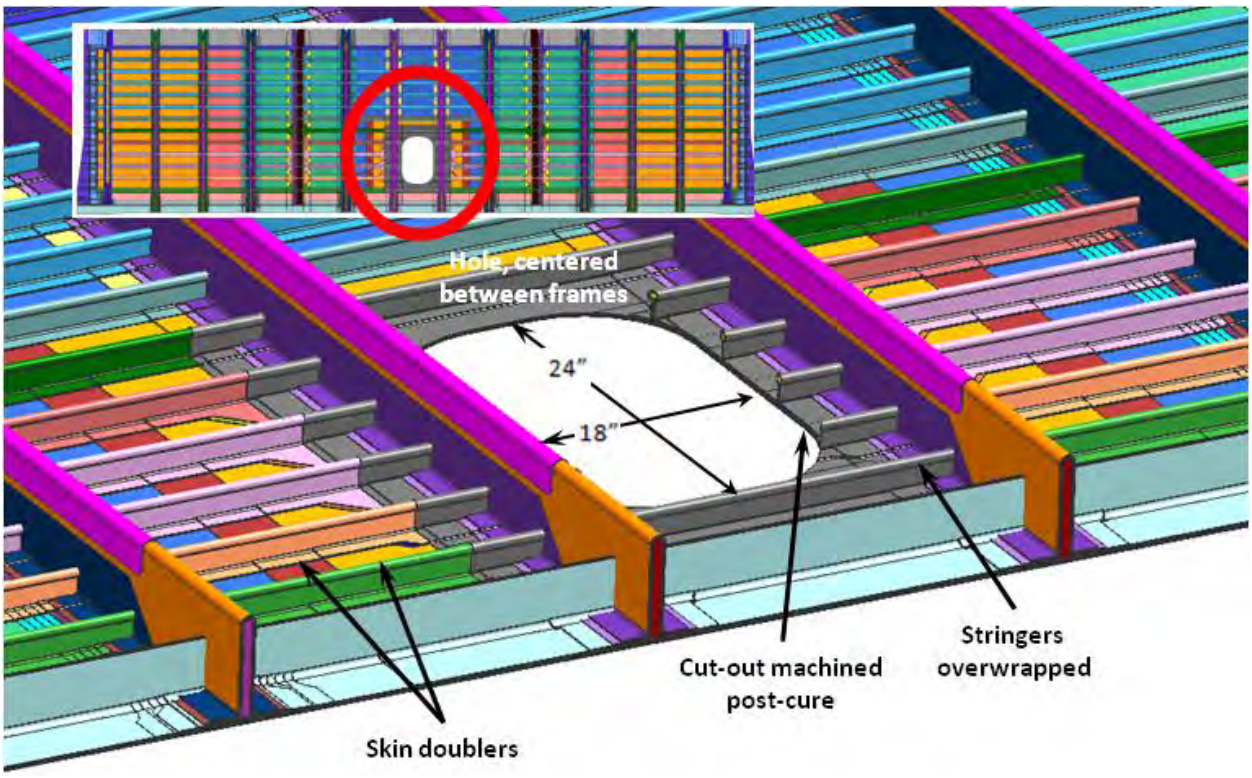

Figure 3-27. Upper Bulkhead Panel Access Hole

3.3.4 Lower Bulkhead Panel Assembly (ZJ153354)

Although smaller in footprint, the lower bulkhead panel was similar in concept to the upper bulkhead. Standard 24-in. frame spacing aligned with the frames on the upper bulkhead. The stringers on the lower bulkhead departed from the standard pitch, which was required so that the ends of the lower bulkhead stringers would not align with the stringers on the side keel panels. The stringer pitch on the lower bulkhead varied so that the stringer ends at the edge of the panel and just above the side keel panel stringer could be tied together. It was judged to be more workable to vary the pitch of the stringers on the lower bulkhead than on the side keel panel. The design intent was to carry load around the corners formed by the keel panel and bulkhead panel interface.

The location of the lower bulkhead panel in the MBB assembly is shown in Figure 3-28. The panel attached to the upper bulkhead panel, the floor panel, the lower center rib panels, and all three keel panels. The lower bulkhead had only two rib T-caps at the lower center rib locations and no T-caps present at the panel edges. It was designed to tie into caps on the interfacing panels.

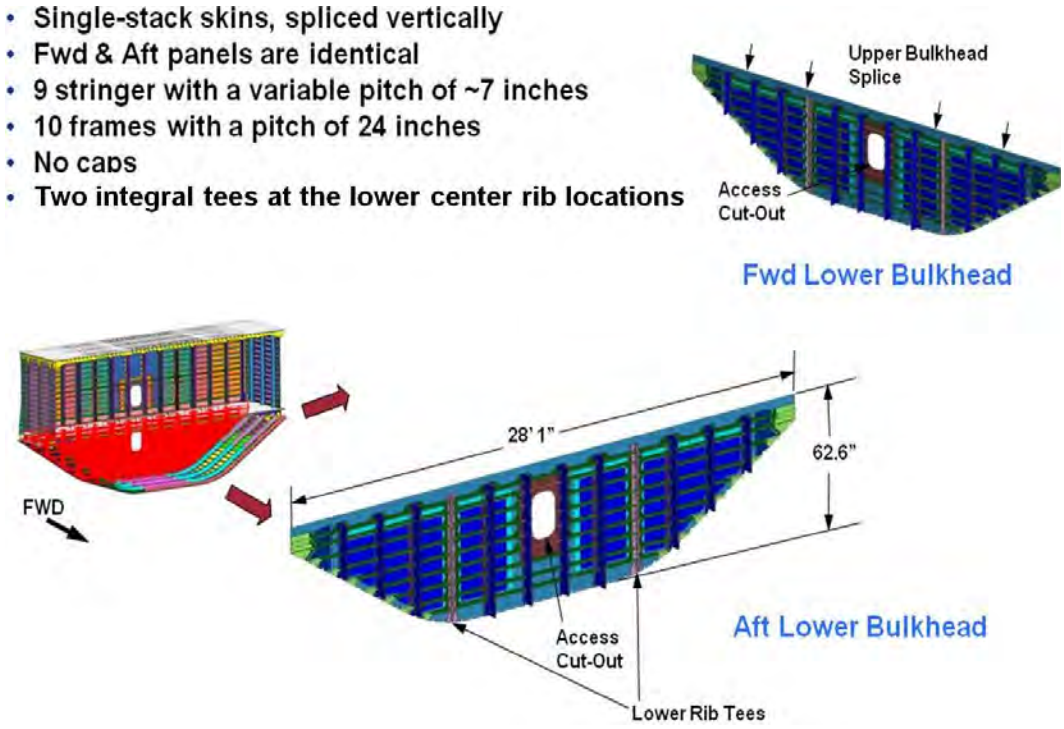

Figure 3-28. Lower Bulkhead Panel Assembly

Figure 3-29 highlights the structural features of the lower bulkhead panel. The four skin splice locations lined up with those on the upper bulkhead panel, as did all of the frames locations. This improved the load distribution in the structure and decreased the number of fittings that tied the upper and lower bulkhead frames together. Doublers were added to the periphery of the panel and the door cutout region in a similar manner as used in the upper bulkhead panel design.

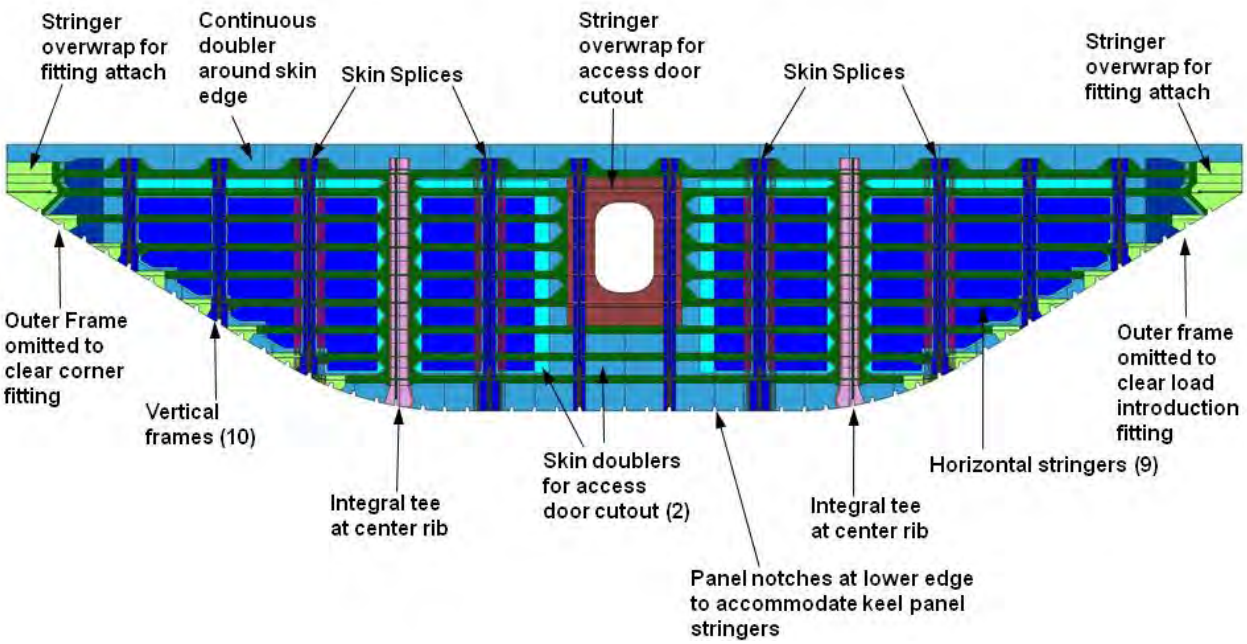

Figure 3-29. Lower Bulkhead Panel Features

The lower bulkhead panel skin was spliced together due to material width constraints. The splice design was identical to the one used for the upper bulkhead shown in Figure 3-30. Four splice straps of Class 75/78 material spanned a butt splice of the Class 72 skin parent material. Orientation of the splice strap material plies followed that in the upper bulkhead panel: 45/-45/0/90/(skin)/90/0/-45/45 deg. The idea was to approximate the parent skin material properties as much as possible using a two-ply stack of material.

The frame design on the lower bulkhead was the baseline construction for the MBB. The basic design geometry for the lower bulkhead was straightforward except for the edge trim and varied stringer spacing, as shown in Figure 3-31.

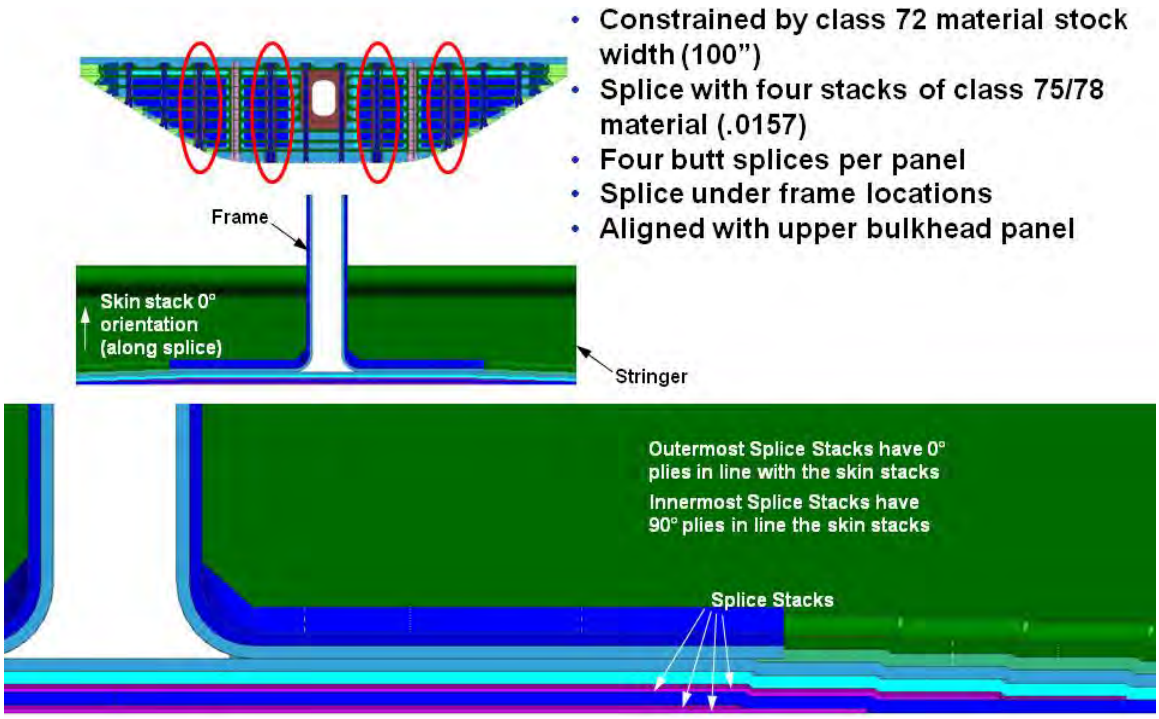

Figure 3-30. Lower Bulkhead Panel Skin Splices

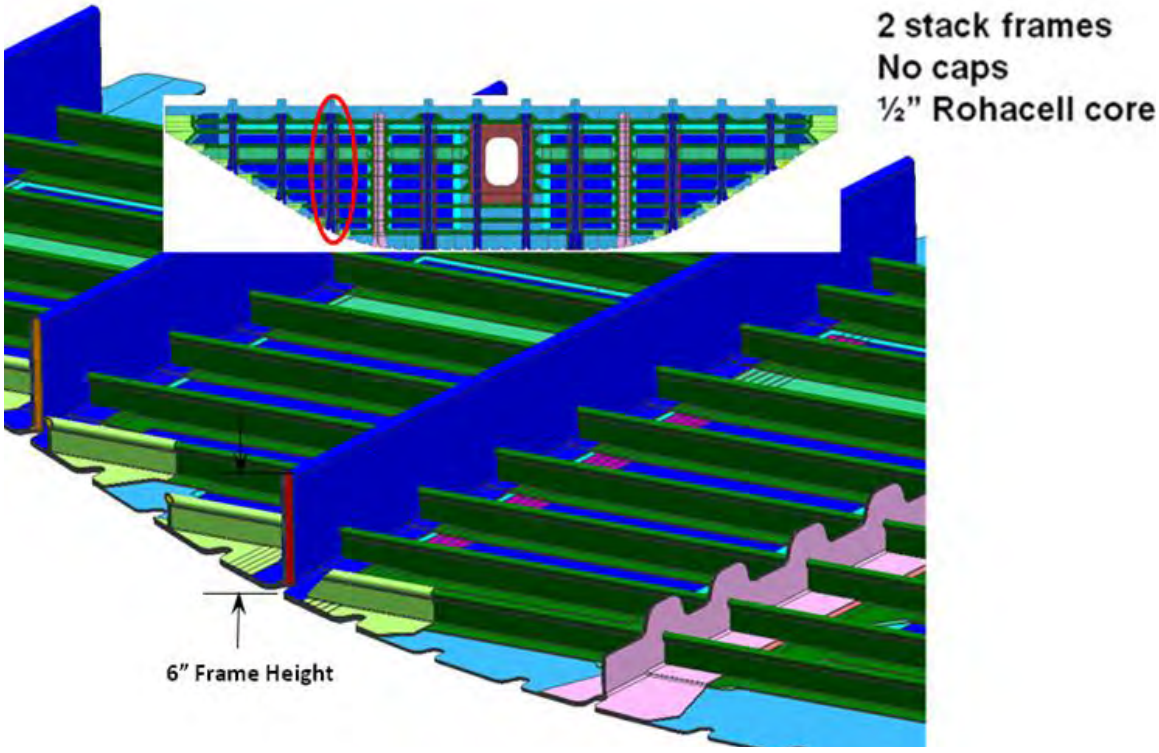

Figure 3-31. Lower Bulkhead Details

Figure 3-32 shows the complexity of the edge trim on the lower bulkhead as well as the rib T-cap construction. Four Class 72 fabric stacks were used to build up the T-cap with a 0.3-in. radius fillet at the base of each of the T-caps. The rib T-web was subsequently machined post-cure to obtain the scalloped design shown. The intent was to reduce the weight of the panel by trimming excess material. Although it was not required for a test article, it was what would be expected in the design of an actual HWB-type structural panel.

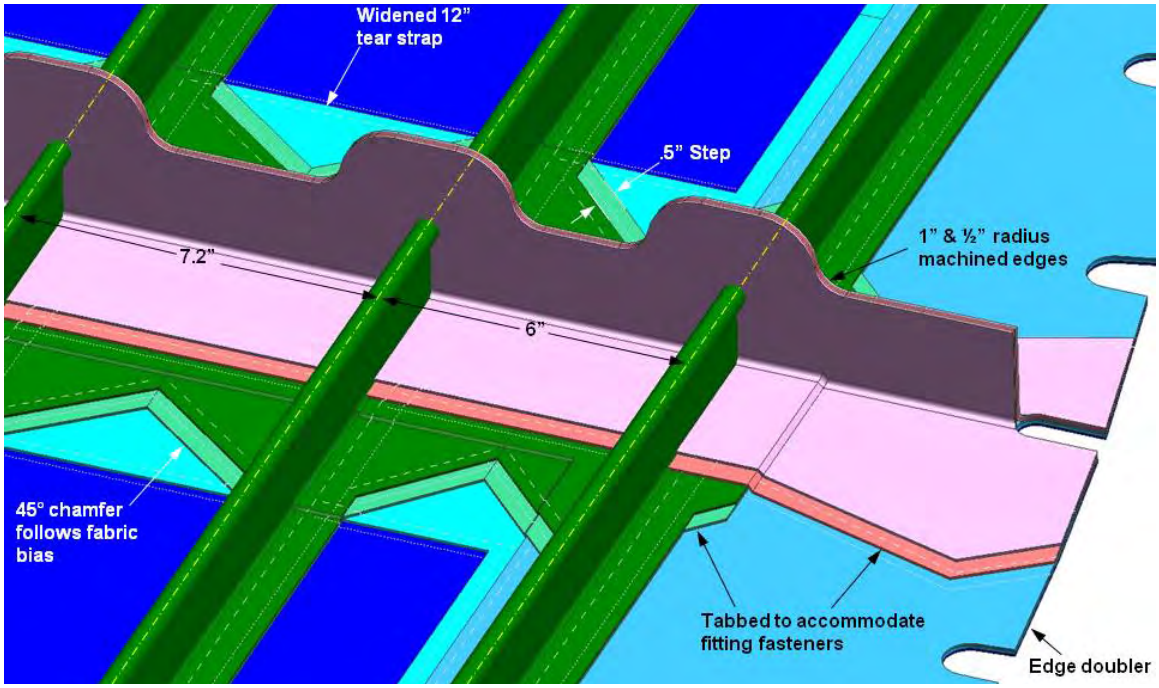

Figure 3-32. Lower Bulkhead Panel Rib T-cap

Figure 3-33 details the geometry of the access door cutout on the lower bulkhead panel as well as the material buildups. The stringers were overwrapped as in the upper bulkhead design. The extra material reinforced the edge of the cutout and carried the door fastener bearing loads.

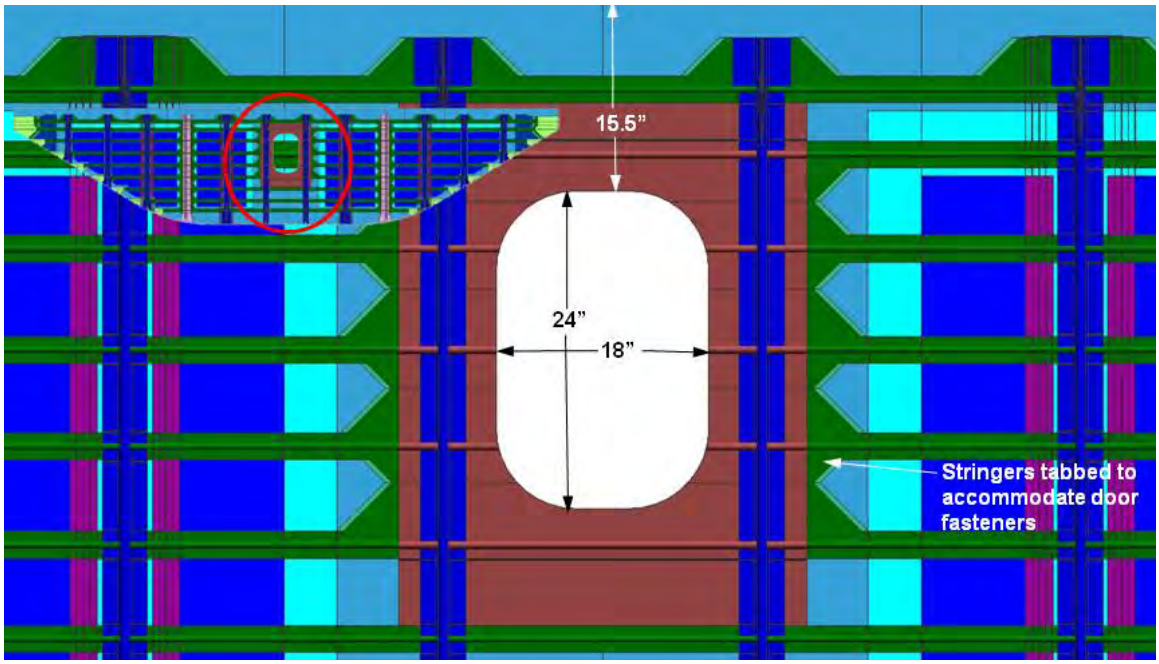

Figure 3-33. Lower Bulkhead Panel Access Hole

3.3.5 Side Keel Panel Assembly (ZJ153355)

The side and center keel panels comprised the bottom closeout section of the MBB. They were roughly comparable in form and shape to the expected lower fuselage of a typical HWB-type aircraft. It is likely that the panels would be designed and built as one panel in a production environment, but for the purposes of this effort, three built-up panels were judged to be the best approach to reduce the tool effort. The two side keel panels were identical, with curvature only at one end, and the center keel panel was flat, similar to the center section of the crown panel.

Integral caps were present on three of the four side keel panel edges, as shown in Figure 3-34. A T-cap was also located on the side keel panel to tie to the lower center rib panel. The inner end of the side keel panel terminated at the splice fittings that tied together the side keel panel to the center keel panel.

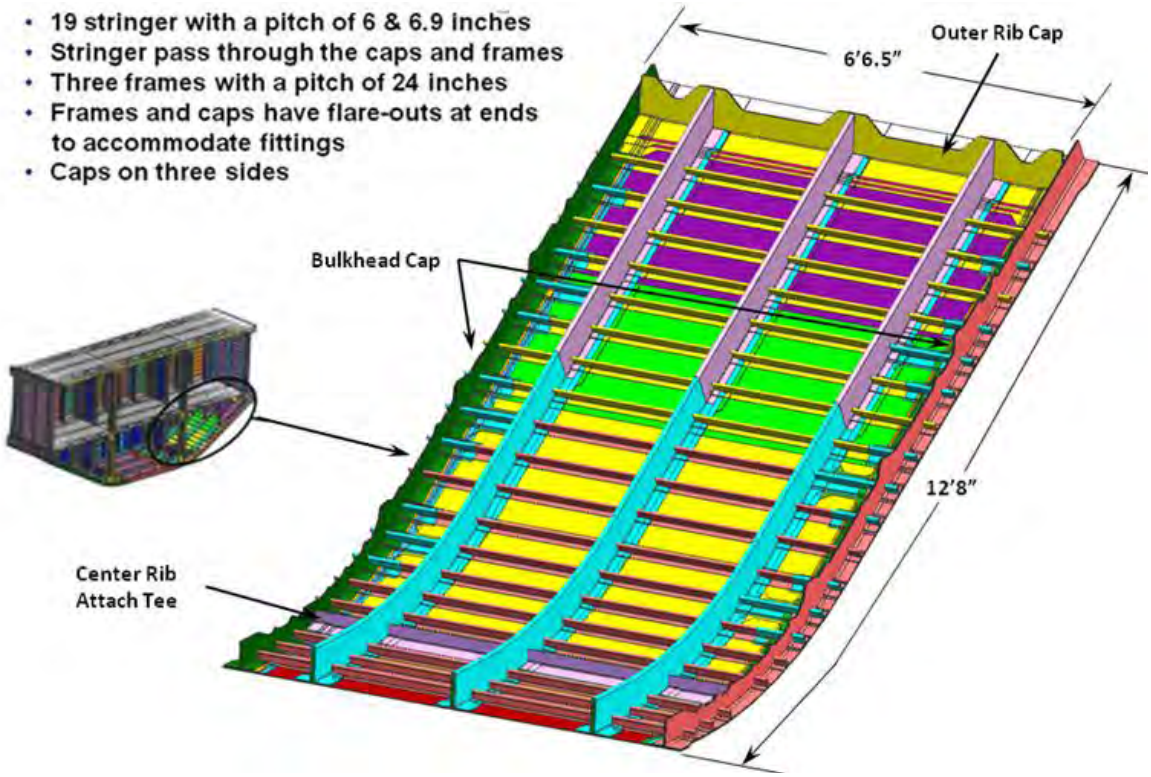

Figure 3-34. Side Keel Panel Assembly

The side keel panel was composed of two skin stacks and two skin doubler stacks. The outer frame tear straps were constructed in one piece with the cap tear straps. All skin stacks and frame tear straps were aligned in the 0-deg direction, as shown in Figure 3-35.

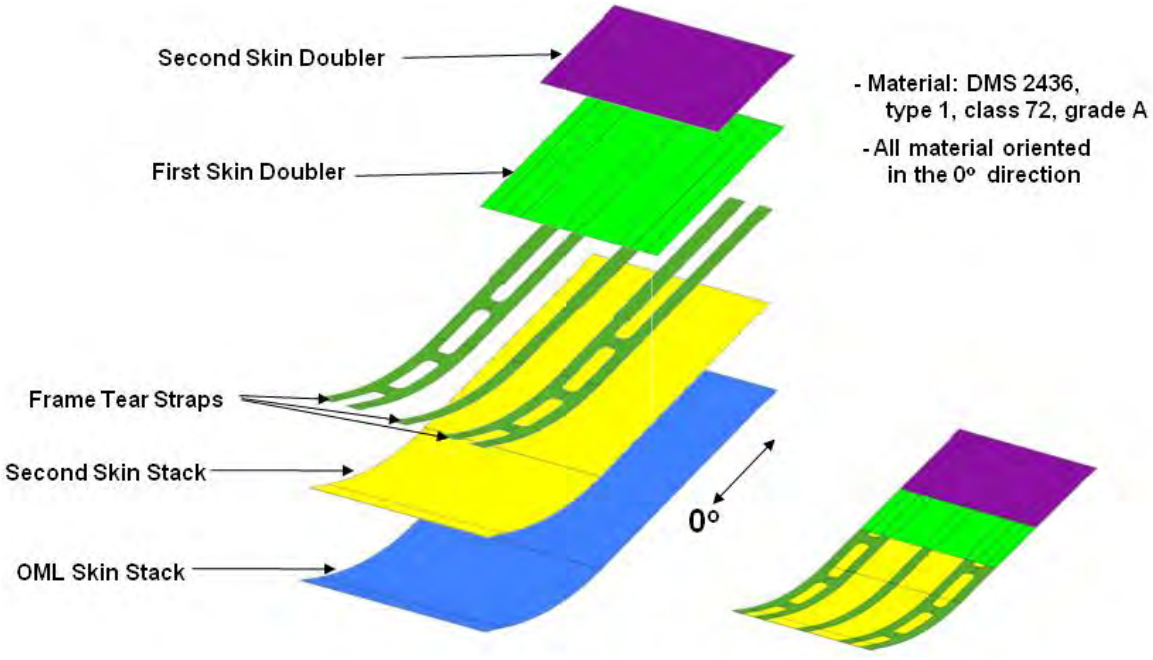

Figure 3-35. Side Keel Panel Skin Layup

The stringer and stringer tear strap stacks were oriented with the fabric 90 deg from the skin direction, as shown in Figure 3-36 and Figure 3-37.

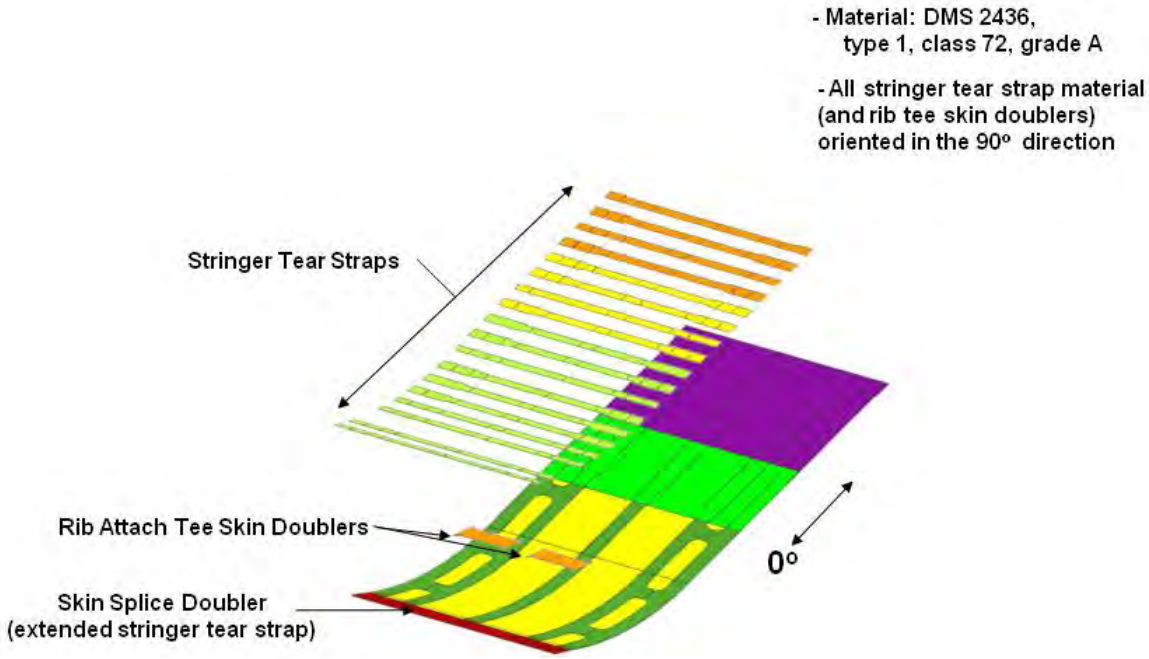

Figure 3-36. Side Keel Panel Tear Strap Layup

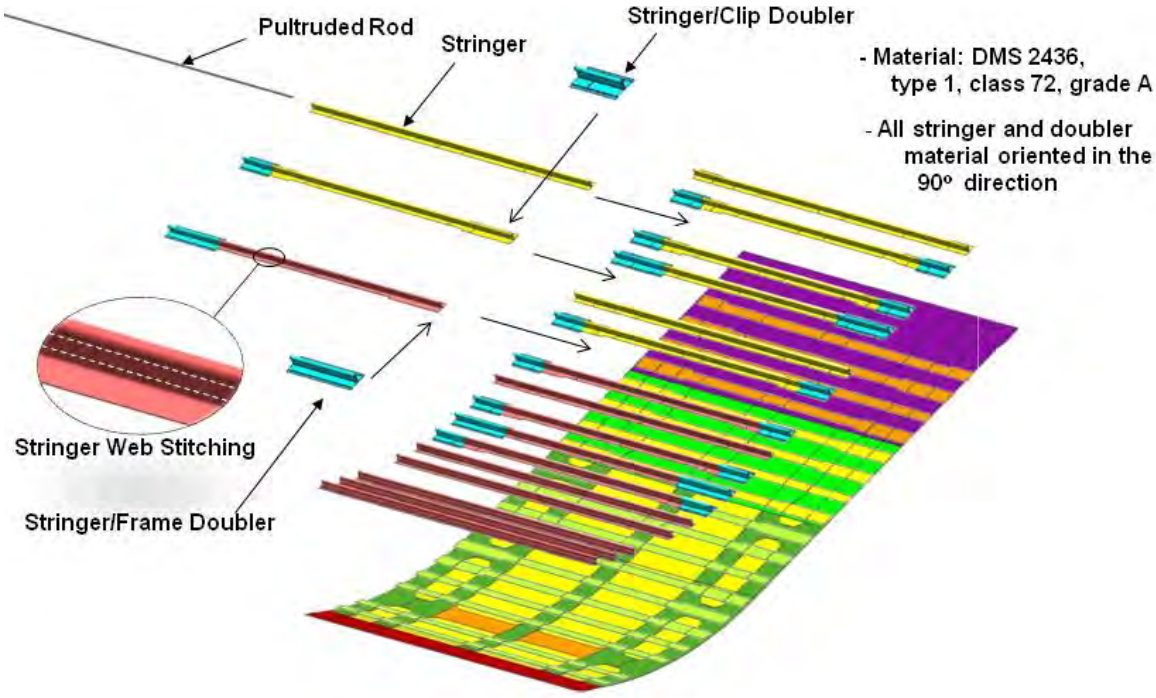

Figure 3-37. Side Keel Panel Stringer Construction

Bulkhead T-caps interfaced with the forward and aft lower bulkheads, simplifying installation and eliminating some fittings and fasteners. The stack-up was balanced, as shown in the small table in Figure 3-38.

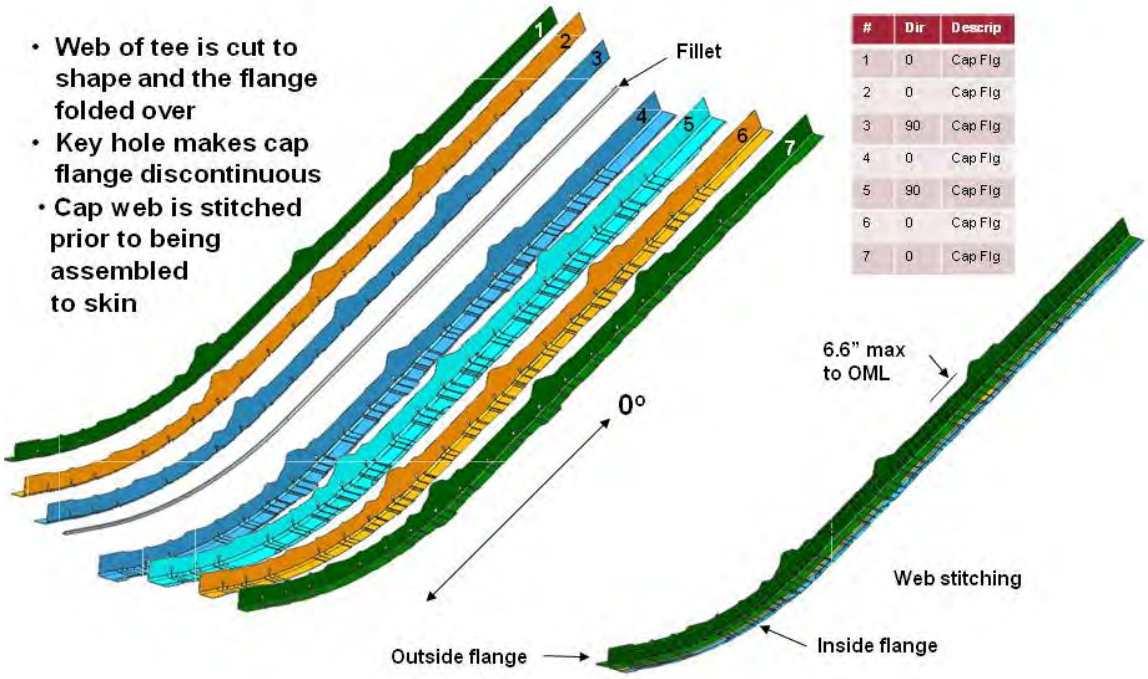

Figure 3-38. Keel Panel Bulkhead Cap Construction

Consistent with the design of the crown and floor panels, the side keel panels had three frames that ran lengthwise along the curvature of the panel. However, the stack-up of material for the frame webs, as shown in Figure 39, was unique to the side keel panel. Class 75 and 78 two-ply fabric was used instead of the baseline Class 72 seven-ply material. A total of ten stacks of Class 75/78 fabric were used to assemble the frame preforms. Additionally, a single stack of Class 72 fabric was overlaid on the end of the frame assembly, as shown in the figure. This added material functioned as a doubler to stiffen the frame where it tied into the auxiliary rib and floor panels. The frame core buildup is shown with Rohacell foam core and G11 fiberglass core end pieces. These core pieces once again interlocked using the “jigsaw puzzle” tongue-and-groove joint to eliminate bond tools.

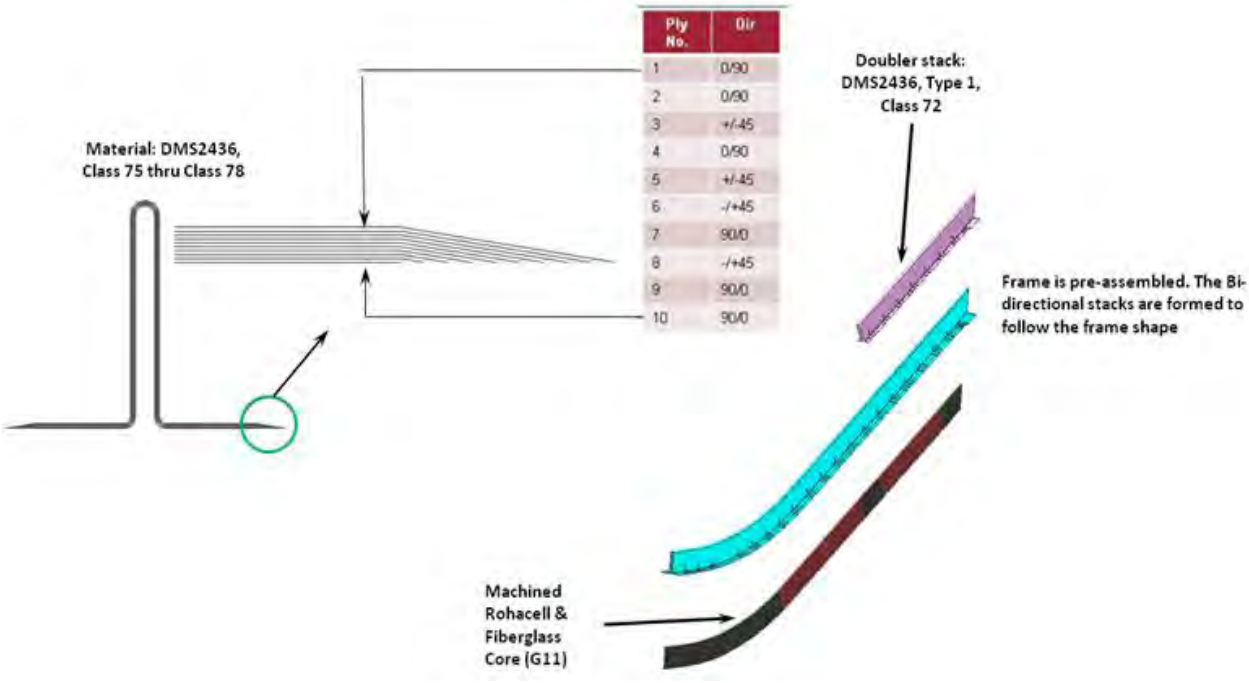

Figure 3-39. Side Keel Panel Frame Construction

Side keel panel caps at the outer and center ribs were constructed in a manner similar to the crown and floor. A total of eight stacks of Class 72 material were used to construct the outer rib cap, and they were oriented as shown in the larger table in Figure 3-40. The smaller table in Figure 3-40 details the stack-up for the T-cap at the center rib location.

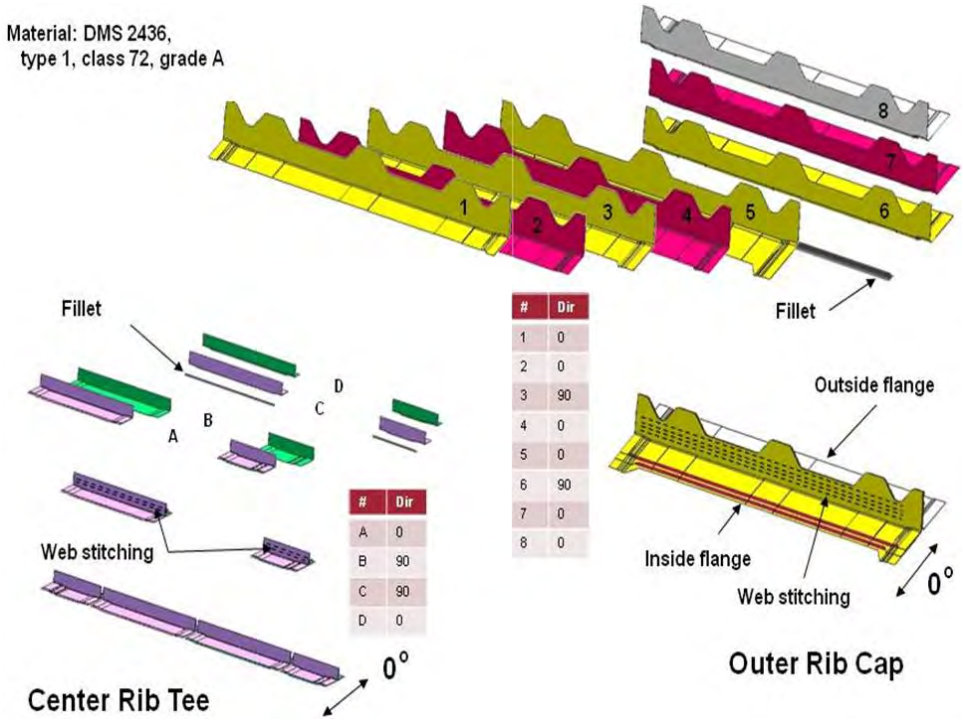

Figure 3-40. Side Keel Panel Rib and T-cap Construction

As with the crown and floor panels, the stiffeners on the side keel panel were all stitched to the skin with single-sided (robotic) stitching as part of the preform preparation. Figure 3-41 indicates the locations where the stitching occurred, complete with typical needle penetrations.

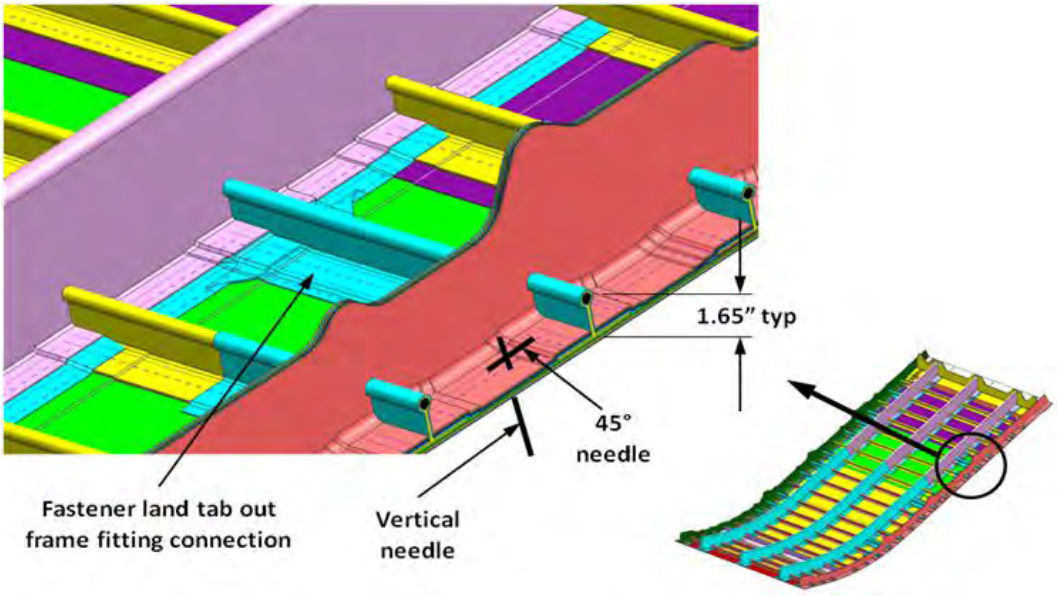

Figure 3-41. Side Keel Panel Edge Feature

Note the extensive stitching shown in Figure 3-42 as well as the flaring of the stiffener flange ends at the panel periphery. The side keel panel, as with all MBB panels, went through an edge machining operation post-cure. The extra material was required to meet the minimum edge distance for the fasteners in the fittings that spliced the keel panels together and the load-introduction fittings.

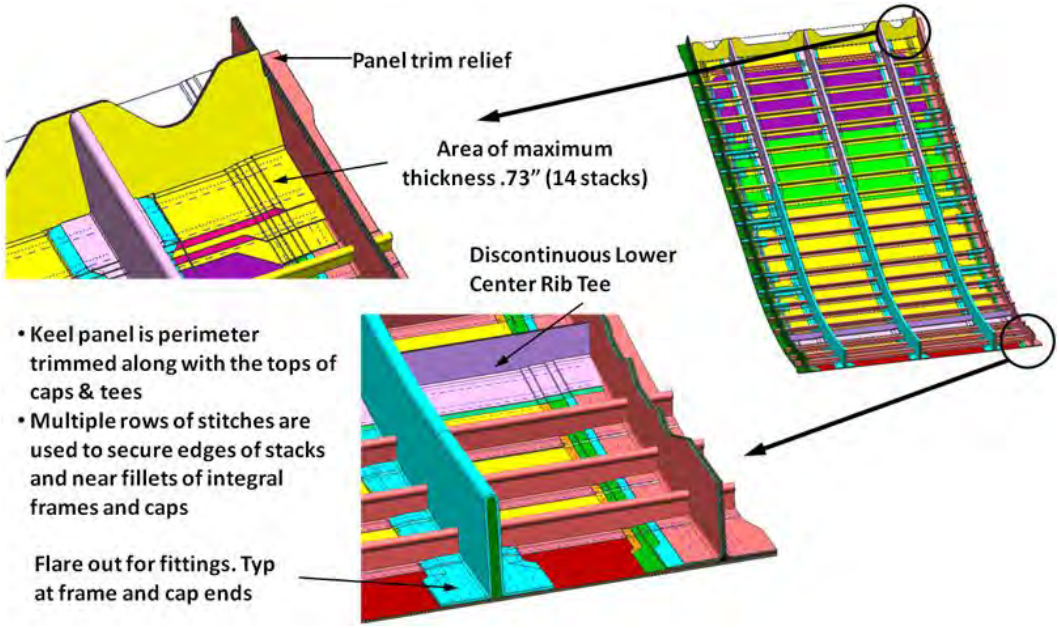

Figure 3-42. Side Keel Panel Corner Feature

3.3.6 Center Keel Panel Assembly (ZJ153356)

Figure 3-43 shows the center keel panel, which was installed at the bottom of the MBB between the two side keel panels and the forward and aft lower bulkhead panels. This panel is analogous to the lower keel section of a typical HWB-type aircraft and would encompass the bilge area. It is likely that a cargo floor would be emplaced on top of this panel in an actual aircraft design.

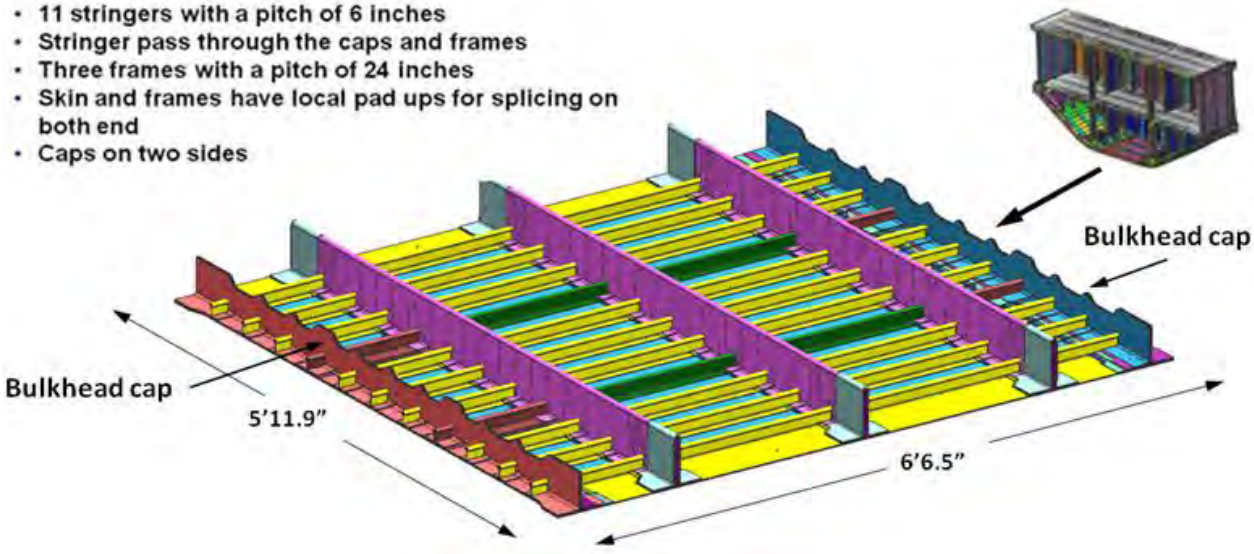

Figure 3-43. Center Keel Panel Assembly

The center keel panel retained the baseline structural design for the MBB, as shown in Figure 3-44. A one-stack skin of Class 72 material was used as opposed to the two-stack skins of the side keel panels. The tear straps were similar in configuration to those used on the side keel panel, where the tear straps for the outermost frames and bulkhead cap teams were designed as one piece.

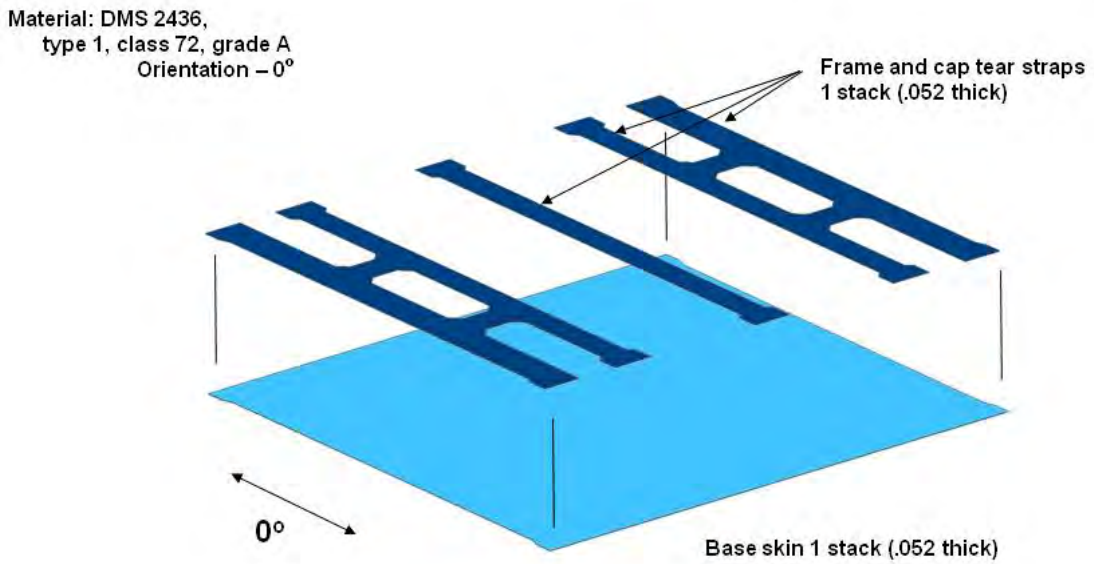

Figure 3-44. Center Keel Panel Skin Construction

As shown in Figure 3-45, the center keel structure consisted of nine PRSEUS stringers, three frames, and two bulkhead caps. The bulkhead T-caps tied in with the forward and aft lower bulkhead panels.

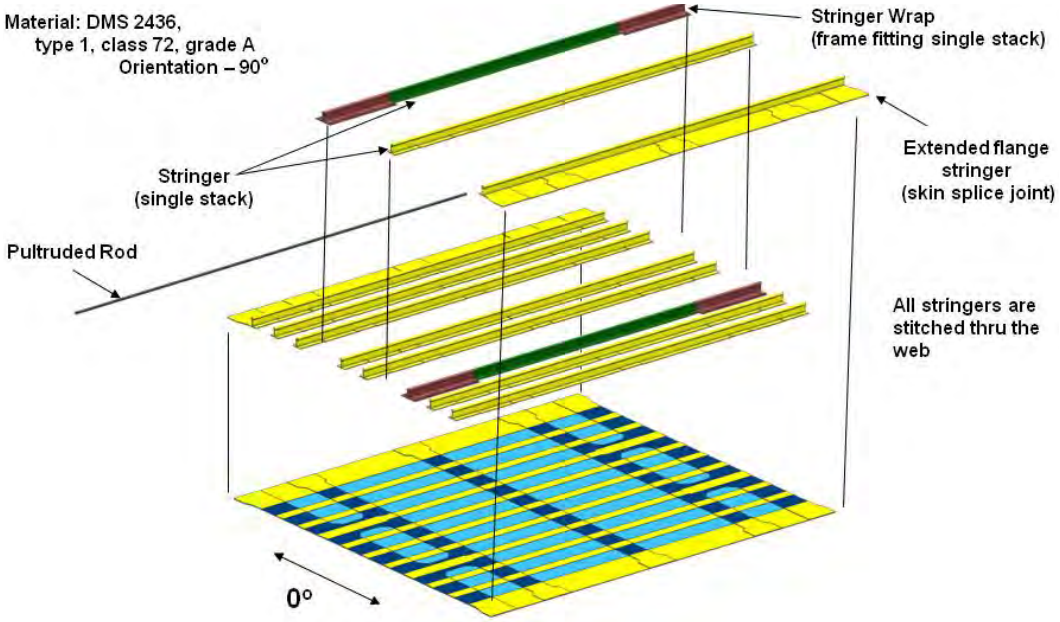

Figure 3-45. Center Keel Panel Stringer Construction

Figure 3-46 shows the detailed construction of the bulkhead T-caps and the frames on the center keel panel. Frames were the standard two-stack construction with overwrap doublers added at each frame end where the center keel panel would be attached to the side keel panels.

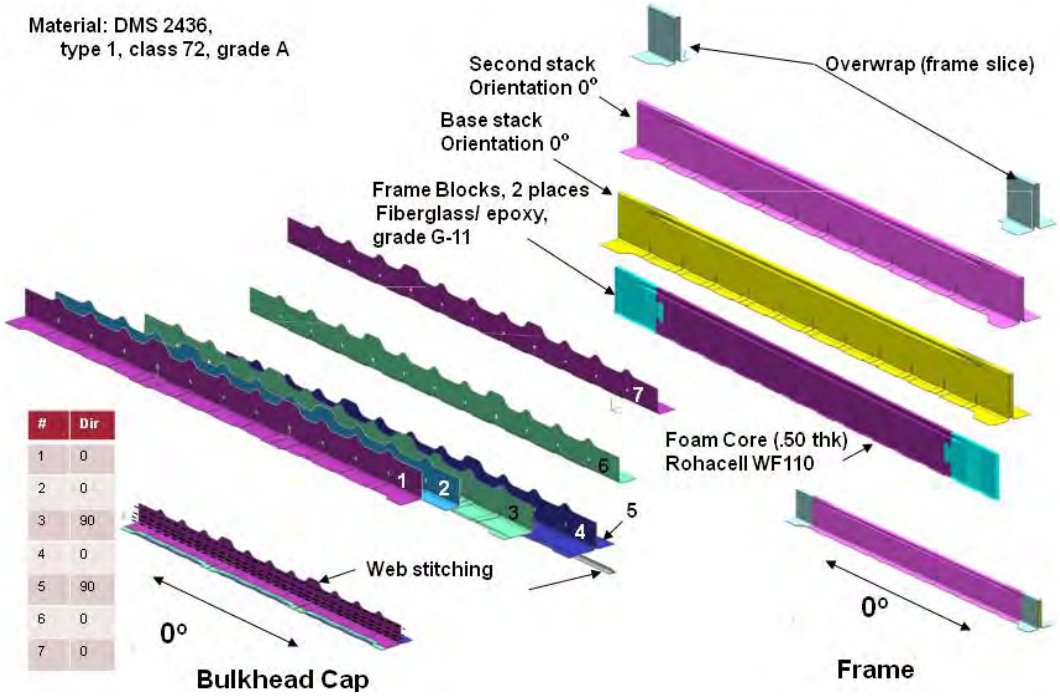

Figure 3-46. Center Keel Panel Frame Construction

As shown in Figure 3-47, the stringer stack direction was 90 deg to the orientation of the skin stack and frame stacks as installed in the preform.

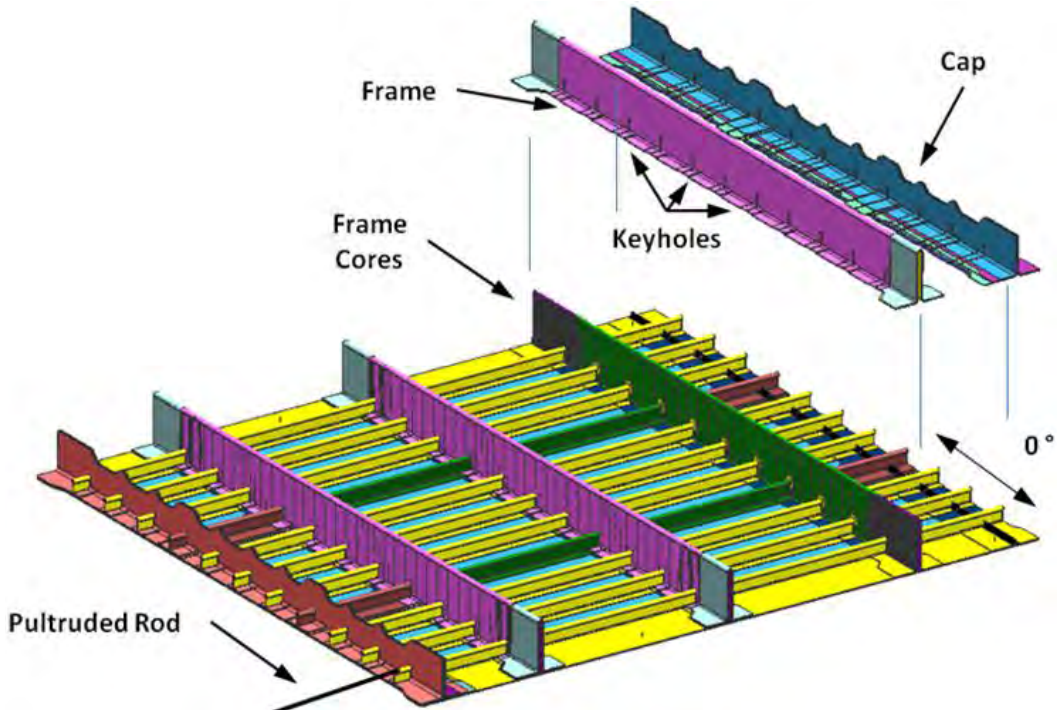

Figure 3-47. Center Keel Panel Cap Construction

As shown in Figure 3-48, the center keel panel was stitched with the flanges of stiffening features flared at the panel periphery, as was done in the side keel design. The flange ends were widened to provide additional material in fastener bearing area at the keel splice.

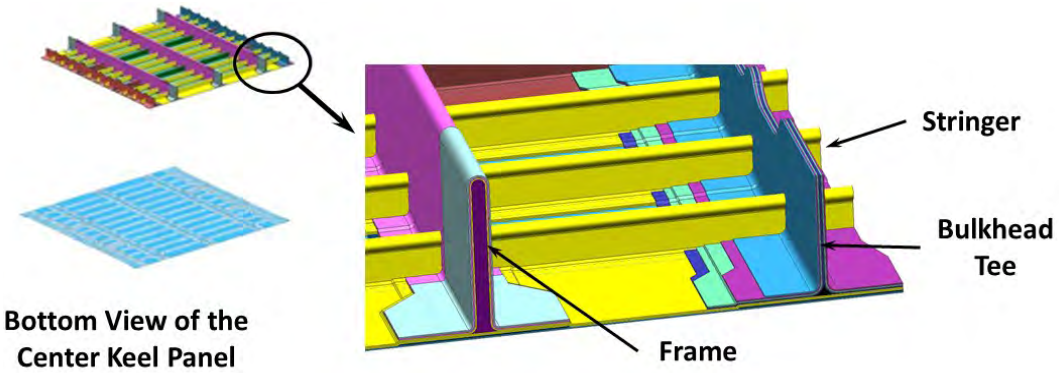

Figure 3-48. Center Keel Panel Edge Features

3.3.7 Outer Rib Panel Assembly (ZJ153357)

The outer rib panels closed out the sides of the MBB. The two panels were identical in geometry and construction, facilitating manufacture. As shown in Figure 3-49, they were typical flat panels and followed the stringer and frame pitch baseline. Stringer overwraps were used to reinforce the ends for fitting attachment, as was done on other MBB panels.

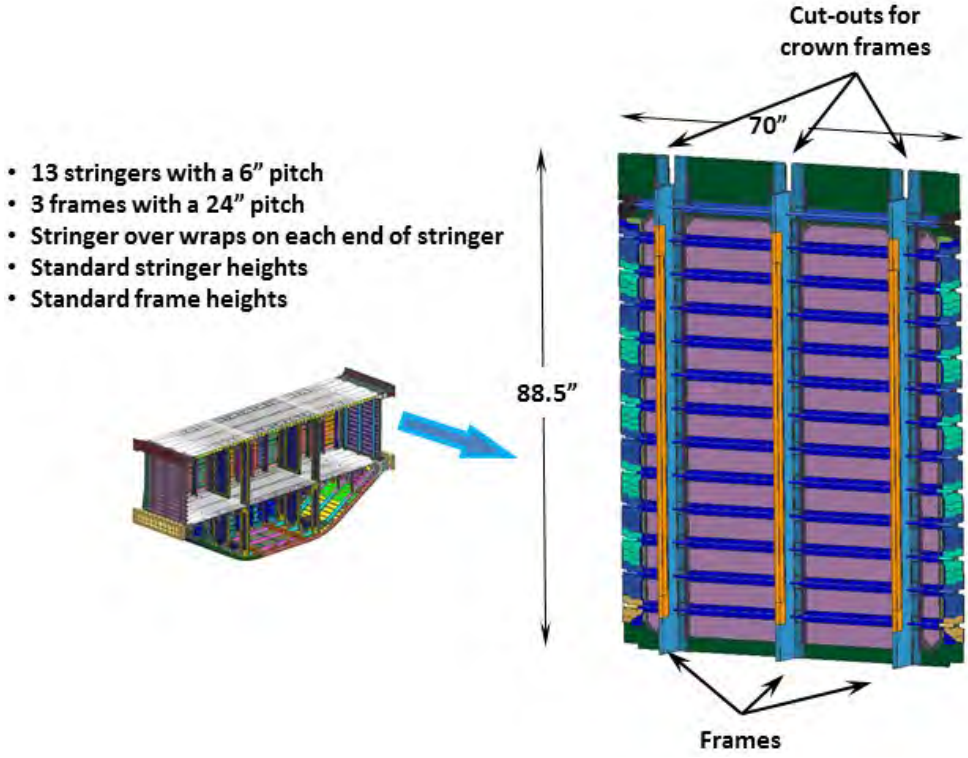

Figure 3-49. Outer Rib Panel Assembly

Figure 3-50 indicates the fabric roll orientation of the stringer tear straps. The stringer material was oriented in line with the tear straps. The skin was oriented in the direction of the frames, 90 deg to the direction of the stringers and stringer tear straps. Figure 3-51 provides a more detailed view of the stringer end overwrap doublers mentioned in the previous section. The doubler material was oriented parallel to the stringer and stringer tear strap.

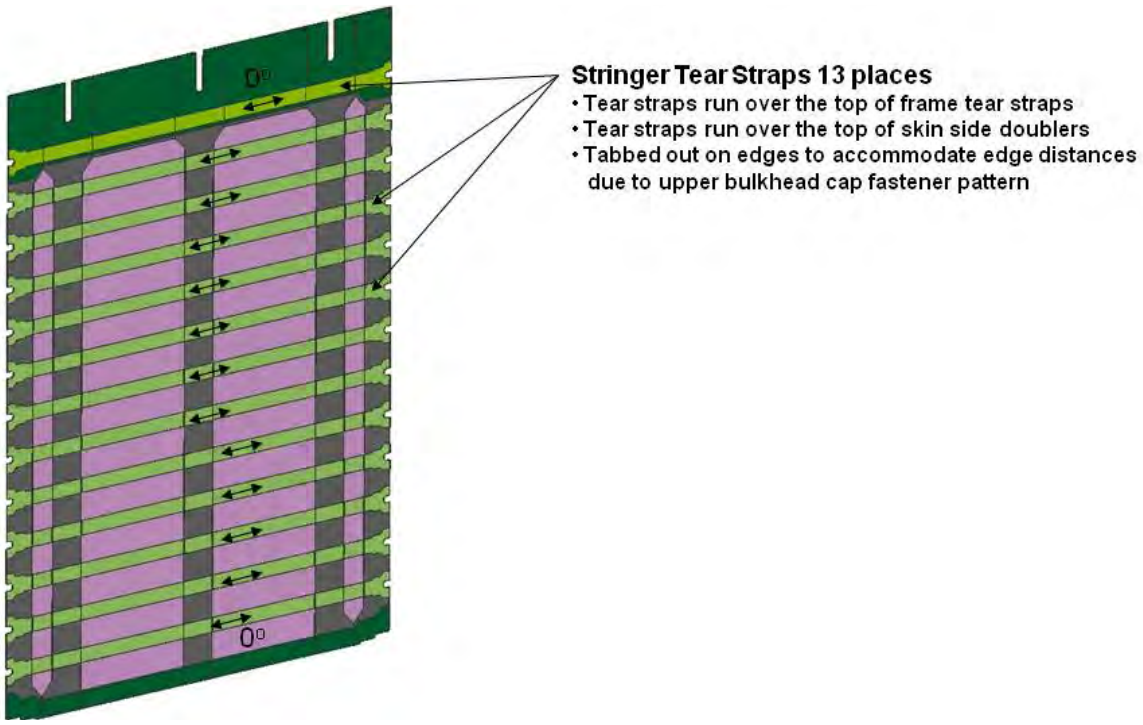

Figure 3-50. Outer Rib Panel Skin and Tear Straps

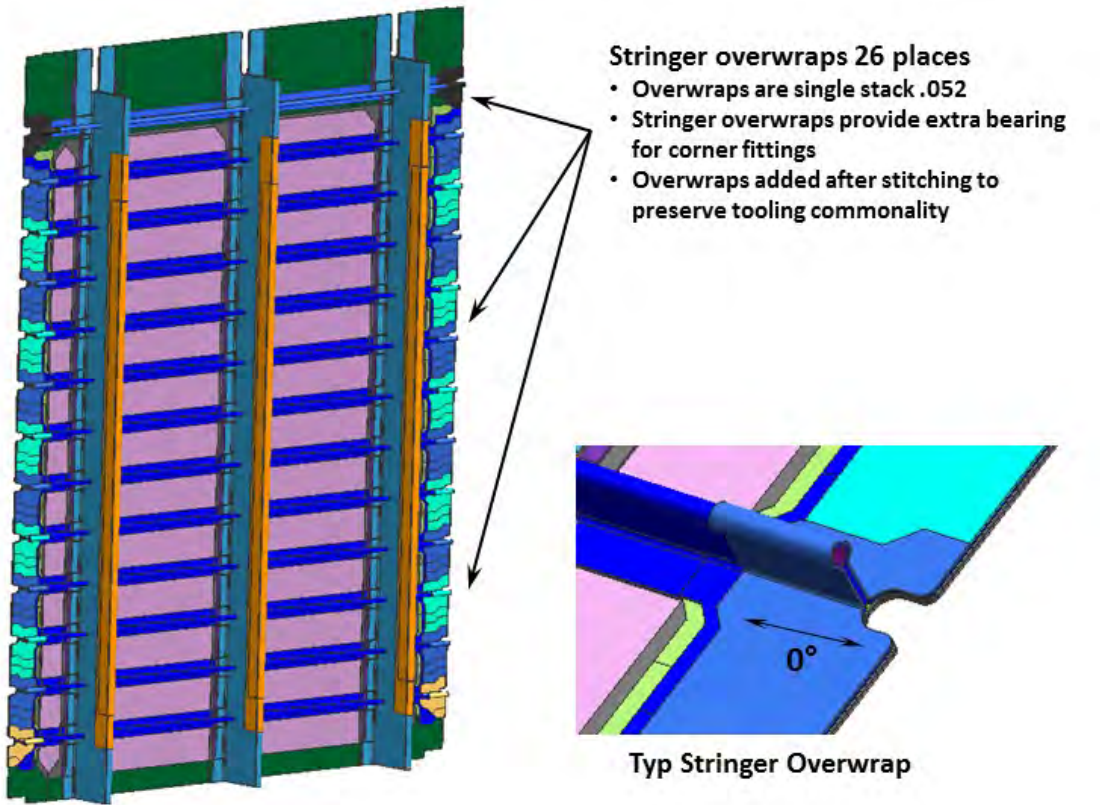

Figure 3-51. Outer Rib Panel Stringers

Figure 3-52 shows the outer rib panel frames. The three frames were the baselined two-stack Class 72 fabric design with an additional cap doubler. Rohacell core with G11 fiberglass inserts at the frame ends supported the frame profile and stringers.

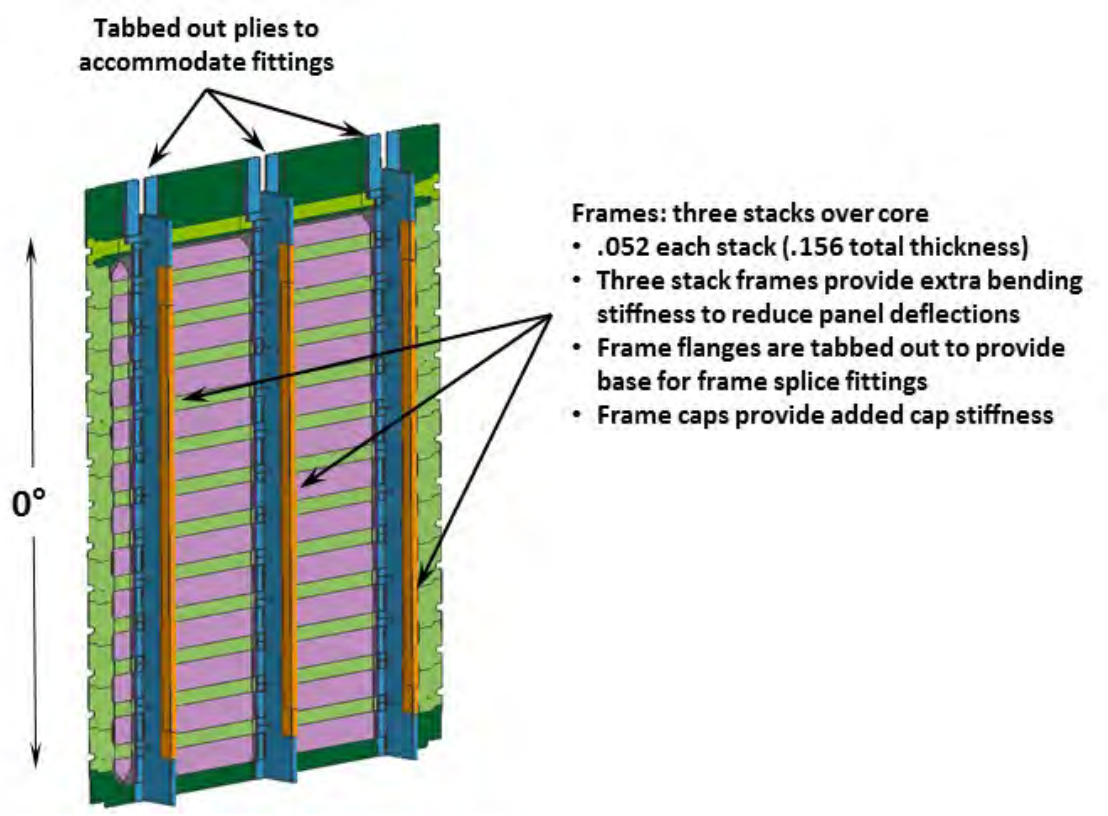

Figure 3-52. Outer Rib Panel Frames

3.3.8 Center Rib Panel Assemblies (ZJ153358 and ZJ153359)

The four inner rib panels functioned to transfer shear loads between the forward and aft bulkhead panels as well as tying the crown panel, floor panel, and keel panels to the bulkheads. The inner rib panels differed from other MBB panels in that they were constructed from carbon-fiber prepreg, which was cured and, secondarily, bonded to the Nomex honeycomb core. Sandwich construction was utilized to simplify manufacture in areas where the greater damage tolerance of PRSEUS panels was not required. This was characteristic of expected construction in a typical HWB aircraft, and many interior panels in current production aircraft are also of the sandwich type.

Vertical edges of the upper center rib panels were scalloped to clear the stringers on the forward and aft bulkheads, as shown in Figure 53. At the upper edge of the rib, longer mouse holes were scalloped into the panel for the crown frames to pass through. An opening was provided in each panel to gain access into the MBB side bays. The facesheets were a constant 10 plies thick to eliminate any special tooling or complex machining of the core. Full-height solid laminate edge supports were used at the fastener locations to support the clamp-up loads from the fasteners (Figure 3-54). The edge of the large pass-through cutout was also reinforced with the full-height solid laminate. Full-length embedded struts tied the crown and floor frames together. These full-height solid laminates added weight but eliminated scarfing the core around the edges as well as the tooling needed to support the assembly during bonding. The supports were fabricated using 156 plies of cloth. Foaming adhesive (FM410) was used to make the shear tie between the core and the thick laminate. Film adhesive (FM73) was used to bond the facesheets, supports, and core together.

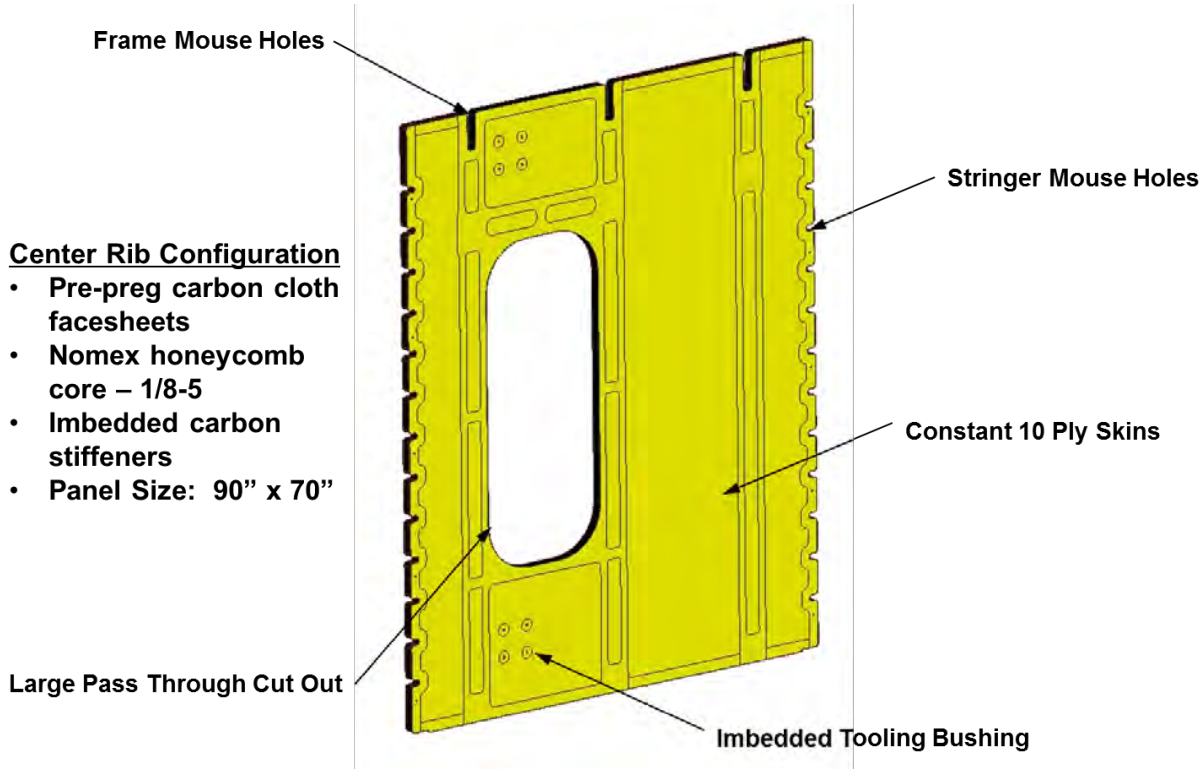

Figure 3-53. Upper Center Rib Panel Assembly

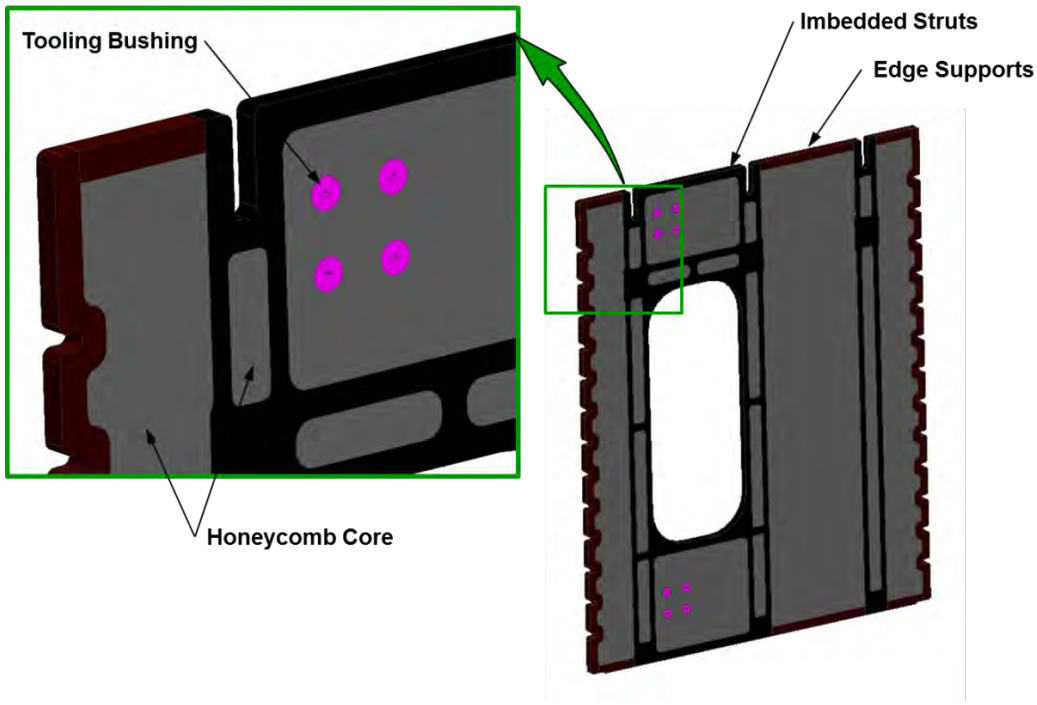

Figure 3-54. Upper Center Rib Substructure

Figure 3-55 shows the lower center rib panel design, which was very similar to the upper center rib panel but smaller due to the shorter height of the lower bay of the MBB. The corresponding pass-through cutout was thus also smaller. Construction was otherwise identical, with the same facesheet layup, Nomex honeycomb core, and embedded carbon-fiber stiffeners.

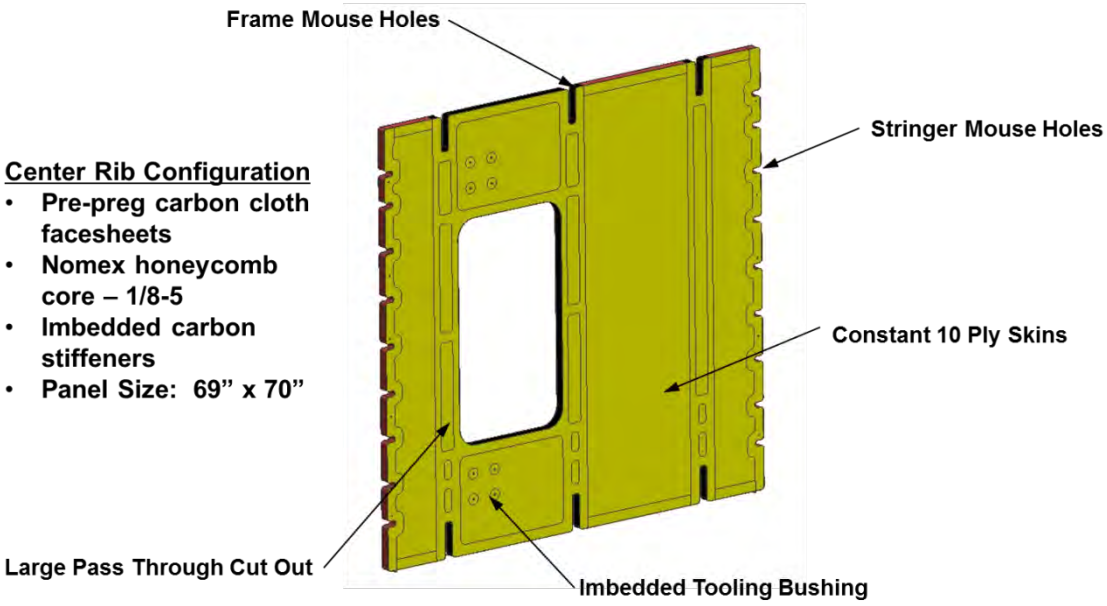

Figure 3-55. Lower Center Rib Panel Assembly

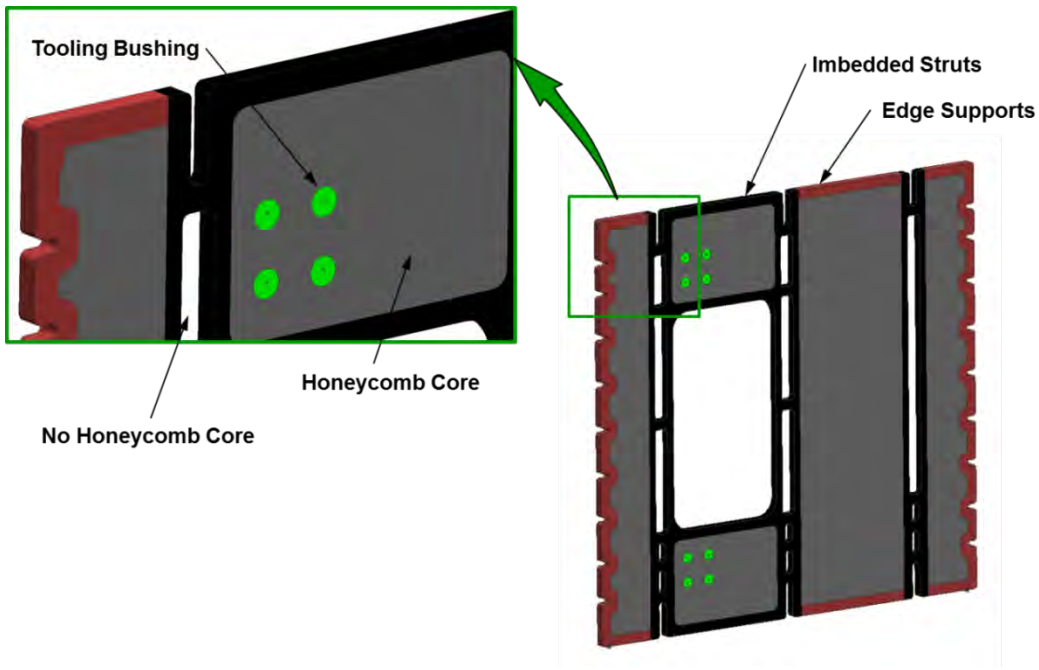

Figure 3-56. Lower Center Rib Substructure

3.4 Multi-bay Box Assembly Features

Integral features were utilized wherever possible in the MBB design, and the caps constituted one such design feature. Nevertheless, a number of metallic fittings were still necessary to transfer the load from one stiffening member to another on an adjacent panel. Fittings were also required in the load-introduction areas to distribute the external input loads from the COLTS platens. Figure 3-57 shows all fittings required to assemble and test an MBB in the COLTS facility. In total, 735 metallic details were required to construct the MBB. The load-introduction fittings accounted for 108 of the fittings.

The MBB represented a compressed version of an HWB fuselage section. In the MBB, the forward and aft pressure bulkheads were only 7 ft apart; however, for an actual HWB aircraft, the pressure bulkheads would be more than 100 ft apart. Figure 3-58 shows a view of a fuselage section where all of the pressure bulkhead and load-introduction fitting were omitted. Considering only the interior (not including the load-introduction and bulkhead) fittings and fasteners, there were only 152 fittings (22/ft) and 1,370 fasteners (196/ft) for an HWB 30-ft-wide by 7-ft-long fuselage test article. The table in the figure illustrates that an actual HWB would be 14 times longer than the MBB. However, the number of panels required would stay the same. The number of fittings would increase by only 3 times (versus the 14 times in length), and the number of fasteners would increase by only 4 times.

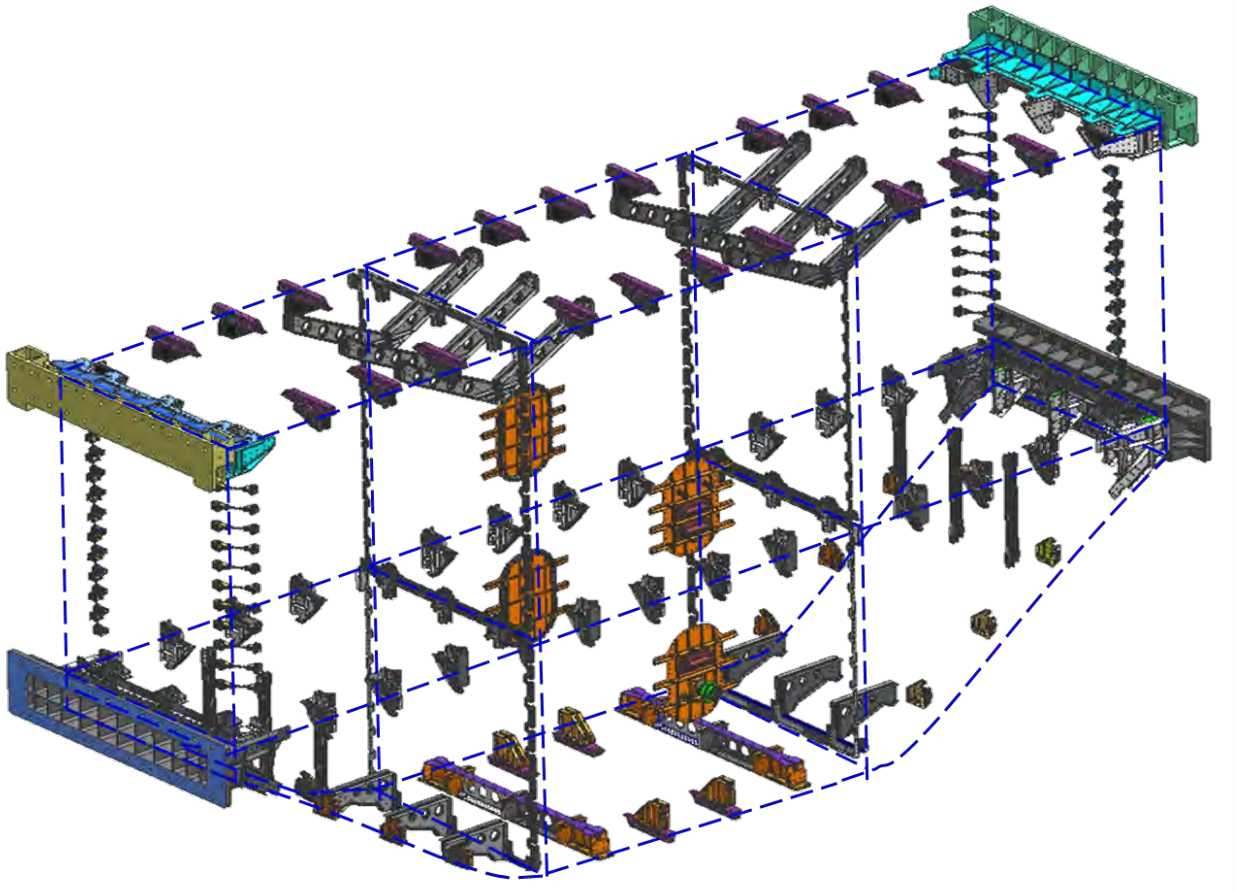

Figure 3-57. MBB Assembly Fittings

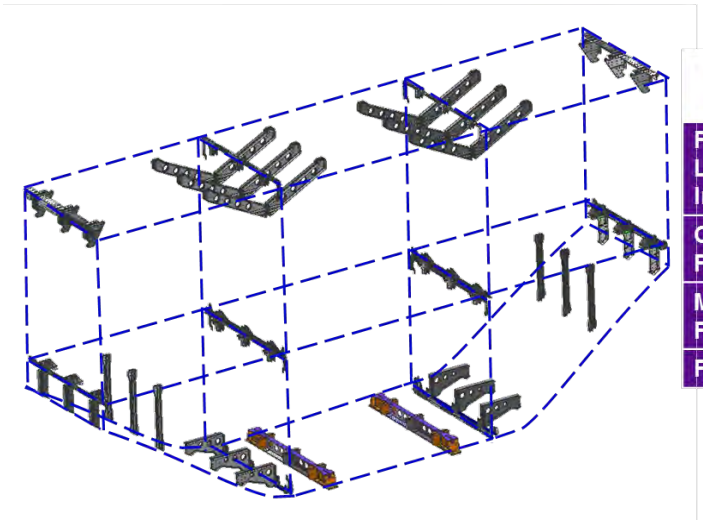

	7 ft Fuselage	100 ft Fuselage	Increase
Fuselage Length Increase	----	93	14 times
Composite Panels	15	15	0
Metallic Fittings	615	1,985	3 times
Fasteners	11,652	51,762	4 times

Figure 3-58. Fittings Required Without the Pressure Bulkhead and Load-Introduction Fittings

Stitched composites that integrate the stiffening members into a single panel can greatly reduce the number of details and fasteners required for a built-up structure. Figure 3-59 provides an approximate estimate for the number of fasteners required to assemble a cube, an MBB, and a theoretical fuselage for three different concepts. For each type of structure, the advanced state-of-the-art composite concept significantly reduced the number of fasteners required to assemble the structure compared to an aluminum structure. However, the stitched integrated composite concept again significantly reduced the number of fasteners required to assemble the structure compared to an advanced state-of-the-art composite concept.

In every case, the number of fasteners required for a stitched concept can be reduced by more than 80% versus an aluminum concept structure or 60% versus a state-of-the-art concept composite structure. Another way to evaluate the integrated structure is to compare different concepts at the assembled (stiffened) panel level. Figure 3-60 shows an estimate for the number of detail parts and fasteners required to assemble a stiffened panel. From strictly a part count (details plus fasteners) perspective, stitched composites would have a 99% reduction. Reducing purchasing, inventory control, planning, tooling, and assembly tasks would correspondingly net large cost savings for a stiffened panel.

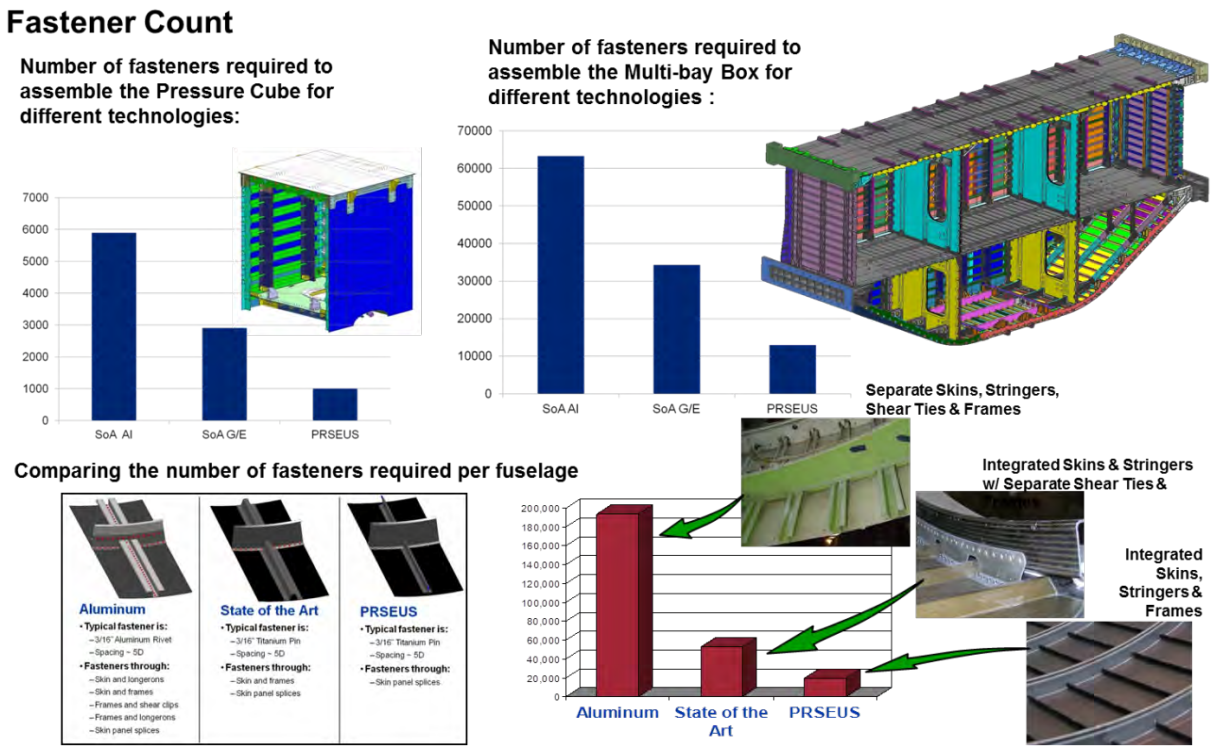

Figure 3-59. Required Number of Fasteners for Different Structural Concepts

- **Integral PRSEUS Design:**
  - 11 Panels

Total Parts = 11
Total Fasteners = 0

- **Current State-of-the-Art Composite Design** ("C"&"L" x-sections):
  - 11 Panels
  - 64 Frames
  - 64 Shear Ties
  - 26 Caps
  - 13,000 Frame and Shear Tie Fasteners
  - 4,100 Cap Fasteners

Total Parts = 165
Total Fasteners = 17,100

- **Current State-of-the-Art Aluminum Design** ("Z" x-section stringers):
  - 11 Panels
  - 64 Frames
  - 64 Shear Ties
  - 223 Stringers
  - 26 Caps
  - 13,000 Frame and Shear Tie Fasteners
  - 4,100 Cap Fasteners
  - 26,000 Stringer Rivets

Total Parts = 388
Total Fasteners = 43,100

Figure 3-60. Stiffened Panel Level Part Count for Different Concepts

3.4.1 Multi-bay Box Internal Fittings

Figure 3-61 shows the locations and part numbers for some of the fittings used to assemble the MBB. Aluminum (versus titanium) was used wherever possible to save on material cost. Because the life span of the MBB was less than 1 year, galvanic corrosion was not an issue; however, all parts were primed to add some corrosion protection. (The parts are shown with varying colors simply for contrast.)

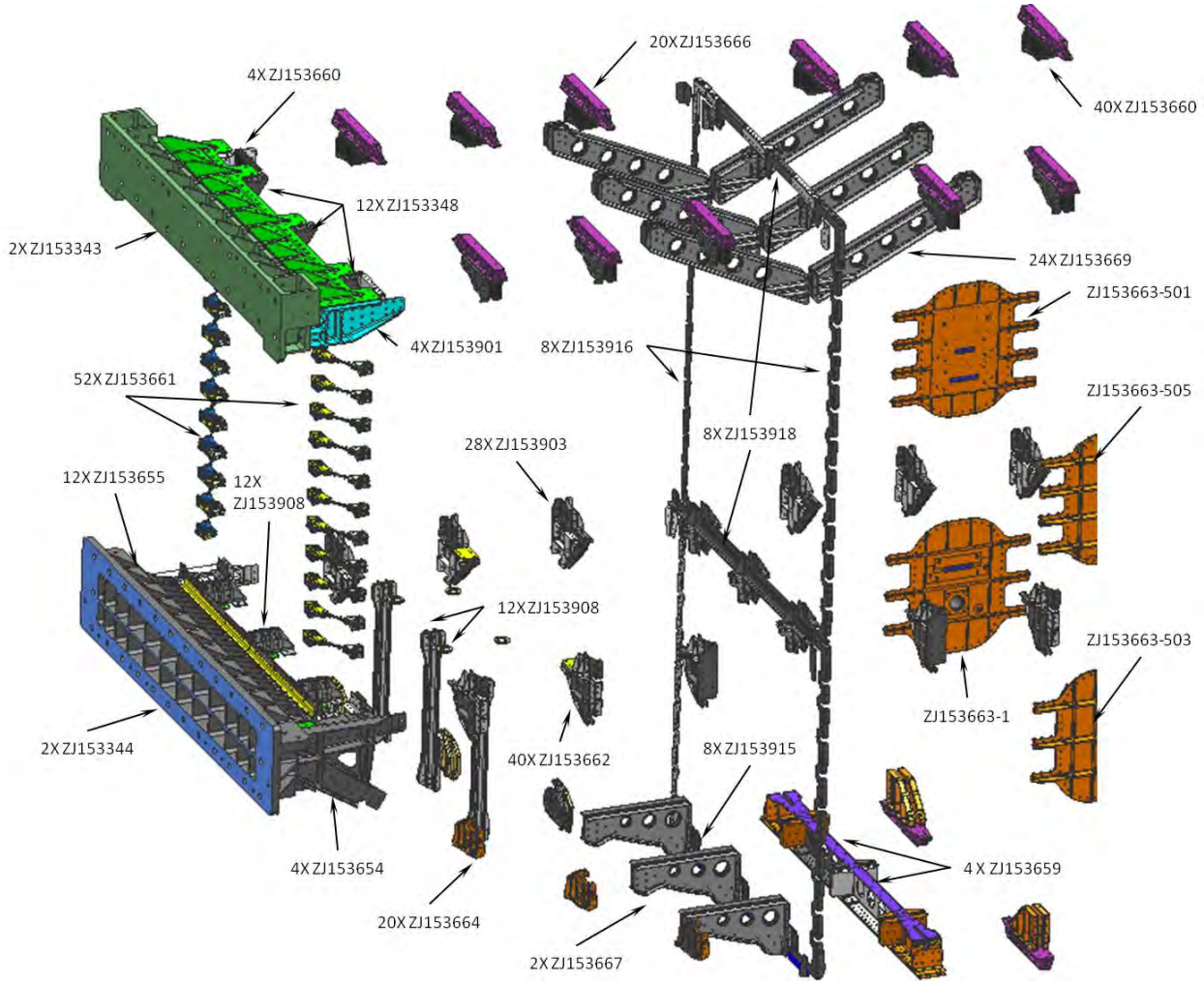

Figure 3-61. MBB Assembly Fittings Details with Part Numbers

High bending loads from the upper bulkhead frames were reacted on only one side by the crown panel at the crown stringer locations. An actual aircraft configuration would have structure on both sides of the pressure bulkhead and could share the loads. For the MBB, external stringers fittings were added to reduce the artificially high pull-off loads at the last fastener of the internal frame fitting shown in Figure 3-62. Local buildups at the fitting locations in the crown panel eliminated most of the joggles and created a nearly flat, uniform surface for the fitting to sit on. This reduced the complexity of the fitting, eliminated fit-up issues at the ply drop-offs, and reduced the amount of liquid shimming required during assembly. Initial fitting designs tied the fitting to the web of the stringer; however, the analysis indicated that the loads were much too high for the web even when doublers were added. So to reduce the complexity of the fitting

and the panel, the fitting was attached only to the stringer flange on the crown panel. Analysis also indicated that it was better not to attach the fitting directly to the frame of the crown panel. This drove too much load into the frame and in the adjacent skin bay, affecting the test section of the crown panel.

Figure 3-63 shows an internal view of the upper bulkhead to crown attachment. Mouse holes trimmed in the edge of the bulkhead panel allowed the continuous stringers on the crown panel to pass through the joint and integral bulkhead cap on the crown panel. The approach also allowed the upper edge of the upper bulkhead panel to fit near the fillet radius of the crown integral cap, reducing the height of the rows of fasteners. This arrangement, in turn, reduced the moment on the web of the integral cap.

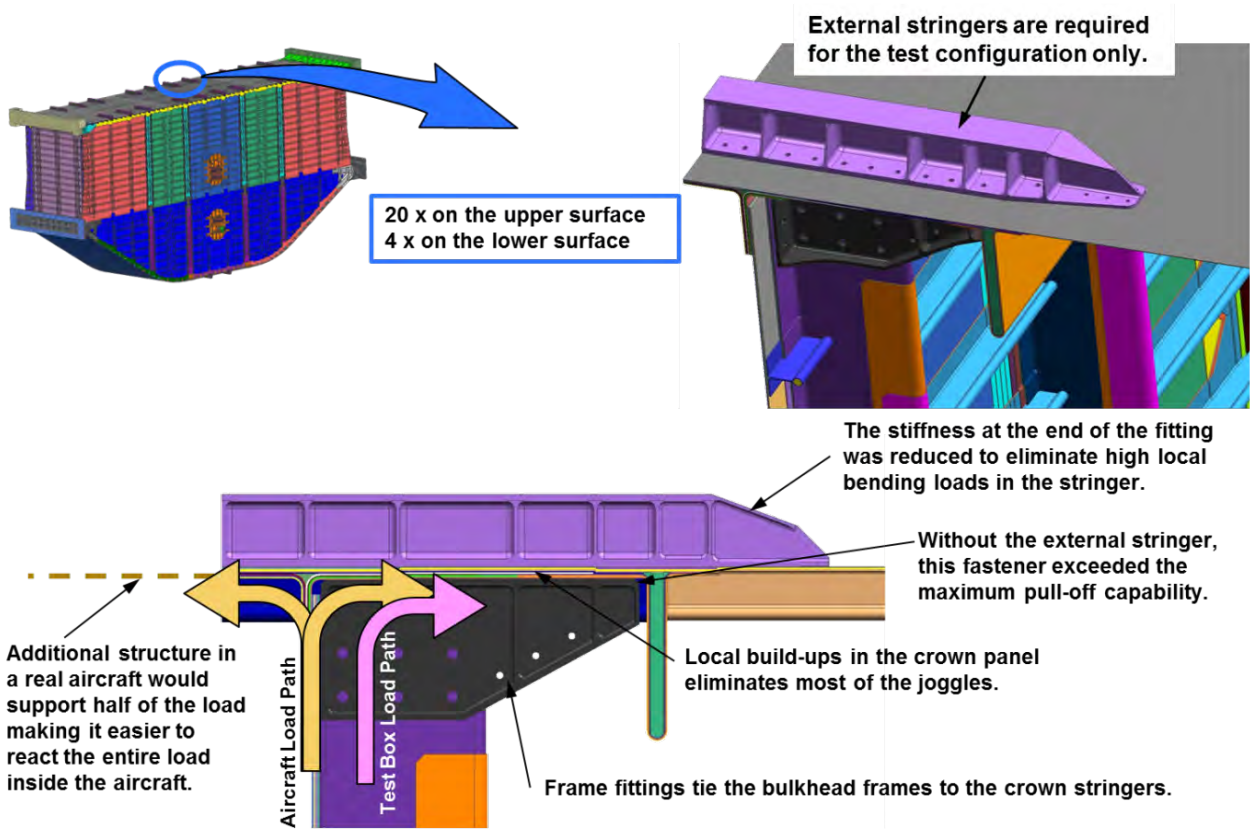

Figure 3-62. Crown-to-Upper Bulkhead Joint

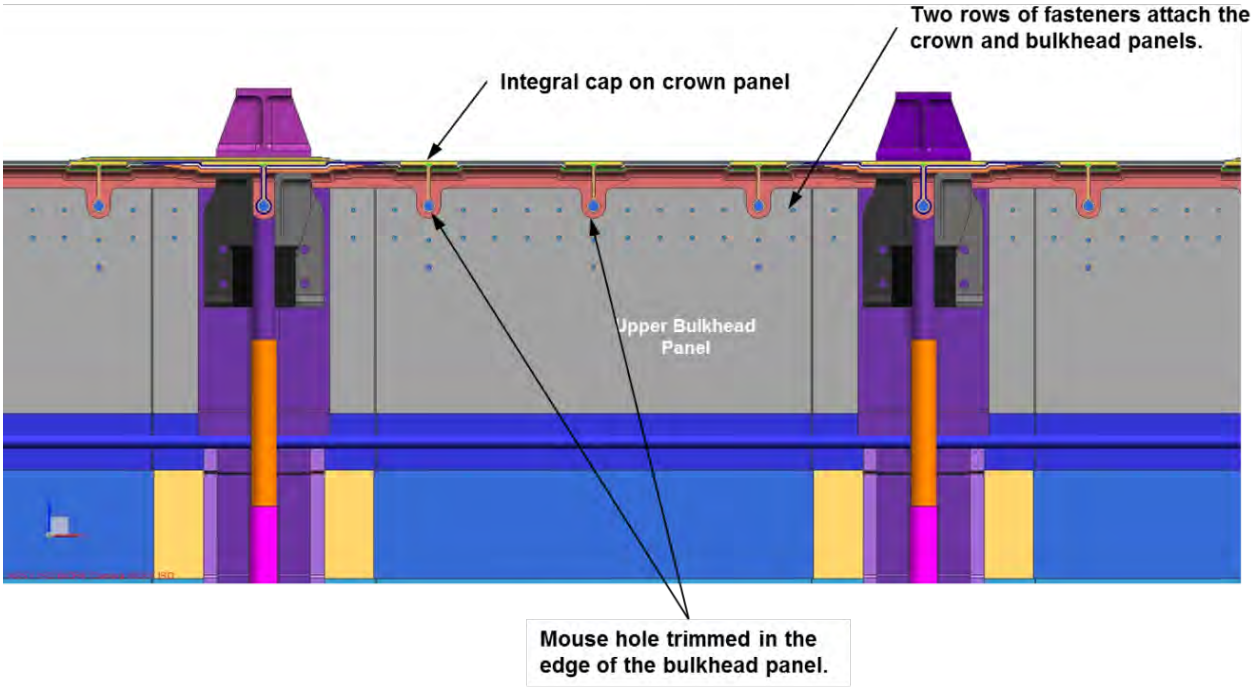

Figure 3-63. Crown-to-Upper Bulkhead View

The crown to outer rib panel joint was very similar to the crown to upper bulkhead panel joint. The skin with doublers along the upper edge of the outer rib panel attached to an integral cap on the crown panel. The difference was that along the short end of the crown, the crown and outer rib frames were spliced together. Long 6-in.-deep slots machined into the end of the outer rib panel allowed the crown frame to extend to the cap (see the lower view in Figure 3-64). Back-to-back frame fittings spliced the two frames together and guided load directly into the crown frames from the platens (see the upper view in Figure 3-64). These fittings wrapped around the first stringer, reinforcing the keyhole cutout in the frame web. The fitting flange that sat on the outer rib was trimmed back to allow the fitting to be positioned in place after the panels were spliced together. To help ease the loads into the crown frames, additional fittings between the frames were used to load up the thick skin on the crown panel.

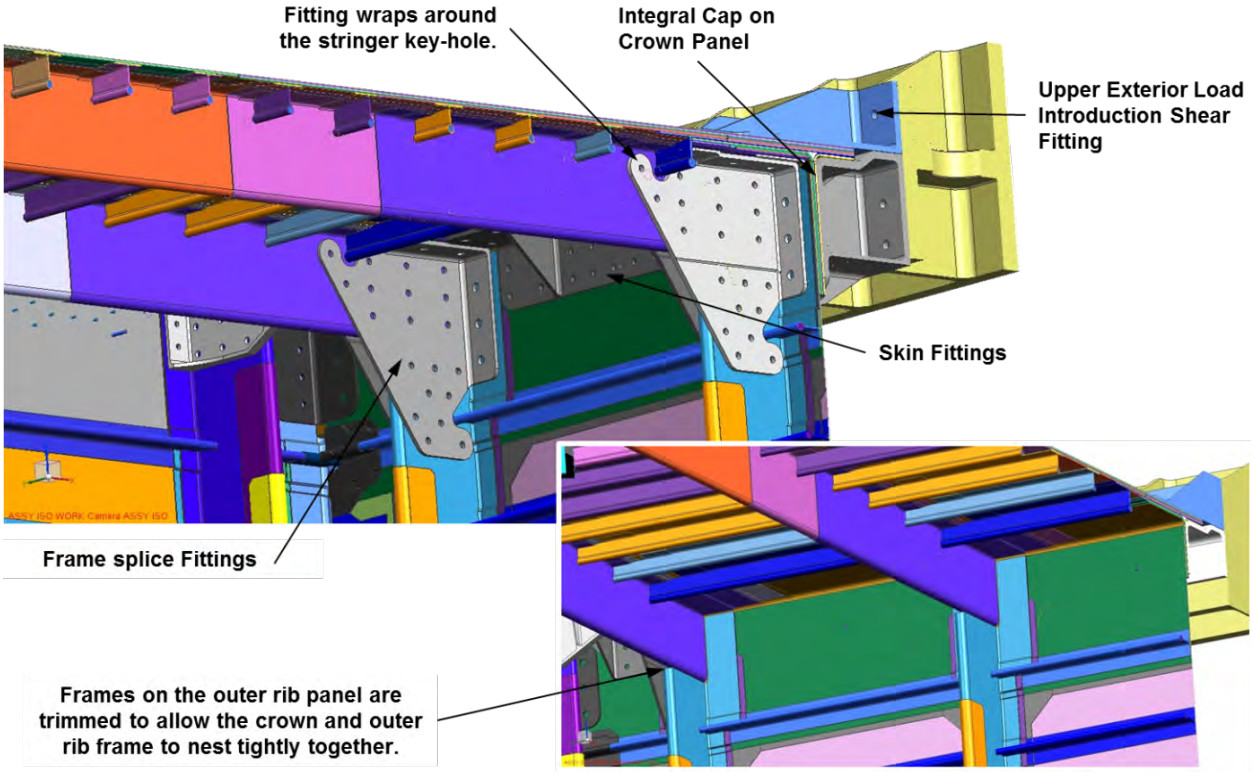

Figure 3-64. Crown-to-Outer Rib Joint

Figure 3-65 shows an external view of the outer rib to crown and upper bulkhead attachment to the integral caps. The crown cap scallops were extended down to create a flat surface for the entire external load-introduction fitting to sit on to reduce the complexity of the fitting. Because large load-introduction fittings were required along the short end of the crown to get the loads in the panel, the crown frames were stopped short at the cap. The bulkhead stringers were extended to the end of the panel. Integrating the caps with the panels and stitching the flanges in place eliminated 50% of the fasteners that would normally be required to join two panels. (Conventional aircraft design would have joined the panels using a separate "*L*" or in some cases a "*T*" section detail.) For a pressurized structure, that would require two rows of fasteners to be installed on each leg of the separate cap detail. The integral cap also eliminated all of the shimming at the interface and allowed the stringers to be continuous to the end of the panel. Because the cap could be fully integrated into the panel during preform assembly, continuous cap plies were located under the stringers that passed through the cap, which required only small keyholes in the web of the cap. The flanges of the caps joggled onto the stringer flanges, and both stringer and cap flanges were stitched into place, which created a stiff and uniform panel that was able to carry the loads efficiently in all directions. The OML of the mating panel simply attached to the tooled surface of the cap and only two rows of fasteners were required. No extra details to be fabricated and tracked, no fit-up issues requiring shimming, no extra fasteners to be ordered and requiring hours to install, and no extra clips to tie off the ends of the stringers were required—just continuous load paths that were all stitched together. Figure 66 shows an internal view of the corner joint. The decision on how the upper bulkhead and outer rib stringers would interface had to be made before the cube test had been completed. The cube employed a more aggressive approach and staggered the stringers so that the stringers could be extended to the end

of the panel. At the time, a more conservative approach was taken with the MBB. For the MBB, the stringers on the two panels were aligned.

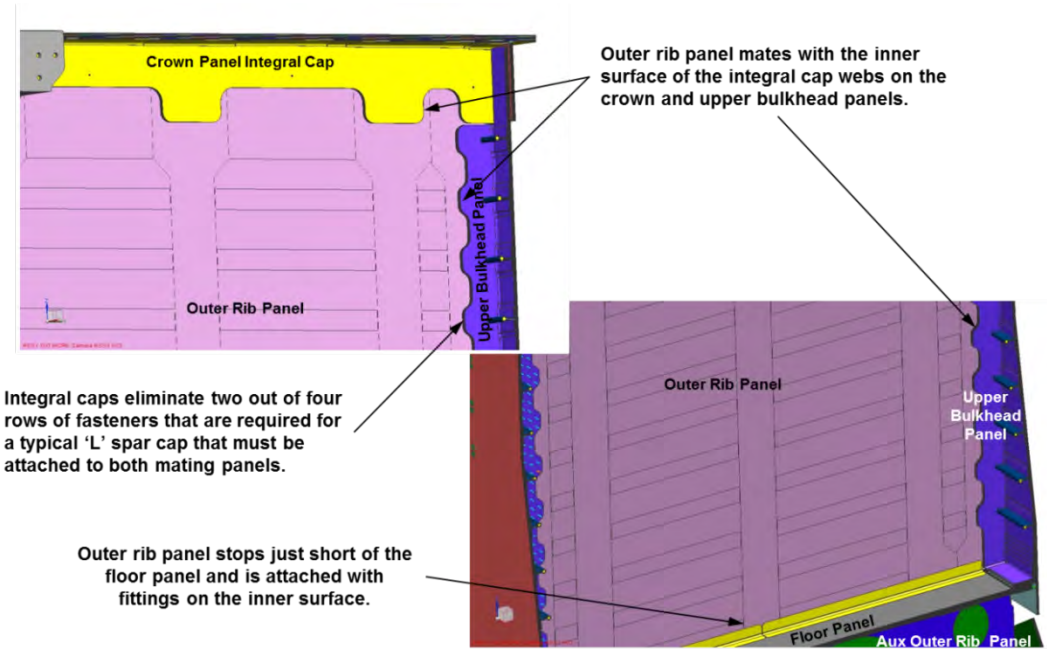

Figure 3-65. Outer Rib Panel Attached to Integral Caps on the Crown and Upper Bulkhead Panels

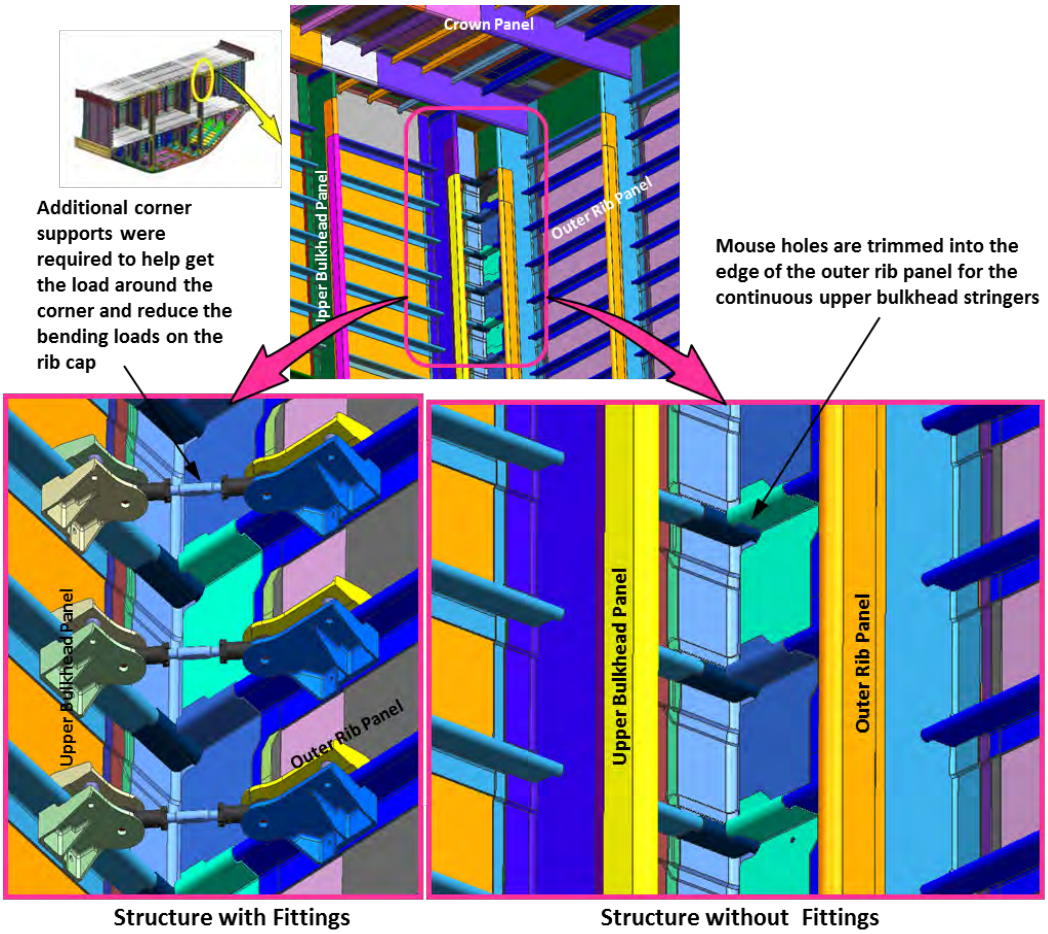

Figure 3-66. Crown Panel Upper Corner View

Stringers on the outer rib were trimmed back to allow the upper bulkhead stringers to extend to the end of the panel, and a small clip tied off the outer rib stringers. It turned out that the staggered approach used on the cube worked very well. Testing indicated that there was no need to tie off the end of the outer rib stringers if they were extended to the end of the panel, which was at the base of the integral cap on the upper bulkhead panel. Well into the design of the MBB, analysis indicated that the outer rib stringers that were stopped a couple of inches away from the base of the integral cap on the upper bulkhead had significantly increased the moments on the web of the cap. The fittings that were designed were much too small to be effective. Compounding the problem on the larger MBB test article was the fact that the upper bulkhead panel was cut off at the joint, requiring all bending loads from the outer rib to be reacted on one side of the upper bulkhead panel. For an actual aircraft, the panel would have continued and stabilized the joint. Therefore, larger corner supports were required for the MBB. Figure 3-67 shows the fitting/strut arrangement. There was very little room available to install a one-piece fitting in the corner after the two panels had been joined. These smaller fittings linked together could be installed any time during the build process.

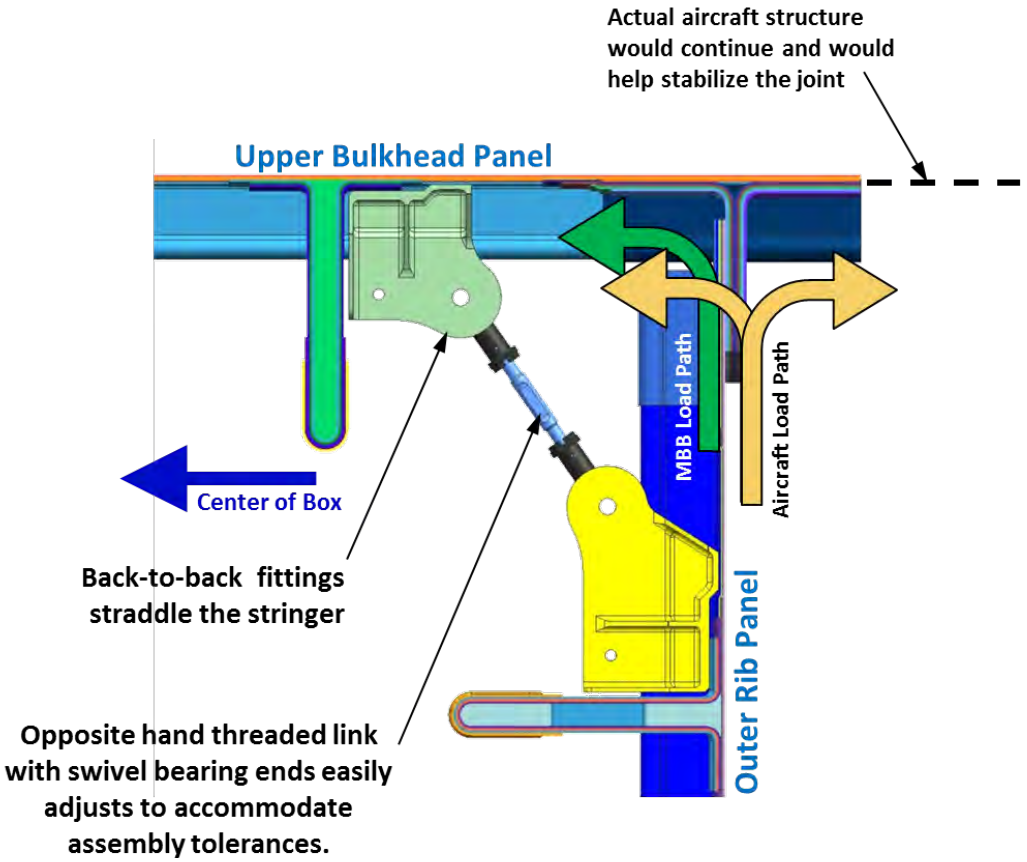

Figure 3-67. Upper-Bulkhead-to-Outer-Rib-Corner Supports

Due to limitations on the size of the oven, the forward and aft bulkhead panels were fabricated in two pieces, an upper and a lower. This meant that the two panels had to be spliced together. To minimize the manufacturing effort, the bulkhead splice was located at the floor line, which had several advantages. To reduce the eccentricity at the joint, double shear joints could be used, requiring four rows of fasteners, two on each side of the joint plus several details. Single-lap splice joints could also be used, which could eliminate one row of fasteners and the splice details. However, overlapping skins create eccentricity at the splice, which degrades the performance of the splice/material. So the splice is typically made at a stringer location, doublers are added to both skins, and the width of the joint is increased (using three rows of fasteners) to help stabilize the joint. The MBB design took advantage of the integral cap feature on the upper bulkhead panel to completely stabilize the joint (Figure 3-68). The integral cap flanges already build up the skin thickness so no additional doublers were required on the upper bulkhead panel.

With the floor attached to the web of the cap, the splice was stabilized even more. Doublers were added to the lower bulkhead skin for increased bearing strength. With a very stable splice area, the joint utilized only two rows of fasteners for a 50% fastener reduction and no additional parts. Frame fittings spliced the upper and lower bulkhead frames together, supporting the end of the floor stringers, minimizing the bulkhead frame rotation, and reducing the overall panel deflections. The edge of the floor panel was attached to the cap using two rows of fasteners. The floor panel stringers were extended to the edge of the panel and did not require any attachment to the upper bulkhead panel. Slots were cut into the floor to allow the upper bulkhead panels to pass through, as shown in Figure 3-69.

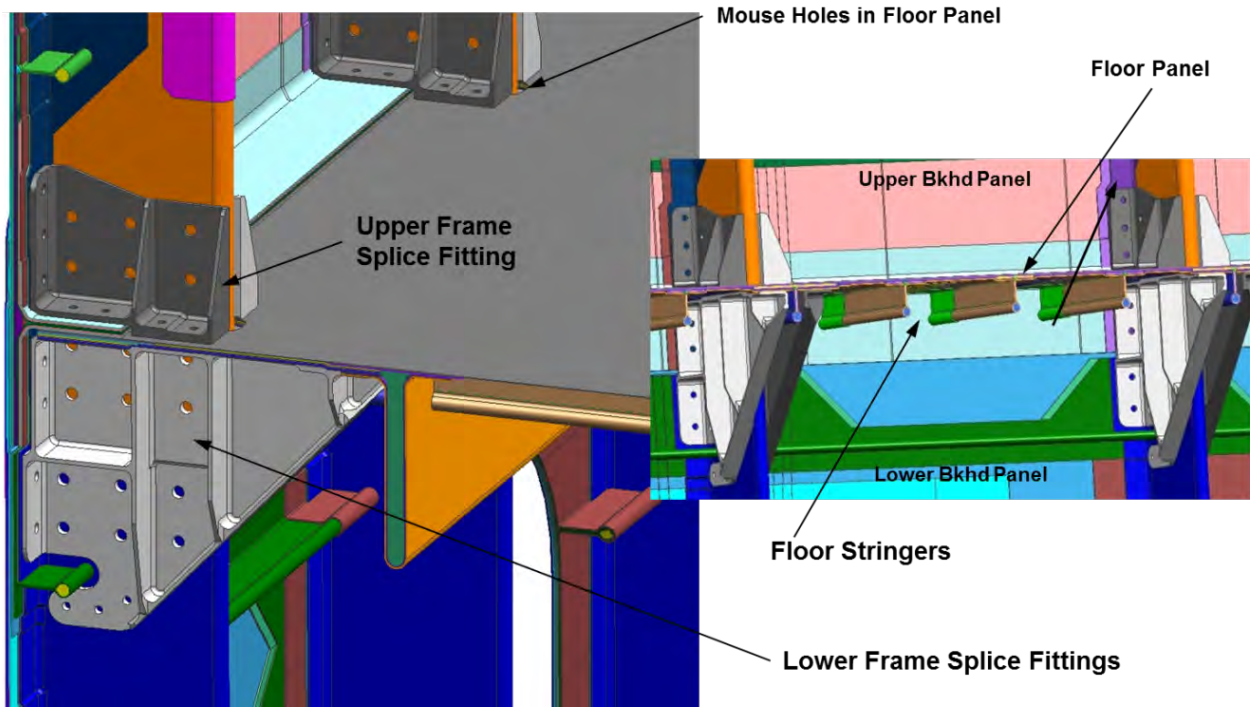

Figure 3-68. Bulkhead Splice View

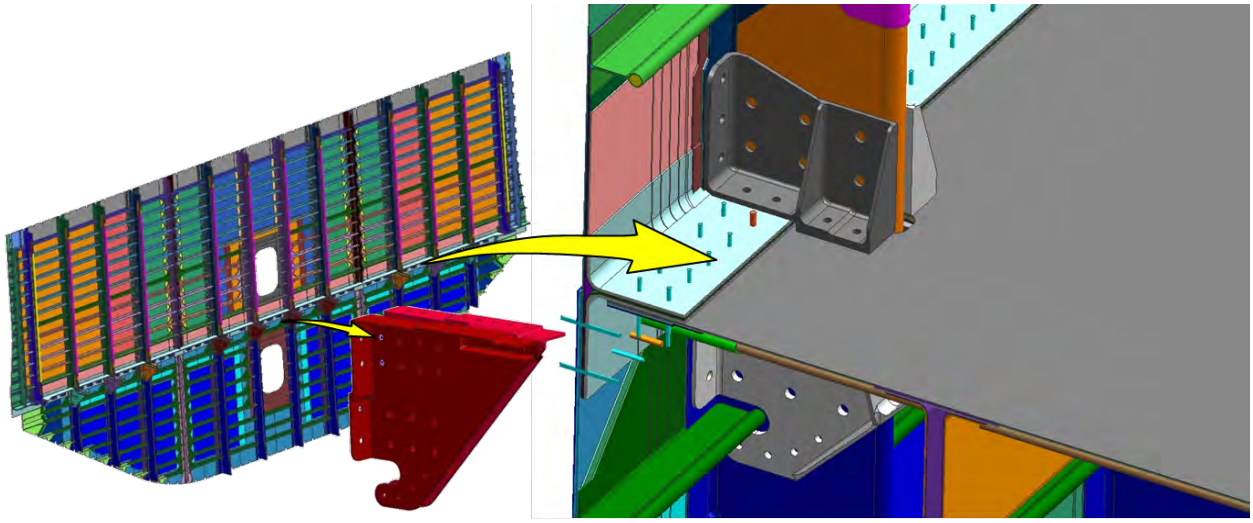

Figure 3-69. Floor Attachment

The lower bulkhead panel was attached to the integral cap on the center and side keel panels (Figure 3-70). Mouse holes were cut into the lower bulkhead to allow the keel panel stringers to pass through to the edge of the panel. The lower bulkhead stringers were located such that the end of the stringer could extend to the base of the cap on the keel panel. This reduced the bending moment on the cap and just above the stringers on the side keel panel so that they could be tied together with small clips. After the cube testing was completed with the staggered stringer arrangement, the additional stringer clips were eliminated. Back-to-back fittings were used to tie off the lower bulkhead frames to the keel panel stringers.

The side keel panels were also stabilized by the addition of struts between the floor and the side keel panel frames. These struts acted to limit deflection of the side keel under pressure and reduced the unsupported span of the side keel. Bending of the side keel was reacted as tension in the strut, which was transferred into the otherwise relatively lightly loaded floor. The design was making use of the floor as a keel beam and one that would otherwise not be heavily loaded at the MBB midsection and unexposed to pressure.

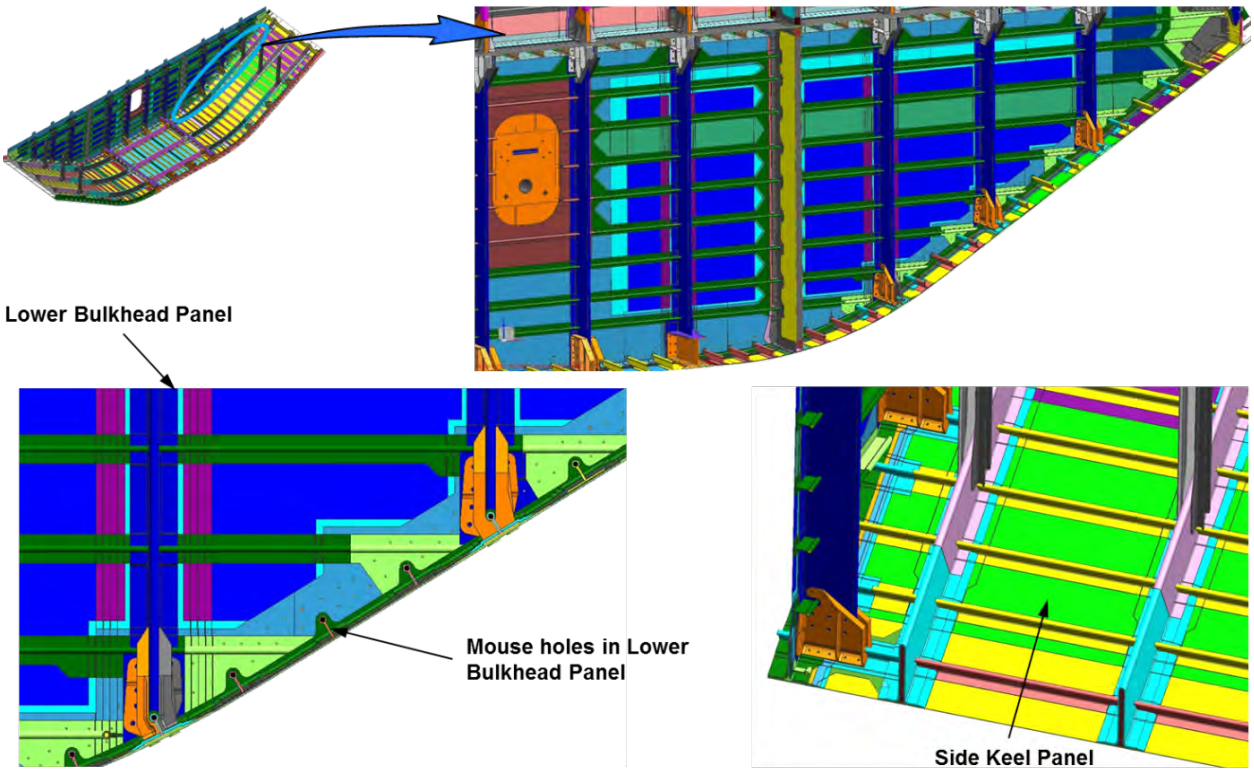

Figure 3-70. Lower Bulkhead-to-Keel Attachment

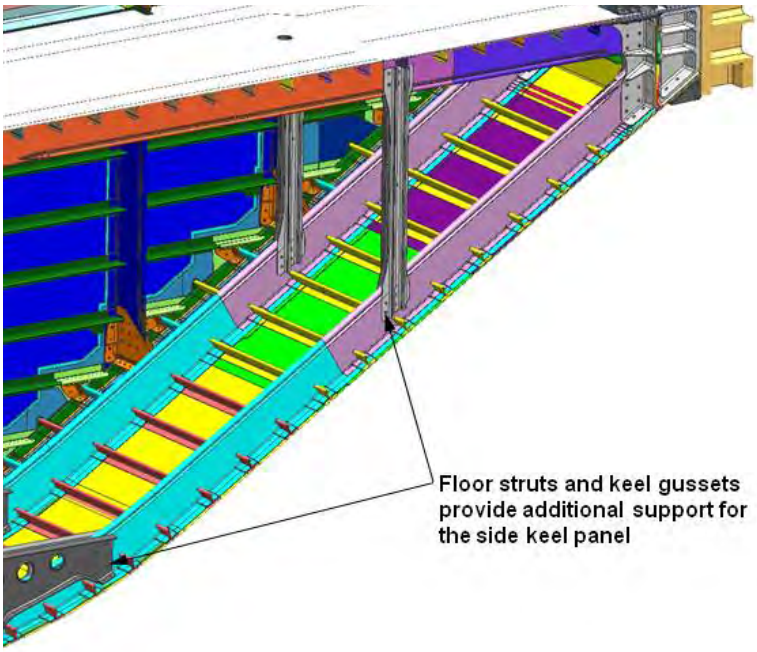

Figure 3-71. Side Keel Supports

Large access holes were machined into the upper and lower bulkhead panels during trimming of the panels (see Figure 3-28 and Figure 3-33). These holes allowed technicians and equipment access into the MBB during assembly and testing. The 24.0- by 18.0-in. access holes were located in both the forward and aft bulkheads. Because the MBB was assembled on its side, the holes in the aft bulkheads were on the lower side, and once the MBB was closed out, these holes were the only way in and out. The holes in the forward bulkheads (upper side during assembly) were used to feed in the pneumatic lines, air ducts, and electrical lines.

Several features were incorporated into the doors. The upper access hole severed four stringers and the lower severed three stringers. To maintain structural integrity of the panel, external stringers were incorporated into the doors. The stringer extensions on the doors created an overlap region where the loads could be transferred from the internal stringers to the external door stringers and then back into the internal stringers. Access slots were added to the aft access doors to enable the internal instrumentation wires to exit the MBB and maintain pressurization. A 3-in. air inlet/outlet port and four 1-in. pressure transducer ports were also included in the aft doors (see Figure 3-72). The forward doors incorporated only the external stringers (see Figure 3-73). All access doors were machined out of 7075-T651 aluminum plate. The aft access doors were completely sealed during the assembly operation. The forward access doors were shipped separately and installed by NASA after all internal test setup had been completed.

Figure 3-72 also shows the external splice straps that spliced the lower bulkhead skin together where the internal skin splice straps were cut short to maintain a constant thickness land for the upper to lower bulkhead splice.

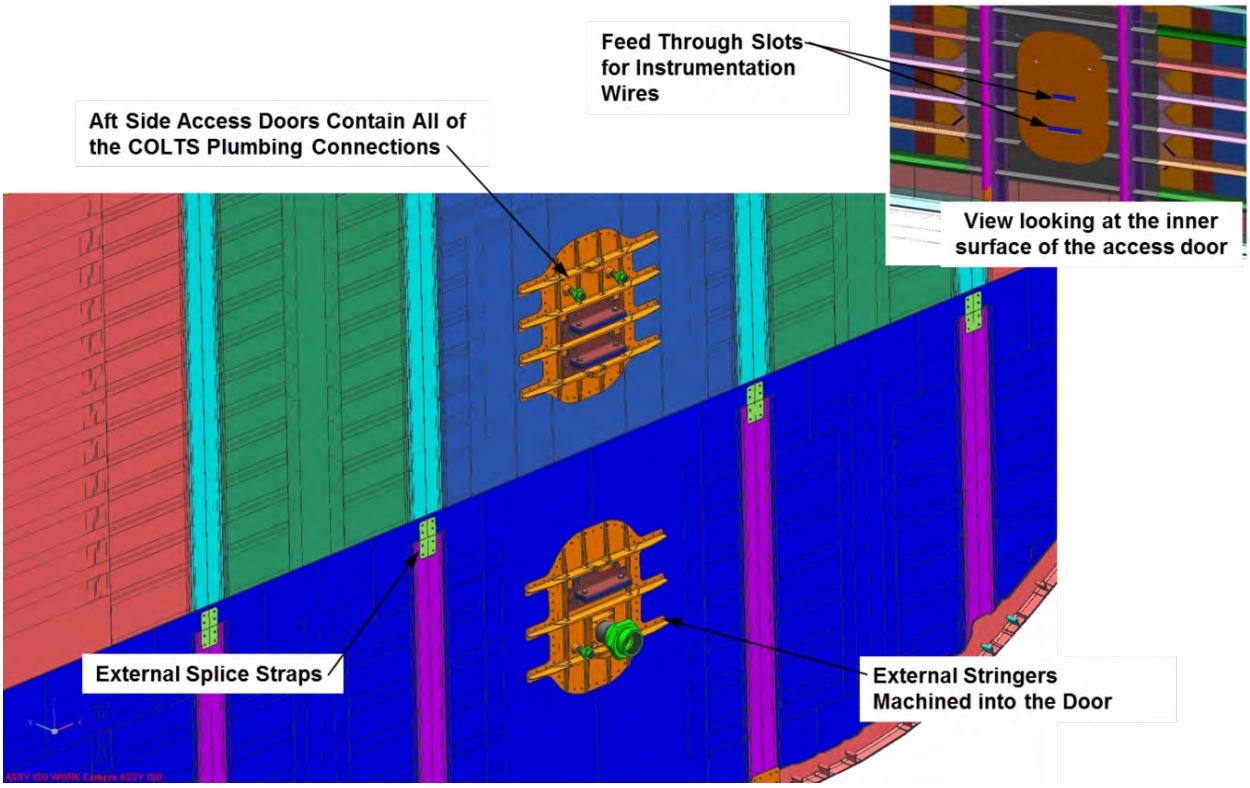

Figure 3-72. Aft Access Covers

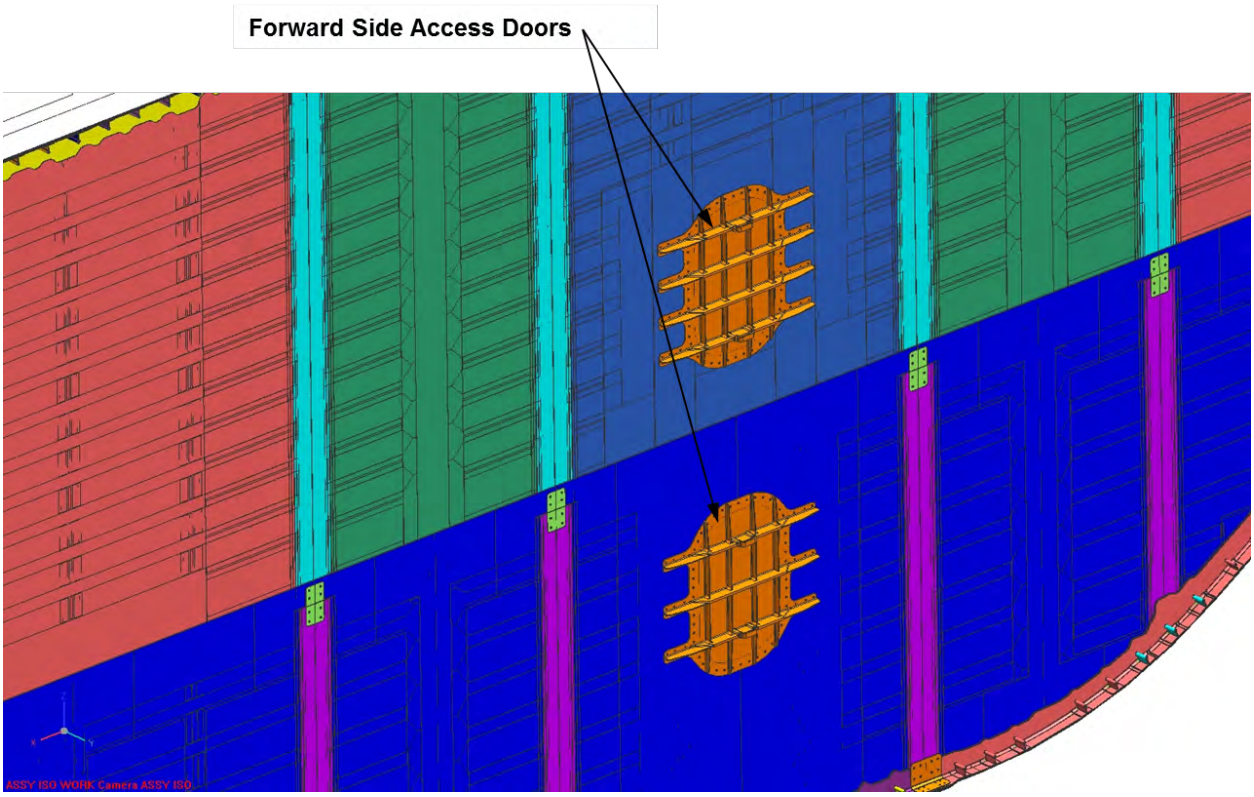

Figure 3-73. Forward Access Doors

The upper and lower center ribs attached to integral T-webs on the adjacent panel (Figure 3-74). Metallic angles were used on the other side of the center ribs to complete the attachment. Initial panel designs incorporated an integral pi member to attach the center ribs. However, to reduce risk on these first-time scale-up panels, the pi joint design was revised to a T-joint and a separate angle that could absorb any tolerance buildup between the mating panels. The bottom of the upper center rib used metallic angles on both sides to attach to the OML (flat side) of the floor to reduce tool complexity for the floor panel. Crown Y-Brace fittings that would be located between the overhead baggage compartments were used to support the crown panel, reducing the unsupported column length. The lower center rib installation was roughly a mirror image at the floor line with gussets at the interface with the side keel panels (Figure 3-74). Keel gusset fittings would be located under the cargo floor and add strength at the curved section of the keel panel. These gusset fittings connected the lower center rib panels to the frames on the side keel panels, and they were required on only one side of the lower center rib panels because the center keel had splice fittings.

Center keel splice fittings shown in Figure 3-75 were located at a stringer location between the two center ribs. They stabilized the frames from rolling/buckling by reducing the effective column length. This low-profile approach was designed as an I-beam section profile for increased stiffness to maximize the height of the center compartment for cargo freight. Because the splice fittings replaced a standard stringer, manufacturing clearances were maximized for assembly. Theses fittings incorporated the skin splice and one frame splice on one end into a single part to reduce part count and assembly time. The frame splice for the other side was a separate detail to allow for some adjustments in the span width between integral frames. OML longitudinal splice straps were used to make a double shear joint because it would have very little effect on the aerodynamic performance of the aircraft. These straps are common in production aircraft and serve to close out joints while limiting interruption to the airflow. The metallic straps enable the use of reduced-height countersunk shear head fasteners to reduce a massive buildup of composite material on the OML. (It is preferable to have countersunk heads in metal rather than in composite due to pull-out issues.) The OML straps have an equivalent weight penalty of only 2.4 lb for both keel splice straps along the entire length of the aircraft.

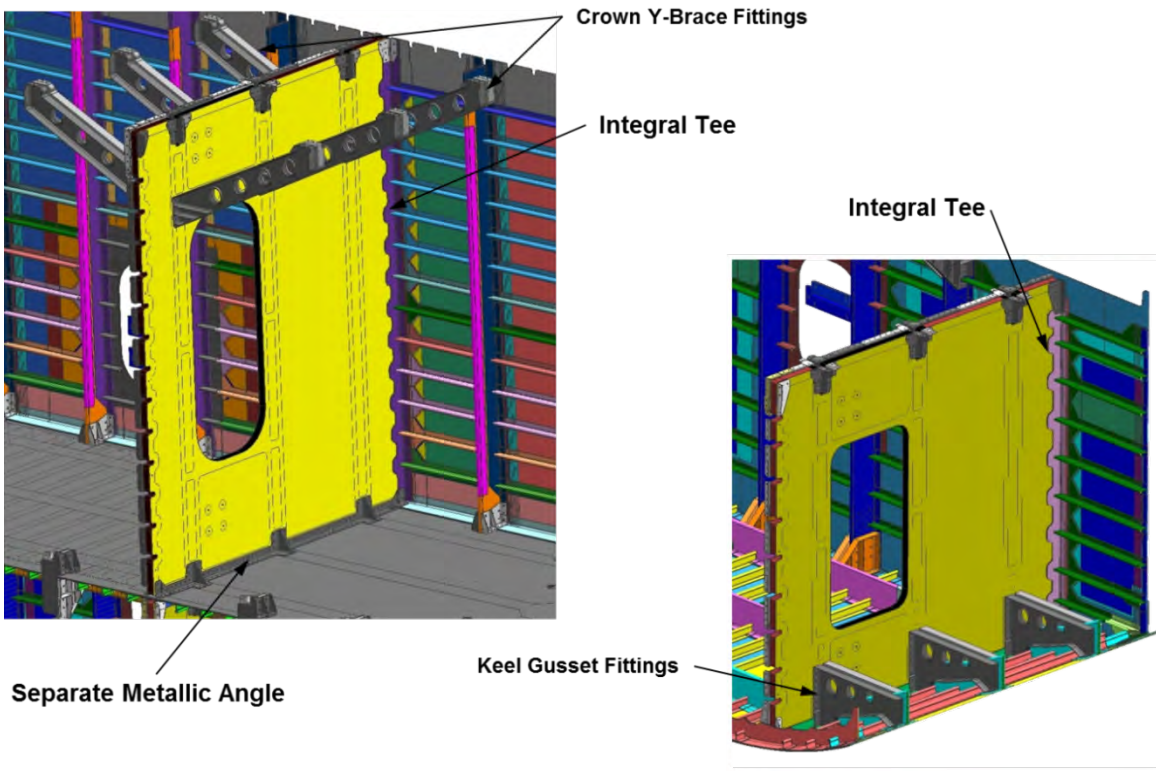

Figure 3-74. Upper and Lower Center Rib Attachment

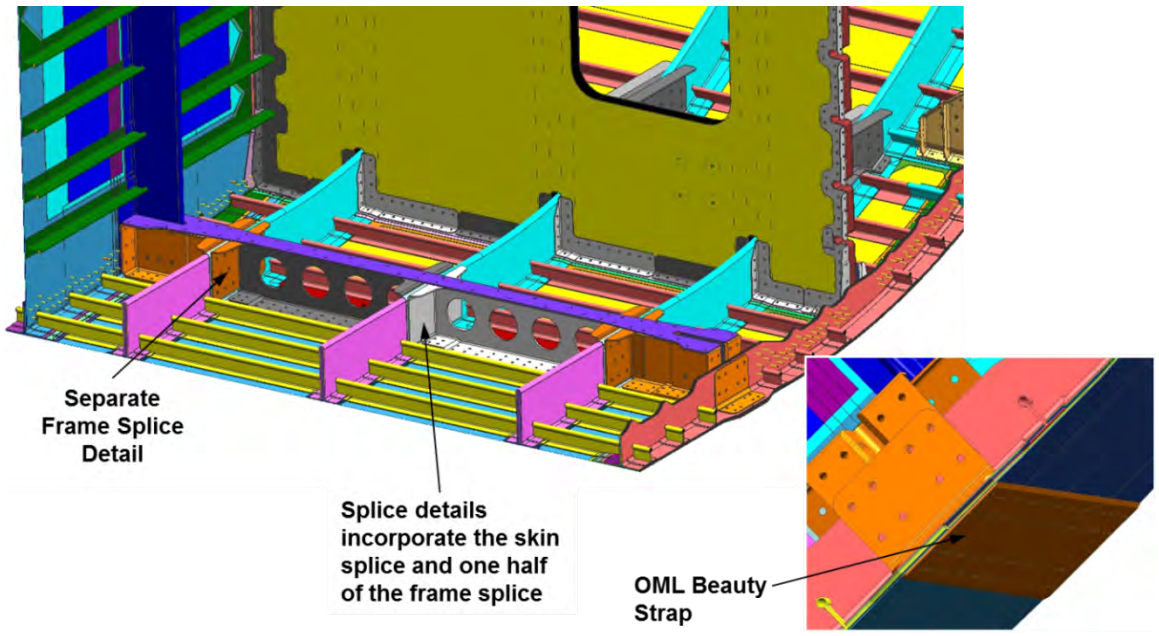

Figure 3-75. Keel Splice Region

3.4.2 Load-Introduction Fittings

As shown in Figure 3-76, four points of contact were created by load-introduction fittings that bolted to the COLTS platens (shown in green) at both ends of the MBB. These fittings attached to the edges of the MBB, with two adaptor fittings attached to each platen. Because the emplacement of the MBB did not afford much clearance, the adaptor fittings had to be designed in such a way that access to the platen bolts was facilitated when the MBB was installed in the COLTS facility.

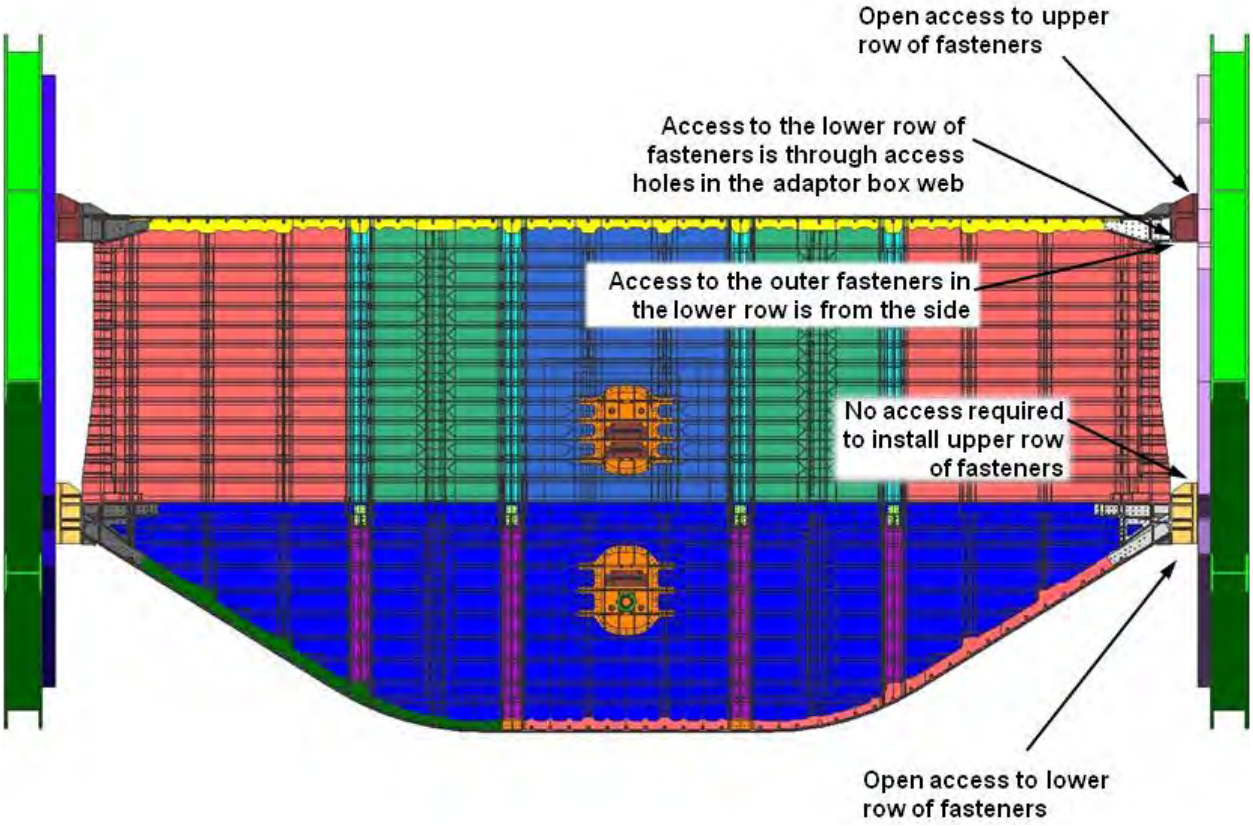

Figure 3-76. Platen Access

Figure 3-77 shows the fittings that transferred load into the upper corner of the MBB. The adapter fitting (ZJ153343) isolated the bolts on the structure from those of the platen. This made it possible to create a symmetric bolt pattern in the MBB that did not interfere with the bolt pattern on the platens.

Figure 3-78 provides detail views of the upper load-introduction fittings at the MBB corner. Key to this design was internal frame fittings (shown in Figure 3-64), which interfaced directly with the exterior load-introduction frame fittings. These, combined with the discontinuous upper shear fittings, served to distribute loading into the frames and skin members. The goal was to distribute the load at the platen interface into the test section without overloading the frames and causing a premature failure outside the test area in the middle of the crown panel.

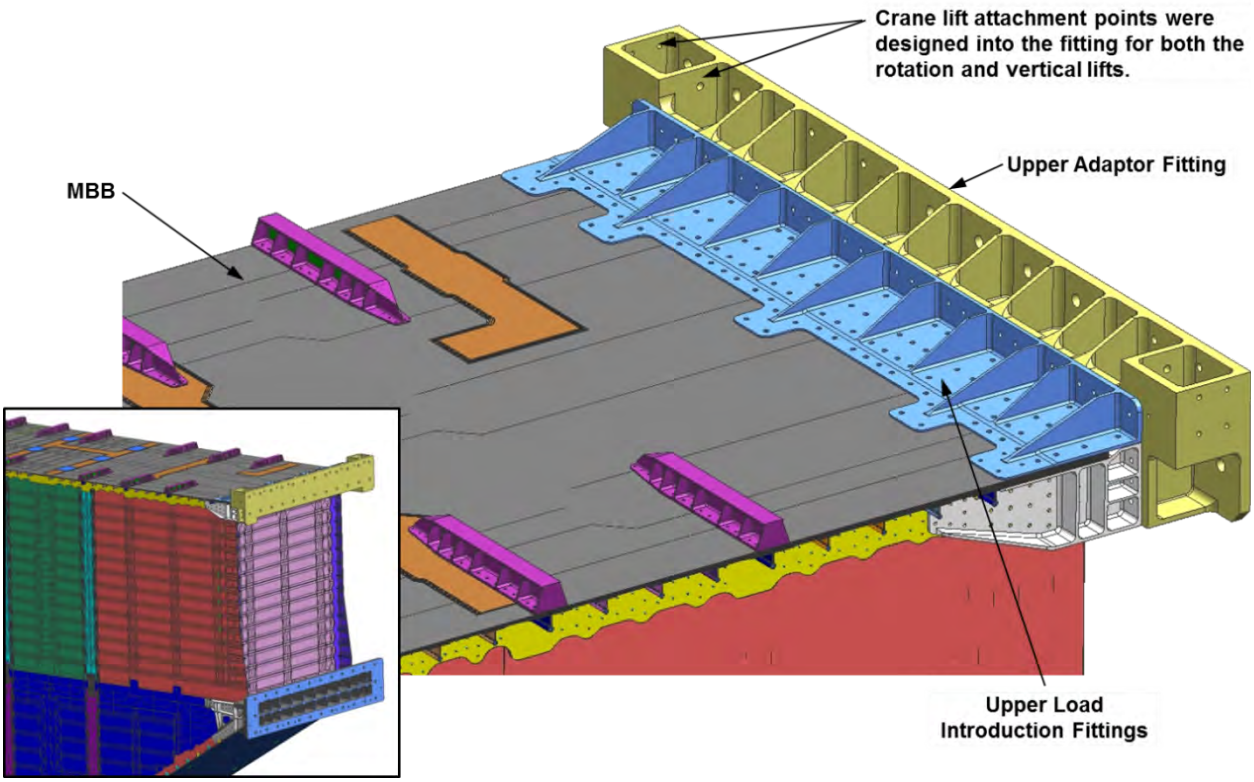

Figure 3-77. Upper Load-Introduction Adaptor Fitting

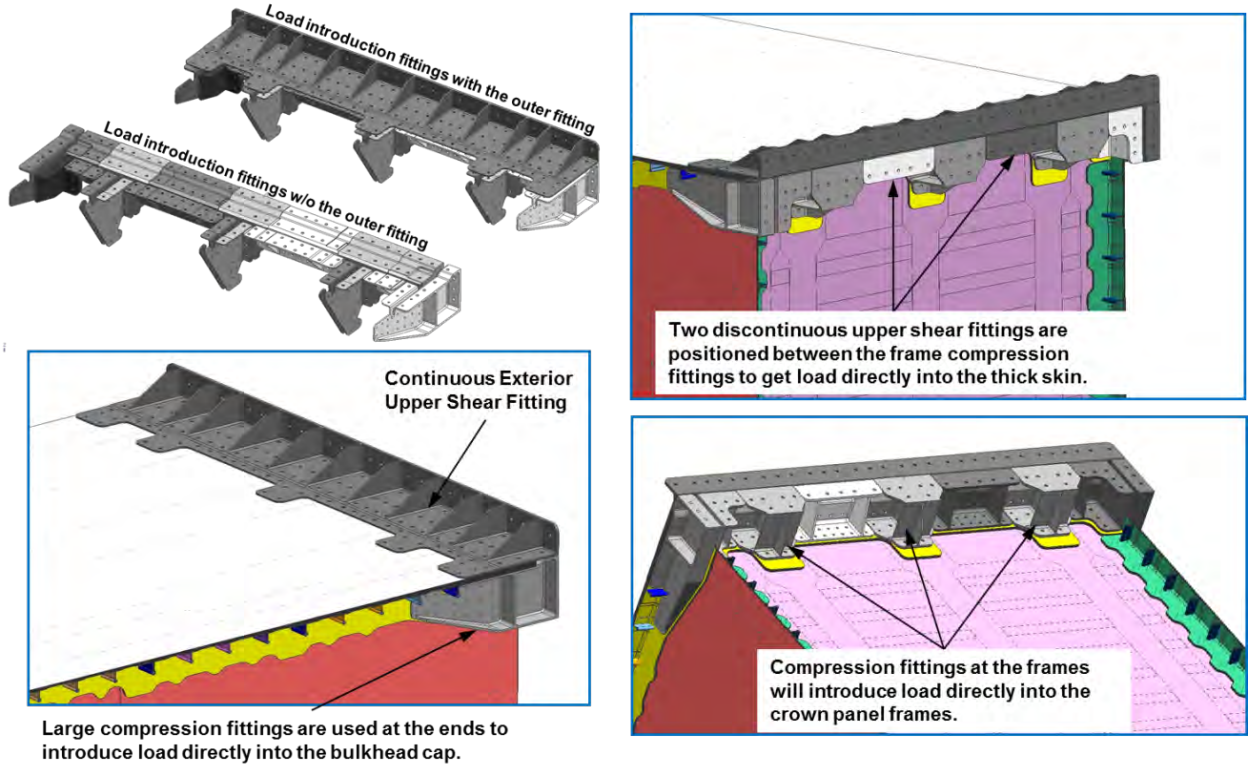

Figure 3-78. Upper Load-Introduction Fittings

Figure 3-79 shows the lower load-introduction and adaptor fittings that transferred load from the platens to the side keel, bulkheads, and the floor panels. The lower load-introduction area was built up with several fittings (Figure 3-80). The bulkhead fittings sheared load from the platens into the upper and lower bulkhead skins. Continuous and discontinuous shear fittings directed loads into the floor and side keel skins. Figure 3-81 shows a sectioned detail view at the floor line of the lower load-introduction fittings. Here, the internal and external frame fittings worked together to get load directly in the floor and side keel frames.

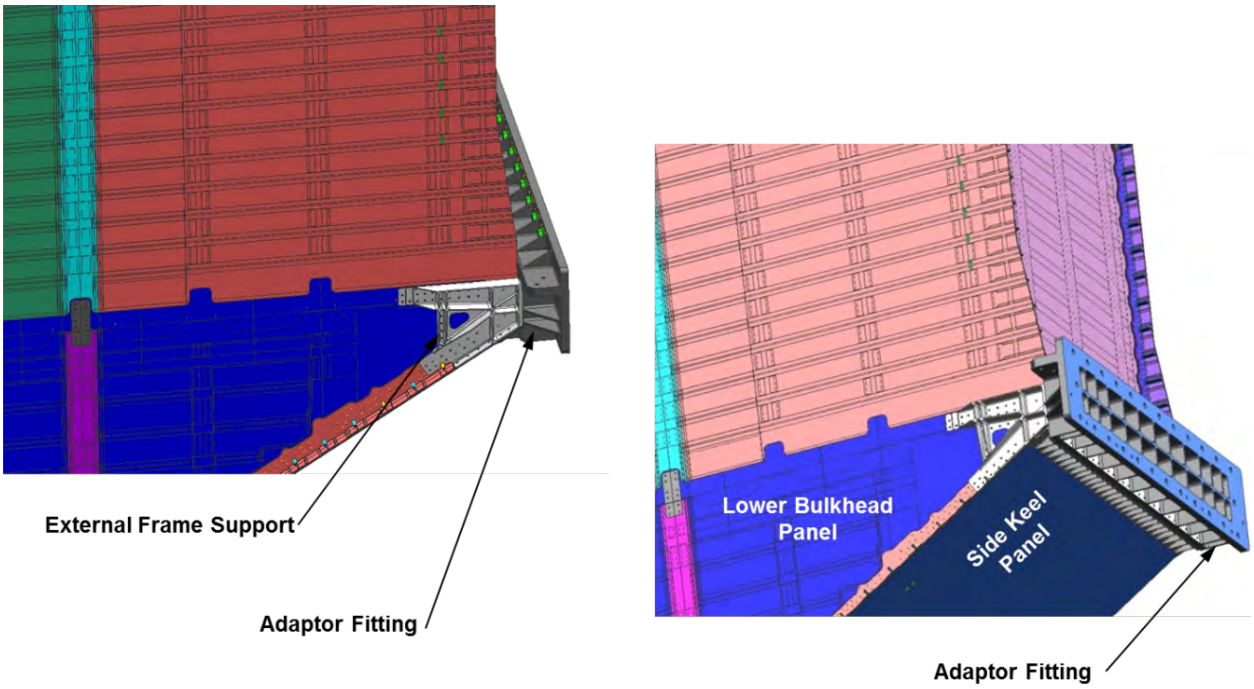

Figure 3-79. Lower Adaptor Fitting

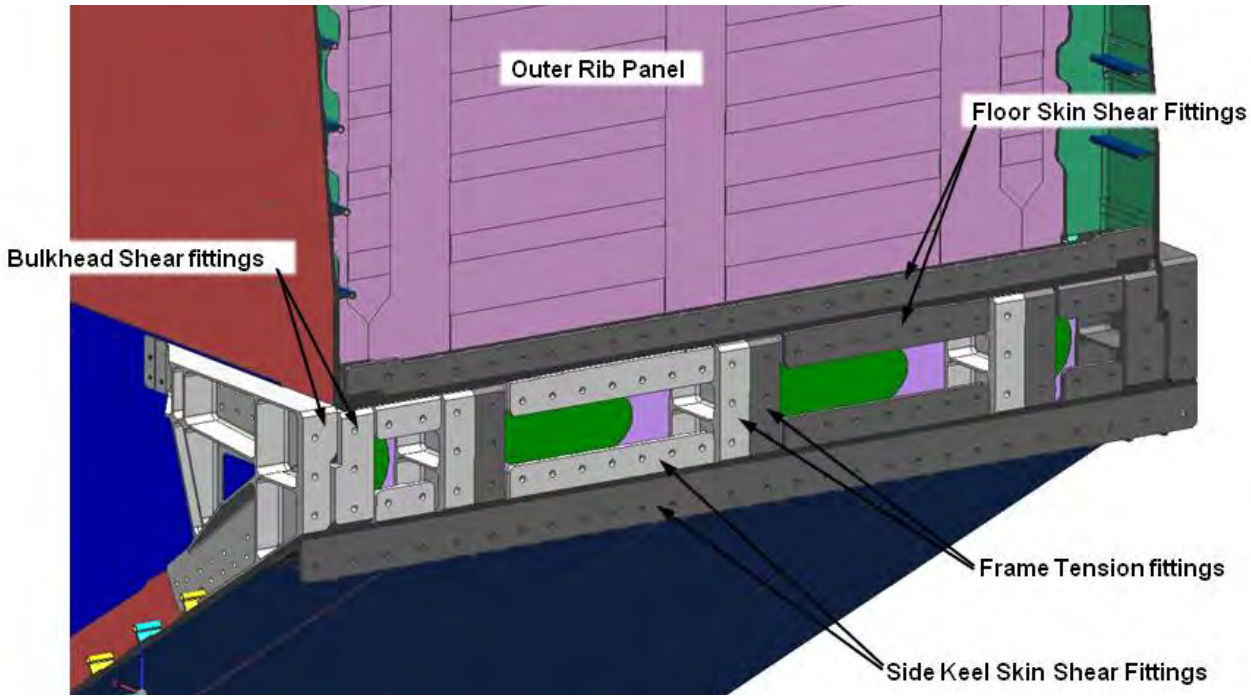

Figure 3-80. Lower Cover Fittings

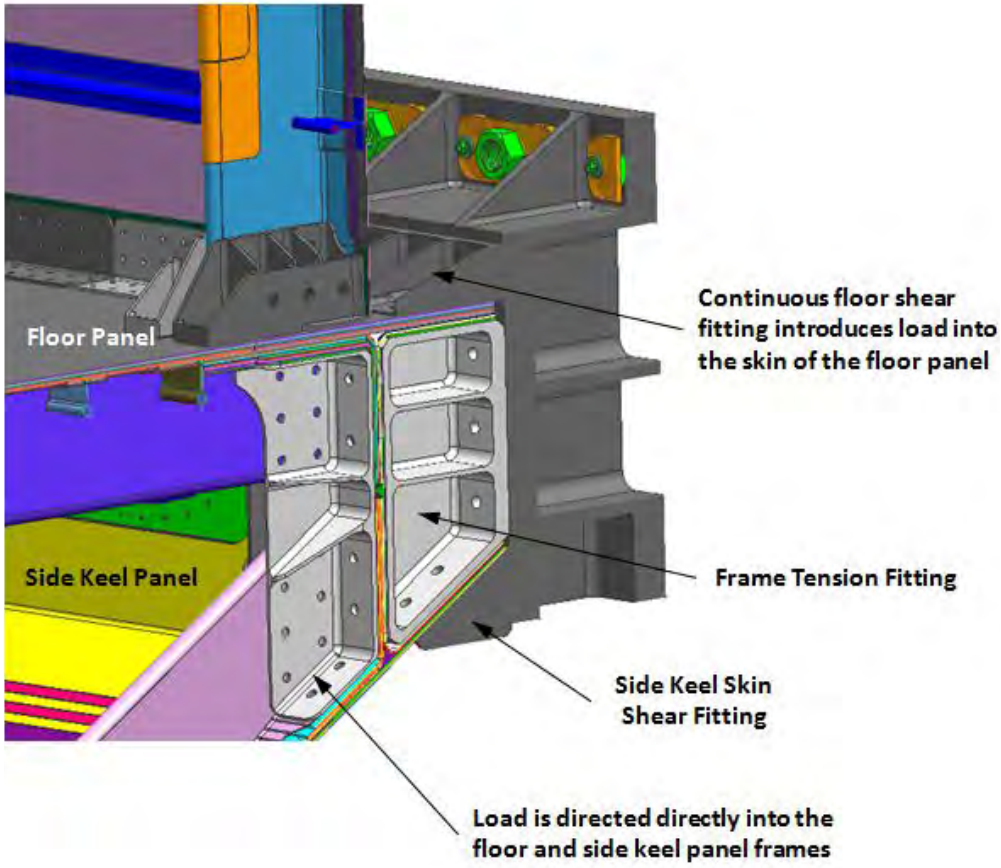

Figure 3-81. Lower Cover Load Introduction at Frame

4.0 STRUCTURAL ANALYSIS

To validate the design of the MBB, strength and stability analyses were performed under the most critical HWB loading conditions. These analyses included creating a global Finite Element Model (FEM) for linear static and linear buckling analyses as well as detailed localized studies. The MBB was designed and sized based on the results obtained from linear analyses only; however, nonlinear analyses were performed later for failure predictions of the tests. Several design and analysis iterations were performed to reach the final design. Positive margins of safety at Design Ultimate Loads (DUL) were derived from the results of linear static analysis of all composite panels, metallic fittings, and fasteners. The goal of the MBB structural analysis was to understand how the MBB would behave under critical loading conditions and make final failure predictions for the testing.

4.1 FEM Development

A global FEM was generated to simulate the structural behavior of the MBB (Figure 4-1). The purpose of this FEM was twofold. Initially, it was used to validate the MBB design according to margins of safety computed from linear static and linear buckling analyses. Later, it was used for test predictions that included nonlinear analyses. The FEM contained enough structural detail and mesh density to calculate internal loads as well as panel stresses and strains in the structure, except at features such as frame keyholes, skin splices, floor venting holes, and T-cap noodles, for which detailed standalone models were created to reduce run time.

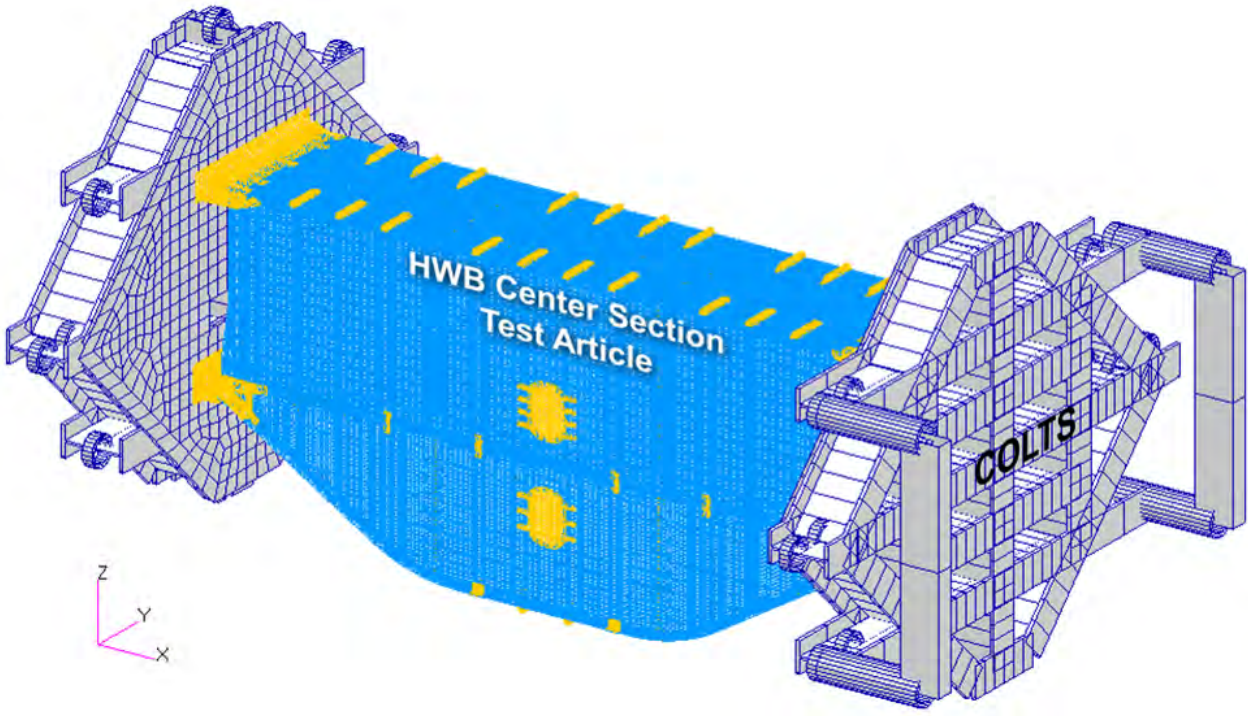

Figure 4-1. Global FEM of the MBB and COLTS Test Fixture

The modeling approach was to use Patran 2008r2 as the pre- and post-processor and MD NASTRAN R3b as the solver for these analyses. The MBB structural weight was assumed to be negligible compared to the test loads, although completing an assessment with the weight was considered. The Finite Element (FE) size used was approximately 1 in. throughout the global model to maintain a mesh size fine enough for the detailed regions. While running the global model to identify critical regions, additional detailed analyses would be added to the plan to ensure that these regions would not fail.

The global FEM comprised 15 composite panels (crown, floor, two upper bulkheads, two lower bulkheads, two outer ribs, two side keels, center keel, and four center rib panels), aluminum fittings and access doors, and titanium bolts. One-dimensional (1D) bar elements were used in modeling the "stringer bulbs," which contained the pultruded rod and the fabric plies that wrapped around the rod. Two-dimensional (2D) shell elements were used in modeling skins, stringer flanges and webs, T-caps, frame webs, and aluminum fittings. 1D bar elements, with cross-section area properly calculated, were used at the frame cap locations to simulate frame cap stiffness. Titanium fasteners were modeled by special NASTRAN fastener connector elements. There were 745,635 nodes, 744,594 elements, and 18,967 fastener connector elements in the global FEM.

More than one fastener connector element was needed when fastener connector elements were used to join more than two plates together. That is why the number of fastener connector elements was significantly higher than the actual number of bolts used in the MBB assembly (by nearly double). Details of each panel's global model are shown in Figure 4-2 through Figure 4-7, and the FEM of the COLTS fixture is shown in Figure 4-8. The fittings are shown in Figure 4-9, and the fastener elements are shown in Figure 4-10. Finally, the COLTS structure was modeled for appropriate load-introduction and boundary conditions, as shown in Figure 4-11.

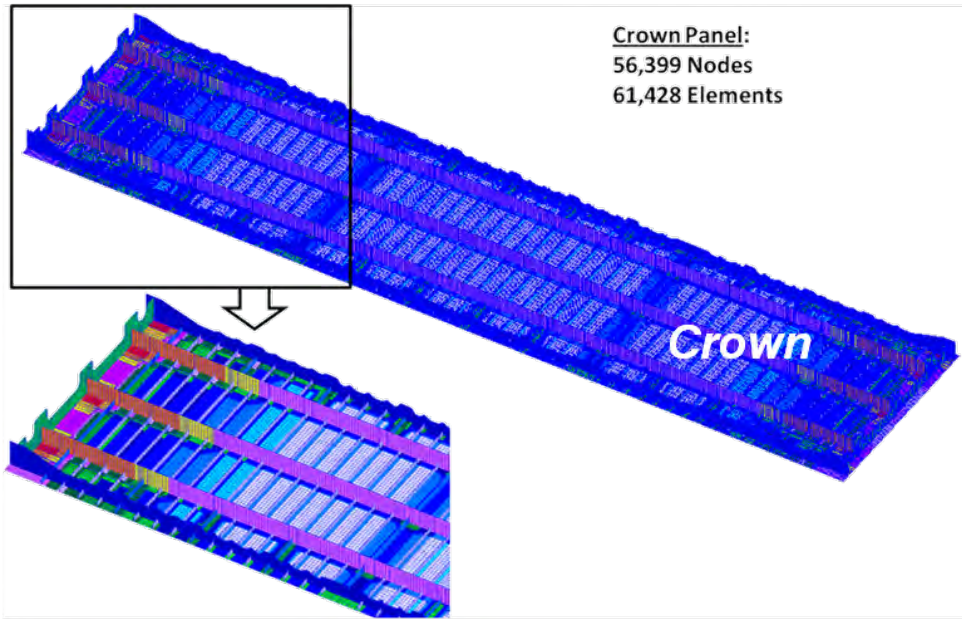

Figure 4-2. Crown Panel FEM Consisted of 56,399 Nodes and 61,428 Elements

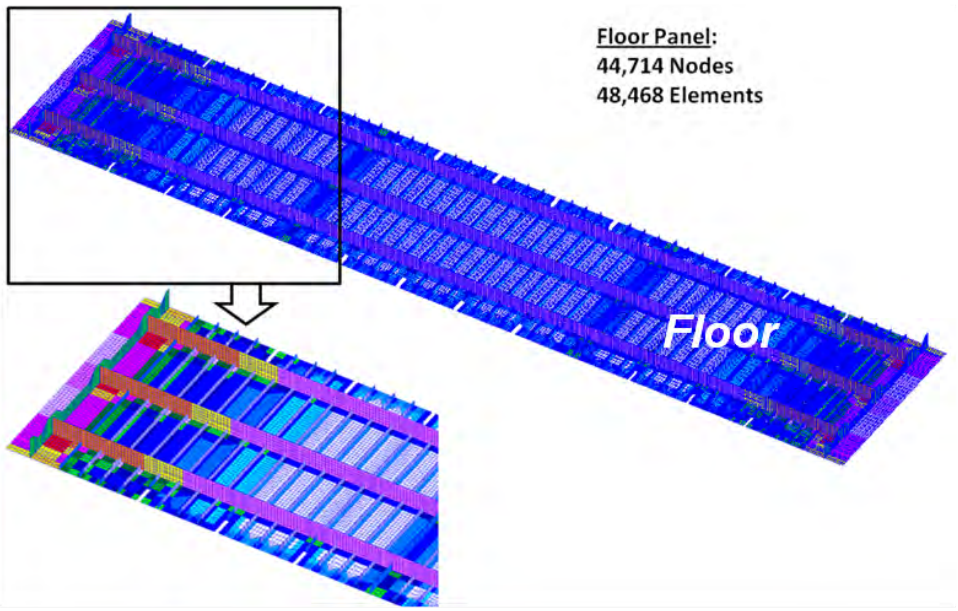

Figure 4-3. Floor Panel FEM Consisted of 44,714 Nodes and 48,468 Elements

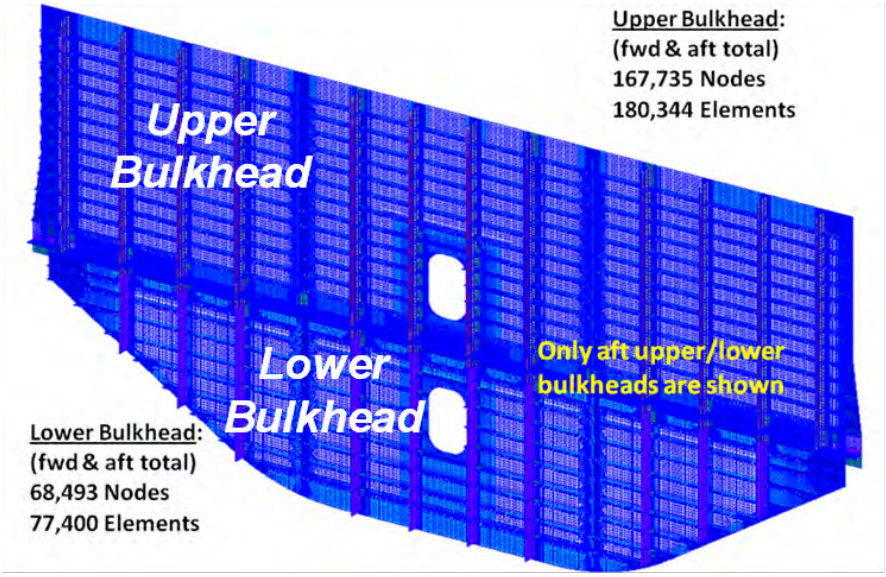

Figure 4-4. Bulkhead Panel FEMs Consisted of 136,228 Nodes and 257,744 Elements

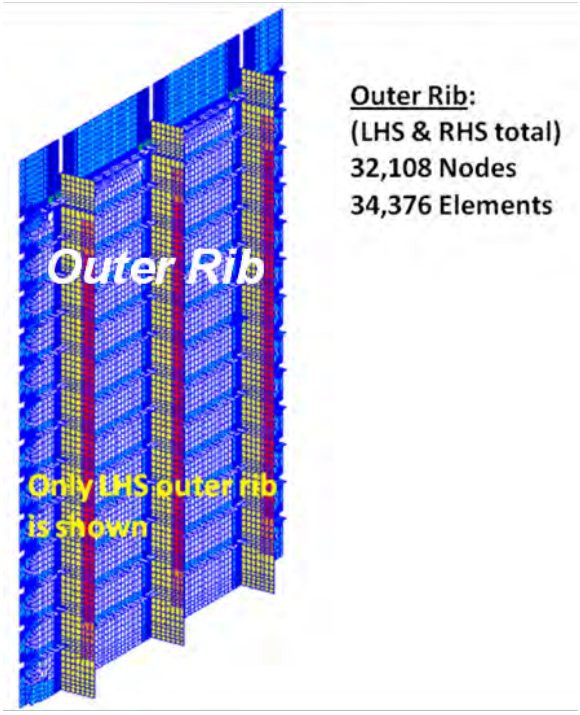

Figure 4-5. Outer Rib Panel FEMs Consisted of 32,108 Nodes and 34,376 Elements

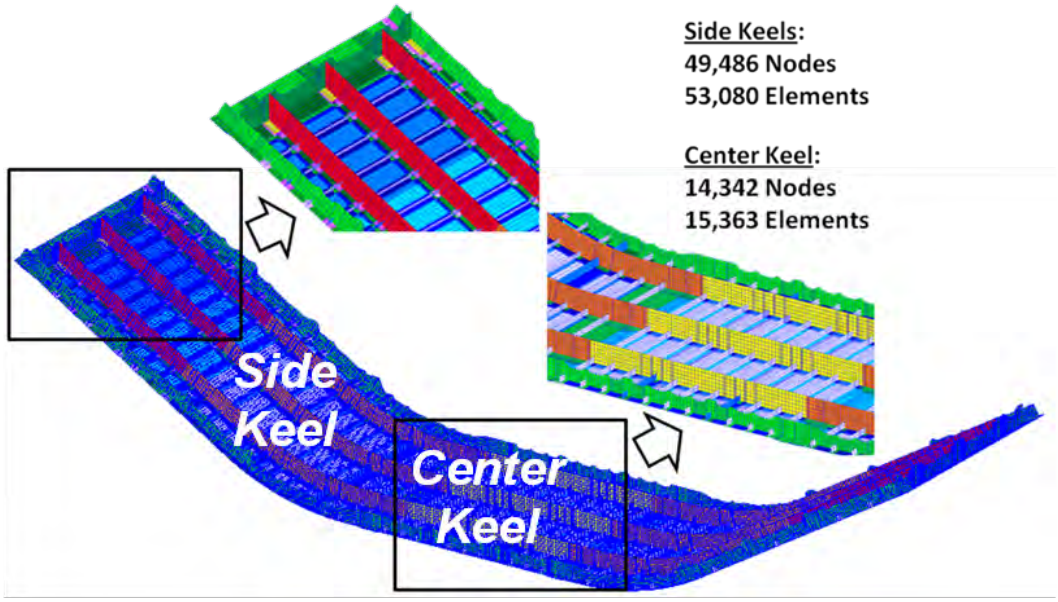

Figure 4-6. Keel Panel FEMs Consisted of 63,828 Nodes and 68,443 Elements

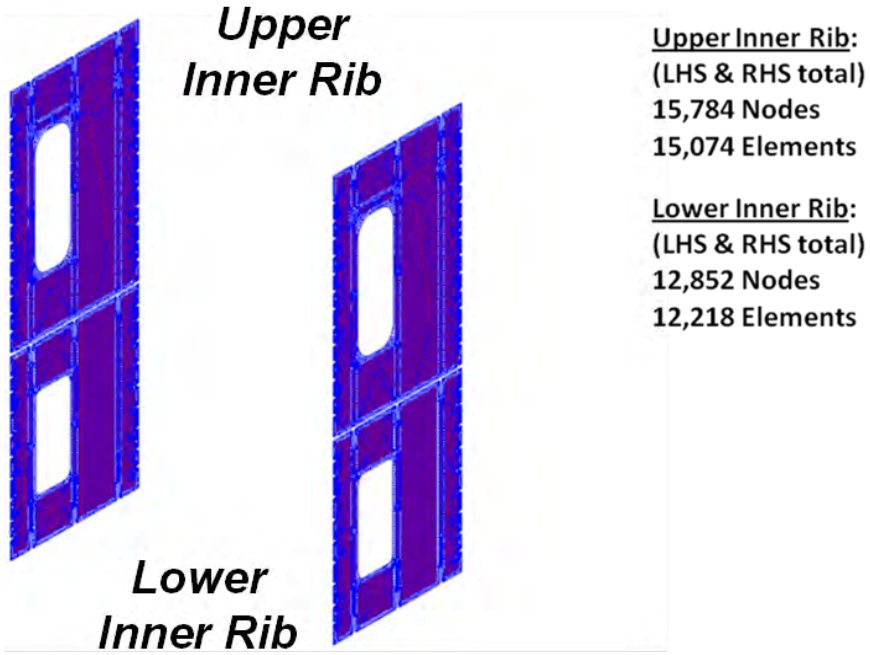

Figure 4-7. Center Rib Panel FEMs Consisted of 28,636 Nodes and 27,292 Elements

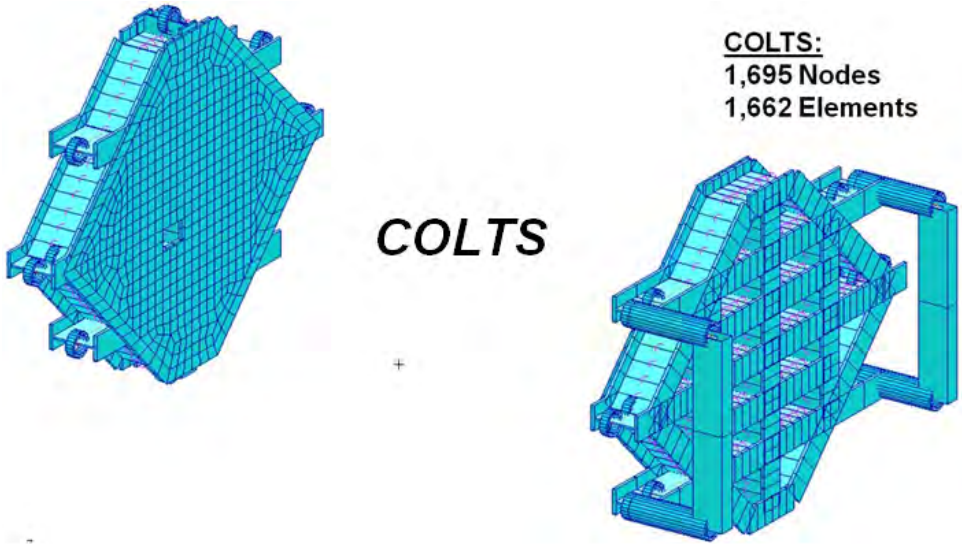

Figure 4-8. COLTS Test Fixture Consisted of 1,695 Nodes and 1,662 Elements

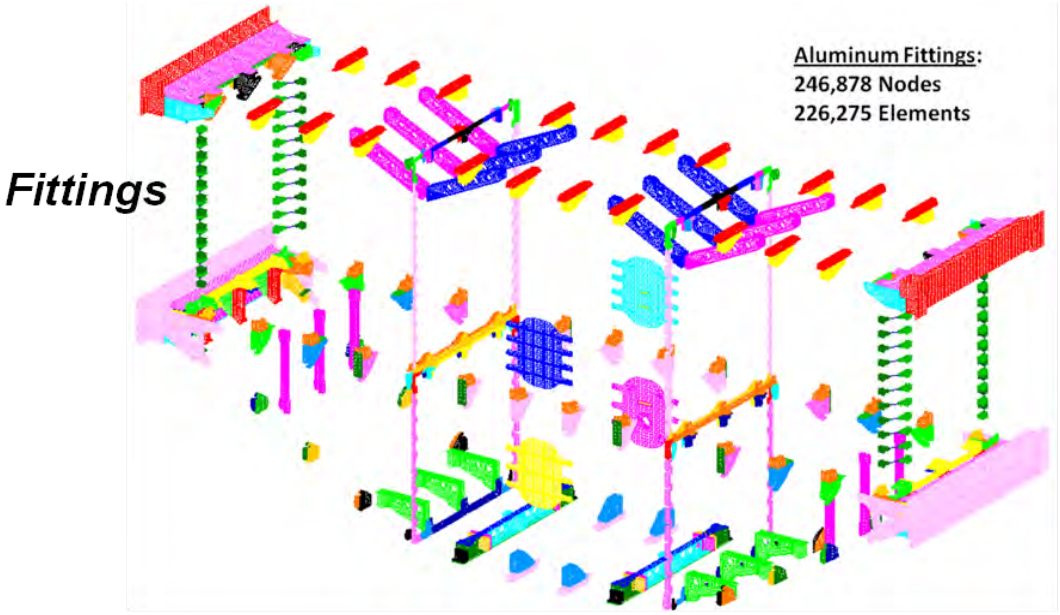

Figure 4-9. Aluminum Fitting FEMs Consisted of 246,878 Nodes and 226,275 Elements

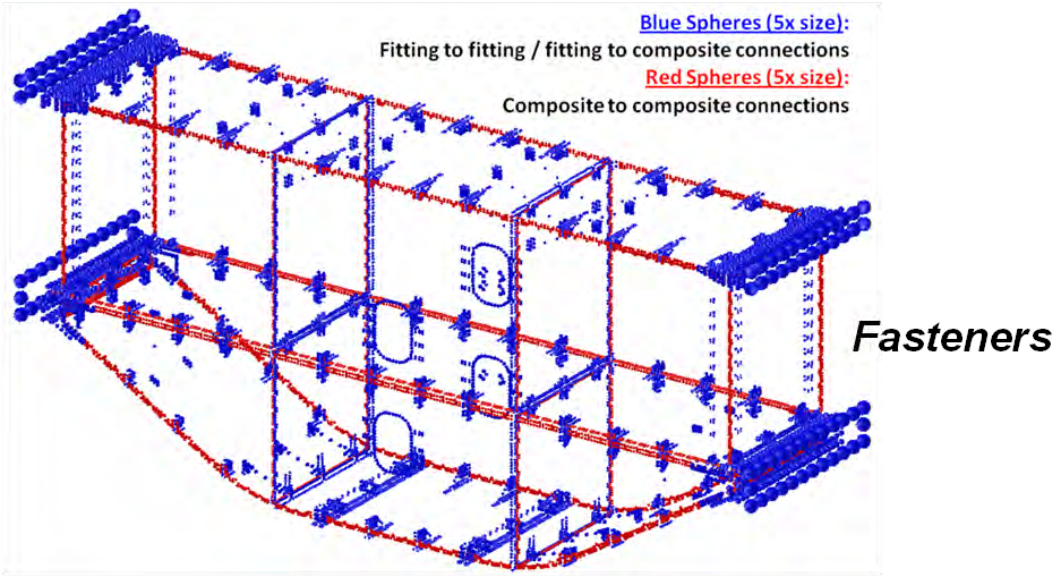

Figure 4-10. Fastener Elements Were Shown Either Connecting Fittings to Fittings, Fittings to Composite, or Composite to Composite

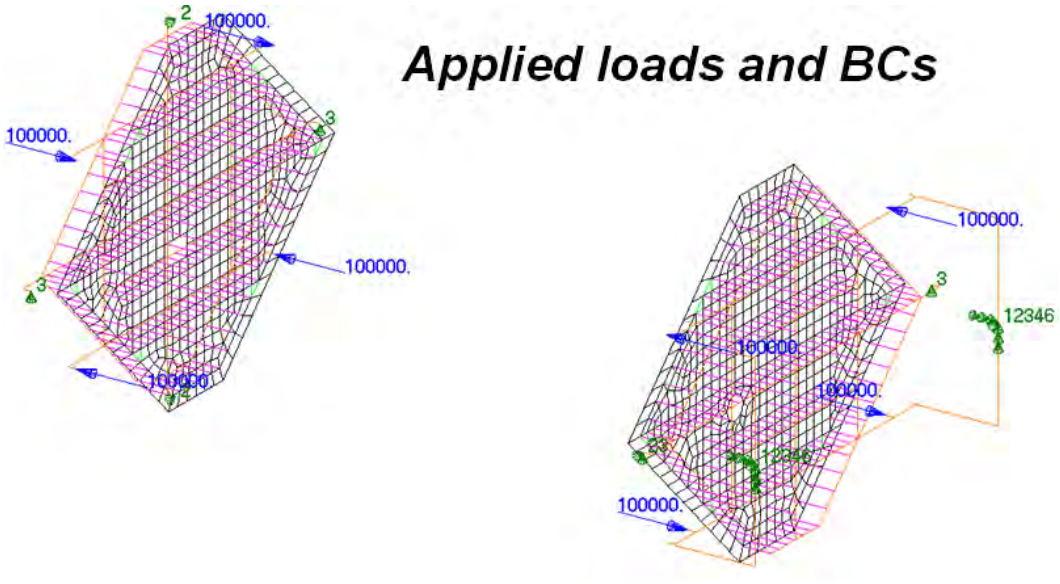

Figure 4-11. Applied Loads and Boundary Conditions on the COLTS Test Fixture

Properties of the composite material (DMS 2436, Type 1, Class 72, Grade A) used for skins, stringers, T-section caps, and frames are listed in Table 4-1. These values were derived by averaging the tensile and compressive laminate stiffness values of DMS 2436 T1C72 material properties used in Advanced Subsonic Technology (AST) composite wing and BWB studies. The properties were derived from Boeing in-house test data (Refs. 4-1, 4-2). Even though the composite parts of the MBB were mainly made of DMS 2436 T1C72, different allowable values were used at different locations based on their Tension After Impact (TAI), Compression After Impact (CAI), Barely Visible Impact Damage (BVID), repair, and other failure criteria. (The allowable values are documented in Section 4.2.8.)

Table 4-1. Composite Material Properties of DMS 2436 T1C72 Grade A

DMS 2436, Type 1, Class 72, Grade A				
E11 (psi)	**E22 (psi)**	**ν12**	**G12 (psi)**	**Density (lb/in^3)**
9,740,000	4,865,000	0.4	2,370,000	0.057

Other composite materials (DMS 2436, Type 1, Class 75/76/77/78, Grade A) were used for skin splices on the bulkhead and curved frames on the side keel. The properties of these composite materials (DMS 2436, Type 1, Class 75/76/77/78, Grade A) are listed in Table 4-2. Values listed in the table were calculated by averaging the tensile and compressive laminate stiffness values of DMS 2436 T1C75/C76/C77/C78 derived from Boeing in-house test data (Ref. 4-3).

Table 4-2. Composite Material Properties of DMS 2436 T1C75/76/77/78 Grade A

DMS 2436 Type 1 Grade A	E11 (psi)	E22 (psi)	**ν12**	G12 (psi)	Density (lb/in^3)
Class 75	1,804,500	1,804,500	0.8045	4,170,000	0.057
Class 76	8,760,000	8,760,000	0.05	500,000	0.057
Class 77	8,760,000	8,760,000	0.05	500,000	0.057
Class 78	1,804,500	1,804,500	0.8045	4,170,000	0.057

Frame cores were made of either fiberglass (Garolite, Grade G-11) or foam (DMS 2278 Class 4, Rohacell WF-110) materials. These fiberglass and foam cores were wrapped with two stacks of composite material. Fiberglass core was used (instead of foam core) where fasteners bolted through the frame. Foam core was considered to be either flyaway structure (removed from the buckling analysis) or a structural part (kept in the buckling analysis). For HWB structure, the foam was considered to be a structural member for critical cases other than 2P. Material properties of the fiberglass and foam materials were derived from the BWB study (Ref. 4-2) and are listed in Table 4-3. The material properties of stringer rods (Toray Uni T800/3900-2B fiber/resin system) were also derived from the BWB study (Ref. 4-2) and are listed in Table 4-3. Material properties of stringer rods were derived by averaging the tensile and compressive axial stiffness values of the unidirectional rod material properties.

Table 4-3. Fiberglass and Foam for Frame Core, and Stringer Rod Material Properties

Isotropic Material	Material Name	E (psi)	ν	G (psi)	Density (lb/in^3)
Fiberglass	Garolite, Grade G-11	1,700,000	0.3	-	0.069
Foam	DMS 2278 class 4 Rohacell WF-110	18,820	-	7,250	0.004
Stringer Rod	Toray Uni T800/3900-2B	20,100,000	0.3	-	0.057

The upper and lower inner ribs were composite sandwich structures with facesheets made of woven composite fabric (BMS 8-276 Class 2A, Style 6K-70-PW, Form 1) and the core made of Hexcel Hexagonal Honeycomb HRH-10, with a cell size of 0.125 in and 5.0 pcf density (HRH-10-1/8-5.0). The properties of the composite material (BMS 8-276, Class 2A, Style 6K-70-PW, Form 1) are listed in Table 4-4 and the properties of the honeycomb core (HRH-10-1/8-5.0) are listed in Table 5.

Table 4-4. BMS 8-276 Class 2A, Style 6K-70-PW, Form 1 Material Properties

BMS 8-276, Class 2A, Style, 6K-70-PW, Form 1				
E11 (psi)	**E22 (psi)**	**ν12**	**G12 (psi)**	**Density (lb/in^3)**
8,000,000	8,000,000	0.3	2,000,000	0.057

Table 5. Honeycomb Core HRH-10-1/8-5.0 Material Properties

Honeycomb Core HRH-10-1/8-5.0						
E11 (psi)	**E22 (psi)**	**Ecc (psi)**	**G12 (psi)**	**$G_{L\text{-}Dir}$ (psi)**	**$G_{W\text{-}Dir}$ (psi)**	**Density (lb/in^3)**
100	100	37,000	100	10,200	5,400	0.0029

Metallic fittings were made of 2219-T851, 7050-T7451, 7075-T6, and 7075-T651 aluminum alloys. These aluminum alloys have the same elastic moduli and density, and their properties are listed in Table 4-6. Fasters were made of titanium with the exception that some were made of Inconel where high strength was needed. The material properties of these fasteners are also listed in Table 4-6.

Table 4-6. Aluminum Alloy Material Properties

Isotropic Material	E (psi)	ν	Density (lb/in^3)
Aluminum Fitting	10,300,000	0.33	0.101
Titanium Fastener	19,900,000	0.31	0.160
Inconel Fastener	29,400,000	0.29	0.304

4.2 Model Checkout and Results

To ensure the integrity of the global FEM and accuracy of analysis results, assessments and result investigations of the FEM were performed before the Critical Design Review (CDR). Several critical load cases were identified for the analyses, and the first case for model checkout was the 2P pressure condition. A check of the model under 2P showed reasonable displacement (Figure 4-12). The f06 result file from NASTRAN analysis was also checked, showing the epsilon value (a measure of numerical accuracy and round-off error) to be less than 1.E-10, indicating that the model was numerically stable and running properly.

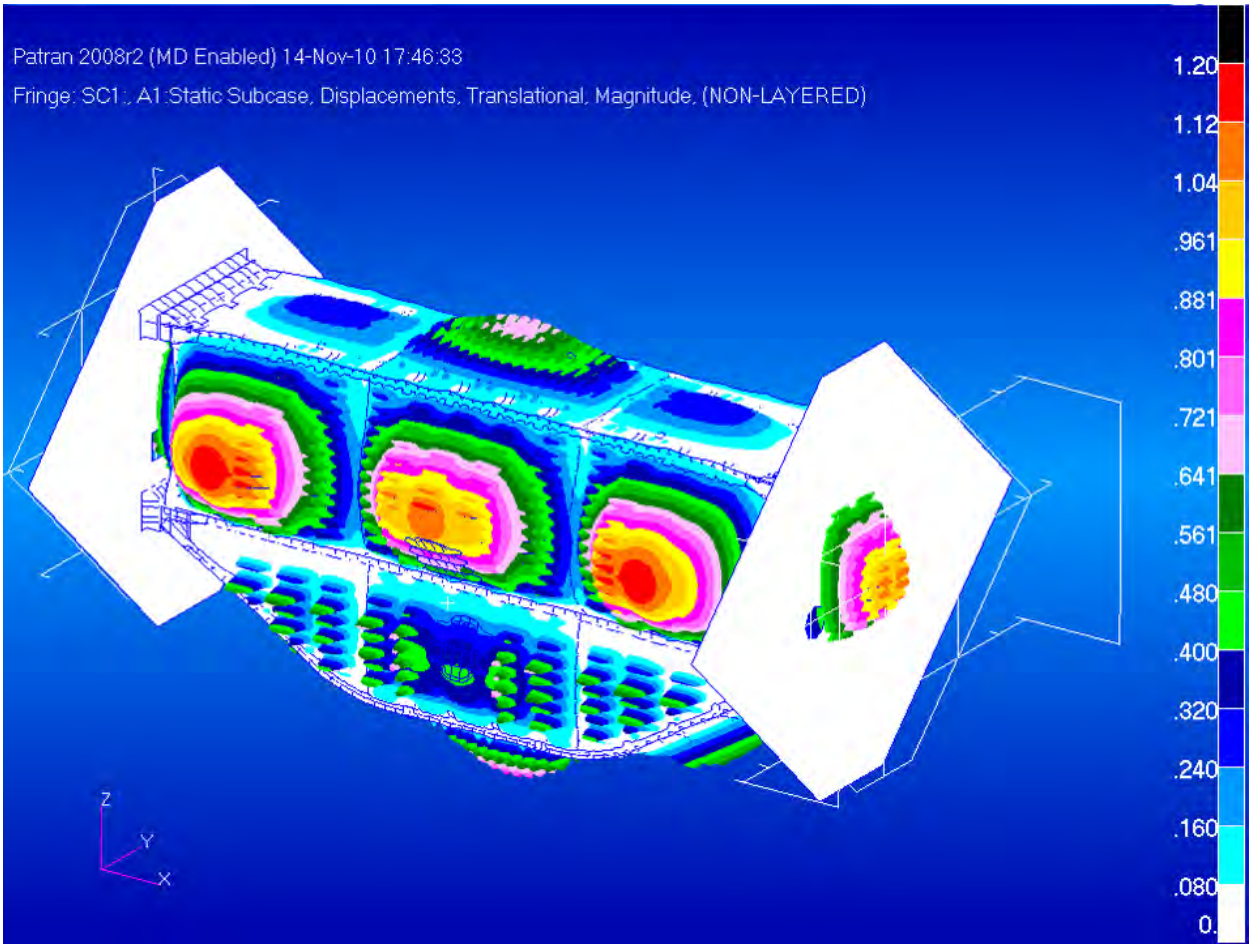

Figure 4-12. Initial Model Checkout of 2P Condition Showed Reasonable Displacement

After the CDR, iterations between analysis and design efforts continued to improve the model and design, and to eliminate negative margins on composite panels, fittings, and fasteners. During these iterative processes, the global FEM was continually modified to incorporate design changes to the structures. At the end of design revision/change efforts, positive margins of safety were shown for all structures. Assessments and result investigations for the final version of the global FEM were performed again and showed that structural integrity and result accuracy were maintained with all post-CDR modifications to the global FEM.

4.2.1 Load Cases Run

Load cases for the MBB analysis were determined by the optimization and sizing performed under contract NNL07AA48C (Refs. 2-1, 2-2). Of the 14 load cases used in the vehicle sizing trades, the most critical five were used in this study. These cases were the 2P pressure condition, the 2.5-g and -1.0-g maneuver conditions, and the 2.5-g + 1P and -1.0-g + 1P combined loading conditions. Among the five, the 2.5-g load case was shown to be critical on the upper cover of the aft end of the HWB, whereas the -1.0-g load case was critical on the lower cover of the aft end, where the wing bending loads are introduced into the fuselage. The 2P pressure condition was critical for the forward section of the HWB. Demonstrating the effects of the combined loading conditions was of particular interest because high stresses were expected on the metallic fittings joining composite panels together. The 2.5-g load case was used to determine the applied running load and the maximum load through the frame, as shown in Figure 4-13. The HWB design ultimate load was 80,000 lb per frame based on the calculation of the 2.5-g load case. Each of these load cases was assessed to determine the critical load case and the final test sequence.

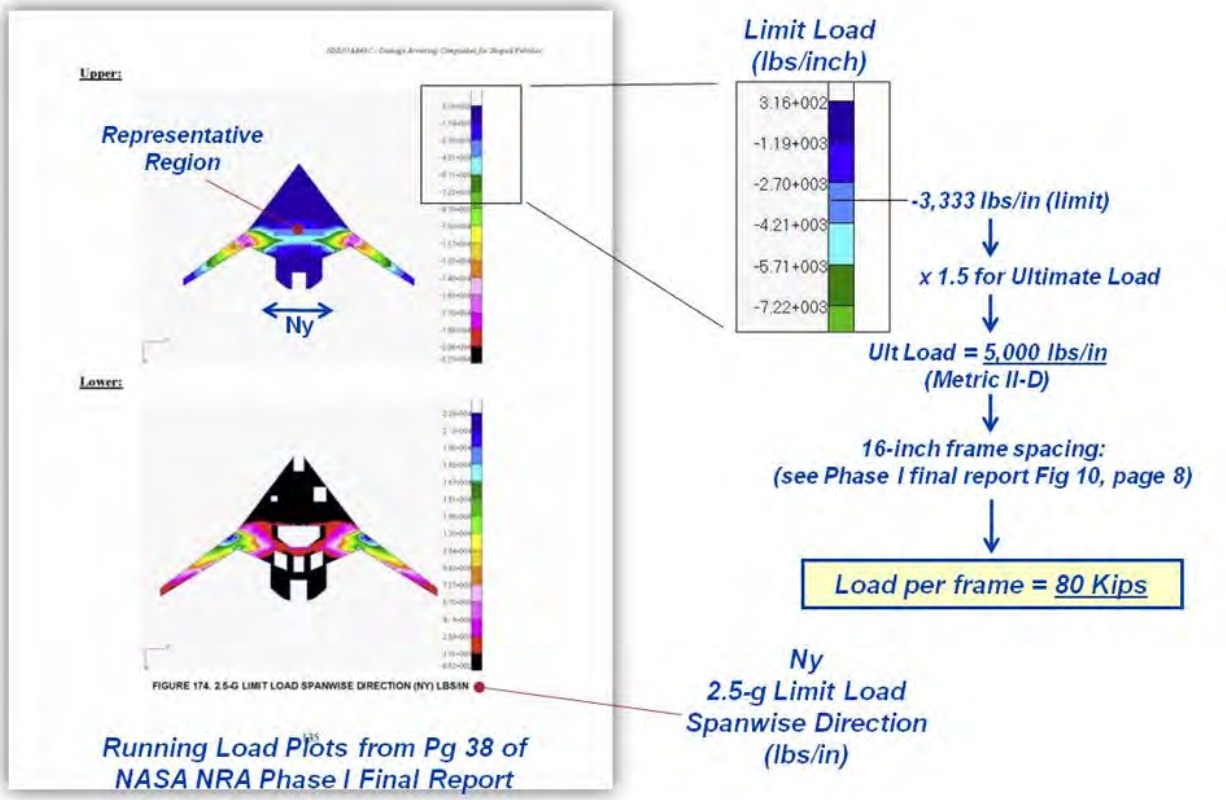

Figure 4-13. HWB Design Ultimate Running Load Calculation Was Based on 2.5-g Load Case

Results of the five critical cases showed that, in general, the most critical cases were those with pressure in the MBB. The 2P pressure condition had the highest strain values and appeared to be the most critical case for the MBB, especially at the interfaces between composite panels. This was because the upper and lower bulkhead panels were joined perpendicularly with crown, floor, keel, and rib panels by fasteners and metallic fittings. The MBB relied on these joints to maintain its structural integrity. Analysis showed that the perpendicularly joined MBB design

was not the most efficient way for a structure to withstand 2P internal pressure. To ensure that the perpendicularly joined MBB would work, stronger and heavier structures were needed at the panel joints, causing weight penalties for the HWB vehicle design. Due to the large size of the MBB, in addition to the five load cases, a static case with the gravitational weight of the MBB was also studied, representing the MBB mounted in the COLTS fixture. This weight-check case was not expected to be critical and should not have caused any high stresses on the MBB. The results from the 1.0-g weight-check confirmed that the internal load, stress, and strain values were negligible compared to those from the five load cases. Therefore, the effects of gravity on the MBB were omitted from the study of the five load cases. The maximum and minimum principal strains of composites were calculated and compared with the strain design values for margin-of-safety calculations. Positive margins were derived on all composite materials of the MBB in all five critical cases. Detailed margins of safety for the composite materials are summarized in Section 4.2.9.

4.2.2 2P Pressure Condition

The 2P pressure condition was a DUL condition. In this condition, a pressure of 18.4 psi was applied to the interior surfaces of the MBB. The resulting displacements are shown in Figure 4-14, and the maximum displacement was 1.08 in. at the center of the forward upper bulkhead.

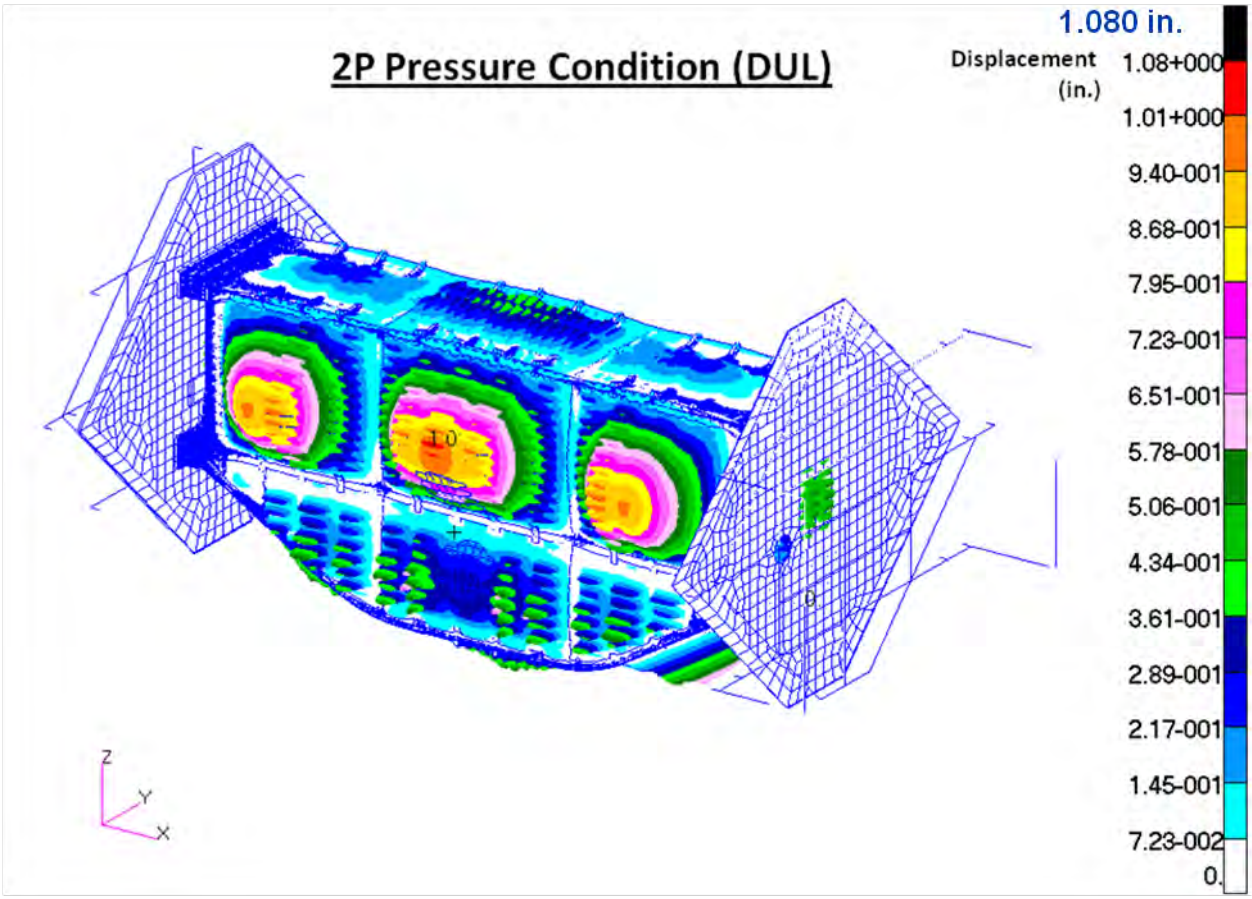

Figure 4-14. Displacements in 2P Condition

The calculated maximum and minimum principal strains are shown in Figure 4-15 through Figure 4-18. The design values of composite skins and composite stringer/frame/T-cap webs were different, and they are described in detail in Section 4.2.8. Therefore, for easier comparisons with their design values, strains for composite skins and strains for composite stringer/frame/T-cap webs are shown in different figures. For the composite skins, the maximum principal strains are shown in Figure 4-15, and the minimum principal strains are shown in Figure 4-16. For the composite stringer/frame/T-cap webs, the maximum principal strains are shown in Figure 4-17, and the minimum principal strains are shown in Figure 4-18.

In addition to plotting the strains of composite skins and the composite stringer/frame/T-cap webs separately, in Figure 4-15 through Figure 4-18, separate plots are shown (in the same figure) for areas that were not influenced (or only slightly influenced) by contact between composite skins and external fittings due to internal pressure in the MBB, and for areas that were heavily influenced by contact. Strains in the areas that were heavily influenced by contact were calculated by modifying the global FEM with locally refined meshes and by modeling contacts between composite skins and fittings. Analysis of this modified global FEM would provide more accurate results for the design cases that included pressure loads.

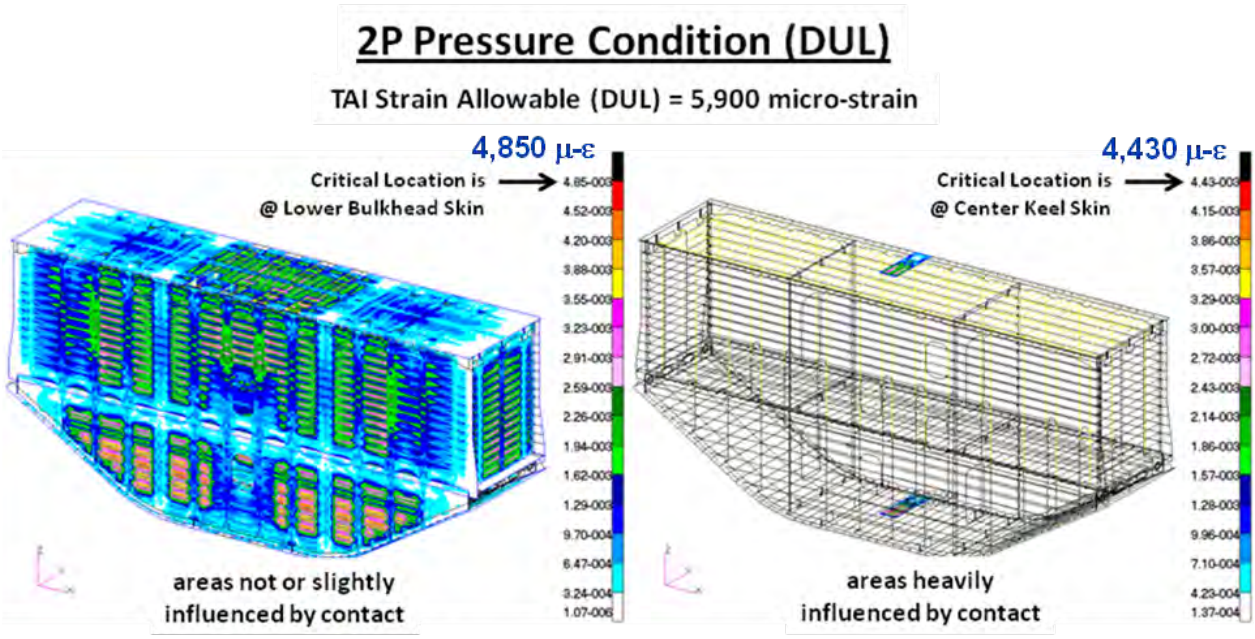

Figure 4-15. Maximum Principal Strains on Composite Skins in 2P Condition

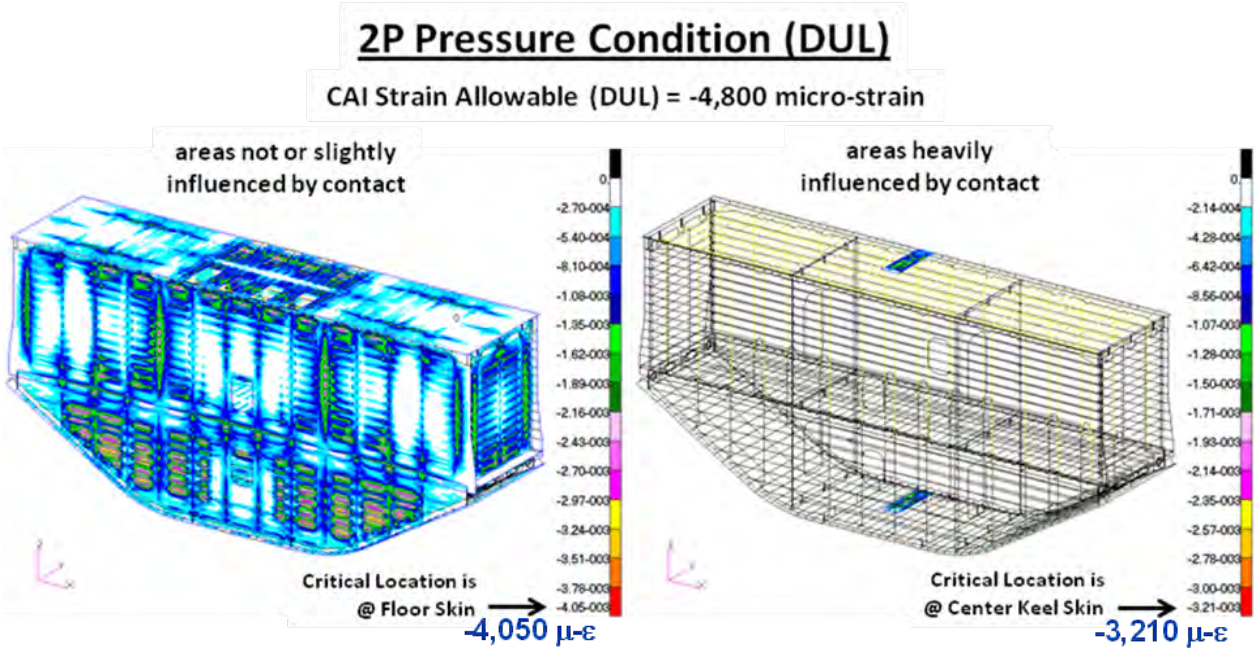

Figure 4-16. Minimum Principal Strains on Composite Skins in 2P Condition

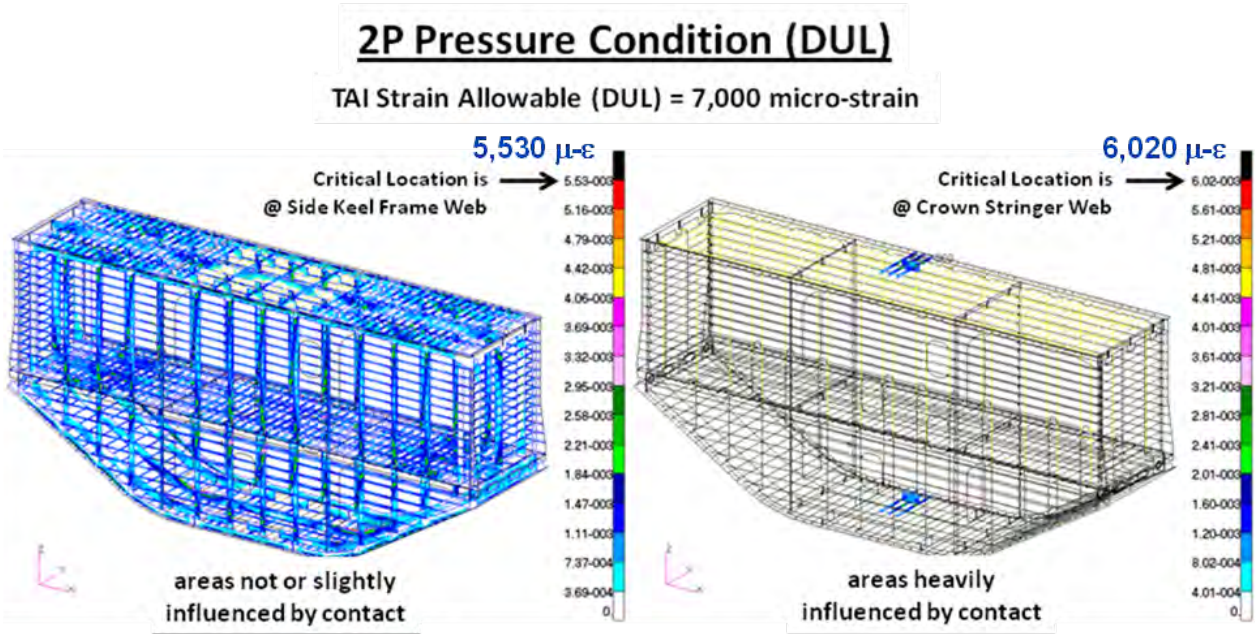

Figure 4-17. Maximum Principal Strains on Composite Stringer/Frame/T-cap Webs in 2P Condition

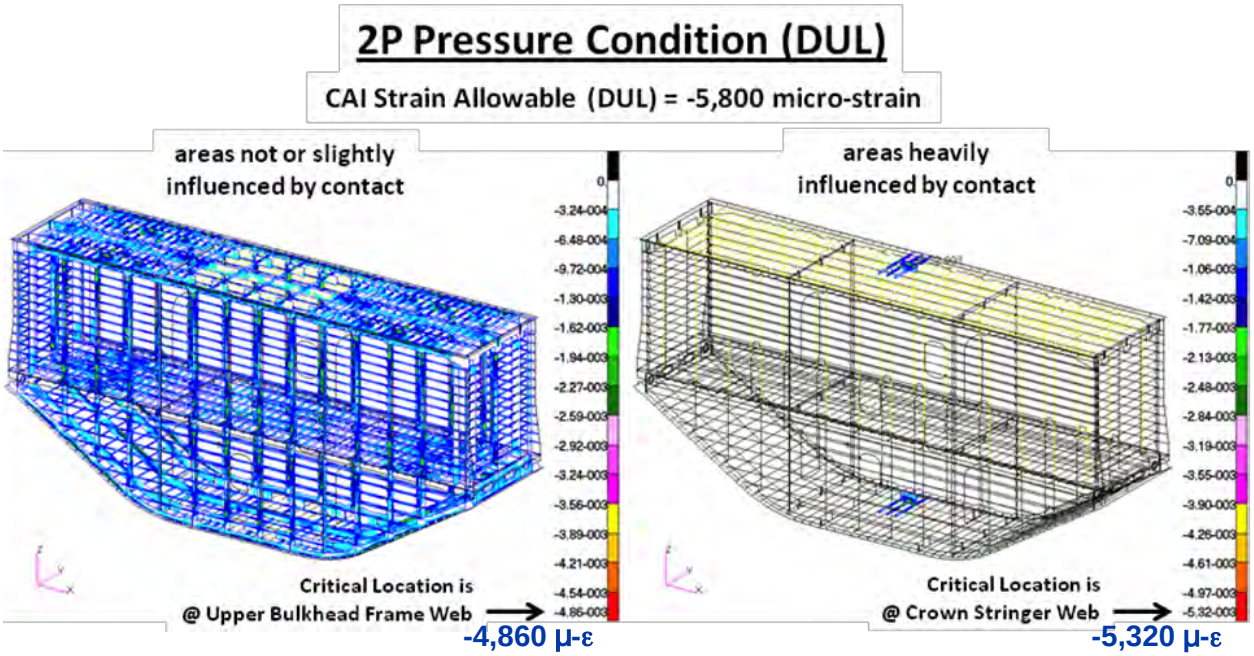

Figure 4-18. Minimum Principal Strains on Composite Stringer/Frame/T-cap Webs in 2P Condition

For the aluminum fittings, von Mises stresses are plotted in Figure 4-19 for the 2P pressure condition. The design values of the aluminum fitting are described in detail in Section 4.2.8. The calculated von Mises stresses on the aluminum fittings were compared with the strength design values of aluminum alloys for margin-of-safety calculations. Positive margins were derived on all metallic fittings of the MBB in the 2P pressure condition. Detailed margins of safety for the metallic fittings are summarized in Section 4.2.9.

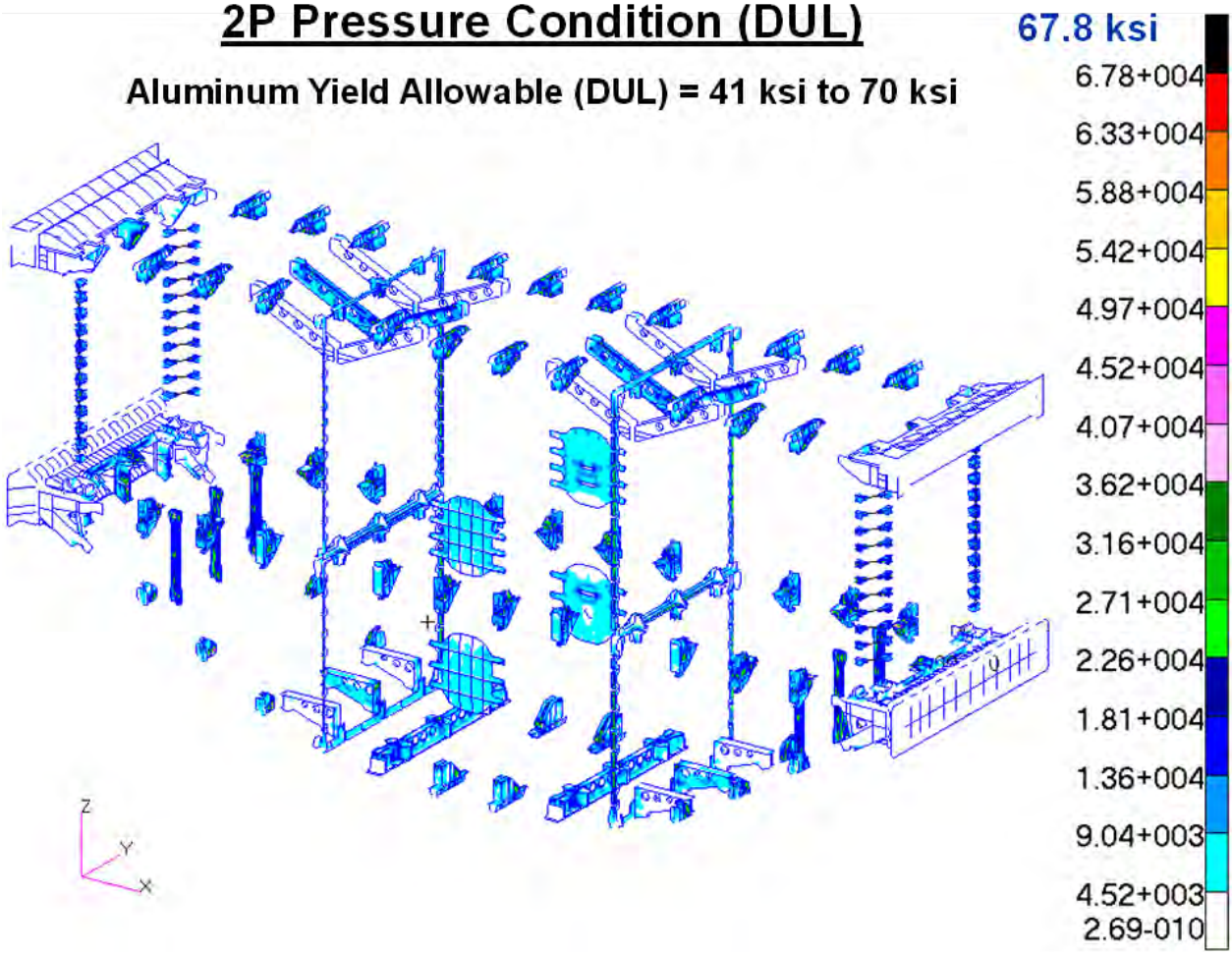

Figure 4-19. von Mises Stresses on Metallic Fittings in 2P Condition

For fasteners, axial and shear forces on each bolt were extracted from the global FEM and checked for fastener-related failure modes, such as bolt axial tension failure, bolt shear failure, bolt bending failure, composite/metallic panel pull-through failure, and composite/metallic panel bearing failure modes. Margins of safety were calculated by comparing the axial and shear forces/stresses on each fastener with the tensile, shear, and bearing allowables of fasteners, and the pull-through and bearing allowables of composite/metallic panels. Positive margins were derived for all fasteners of the MBB in the 2P pressure condition. Detailed margins of safety for the fasteners are summarized in Section 4.2.9.

4.2.3 2.5-g Maneuver Condition

The 2.5-g maneuver condition was a Design Limit Load (DLL) condition without pressure. In this condition, concentrated loads were applied on the COLTS fixture to simulate 2.5-g up-bending wing loads. Linear analysis results for the DLL condition are presented in this section. DLL results must be multiplied by a 1.5 factor-of-safety to achieve the final DUL state. DLL displacements are shown in Figure 4-20 for the 2.5-g maneuver condition, and the maximum displacement was 0.544 in. at the upper edge of the COLTS loading platen.

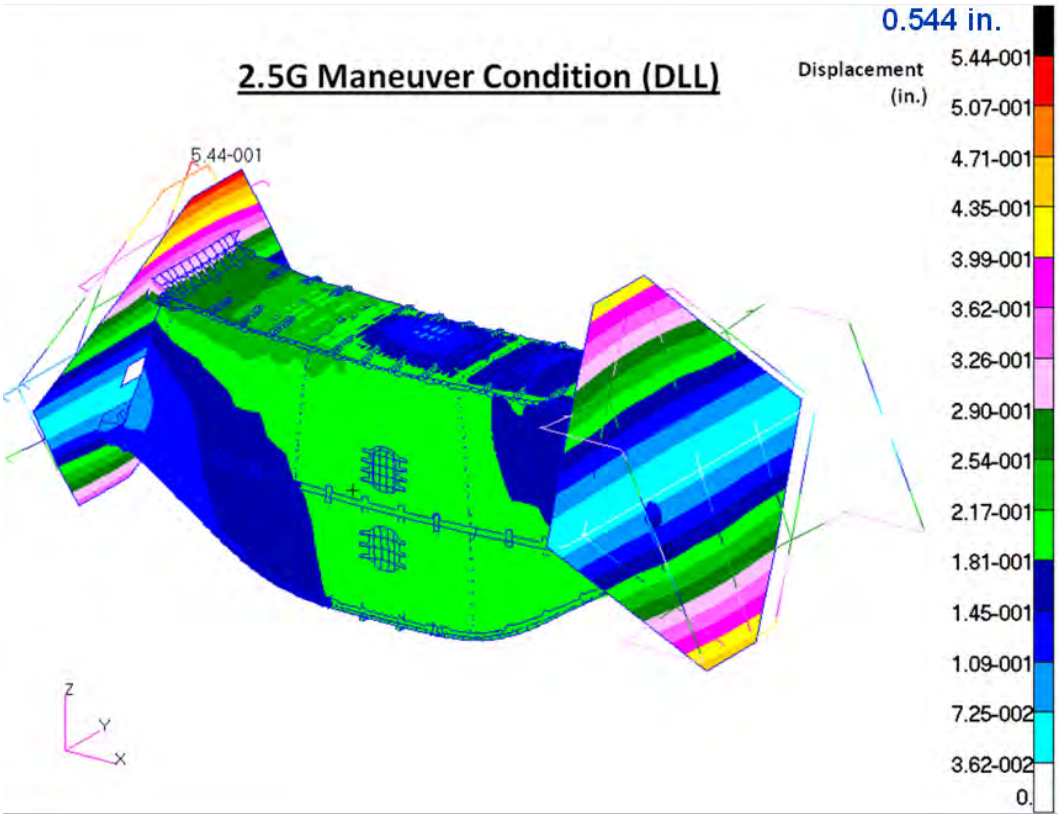

Figure 4-20. Displacements in 2.5-g Condition

Results of maximum and minimum principal strains are shown in Figure 4-21 through Figure 4-24 for the 2.5-g maneuver condition. The design values of composite skins and composite stringer/frame/T-cap webs were different, and they are described in detail in Section 4.2.8. Therefore, for easier comparisons with their design values, strains for composite skins and strains for composite stringer/frame/T-cap webs are shown in different figures. For the composite skins, the maximum principal strains are shown in Figure 4-21, and the minimum principal strains are shown in Figure 4-22. For the composite stringer/frame/T-cap webs, the maximum principal strains are shown in Figure 4-23, and the minimum principal strains are shown in Figure 4-24.

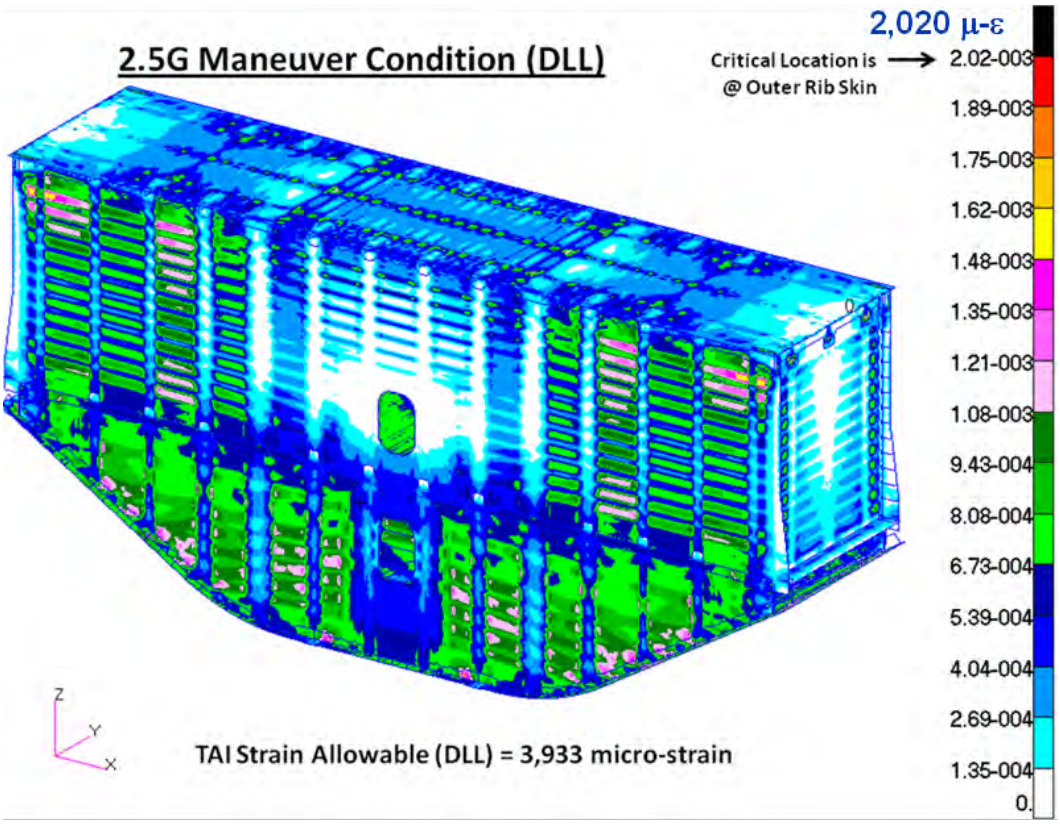

Figure 4-21. Maximum Principal Strains on Composite Skins in 2.5-g Condition

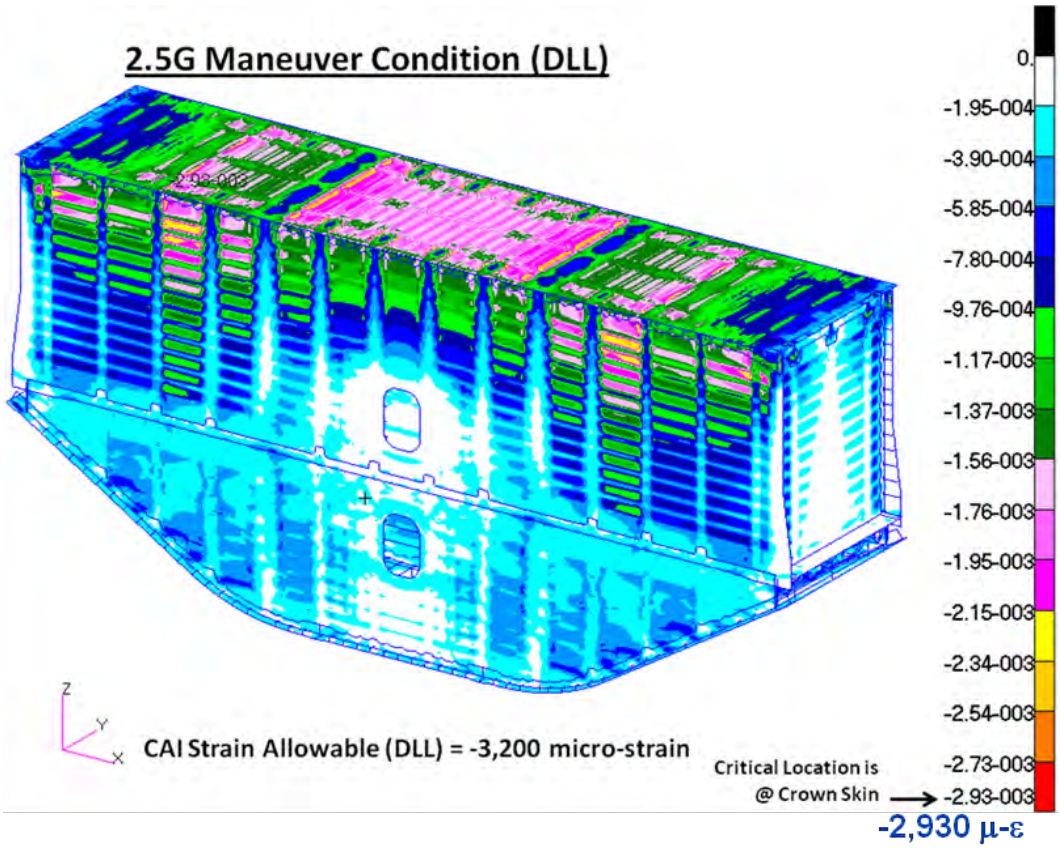

Figure 4-22. Minimum Principal Strains on Composite Skins in 2.5-g Condition

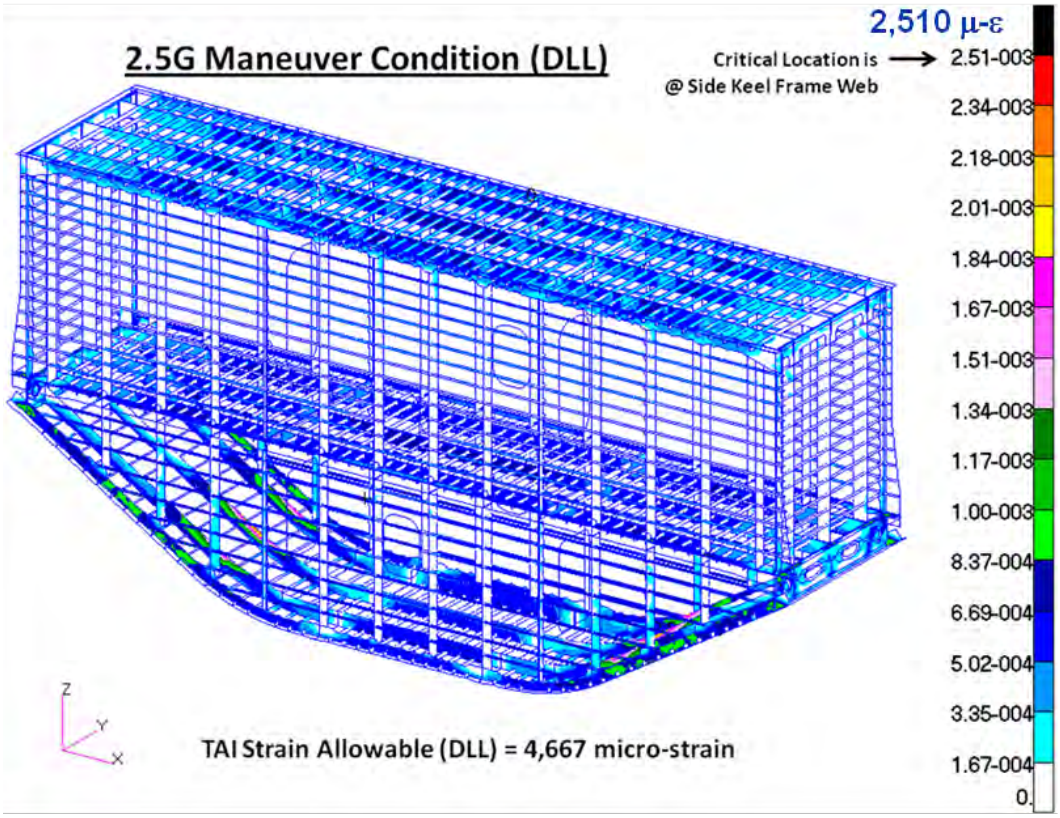

Figure 4-23. Maximum Principal Strains on Composite Stringer/Frame/T-cap Webs in 2.5-g Condition

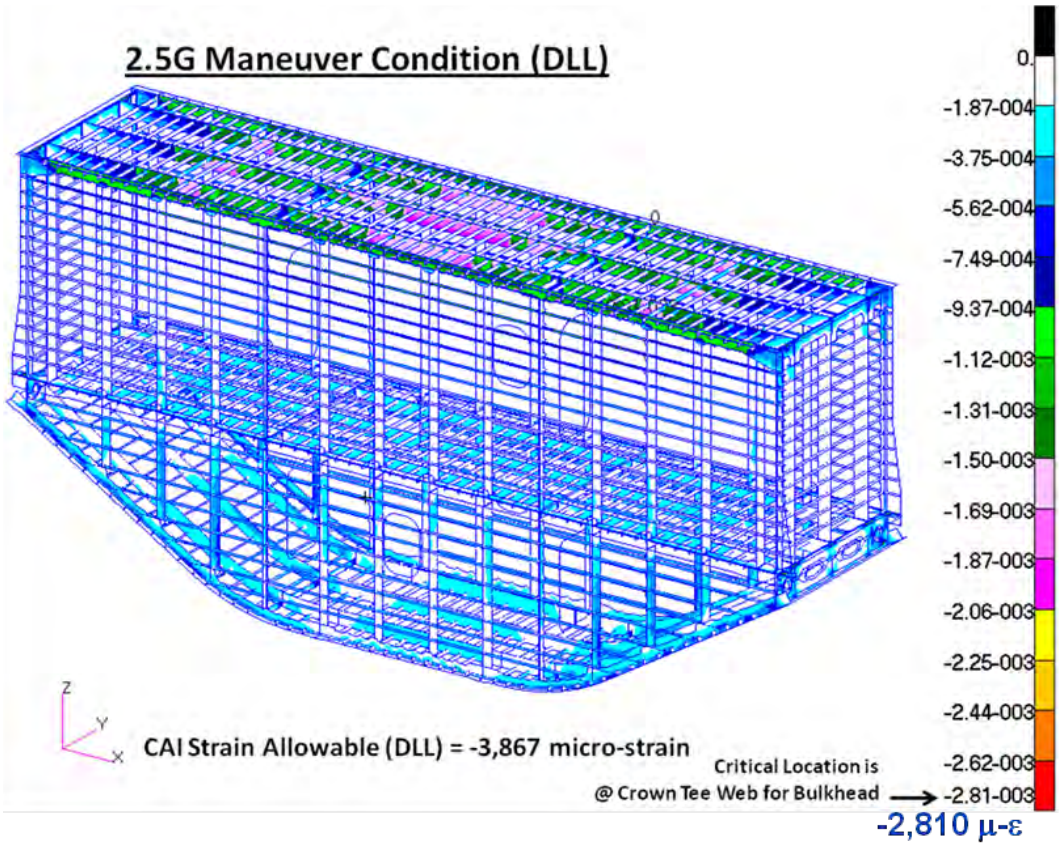

Figure 4-24. Minimum Principal Strains on Composite Stringer/Frame/T-cap Webs in 2.5-g Condition

For aluminum fittings, von Mises stresses are plotted in Figure 4-25 for the 2.5-g maneuver condition. The design values of the aluminum fitting are described in detail in Section 4.2.8. The calculated von Mises stresses on the aluminum fittings were compared with the strength design values of aluminum alloys for margin-of-safety calculations. Positive margins were derived on all metallic fittings of the MBB in the 2.5-g maneuver condition. Detailed margins of safety of the metallic fittings are summarized in Section 4.2.9.

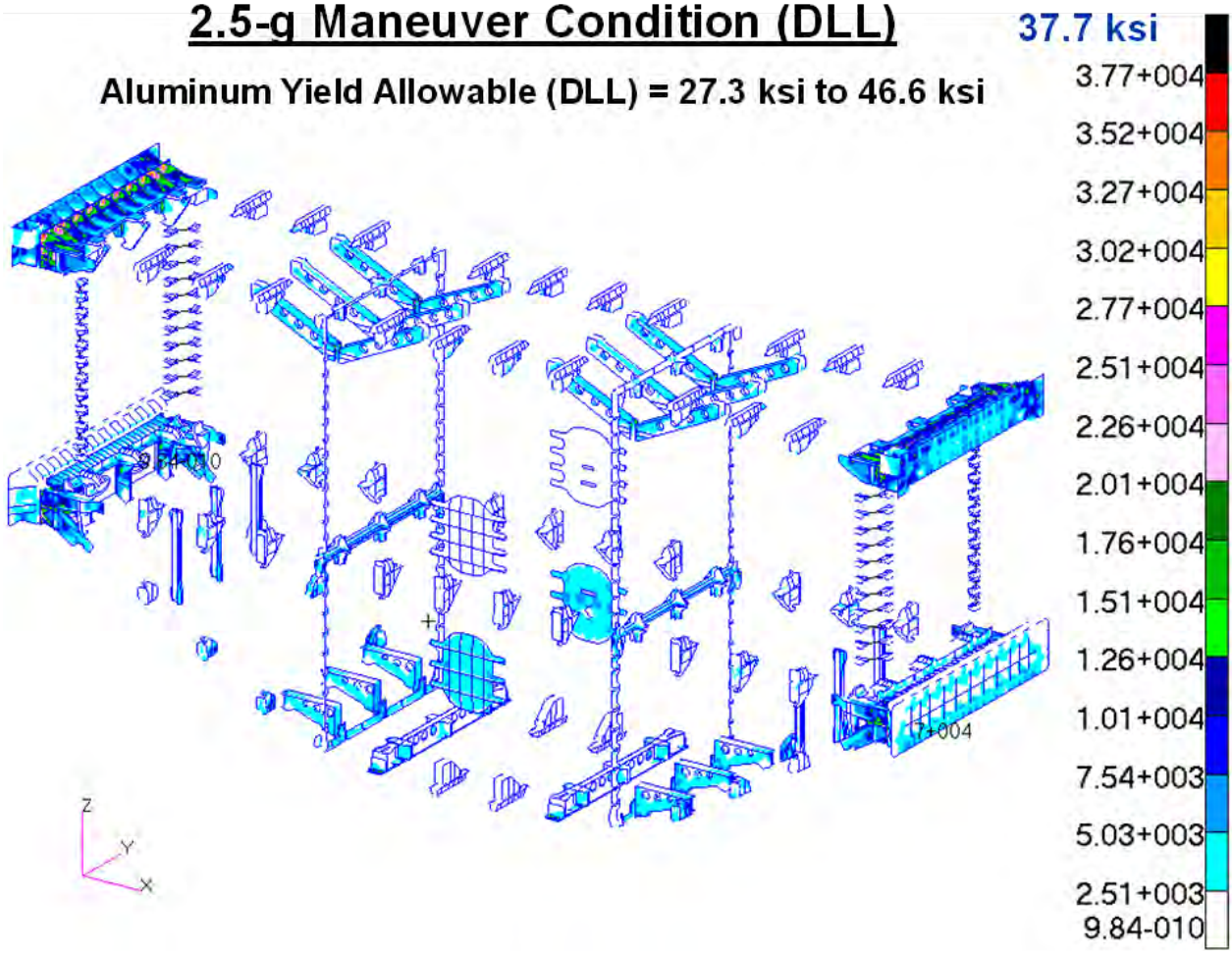

Figure 4-25. von Mises Stresses on Metallic Fittings in 2.5-g Condition

For fasteners, axial and shear forces on each bolt were extracted from the global FEM and checked for fastener-related failure modes, such as bolt axial tension failure, bolt shear failure, bolt bending failure, composite/metallic panel pull-through failure, and composite/metallic panel bearing failure modes. Margins of safety were calculated by comparing the axial and shear forces/stresses on each fastener with the tensile, shear, and bearing allowables of fasteners, and the pull-through and bearing allowables of composite/metallic panels. Positive margins were derived for all fasteners of the MBB in the 2.5-g maneuver condition. Detailed margins of safety for the fasteners are summarized in Section 4.2.9.

4.2.4 2.5-g + 1P Combined Loading Condition

The 2.5-g + 1P combined loading condition was a DLL condition with pressure. For DLL, 1P was 9.2 psi. In this 2.5-g + 1P combined loading condition, concentrated loads were applied on the COLTS fixture to simulate 2.5-g up-bending wing loads, and a 9.2-psi pressure was applied to the interior surfaces of the MBB. Linear analysis results are shown here. DLL results must be multiplied by a 1.5 factor-of-safety to achieve the final DUL state. DLL displacements are shown in Figure 4-26 for the 2.5-g + 1P combined loading condition, and the maximum displacement was 0.550 in. at the center of the aft upper bulkhead.

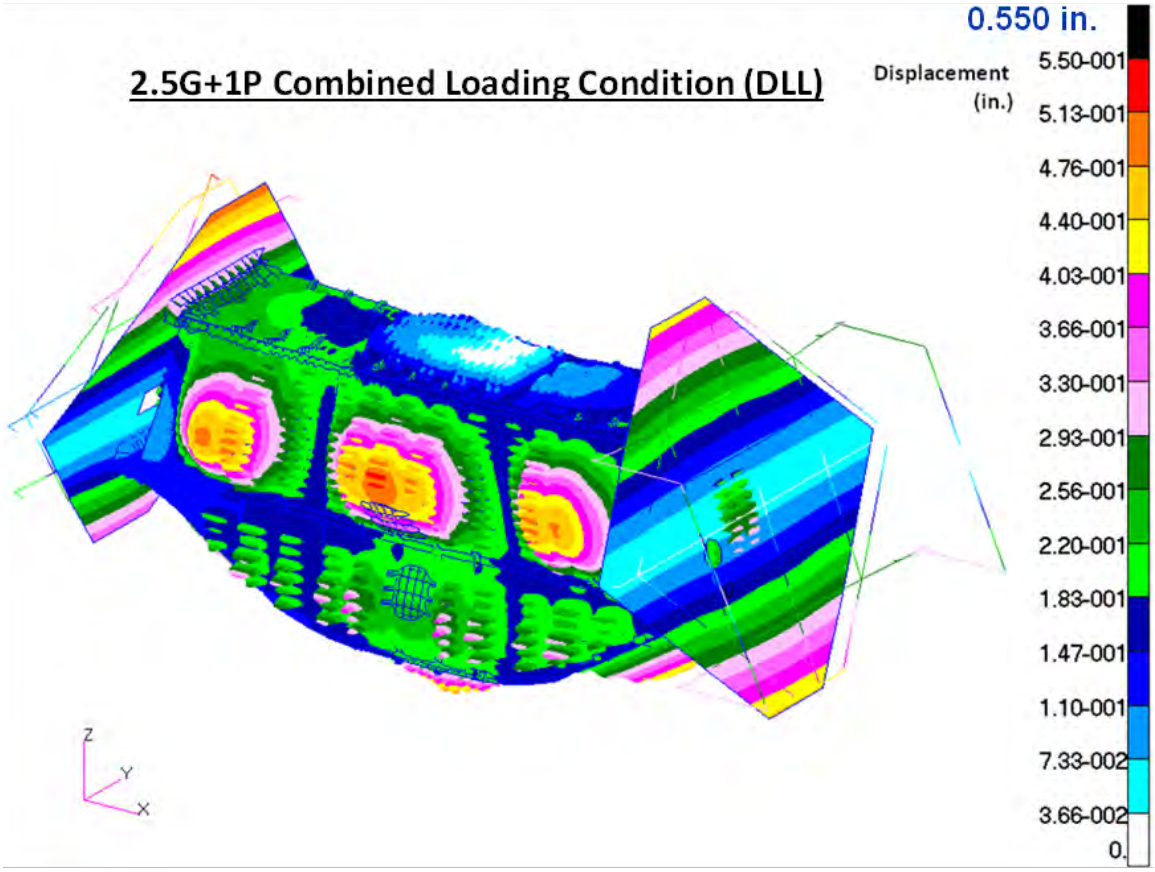

Figure 4-26. Displacements in 2.5-g + 1P Condition

Results of maximum and minimum principal strains are shown in Figure 4-27 through Figure 4-30 for the 2.5-g + 1P combined loading condition. The design values of composite skins and composite stringer/frame/T-cap webs were different, and they are described in detail in Section 4.2.8. Therefore, for easier comparisons with their design values, strains for composite skins and strains for composite stringer/frame/T-cap webs are shown in different figures. For the composite skins, the maximum principal strains are shown in Figure 4-27, and the minimum principal strains are shown in Figure 4-28. For the composite stringer/frame/T-cap webs, the maximum principal strains are shown in Figure 4-29, and the minimum principal strains are shown in Figure 4-30. In addition to plotting the strains of composite skins and the composite stringer/frame/T-cap webs separately, in Figure 4-27 through Figure 4-30, separate plots are shown (in the same figure) for areas that were not influenced (or only slightly influenced) by contact between composite skins and external fittings due to internal pressure in the MBB, and for areas that were heavily influenced by contact. Strains in the areas that were heavily influenced by contact were calculated by modifying the global FEM with locally refined meshes and by modeling contacts between composite skins and fittings. Analysis of this modified global FEM would provide more accurate results for the design cases that included pressure loads.

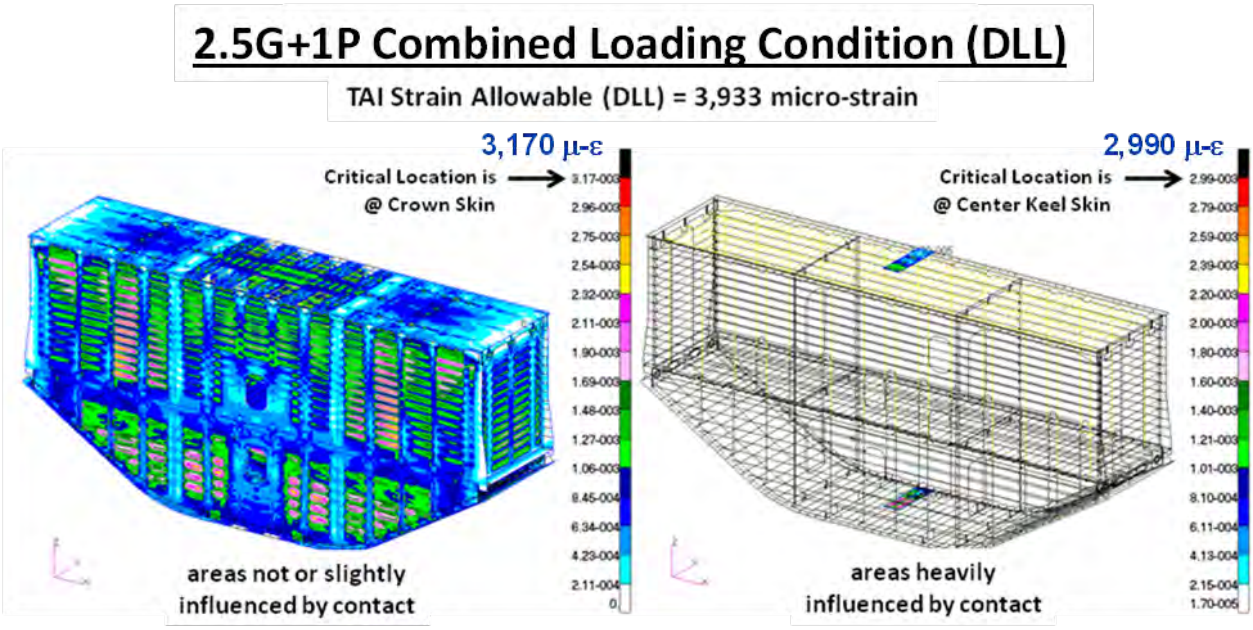

Figure 4-27. Maximum Principal Strains on Composite Skins in 2.5-g + 1P Condition

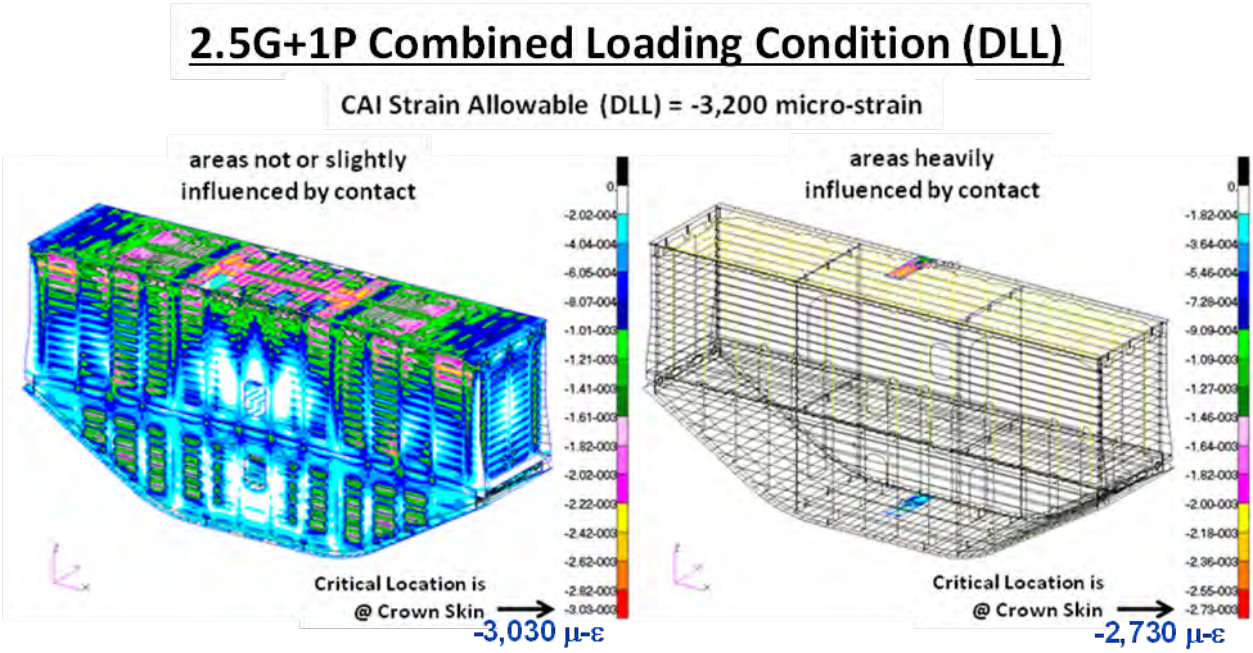

Figure 4-28. Minimum Principal Strains on Composite Skins in 2.5-g + 1P Condition

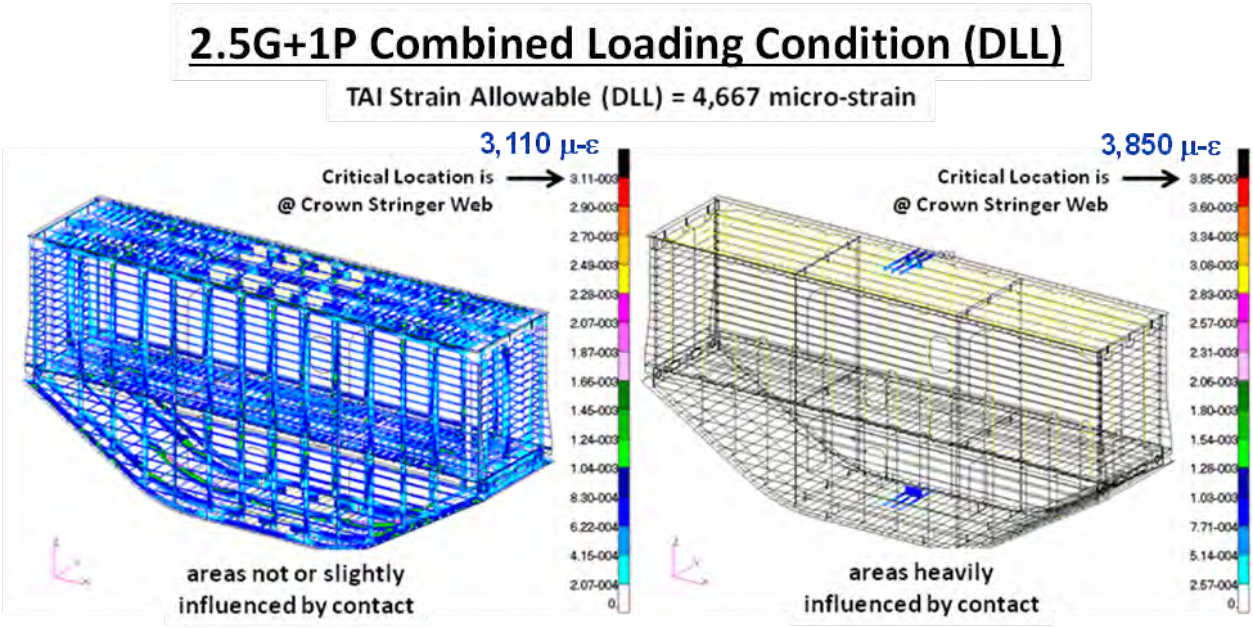

Figure 4-29. Maximum Principal Strains on Composite Stringer/Frame/T-cap Webs in 2.5-g + 1P Condition

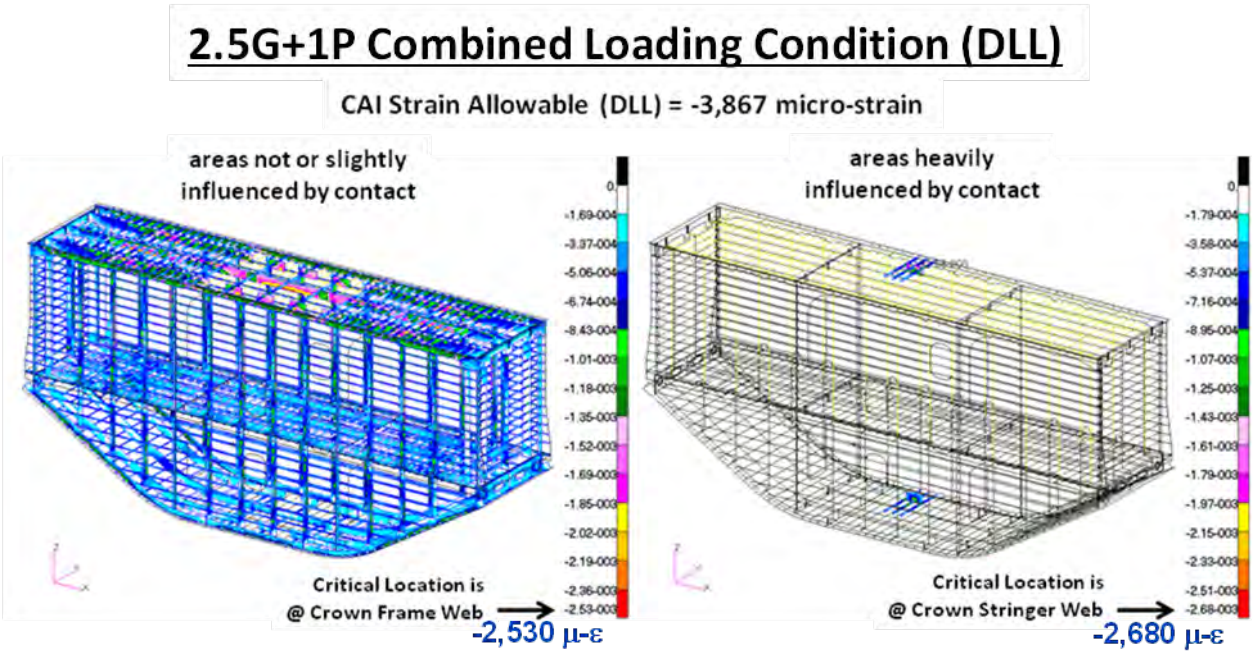

Figure 4-30. Minimum Principal Strains on Composite Stringer/Frame/T-cap Webs in 2.5-g + 1P Condition

For aluminum fittings, von Mises stresses are plotted in Figure 4-31 for the 2.5-g + 1P combined loading condition. The design values of the aluminum fitting are described in detail in Section 4.2.8. The calculated von Mises stresses on the aluminum fittings were compared with the strength design values of aluminum alloys for margin-of-safety calculations. Positive margins were derived on all metallic fittings of the MBB in the 2.5-g + 1P combined loading condition. Detailed margins of safety for the metallic fittings are summarized in Section 4.2.9.

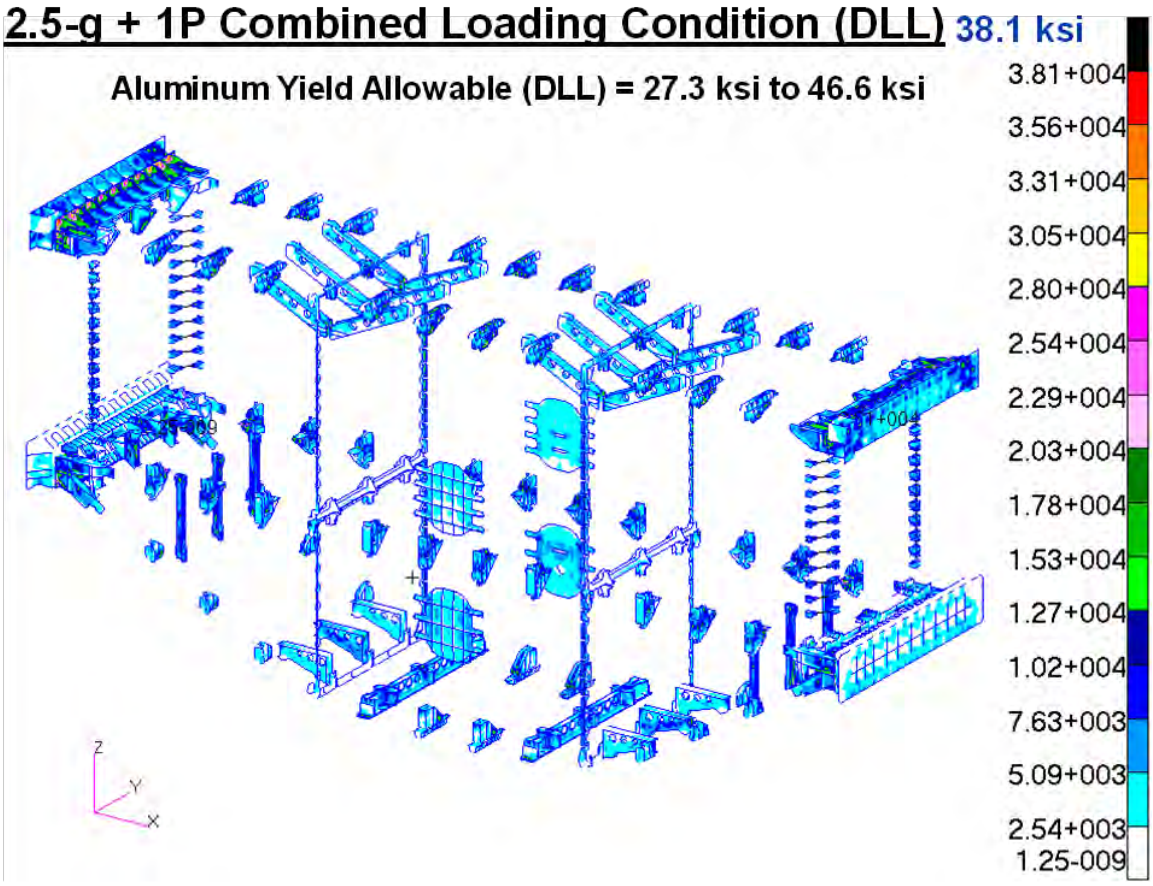

Figure 4-31. von Mises Stresses on Metallic Fittings in 2.5-g + 1P Condition

For fasteners, axial and shear forces on each bolt were extracted from the global FEM and checked for fastener-related failure modes, such as bolt axial tension failure, bolt shear failure, bolt bending failure, composite/metallic panel pull-through failure, and composite/metallic panel bearing failure modes. Margins of safety were calculated by comparing the axial and shear forces/stresses on each fastener with the tensile, shear, and bearing allowables of fasteners, and the pull-through and bearing allowables of composite/metallic panels. Positive margins were derived for all fasteners of the MBB in the 2.5-g + 1P combined loading condition. Detailed margins of safety for the fasteners are summarized in Section 4.2.9.

4.2.5 -1.0-g Maneuver Condition

The -1.0-g maneuver condition was a DLL condition without pressure. In this condition, concentrated loads were applied on the COLTS fixture to simulate -1.0-g down-bending wing loads. Linear analysis results are presented in this section. DLL results must be multiplied by a 1.5 factor-of-safety to achieve the final DUL state. DLL displacements are shown in Figure 4-32 for the -1.0-g maneuver condition, and the maximum displacement is 0.217 in. at the upper edge of the COLTS loading platen.

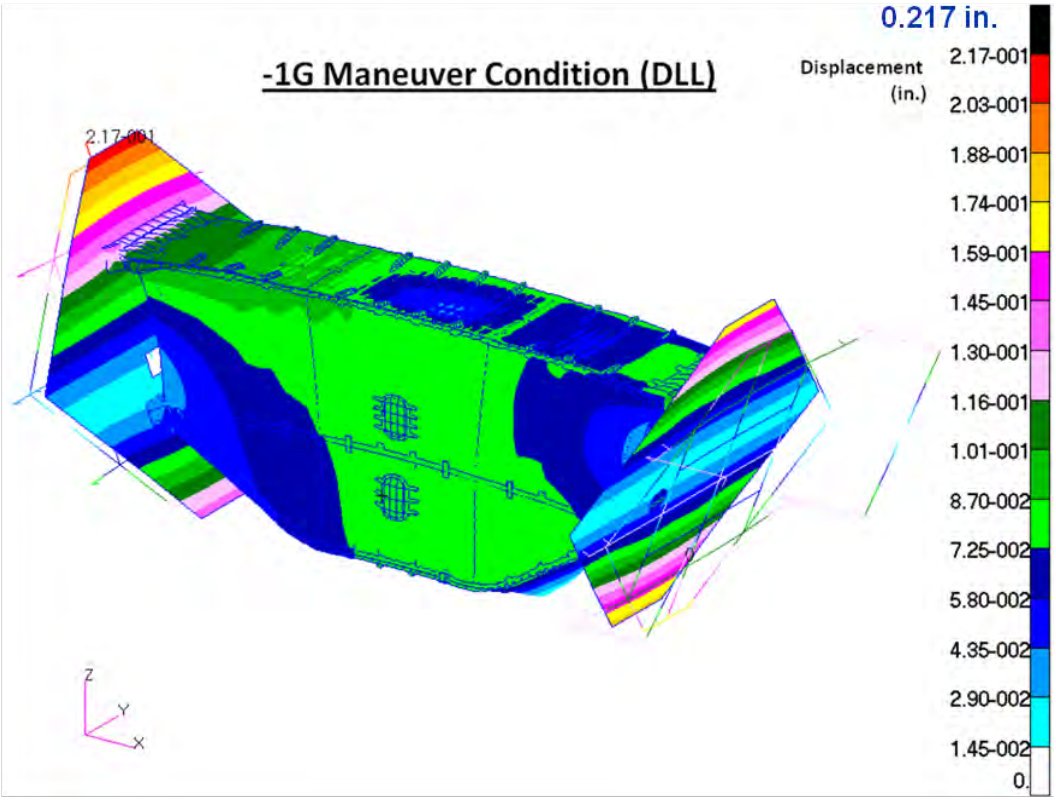

Figure 4-32. Displacements in -1.0-g Condition

The results of maximum and minimum principal strains are shown in Figure 4-33 through Figure 4-36 for the -1.0-g maneuver condition. The design values of composite skins and composite stringer/frame/T-cap webs were different, and they are described in detail in Section 4.2.8. Therefore, for easier comparisons with their design values, strains for composite skins and strains for composite stringer/frame/T-cap webs are shown in different figures. For the composite skins, the maximum principal strains are shown in Figure 4-33, and the minimum principal strains are shown in Figure 4-34. For the composite stringer/frame/T-cap webs, the maximum principal strains are shown in Figure 4-35, and the minimum principal strains are shown in Figure 4-36.

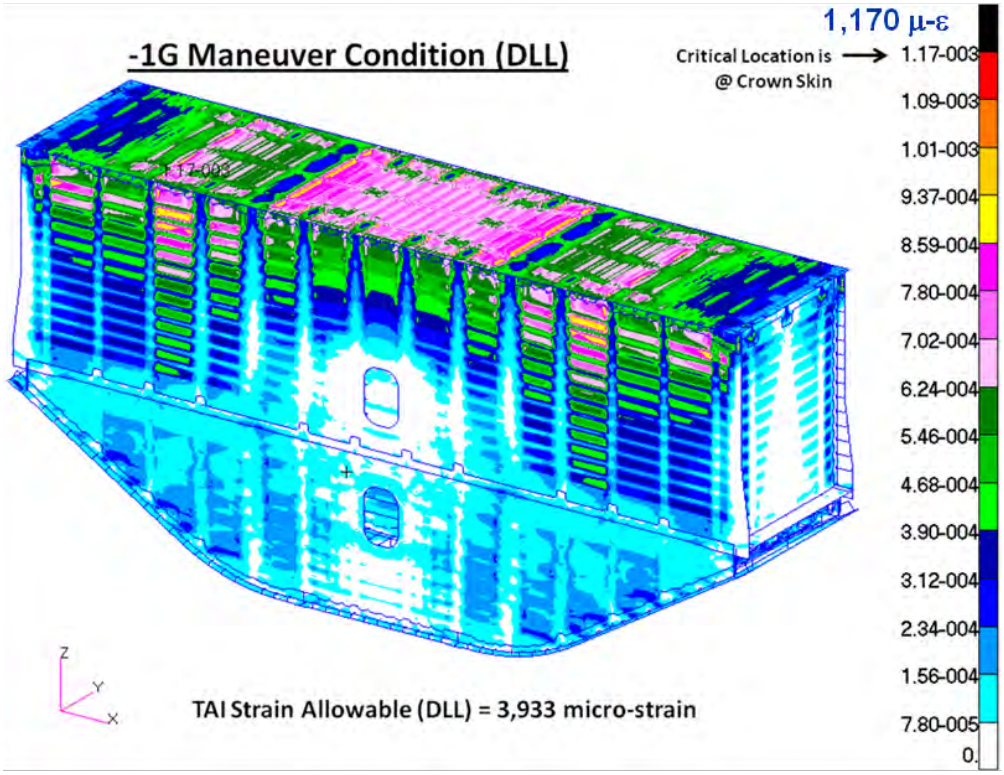

Figure 4-33. Maximum Principal Strains on Composite Skins in -1.0-g Condition

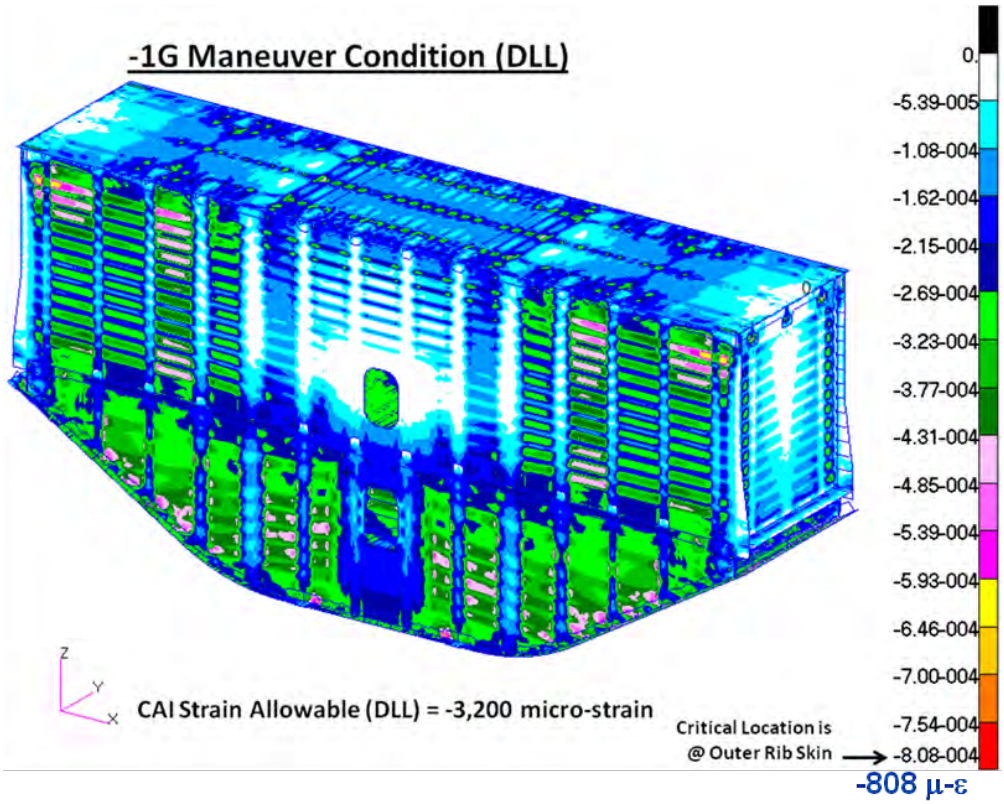

Figure 4-34. Minimum Principal Strains on Composite Skins in -1.0-g Condition

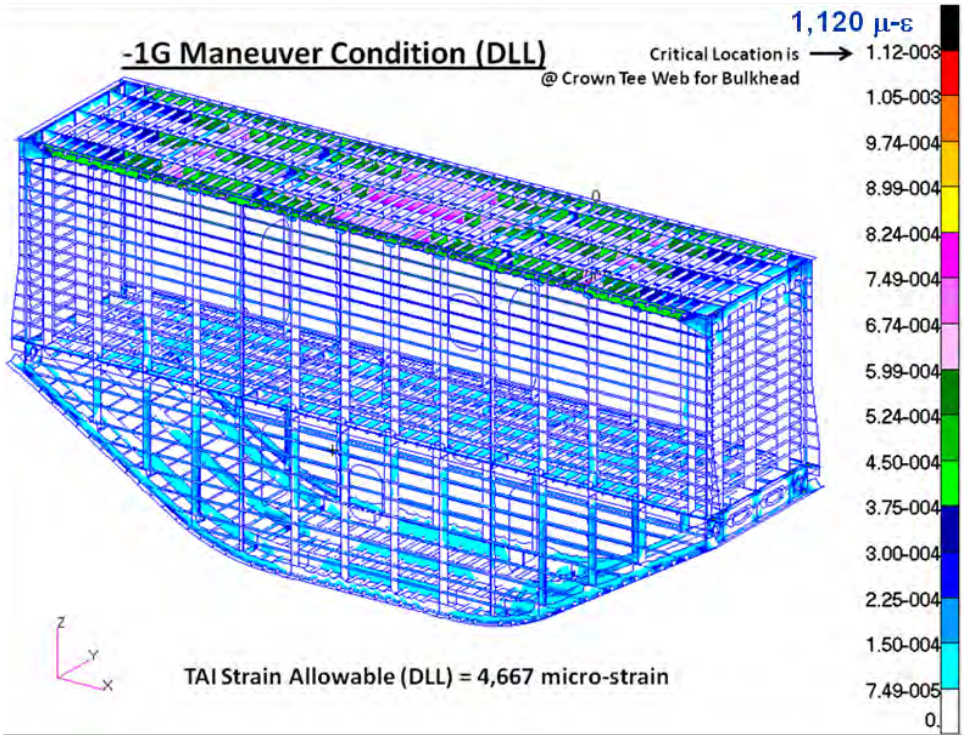

Figure 4-35. Maximum Principal Strains on Composite Stringer/Frame/T-cap Webs in -1.0-g Condition

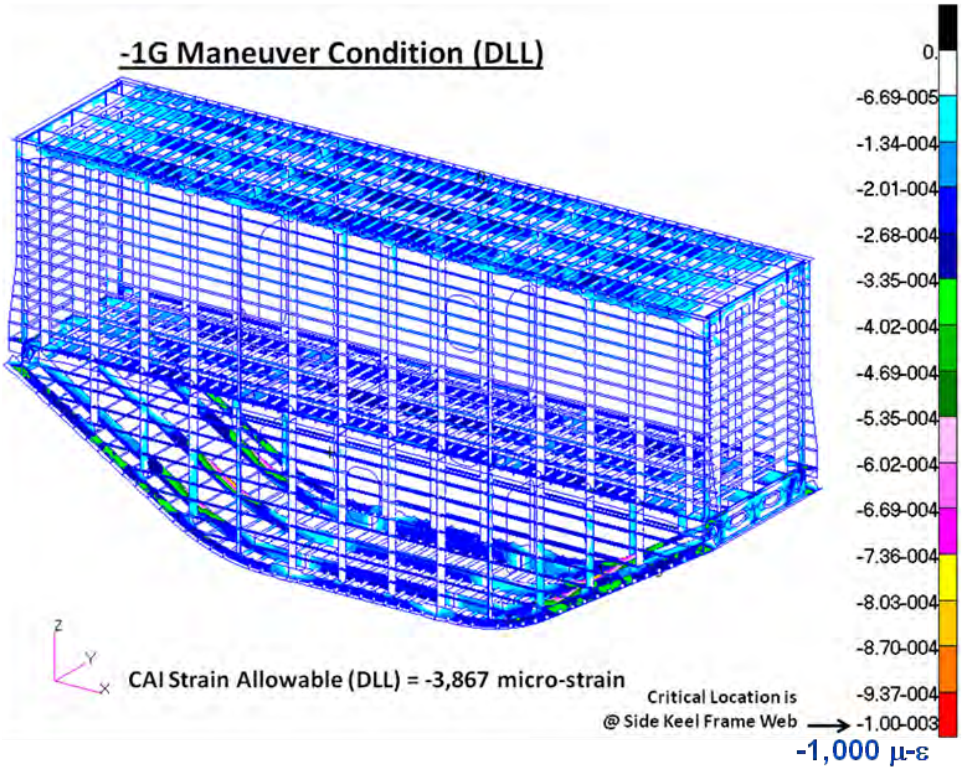

Figure 4-36. Minimum Principal Strains on Composite Stringer/Frame/T-cap Webs in -1.0-g Condition

For aluminum fittings, von Mises stresses are plotted in Figure 4-37 for the -1.0-g maneuver condition. The design values of the aluminum fitting are described in detail in Section 4.2.8. The calculated von Mises stresses on the aluminum fittings were compared with the strength design values of aluminum alloys for margin-of-safety calculations. Positive margins were derived on all metallic fittings of the MBB in the -1.0-g maneuver condition. Detailed margins of safety for the metallic fittings are summarized in Section 4.2.9.

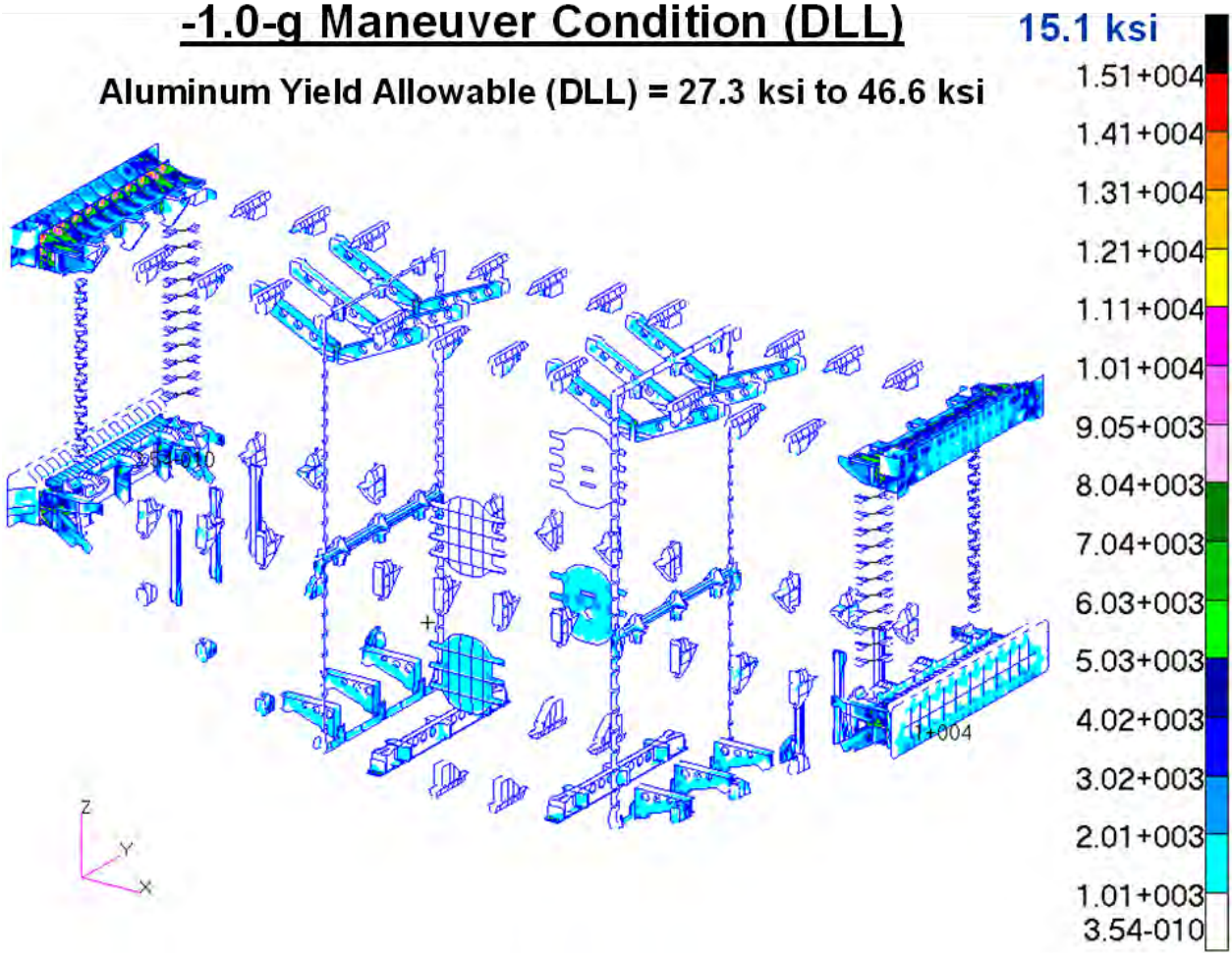

Figure 4-37. von Mises Stresses on Metallic Fittings in -1.0-g Condition

For fasteners, axial and shear forces on each bolt were extracted from the global FEM and checked for fastener-related failure modes, such as bolt axial tension failure, bolt shear failure, bolt bending failure, composite/metallic panel pull-through failure, and composite/metallic panel bearing failure modes. Margins of safety were calculated by comparing the axial and shear forces/stresses on each fastener with the tensile, shear, and bearing allowables of fasteners, and the pull-through and bearing allowables of composite/metallic panels. Positive margins were derived for all fasteners of the MBB in the -1.0-g maneuver condition. Detailed margins of safety for the fasteners are summarized in Section 4.2.9.

4.2.6 -1.0-g + 1P Combined Loading Condition

The -1.0-g + 1P combined loading condition was a DLL condition with pressure. For DLL, 1P was 9.2 psi. In this condition, concentrated loads were applied on the COLTS fixture to simulate -1.0-g down-bending wing loads, and a 9.2-psi pressure was applied to the interior surfaces of the MBB. Linear analysis results are presented in this section. DLL results must be multiplied by a 1.5 factor-of-safety to achieve the final DUL state. DLL displacements are shown in Figure 4-38 for the -1.0-g + 1P combined loading condition, and the maximum displacement is 0.563 in. at the center of the forward upper bulkhead.

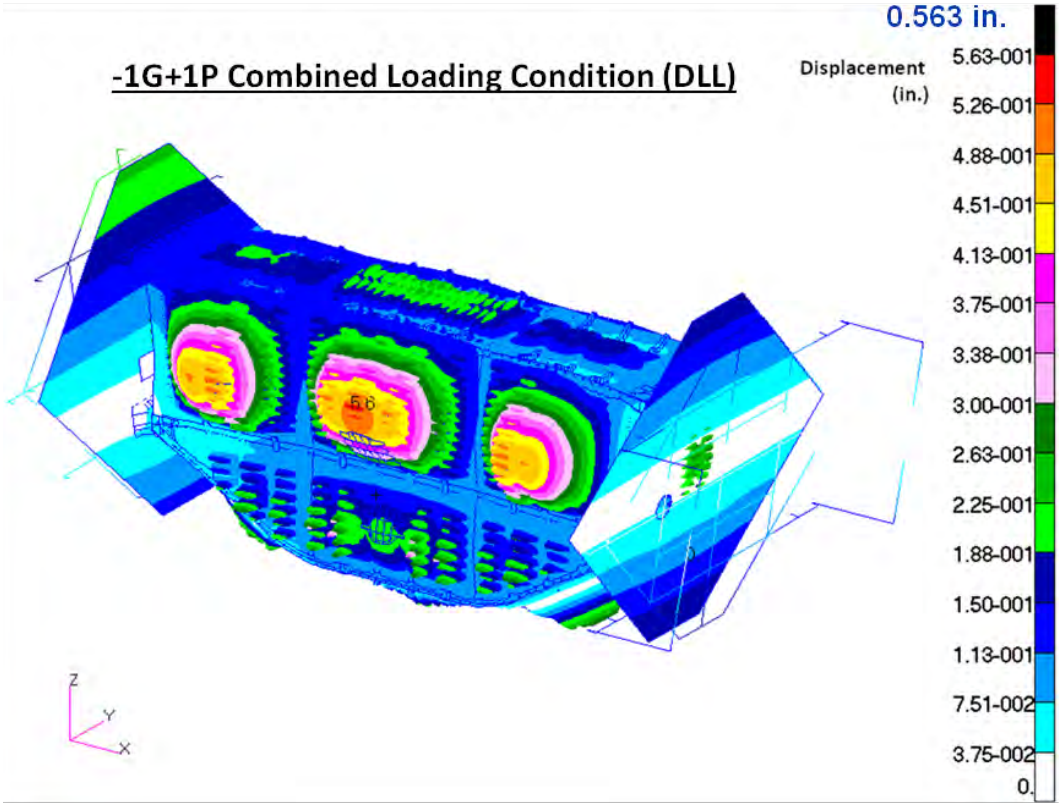

Figure 4-38. Displacements in -1.0-g + 1P Condition

The results of maximum and minimum principal strains are shown in Figure 4-39 through Figure 4-42 for the -1.0-g + 1P combined loading condition. The design values of composite skins and composite stringer/frame/T-cap webs were different, and they are described in detail in Section 4.2.8. Therefore, for easier comparisons with their design values, strains for composite skins and strains for composite stringer/frame/T-cap webs are shown in different figures. For the composite skins, the maximum principal strains are shown in Figure 4-39, and the minimum principal strains are shown in Figure 4-40. For the composite stringer/frame/T-cap webs, the maximum principal strains are shown in Figure 4-41, and the minimum principal strains are shown in Figure 4-42. In addition to plotting the strains of composite skins and the composite stringer/frame/T-cap webs separately, in Figure 4-39 through Figure 4-42, separate plots are shown (in the same figure) for areas that were not influenced (or only slightly influenced) by contact between composite skins and external fittings due to internal pressure in the MBB, and for areas that were heavily influenced by contact. Strains in the areas that were heavily influenced by contact were calculated by modifying the global FEM with locally refined meshes,

and by modeling contacts between composite skins and fittings. Analysis of this modified global FEM would provide more accurate results for the design cases that included pressure loads.

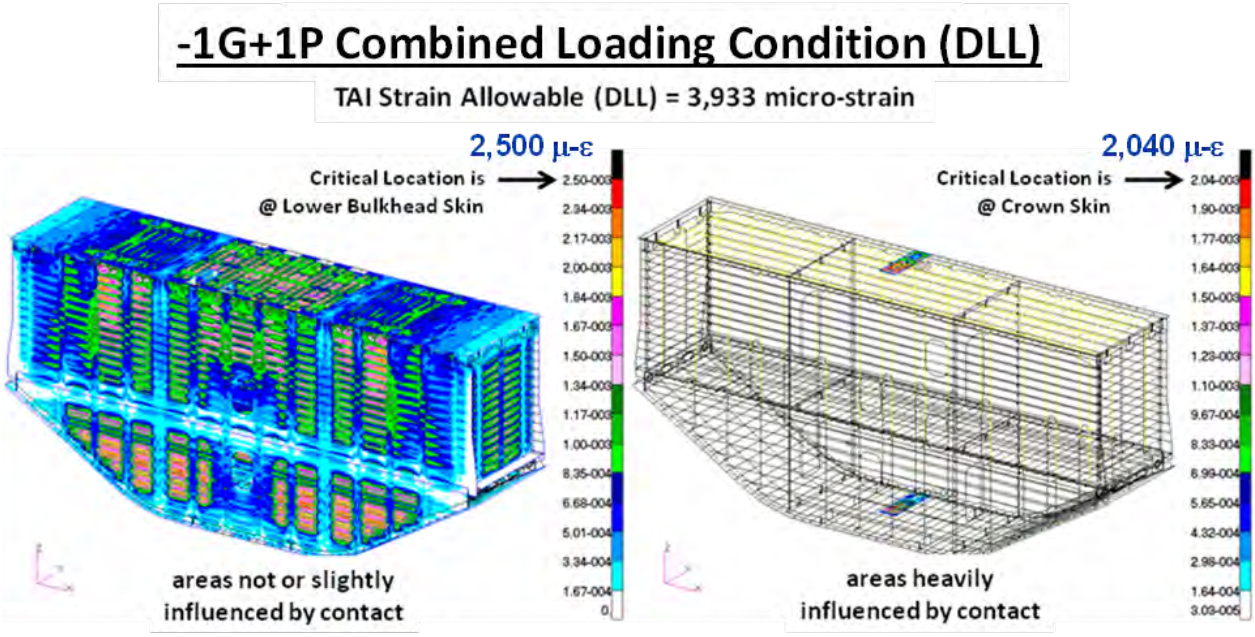

Figure 4-39. Maximum Principal Strains on Composite Skins in -1.0-g + 1P Condition

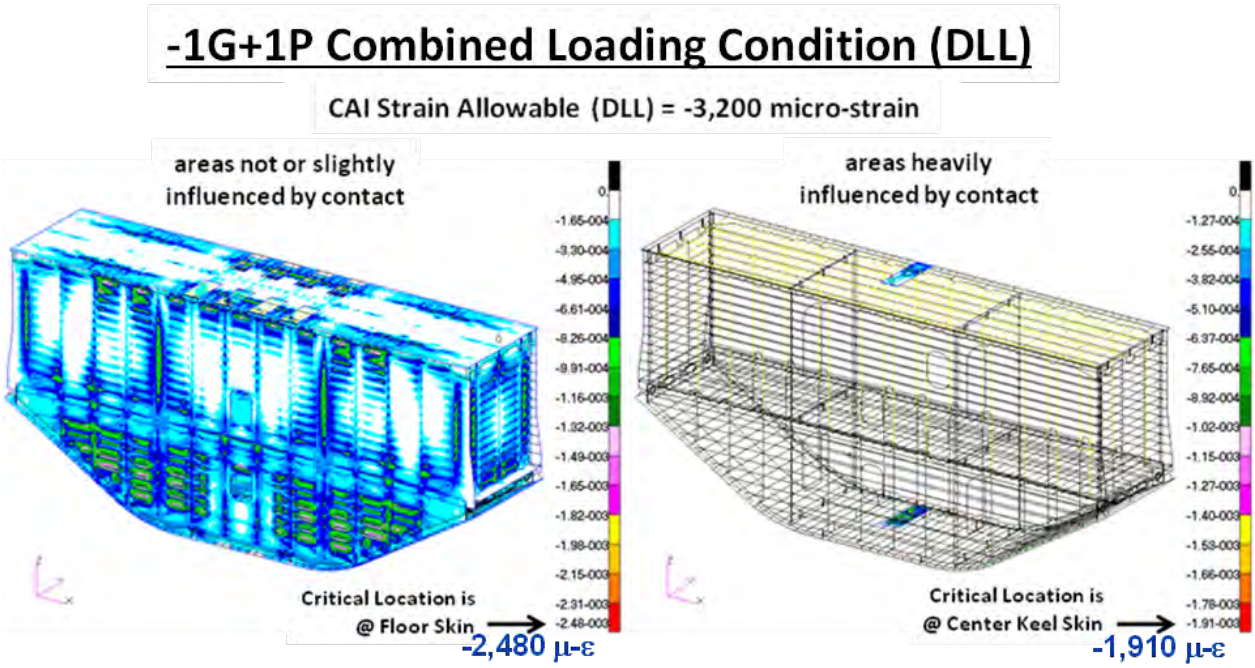

Figure 4-40. Minimum Principal Strains on Composite Skins in -1.0-g + 1P Condition

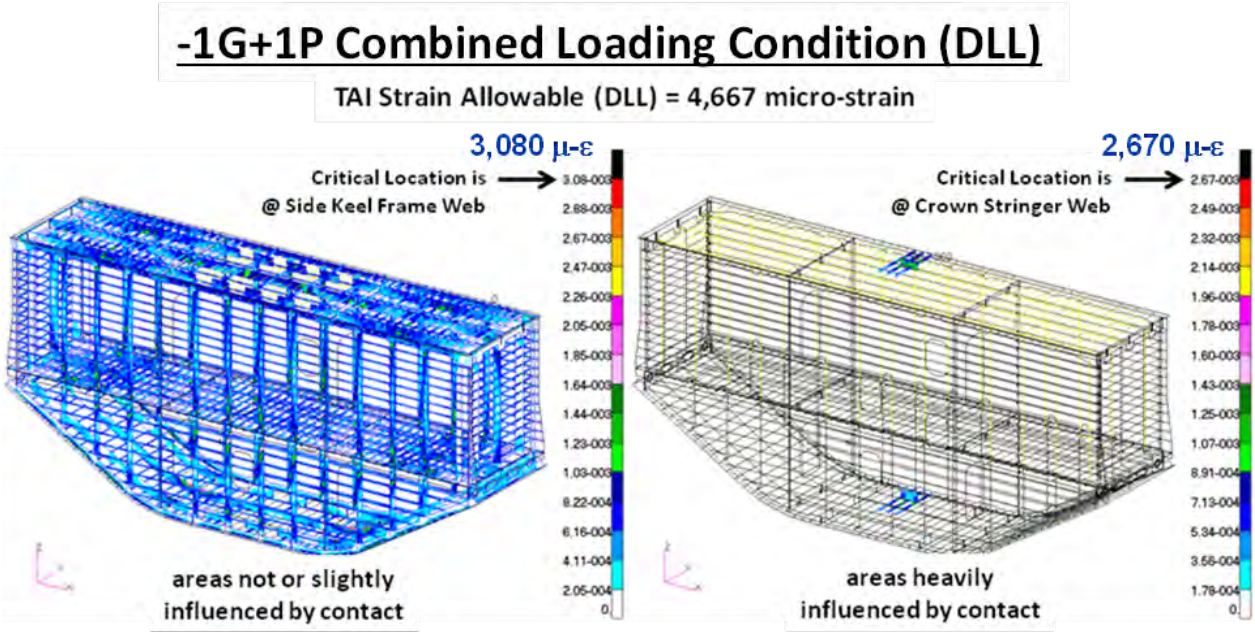

Figure 4-41. Maximum Principal Strains on Composite Stringer/Frame/T-cap Webs in -1.0-g + 1P Condition

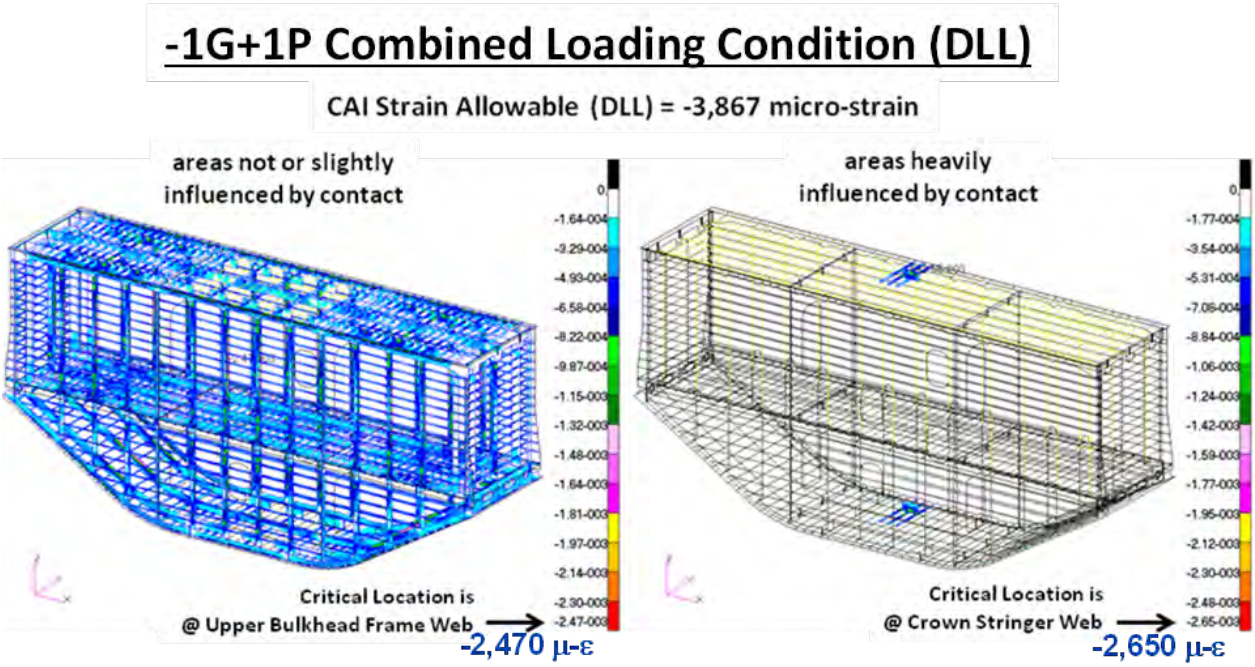

Figure 4-42. Minimum Principal Strains on Composite Stringer/Frame/T-cap Webs in -1.0-g + 1P Condition

For aluminum fittings, von Mises stresses are plotted in Figure 4-43 for the -1.0-g + 1P combined loading condition. The design values of the aluminum fitting are described in detail in Section 4.2.8. The calculated von Mises stresses on the aluminum fittings were compared with the strength design values of aluminum alloys for margin-of-safety calculations. Positive margins were derived on all metallic fittings of the MBB in the -1.0-g + 1P combined loading condition. Detailed margins of safety for the metallic fittings are summarized in Section 4.2.9.

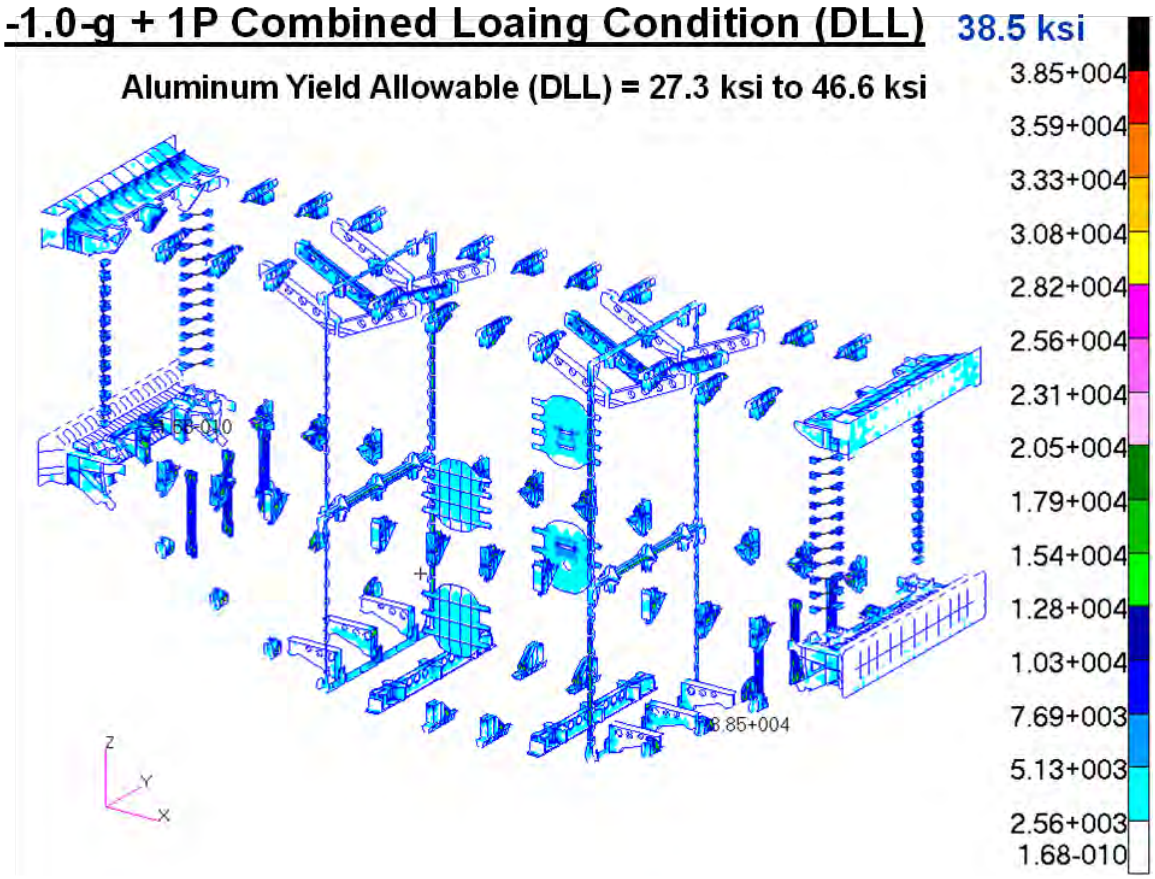

Figure 4-43. von Mises Stresses on Metallic Fittings in -1.0-g + 1P Condition

For fasteners, axial and shear forces on each bolt were extracted from the global FEM and checked for fastener-related failure modes, such as bolt axial tension failure, bolt shear failure, bolt bending failure, composite/metallic panel pull-through failure, and composite/metallic panel bearing failure modes. Margins of safety were calculated by comparing the axial and shear forces/stresses on each fastener with the tensile, shear, and bearing allowables of fasteners, and the pull-through and bearing allowables of composite/metallic panels. Positive margins were derived for all fasteners of the MBB in the -1.0-g + 1P combined loading condition. Detailed margins of safety for the fasteners are summarized in Section 4.2.9.

4.2.7 1.0-g Weight Check

Due to the large size of the MBB, a 1.0-g down static case of the MBB was also studied. The results of displacement are shown in Figure 4-44 for the 1.0-g down static case, and the maximum displacement was 0.0000698 in. at the center of the keel. The results of maximum principal strains are shown in Figure 4-45, and the results of minimum principal strains are shown in Figure 4-46 for the composite structures. The maximum and minimum principal strains were both less than 1 micro-strain, which confirmed that they were much lower than the strain results from the five critical load cases shown above.

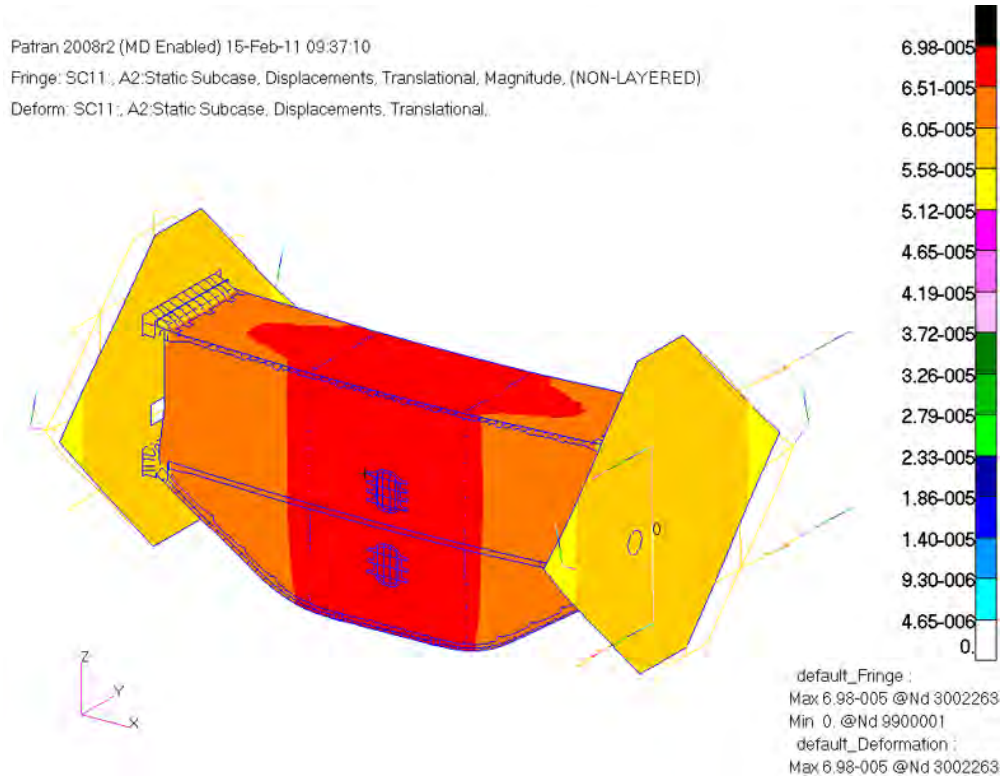

Figure 4-44. Displacements in 1.0-g Weight Condition

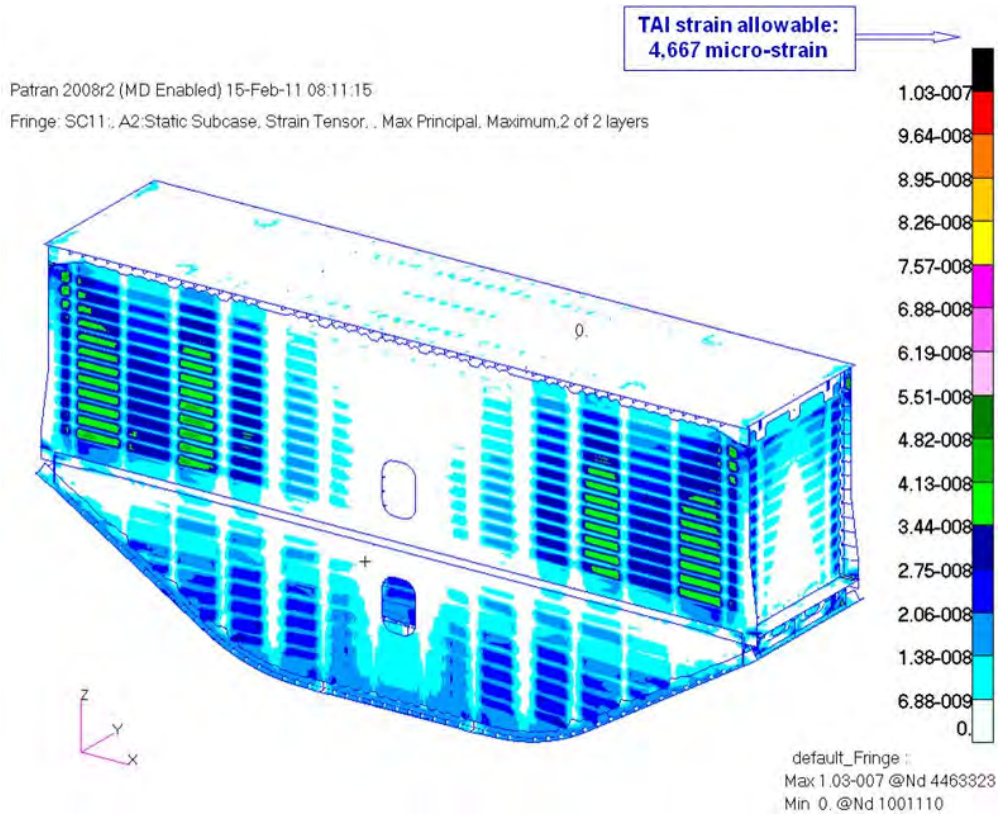

Figure 4-45. Maximum Principal Strains on Composite Structures in 1.0-g Weight Condition

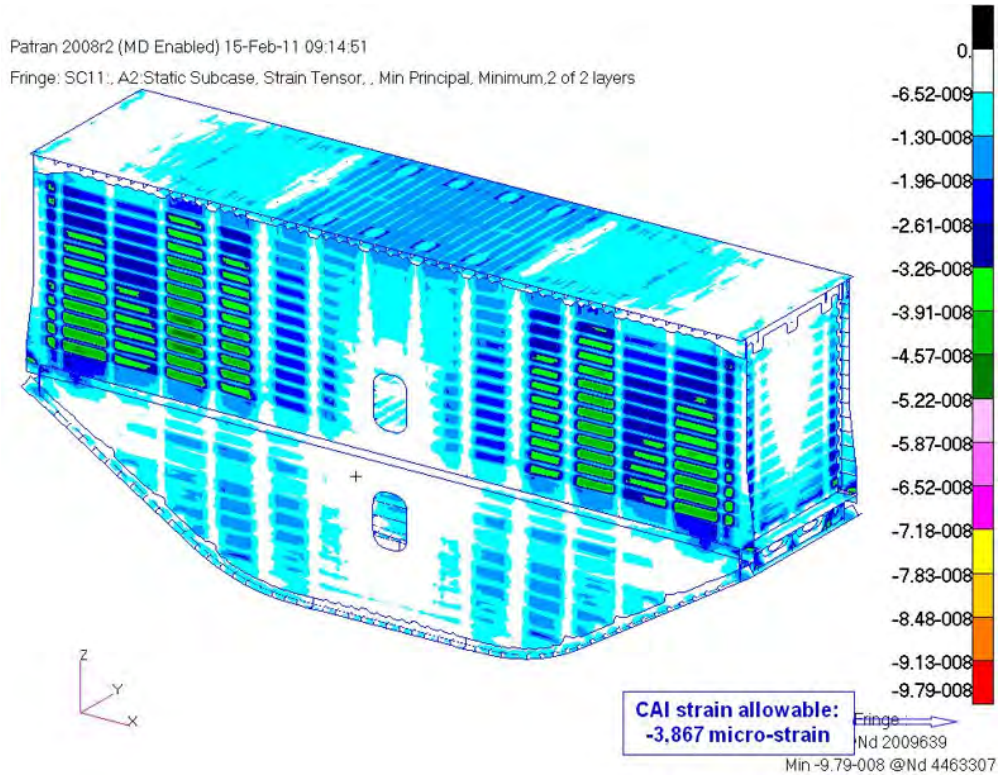

Figure 4-46. Minimum Principal Strains on Composite Structures in 1.0-g Weight Condition

4.2.8 Design Allowables

Design values for different structural parts of the MBB are listed in Table 4-7. The design values of composite material were obtained from various previous development programs (Refs. 4-1, 2-1, 2-2, 4-4, and 4-5), and they were derived primarily from testing. Even though most of the composite parts of the MBB were made of the same material (DMS 2436 T1C72), different allowable values were used at different locations based on their TAI, CAI, BVID, repair, and other failure criteria. As shown in Table 4-7, different allowable values were used at different locations in the margin-of-safety calculations. In designing the MBB, notched design values were used for the composites, and yielding strength design values were used for the metal parts. In the MBB design, metallic fittings and fasteners were used to join the composite panels together. To reduce the likelihood of premature failures on the fittings and fasteners, a conservative approach of using yielding strengths as the metallic design values at DUL was adopted. In other words, no yielding was allowed on metallic fittings and fasteners of the MBB at DUL. In addition to design allowable values, Table 4-7 also lists un-notched (pristine) design values for the composites. The un-notched design values were used in the final two-part (catastrophic) failure prediction because (1) the stitching threads of the PRSEUS would provide excellent crack (or failure) arresting capabilities, for initial inter-laminar failures such as delamination, and (2) they would result in a much higher final failure load. From previous tests, it was proven that the final two-part failure loads of stitched composites were much higher than the initial failure loads. In margin-of-safety calculations for composite structures, point strain failure criteria were used. Maximum principal strains were calculated and compared with the design allowable values for tension, and minimum principal strains were calculated and compared with the design allowable values for compression of composite parts. Detailed margin-of-safety results are summarized in Section 4.2.9.

Table 4-7. Composite and Metallic Material Design Values of the MBB

Design Regions	Loading Type	Notched Design Values (micro-in/in)	Un-notched Design Values (micro-in/in)	Strength Design Values (psi)
Skin	Compression	-4,800	-8,000	n.a.
	Tension	5,900	10,000	n.a.
Stringer Web	Compression	-5,800	-8,000	n.a.
	Tension	7,000	10,000	n.a.
Stringer Flange	Compression	-4,800	-8,000	n.a.
	Tension	5,900	10,000	n.a.
Frame & T-cap Web	Compression	-5,800	-8,000	n.a.
	Tension	7,000	10,000	n.a.
Frame & T-cap Flange	Compression	-4,800	-8,000	n.a.
	Tension	5,900	10,000	n.a.
Inter-laminar	Tension	n.a.	n.a.	6,452
Foam Core Rohacell 110WF	Compression	n.a.	n.a.	319
	Tension	n.a.	n.a.	441
	Shear	n.a.	n.a.	253
Fiberglass Garolite G-11	Compression	n.a.	n.a.	32,900
	Tension	n.a.	n.a.	37,000
Aluminum Fitting (Strength Study)	Tension (Yielding)	n.a.	n.a.	41,000 to 70,000*

Design Regions	Loading Type	Notched Design Values (micro-in/in)	Un-notched Design Values (micro-in/in)	Strength Design Values (psi)
Aluminum Fitting (Fastener Study)	Bearing	n.a.	n.a.	105,000
	Pull-through	n.a.	n.a.	48,000
Composite Panel (Fastener Study)	Bearing	n.a.	n.a.	70,000
	Pull-through	n.a.	n.a.	5,230
Titanium Fastener (Fastener Study)	Tension	n.a.	n.a.	160,000
	Shear	n.a.	n.a.	95,000
Inconel Fastener (Fastener Study)	Tension	n.a.	n.a.	220,000
	Shear	n.a.	n.a.	125,000

Note: *Aluminum fittings are made of 7050-T7451, 7075-T6, or 7075-T651.
Their tensile yielding allowables depend on material types and stock sizes

In Table 4-7, the inter-laminar tension strength design value was derived from pressure cube testing (Ref. 4-6), the strength design values of foam core were from the BWB material allowable (Ref. 4-2), and the strength design values of fiberglass were derived from vendor data. Also shown in Table 4-7 are the design values of metallic fittings and fasteners, which were derived from the Military Handbook (MIL-HDBK), Boeing design manual, and vendor data. To be conservative, tensile yield allowables were used as the design values of metallic fittings and fasteners at DULs. The calculated von Mises stresses on each aluminum fitting were compared with the aluminum strength design values, and the axial and shear forces of each bolt were checked for fastener-related failure modes, such as bolt axial tension failure, bolt shear failure, bolt bending failure, composite/metallic panel pull-through failure, and composite/metallic panel bearing failure modes.

4.2.9 Results Summary

The results of strains, stresses, and margins of safety for the composite panels, fittings, and fasteners are documented in this section. These results were compared with the allowable design values presented in Section 4.2.8. Margins of safety of each structural component were calculated, and they are documented in detail here. Results of composite panels, metallic fittings, and fasteners are listed separately in the following sections.

4.2.9.1 Composite Panel Results Summary

A detailed summary of the critical maximum and minimum principal strains is shown in Table 4-8, and a detailed summary of the margins of safety is shown in Table 4-9 for the composite panels. These margins of safety were calculated by comparing the critical maximum and minimum principal strains of the composite parts on each panel with the allowable design values shown in Table 4-7. In Table 4-9, the margins of safety are positive for all composite panels in the MBB. Among all these composite structural parts, there were six critical locations with margins of safety less than or equal to 10%. The maximum or minimum principal strains at these locations are plotted in Figure 4-47 through Figure 4-52. The lowest margin was 2% and was located at the crown stringer web in the 2P pressure condition, as shown in Figure 4-48.

Table 4-8. Summary of Maximum/Minimum Principal Strains (micro-strain) for Composite Panels

Description	2P (DUL)		2.5-g (DLL)		2.5-g + 1P (DLL)		-1.0-g (DLL)		-1.0-g + 1P (DLL)	
Crown	Tension	Comp.	Tension	Comp.	Tension	Comp.	Tension	Comp.	Tension	Comp.
Crown Frame Web	2900	-4030	1100	-2060	1650	-2530	824	-424	1680	-1920
Crown Stringer Web	6360	-5670	1770	-744	4130	-2810	298	-708	2810	-2850
Crown T-caps for Bulkhead	2970	-3070	942	-2810	1910	-2530	1120	-377	1600	-1560
Crown T-caps for Rib	2420	-1640	841	-1600	1990	-1560	641	-337	928	-707
Crown Skin	3810	-2690	1730	-2930	3170	-3030	1170	-691	2130	-1510
Floor	Tension	Comp.	Tension	Comp.	Tension	Comp.	Tension	Comp.	Tension	Comp.
Floor Frame Web	5350	-2410	812	-397	2950	-1170	159	-325	2570	-1400
Floor Stringer Web	3970	-4130	323	-371	1660	-1800	148	-129	2130	-2170
Floor T-caps for Center Rib	1390	-1280	1580	-1390	1600	-1330	554	-631	849	-648
Floor Skin	4810	-4050	1710	-592	2540	-942	237	-685	2410	-2480
Center Keel	Tension	Comp.	Tension	Comp.	Tension	Comp.	Tension	Comp.	Tension	Comp.
Center Keel Frame Web	2270	-3310	733	-356	1440	-1780	143	-293	1150	-2370
Center Keel Stringer Web	5650	-5360	364	-264	2830	-2760	106	-138	2830	-2650
Center Keel T-cap for bulkhead	2190	-2400	926	-327	1230	-1290	131	-370	1140	-1160
Center Keel Skin	4430	-3210	1160	-670	2990	-1550	268	-462	1920	-1910
Side Keel	Tension	Comp.	Tension	Comp.	Tension	Comp.	Tension	Comp.	Tension	Comp.
Side Keel Frame Web	5530	-3210	2510	-860	2860	-891	344	-1000	3080	-2090
Side Keel Stringer Web	4870	-3830	1030	-1150	1760	-1440	460	-416	2710	-2170
Side Keel T-cap for bulkhead	4170	-4080	1330	-1040	1990	-2100	417	-531	2170	-2030
Side Keel T-cap for Rib	2020	-1740	915	-1320	924	-1220	530	-366	1530	-1000
Side Keel Skin	2940	-3810	1970	-1080	1930	-1450	433	-789	1730	-2150
Lower Bulkhead	Tension	Comp.	Tension	Comp.	Tension	Comp.	Tension	Comp.	Tension	Comp.
Lower Bulkhead Frame Web	4150	-3490	611	-1030	1850	-1770	412	-244	2180	-1760
Lower Bulkhead Stringer Web	3130	-4450	1350	-895	1940	-2410	358	-538	1460	-2240
Lower Bulkhead T-cap for Rib	2130	-1050	633	-469	1040	-610	187	-253	1090	-586
Lower Bulkhead Skin	4850	-3890	1610	-820	2810	-2180	328	-643	2500	-2230
Upper Bulkhead	Tension	Comp.	Tension	Comp.	Tension	Comp.	Tension	Comp.	Tension	Comp.
Upper Bulkhead Frame Web	4110	-4860	738	-477	1960	-2540	191	-295	2110	-2470
Upper Bulkhead Stringer Web	5120	-3950	747	-1340	2330	-1970	535	-299	2660	-1990
Upper Bulkhead T-cap for Floor	5130	-2570	1870	-2160	2890	-2130	864	-748	2460	-1600
Upper Bulkhead T-cap for Rib	1850	-1570	848	-714	1010	-834	308	-339	1190	-765
Upper Bulkhead Skin	4210	-3670	1650	-2640	2860	-2960	1060	-660	2430	-1780
Outer Rib	Tension	Comp.	Tension	Comp.	Tension	Comp.	Tension	Comp.	Tension	Comp.
Outer Rib Frame Web	2610	-2720	400	-1720	1540	-2090	687	-160	1220	-1370
Outer Rib Stringer Web	3010	-2930	619	-348	1510	-1420	139	-284	1510	-1490
Outer Rib Skin	3660	-2940	2020	-1840	2300	-2080	736	-808	1740	-1540
Upper Center Rib	2800	-1610	321	-328	1510	-899	131	-129	1380	-772
Lower Center Rib	1740	-939	341	-611	897	-710	244	-136	975	-423

Table 4-9. Summary of Margins of Safety for Composite Panels

Description	2P (DUL)		2.5-g (DUL)		2.5-g + 1P (DUL)		-1.0-g (DUL)		-1.0-g + 1P (DUL)	
Crown	Tension	Comp.	Tension	Comp.	Tension	Comp.	Tension	Comp.	Tension	Comp.
Crown Frame Web	141%	44%	324%	88%	183%	53%	466%	812%	178%	101%
Crown Stringer Web	10%	2%	164%	420%	13%	38%	1466%	446%	66%	36%
Crown T-caps for Bulkhead	136%	89%	395%	38%	144%	53%	317%	926%	192%	148%
Crown T-caps for Rib	189%	254%	455%	142%	135%	148%	628%	1047%	403%	447%
Crown Skin	55%	78%	127%	9%	24%	6%	236%	363%	85%	112%
Floor	Tension	Comp.	Tension	Comp.	Tension	Comp.	Tension	Comp.	Tension	Comp.
Floor Frame Web	31%	141%	475%	874%	58%	230%	2835%	1090%	82%	176%
Floor Stringer Web	76%	40%	1345%	942%	181%	115%	3053%	2897%	119%	78%
Floor T-caps for Center Rib	404%	353%	195%	178%	192%	191%	742%	513%	450%	497%
Floor Skin	23%	19%	130%	441%	55%	240%	1560%	367%	63%	29%
Center Keel	Tension	Comp.	Tension	Comp.	Tension	Comp.	Tension	Comp.	Tension	Comp.
Center Keel Frame Web	208%	75%	537%	986%	224%	117%	3163%	1220%	306%	63%
Center Keel Stringer Web	24%	8%	1182%	1365%	65%	40%	4303%	2702%	65%	46%
Center Keel T-cap for bulkhead	220%	142%	404%	1082%	279%	200%	3462%	945%	309%	233%
Center Keel Skin	33%	50%	239%	378%	32%	106%	1368%	593%	105%	68%
Side Keel	Tension	Comp.	Tension	Comp.	Tension	Comp.	Tension	Comp.	Tension	Comp.
Side Keel Frame Web	27%	81%	86%	350%	63%	334%	1257%	287%	52%	85%
Side Keel Stringer Web	44%	51%	353%	236%	165%	169%	914%	829%	72%	78%
Side Keel T-cap for bulkhead	68%	42%	251%	272%	135%	84%	1019%	628%	115%	90%
Side Keel T-cap for Rib	247%	233%	410%	193%	405%	217%	781%	956%	205%	287%
Side Keel Skin	101%	26%	100%	196%	104%	121%	808%	306%	127%	49%
Lower Bulkhead	Tension	Comp.	Tension	Comp.	Tension	Comp.	Tension	Comp.	Tension	Comp.
Lower Bulkhead Frame Web	69%	66%	664%	275%	152%	118%	1033%	1485%	114%	120%
Lower Bulkhead Stringer Web	124%	30%	246%	332%	141%	60%	1204%	619%	220%	73%
Lower Bulkhead T-cap for Rib	229%	452%	637%	724%	349%	534%	2396%	1428%	328%	560%
Lower Bulkhead Skin	22%	23%	144%	290%	40%	47%	1099%	398%	57%	43%
Upper Bulkhead	Tension	Comp.	Tension	Comp.	Tension	Comp.	Tension	Comp.	Tension	Comp.
Upper Bulkhead Frame Web	70%	19%	532%	711%	138%	52%	2343%	1211%	121%	57%
Upper Bulkhead Stringer Web	37%	47%	525%	189%	100%	96%	772%	1193%	75%	94%
Upper Bulkhead T-cap for Floor	36%	126%	150%	79%	61%	82%	440%	417%	90%	142%
Upper Bulkhead T-cap for Rib	278%	269%	450%	442%	362%	364%	1415%	1041%	292%	405%
Upper Bulkhead Skin	40%	31%	138%	21%	38%	8%	271%	385%	62%	80%
Outer Rib	Tension	Comp.	Tension	Comp.	Tension	Comp.	Tension	Comp.	Tension	Comp.
Outer Rib Frame Web	168%	113%	1067%	125%	203%	85%	579%	2317%	283%	182%
Outer Rib Stringer Web	133%	98%	654%	1011%	209%	172%	3257%	1262%	209%	160%
Outer Rib Skin	61%	63%	95%	74%	71%	54%	434%	296%	126%	108%
Upper Center Rib	72%	125%	899%	637%	112%	169%	2348%	1773%	132%	213%
Lower Center Rib	176%	286%	1053%	424%	338%	351%	1512%	2253%	303%	657%

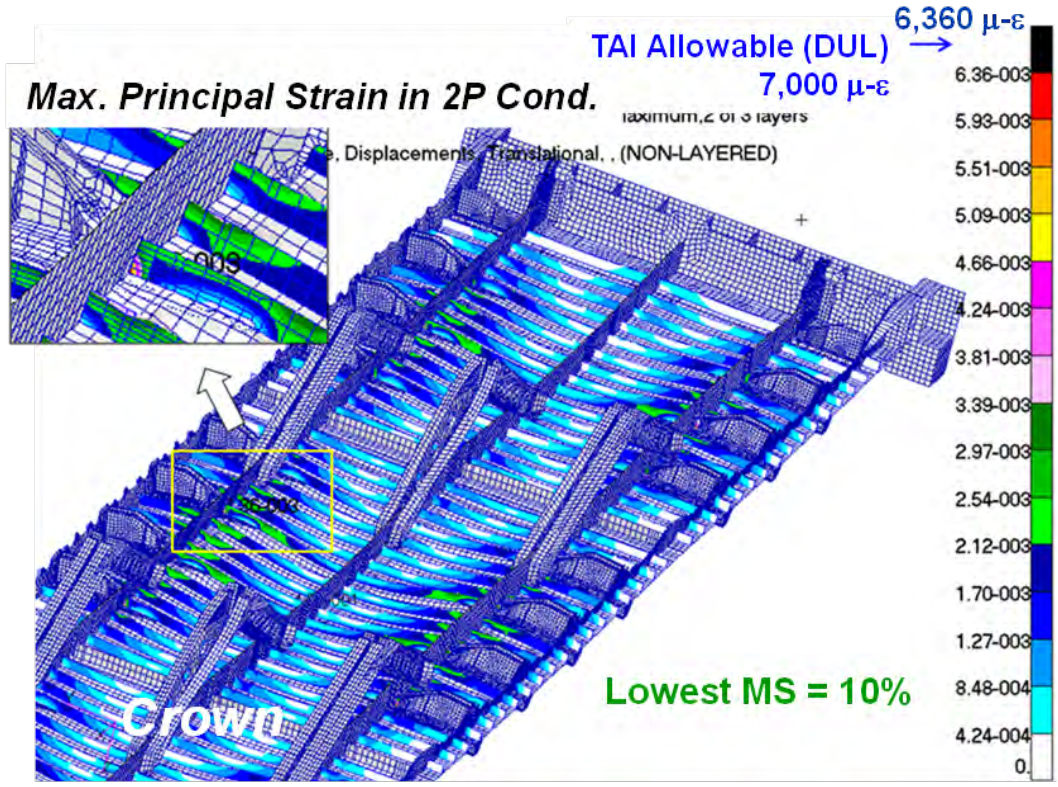

Figure 4-47. Maximum Principal Strains on Crown Stringer Web in 2P Condition

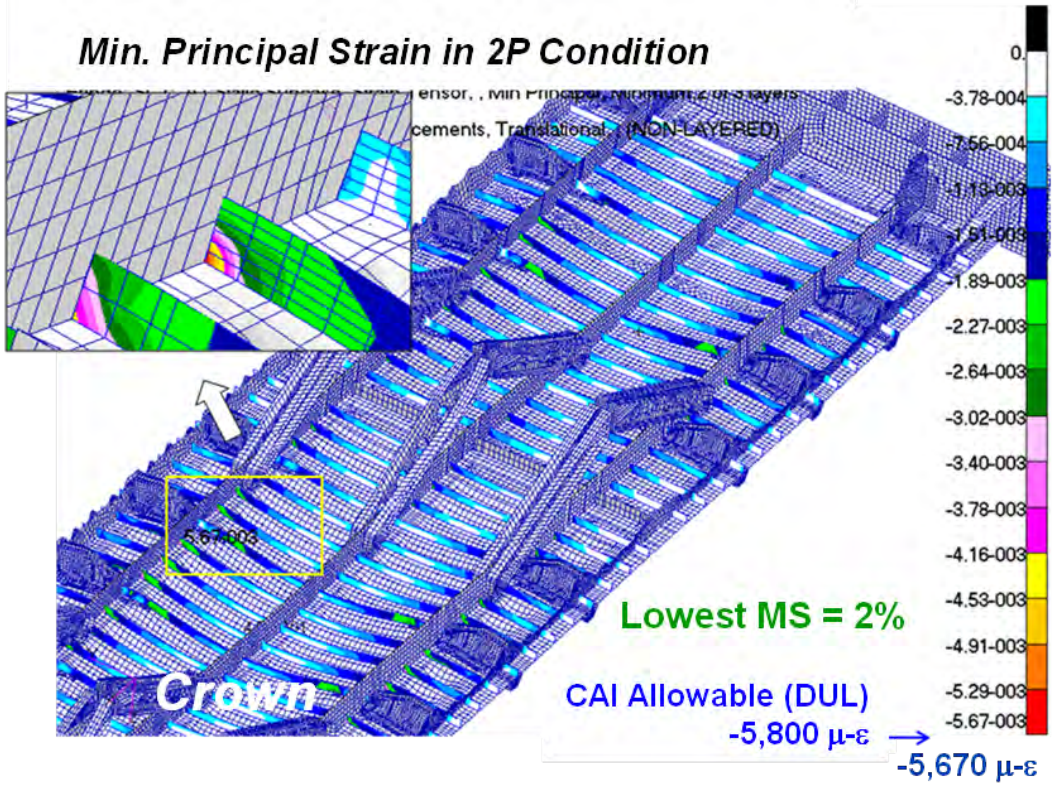

Figure 4-48. Minimum Principal Strains on Crown Stringer Web in 2P Condition

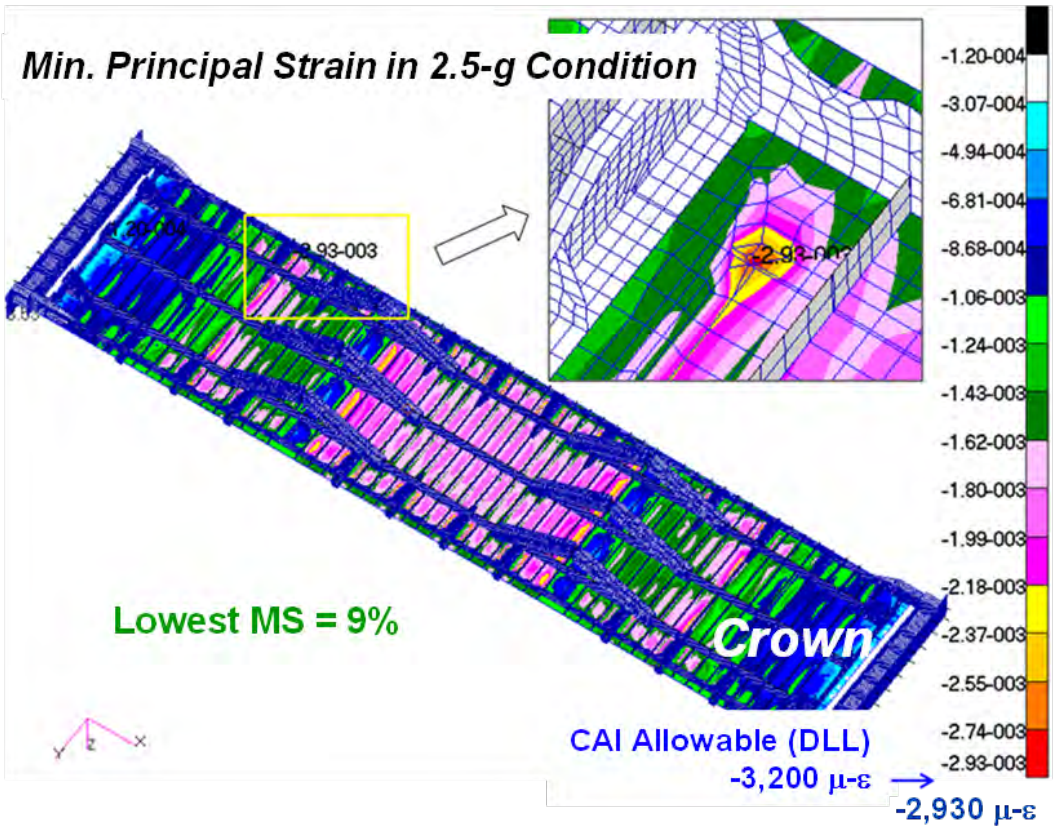

Figure 4-49. Minimum Principal Strain on Crown Skin in 2.5-g Condition

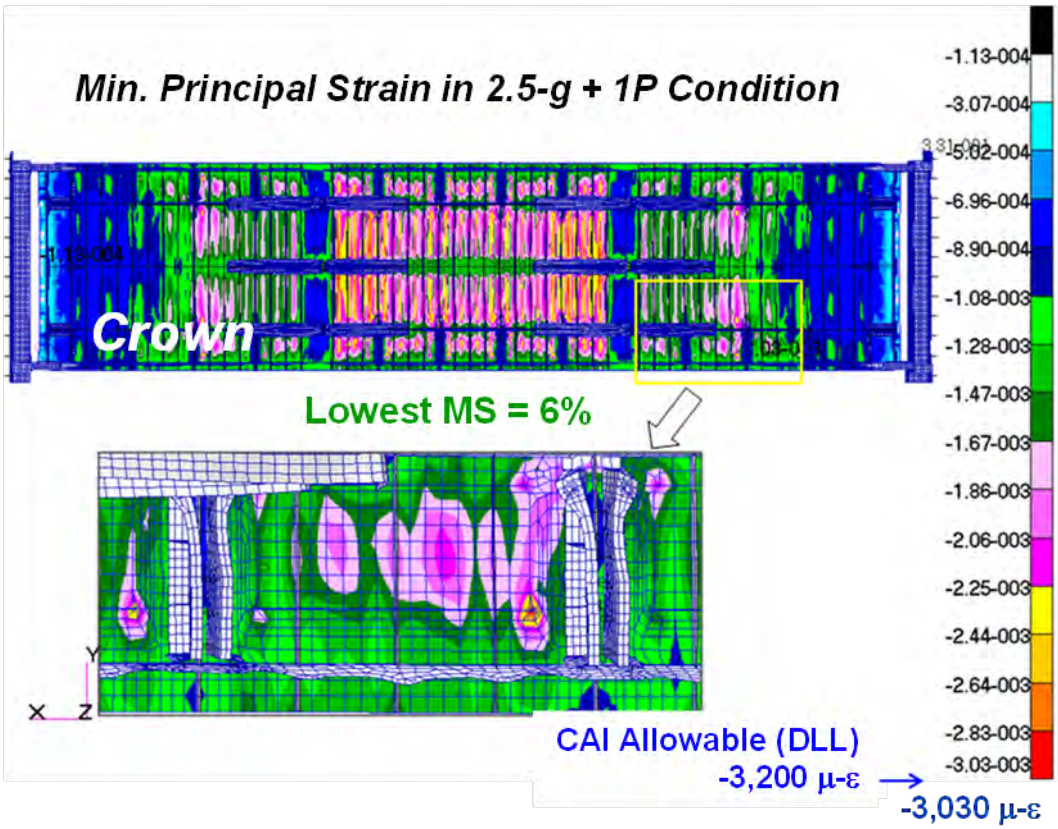

Figure 4-50. Minimum Principal Strain on Crown Skin in 2.5-g + 1P Condition

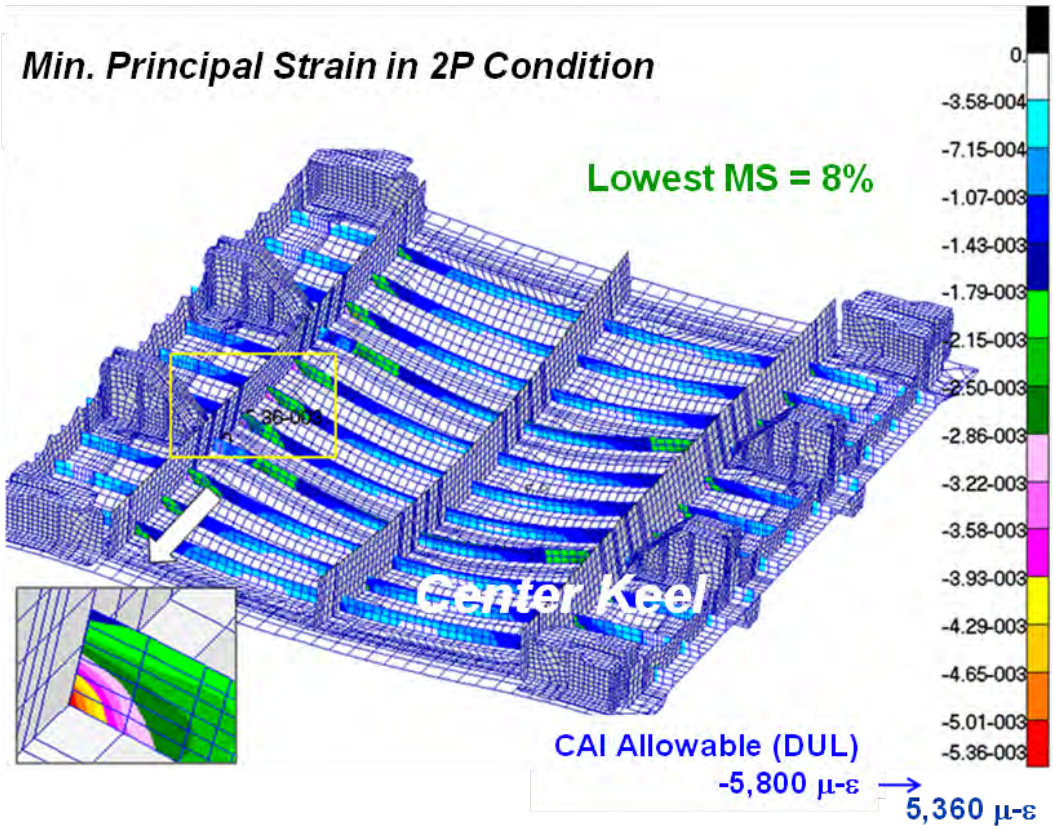

Figure 4-51. Minimum Principal Strain on Center Keel Stringer Web in 2P Condition

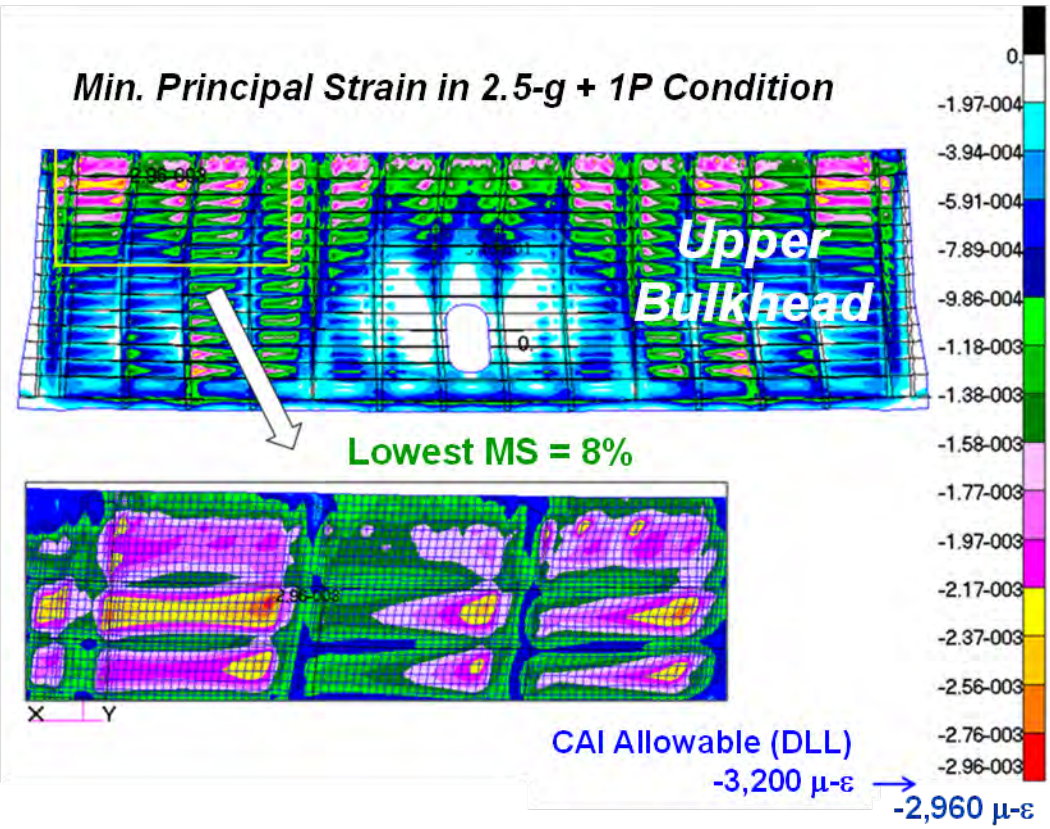

Figure 4-52. Minimum Principal Strain on Upper Bulkhead Skin in 2.5-g + 1P Condition

4.2.9.2 Metallic Fitting Results Summary

Critical von Mises stresses for the metallic fittings are shown in Table 4-10 and Table 4-11, and the corresponding margins of safety are shown in Table 12 and Table 13. These margins of safety were calculated by comparing the critical von Mises stresses of the metallic fittings with the metallic strength design values. In Table 12 and Table 13, the margins of safety are positive for all metallic fittings. There were five locations with margins of safety less than or equal to 10%. The lowest margin was 1.8% on the Bulkhead Frame to Canted Stringer no. 18 Fittings (ZJ153664-505) that connected to the lower bulkhead frame and canted stringer no. 18 of the side keel in the 2P pressure condition, as shown in Figure 4-53.

Table 4-10. Summary of Maximum von Mises Stresses (ksi) for Metallic Fittings (Part 1 of 2)

Description	Part No.	2P (DUL)	2.5-g (DLL)	2.5-g + 1P (DLL)	-1.0-g (DLL)	-1.0-g + 1P (DLL)	Allowable (ksi) DUL	DLL
Upper Test Adapter Box	ZJ153343-1/-2	1.27	16.8	17.1	6.72	6.43	41	27.3
Lower Test Adaptor Box	ZJ153344-1/-2	1.54	12.7	12.2	5.07	5.54	41	27.3
Upper OML Load Introduction Fitting	ZJ153345-1	5.29	37.2	38.1	14.9	13.9	64	42.7
Upper IML Load Introduction Fitting	ZJ153346-1/-2	2.93	32.0	32.2	12.8	12.6	62	41.3
	ZJ153346-501/-502	2.26	29.7	29.1	11.9	12.6	64	42.7
	ZJ153346-503/-504	9.94	9.90	11.9	3.96	4.93	64	42.7
	ZJ153346-505/-506	1.53	19.9	20.4	9.75	7.38	64	42.7
Upper IML External Frame Load Intro Fitting	ZJ153347-1	6.61	25.6	25.8	10.2	9.96	62	41.3
Upper IML Internal Frame Load Intro Fitting (outside frames)	ZJ153348-1/-2	10.6	23.6	25.8	9.45	9.98	66	44
Upper IML Internal Frame Load Intro Fitting (Center frame)	ZJ153348-501/-502	38.2	15.4	20.1	6.16	18.7	66	44
Lower OML Load Introduction Fitting	ZJ153650-1	4.04	31.7	31.1	12.7	13.2	65	43.3
Lower IML Load Introduction Fitting	ZJ153651-1	1.41	9.55	9.16	3.82	4.23	66	44
	ZJ153651-501	1.47	24.8	24.3	9.92	10.4	66	44
Lower IML External Frame Load Intro Fitting	ZJ153652-1/-2	2.02	21.0	21.1	8.41	8.38	56	37.3
	ZJ153652-501/-502	5.52	15.2	14.3	6.06	6.90	63	42
Lower IML Internal Frame Load Introduction Fitting (Keel & Floor)	ZJ153653-1/-2	54.1	16.8	27.4	6.71	28.2	66	44
Lower External Side Load Introduction Fitting	ZJ153654-1/-2	13.3	37.7	37.6	15.1	15.7	65	43.3
Mid Continuous Load Introduction Fitting	ZJ153655-1	6.43	21.5	22.4	8.58	7.66	63	42
Mid Discontinuous Load Introduction Fitting	ZJ153656-1/-2	3.06	16.3	15.9	6.53	7.35	63	42
	ZJ153656-501	0.630	25.6	25.7	10.2	10.1	63	42
OML Skin Splice Plate	ZJ153657-1	9.12	10.7	12.0	4.28	4.81	70	46.7
Keel Splice/ Bulkhead Intercostal Fitting (frame to cap)	ZJ153658-1	29.3	15.0	19.9	5.98	14.7	62	41.3
	ZJ153658-501	19.9	7.66	16.1	3.06	10.9	69	46
Keel Cap Flange Splice Plate	ZJ153658-503	9.04	20.0	24.4	7.98	5.42	70	46.7
Keel Cap Splice Fitting	ZJ153658-505	6.20	25.6	27.6	10.2	9.03	63	42
Keel Splice Intercostal Fitting	ZJ153659-1	26.3	8.00	14.5	3.20	12.6	62	41.3
	ZJ153659-501	14.6	9.37	14.5	3.75	7.27	69	46
	ZJ153659-503	46.3	3.09	26.2	1.23	21.9	70	46.7
Bulkhead Frame to Crown Panel Fitting	ZJ153660-1/-2	62.1	7.00	37.4	2.80	29.5	69	46
	ZJ153660-501/-502	17.1	2.97	6.00	1.19	9.70	69	46
Bkhd Frame Splice Fitting	ZJ153662-1/-2	57.5	6.11	27.2	2.44	29.4	69	46
	ZJ153662-501/-502	43.4	5.26	21.1	2.10	22.6	69	46
	ZJ153662-503/-504	66.0	5.48	28.2	2.19	35.1	69	46
	ZJ153662-505/-506	61.9	5.03	29.3	2.01	31.6	69	46
Access Cover, Lower Bulkhead	ZJ153663-1	22.3	8.70	10.8	3.48	12.3	66	44
Access Cover, Upper Bulkhead	ZJ153663-501	16.4	3.14	8.00	1.25	8.34	66	44
Access Cover, Lower Bulkhead w/ Instrumentation Holes	ZJ153663-503	29.2	14.4	15.7	5.78	15.9	66	44

Description	Part No.	2P (DUL)	2.5-g (DLL)	2.5-g + 1P (DLL)	-1.0-g (DLL)	-1.0-g + 1P (DLL)	Allowable (ksi) DUL	DLL
Access Cover, Upper Bulkhead w/ Instrumentation Holes	ZJ153663-505	31.9	3.15	14.4	1.26	16.6	66	44
Bkhd Frame to Canted Stringer #14 Fitting	ZJ153664-1/-2	60.9	16.9	13.8	6.75	37.1	63	42.0
	ZJ153664-501/-502	47.8	16.3	10.9	6.51	30.3	69	46.0
Bkhd Frame to Canted Stringer #18 Fitting	ZJ153664-503/-504	56.5	13.1	19.8	5.23	33.0	63	42.0
	ZJ153664-505/-506	67.8	11.5	22.6	4.62	38.5	69	46.0
Bkhd Frame to Canted Stringer #22 Fitting	ZJ153664-507/-508	34.1	4.51	18.3	1.80	16.6	63	42.0
	ZJ153664-509/-510	39.3	3.49	20.5	1.39	19.4	69	46.0
Bkhd Frame to Stringer #2 Fitting	ZJ153664-511/-512	62.4	1.08	31.1	0.431	31.3	69	46
Lower Center Rib to Side Keel Fitting	ZJ153664-515/-516	19.0	6.39	8.28	2.55	9.97	66	44.0

Table 4-11. Summary of Maximum von Mises Stresses (ksi) for Metallic Fittings (Part 2 of 2)

Description	Part No.	2P (DUL)	2.5-g (DLL)	2.5-g + 1P (DLL)	-1.0-g (DLL)	-1.0-g + 1P (DLL)	Allowable (ksi) DUL	DLL
External Center Keel Stringer Support	ZJ153666-1	62.6	1.64	30.6	0.656	31.6	65	43.3
External Crown Stringer Support	ZJ153666-501	50.1	4.97	30.0	1.99	24.6	65	43.3
Keel Gusset	ZJ153667-1/-2	54.2	14.0	22.4	5.62	29.3	69	46
Wire Clamp Fitting	ZJ153668-1	6.03	3.85	6.04	1.54	2.33	69	46
Crown/ Floor Gusset	ZJ153669-1/-2	50.5	20.2	24.6	8.07	30.8	69	46
	ZJ153669-501/-502	56.5	25.6	29.7	10.2	31.8	69	46
External Bulkhead Cap Load Introduction Fitting	ZJ153901-1/-2	7.66	36.6	37.4	14.6	13.8	63	42
Internal Bulkhead Cap Crown Load Intro Fitting	ZJ153902-1/-2	3.26	15.0	14.1	6.00	6.90	60	40
Bkhd Frame to Floor Cap Clip	ZJ153903-1/-2	59.1	4.43	28.2	1.77	30.1	69	46
	ZJ153903-501/-502	22.2	6.80	17.9	2.72	8.44	69	46.0
Lower Bkhd Skin Splice Strap	ZJ153904-1	14.5	2.33	9.35	0.934	6.57	70	46.7
Floor Skin Back-Up Plate	ZJ153904-501	16.5	5.48	7.22	2.19	8.76	70	46.7
Lower Center Rib Clip	ZJ153905-1/-2	33.1	8.66	7.91	3.46	20.0	65	43
Upper Center Rib Clip	ZJ153905-501/-502	21.8	7.09	17.1	2.84	8.43	69	46
	ZJ153905-503/-504	23.5	6.91	18.7	2.76	9.00	69	46
	ZJ153905-505/-506	34.2	5.16	22.2	2.07	15.0	65	43.3
Outer Rib Frame to Floor Fitting	ZJ153906-1/-2	22.8	13.4	15.6	5.37	11.7	64	42.7
	ZJ153906-501/-502	49.4	13.3	23.1	5.32	25.7	65	43.3
	ZJ153906-503/-504	4.48E-09	1.25E-08	1.31E-08	4.86E-09	5.26E-09	70	46.7
Floor Strut	ZJ153908-1/-2	48.8	7.97	25.4	3.19	24.2	69	46
Floor Corner Fitting – Lower Center Rib	ZJ153909-1/-2	8.55	25.2	24.5	10.1	10.9	70	46.7
Keel Corner Fitting – Lower Center Rib	ZJ153910-1/-2	12.3	3.88	3.91	1.55	7.07	70	46.7
Mid Internal Side Load Introduction Fitting	ZJ153911-1/-2	11.5	17.2	18.9	6.89	5.34	64	42.7
Lower Internal Side Load Introduction Fitting	ZJ153912-1/-2	17.2	12.4	15.6	4.94	6.36	60	40.0

Description	Part No.	2P (DUL)	2.5-g (DLL)	2.5-g + 1P (DLL)	-1.0-g (DLL)	-1.0-g + 1P (DLL)	Allowable (ksi) DUL	DLL
Stringer Shear Fitting (Lower Bkhd Panel)	ZJ153912-501/-502	1.34	4.23	4.79	1.69	1.32	70	46.7
Corner Fitting – Upper Center Rib	ZJ153913-1/-2	14.8	3.58	6.12	1.43	7.96	70	46.7
Lower Center Rib to Side Keel Fitting	ZJ153915-1/-2	29.7	15.1	5.52	6.04	20.7	69	46
	ZJ153915-501/-502	23.2	16.0	4.80	6.39	17.9	69	46
Center Rib to Bulkhead Fitting	ZJ153916-1/-2	34.3	8.98	15.4	3.59	18.1	70	46.7
	ZJ153916-501/-502	33.3	4.62	15.6	1.85	17.1	70	46.7
Center Rib to Crown/Floor Corner Fitting	ZJ153917-1/-2	27.2	14.3	17.7	5.70	12.2	69	46
	ZJ153917-501/-502	40.2	3.48	18.6	1.39	20.7	69	46
Center Rib to Floor Center Fitting	ZJ153918-1/-2	29.0	14.6	7.65	5.85	18.3	65	43.3
Center Rib to Crown Center Fitting	ZJ153918-501/-502	18.3	7.46	15.8	2.98	9.10	69	46
Center Rib to Crown Center Fitting	ZJ153918-503/504	21.8	5.28	16.0	2.11	8.87	69	46
Center Rib to Floor Center Fitting	ZJ153918-505/506	25.2	13.0	4.71	5.20	17.6	65	43.3
Center Rib to Crown Center Fitting	ZJ153918-507/508	37.9	5.76	24.4	2.30	16.8	65	43.3
Upper Center Rib to Floor Fitting (flat side)	ZJ153919-1	33.5	15.4	6.41	6.17	21.5	65	43.3
	ZJ153919-501	40.0	17.6	3.86	7.04	27.0	65	43.3
Coner Strut Fitting - Bulkhead	ZJ153945-1/-2	59.6	6.63	29.3	2.65	30.2	65	43.3
Coner Strut Fitting - Outer Rib	ZJ153945-501/-502	56.0	6.52	27.8	2.61	28.4	65	43.3
Strut, Corner Brace	ZJ153956-1	5461	599	2678	239	2770	7671	5114

Table 12. Summary of Margins of Safety for Metallic Fittings (Part 1 of 2)

Description	Part No.	2P	2.5-g	2.5-g + 1P	-1.0-g	-1.0-g + 1P	Comments
Upper Test Adapter Box	ZJ153343-1/-2	3128%	63%	60%	307%	325%	MS=60% (2.5-g+1P)
Lower Test Adaptor Box	ZJ153344-1/-2	2562%	115%	124%	439%	393%	MS=115% (2.5-g)
Upper OML Load Introduction Fitting	ZJ153345-1	1110%	15%	12%	186%	207%	MS=12% (2.5-g+1P)
Upper IML Load Introduction Fitting	ZJ153346-1/-2	2016%	29%	28%	223%	228%	MS=28% (2.5-g+1P)
	ZJ153346-501/-502	2732%	44%	47%	259%	239%	MS=44% (2.5-g)
	ZJ153346-503/-504	544%	331%	259%	977%	765%	MS=259% (2.5-g+1P)
	ZJ153346-505/-506	4083%	114%	109%	338%	478%	MS=109% (2.5-g+1P)
Upper IML External Frame Load Intro Fitting	ZJ153347-1	838%	61%	60%	305%	315%	MS=60% (2.5-g+1P)
Upper IML Internal Frame Load Intro Fitting (outside frames)	ZJ153348-1/-2	523%	86%	71%	366%	341%	MS=71% (2.5-g+1P)
Upper IML Internal Frame Load Intro Fitting (Center frame)	ZJ153348-501/-502	73%	186%	119%	614%	135%	MS=73% (2P)
Lower OML Load Introduction Fitting	ZJ153650-1	1509%	37%	39%	241%	228%	MS=37% (2.5-g)
Lower IML Load Introduction Fitting	ZJ153651-1	4581%	361%	380%	1052%	940%	MS=361% (2.5-g)
	ZJ153651-501	4390%	77%	81%	344%	323%	MS=77% (2.5-g)
Lower IML External Frame Load Intro Fitting	ZJ153652-1/-2	2672%	78%	77%	344%	346%	MS=77% (2.5-g+1P)
	ZJ153652-501/-502	1041%	176%	194%	593%	509%	MS=176% (2.5-g)

Description	Part No.	2P	2.5-g	2.5-g + 1P	-1.0-g	-1.0-g + 1P	Comments
Lower IML Internal Frame Load Introduction Fitting (Keel & Floor)	ZJ153653-1/-2	22%	162%	61%	556%	56%	MS=22% (2P)
Lower External Side Load Introduction Fitting	ZJ153654-1/-2	389%	15%	15%	187%	176%	MS=15% (2.5-g)
Mid Continuous Load Introduction Fitting	ZJ153655-1	880%	95%	88%	390%	448%	MS=88% (2.5-g+1P)
Mid Discontinuous Load Introduction Fitting	ZJ153656-1/-2	1959%	158%	164%	543%	471%	MS=158% (2.5-g)
	ZJ153656-501	9900%	64%	63%	312%	316%	MS=63% (2.5-g+1P)
OML Skin Splice Plate	ZJ153657-1	668%	336%	289%	990%	870%	MS=289% (2.5-g+1P)
Keel Splice/ Bulkhead Intercostal Fitting (frame to cap)	ZJ153658-1	112%	176%	108%	591%	181%	MS=108% (2.5-g+1P)
	ZJ153658-501	247%	501%	186%	1403%	322%	MS=186% (2.5-g+1P)
Keel Cap Flange Splice Plate	ZJ153658-503	674%	133%	91%	485%	761%	MS=91% (2.5-g+1P)
Keel Cap Splice Fitting	ZJ153658-505	916%	64%	52%	312%	365%	MS=52% (2.5-g+1P)
Keel Splice Intercostal Fitting	ZJ153659-1	136%	417%	185%	1192%	228%	MS=136% (2P)
	ZJ153659-501	373%	391%	217%	1127%	533%	MS=217% (2.5-g+1P)
	ZJ153659-503	51%	1410%	78%	3694%	113%	MS=51% (2P)
Bulkhead Frame to Crown Panel Fitting	ZJ153660-1/-2	11%	557%	23%	1543%	56%	MS=11% (2P)
	ZJ153660-501/-502	304%	1449%	667%	3766%	374%	MS=304% (2P)
Bkhd Frame Splice Fitting	ZJ153662-1/-2	20%	653%	69%	1785%	56%	MS=20% (2P)
	ZJ153662-501/-502	59%	775%	118%	2090%	104%	MS=59% (2P)
	ZJ153662-503/-504	4.5%	739%	63%	2000%	31%	MS=4.5% (2P)
	ZJ153662-505/-506	11%	815%	57%	2189%	46%	MS=11% (2P)
Access Cover, Lower Bulkhead	ZJ153663-1	196%	406%	307%	1164%	258%	MS=196% (2P)
Access Cover, Upper Bulkhead	ZJ153663-501	302%	1301%	450%	3420%	428%	MS=302% (2P)
Access Cover, Lower Bulkhead w/ Instrumentation Holes	ZJ153663-503	126%	206%	180%	661%	177%	MS=126% (2P)
Access Cover, Upper Bulkhead w/ Instrumentation Holes	ZJ153663-505	107%	1297%	206%	3392%	165%	MS=107% (2P)
Bkhd Frame to Canted Stringer #14 Fitting	ZJ153664-1/-2	3.4%	149%	204%	522%	13%	MS=3.4% (2P)
	ZJ153664-501/-502	44%	182%	322%	607%	52%	MS=44% (2P)
Bkhd Frame to Canted Stringer #18 Fitting	ZJ153664-503/-504	12%	221%	112%	703%	27%	MS=12% (2P)
	ZJ153664-505/-506	1.8%	300%	104%	896%	19%	MS=1.8% (2P)
Bkhd Frame to Canted Stringer #22 Fitting	ZJ153664-507/-508	85%	831%	130%	2233%	153%	MS=85% (2P)
	ZJ153664-509/-510	76%	1218%	124%	3209%	137%	MS=76% (2P)
Bkhd Frame to Stringer #2 Fitting	ZJ153664-511/-512	11%	4159%	48%	10573%	47%	MS=11% (2P)
Lower Center Rib to Side Keel Fitting	ZJ153664-515/-516	247%	589%	431%	1625%	341%	MS=247% (2P)

Table 13. Summary of Margins of Safety for Metallic Fittings (Part 2 of 2)

Description	Part No.	2P	2.5-g	2.5-g + 1P	-1.0-g	-1.0-g + 1P	Comments
External Center Keel Stringer Support	ZJ153666-1	3.8%	2542%	42%	6506%	37%	MS=3.8% (2P)
External Crown Stringer Support	ZJ153666-501	30%	772%	44%	2078%	76%	MS=30% (2P)
Keel Gusset	ZJ153667-1/-2	27%	229%	105%	719%	57%	MS=27% (2P)
Wire Clamp Fitting	ZJ153668-1	1044%	1095%	662%	2887%	1874%	MS=662% (2.5-g+1P)
Crown/ Floor Gusset	ZJ153669-1/-2	37%	128%	87%	470%	49%	MS=37% (2P)
	ZJ153669-501/-502	22%	80%	55%	351%	45%	MS=22% (2P)
External Bulkhead Cap Load Introduction Fitting	ZJ153901-1/-2	722%	15%	12%	188%	204%	MS=12% (2.5-g+1P)
Internal Bulkhead Cap Crown Load Intro Fitting	ZJ153902-1/-2	1740%	167%	184%	567%	480%	MS=167% (2.5-g)
Bkhd Frame to Floor Cap Clip	ZJ153903-1/-2	17%	938%	63%	2499%	53%	MS=17% (2P)
	ZJ153903-501/-502	211%	576%	157%	1591%	445%	MS=157% (2.5-g+1P)
Lower Bkhd Skin Splice Strap	ZJ153904-1	383%	1903%	399%	4896%	610%	MS=383% (2P)
Floor Skin Back-Up Plate	ZJ153904-501	324%	752%	546%	2031%	433%	MS=324% (2P)
Lower Center Rib Clip	ZJ153905-1/-2	96%	400%	448%	1152%	117%	MS=96% (2P)
Upper Center Rib Clip	ZJ153905-501/-502	217%	549%	169%	1520%	446%	MS=169% (2.5-g+1P)
	ZJ153905-503/-504	194%	566%	146%	1567%	411%	MS=146% (2.5-g+1P)
	ZJ153905-505/-506	90%	740%	95%	1993%	189%	MS=90% (2P)
Outer Rib Frame to Floor Fitting	ZJ153906-1/-2	181%	218%	174%	695%	265%	MS=174% (2.5-g+1P)
	ZJ153906-501/-502	32%	226%	88%	715%	69%	MS=32% (2P)
	ZJ153906-503/-504	Infinite	Infinite	Infinite	Infinite	Infinite	MS=Infinite (2.5-g+1P)
Floor Strut	ZJ153908-1/-2	41%	477%	81%	1342%	90%	MS=41% (2P)
Floor Corner Fitting – Lower Center Rib	ZJ153909-1/-2	719%	85%	90%	362%	328%	MS=85% (2.5-g)
Keel Corner Fitting – Lower Center Rib	ZJ153910-1/-2	469%	1103%	1094%	2911%	560%	MS=469% (2P)
Mid Internal Side Load Introduction Fitting	ZJ153911-1/-2	457%	148%	126%	519%	699%	MS=126% (2.5-g+1P)
Lower Internal Side Load Introduction Fitting	ZJ153912-1/-2	249%	223%	156%	710%	529%	MS=156% (2.5-g+1P)
Stringer Shear Fitting (Lower Bkhd Panel)	ZJ153912-501/-502	5124%	1003%	874%	2661%	3435%	MS=874% (2.5-g+1P)
Corner Fitting – Upper Center Rib	ZJ153913-1/-2	373%	1204%	663%	3163%	486%	MS=373% (2P)
Lower Center Rib to Side Keel Fitting	ZJ153915-1/-2	132%	205%	733%	662%	122%	MS=122% (-1.0-g+1P)
	ZJ153915-501/-502	197%	188%	858%	620%	157%	MS=157% (-1.0-g+1P)
Center Rib to Bulkhead Fitting	ZJ153916-1/-2	104%	420%	203%	1200%	158%	MS=104% (2P)
	ZJ153916-501/-502	110%	910%	199%	2423%	173%	MS=110% (2P)
Center Rib to Crown/Floor	ZJ153917-1/-2	154%	222%	160%	707%	277%	MS=154% (2P)

Description	Part No.	2P	2.5-g	2.5-g + 1P	-1.0-g	-1.0-g + 1P	Comments
Corner Fitting	ZJ153917-501/-502	72%	1222%	147%	3209%	122%	MS=72% (2P)
Center Rib to Floor Center Fitting	ZJ153918-1/-2	124%	197%	466%	641%	137%	MS=124% (2P)
Center Rib to Crown Center Fitting	ZJ153918-501/-502	277%	517%	191%	1444%	405%	MS=191% (2.5-g+1P)
Center Rib to Crown Center Fitting	ZJ153918-503/504	217%	771%	188%	2080%	419%	MS=188% (2.5-g+1P)
Center Rib to Floor Center Fitting	ZJ153918-505/506	158%	233%	820%	733%	146%	MS=146% (-1.0-g+1P)
Center Rib to Crown Center Fitting	ZJ153918-507/508	72%	652%	78%	1784%	158%	MS=72% (2P)
Upper Center Rib to Floor Fitting (flat side)	ZJ153919-1	94%	181%	576%	602%	102%	MS=94% (2P)
	ZJ153919-501	63%	146%	1023%	516%	60%	MS=60% (-1.0-g+1P)
Coner Strut Fitting - Bulkhead	ZJ153945-1/-2	9.1%	554%	48%	1535%	43%	MS=9.1% (2P)
Coner Strut Fitting - Outer Rib	ZJ153945-501/-502	16%	565%	56%	1560%	53%	MS=16% (2P)
Strut, Corner Brace	ZJ153956-1	40%	754%	91%	2040%	85%	MS=40% (2P)

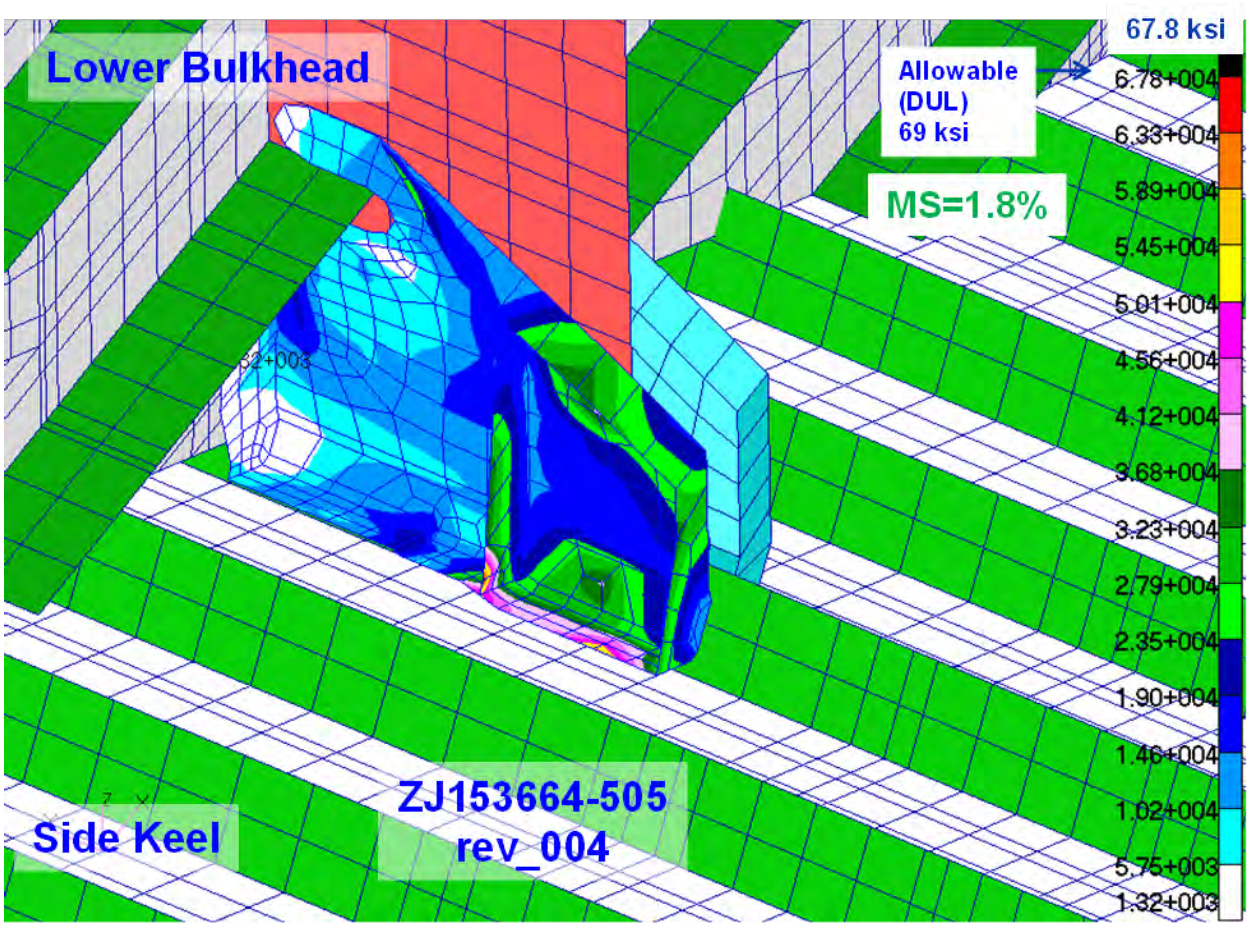

Figure 4-53. Critical von Mises Stresses on ZJ153664-505 in 2P Condition

4.2.9.3 Fastener Results Summary

In this section, margins of safety are summarized for the critical bolts in accordance with their fastener-related failure modes. These failure modes were bolt axial tension failure, bolt shear failure, bolt bending failure, composite/metallic panel pull-through failure, and composite/metallic panel bearing failure modes. Margins of safety were calculated in all five critical load cases, and it was found that the 2P pressure condition was the most critical case in the fastener-related failure calculations. Similar to the margin-of-safety summaries for composite panels and metallic fittings, fasteners with margins greater than 10% are not discussed in this report.

Margins of safety in bolt shear failure calculations were all found to be greater than 10% and are not shown here. The margins of safety in bolt axial tension failure were found to be mostly greater than 10%. The lowest margins were at the locations of two bolts on the External Crown Fitting (ZJ153660-1), which had margins of safety equal to 6% and 8%, respectively, in the 2P pressure condition. To increase the margins of these bolts, higher strength tension bolts were used instead of the shear bolts specified in the baseline design of the MBB. Using high-strength tension-bolts, the margins of safety became greater than 10%. Locations of these fasteners and detailed margin-of-safety results are shown in Figure 4-54.

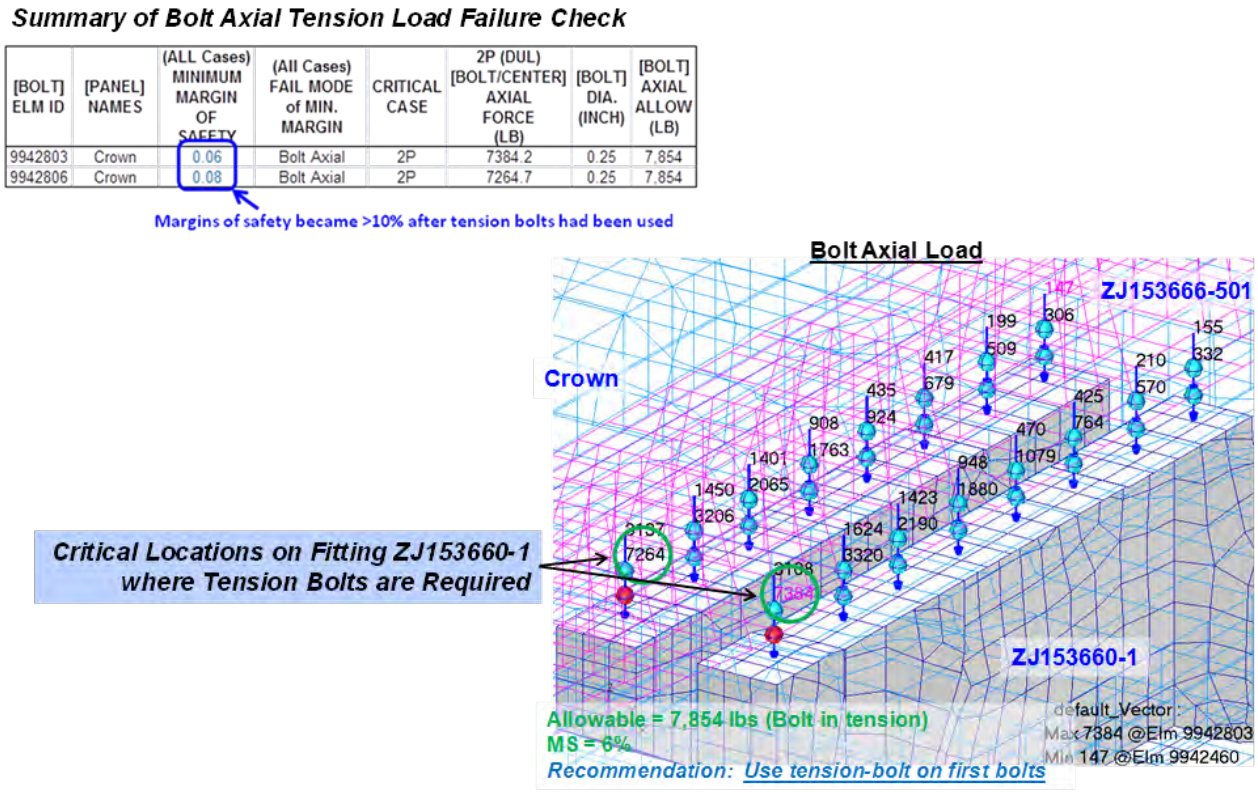

Figure 4-54. Fastener Axial Tension Failure Results on the Crown

The margins of safety in composite/metallic panel pull-through failure calculations were found to be mostly greater than 10%. The lowest margins were at the locations of four locations on the MBB in the 2P pressure condition. To increase margins at these four locations, washers were added to increase the footprint of the transverse shear on composite, and therefore increase the pull-through strengths of the composite panels. The four locations are listed below.

1. Corner-Strut Fitting for Bulkhead (ZJ153945-1)—In the four corners of the upper bulkheads and outer ribs of the MBB, washers were added to the outside of the upper bulkhead panels on the five middle fittings, as shown in Figure 4-55. Without washers, margins of safety ranged from 1 to 9%. After adding washers to the outside of the upper bulkhead panels, margins of safety became greater than 10%.
2. External Center Keel Stringer Support Fitting (ZJ153666-1)—Washers were added to the inside of the center keel panel, as shown in Figure 4-56. Without washers, margins of safety ranged from -18 to -20%. After adding washers to the inside of the center keel panel, margins of safety became greater than 10%.
3. Bulkhead Frame to Side Keel Canted Stringer Fittings (ZJ153664-1/-501/-503/-505/-507/-509)—Washers were added to the outside of the side keel panel, as shown in Figure 4-57. Without washers, margins of safety ranged from -11 to -57%. After adding washers to the outside of the side keel panel, margins of safety became greater than 10%.
4. Bulkhead Frame to Crown Fitting (ZJ153660-1)—Without washers, the margin of safety was 9%. Because the margin of safety was so close to 10%, it was decided that washers would not be added at this location. Locations of these fasteners and detailed margins of safety results are shown in Figure 4-58.

Summary of Composite Panel Pull-Thru Check on Upper Bulkhead

[BOLT] ELM ID	[PANEL] NAMES	(ALL Cases) MINIMUM MARGIN OF SAFETY	(All Cases) FAIL MODE of MIN. MARGIN	CRITICAL CASE	2P (DUL) [BOLT/CENTER] AXIAL FORCE (LB)	[BOLT] DIA. (INCH)	[BOLT] PROTRUDED/ COUNTERSINK	[PANEL] MATERIAL TYPES	[PANEL] THICKNESS (INCH)	[PANEL] PULL-THRU ALLOW (LB)
9946521	Blkhd_Up	0.01	Panel Pull-Thru	2P	1843.6	0.1875	PRTD	COMP	0.364	1,866
9946520	Blkhd_Up	0.01	Panel Pull-Thru	2P	1842.1	0.1875	PRTD	COMP	0.364	1,866
9946510	Blkhd_Up	0.01	Panel Pull-Thru	2P	1841.5	0.1875	PRTD	COMP	0.364	1,866
9946565	Blkhd_Up	0.01	Panel Pull-Thru	2P	1841.8	0.1875	PRTD	COMP	0.364	1,866
9946532	Blkhd_Up	0.02	Panel Pull-Thru	2P	1836.6	0.1875	PRTD	COMP	0.364	1,866
9946609	Blkhd_Up	0.02	Panel Pull-Thru	2P	1835.1	0.1875	PRTD	COMP	0.364	1,866
9946499	Blkhd_Up	0.02	Panel Pull-Thru	2P	1834.1	0.1875	PRTD	COMP	0.364	1,866
9946576	Blkhd_Up	0.02	Panel Pull-Thru	2P	1834.4	0.1875	PRTD	COMP	0.364	1,866
9946522	Blkhd_Up	0.02	Panel Pull-Thru	2P	1824.9	0.1875	PRTD			
9946566	Blkhd_Up	0.02	Panel Pull-Thru	2P	1822.6	0.1875	PRTD			
9946621	Blkhd_Up	0.02	Panel Pull-Thru	2P	1822.5	0.1875	PRTD			
9946511	Blkhd_Up	0.02	Panel Pull-Thru	2P	1821.5	0.1875	PRTD			
9946533	Blkhd_Up	0.03	Panel Pull-Thru	2P	1814.5	0.1875	PRTD			
9946610	Blkhd_Up	0.03	Panel Pull-Thru	2P	1812	0.1875	PRTD			
9946577	Blkhd_Up	0.03	Panel Pull-Thru	2P	1811.8	0.1875	PRTD			
9946500	Blkhd_Up	0.03	Panel Pull-Thru	2P	1810.7	0.1875	PRTD			
9946520	Blkhd_Up	0.03	Panel Pull-Thru	2P	1806.1	0.1875	PRTD			
9946619	Blkhd_Up	0.03	Panel Pull-Thru	2P	1804.9	0.1875	PRTD			
9946509	Blkhd_Up	0.03	Panel Pull-Thru	2P	1804.8	0.1875	PRTD			
9946564	Blkhd_Up	0.03	Panel Pull-Thru	2P	1804.7	0.1875	PRTD			
9946531	Blkhd_Up	0.04	Panel Pull-Thru	2P	1802.6	0.1875	PRTD			
9946608	Blkhd_Up	0.04	Panel Pull-Thru	2P	1801.4	0.1875	PRTD			
9946496	Blkhd_Up	0.04	Panel Pull-Thru	2P	1800.9	0.1875	PRTD			
9946575	Blkhd_Up	0.04	Panel Pull-Thru	2P	1800.8	0.1875	PRTD			
9946523	Blkhd_Up	0.07	Panel Pull-Thru	2P	1748.3	0.1875	PRTD			
9946622	Blkhd_Up	0.07	Panel Pull-Thru	2P	1745.6	0.1875	PRTD			
9946567	Blkhd_Up	0.07	Panel Pull-Thru	2P	1745.4	0.1875	PRTD			
9946512	Blkhd_Up	0.07	Panel Pull-Thru	2P	1742.8	0.1875	PRTD			
9946534	Blkhd_Up	0.08	Panel Pull-Thru	2P	1735	0.1875	PRTD			
9946611	Blkhd_Up	0.08	Panel Pull-Thru	2P	1732.2	0.1875	PRTD			
9946578	Blkhd_Up	0.08	Panel Pull-Thru	2P	1731.7	0.1875	PRTD			
9946501	Blkhd_Up	0.08	Panel Pull-Thru	2P	1729	0.1875	PRTD			
9946530	Blkhd_Up	0.09	Panel Pull-Thru	2P	1712.7	0.1875	PRTD			
9946607	Blkhd_Up	0.09	Panel Pull-Thru	2P	1711.7	0.1875	PRTD			
9946519	Blkhd_Up	0.09	Panel Pull-Thru	2P	1712.6	0.1875	PRTD			
9946618	Blkhd_Up	0.09	Panel Pull-Thru	2P	1711.6	0.1875	PRTD			
9946508	Blkhd_Up	0.09	Panel Pull-Thru	2P	1711.3	0.1875	PRTD			
9946563	Blkhd_Up	0.09	Panel Pull-Thru	2P	1711.2	0.1875	PRTD			
9946497	Blkhd_Up	0.09	Panel Pull-Thru	2P	1710.9	0.1875	PRTD			
9946574	Blkhd_Up	0.09	Panel Pull-Thru	2P	1711	0.1875	PRTD			

Margins of safety became >10% after washers had been used

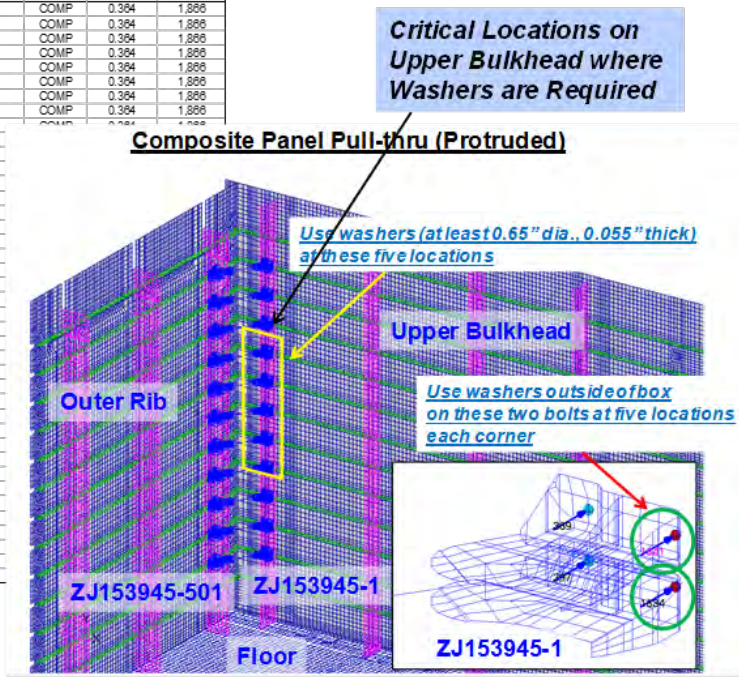

Figure 4-55. Composite Panel Pull-Through Failure Results on the Upper Bulkheads

Summary of Composite Panel Pull-Thru Check on Center Keel

[BOLT] ELM ID	[PANEL] NAMES	(ALL Cases) MINIMUM MARGIN OF SAFETY	(All Cases) FAIL MODE of MIN. MARGIN	CRITICAL CASE	2P (DUL) [BOLT/CENTER] AXIAL FORCE (LB)	[BOLT] DIA. (INCH)	[BOLT] PROTRUDED/ COUNTERSINK	[PANEL] MATERIAL TYPES	[PANEL] THICKNESS (INCH)	[PANEL] PULL-THRU ALLOW (LB)
9943012	Keel_Ctr	-0.20	Panel Pull-Thru	2P	995.3	0.1875	PRTD	COMP	0.156	800
9943009	Keel_Ctr	-0.18	Panel Pull-Thru	2P	978	0.1875	PRTD	COMP	0.156	800

Margins of safety became >10% after washers had been used

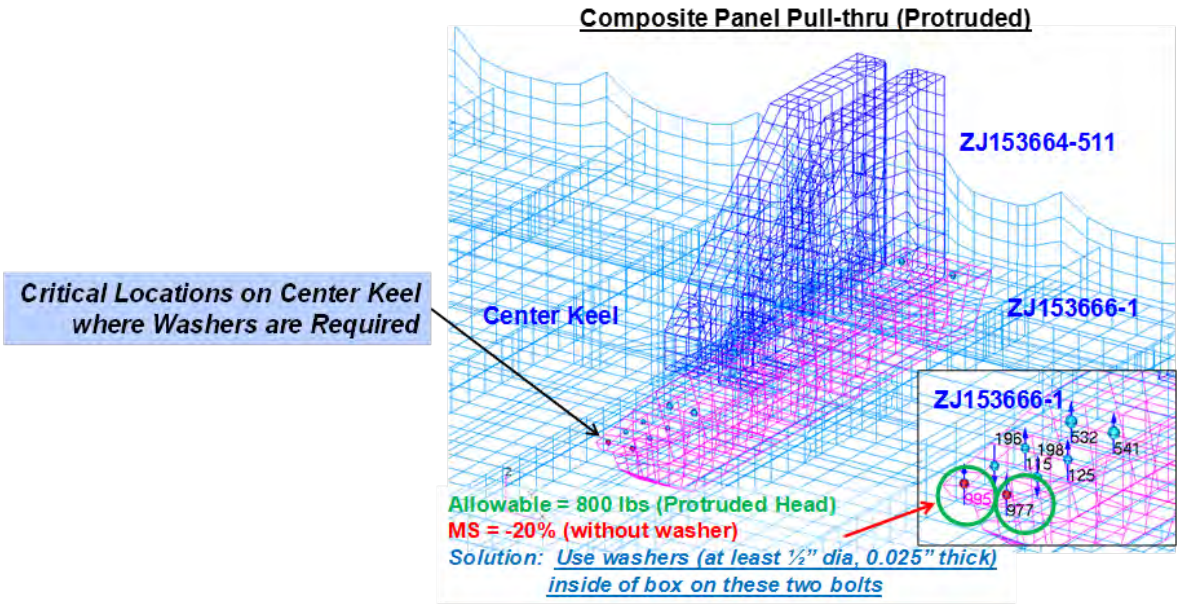

Figure 4-56. Composite Panel Pull-Through Failure Results on the Center Keel

Summary of Composite Panel Pull-Thru Check on Side Keel

[BOLT] ELM ID	[PANEL] NAMES	(ALL Cases) MINIMUM MARGIN OF SAFETY	(All Cases) FAIL MODE of MIN. MARGIN	CRITICAL CASE	2P (DUL) [BOLT/CENTER] AXIAL FORCE (LB)	[BOLT] DIA. (INCH)	[BOLT] PROTRUDED/ COUNTERSINK	[PANEL] MATERIAL TYPES	[PANEL] THICKNESS (INCH)	[PANEL] PULL-THRU ALLOW (LB)
9931482	Keel_Side	-0.57	Panel Pull-Thru	2P	4566.3	0.25	CSK	COMP	0.312	1,949
9931474	Keel_Side	-0.57	Panel Pull-Thru	2P	4559.4	0.25	CSK	COMP	0.312	1,949
9931490	Keel_Side	-0.57	Panel Pull-Thru	2P	4565	0.25	CSK	COMP	0.312	1,949
9931466	Keel_Side	-0.57	Panel Pull-Thru	2P	4561.5	0.25	CSK	COMP	0.312	1,949
9931587	Keel_Side	-0.47	Panel Pull-Thru	2P	3685.1	0.25	CSK	COMP	0.312	1,949
9931579	Keel_Side	-0.47	Panel Pull-Thru	2P	3684.6	0.25	CSK	COMP	0.312	1,949
9931603	Keel_Side	-0.47	Panel Pull-Thru	2P	3680.2	0.25	CSK	COMP	0.312	1,949
9931595	Keel_Side	-0.47	Panel Pull-Thru	2P	3680	0.25	CSK	COMP	0.312	1,949
9931703	Keel_Side	-0.35	Panel Pull-Thru	2P	2983.1	0.25	CSK	COMP	0.312	1,949
9931687	Keel_Side	-0.35	Panel Pull-Thru	2P	2978.6	0.25	CSK	COMP	0.312	1,949
9931694	Keel_Side	-0.34	Panel Pull-Thru	2P	2968.7	0.25	CSK	COMP	0.312	1,949
9931679	Keel_Side	-0.34	Panel Pull-Thru	2P	2943.2	0.25	CSK	COMP	0.312	1,949
9931041	Keel_Side	-0.33	Panel Pull-Thru	2P	2906.7	0.25	CSK	COMP	0.312	1,949
9931057	Keel_Side	-0.33	Panel Pull-Thru	2P	2903.8	0.25	CSK	COMP	0.312	1,949
9931049	Keel_Side	-0.32	Panel Pull-Thru	2P	2872.5	0.25	CSK	COMP	0.312	1,949
9931036	Keel_Side	-0.32	Panel Pull-Thru	2P	2871.7	0.25	CSK	COMP	0.312	1,949
9931786	Keel_Side	-0.16	Panel Pull-Thru	2P	2315.1	0.25	CSK	COMP	0.312	1,949
9931802	Keel_Side	-0.16	Panel Pull-Thru	2P	2309.9	0.25	CSK	COMP	0.312	1,949
9931779	Keel_Side	-0.16	Panel Pull-Thru	2P	2307.1	0.25	CSK	COMP	0.312	1,949
9931794	Keel_Side	-0.16	Panel Pull-Thru	2P	2306.4	0.25	CSK	COMP	0.312	1,949
9931152	Keel_Side	-0.11	Panel Pull-Thru	2P	2198.6	0.25	CSK	COMP	0.312	1,949
9931168	Keel_Side	-0.11	Panel Pull-Thru	2P	2196.9	0.25	CSK	COMP	0.312	1,949
9931145	Keel_Side	-0.11	Panel Pull-Thru	2P	2181.3	0.25	CSK	COMP	0.312	1,949
9931160	Keel_Side	-0.11	Panel Pull-Thru	2P	2177.7	0.25	CSK	COMP	0.312	1,949

Margins of safety became >10% after washers had been used

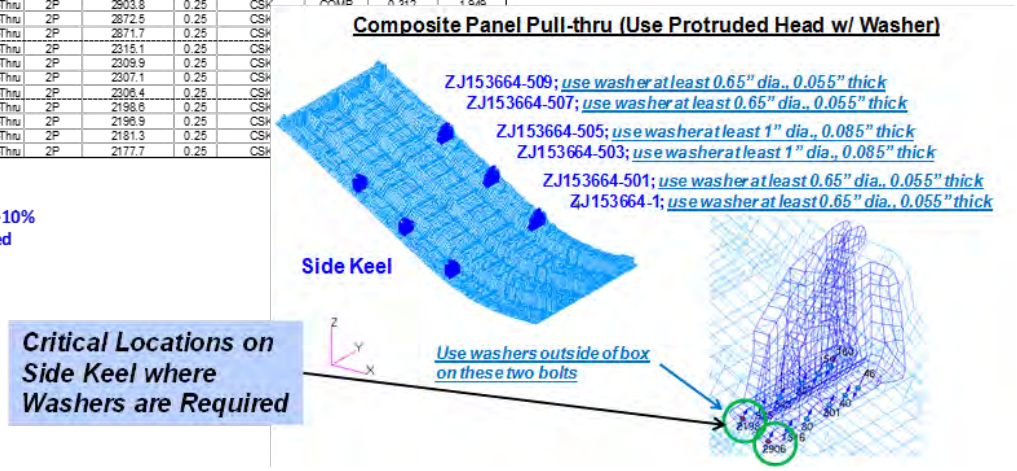

Figure 4-57. Composite Panel Pull-Through Failure Results on the Side Keels

Summary of Composite Panel Pull-Thru Check on Crown

[BOLT] ELM ID	[PANEL] NAMES	(ALL Cases) MINIMUM MARGIN OF SAFETY	(All Cases) FAIL MODE of MIN. MARGIN	CRITICAL CASE	2P (DUL) [BOLT/CENTER] AXIAL FORCE (LB)	[BOLT] DIA. (INCH)	[BOLT] PROTRUDED/ COUNTERSINK	[PANEL] MATERIAL TYPES	[PANEL] THICKNESS (INCH)	[PANEL] PULL-THRU ALLOW (LB)
9942133	Crown	0.09	Panel Pull-Thru	2P	733.5	0.1875	PRTD	COMP	0.156	800

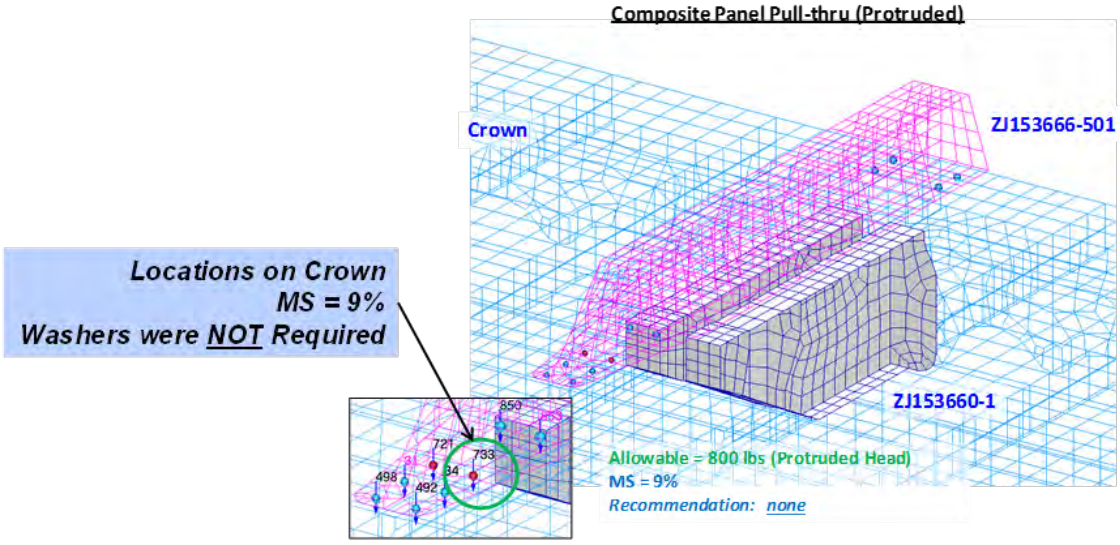

Figure 4-58. Composite Panel Pull-Through Failure Results on the Crown

Margins of safety in the composite/metallic panel bearing failure calculations were found to be mostly greater than 10%. The lowest margins were at the locations of two bolts on the Bulkhead Frame Splice Fitting (ZJ153662-503) and the Bulkhead Frame to Floor Cap Clip Fitting (ZJ153903-1). In those locations, the floor panel had margins of safety ranging from 4 to 10% in the 2P pressure condition. To increase the margins of safety of the critical bolts, diameters of the two adjacent fasteners were increased to draw more shear loads to the adjacent fasteners and reduce shear loads on the critical fasteners. After increasing fastener size on the two adjacent fasteners, the margins of safety of all fasteners became greater than 10%. Locations of these fasteners and detailed margin-of-safety results are shown in Figure 4-59.

Summary of Composite Panel Bearing Failure Check on Floor

[BOLT] ELM ID	[PANEL] NAMES	(ALL Cases) MINIMUM MARGIN OF SAFETY	(All Cases) FAIL MODE of MIN. MARGIN	CRITICAL CASE	2P (DUL) [NODAL/PANEL] SHEAR RESULTANT (LB)	[BOLT] DIA. (INCH)	[PANEL] MATERIAL TYPES	[PANEL] THICKNESS (INCH)	[PANEL] BEARING ALLOW (LB)
9928729	Floor	0.04	Panel Bearing	2P	4382.4	0.25	COMP	0.26	4,550
9943581	Floor	0.04	Panel Bearing	2P	4382.4	0.25	COMP	0.26	4,550
9928841	Floor	0.05	Panel Bearing	2P	4349	0.25	COMP	0.26	4,550
9943533	Floor	0.05	Panel Bearing	2P	4349	0.25	COMP	0.26	4,550
9928737	Floor	0.10	Panel Bearing	2P	4135.7	0.25	COMP	0.26	4,550
9943573	Floor	0.10	Panel Bearing	2P	4135.7	0.25	COMP	0.26	4,550

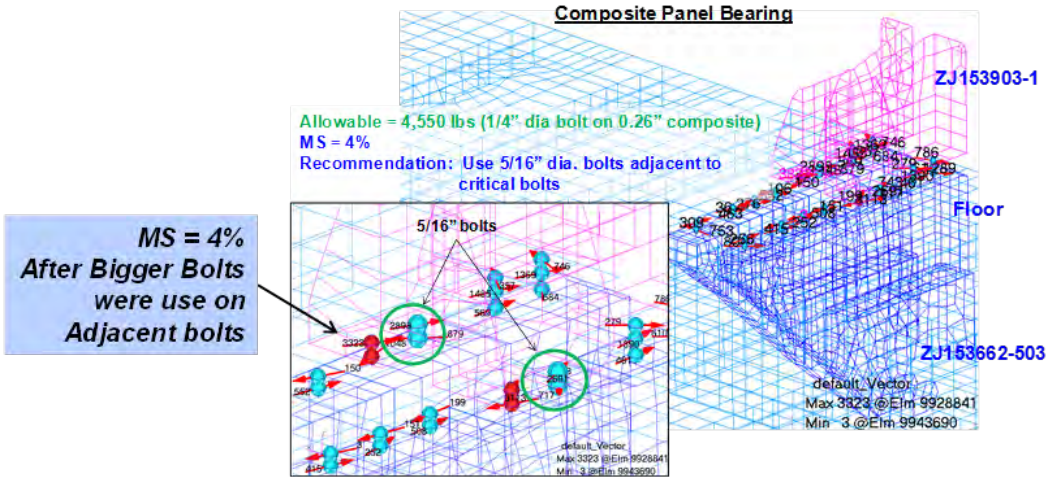

Figure 4-59. Composite Panel Bearing Failure Results on the Floor

Margins of safety for fasteners in the bending failure mode were greatly influenced by the shimming thicknesses between fastening panels or plates. Different shimming thicknesses were used at different fastener locations, and the exact shimming thicknesses were not known until final assembly of the MBB. In the analysis of fastener bending failure, a baseline shimming thickness of 0.050 in. was assumed for all fastener locations. Additional margin-of-safety calculations would be performed only when shimming thicknesses greater than 0.050 in. were needed. With shimming thickness of 0.050 in., fasteners that had margins of safety less than 10% were identified, and design changes (such as using higher strength fastener material or increasing bolt size) were implemented for these bolts. After implementing these design changes, margins of safety in fastener bending failure calculations with shimming thickness of 0.050 in. became greater than 10%. Fasteners that required design changes are described below.

On the Bulkhead Frame Splice Fitting (ZJ153662-1), as shown in Figure 4-60, a fastener material change was needed on one of the bolts. In addition, on the other Bulkhead Frame Splice Fittings (ZJ153662-1/-501/-503/-505), as shown in Figure 4-61, some bolts did not require any design change, some bolts required a fastener material change, some bolts required a bigger fastener diameter, and some bolts required both material and diameter changes. On the Bulkhead Frame Splice to Crown Panel Fitting (ZJ153660-1) and the External Crown Stringer Support Fitting (ZJ153666-501), as shown in Figure 4-62, some bolts required a fastener material change and some bolts required both material and diameter changes. The same was true on the Bulkhead Frame to Floor Cap Clip Fitting (ZJ153903-1), as shown in Figure 4-63. On the Bulkhead Frame to Side Keel Canted Stringer Fitting (ZJ153664-503), as shown in Figure 4-64, a fastener material change was needed on one of the bolts. On the Bulkhead Frame to Center Keel Stringer Fitting (ZJ153664-511), as shown in Figure 4-65, a fastener material change was needed on one of the bolts. On the Lower Test Adaptor Box Fitting (ZJ153344-1) and the Lower External Side

Load Introduction Fitting (ZJ153654-10), as shown in Figure 4-66, a fastener material change was needed on one of the bolts.

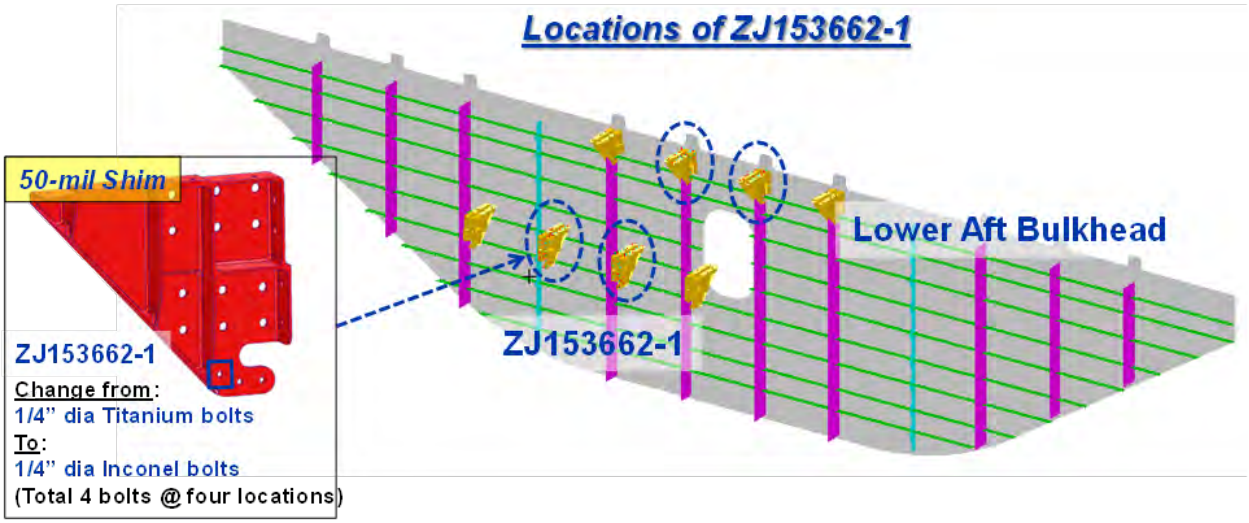

Figure 4-60. Fastener Change on ZJ153662-1 From the Fastener Bending Calculation

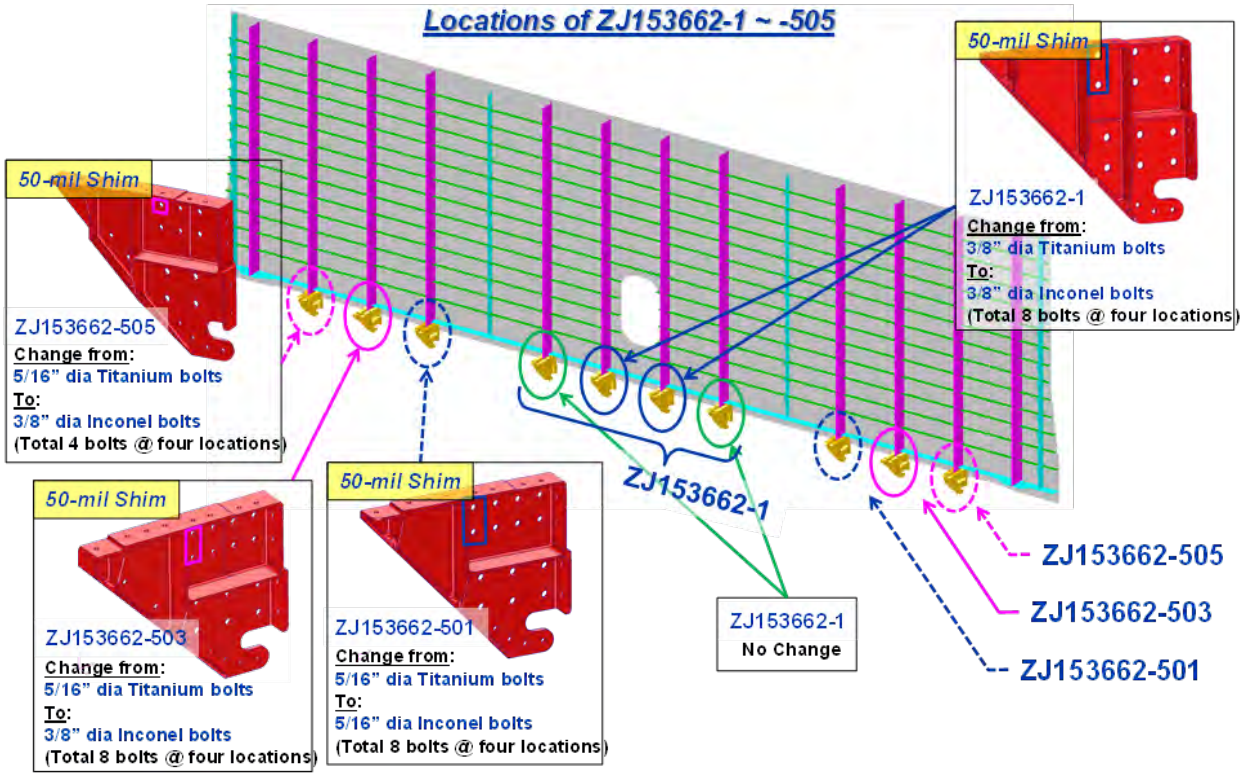

Figure 4-61. Fastener Changes on ZJ153662-1 to -505 From the Fastener Bending Calculation

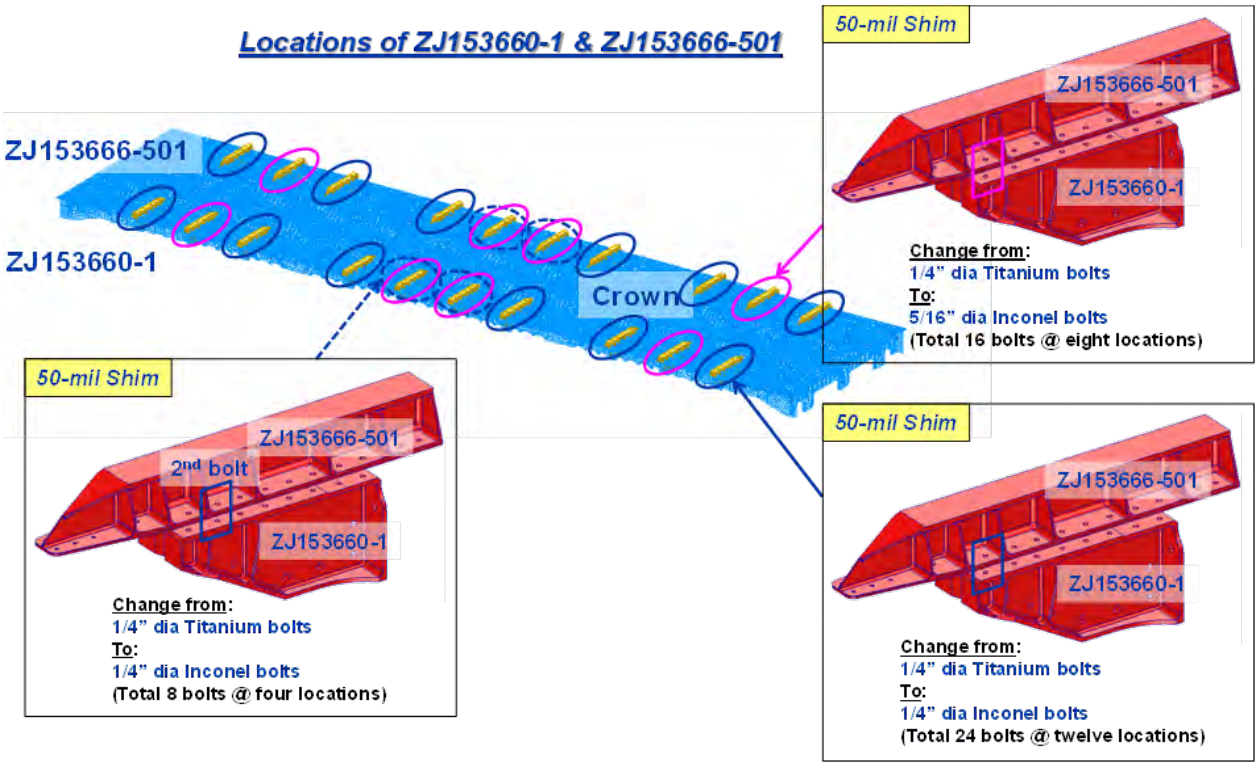

Figure 4-62. Fastener Changes on ZJ153660-1 and ZJ153666-501 From the Fastener Bending Calculation

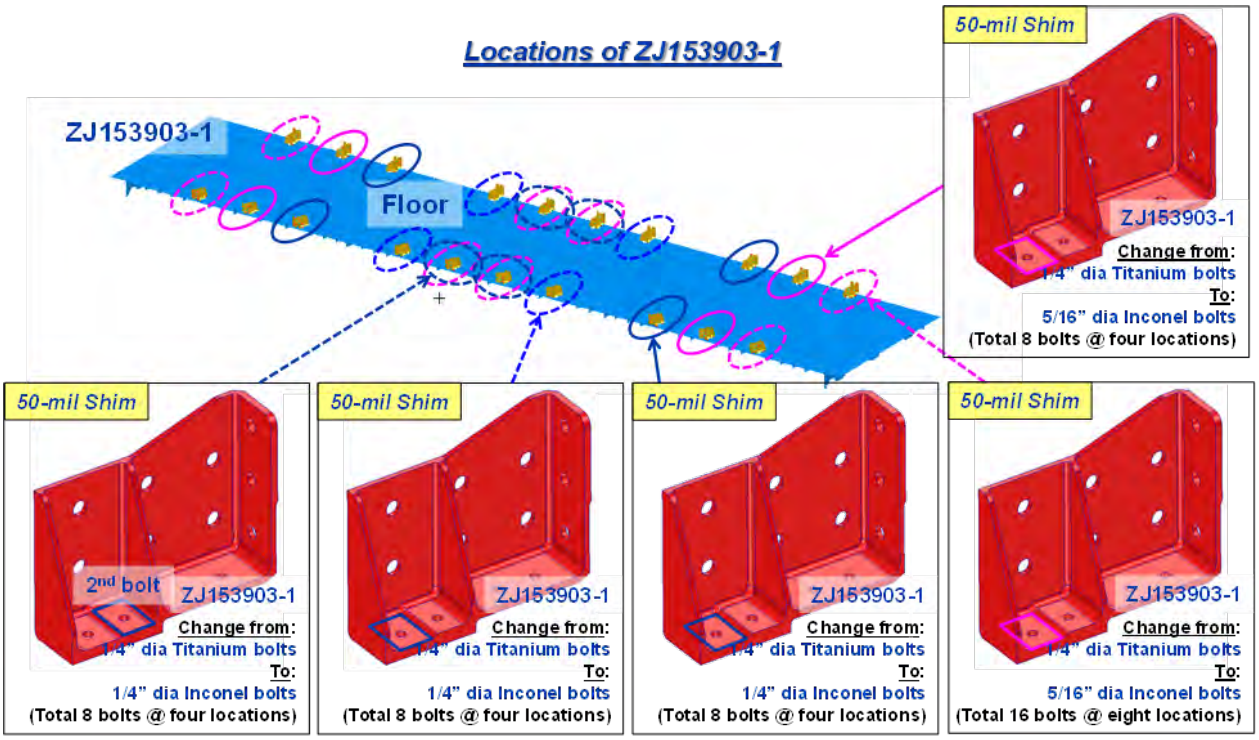

Figure 4-63. Fastener Changes on ZJ153903-1 From the Fastener Bending Calculation

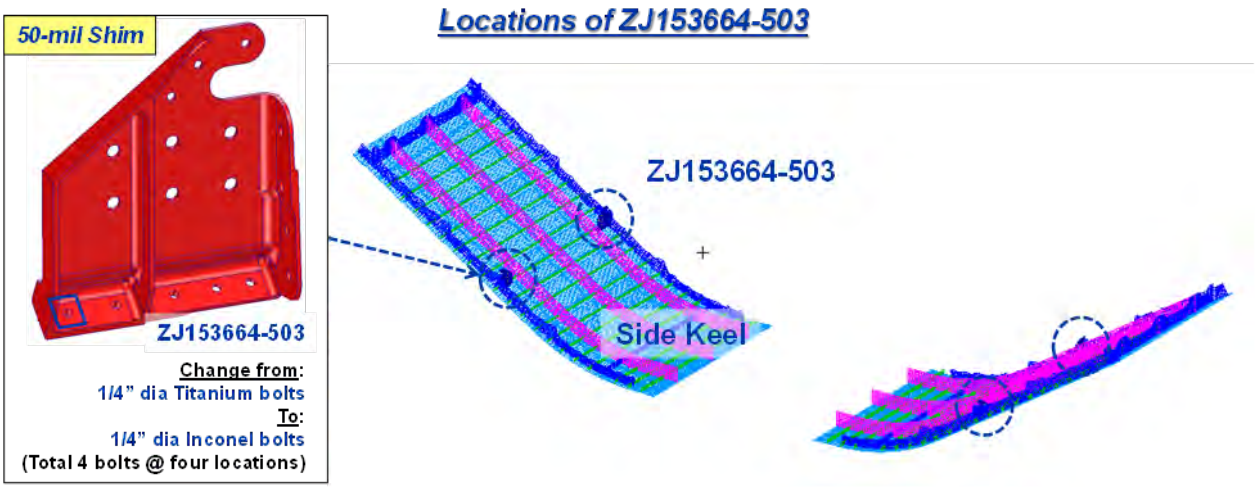

Figure 4-64. Fastener Change on ZJ153664-503 From the Fastener Bending Calculation

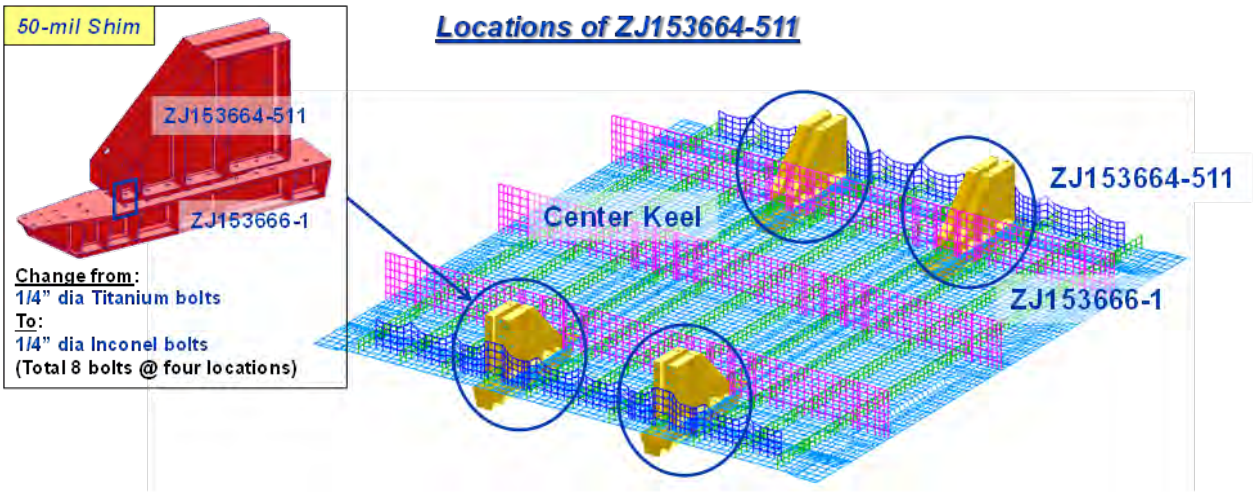

Figure 4-65. Fastener Change on ZJ153664-511 From the Fastener Bending Calculation

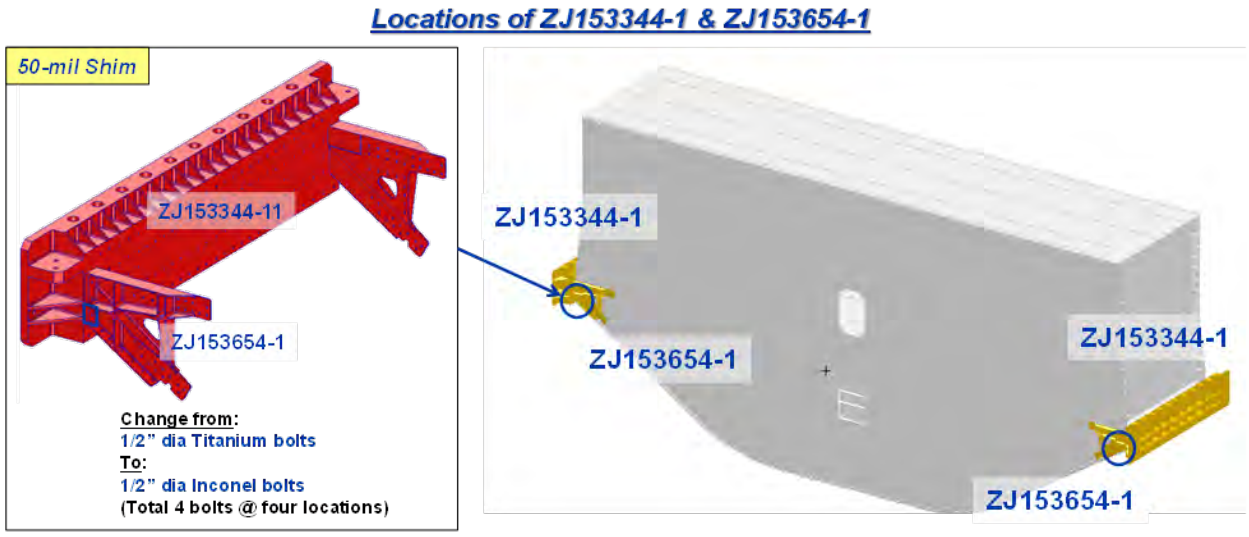

Figure 4-66. Fastener Change on ZJ153344-1 and ZJ153654-1 From the Fastener Bending Calculation

4.3 Local Detailed Analysis Studies

Several local detailed analysis studies were performed to investigate regions of concern or locations with a high concentration of stresses and strains. These local detailed studies included the analyses of bulkhead frame bending under the 2P pressure condition, crown panel keyhole stress/strain concentrations, crown panel stringer refined mesh, skin splice joint, floor panel venting holes, linear buckling of the MBB, composite bearing/bypass interaction, and T-cap noodle failure. All studies showed positive margins of safety except the T-cap noodle failure study. In that study, results showed that an inter-laminar crack would occur at the stringer radius-laminate due to a high inter-laminar tensile stress at 8.7 psi. Although this pressure loading value was lower than 2P DUL, the area with high inter-laminar tensile stress was localized and surrounded by stitching threads. This localized resin cracking would not spread beyond the surrounding stitches, and a catastrophic failure was not expected from this failure mode. Analyses and results of these local detailed studies are described in the following sections.

4.3.1 Bulkhead Frame Keyhole Stress Concentration in 2P Load Case

In the detailed Finite Element Analysis (FEA) of bulkhead frames, fine-mesh FEMs were created at critical locations, such as keyholes on the frames, where high stress/strain concentration values were expected. These stress/strain concentrations are inherent in structures with cutouts, with the highest stress/strain values typically located at the edges of cutouts. The magnitude, location, and extent for a frame keyhole stress/strain concentration depend on the amounts of axial load and bending moment acting on the frame. The area with high stress/strain values is usually small and located at the edge of keyhole. Detailed analyses were performed on the bulkhead frame keyholes to evaluate the magnitudes, locations, and extents of stress/strain concentrations.

The 2P pressure condition was found to be the most critical condition for the bulkhead frames. In the global FEM, frames and stringers were modeled with coarse-mesh elements of approximately 1.0-in. element size, as shown in Figure 4-67. Although this element size was appropriate in stress/strain calculations for the majority of the MBB structure, it was by no means sufficient for calculating the stress/strain concentration of a frame keyhole. Therefore,

fine-mesh FEMs with element sizes ranging from 0.1 to 1.0 in., and with keyhole cutouts modeled in the frame with gaps around continuous stringers, were created. A graphic comparison of the coarse-mesh model in the global FEM and the detailed fine-mesh FEM are shown in Figure 4-67. In the detailed analysis of bulkhead frames, as shown in Figure 4-68, the middle five stringer/frame intersections for the two critical frames on the upper bulkhead were modeled in detail. This was done to capture the stress/strain concentrations on frame keyholes where stringers passed through.

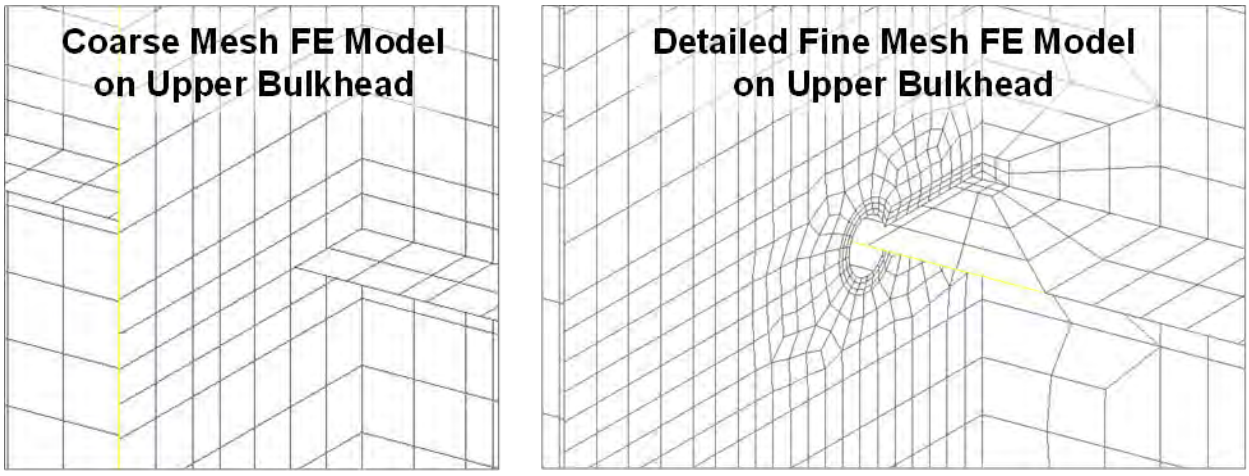

Figure 4-67. Coarse-Mesh and Detailed Fine-Mesh FEMs on Keyholes of the Upper Bulkhead

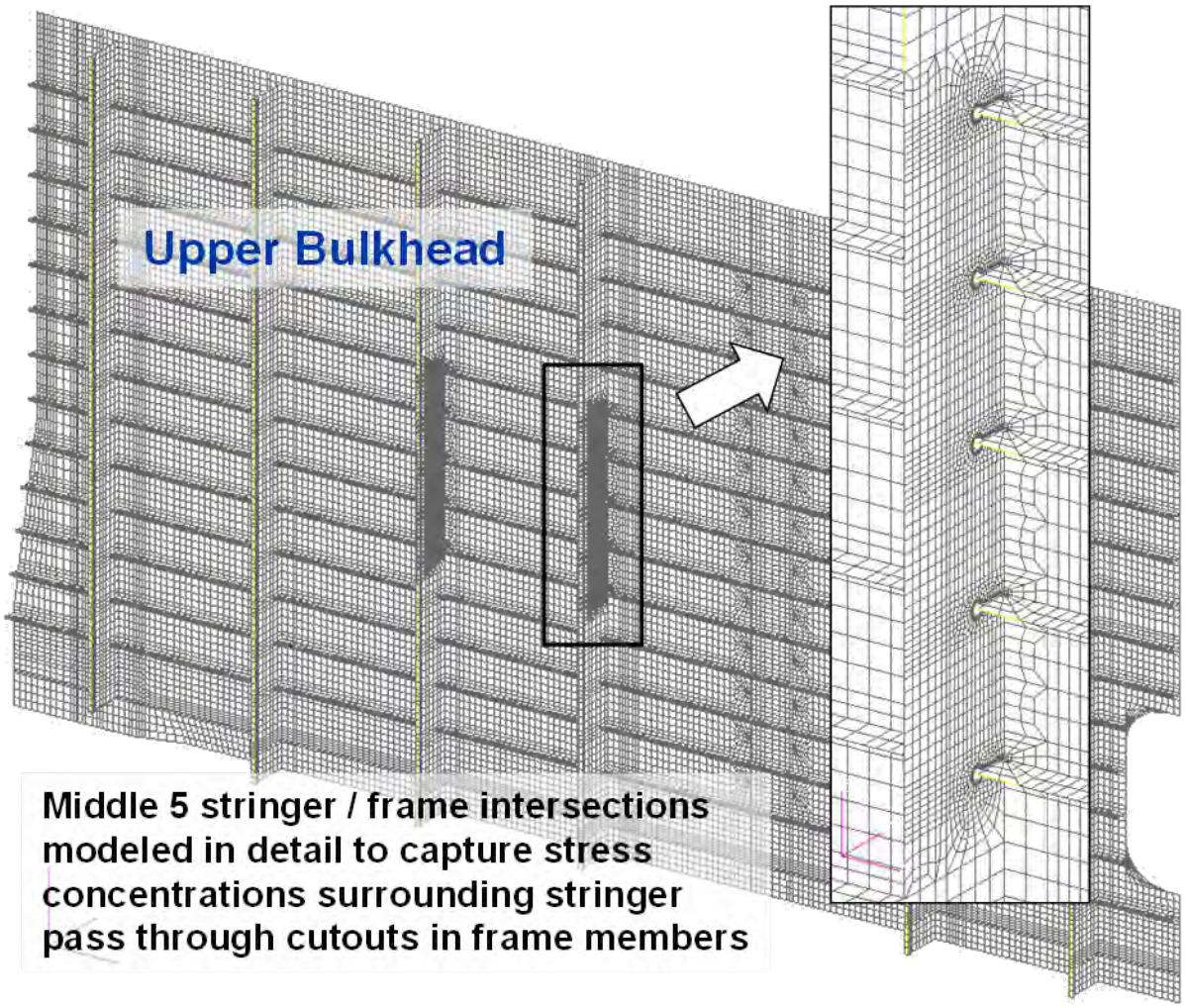

Figure 4-68. Fine-Mesh Modeling in Keyholes of the Frames on the Upper Bulkhead

Results from the local detailed analysis of keyholes on bulkhead frames showed that tension strains in the frame and skin increased at the keyhole of frame, but compression strains were essentially unchanged, as shown in Table 4-14 and Figure 4-69. In Table 4-14, the critical minimum principal strain was -5,400 micro-strain from the baseline (or global) FEM and was -5,700 micro-strain from the detailed FEM calculations. Both results were within the composite notched design value of -5,800 micro-strain for frame web design shown in Table 4-7.

From Figure 4-69, the highest maximum principal strain peaked at the keyhole notch of the frame-to-skin connection on the upper bulkhead, with a value of 10,700 micro-strain shown in the plot. This high strain value was caused by a finite element discontinuity on the frame at the location where a frame web, stringer, and skin were joined. This FE discontinuity was unavoidable in the modeling of the frame, stringer, and skin using 2D elements. The peaking of strain results of the frame at the conjunction of the frame/stringer/skin was not real and therefore was discounted. Excluding this unreal peaking, the maximum principal strain at the frame keyhole became 6,410 micro-strain, as shown in Figure 4-69. This strain value of 6,410 micro-strain is within the notched design value of 7,000 micro-strain for frame web design shown in Table 4-7.

Table 4-14. Summary of Maximum and Minimum Principal Strains in Keyholes of the Frames on the Upper Bulkhead

Strains	Maximum Principal Strain (micro-strain)	Load Case	Minimum Principal Strain (micro-strain)	Load Case
Allowable Strain (Notched Design Values)	7,000	LC1: 2P	-5,800	LC1: 2P
Baseline (Coarse) FEM Strain	2,800	LC1: 2P	-5,400	LC1: 2P
Fine-Mesh FEM Strain	10,700	LC1: 2P	-5,700	LC1: 2P

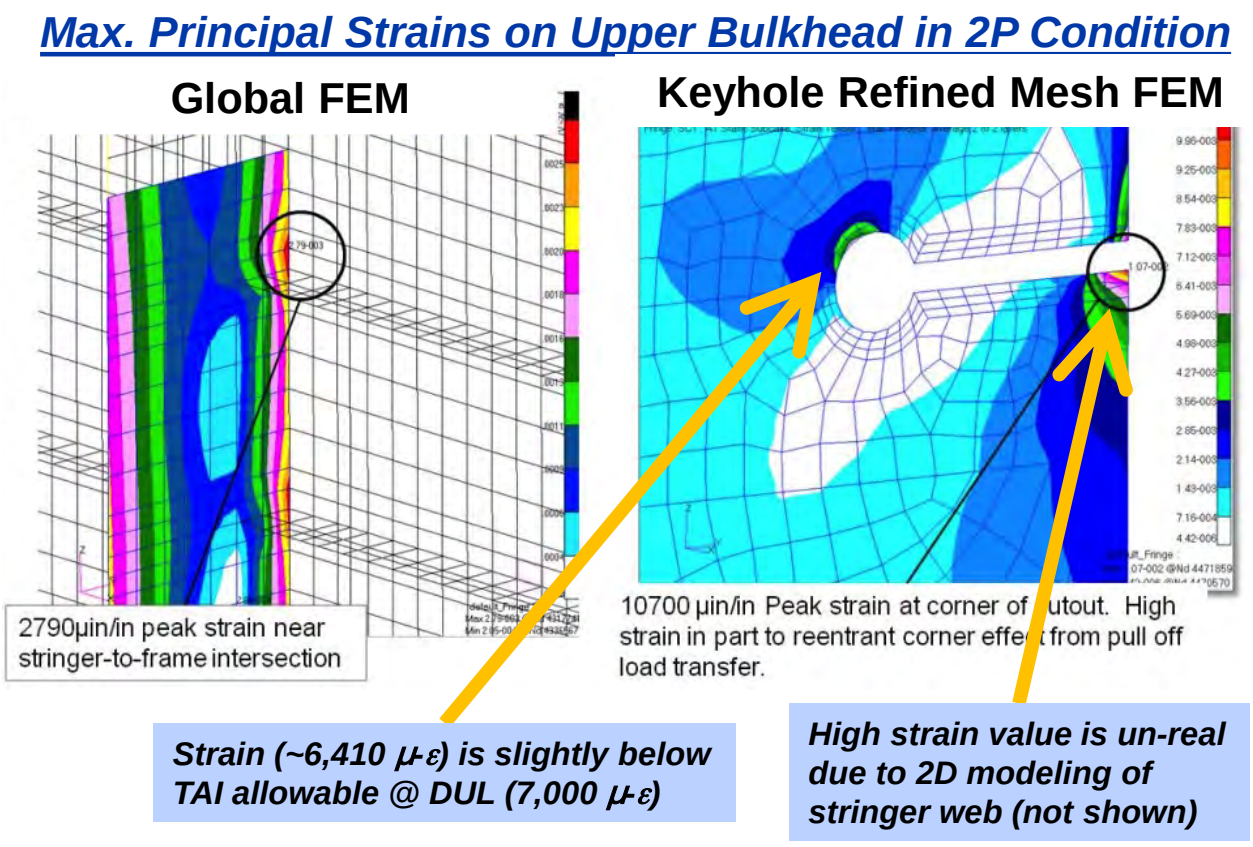

Figure 4-69. Fine-Mesh Model Shows Much Higher Strains Than the Baseline Model

4.3.2 Crown Frame Keyhole Stress Concentrations in 2P and 2.5-g Load Cases

Similar to the frames on the upper bulkhead, frames on the crown were also highly loaded in 2P and 2.5-g loading conditions. Several keyhole cutouts where stringers passed through the center and outer frames of the crown panel showed high strains, and they required refined meshes to determine the stress/strain concentrations. Locations of the crown frames where detailed meshes were selected as areas of interest are shown in Figure 4-70. In the detailed analysis of crown frames, as shown in Figure 4-71, the middle three stringer/frame intersections of the two frames on crown were modeled in detail to capture the stress/strain concentrations on frame keyholes.

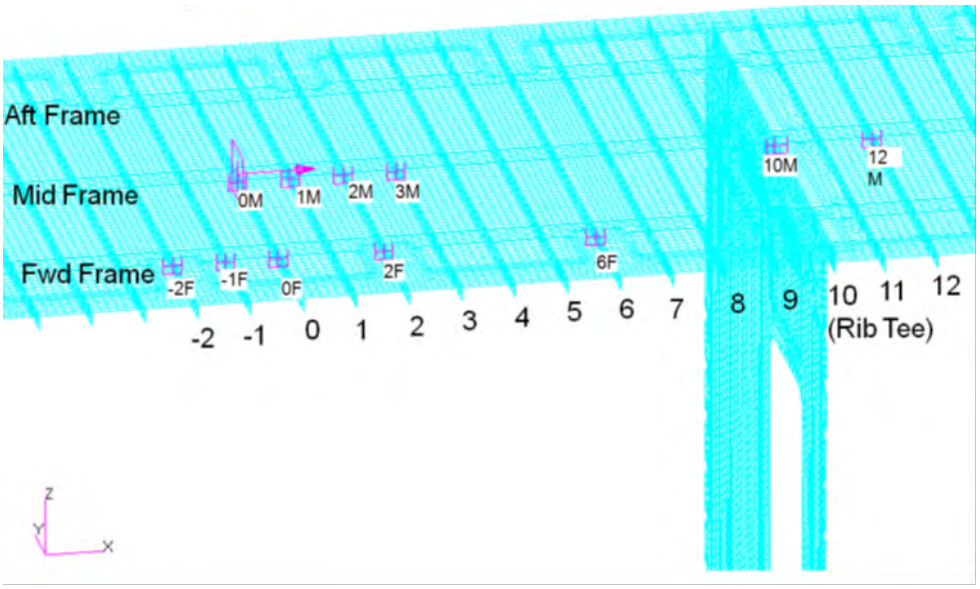

Figure 4-70. Locations of Fine-Mesh Modeling in Keyholes of the Frames on the Crown

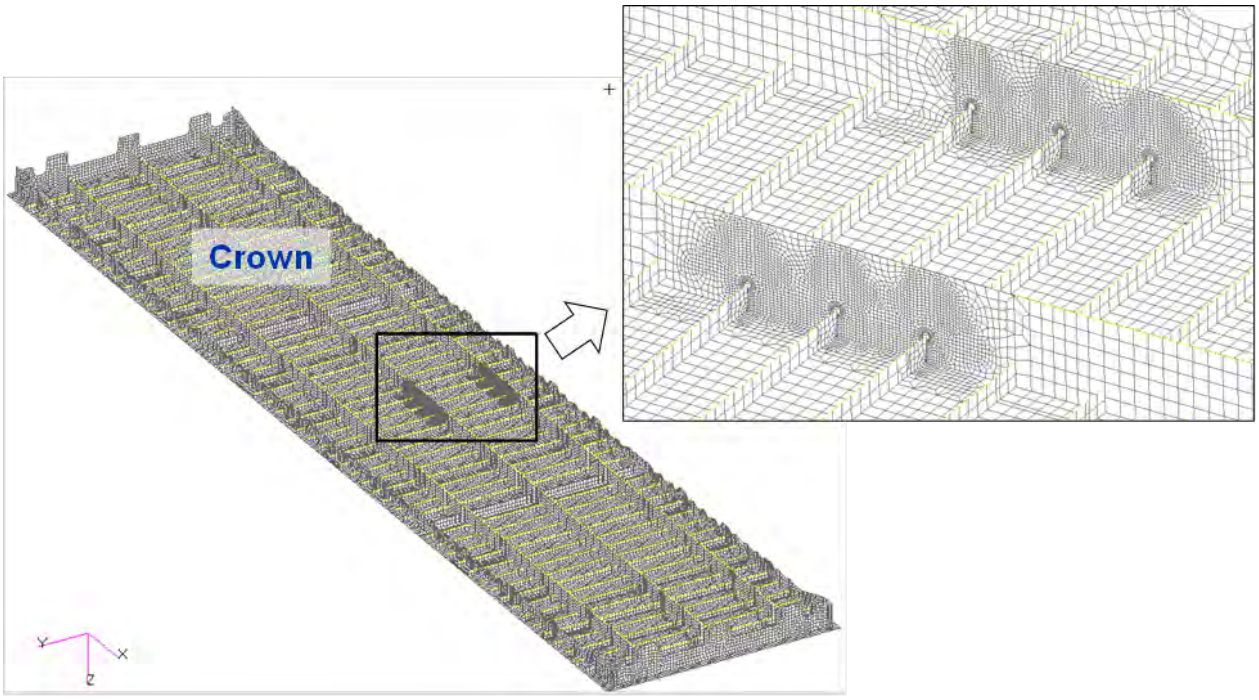

Figure 4-71. Fine-Mesh Modeling in Keyholes of the Frames on the Crown

Results from the local detailed analysis of keyholes on crown frames showed that the strain values of the center and forward frames on the crown increased significantly for both 2P and 2.5-g loading conditions. In the 2P pressure condition, the maximum principal strain increased on both frames, as shown in Figure 4-72. Similar to the results of the upper bulkhead, the highest maximum principal strain peaked at the keyhole notch of the frame-to-skin connection of the crown, with a value of 9,200 micro-strain shown in the plot. As discussed earlier, this high strain value was caused by a finite element discontinuity on the frame at the location where a frame web, stringer, and skin were joined. This FE discontinuity was unavoidable in the modeling of

frame, stringer, and skin using 2D elements. The peaking of strain in the frame at the conjunction of the frame/stringer/skin was not real and was therefore discounted. Excluding this unreal result, the maximum principal strain at the keyhole location became 6,530 micro-strain, as shown in Figure 4-72. This strain value of 6,530 micro-strain is within the notched design value of 7,000 micro-strain for frame web design shown in Table 4-7.

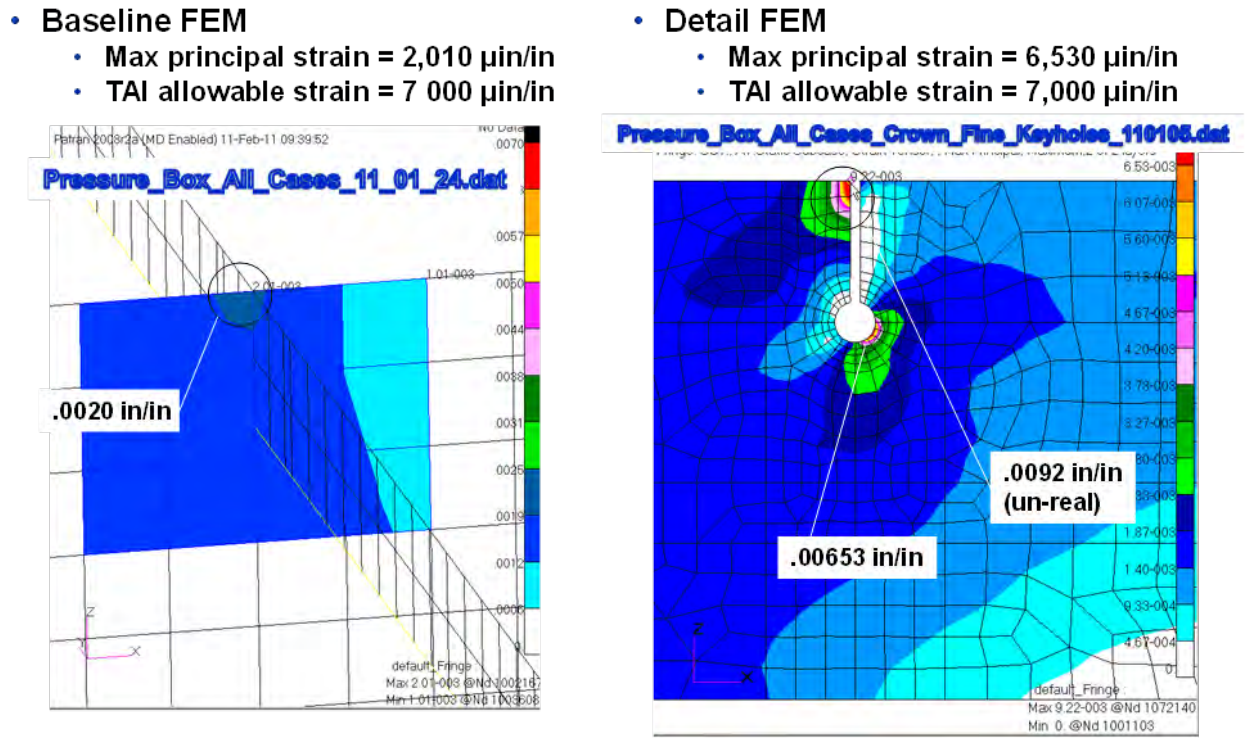

Figure 4-72. Maximum Principal Strains on the Center Frame of the Crown in 2P Condition

In the 2.5-g DLL case, the minimum principal strain increased for both frames at two critical locations, as shown in Figure 4-73. The compression strain peaked at the top edge of the keyhole, with a value of -8,250 micro-strain shown in the plot. This compressive strain exceeded both the notched DLL value of -3,867 micro-strain (or -5,800 micro-strain in DUL) and the un-notched DLL value of -5,333 micro-strain (or -8,000 micro-strain in DUL) for frame web design, as shown in Table 4-7. A summary of these results is provided in Table 4-15, as shown in Figure 4-70, for their locations on the crown. To reduce the compressive strain levels on the keyhole edges, ring-shaped DMS 2436 C1T72 fabric pieces were added to both facesheets of the frames at critical locations. Increasing frame facesheet thickness at keyhole edges reduced the minimum principal strains on keyhole edges to values below the un-notched design value of the composite. From the results of the detailed frame keyhole cutout study on the crown, it was concluded that local facesheet thickness increases at critical keyhole locations on frames were required. Design changes of the critical frames on the crown were incorporated with ring-shaped DMS 2436 C1T72 fabric pieces added to both facesheets of the frames at critical locations.

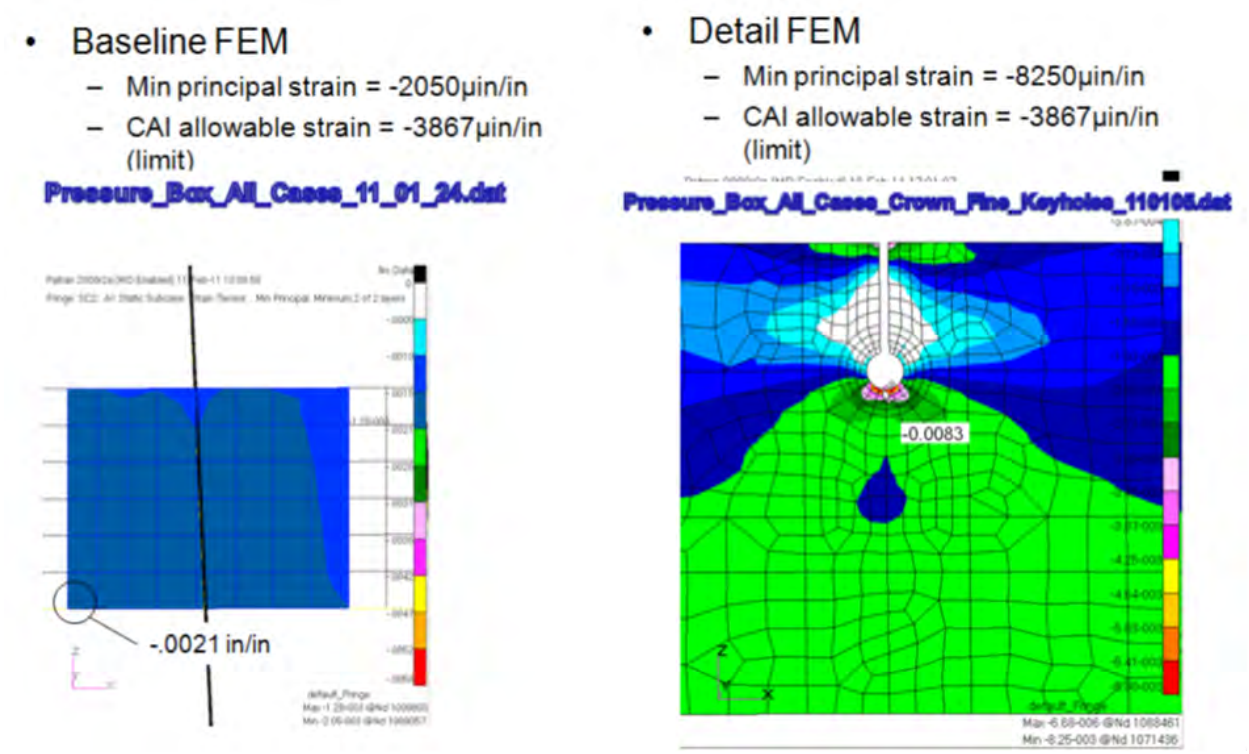

Figure 4-73. Minimum Principal Strains on the Center Frame of the Crown in 2.5-g Condition

Table 4-15. Summary of Maximum and Minimum Principal Strains in Keyholes of Frames on Crown

Crown Frame	Load Case	Load Condition	Tension			Compression		
			TAI Allowable (ULT) = 7,000 µin/in			CAI Allowable (ULT) = -5,800 µin/in		
			TAI Allowable (Limit) = 4,667 µin/in			CAI Allowable (Limit) = -3,867 µin/in		
			Stringer Location	Max Principal Strain (µ-in/in)		Stringer Location	Max Principal Strain (µ-in/in)	
				Baseline (Coarse) Mesh	Fine Mesh		Baseline (Coarse) Mesh	Fine Mesh
Center Frame	LC1: 2P	Ultimate	12M	2,010	9,200	12M	-1,500	-5,230
	LC2: 2.5-g	Limit	3M	1,340	2,930	3M	-2,050	-8,250
	LC3: 2.5-g +1P	Limit	12M	1,060	4,690	3M	-2,510	-7,490
Fwd Frame	LC1: 2P	Ultimate	1F	2,850	8,540	-2F	-3,450	-6,870
	LC2: 2.5-g	Limit	-1F	773	2,460	-1F	-1,390	-7,260
	LC3: 2.5-g +1P	Limit	1F	1,640	4,440	-2F	-2,480	-8,050

4.3.3 Crown Panel Stringer Study

At the location where upper bulkhead frames attached to the crown stringer webs by means of the External Crown Fitting (ZJ153660-1), high principal strains were found on these webs in the 2P pressure condition. To calculate more accurate strain distributions on the stringer webs, a detailed study using locally refined stringer web meshes was performed. The element length was reduced from 1.0 in. in the global FEM to 0.25 in. in the refined local FEM, as shown in Figure 4-74.

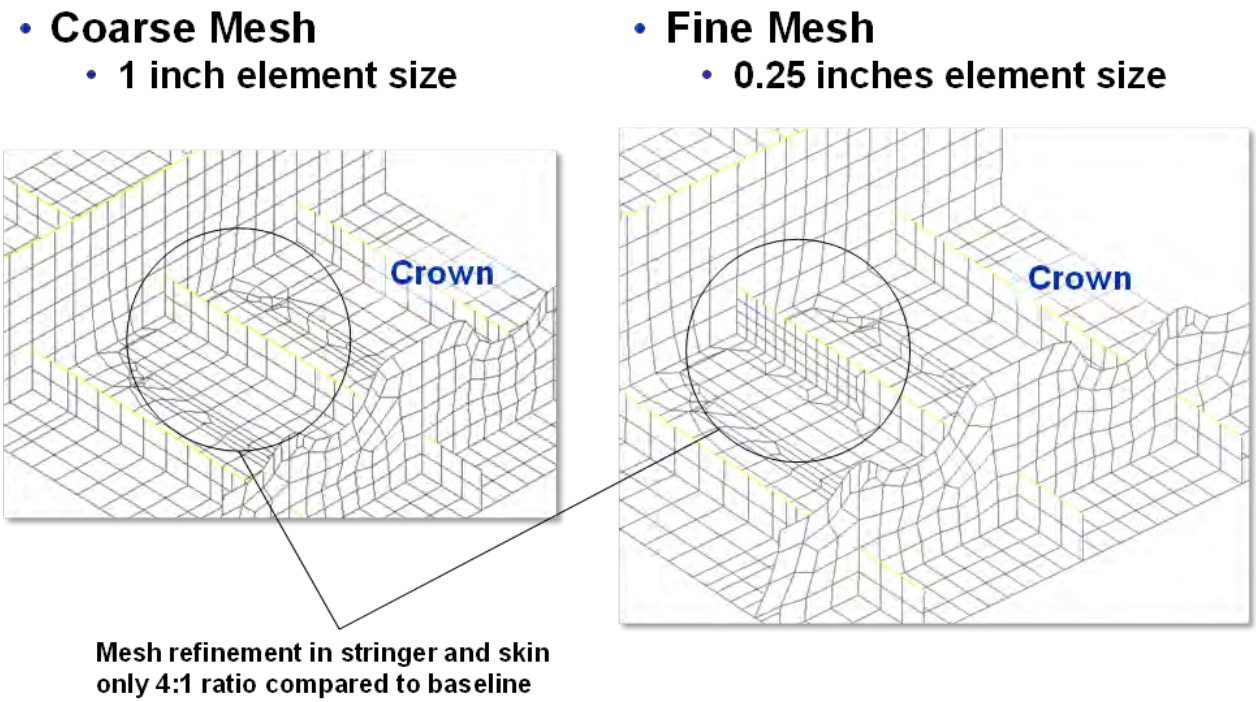

Figure 4-74. Comparison of Coarse-FEM to Fine-Mesh FEM With Refined Stringer Meshing

Maximum principal strain results from the fine-mesh study were plotted (Figure 4-75) and compared with the results from the coarse mesh from the global FEM. The results showed that refining the stringer mesh locally reduced the maximum principal strain by 8%. However, while checking the minimum principal strain, no reduction of strain was found. The minimum principal strain from the fine-mesh model was similar to the minimum principal strain from the global FEM with the baseline coarse mesh. Summaries of the maximum and minimum principal strains from the baseline and fine-mesh models are listed in Table 4-16. Because the baseline coarse-mesh FEM gave more conservative results for the stringer webs, no local stringer web mesh refinement was necessary on the global FEM.

Baseline FEM

- Max principal strain = 6510µin/in
- Allowable Strain = 7000 µin/in
- MS = 0.075

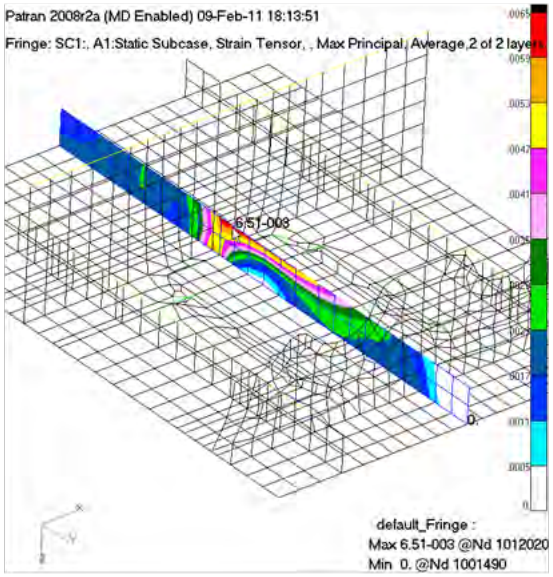

Fine Mesh FEM

- Max principal strain = 5990 µin/in
- Allowable Strain = 7000 µin/in
- MS = 0.169
- Approx. 8% strain reduction due to mesh density

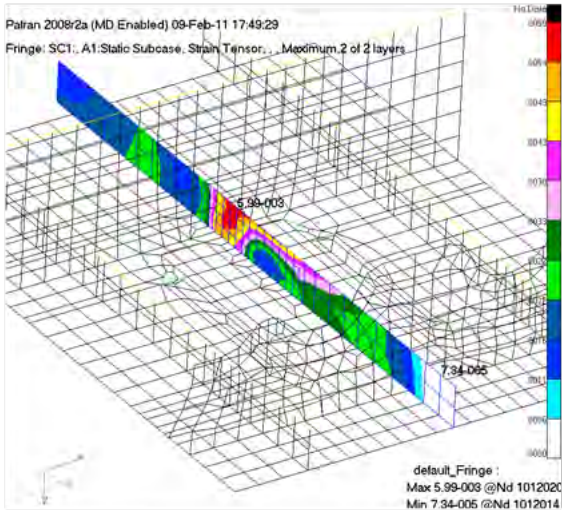

Figure 4-75. Comparison of Maximum Principal Strains from Coarse- and Fine-Mesh Models

Table 4-16. Summary of Maximum and Minimum Principal Strains from Coarse- and Fine-Mesh Models

Strains	Maximum Principal Strain (micro-strain)	Load Case	Minimum Principal Strain (micro-strain)	Load Case
Allowable Strain (Notched Design Values)	7,000	LC1: 2P	-5,800	LC1: 2P
Baseline (Coarse) FEM Strain	6,500	LC1: 2P	-5,700	LC1: 2P
Fine-Mesh FEM Strain	6,000	LC1: 2P	-5,700	LC1: 2P

4.3.4 Bulkhead Skin Splice Joint Study

A detailed analysis of the skin splice joint on the bulkhead panel was determined to be necessary. The global FEM did not include a representation of the skin butt splice used on the bulkhead panel, creating the potential to miss a possible failure location. This detailed study generated a FEM of the splice to demonstrate that the splice joint on the bulkhead was not a primary failure location. Because the splice was parallel to the frames, the primary load case of concern would be pressure loading. In this case, the frame would provide a node point or point of minimal deflection, as shown in Figure 4-76. The skin splice design was based on coupon testing completed under IRAD funding and is shown in Figure 4-77.

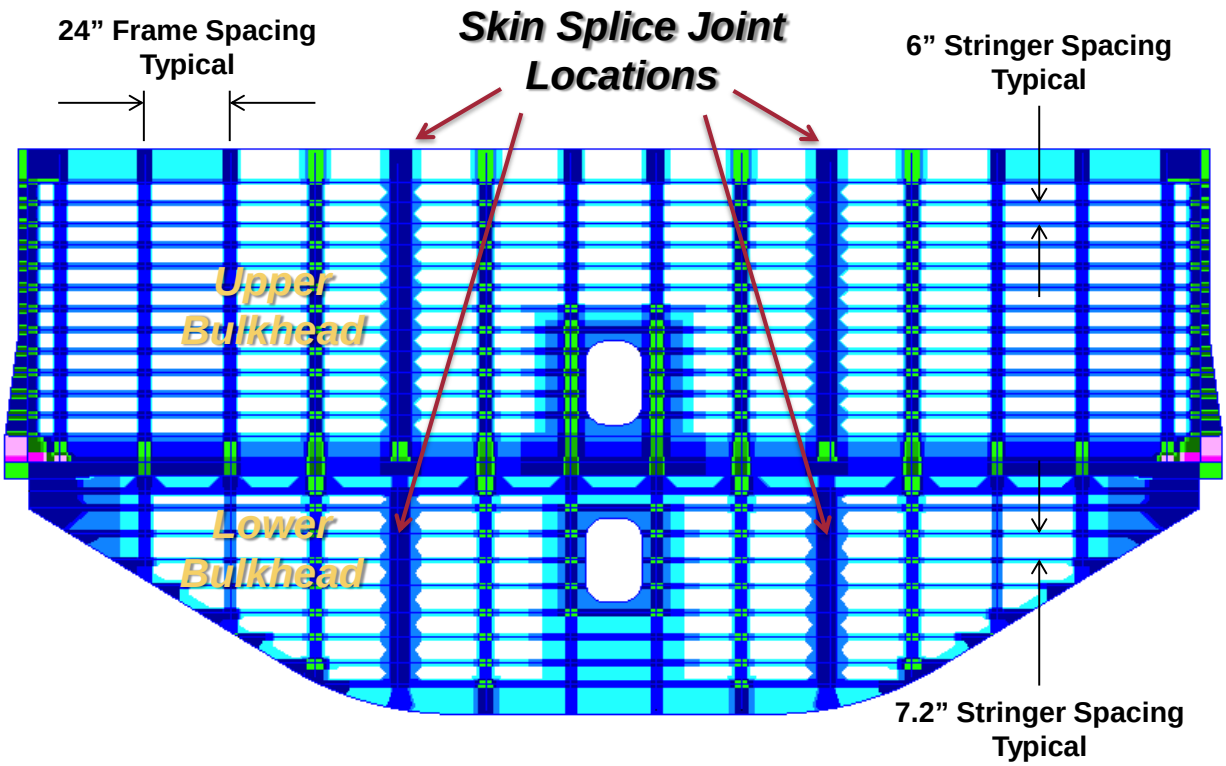

Figure 4-76. Skin Splice Joint Located on a Frame of the Bulkhead Panel

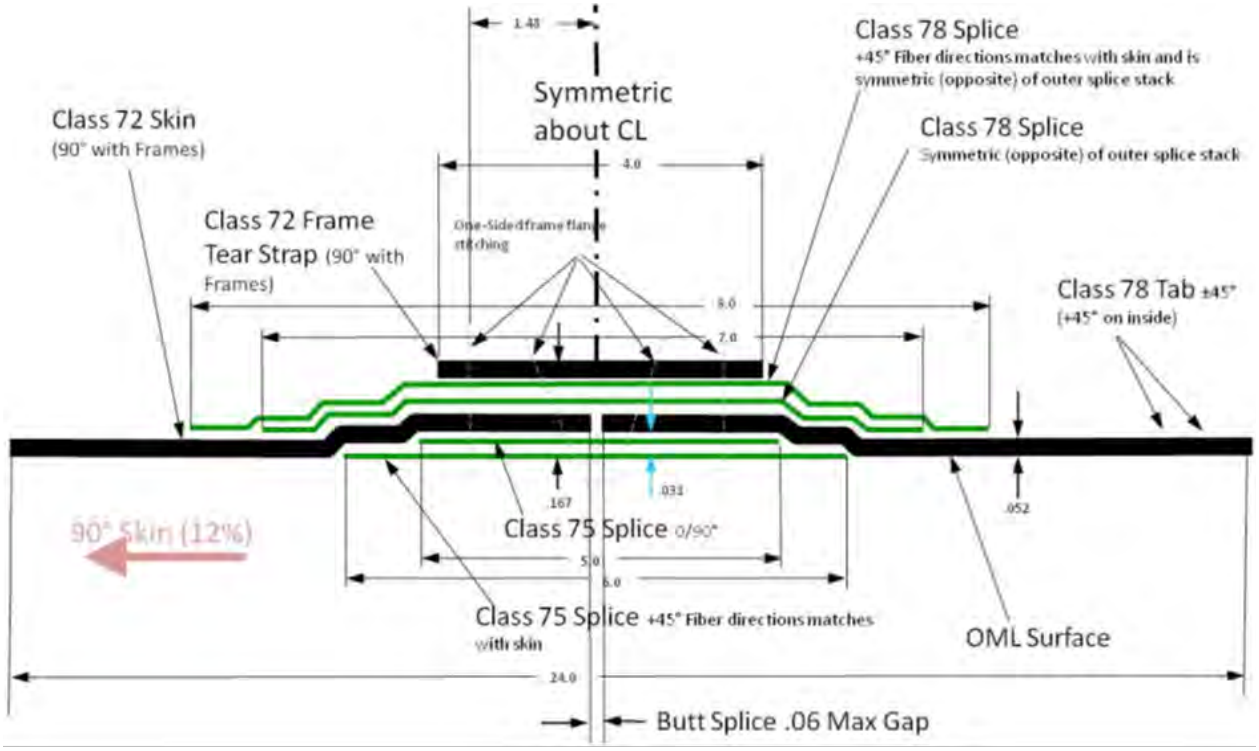

Figure 4-77. Schematic of the Skin Splice Joint Design

The detailed FEM of the skin splice joint was a planar shell model corresponding to Figure 4-77, with the thickness of the shell being 0.10 in. into the page. Modeling assumptions included that plane strain was of concern and there would be no stitching. A 0.050-in. butt joint gap was also assumed in the modeling. For modeling ease, the extensional material properties for each ply were isotropic. The frame itself was not modeled because it would not draw axial load away from the splice plies and, therefore, would have little influence on the splice.

Two loading and boundary conditions were used in this assessment. The first condition was a pressure condition with a section between stringers across the frame flange under 2P pressure loading. Modeling of the 2P pressure condition is shown in Figure 4-78, and the results are shown in Figure 4-79. The second condition was an axial loading condition, modeled as shown in Figure 4-80, with results shown in Figure 4-81. In both conditions, the strains at the splice location were small compared with the strains on the skin. The failure occurred at the skin joggle in the 45-deg OML ply and not the skin splice. This study demonstrated that the splice was not a critical region, and it was acceptable to use the global model without detailed modeling of the splice.

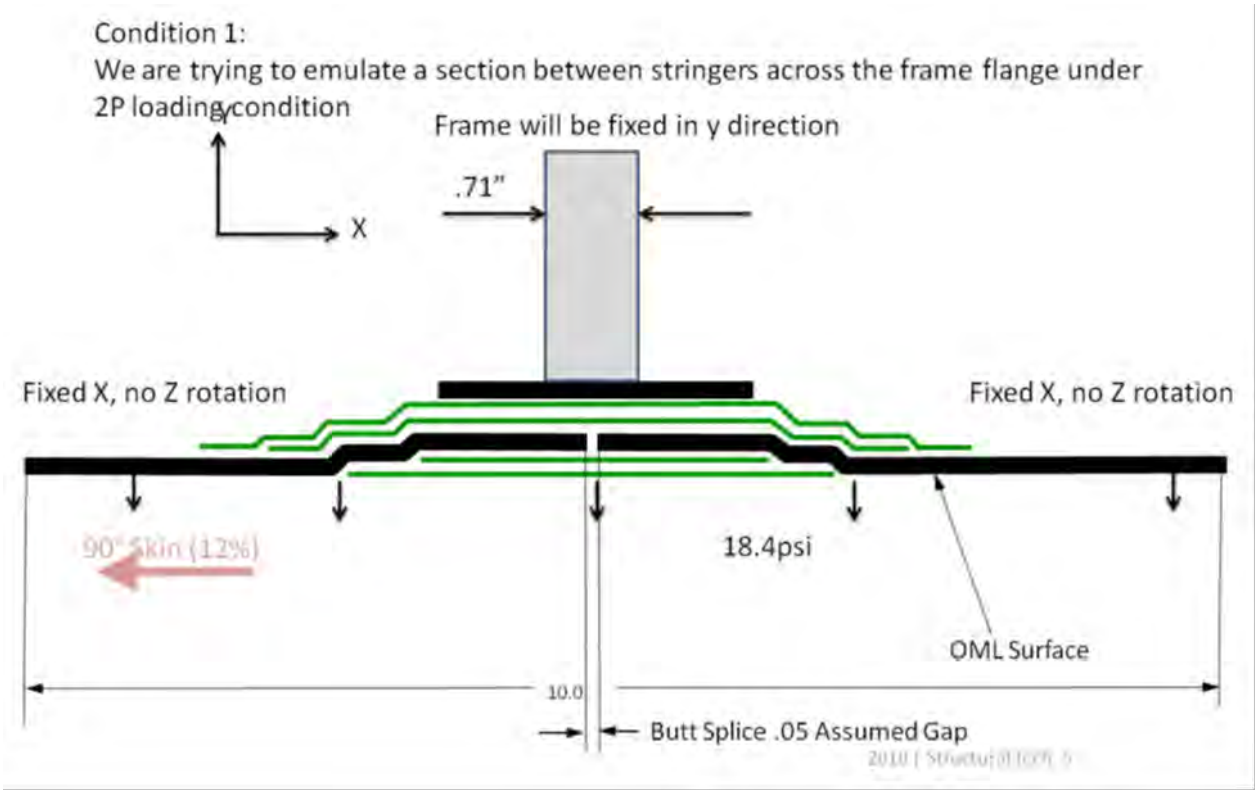

Figure 4-78. 2P Pressure Loading on the Skin Splice Joint

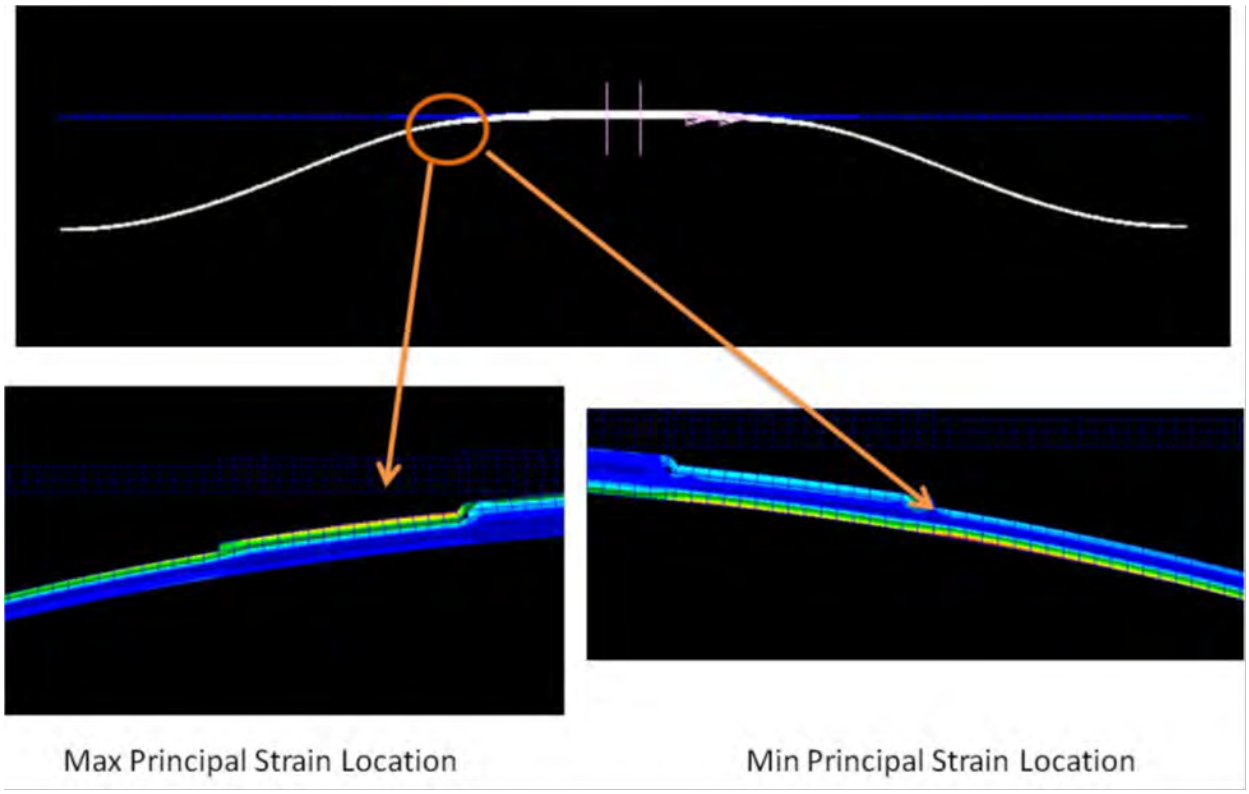

Figure 4-79. Deformed Shape and Maximum/Minimum Principal Strains of the Skin Splice Joint in 2P Loading

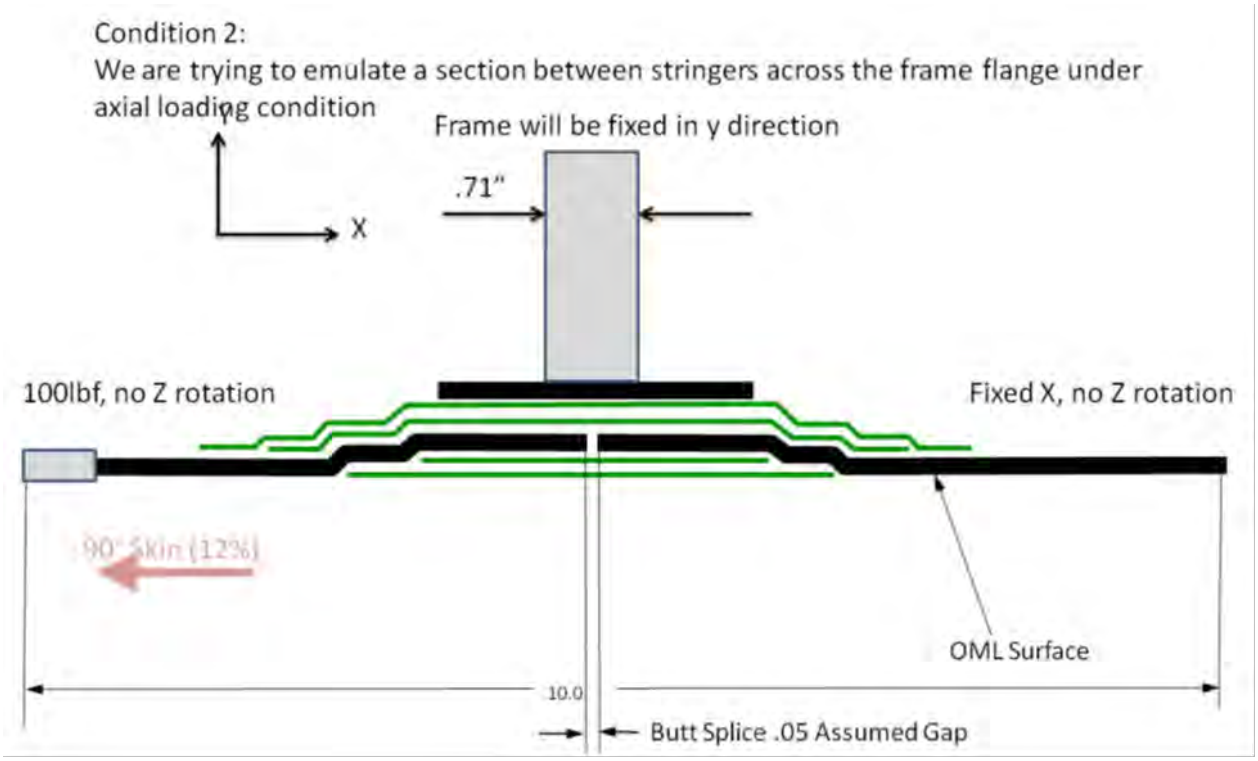

Figure 4-80. Skin Axial Loading on the Skin Splice Joint

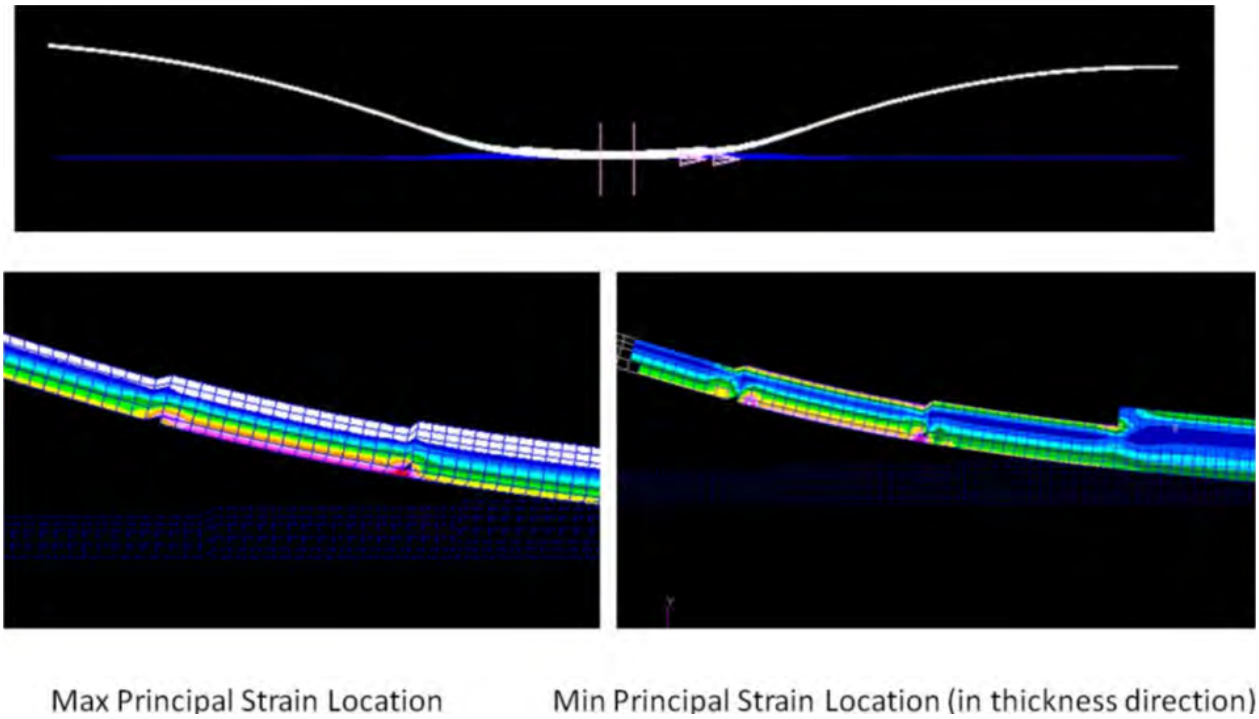

Figure 4-81. Deformed Shape and Maximum/Minimum Principal Strains of Skin Splice Joint in Axial Loading

4.3.5 Floor Panel Vent Hole Study

During the detailed design stage, it was determined that additional venting holes would be added to the floor panel for blowout safety in pressure loads. A study was performed to show that the peak concentrated strain on the edges of these venting holes would be within the MBB design values. A detailed mesh FEM of the venting holes was built and run under all five loading conditions. The maximum and minimum principal strain results from the detailed study are summarized in Table 4-17. For all five loading cases, the results showed that the maximum principal strains were within the notched tension design values, and the minimum principal strains were within the notched compression design values of the MBB. The two critical locations with the lowest margins of safety of 72% came from the 2.5-g and 2.5-g + 1P loading conditions. The maximum principal strain plots in these two loading cases are shown in Figure 4-82 and Figure 4-83, respectively. The high margins of safety derived from this detailed study indicated that the concentration of strains on the floor venting holes would not become critical for the MBB.

Table 4-17. Summary of Maximum and Minimum Principal Strains on the Floor Venting Holes

Load Case	Notched Tension Design Values (micro-strain)	Maximum Principal Strain (micro-strain)	MS	Notched Compression Design Values (micro-strain)	Minimum Principal Strain (micro-strain)	MS
LC1: 2P	5,900	1,710	2.45	-4,800	-682	6.04
LC2: 2.5-g	3,933	2,290	0.72	-3,200	-783	3.09
LC3: 2.5-g +1P	3,933	2,290	0.72	-3,200	-783	3.09
LC4: -1.0-g	3,933	313	11.57	-3,200	-914	2.50
LC5: -1.0-g + 1P	3,933	954	3.12	-3,200	-1,030	2.11

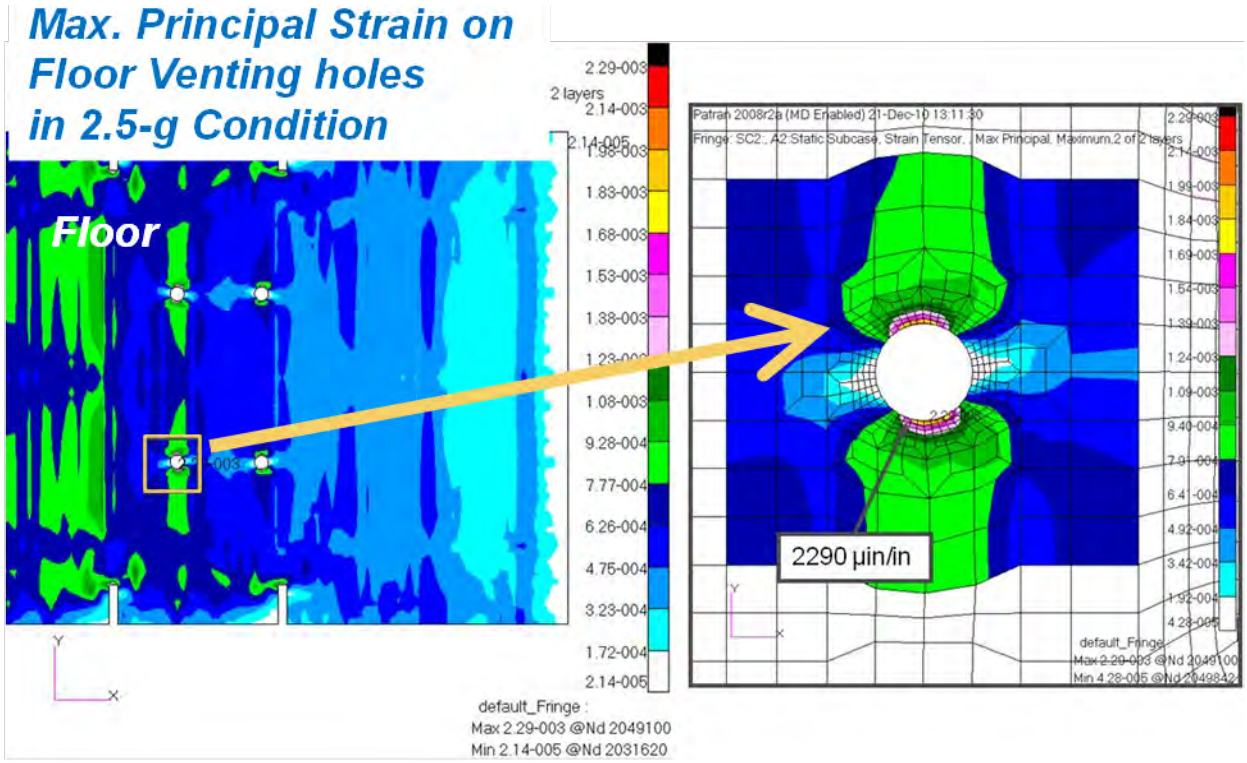

Figure 4-82. Maximum Principal Strain Results on the Floor Venting Hole in 2.5-g Condition

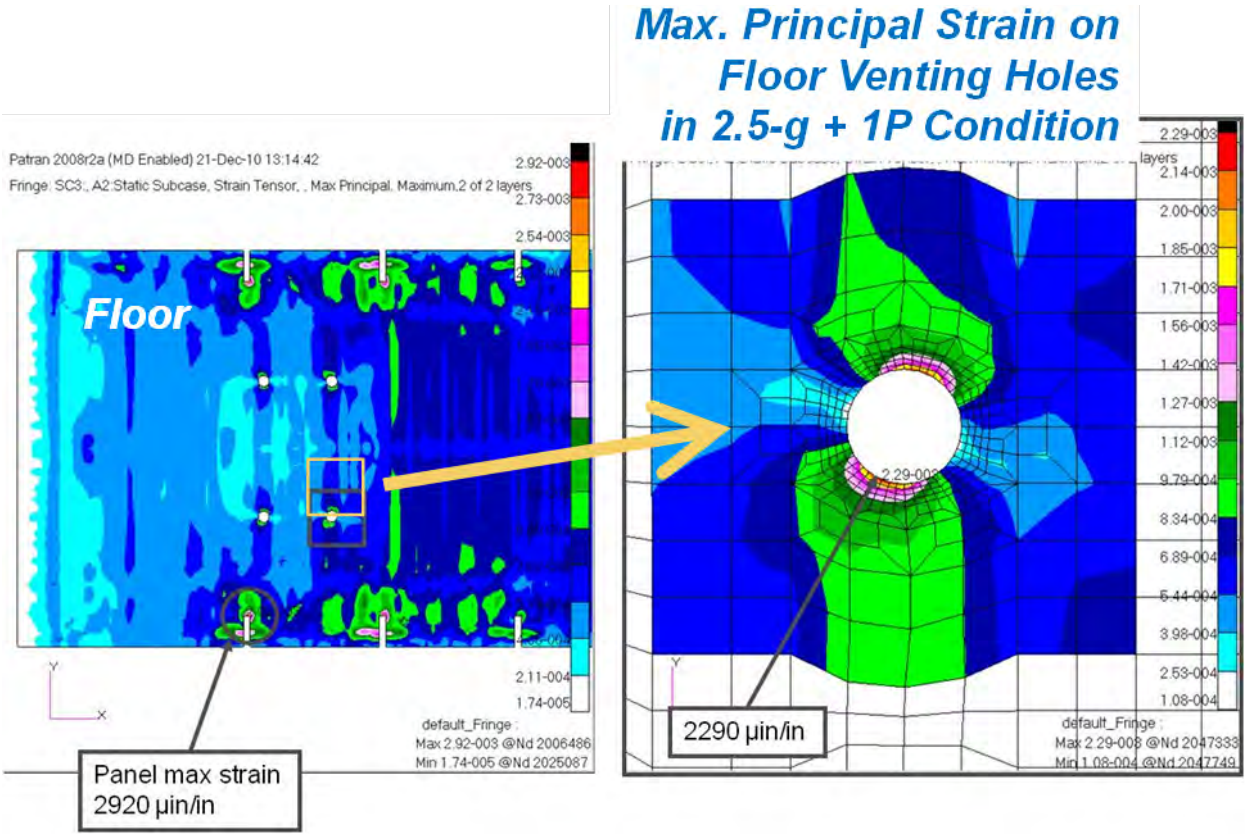

Figure 4-83. Maximum Principal Strain Results on the Floor Venting Hole in 2.5-g + 1P Condition

To confirm that the FEM results were correct, a free-body-force calculation of axial load for the 2.5-g load condition was completed to check the strain concentration value. Using the sum of the forces in the frame direction (x-direction) of the three-stack region gave a load of 18,957 lb, and a net section strain of 701 micro-strain with a stress concentration of 3.25, showing that the concentration of strains on the vent holes was not critical. Details of the stress concentration factor calculation are shown in Figure 4-84.

- Sum of the forces in x-dir of 3 stack area yields:

$$\sum P_x = 18956 lb$$

- Net section strain would be:

$$\varepsilon_x \approx \frac{P_x}{A_{net} \cdot E_x} = \frac{18958\,lb}{2.78 in^2 \cdot 9.74 msi} = 701\,\mu in/in$$

- Strain conc. factor is reasonable value, calculated as:

$$\frac{2280}{701} = 3.25$$

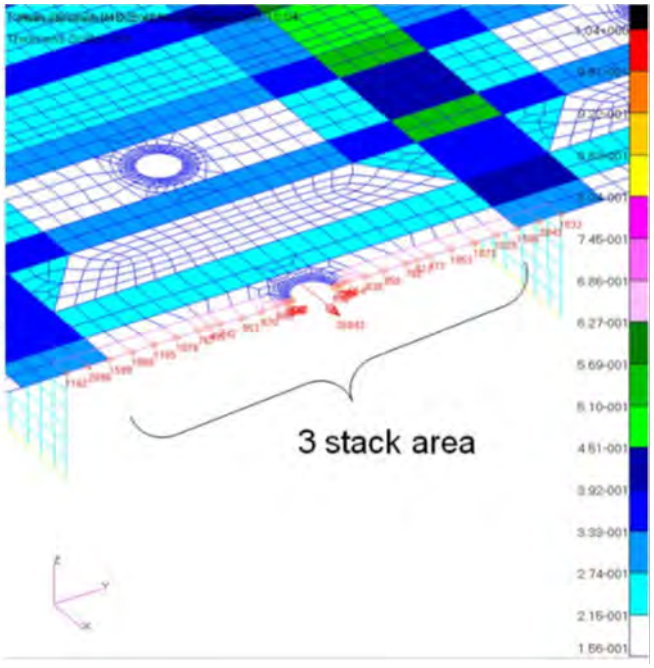

Figure 4-84. Stress/Strain Concentration Calculation on the Floor Venting Holes

4.3.6 Linear Buckling Analyses

Because most composite skins on the MBB were made of minimum gage (one-stack) laminates, it was possible that local skin buckling would appear well before a global instability occurred on a primary load-carrying structural member (e.g., a frame or T-cap) while loaded in compression. To investigate if, when, and how the MBB would buckle locally and globally in different design cases, linear buckling analyses using the global FEM were performed.

While performing the linear buckling analyses, an unexpected buckling mode appeared at one of the frame webs on the upper bulkhead, as shown in Figure 4-85. This buckling mode had a checker-board buckling shape on the frame web, and its buckling shape seemed to be dependent on the finite element mesh. Further investigation showed this buckling mode to be a spurious (or fictitious) mode resulting from a calculation error in the eigenvalue solution for buckling analysis. This error was associated with the NASTRAN composite 2D plate formulation using the classical laminate theory. The transverse shear modulus values of Rohacell foam core were simply too low compared to the modulus values of composite facesheets on frames, resulting in a misrepresentation of the transverse shear stiffness of the sandwich frames. The MSC Software Corporation confirmed this spurious buckling mode while using 2D plate elements with PCOMP and MAT8 entries for their material properties. Similar miscalculations also exist in the buckling analysis of sandwich frames using ABAQUS software. A 3D model of the PRSEUS frames, representing the core with 3D solid elements, would eliminate this spurious

mode in buckling analyses. However, using 3D elements for frames in the global model of the MBB was not feasible. Therefore, a simpler approach was taken to solve this numerical issue. The transverse shear moduli of the Rohacell foam core were increased by a factor of 10. After this modification to the frames, the spurious mode was reduced in the buckling analyses. Later, in the nonlinear analyses of the MBB, it was found that the misrepresentation of the transverse shear stiffness of sandwich frames also caused some numerical convergence difficulties. Similar changes were made to the transverse shear stiffness of frames, which enabled better convergence in nonlinear analyses. To investigate the influence of this transverse shear modulus change on the strains in frames, linear static results from the FEM with modified frame stiffness and the original global FEM were compared. It was found that the strain values on the frames and their adjacent structure were almost identical, authenticating the use of modified frame stiffness in the buckling and nonlinear analyses.

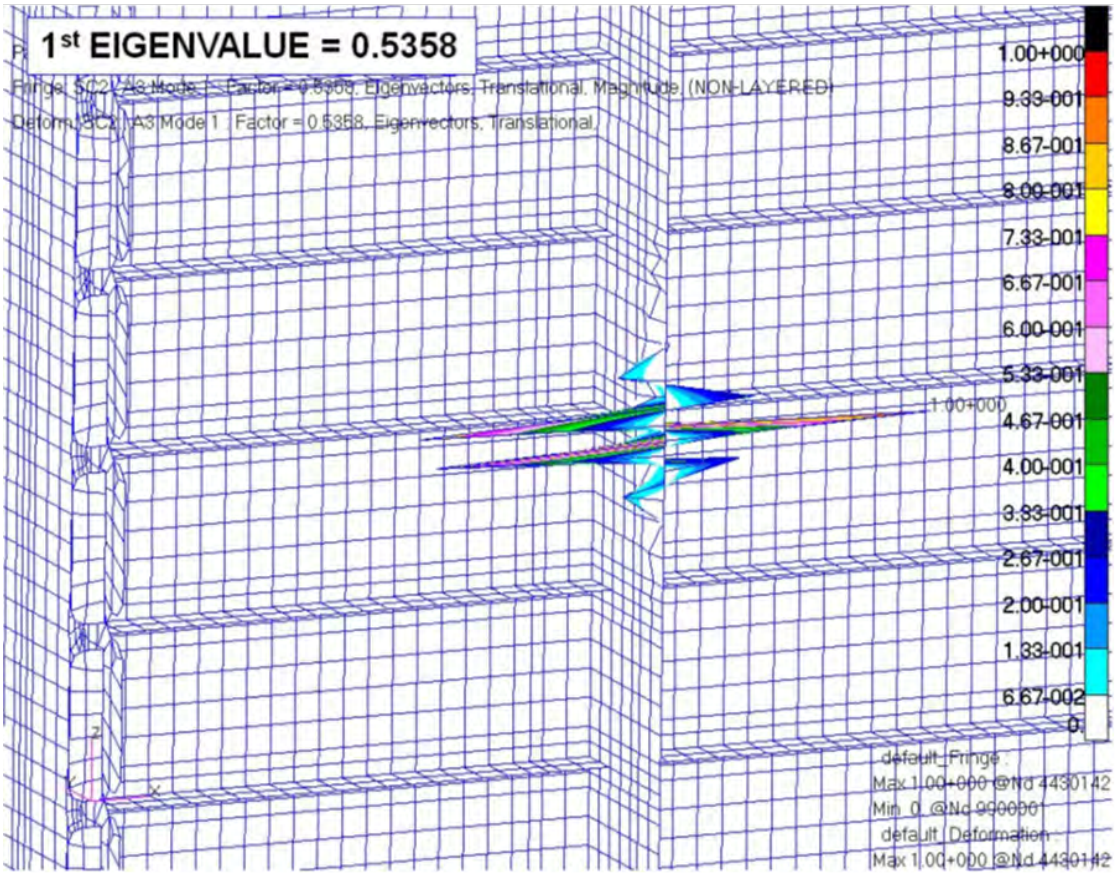

Figure 4-85. Spurious Mode at Frame Web on the Upper Bulkhead in Linear Buckling Analysis

In the structural stability studies of the MBB, linear buckling analyses were performed for the 2P pressure condition, and the 2.5-g and -1.0-g maneuver conditions. Linear buckling analyses were not performed for the 2.5-g + 1P and -1.0-g + 1P combined loading conditions because the structural response in these cases calls for geometrically nonlinear behavior to be captured. The structural stability studies for the 2.5-g + 1P and -1.0-g + 1P conditions can only be performed using nonlinear analyses.

Results from the linear buckling analyses showed that the skin locations on the crown, floor, and center keel that buckled were flat and had the minimum gage (one-stack) skin thickness.

Although these skins would buckle at load levels below DLL, it is probable that they would support higher loads by entering the post-buckling stage in structural tests. A prior experiment for a compression panel showed that the skin buckled long before the frames failed, allowing the panel to support seven times the skin buckling loads (Ref. 4-7). Results from linear buckling analyses are presented in detail in the following sections.

4.3.6.1 2P Pressure Condition

For the linear buckling analysis in the 2P pressure condition, the first and second buckling modes appeared at the Keel Splice Intercostal Fitting (ZJ153659-503) at 3.57P (or 32.9 psi), as shown in Figure 4-86. This internal pressure of 3.57P was higher than the 2P DUL, which meant that the MBB would not buckle below 2P. The third buckling mode, at 37.2 psi, appeared at a stringer on the center keel and is shown in Figure 4-87. The fourth and fifth buckling modes, at 37.3 psi, appeared at a stringer on the side keel and are shown in Figure 4-88. These buckling modes were local buckling modes, and no global buckling was found on any of the primary structures, such as frames or T-caps, below 2P. In conclusion, the MBB would not experience any structural instability at pressures below 2P.

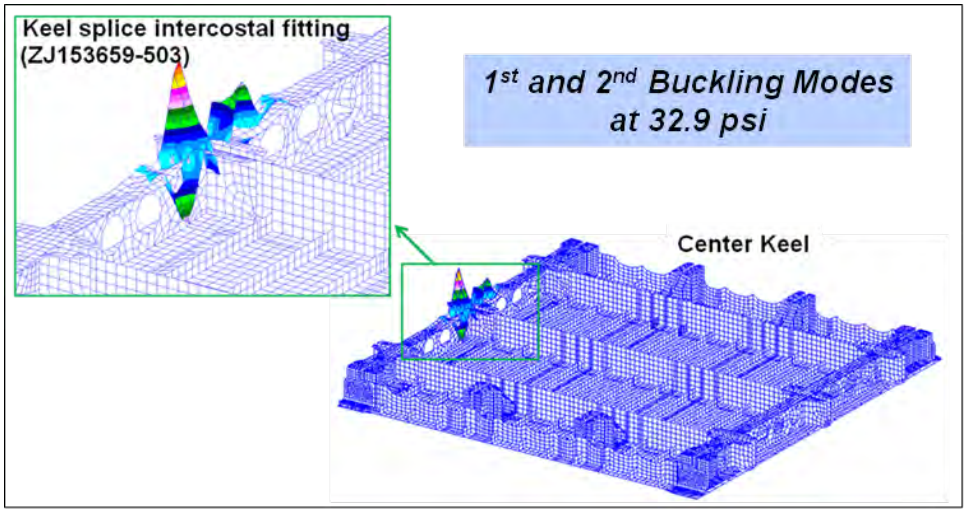

Figure 4-86. First and Second Buckling Modes in 2P Pressure Condition

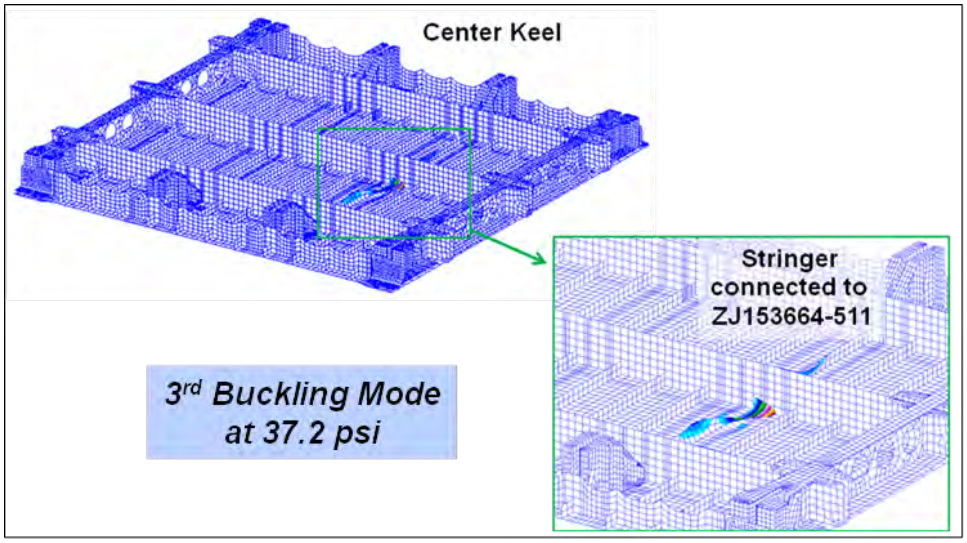

Figure 4-87. Third Buckling Mode in 2P Pressure Condition

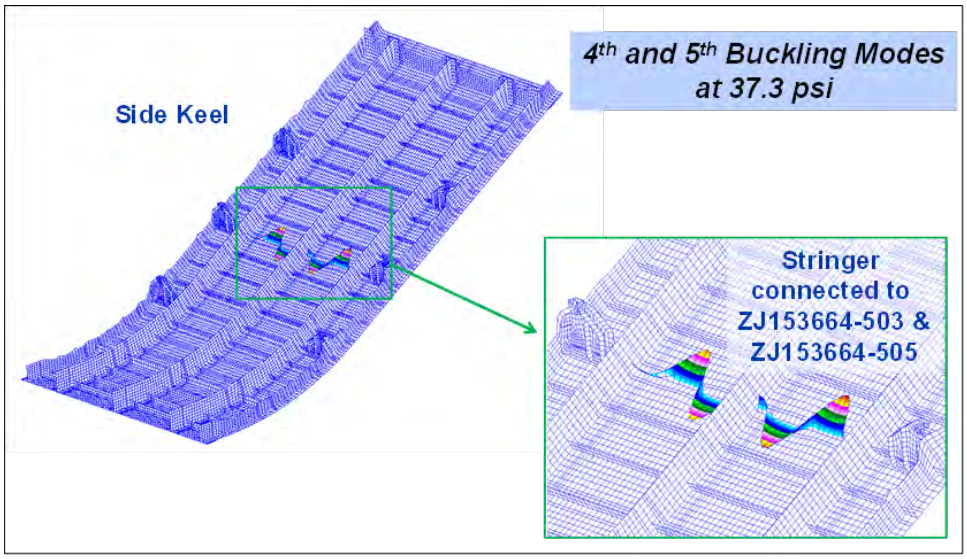

Figure 4-88. Fourth and Fifth Buckling Modes in 2P Pressure Condition

4.3.6.2 2.5-g Maneuver Condition

For the linear buckling analysis in the 2.5-g maneuver condition, as shown in Figure 4-89, the skin at the center section of the crown panel would start to buckle at 0.347-g up-bending load. Plots of the first five modes showed similar mode shapes, all located at the center section of the crown. These buckling modes were local buckling on the skin of the crown. To find out whether a global buckling mode would occur before 2.5-g DLL, linear buckling runs were performed on up to 30 modes. However, with up to 30 buckling modes, buckling modes were found on the skins of crown and no global buckling was found on any of the primary structures, such as frames and T-caps. It was believed that the up-bending load to cause global buckling would be significantly higher than 0.347 g. A nonlinear analysis performed later confirmed that no global instability of the MBB primary structures was found below 2.5-g DUL. No additional runs were performed after the first 30 local buckling modes.

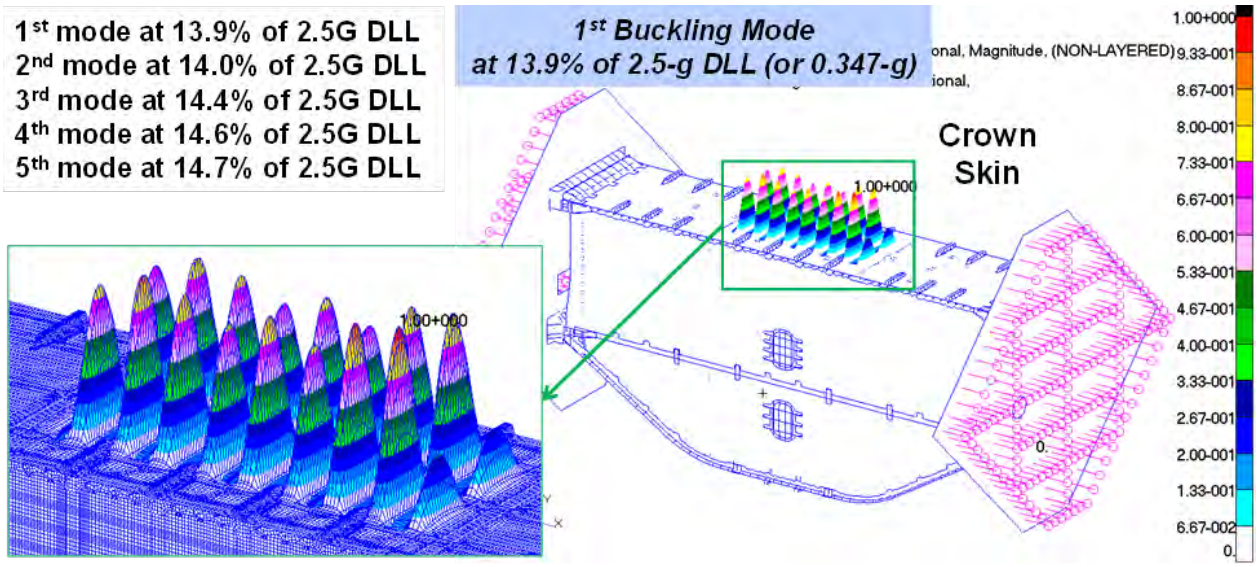

Figure 4-89. First Buckling Mode in 2.5-g Maneuver Condition

4.3.6.3 -1.0-g Maneuver Condition

For the linear buckling analysis in the -1.0-g maneuver condition, the first four buckling modes appeared on the skin of the center keel, as shown in Figure 4-90. The first buckling load was at -0.754-g down-bending load. The fifth buckling mode, as shown in Figure 4-91, appeared on the center section of the floor panel at -0.840-g down-bending load. No global buckling was found on any of the primary structures such as frames and T-caps below -1.0-g DLL. It was believed that the down-bending load for global buckling of the MBB would be significantly higher than -0.754 g. No additional runs were performed for calculating buckling modes beyond -1.0-g DLL.

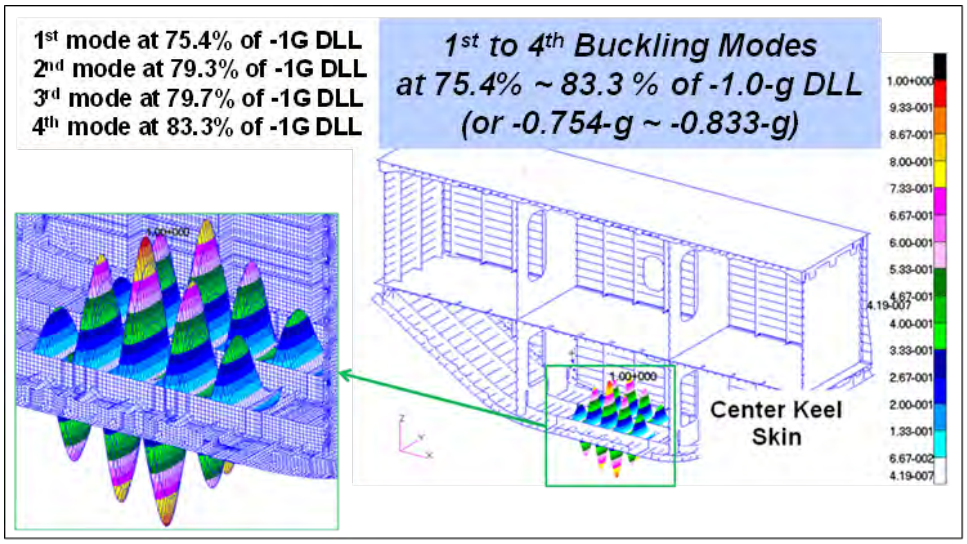

Figure 4-90. First to Fourth Buckling Modes in -1.0-g Maneuver Condition

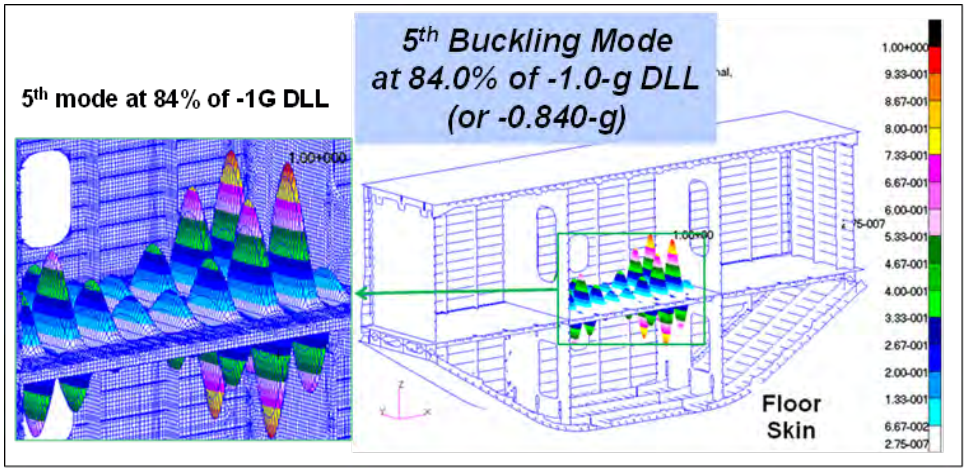

Figure 4-91. Fifth Buckling Mode in -1.0-g Maneuver Condition

4.3.7 Composite Bearing/Bypass Interaction Studies

Another important set of studies performed on the MBB were the bearing/bypass interaction analyses, which were done for fastener locations that showed high bearing and bypass loads in composite structure. These bearing/bypass interaction studies were in addition to typical fastener-related failure checks performed previously and described in Section 4.2.9.3. In the MBB, the critical areas requiring bearing/bypass interaction analyses were located at the panel-to-panel connections, such as at the frames on the upper and lower bulkheads that were connected to the crown, floor, and keel panels.

The 2P pressure condition was found to be the most critical case for the composite bearing/bypass failure mode. While loaded in internal pressure, the upper and lower bulkhead panels of the MBB would bulge outward like a balloon. Consequently, high bearing and bypass loads would be seen on the frames of the upper and lower bulkheads that are connected to the crown, floor, and keel panels. To capture the composite bolted-hole behaviors of these frames, composite bearing/bypass interaction studies were performed on these frames at the fastener locations. Depending on the magnitudes of bearing and bypass loads, a bolted composite may fail along its bearing or bypass loading directions. Therefore, bearing/bypass checks must be performed in both bearing and bypass directions at each fastener location.

In a typical bearing/bypass check, calculated values of composite bypass strain (ε_{pt}) and composite bearing stress (f_{br}) at a critical bolted-hole location are plotted against the bearing/bypass interaction curves. These interaction curves are created by enveloping the composite's bearing strength values (F_{bru}, F_{bry}) and net-section strength values (ε_{uht}, ε_{uhc}, F_{brl}), as shown in Figure 4-92. These composite strength values were determined by tests as a part of NASA's Advanced Subsonic Technology (AST) Composite Wing program (Ref. 4-1). When loaded in tension, as shown in Figure 4-92 for the upper bulkhead frame, the margin of safety was calculated by comparing either the bearing stress (f_{br}) or the principal bypass strain (ε_{pt}) to their failure values (F_{brt} or ε_{byt}) with the formula of MS = F_{brt}/f_{br} - 1 or MS = $\varepsilon_{byt}/\varepsilon_{pt}$ - 1. The results from the bearing/bypass studies showed that margins of safety were all positive for the 2P pressure condition. Details of the bearing/bypass studies of critical frames on the MBB are presented in the following sections.

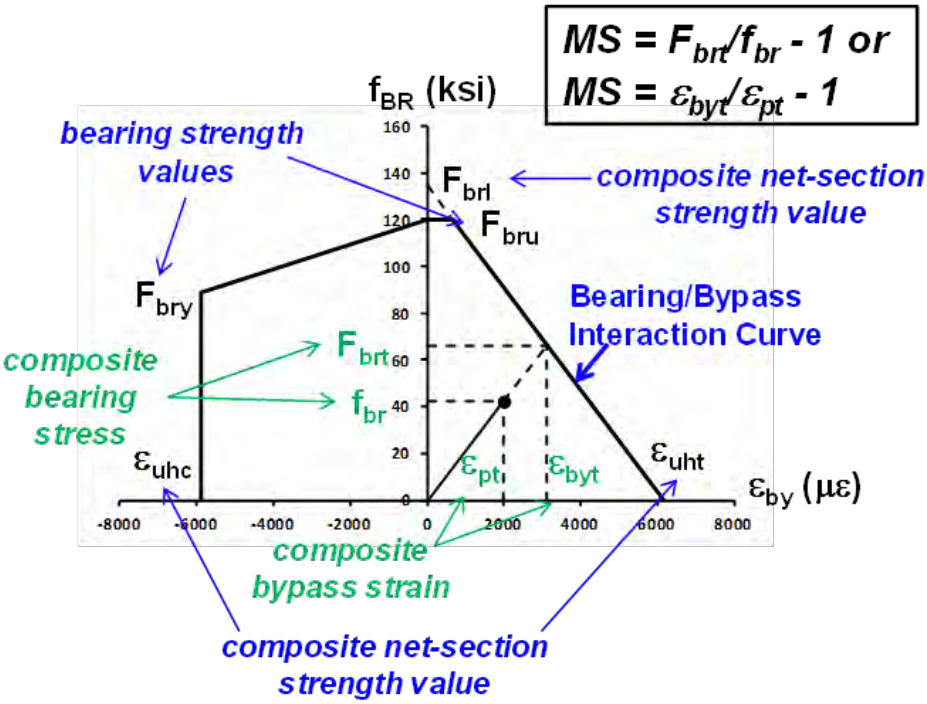

Figure 4-92. Typical Interaction Curve in the Composite Bearing/Bypass Study

In the MBB, frames on PRSEUS panels were made of sandwich structures with either Rohacell foam cores or fiberglass cores. Fiberglass cores were used at locations where these frames were connected to other structural members using mechanical fittings and fasteners. While bolted with mechanical fittings, these fiberglass cores provided out-of-plane stiffness to frames and prevented them from being crushed by fastener clamping forces.

More importantly, the fiberglass cores were able to distribute bolt bearing loads to facesheets more efficiently than did the Rohacell foam cores. In the composite bearing/bypass interaction studies of the MBB, fiberglass cores were assumed to be capable of withstanding bearing loads together with graphite laminate facesheets. To validate this assumption, a post-failure specimen from the pressure cube test (Ref. 4-6) was carefully examined, and a bearing/bypass study of this specimen was also performed. The results from the pressure cube bearing/bypass study showed that fiberglass cores were indeed able to carry bearing loads from fasteners. Details of the pressure cube bearing/bypass study are presented in the following section.

4.3.7.1 Pressure Cube Bearing/Bypass Correlation

To better understand the risk for a flat-sided HWB pressure cabin design in pressure loading, a smaller scale cube specimen was built and successfully tested in 2010. It was subjected to an internal pressure of 5.22P (or 48 psi) (Ref. 4-6). Final failure of the cube started as a crack line on one of the metallic fittings connecting a frame on the crown to a frame on the rib panel, as shown in Figure 4-93. Stress results from linear analysis showed that this critical fitting would start to yield at an internal pressure of 32.4 psi and finally fail at higher pressure. It appeared that the failure of this metallic fitting had caused the final catastrophic failure of the pressure cube.

As shown in Figure 4-93 and Figure 4-94, this metallic fitting has 16 bolts fastened to the frame on the crown and 8 bolts fastened to the frame on the rib. The behavior of the frames at these fastener locations in the pressure cube test provided useful information regarding the

bearing/bypass failure mechanism on PRSEUS frames. Hence, the metallic fitting and fasteners were removed from the composite frames for post-failure inspections of the frames. After removing the metallic fitting and fasteners, as shown in Figure 4-94, it was discovered that the fastener holes were undamaged and showed no sign of any bearing failure. Detailed bearing/bypass interaction studies were performed on the pressure cube at these fastener hole locations and the results are shown in Figure 4-94 and Figure 4-95. The results showed that composite frames on the crown and rib would have negative margins of safety if the facesheets were carrying bolt bearing loads alone. However, where fiberglass cores were included with the facesheets to carry bolt bearing loads, margins of safety from the bearing/bypass studies became positive. In conclusion, it was determined that fiberglass cores in frames should be included in the bearing/bypass study for margin-of-safety calculations.

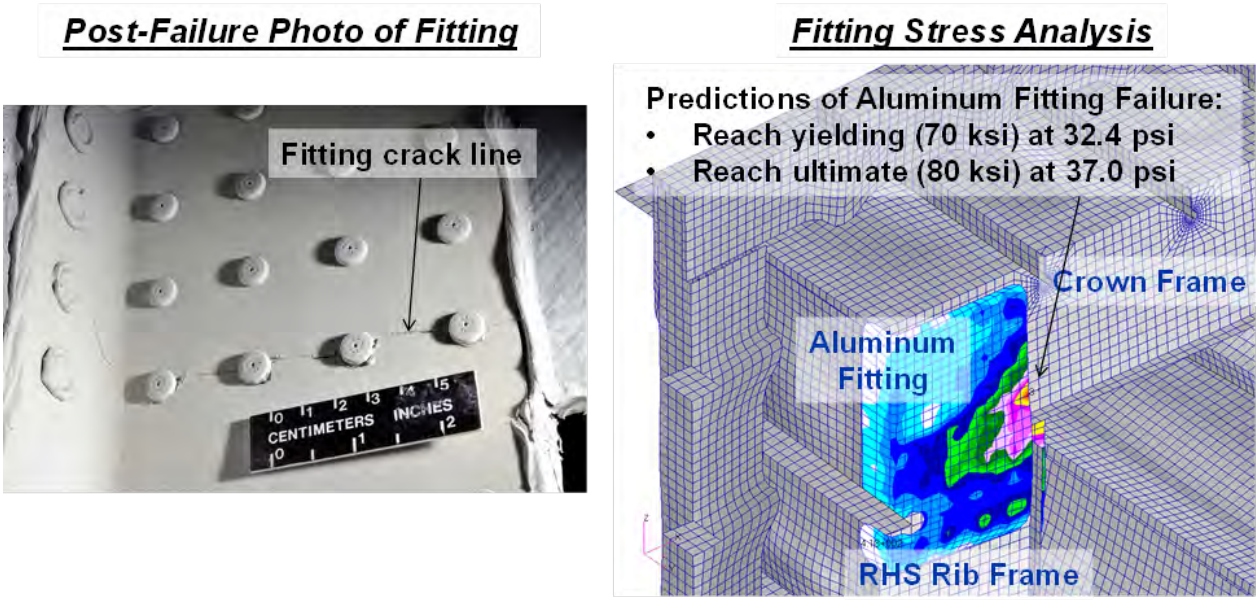

Figure 4-93. Pressure Cube Fitting Post-Failure Photograph and Predictions

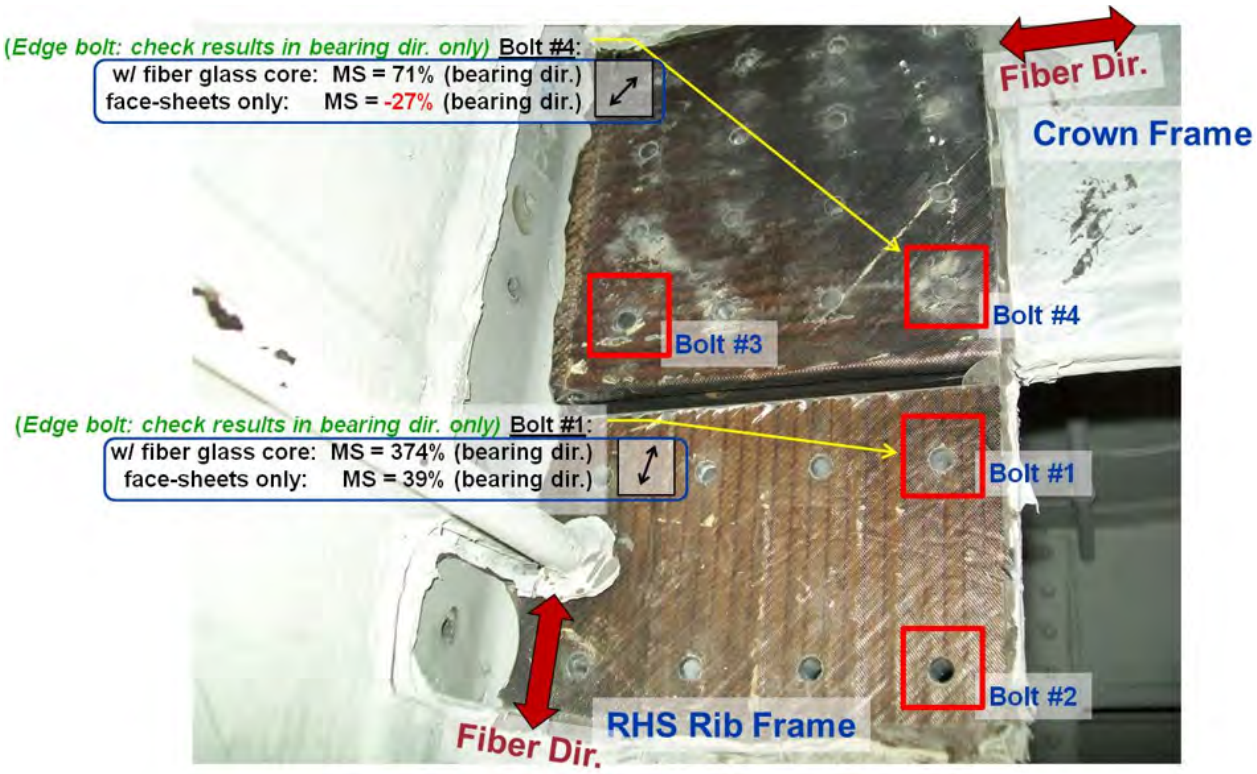

Figure 4-94. Pressure Cube Post-Failure Photograph of Frames on the Crown and Rib

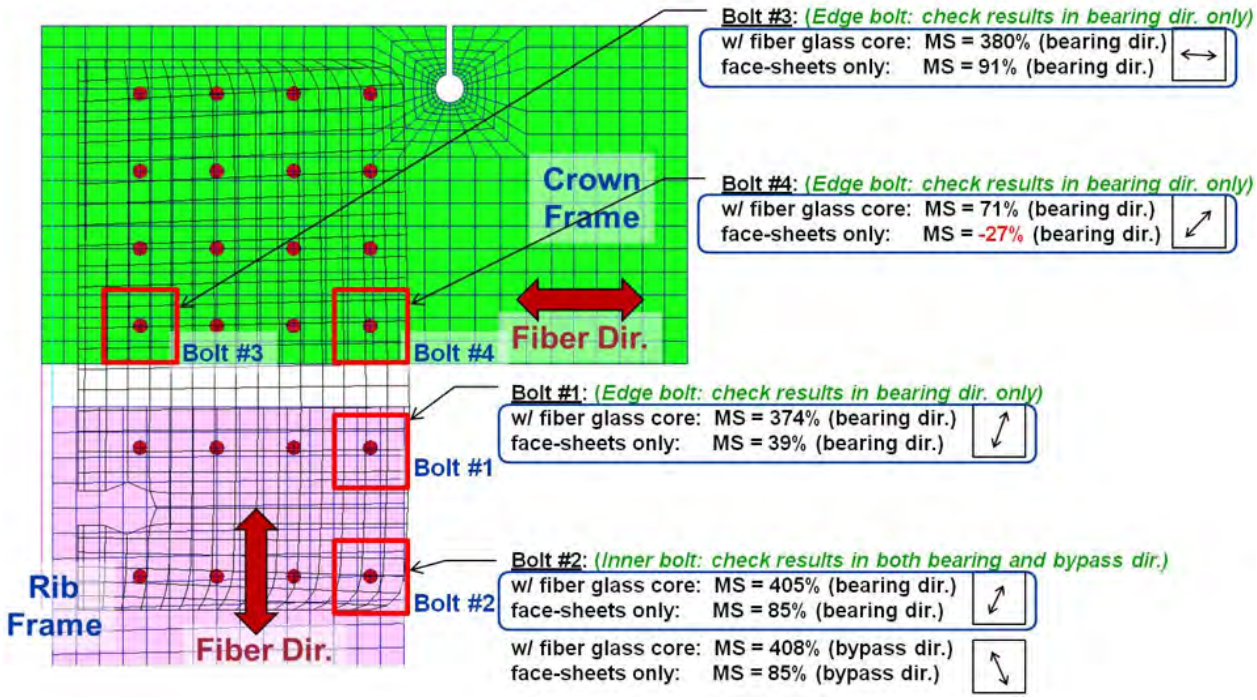

Figure 4-95. Results of Pressure Cube Bearing/Bypass Analysis of Frames on the Crown and Rib

4.3.7.2 Crown to Upper Bulkhead Connection Study

Similar to the pressure cube, the 2P pressure condition is the most critical case for the composite bearing/bypass failure mode for the connection of the upper bulkhead frames to the crown on the MBB. A detailed bearing/bypass interaction study was performed on one of the upper bulkhead frames, which were connected to the crown through mechanical fittings and fasteners. The selected frame had the highest fastener loads in the 2P pressure condition. The location of this frame on the upper bulkhead, and the critical fasteners on this frame, are shown in Figure 4-96. Detailed results, including margins of safety and one of the bearing/bypass interaction curves, are also shown in Figure 4-96. The lowest margin of safety was 56% in the 2P pressure condition.

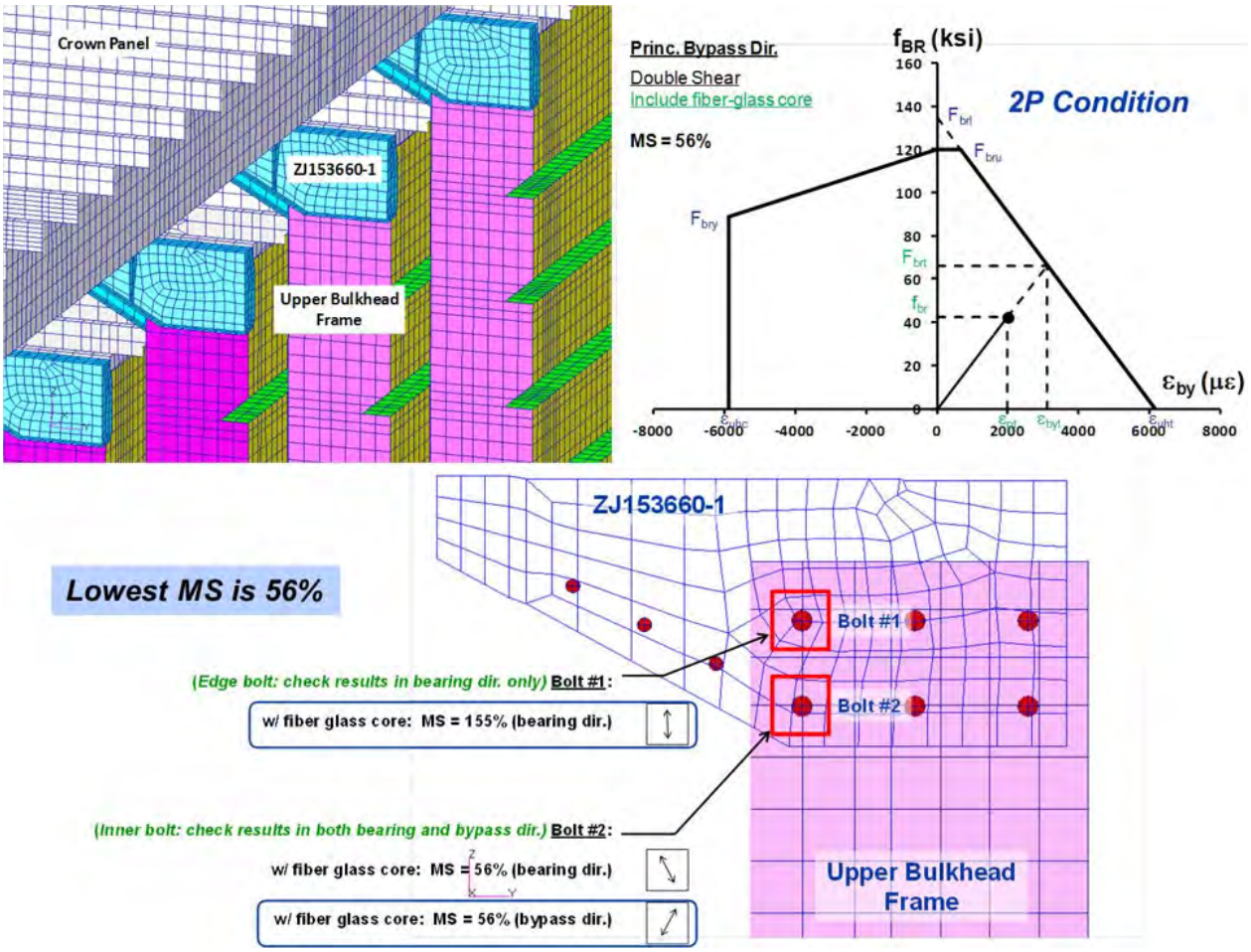

Figure 4-96. Bearing/Bypass Analysis of a Critical Frame on Upper Bulkhead Connected to Crown

4.3.7.3 Floor to Upper/Lower Bulkhead Connection Study

As with the pressure cube and the crown-to-upper-bulkhead connection, the 2P pressure condition is the most critical case for the composite bearing/bypass failure mode for the MBB connection between the upper and lower bulkhead frames and the floor. A detailed bearing/bypass interaction study was performed on one of the upper bulkhead frames and its corresponding lower bulkhead frame, where these two frames connected to the floor through mechanical fittings and fasteners. The selected frames had the highest fastener loads in the 2P pressure condition. The location of these frames on the upper and lower bulkheads, and the critical fasteners on these frames, are shown in Figure 4-97 for fitting ZJ153662-503 and in Figure 4-98 for fitting ZJ153662-505. Detailed results, including margins of safety and one of the bearing/bypass interaction curves, are also shown in Figure 4-97 and Figure 4-98. The lowest margin of safety was 45% for fitting ZJ153662-503 and 44% for fitting ZJ153662-505.

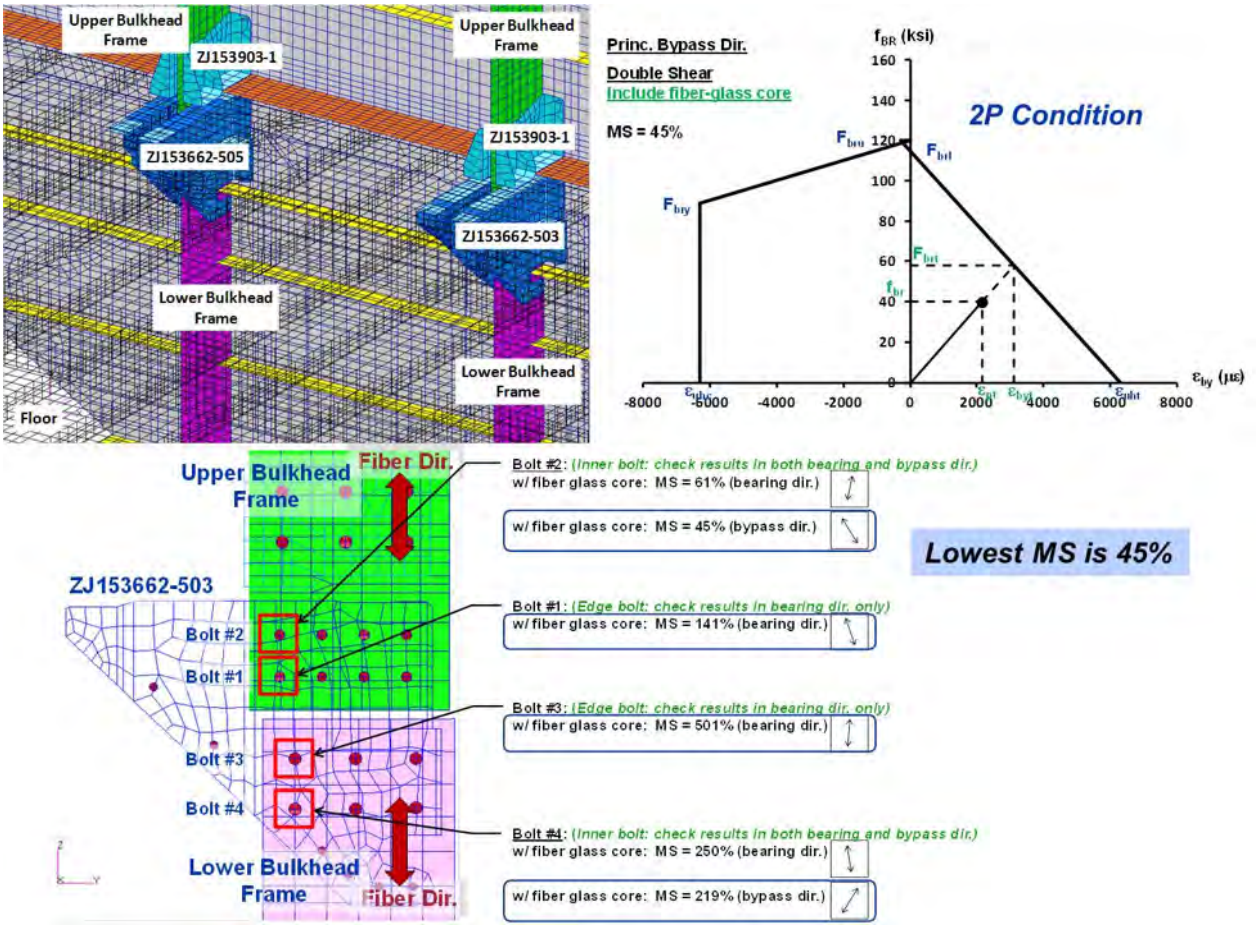

Figure 4-97. Bearing/Bypass Analysis of Critical Frames on the Upper and Lower Bulkheads Connected to the Floor on Fitting ZJ153662-503

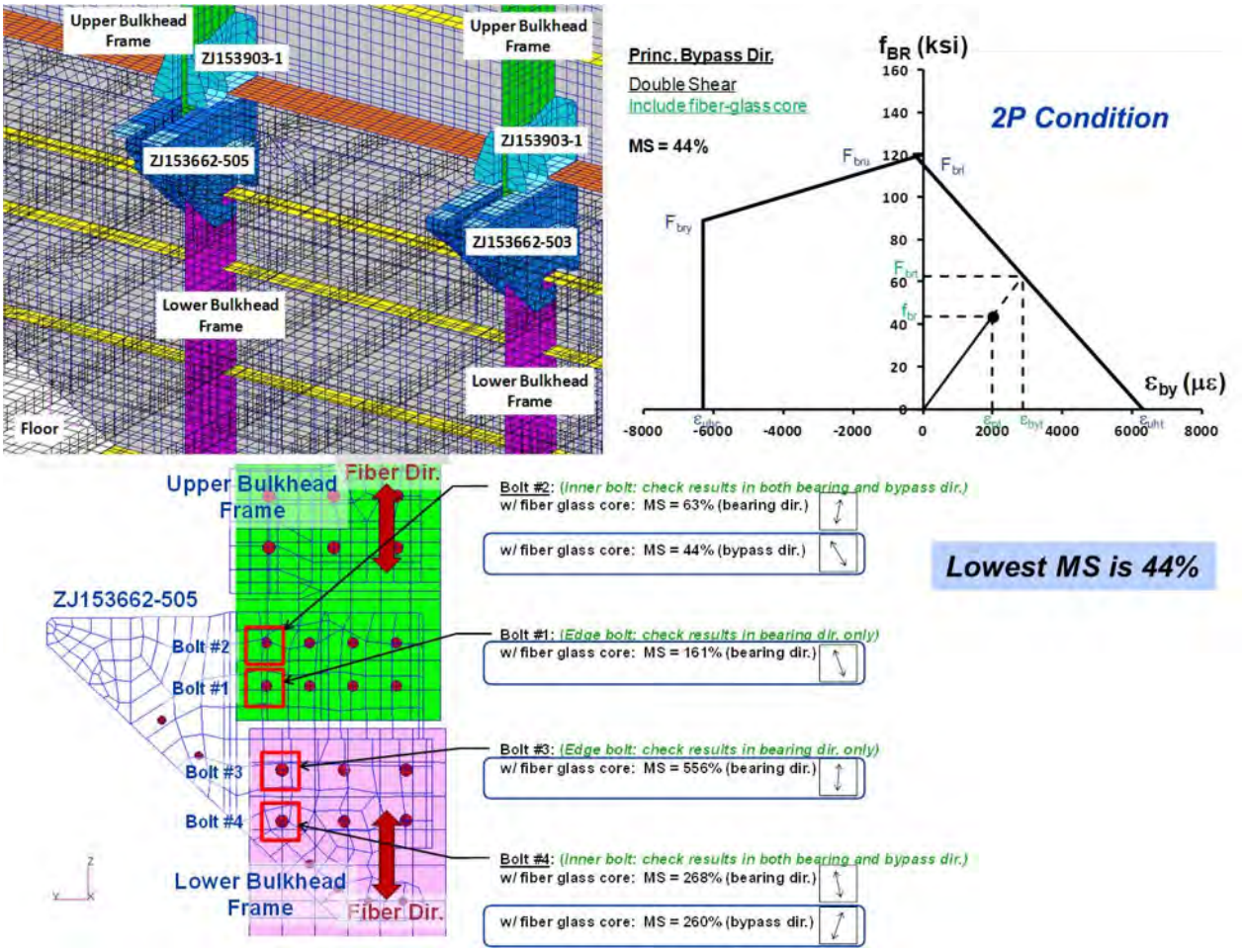

Figure 4-98. Bearing/Bypass Analysis of Critical Frames on the Upper and Lower Bulkheads Connected to the Floor on Fitting ZJ153662-505

4.3.7.4 Center Keel to Lower Bulkhead Connection Study

As with the pressure cube, and the other frame connections at corners in the MBB, the most critical case for composite bearing/bypass failure for the connection between the lower bulkhead frames and the center keel was the 2P pressure condition. A detailed bearing/bypass interaction study was performed on one of the lower bulkhead frames, where it connected to the center keel through mechanical fittings and fasteners. The selected frame had the highest fastener loads. The location of this frame on the upper bulkhead, and the critical fasteners on this frame, are shown in Figure 4-99. Detailed results, including margins of safety, and one of the bearing/bypass interaction curves, are also shown in Figure 4-99. The lowest margin of safety in the 2P pressure condition was 182%.

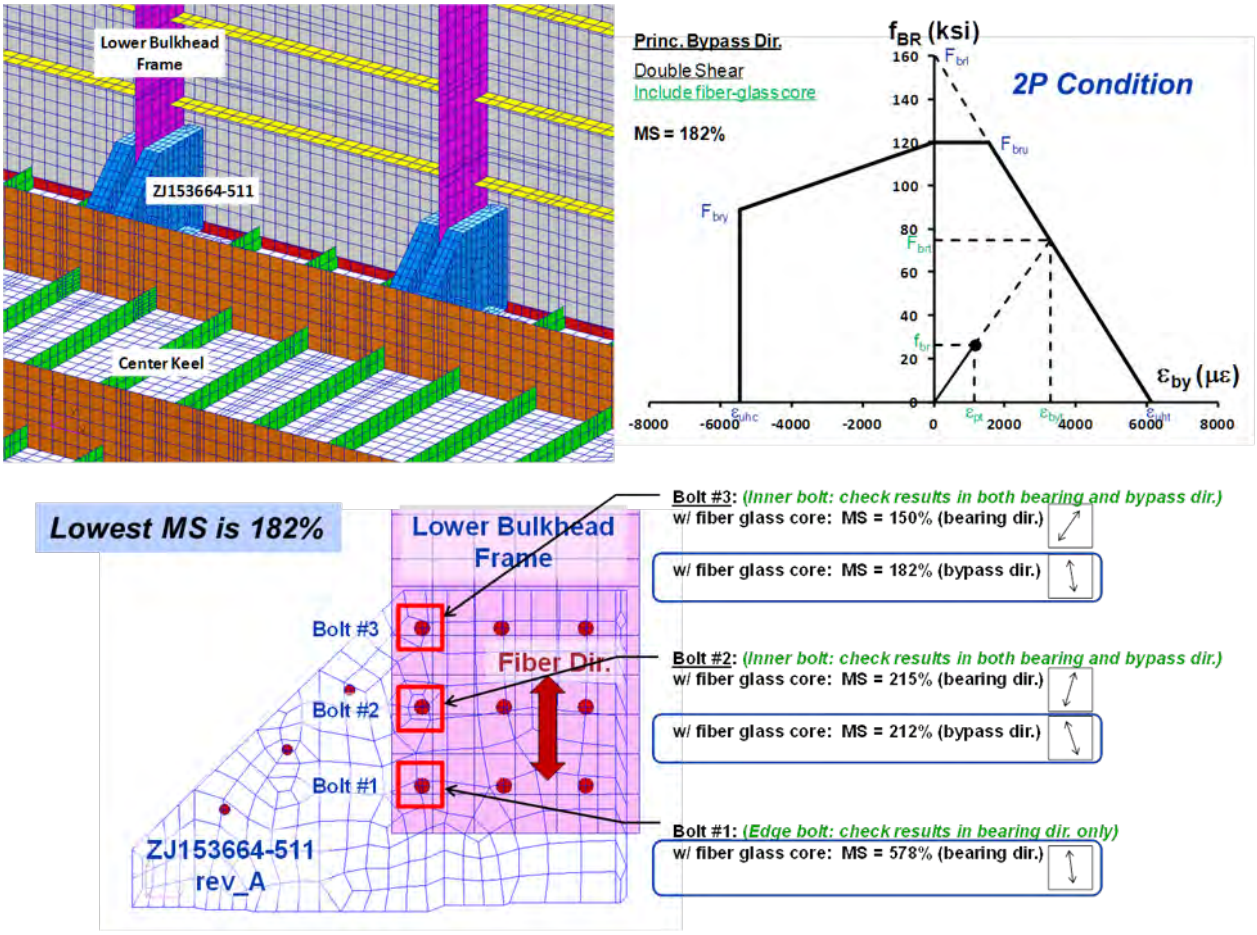

Figure 4-99. Bearing/Bypass Analysis of a Critical Frame on Upper Bulkhead Connected to Crown

4.3.8 T-cap Noodle Failure Studies

The integral cap features in the MBB and the pressure cube were made by folding layers of warp-knit fabric to create a T-cap and skin configuration. A braided fillet detail (or noodle) fills the gap between the T-cap web, T-cap flange, and skin layers. During the testing of the pressure cube (Ref. 4-6), an inter-laminar tension failure (or delamination) was initiated along the fillet on the crown panel at 16 psi. As the fillet delamination progressed, it was contained by the adjacent stitching, enabling the T-cap to continue carrying loading until the final catastrophic failure occurred at 48 psi. Post-test microscopic examination was performed on the pressure cube by sectioning the delaminated T-cap of the pressure cube structure. The examination revealed that the inner radius-laminate of the T-cap had delaminated like an onion peel (Ref. 4-8). A 3D detailed FEA from the pressure cube confirmed that high inter-laminar tensile stresses appeared along the inner radius-laminate of the T-cap. This type of resin failure mode was caused by the high inter-laminar tensile forces generated by pull-off loads and rocking moments on the T-cap due to the internal pressure. The inter-laminar tension allowable was derived from results of the pressure cube test and the pressure cube 3D detailed analysis. This inter-laminar tension allowable was used to predict the initiation of an inter-laminar failure in the T-caps on the MBB. Results from the 3D detailed FEA for the pressure cube are presented in the following section.

The MBB had T-cap features on the crown, floor, keel, and upper bulkhead panels. Based on the test results from the pressure cube, it was reasonable to expect that similar inter-laminar resin failures would occur in the MBB under the 2P pressure condition. Seven locations in the MBB that had integral cap features required further investigations. These locations were at the connections between the following panels: crown/upper bulkhead, upper bulkhead/rib, crown/rib, floor/rib, center keel/lower bulkhead, side keel/lower bulkhead, and floor/bulkhead. At each location, pull-off loads and rocking moments for the MBB and the pressure cube were compared to investigate the likelihood of an inter-laminar resin failure. These locations and their loads are shown in Figure 4-100. The most critical location was the T-cap on the crown, which was connected to the upper bulkhead. A 3D detailed FEM was built for the T-cap on the crown. Results from the 3D detailed FEA of the MBB are presented in the following section.

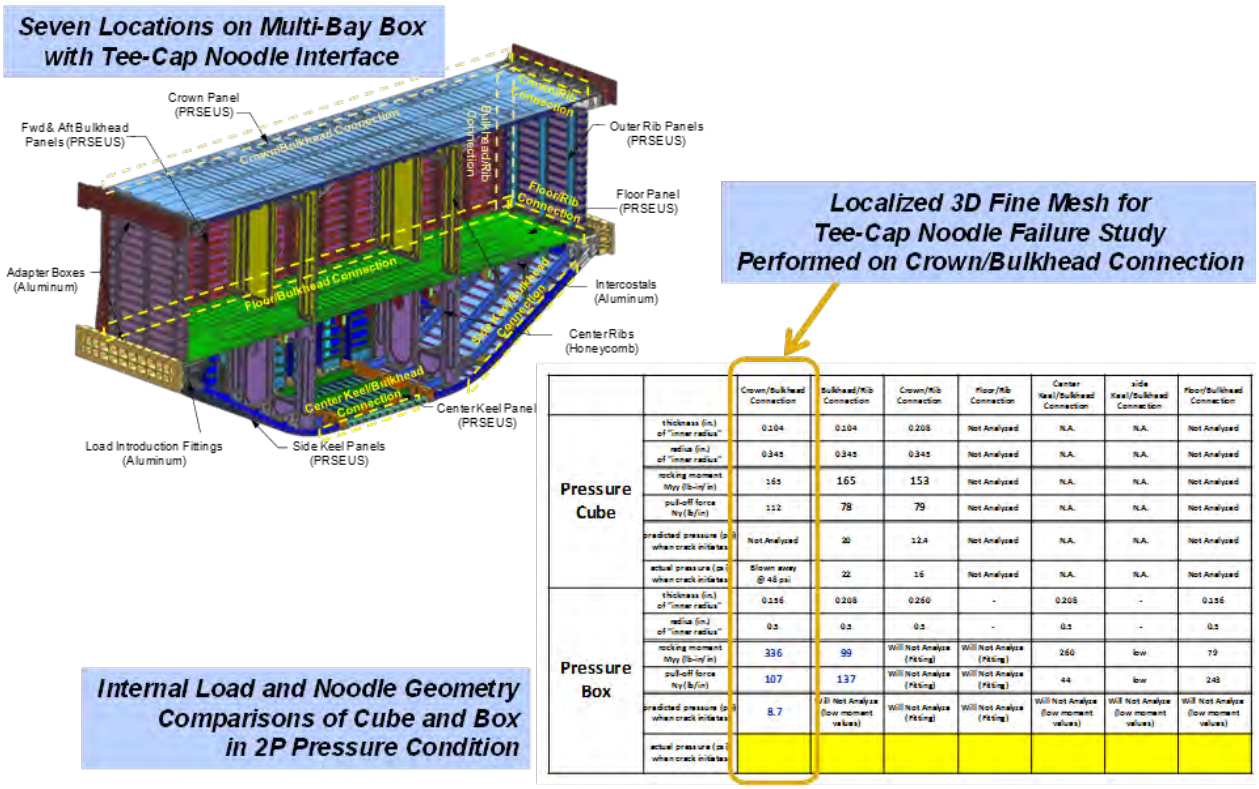

		Crown/Bulkhead Connection	Bulkhead/Rib Connection	Crown/Rib Connection	Floor/Rib Connection	Center Keel/Bulkhead Connection	side Keel/Bulkhead Connection	Floor/Bulkhead Connection
Pressure Cube	thickness (in.) of "inner radius"	0.104	0.104	0.208	Not Analyzed	N.A.	N.A.	Not Analyzed
	radius (in.) of "inner radius"	0.345	0.345	0.345	Not Analyzed	N.A.	N.A.	Not Analyzed
	rocking moment Myy (lb-in/in)	165	165	153	Not Analyzed	N.A.	N.A.	Not Analyzed
	pull-off force Ny (lb/in)	112	78	79	Not Analyzed	N.A.	N.A.	Not Analyzed
	predicted pressure (psi) when crack initiates	Not Analyzed	20	12.4	Not Analyzed	N.A.	N.A.	Not Analyzed
	actual pressure (psi) when crack initiates	Blown away @ 48 psi	22	16	Not Analyzed	N.A.	N.A.	Not Analyzed
Pressure Box	thickness (in.) of "inner radius"	0.156	0.208	0.260	-	0.208	-	0.156
	radius (in.) of "inner radius"	0.5	0.5	0.5	-	0.5	-	0.5
	rocking moment Myy (lb-in/in)	336	99	Will Not Analyze (Pitting)	Will Not Analyze (Pitting)	260	low	79
	pull-off force Ny (lb/in)	107	137	Will Not Analyze (Pitting)	Will Not Analyze (Pitting)	44	low	248
	predicted pressure (psi) when crack initiates	8.7	Will Not Analyze (low moment values)	Will Not Analyze (Pitting)	Will Not Analyze (Pitting)	Will Not Analyze (low moment values)	Will Not Analyze (low moment values)	Will Not Analyze (low moment values)
	actual pressure (psi) when crack initiates							

Figure 4-100. Seven Locations With Integral Cap Features Were Investigated

4.3.8.1 Pressure Cube Noodle Correlation

During pressure cube testing (Ref. 4-6), a sudden jump of strain gage readings at a location near the T-cap on the crown was observed at 16 psi of internal pressure. After internal pressure was released from the test cube, a Nondestructive Inspection (NDI) was performed on the structures adjacent to the T-cap on the crown. The NDI revealed that inter-laminar cracks (delamination) had occurred inside the laminate of the T-cap during the pressure test. With the presence of these inter-laminar cracks in the T-cap, testing was resumed, and the pressure cube continued to carry loads higher than 16 psi until, finally, a two-piece failure occurred at 48 psi. From the pressure cube test, it appeared that these inter-laminar cracks were contained by the adjacent stitching, enabling the T-cap to carry higher internal pressure load until a final catastrophic failure occurred at another location. A post-test sectioning of the T-cap showed that the inner radius-laminate of the T-cap had delaminated like an onion peel, and this delamination was contained by the adjacent stitches (Ref. 4-8). It is believed that this type of resin failure mode was initiated by high inter-laminar tensile stresses created from high pull-off loads and rocking moments imparted on the T-cap from the internal pressure. To calculate the inter-laminar tensile stress when this delamination occurred, a 3D detailed FEM of the T-cap on the pressure cube was built. An FEA was performed to calculate the inter-laminar tensile stresses in the inner radius-laminate of the T-cap at 16 psi when initial cracking occurred.

From the results of pressure cube global FEA, as shown in Figure 4-101, pull-off load (Ny) and rocking moment (Myy) on the T-cap peaked at the center location between frames on the crown. Thus, a high-fidelity 3D detailed FEM was built at this location for inter-laminar tensile stress calculations. In this 3D detailed FEA, CHEXA and CPENTA 3D solid elements were used in modeling the noodle and laminates of the T-cap and skin on the crown. Peel stresses on the

inner-radius laminate of the T-cap were calculated and are shown in Figure 4-102. At 2P (or 18.4 psi), a maximum radial (or peeling) stress of 7,420 psi was seen on the inner-radius laminate of the T-cap. By scaling down the internal pressure from 18.4 psi to 16 psi when the inter-laminar cracks were observed, a critical radial stress on the inner-radius equal to 6,452 psi was derived. This radial (or peeling) stress of 6,452 psi derived from the pressure cube test was used in predicting the inter-laminar cracks of the T-caps on the MBB.

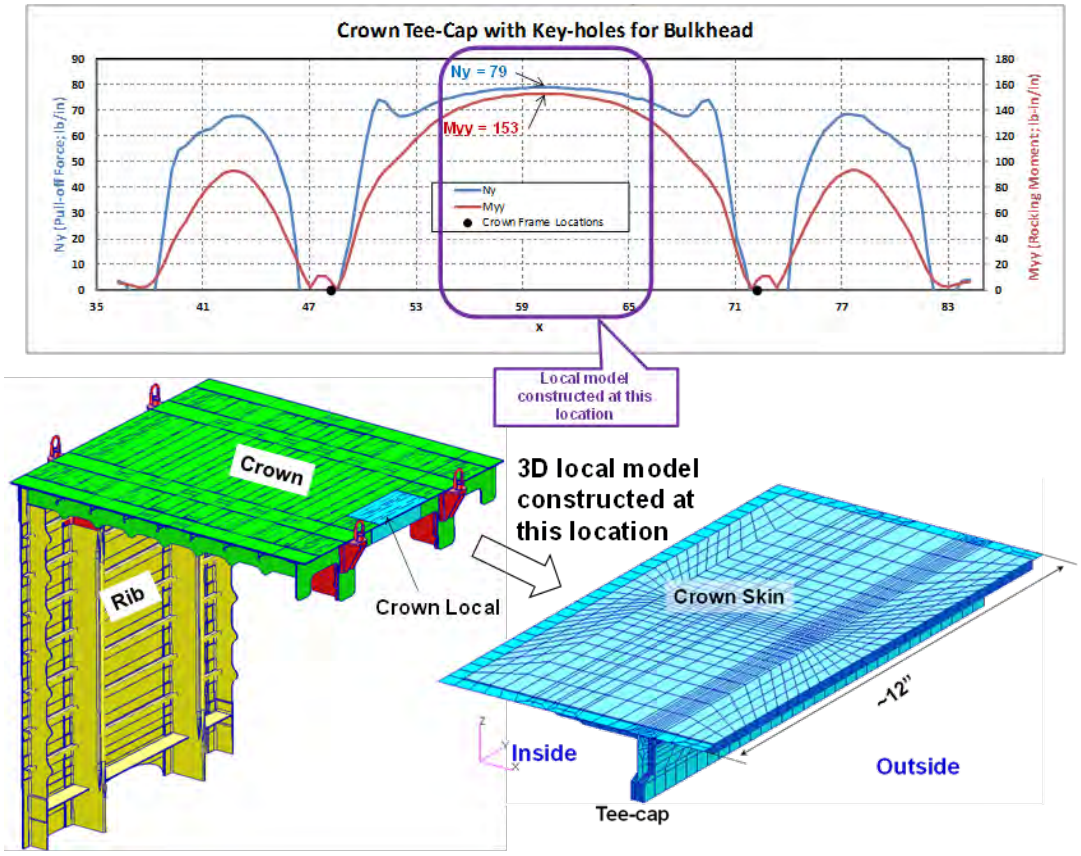

Figure 4-101. Location of 3D Detailed FEM Study of T-cap on the Crown of the Pressure Cube

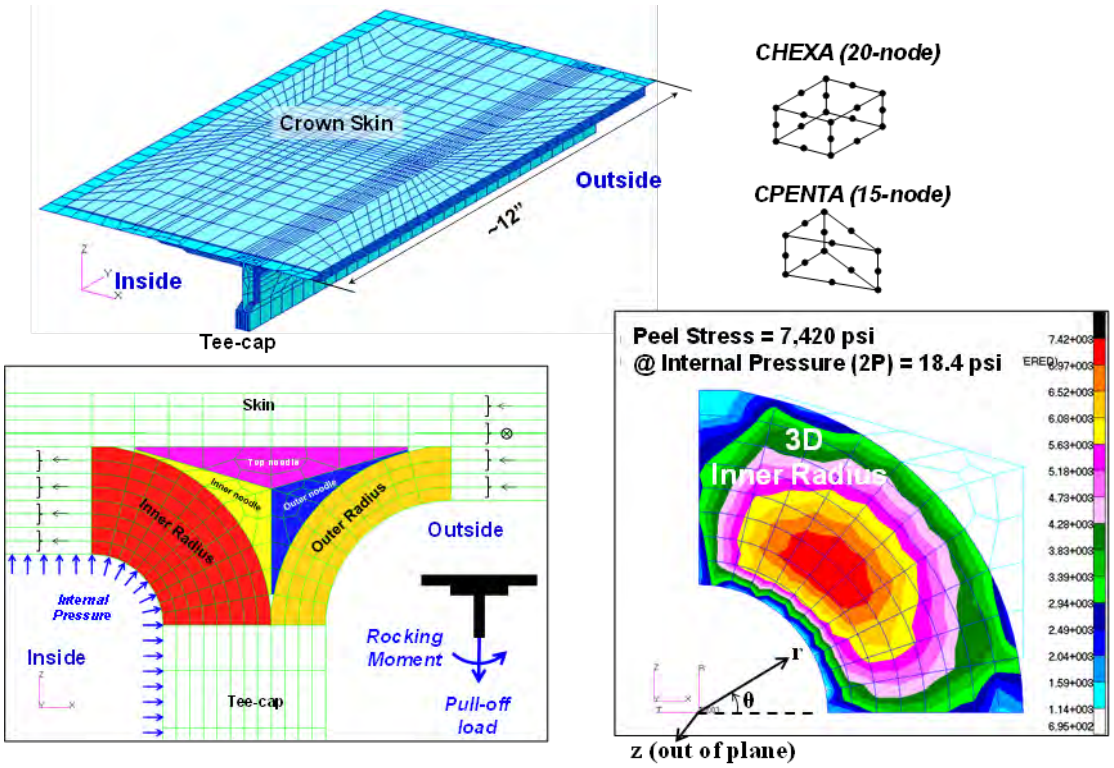

Figure 4-102. Results of Inter-laminar Tensile Stress Calculation From the Pressure Cube 3D FEM

4.3.8.2 Crown to Upper Bulkhead Noodle Study

On the MBB, T-caps that had the highest pull-off loads and rocking moments were at locations where the T-cap on the crown panel and upper bulkheads were connected. As discussed earlier, the inter-laminar crack (delamination) on a T-cap was initiated by high inter-laminar tensile stresses created from high pull-off loads and rocking moments imparted on the T-cap from the internal pressure. To find the most critical T-cap location on the crown, pull-off loads and rocking moments were plotted along the T-caps on the crown, as shown in Figure 4-103. The distributions of these pull-off loads and rocking moments were examined for the most critical location that would be analyzed in the 3D detailed FEA. From Figure 4-103, the values of pull-off load (Ny) and rocking moment (Myy) were both high at a location where a T-cap intersected with stringer-9 of the crown. The inter-laminar tension stress of the T-cap on the crown was most likely the highest at this location. Therefore, a high-fidelity 3D detailed FEM was built at this T-cap location for inter-laminar tensile stress calculations.

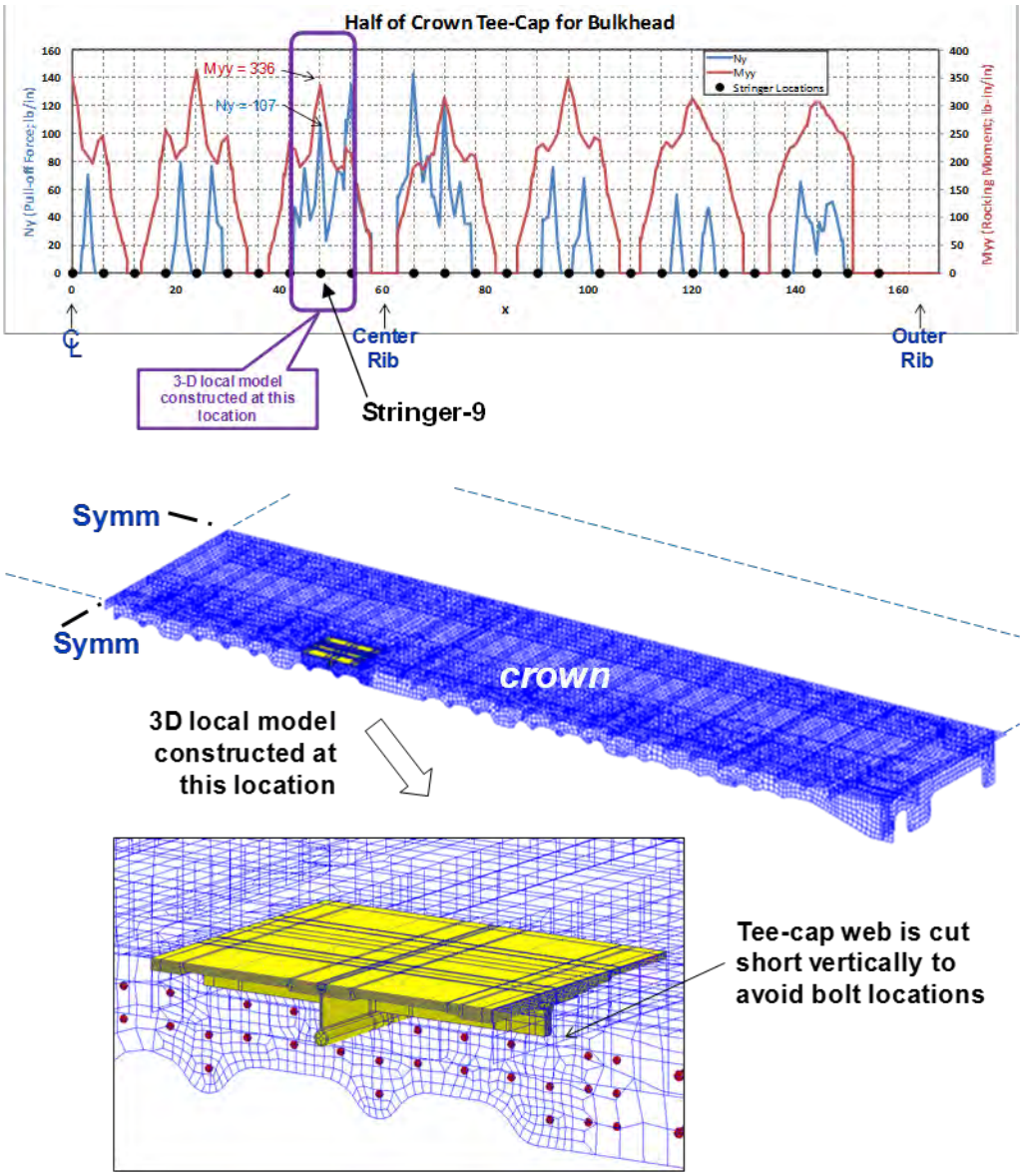

Figure 4-103. Location of 3D Detailed FEM Study of a T-cap on the Crown of the MBB

In this high-fidelity 3D detailed FEM for the T-cap on the MBB, CHEXA and CPENTA 3D solid elements were used in modeling the noodle and laminates of the T-cap, stringer, and skin on the crown. Two solid elements were used in each composite stack to capture the stress variations through the thickness of the stacks. In the in-plane directions of laminates, finer meshes were used at locations where higher stress variations were expected. To represent discontinuity of the T-cap web at keyhole locations where stringers passed through, nodes on the T-cap web and stringer finite elements were not connected. Equivalent laminate moduli (Ref. 4-1) with homogeneous properties were used on these 3D elements. 2P pressure was applied on the internal faces of the T-cap web and crown skin, and the displacements derived from the global FEA were applied at the boundaries of this 3D detailed FEM. As shown in Figure 4-104, there were a total of 461,054 nodes, 103,413 CHEXA and 2 CPENTA solid elements, and 133 RBE2 and 436 RSPLINE rigid body elements in this 3D detailed FEM.

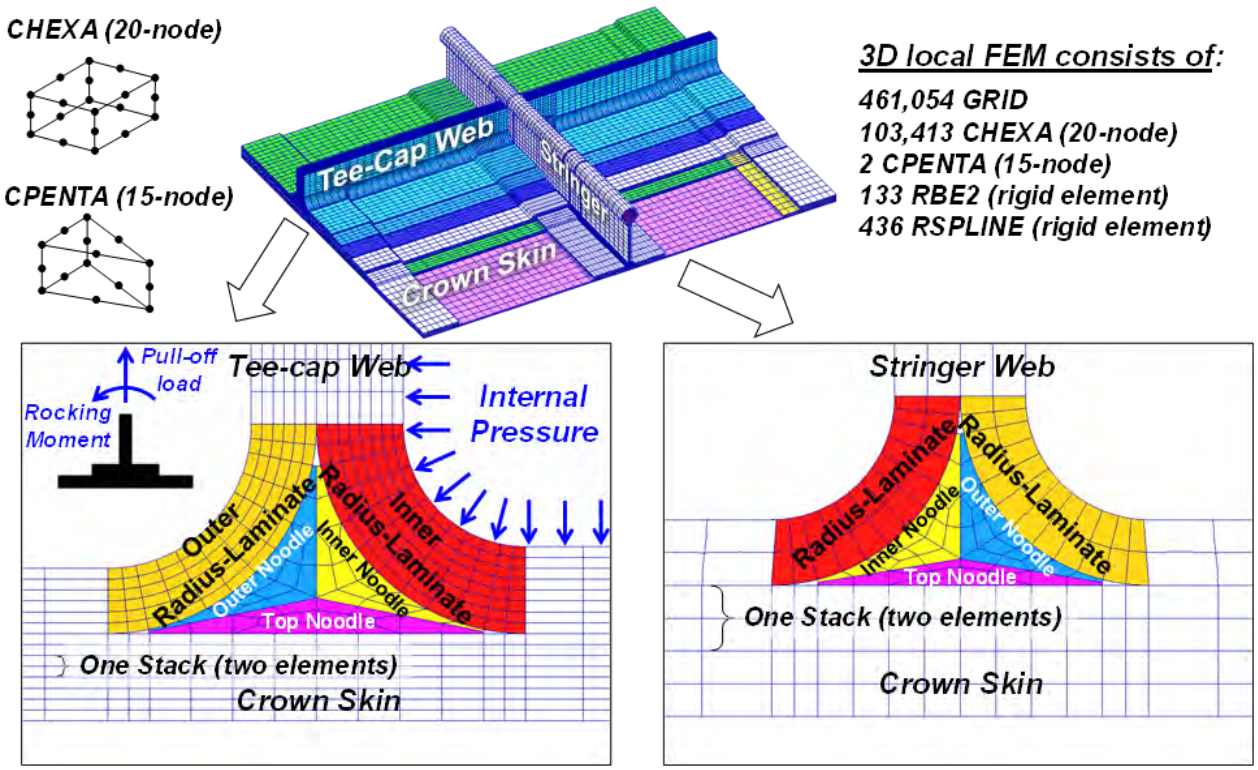

Figure 4-104. 3D Detailed FEM for Inter-laminar Tensile Stress Calculations

From the 3D detailed FEA for the MBB, as shown in Figure 4-105, a high inter-laminar tensile stress of 13.6 ksi was observed on the stringer radius-laminate that was connected to the terminated-end of the T-cap noodle in the 2P pressure condition. This high inter-laminar tensile stress value was likely caused by the stress concentration due to the termination of the T-cap noodle at the intersection with a stringer member. Using the inter-laminar strength allowable derived from the pressure cube test, failure calculations were made for the T-cap and stringers of the crown on the MBB. The results from the failure calculations showed that high inter-laminar tensile stresses in the stringer radius-laminate would cause resin cracking (or delamination) at an internal pressure of 8.7 psi. Although this pressure loading value was lower than 2P DUL, the area with high inter-laminar tensile stress was small and confined to the fillet region by surrounding stitches. When this interface resin cracking in the stringer radius-laminate initiated, this localized resin cracking would likely be contained by the surrounding stitches. The stringer and T-cap would continue to carry higher loads, as they did in the pressure cube test. A catastrophic failure was not expected to be caused by this localized resin cracking failure mode.

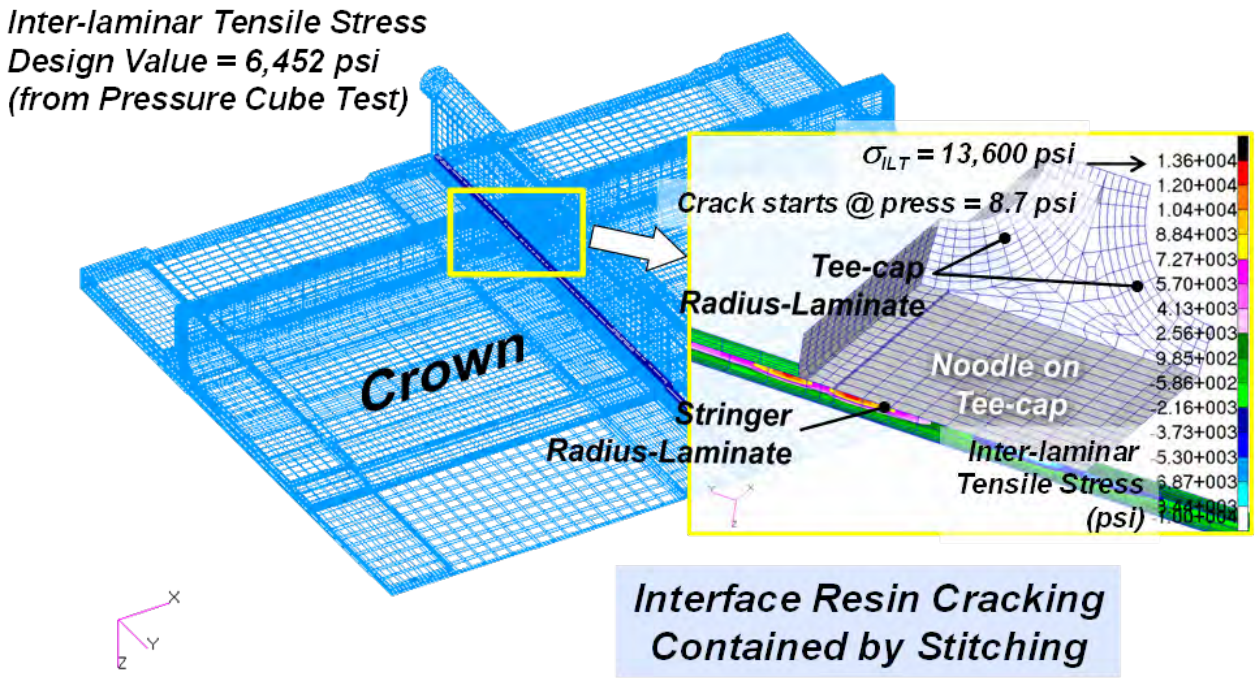

Figure 4-105. Inter-laminar Tensile Stress on Stringer Radius-Laminate in 2P Condition

4.4 Multi-bay Box Test Failure Predictions

The MBB underwent a series of tests, comprising the five critical load cases described in Section 4.2.1. These five critical load cases were the 2P pressure condition, the 2.5-g and -1.0-g maneuver conditions, and the 2.5-g + 1P and -1.0-g + 1P combined loading conditions. The MBB was tested in the DLLs and DULs of these five cases. In addition, the MBB was tested in its pristine structural condition and impact-damaged condition. Upon completing all five critical cases, the MBB was then subjected to final failure load testing, during which a catastrophic failure could occur at any time. The sequence of MBB structural tests is shown in Figure 4-106. Tests of the MBB in DLLs were for validating the structural integrity of the structure, and no structural failure was expected to occur in DLL. Thus, failure predictions in DUL tests were made for the MBB in pristine and impact-damaged conditions, and final failure test of the impact-damaged test article.

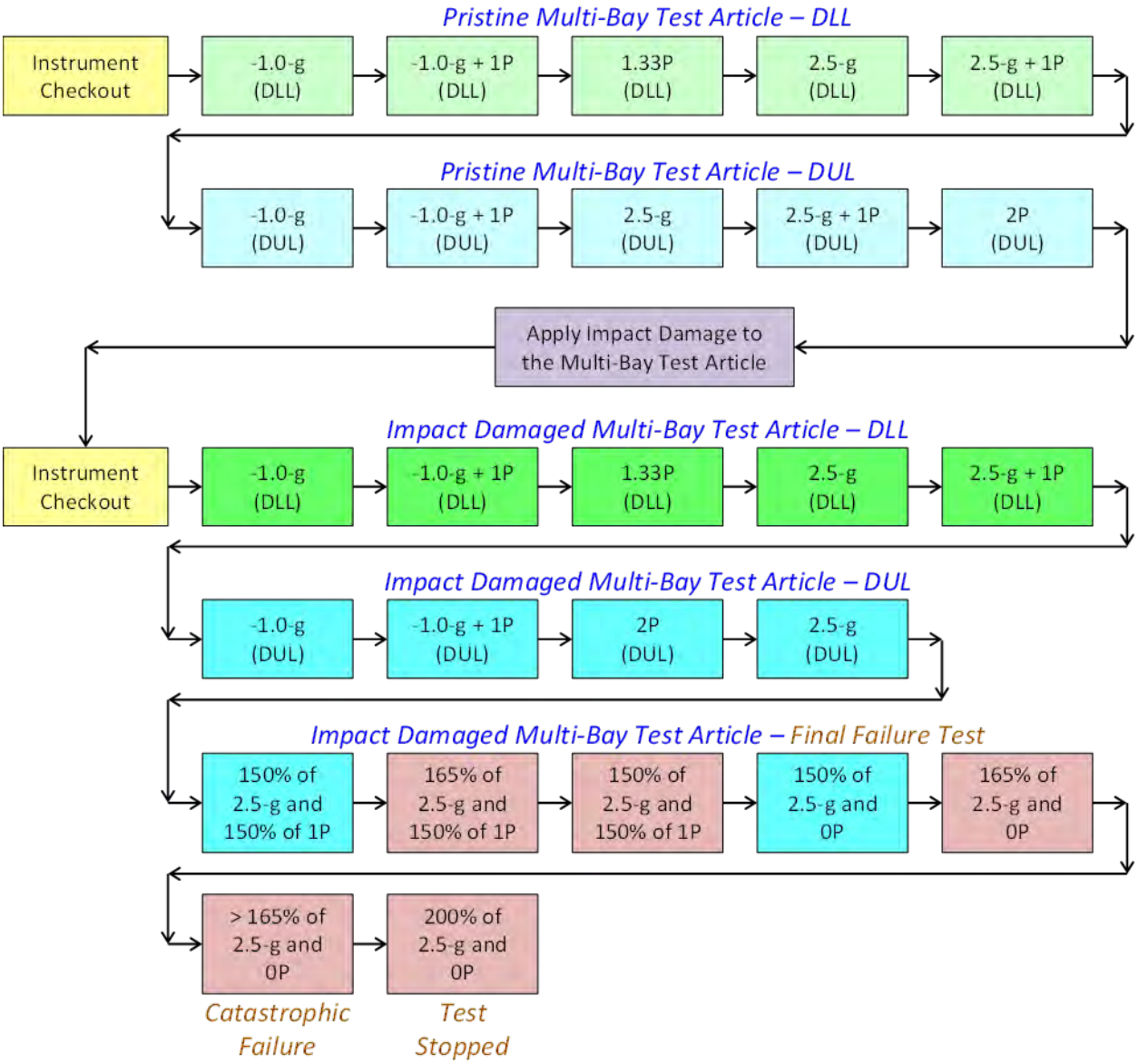

Figure 4-106. Sequence of the MBB Structural Tests

In predicting failures of the MBB, instead of using notched composite strength values for design and in margin-of-safety calculations, un-notched (pristine) composite strength values were used in failure predictions of composites, except at locations of impact damage where notched strength values were used. As shown in Table 4-7, un-notched composite strength values for the MBB were -8,000 micro-in./in. for compression and 10,000 micro-in./in. for tension. For metallic fittings and fasteners, instead of using tensile yield strengths for design and in margin-of-safety calculations, tensile ultimate strengths of metals were used in failure predictions. In Table 4-7, only tensile yield strengths of metals were listed; however, the ultimate strengths of metals were derived from these yield strength values. For instance, strength values of 15% above the yield strengths shown in Table 4-7 were used as the ultimate strengths of metals. This was because ultimate strengths of metals are generally 15% greater than their yielding strengths.

Even though only linear analysis results were available during the designing and sizing phase of the MBB, nonlinear analyses were completed before testing of the structure. Results from nonlinear analyses were more representative and meaningful and would be used in failure predictions for the MBB. The inclusion of nonlinear geometric effects in the analysis made studies possible on composite panel membrane-force and bending-moment coupling effects in pressure conditions and panel skin post-buckling in maneuver cases. Results from nonlinear analysis were used in the failure predictions for the MBB, and, in addition, design modifications to the MBB (such as repairs on the crown) were incorporated into the global FEM. This ensured a more accurate representation of the final configuration and, therefore, yielded better failure predictions for the MBB.

In the following sections, plots of LVDT displacements and strain gage results versus pressure or actuator load are presented. Please note that these plots do not contain test data even though the legends mention test data along with predicted results. The plots were set up for test data to be added after testing. The test data were not available as of this writing, and inclusion of the test results in the report was not in the scope of the contract.

4.4.1 2P Pressure Condition

Failure predictions for the MBB in the 2P pressure condition were made based on results from nonlinear analysis of the global FEM. In the 2P pressure condition, a 2P pressure creates a force normal to the internal skin surface that deforms the crown, bulkhead, and keel panels outward. To understand the structural behavior of the MBB and the crown panel in the 2P pressure load, displacement plots from nonlinear and linear analyses were compared and are shown in Figure 4-107 and Figure 4-108. For the MBB, the maximum displacement at the center of the forward upper bulkhead was 0.951 in. from the nonlinear analysis and 1.080 in. from the linear analysis. For the crown panel, the maximum displacement at the center of the crown was 0.360 in. from the nonlinear analysis and 0.446 in. from the linear analysis. These results showed that displacements from the nonlinear analysis were smaller than those from the linear analysis in the 2P pressure condition. This was because for a large out-of-plane deformation, an appreciable in-plane tensioning occurs, which, in turn, tends to stiffen the deformed structure and effectively suppresses further out-of-plane deformation. Because this coupling mechanism between the bending and in-plane stretching of the panels was included in the nonlinear solution, the out-of-plane displacement of the upper bulkhead from the nonlinear solution was smaller than the one produced by the linear solution.

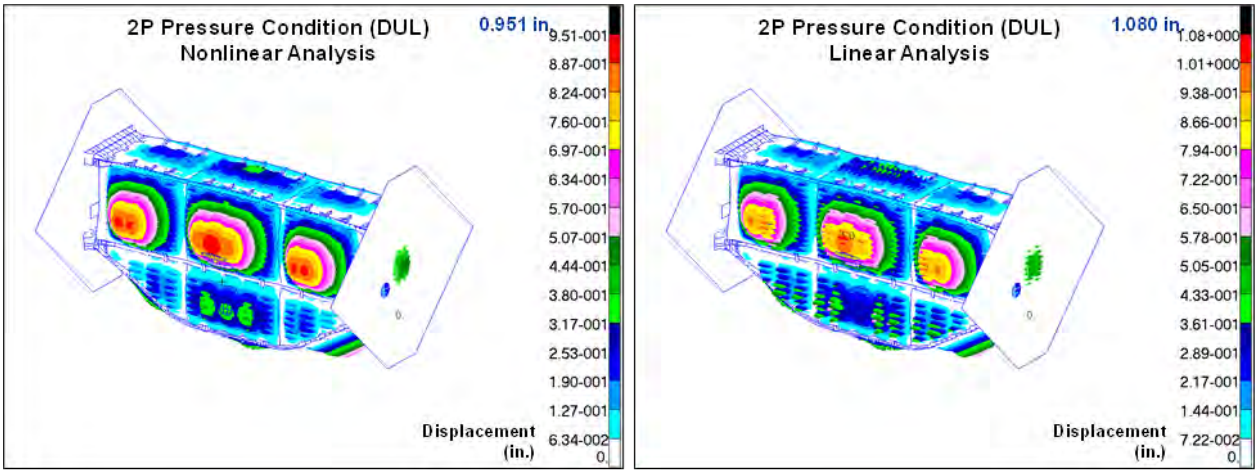

Figure 4-107. Displacements of the MBB from Linear and Nonlinear Analyses in 2P Condition

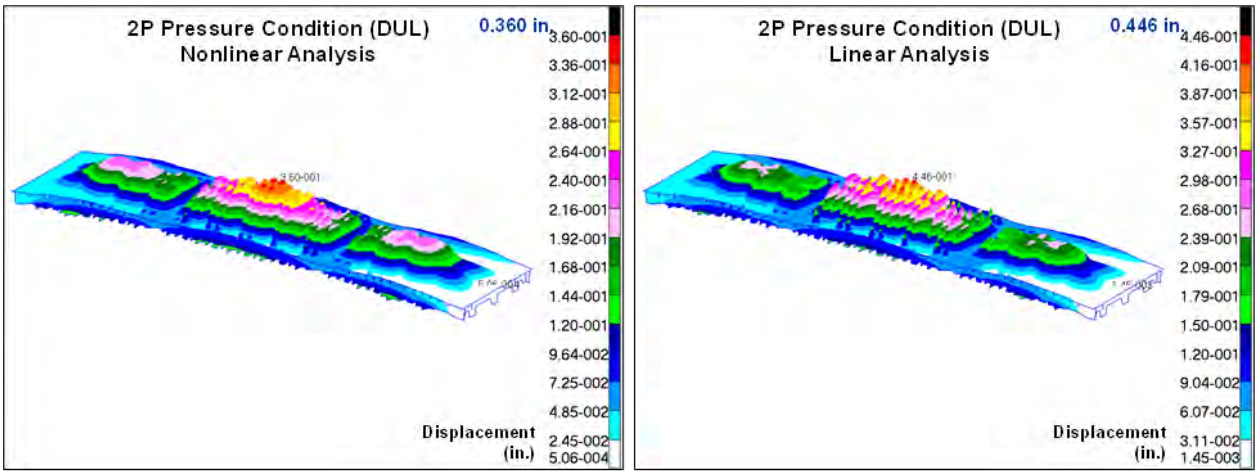

Figure 4-108. Displacements of the Crown From Linear and Nonlinear Analyses in 2P Condition

In testing of the 2P pressure condition, the MBB was loaded up to 2P (18.4 psi). During the test, in-plane strains and out-of-plane deformations were measured by Video Image Correlation in Three Dimensions (VIC-3D) and Linear Variable Displacement Transducers (LVDT), and strain gages. Locations of the VIC-3D, LVDT, and strain gages are shown in the HWB MBB Test Specification (Ref. 4-9). Predictions of VIC-3D plots from nonlinear analysis are shown in Figure 4-109. Also shown in Figure 4-109 are the displacement prediction charts of the two LVDTs for the upper bulkhead and the side keel. Results from linear and nonlinear analyses are plotted and compared. Results from the LVDT charts showed that normal displacements of the upper bulkhead and center keel were lower from the nonlinear analysis than those from the linear analysis in the 2P pressure condition.

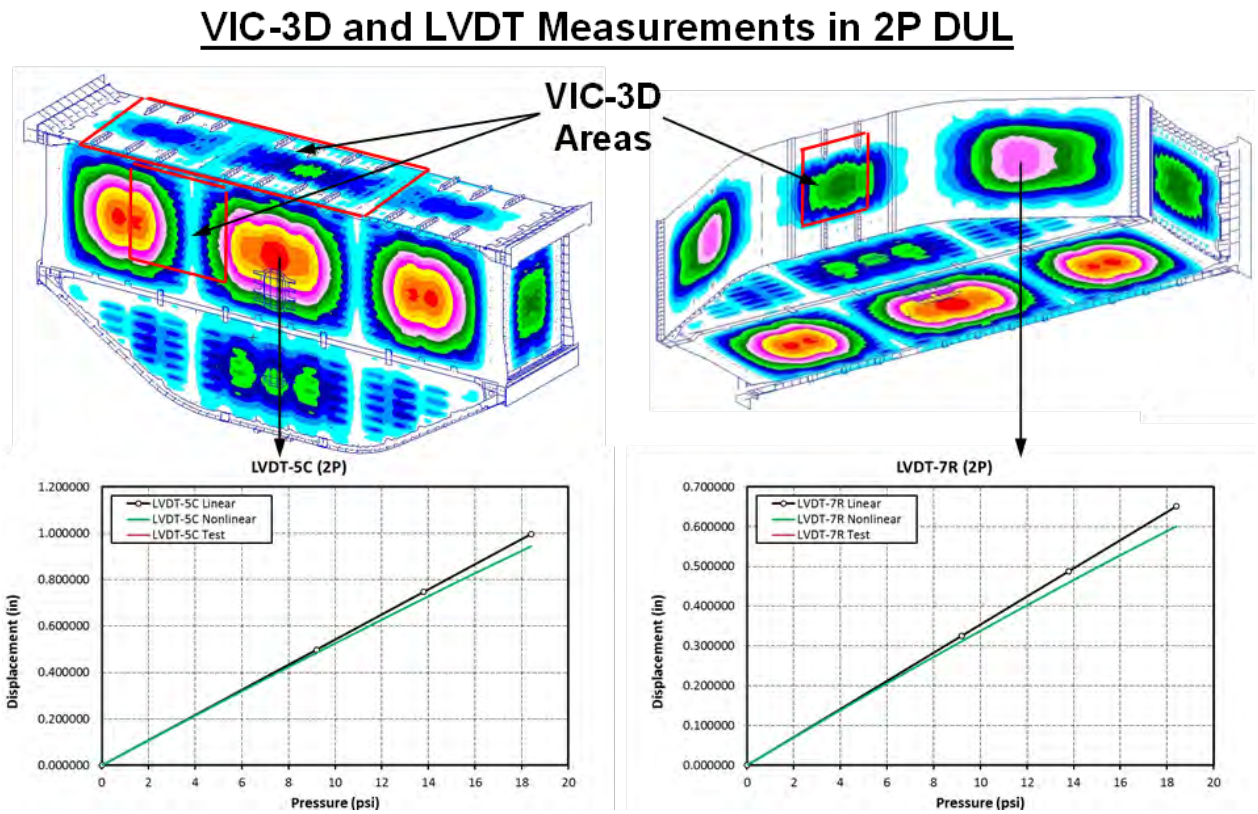

Figure 4-109. VIC-3D and LVDT Measurements of the MBB in 2P Condition

In addition to the VIC-3D and LVDT instruments, strain gages were placed on the MBB where high strains and stresses were expected during tests. As shown in Figure 4-110, for the MBB structures that were considered to be pristine (not impact damaged), the following five critical locations were identified for possible failure locations that warranted evaluation:

1. On the crown stringer webs and stringer rods near the frames.
2. On the upper bulkhead frames.
3. On the upper bulkhead skin.
4. On the center keel external fittings.
5. On the corner struts connecting the upper bulkhead and outer rib.

Strain gages were placed at these critical locations to monitor the structural behavior and integrity of the MBB during tests. Maximum or minimum principal strain distribution plots from nonlinear analysis and strain gage predictions from linear and nonlinear analyses are shown in Figure 4-111 through Figure 4-116. Strain gage predictions from linear and nonlinear analyses were compared to evaluate the extent of geometric nonlinearity of the MBB in the 2P pressure condition. Failure predictions were made by comparing the maximum and minimum principal strain values of the MBB from nonlinear analysis to the un-notched strain design values (in pristine condition) of the composites shown in Table 4-7, and by comparing von Mises stresses of metallic fittings and bolts to the ultimate strengths of metals. In summary, failure prediction results showed that the MBB in its pristine condition would not fail catastrophically at 2P. Detailed results of the five critical locations listed above are presented in the following discussion.

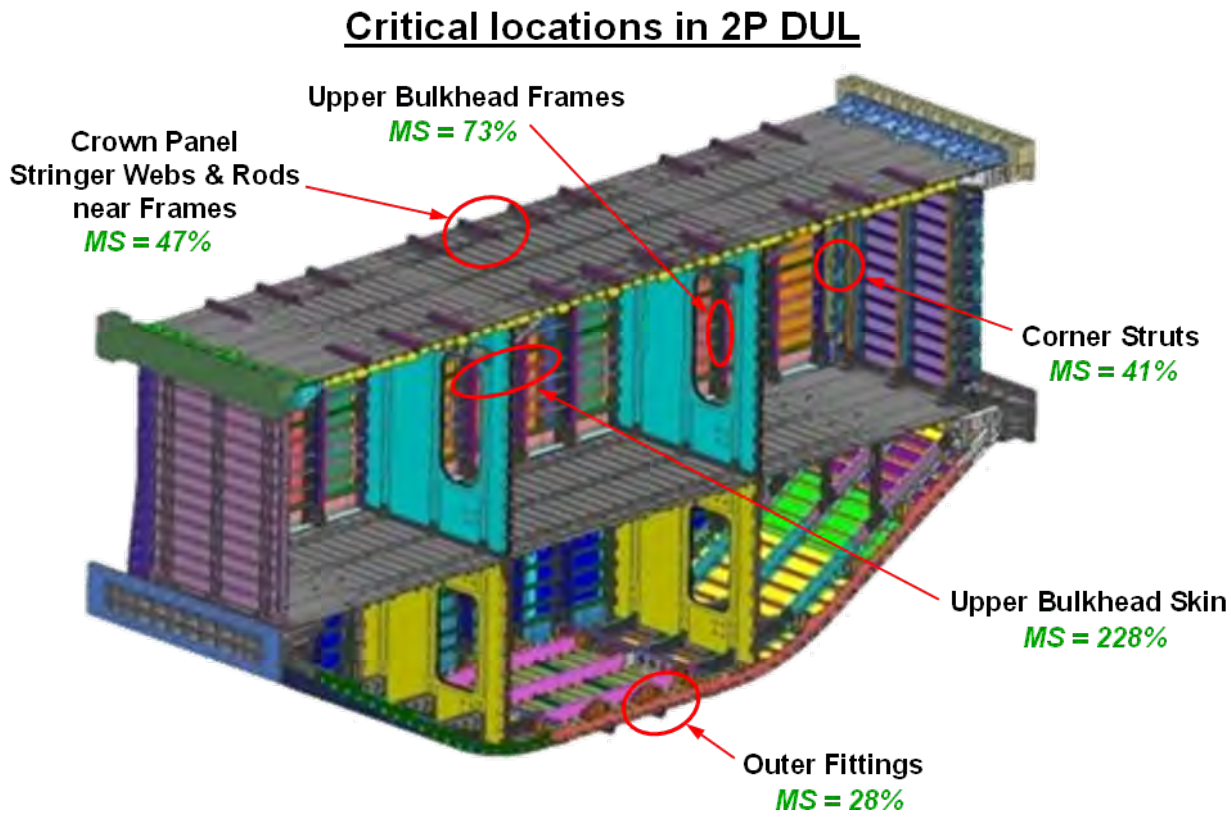

Figure 4-110. Critical Locations in Failure Predictions for the MBB in 2P Condition

Figure 4-111 shows a plot of maximum principal strain on the crown stringer web near the frames and charts of strain versus internal pressure of rosette strain gage locations sg01436C/sg01440C (on the stringer web to measure principal strains) and sg01525/sg01529 (on the stringer rod). A critical maximum principal strain of 5,780 micro-in./in. on the stringer web/rod was seen in the 2P pressure condition. This critical strain was within the un-notched design strain value of 10,000 micro-in./in. for the stringer web. The calculated margin of safety was 73%, which indicated that a failure of the crown stringer web and stringer rod on the MBB was unlikely to occur at 2P pressure load. When comparing strain gage results calculated from linear and nonlinear analyses, a slight reduction of strain values was seen in the results from nonlinear analysis. This was because an appreciable out-of-plane deformation was suppressed and replaced with an in-plane tensioning on the panel skin/stringer/frame in pressure loading. As a result, lower strains were detected on the panel skin/stringer/frame from nonlinear analysis, resembling a stiffening effect to a panel in pressure load.

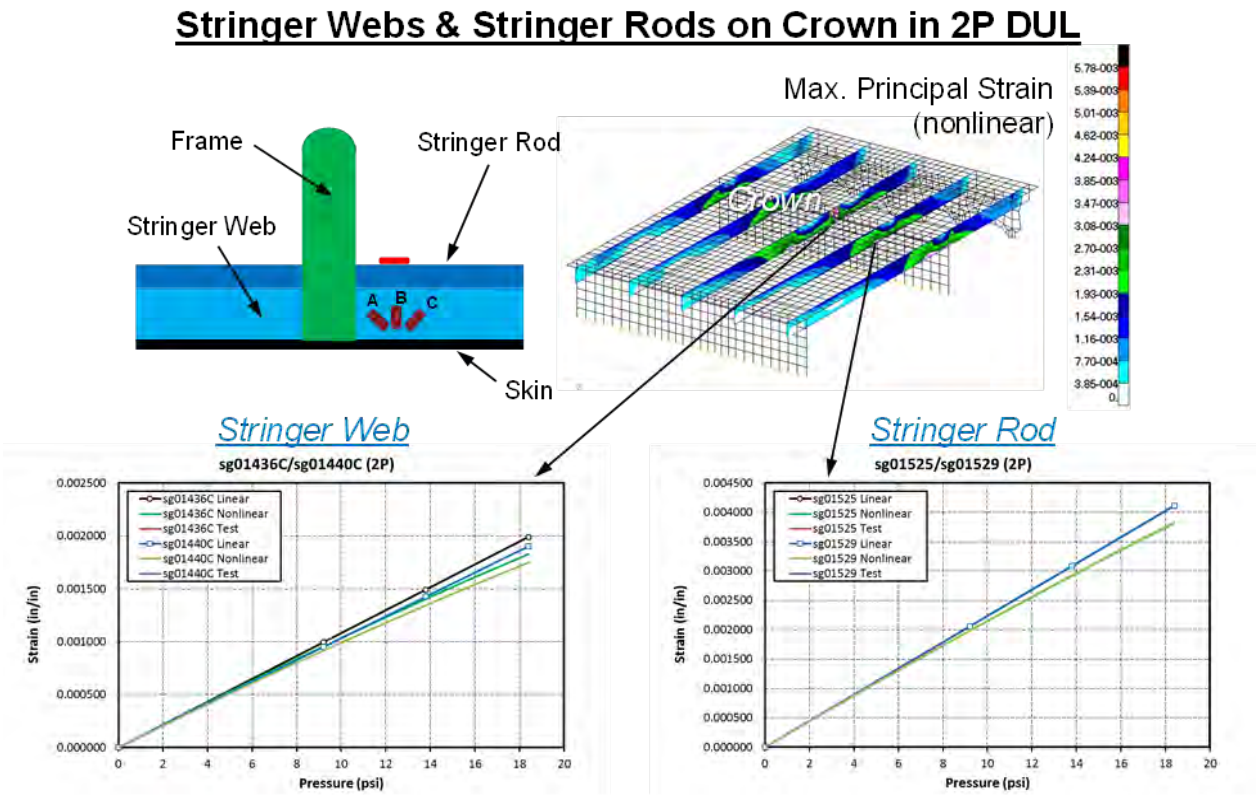

Figure 4-111. Strains on Crown Stringer Webs and Stringer Rods in 2P Condition

Figure 4-112 shows a plot of minimum principal strain on the crown stringer web near the frames and a chart of strain versus internal pressure of rosette strain gage locations sg01420C/sg01424C (on the stringer web to measure principal strains). A critical minimum principal strain of -5,440 micro-in./in. on the stringer web/rod was seen in the 2P pressure condition. This critical strain was within the un-notched design strain value of -8,000 micro-in./in. for the stringer web. The calculated margin of safety was 47%, which indicated that a failure of the crown stringer web and stringer rod on the MBB was unlikely to occur at 2P pressure load. When comparing strain gage results calculated from linear and nonlinear analyses, a slight reduction of strain values was seen in the results from nonlinear analysis. This was because an appreciable out-of-plane deformation was suppressed and replaced with an in-plane tensioning on the panel skin/stringer/frame in pressure loading. As a result, lower strains were detected on the panel skin/stringer/frame from nonlinear analysis, resembling a stiffening effect to a panel in pressure load.

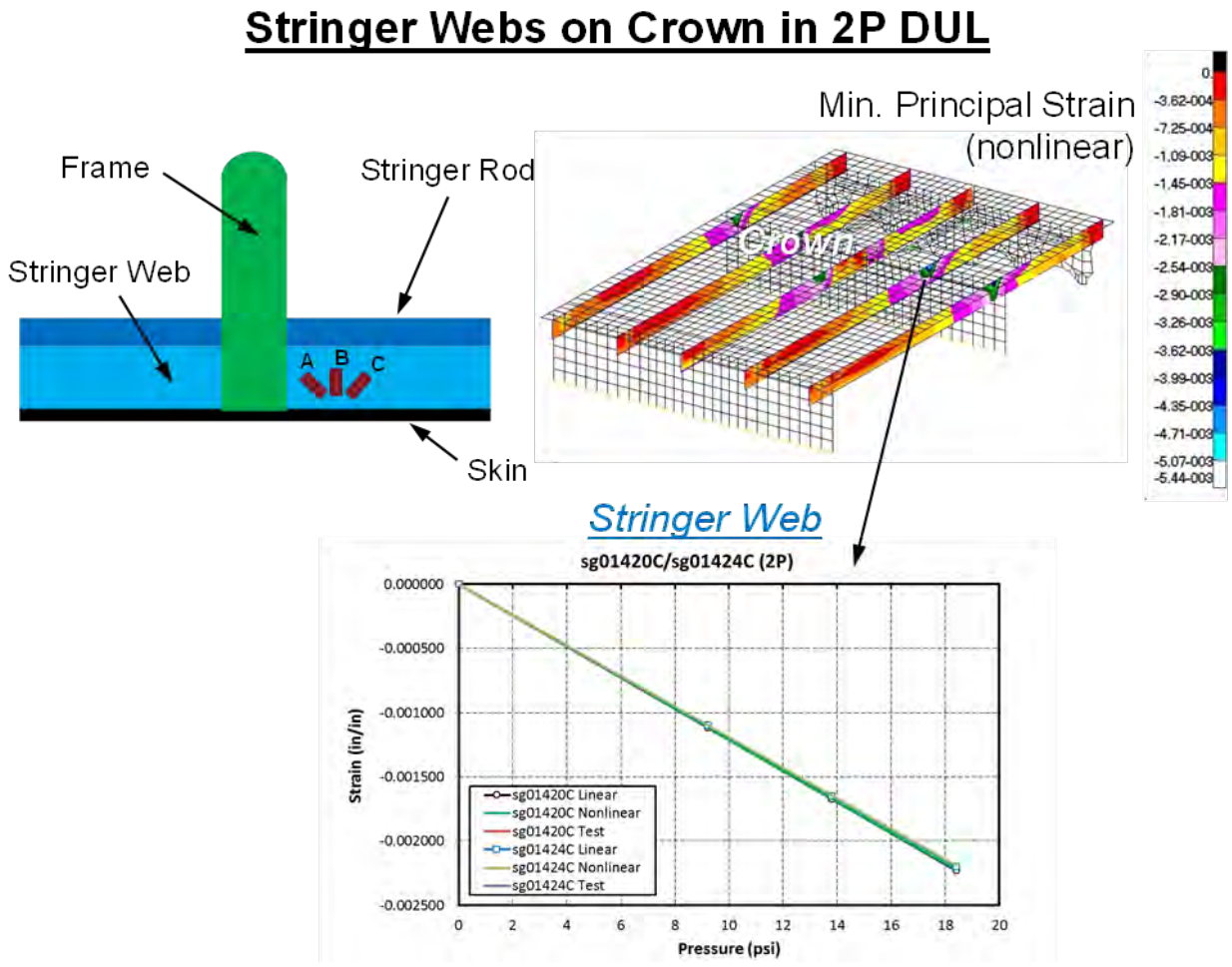

Figure 4-112. Strains on Crown Stringer Webs in 2P Condition

Figure 4-113 shows a plot of the minimum principal strain on the upper bulkhead frame web and a chart of strain versus internal pressure of strain gage locations sg03820/sg03821 (on the frame top). A critical minimum principal strain of -4,630 micro-in./in. on the frame web was seen in the 2P pressure condition. This critical strain was within the un-notched design strain value of -8,000 micro-in./in. for the frame web. The calculated margin of safety was 73%, which indicated that a failure of the upper bulkhead frame web on the MBB was unlikely to occur at 2P pressure load. When comparing strain gage results calculated from linear and nonlinear analyses, a slight reduction of strain values was seen in the results from nonlinear analysis. This was because an appreciable out-of-plane deformation was suppressed and replaced with an in-plane tensioning on the panel skin/stringer/frame in pressure loading. As a result, lower strains were detected on the panel skin/stringer/frame from nonlinear analysis, resembling a stiffening effect to a panel in pressure load.

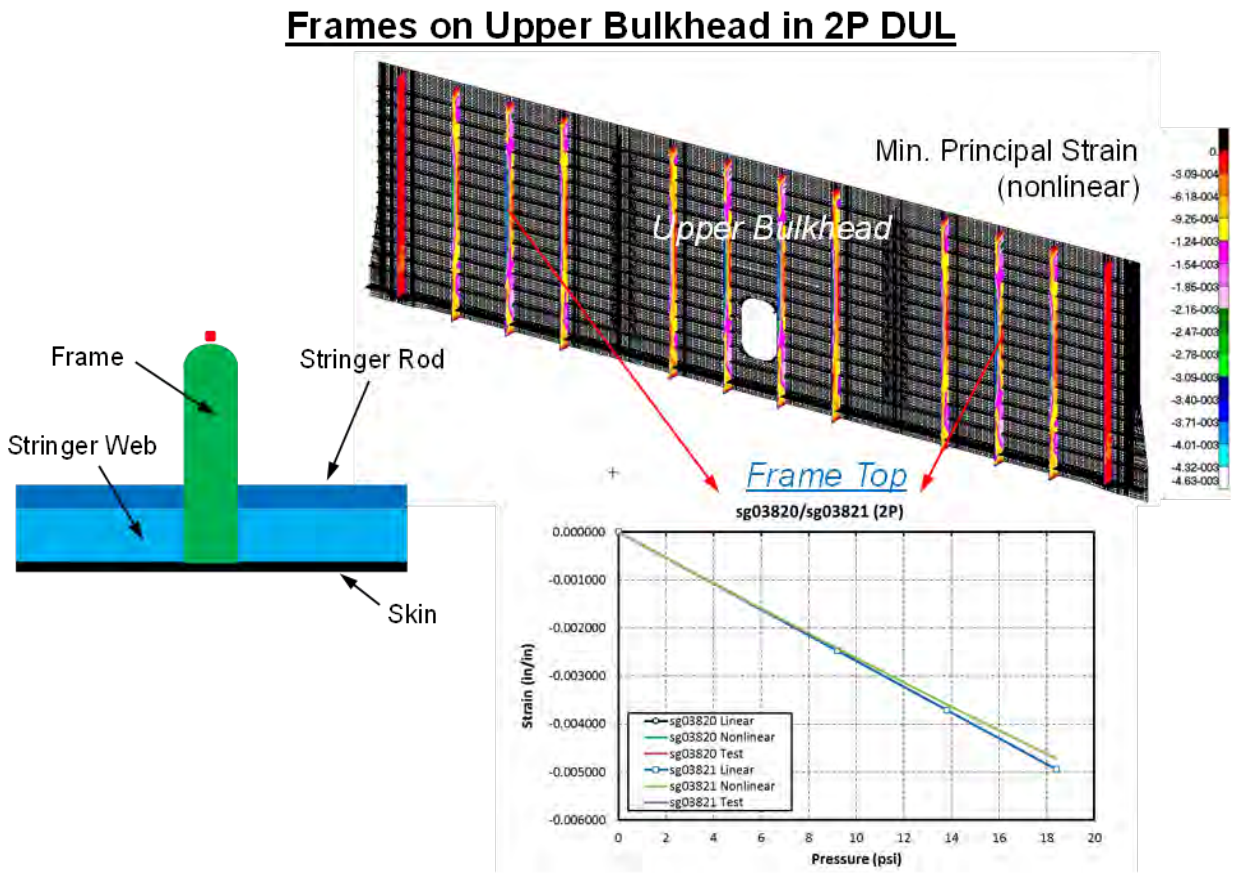

Figure 4-113. Strains on Upper Bulkhead Frames in 2P Condition

Figure 4-114 shows a plot of maximum principal strain on the upper bulkhead skin and a chart of strain versus internal pressure of back-to-back strain gage locations sg03101/sg03201 (on the exterior and interior skin). A critical maximum principal strain of 3,050 micro-in./in. on the skin was seen in the 2P pressure condition. This critical strain was within the un-notched design strain value of 10,000 micro-in./in. for the skin. The calculated margin of safety was 228%, which indicated that a failure of the upper bulkhead skin on the MBB was unlikely to occur at 2P pressure load. When comparing back-to-back skin strain gage results, it was found that in-plane tension strain derived from nonlinear analysis was only slightly higher than the in-plane tension strain from linear analysis, whereas the bending strain derived from nonlinear analysis was significantly lower than the bending strain from linear analysis. This was because an appreciable out-of-plane deformation was suppressed and replaced with an in-plane tensioning on the panel skin/stringer/frame in pressure loading. As a result, lower strains were detected on the panel skin/stringer/frame from nonlinear analysis, resembling a stiffening effect to a panel in pressure load.

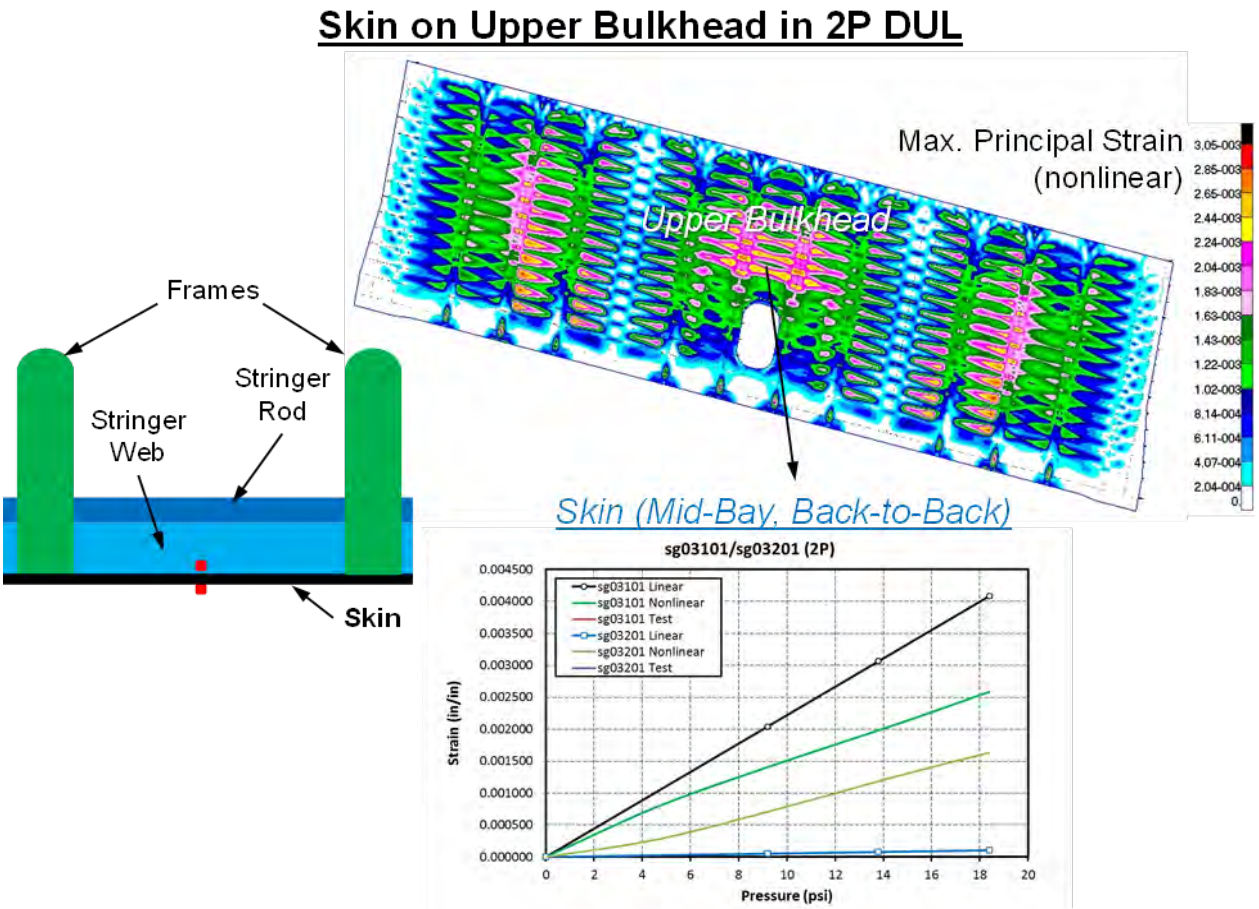

Figure 4-114. Strains on Upper Bulkhead Skin in 2P Condition

Figure 4-115 shows a plot of von Mises strain of the External Center Keel Stringer Support Fitting (ZJ153666-1) and a chart of strain versus internal pressure of strain gage location sg16002 (on the fitting web). A critical strain of 4,930 micro-in./in. located at the fitting web was seen in the 2P pressure condition. Using Young's modulus of 10.3 Msi for aluminum alloy 7050-T7451, this strain was equivalent to a stress of 50.8 ksi. Compared to the yielding allowable of 65 ksi for the External Center Keel Stringer Support Fitting (ZJ153666-1), this critical stress was within the yielding allowable of the fitting. The calculated margin of safety was 28%, which indicated that a failure of the center keel external fitting on the MBB was unlikely to occur at 2P pressure load. When comparing strain gage results, strain values calculated from linear and nonlinear analyses were almost identical, which meant that stress/strain results of metallic fittings on the MBB were mostly linear. Linear analysis was sufficient for the failure predictions for metallic fittings in the 2P pressure condition.

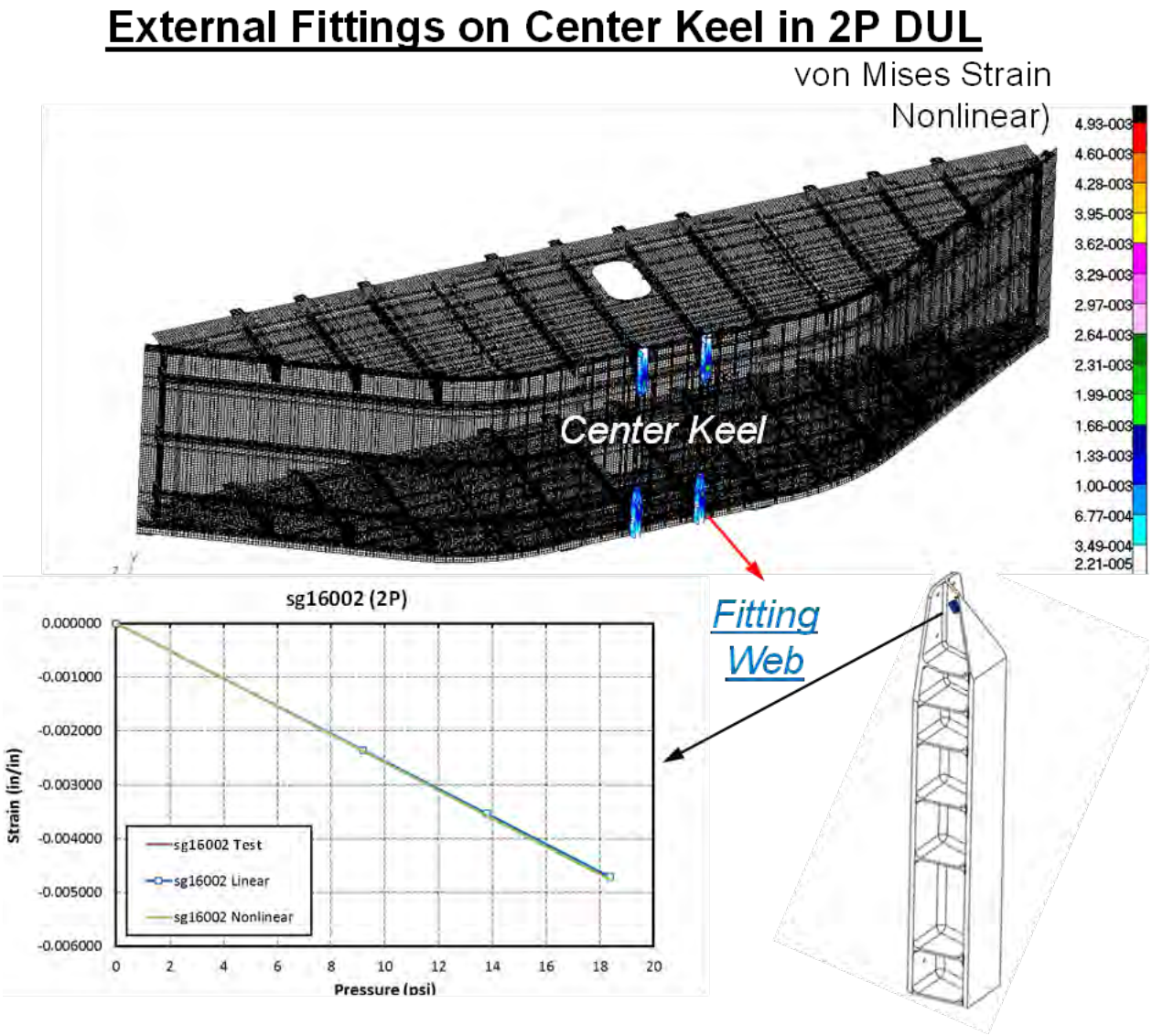

Figure 4-115. Strains on Center Keel External Fittings in 2P Condition

Figure 4-116 shows a chart of strain versus internal pressure of strain gage locations sg17021/17022 on the Corner Brace Strut (ZJ153956-1). A critical strain of 2,856 micro-in./in. on the strain gages was seen in the 2P pressure condition. Using Young's modulus of 26 Msi for stainless steel of MIL-S-5059, this strain was equivalent to a stress of 74.3 ksi. Compared to the yielding allowable of 105 ksi for the Corner Brace Strut (ZJ153956-1), this critical stress was within the yielding allowable of the strut. The calculated margin of safety was 41%, which indicated that a failure of the corner metallic strut on the MBB was unlikely to occur at 2P pressure load. When comparing strain gage results, strain values calculated from linear and nonlinear analyses were almost identical, which meant that stress/strain results of these metallic struts on the MBB were linear. Linear analysis was sufficient for the failure predictions for these metallic struts in the 2P pressure condition.

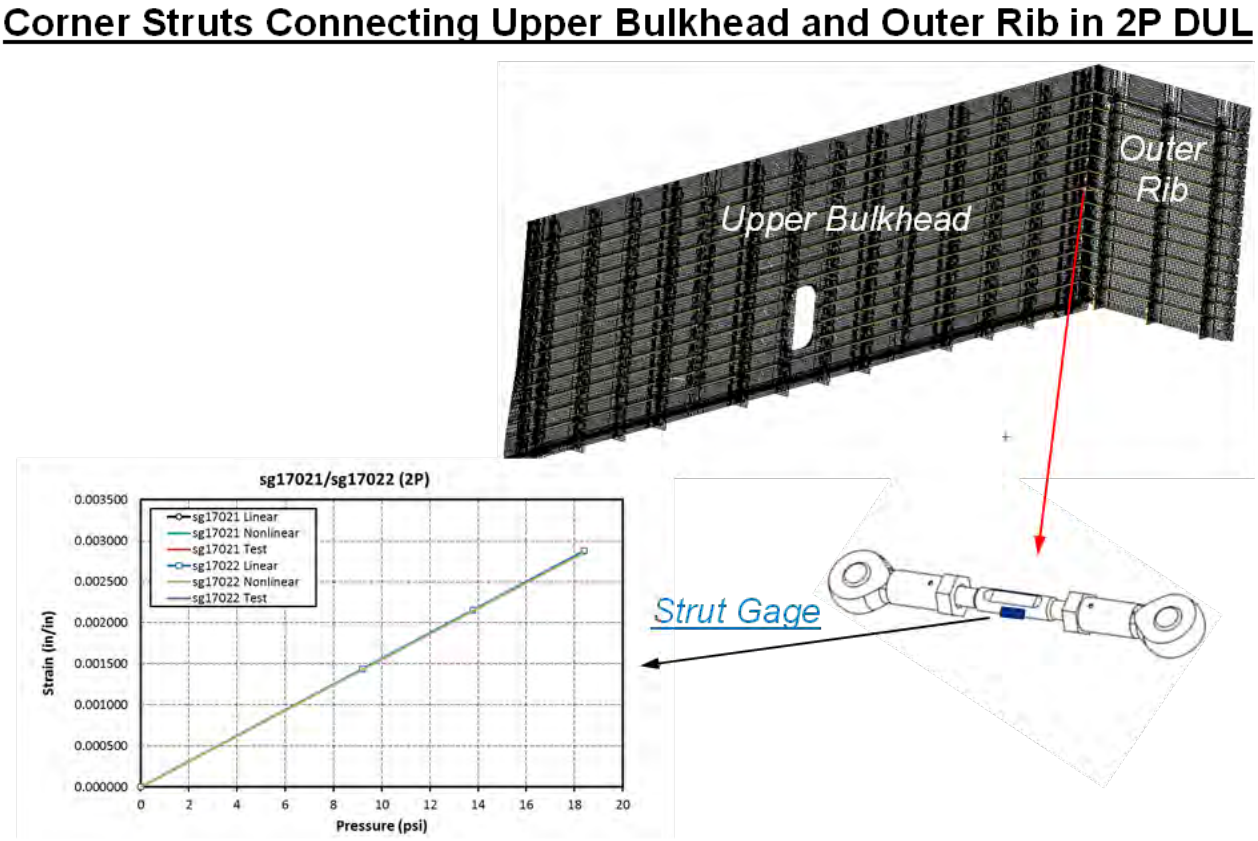

Figure 4-116. Strains on Corner Struts in 2P Condition

For tests of the MBB after impact damage, the following four critical locations were identified near the impact damage for possible failure locations that warranted evaluation:

1. On the exterior impact site no. 2, which was on the stringer flange of the center keel.
2. On the exterior impact site no. 3, which was on the mid-bay skin of the center keel.
3. On the interior impact site no. 1, which was on the frame top of the upper bulkhead.
4. On the interior impact site no. 3, which was on the mid-bay skin of the upper bulkhead.

Strain gages were placed near these impact-damaged locations to monitor the behavior of structure with impact damage during tests. Strain versus internal pressure of the critical strain gages are shown in Figure 4-117 through Figure 4-120. Strain gage predictions from linear and

nonlinear analyses were compared to evaluate the extent of geometric nonlinearity of the test article in the 2P pressure condition. Failure predictions were made by comparing the maximum and minimum principal strain values of the MBB from nonlinear analysis to the notched strain design values (in impact-damaged condition) of the composites shown in Table 4-7.

Figure 4-117 shows charts of strain versus internal pressure of back-to-back strain gage locations sg18103/sg18303 (located 0.5 in. forward from the impact site) and sg18104/sg18304 (located 0.5 in. aft from the impact site) near exterior impact site no. 2 on the stringer flange of the center keel. When comparing strain results of these back-to-back strain gages, it was found that tension strain derived from nonlinear analysis was only slightly higher than the tension strain from linear analysis, whereas the bending strain derived from nonlinear analysis was significantly lower than the bending strain from linear analysis. This was because an appreciable out-of-plane deformation was suppressed and replaced with an in-plane tensioning on the panel skin/stringer/frame in pressure loading. As a result, lower strains were detected on the panel skin/stringer/frame from nonlinear analysis, resembling a stiffening effect to a panel in pressure load. Results from nonlinear analysis showed that the critical compression strain was -132 micro-in./in. and the critical tension strain was 1,497 micro-in./in. near the impact damage site in the 2P pressure condition. These strains were within the notched design strain values of -4,800 and 5,900 micro-in./in. for the stringer flange. The calculated margin of safety was 294%, which indicated that a failure of the stringer flange at exterior impact site no. 2 of the center keel on the MBB was unlikely to occur at 2P pressure load.

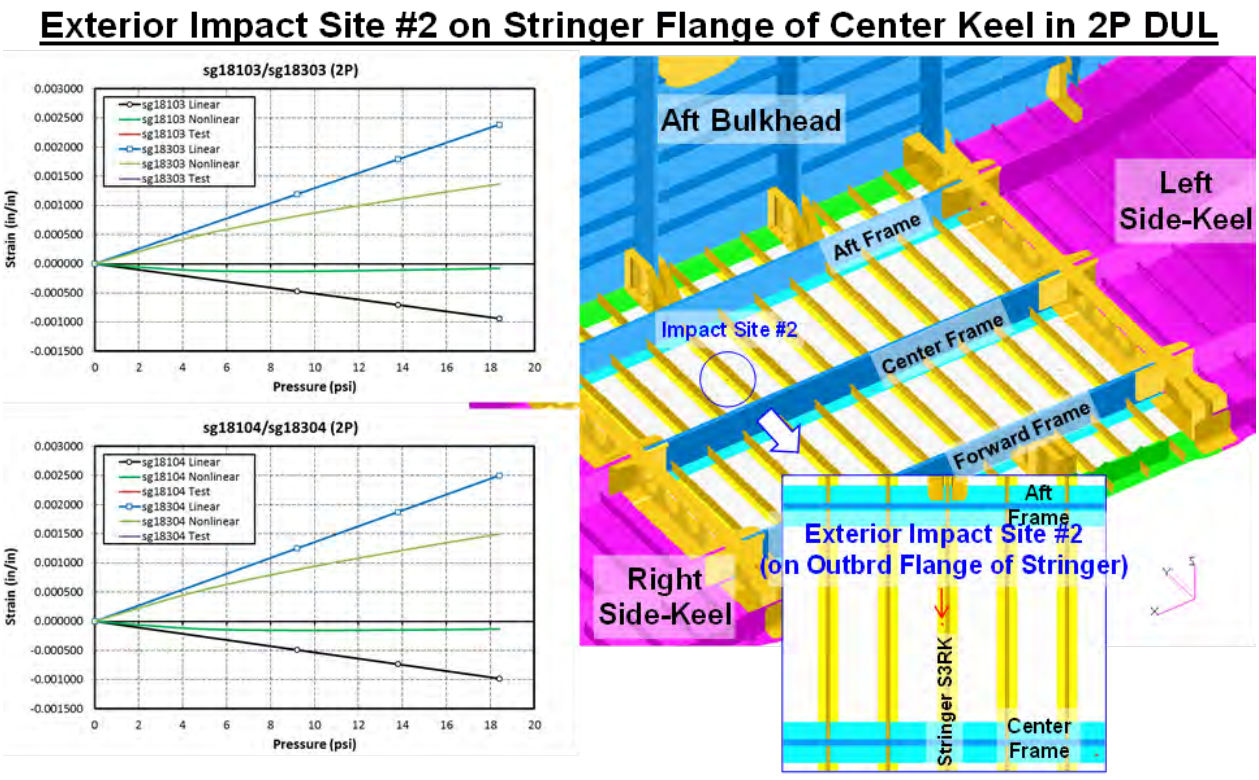

Figure 4-117. Strains on Exterior Impact Site no. 2 in 2P Condition

Figure 4-118 shows charts of strain versus internal pressure of back-to-back strain gage locations sg18105/sg18205 (located 1.0 in. left of the impact site) and sg18106/sg18206 (located 1.0 in. right of the impact site) near exterior impact site no. 3 on the mid-bay skin of the center keel. When comparing strain results of these back-to-back strain gages, it was found that tension strain derived from nonlinear analysis was only slightly higher than the tension strain from linear analysis, whereas the bending strain derived from nonlinear analysis was significantly lower than the bending strain from linear analysis. This was because an appreciable out-of-plane deformation was suppressed and replaced with an in-plane tensioning on the panel skin/stringer/frame in pressure loading. As a result, lower strains were detected on the panel skin/stringer/frame from nonlinear analysis, resembling a stiffening effect to a panel in pressure load. Results from nonlinear analysis showed that the critical tension strain was 1,068 micro-in./in. near the impact damage site in the 2P pressure condition. This strain was within the notched design strain value of 5,900 micro-in./in. for the skin. The calculated margin of safety was 452%, which indicated that a failure of the skin at exterior impact site no. 3 of the center keel on the MBB was unlikely to occur at 2P pressure load.

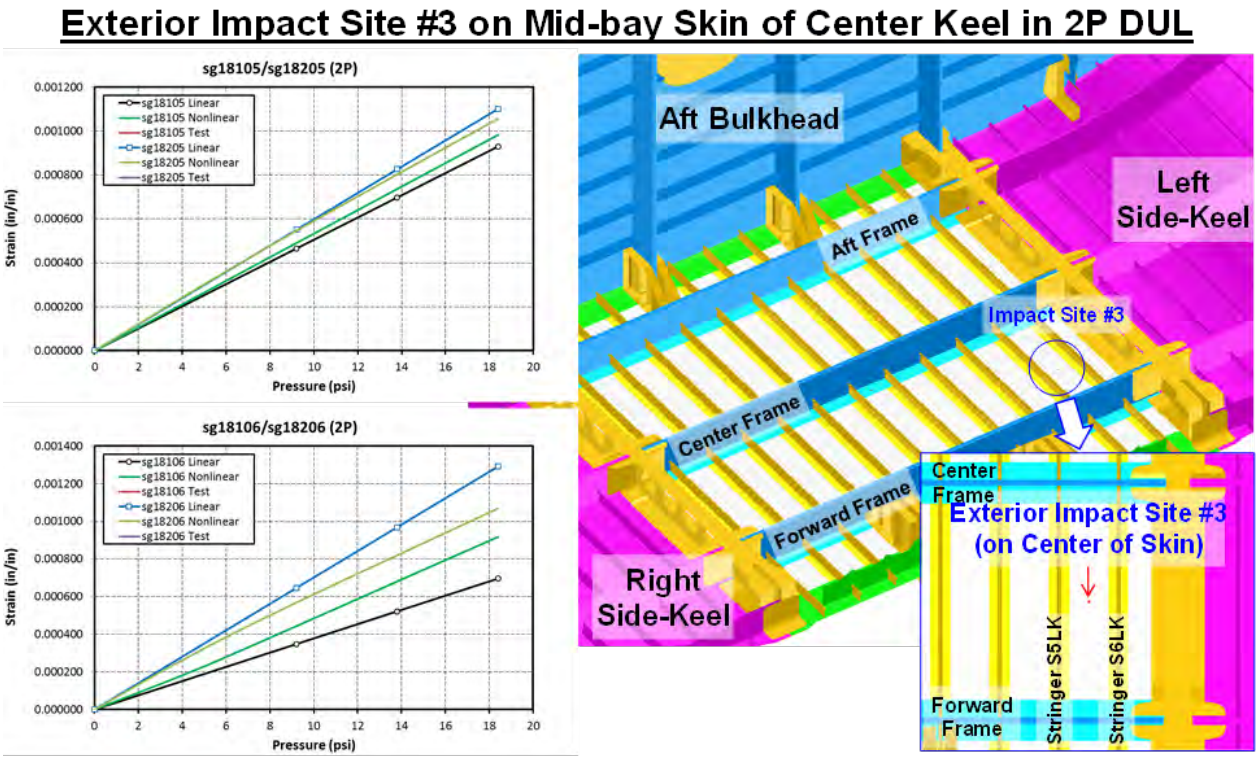

Figure 4-118. Strains on Exterior Impact Site no. 3 in 2P Condition

Figure 4-119 shows charts of strain versus internal pressure of strain gage locations sg18807 (located 1.0 in. upward from the impact site) and sg18808 (located 1.0 in. downward from the impact site) near interior impact site no. 1 on top of the frame cap of the forward upper bulkhead. When comparing strain results of these strain gages, it was found that strain derived from nonlinear analysis was slightly lower than the strain from linear analysis. This was because an appreciable out-of-plane deformation was suppressed and replaced with an in-plane tensioning on the panel skin/stringer/frame in pressure loading. As a result, lower strains were detected on the panel skin/stringer/frame from nonlinear analysis, resembling a stiffening effect to a panel in pressure load. Results from nonlinear analysis showed that the critical compression strain was -4,693 micro-in./in. near the impact damage site in the 2P pressure condition. This strain was within the notched design strain values of -5,800 micro-in./in. for the frame web/cap. The calculated margin of safety was 24%, which indicated that a failure of the frame web/cap at interior impact site no. 1 of the forward upper bulkhead on the MBB was unlikely to occur at 2P pressure load.

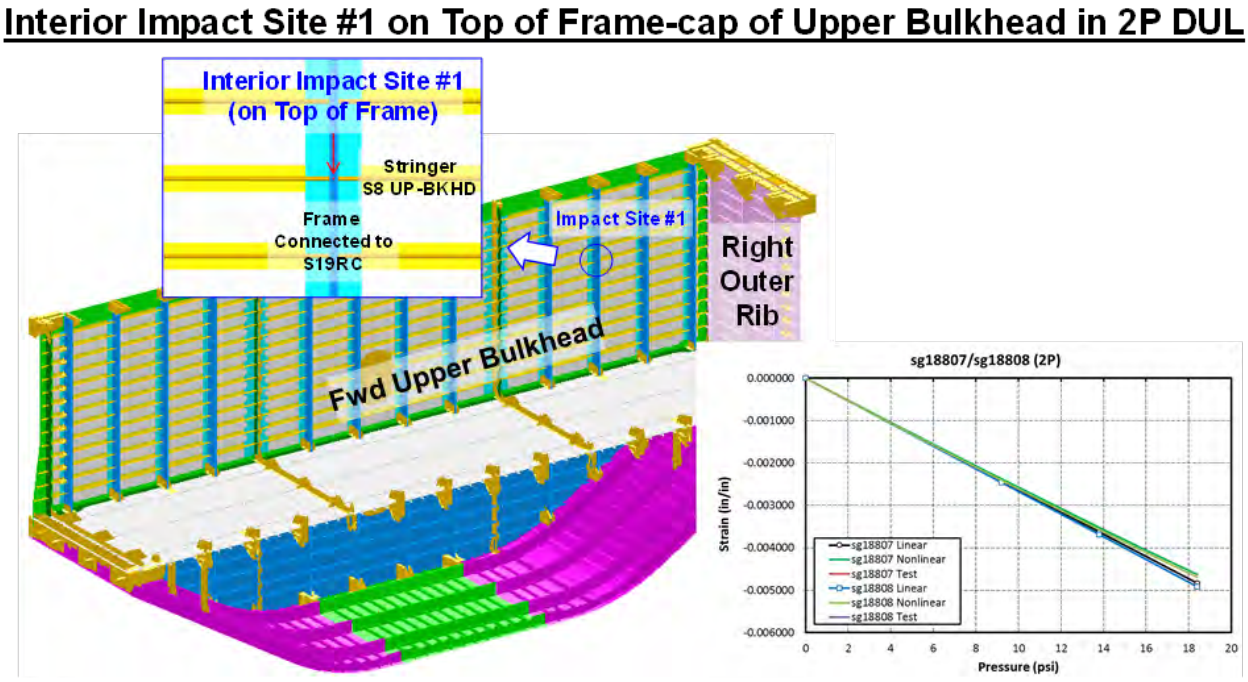

Figure 4-119. Strains on Interior Impact Site no. 1 in 2P Condition

Figure 4-120 shows charts of strain versus internal pressure of back-to-back strain gage locations sg18107/sg18211 (located 1.0 in. up from the impact site) and sg18108/sg18212 (located 1.0 in. down from the impact site) near interior impact site no. 3 on the mid-bay skin of the forward upper bulkhead. When comparing strain results of these back-to-back strain gages, it was found that tension strain derived from nonlinear analysis was only slightly higher than the tension strain from linear analysis, whereas the bending strain derived from nonlinear analysis was significantly lower than the bending strain from linear analysis. This was because an appreciable out-of-plane deformation was suppressed and replaced with an in-plane tensioning on the panel skin/stringer/frame in pressure loading. As a result, lower strains were detected on the panel skin/stringer/frame from nonlinear analysis, resembling a stiffening effect to a panel in pressure load. Results from nonlinear analysis showed that the critical tension strain was 1,668 micro-in./in. near the impact damage site in the 2P pressure condition. This strain was within the notched design strain value of 5,900 micro-in./in. for the skin. The calculated margin of safety was 254%, which indicated that a failure of the skin at interior impact site no. 3 of the forward upper bulkhead on the MBB was unlikely to occur at 2P pressure load.

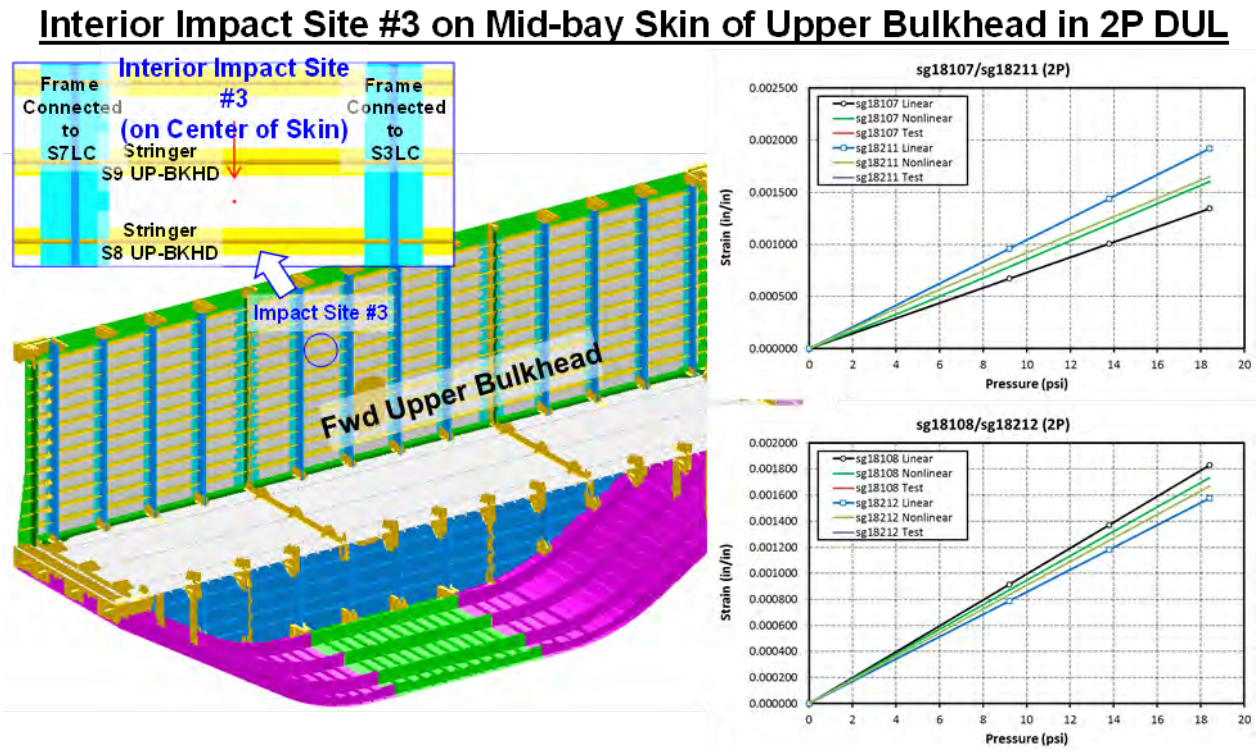

Figure 4-120. Strains on Interior Impact Site no. 3 in 2P Condition

4.4.2 2.5-g DUL Maneuver Condition

Failure predictions for the MBB were made based on results from nonlinear analysis of the global FEM in the 2.5-g DUL maneuver condition. In this condition, concentrated loads were applied on the COLTS fixture to simulate a 2.5-g DUL (3.75-g) up-bending load. To understand the structural behavior of the MBB and the crown panel in 2.5-g DUL up-bending load, displacement plots from nonlinear and linear analyses were compared and are shown in Figure 4-121 and Figure 4-122. For the MBB, the maximum displacement at the upper edge of the COLTS loading platen was 0.875 in. from the nonlinear analysis and 0.807 in. from the linear analysis. For the crown panel, the maximum displacement at the right end of the crown was 0.601 in. from the nonlinear analysis and 0.415 in. from the linear analysis. These results showed that displacements from the nonlinear analysis were higher than those from the linear analysis in the 2.5-g DUL maneuver condition. This was because the skin of the center crown started to buckle at 0.347-g up-bending load (see Section 4.3.6.2), which had resulted in loss of in-plane stiffness of the crown. Because this effect of stiffness reduction from the crown skin buckling was included in the nonlinear analysis, displacements of the upper edge on the loading platen and the right end of the crown from the nonlinear calculation were greater than those produced by the linear solution.

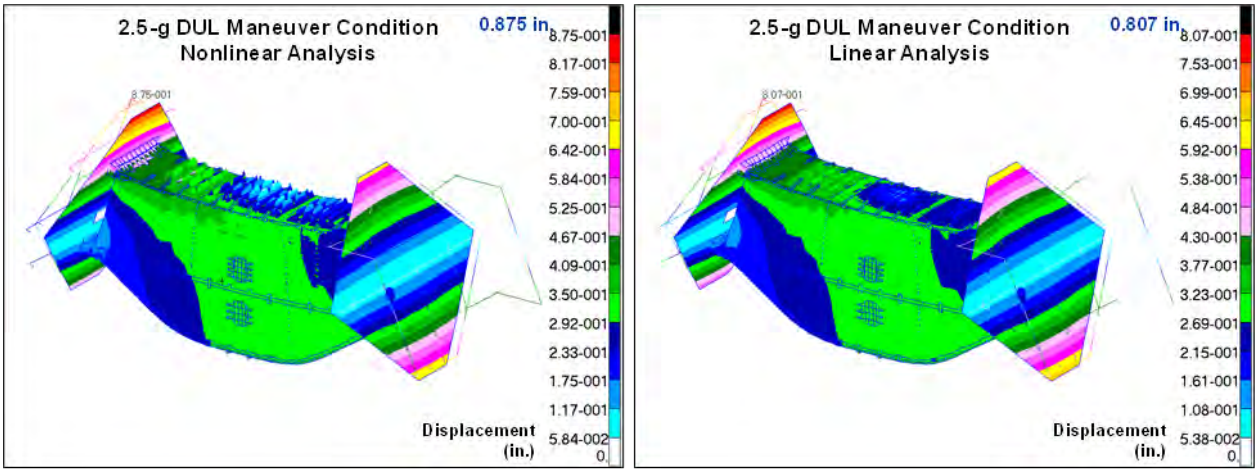

Figure 4-121. Displacements of the MBB From Linear and Nonlinear Analyses in 2.5-g DUL Condition

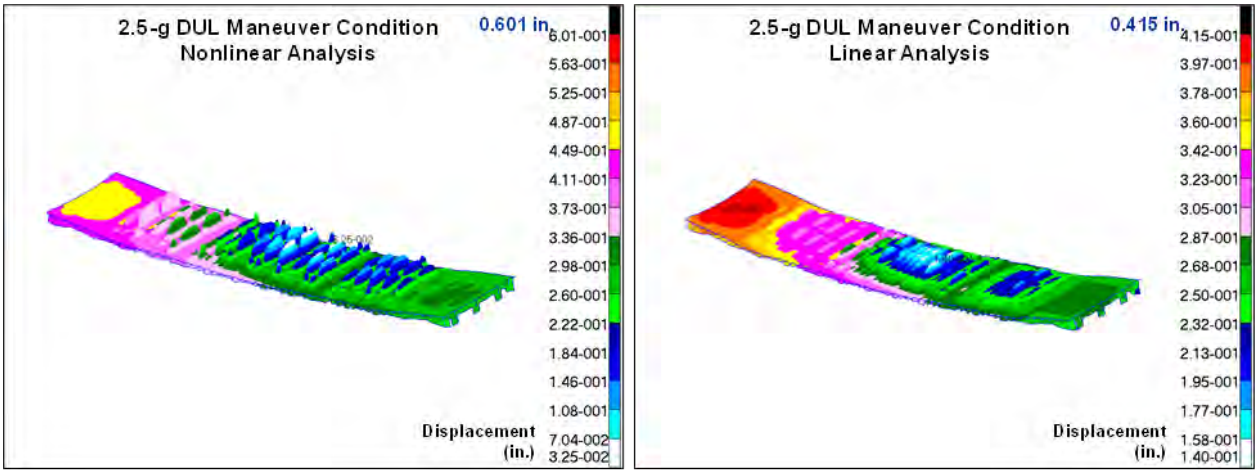

Figure 4-122. Displacements of the Crown from Linear and Nonlinear Analyses in 2.5-g DUL Condition

In testing of the 2.5-g DUL maneuver condition, the MBB was loaded up to 2.5-g DUL (3.75 g). During the test, in-plane strains and out-of-plane deformations were measured by VIC-3D, LVDT, and strain gages. Locations of the VIC-3D, LVDT, and strain gages are shown in the HWB MBB Test Specification (Ref. 4-9). Predictions of VIC-3D plots from nonlinear analysis are shown in Figure 4-123, and the displacement prediction chart of the LVDT is shown in Figure 4-124 for the reacting platen. Results from linear and nonlinear analyses were plotted and compared. Results from the LVDT chart showed that rotation of the reacting platen was slightly higher from the nonlinear analysis than those from the linear analysis in the 2.5-g DUL maneuver condition.

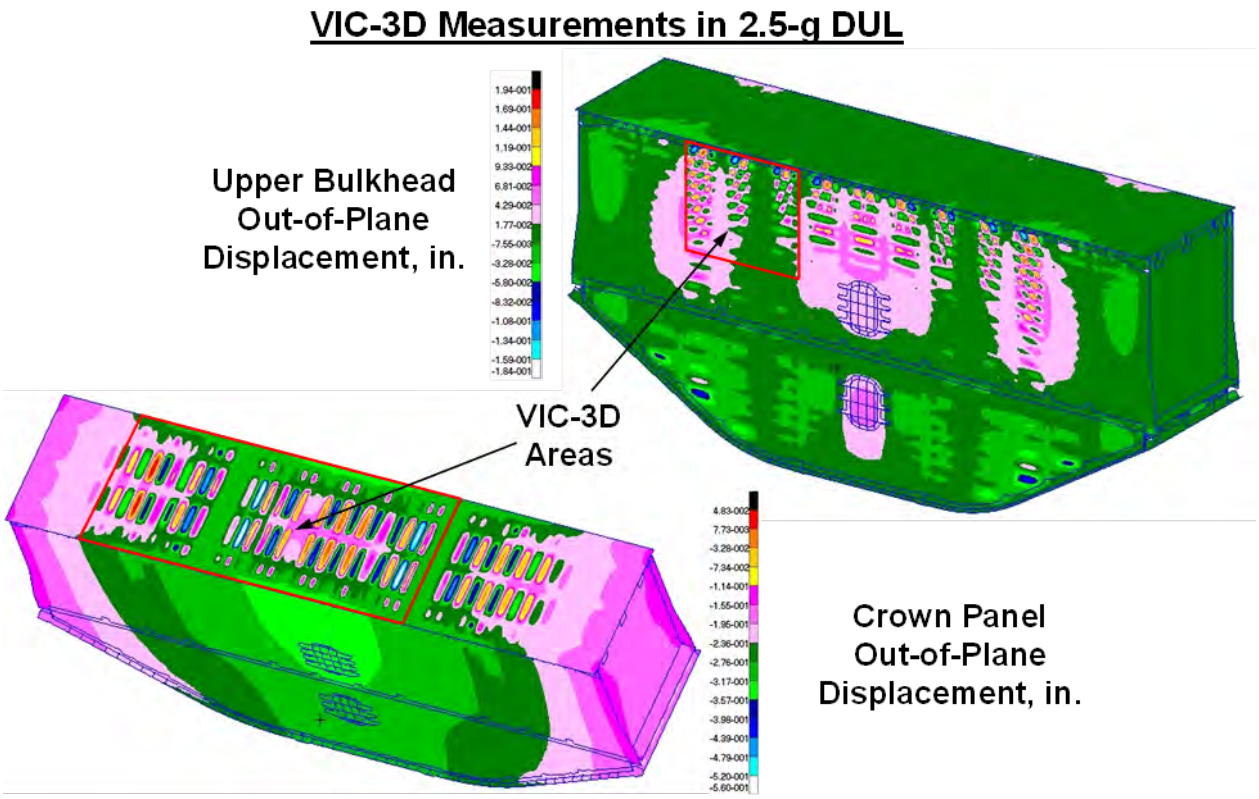

Figure 4-123. VIC-3D Measurements of the MBB in 2.5-g DUL Condition

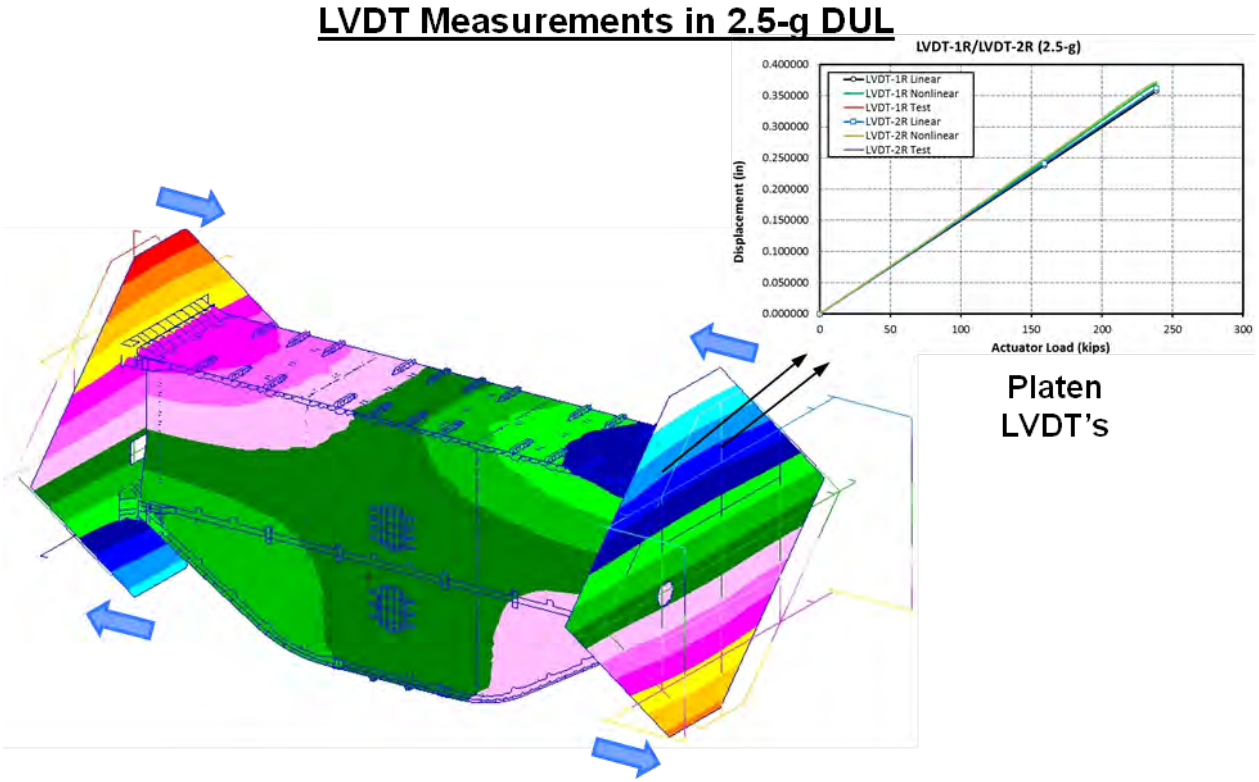

Figure 4-124. LVDT Measurements of the MBB in 2.5-g DUL Condition

In addition to the VIC-3D and LVDT instruments, strain gages were placed on the MBB where high strains and stresses were expected during tests. As shown in Figure 4-125, for the MBB structures that were considered to be pristine (not impact damaged), the following six critical locations were identified for possible failure locations that warranted evaluation:

1. On the crown frames.
2. On the crown T-caps.
3. On the crown skin.
4. On the upper bulkhead skin.
5. On the side keel frames.
6. On the metallic fittings connected to the lower load-introduction fittings.

Strain gages were placed at these critical locations to monitor the structural behavior and integrity of the MBB during tests. Maximum or minimum principal strain distribution plots from nonlinear analysis and strain gage predictions from linear and nonlinear analyses are shown in Figure 4-126 through Figure 4-131. Strain gage predictions from linear and nonlinear analyses were compared to evaluate the extent of geometric nonlinearity of the MBB in the 2.5-g DUL maneuver condition. Failure predictions were made by comparing the maximum and minimum principal strain values of the MBB from nonlinear analysis to the un-notched strain design values (in pristine condition) of the composites shown in Table 4-7, and by comparing von Mises stresses of metallic fittings and bolts to the ultimate strengths of metals. In summary, failure prediction results showed that the MBB in its pristine condition would not fail catastrophically at 2.5-g DUL. Detailed results for these critical locations are presented in the following discussion.

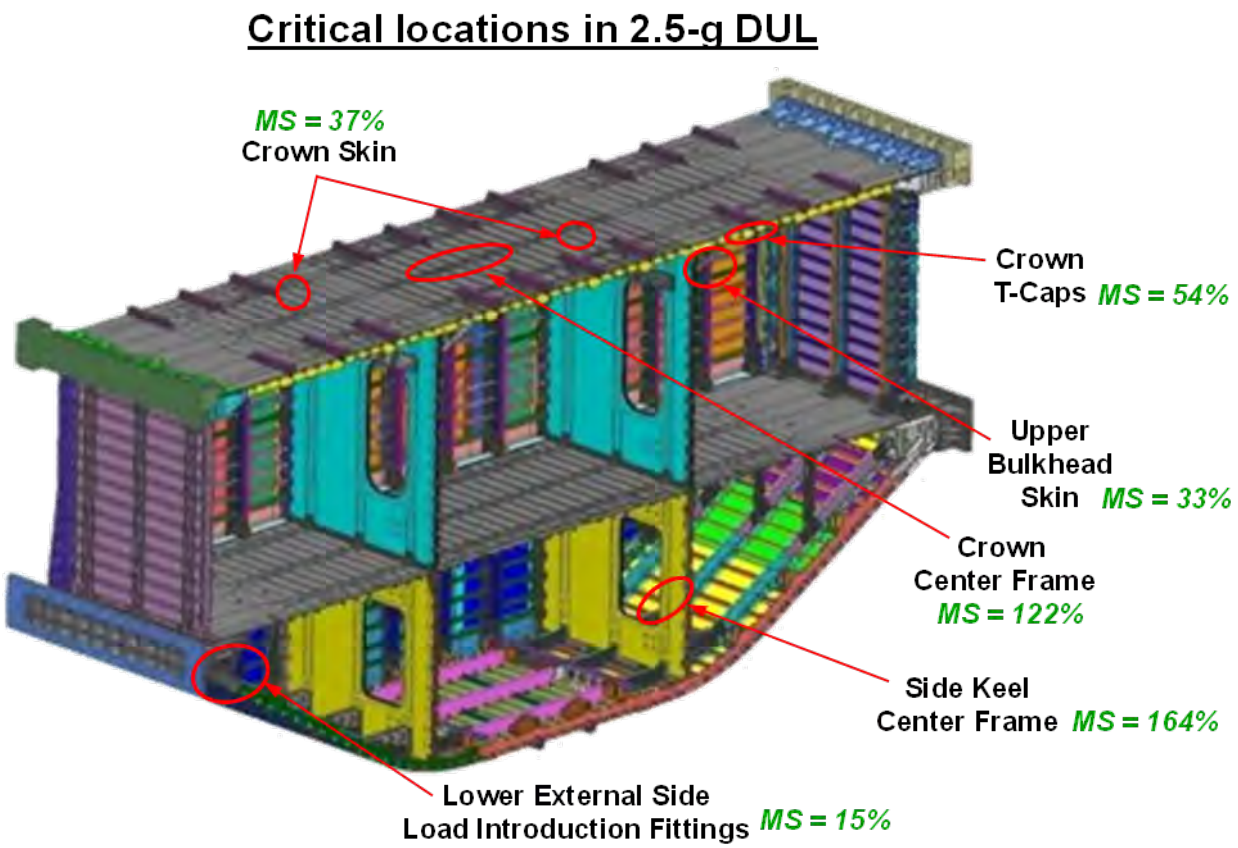

Figure 4-125. Critical Locations in Failure Predictions for the MBB in 2.5-g DUL Condition

Figure 4-126 shows a plot of minimum principal strain on the crown frames and charts of strain versus actuator load of strain gage locations sg01777/sg01778 (on the frame sides near the top) and sg01874 (on the frame top). A critical minimum principal strain of -3,610 micro-in./in. on the frame was seen in the 2.5-g DUL maneuver condition. This critical strain was within the un-notched design strain value of -8,000 micro-in./in. for the frame web. The calculated margin of safety was 122%, which indicated that a failure of crown frame on the MBB was unlikely to occur at 2.5-g DUL. When comparing strain gage results calculated from linear and nonlinear analyses, an increase of strain values was seen in the results from nonlinear analysis. This was because the skin of the center crown started to buckle at 0.347-g up-bending load (see Section 4.3.6.2), which had resulted in more axial loads being taken by the crown frames instead of the crown skin. Because this effect of stiffness reduction from the crown skin buckling was included in the nonlinear analysis, strains of the crown frame from the nonlinear calculation would be higher than those produced by the linear solution, resembling a softening effect to a panel in post-buckling phase.

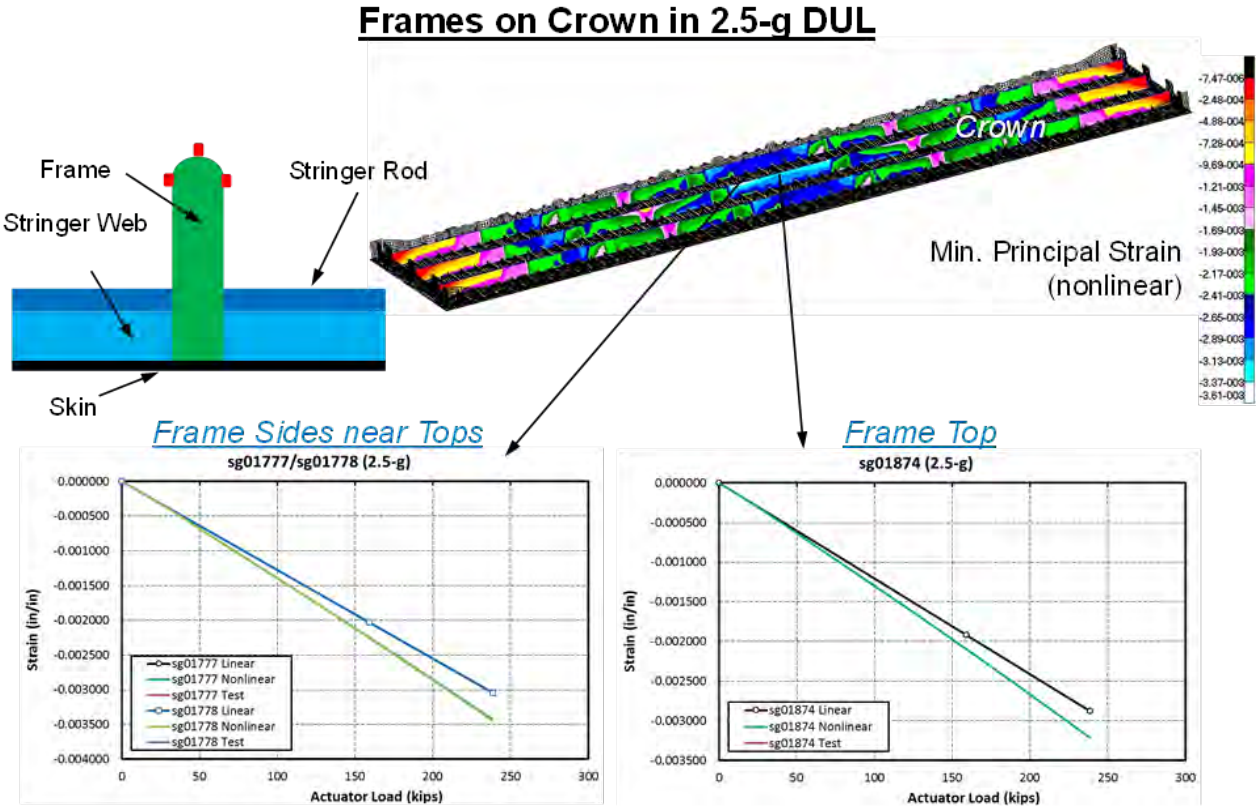

Figure 4-126. Strains on Crown Frames in 2.5-g DUL Condition

Figure 4-127 shows a plot of minimum principal strain on the crown T-caps and a chart of strain versus actuator load of strain gage locations sg01924/sg01922 (on the T-cap web). A critical minimum principal strain of -5,210 micro-in./in. on the T-caps was seen in the 2.5-g DUL maneuver condition. This critical strain was within the un-notched design strain value of -8,000 micro-in./in. for the T-cap web. The calculated margin of safety was 54%, which indicated that a failure of the crown T-cap on the MBB was unlikely to occur at 2.5-g DUL. When comparing strain gage results calculated from linear and nonlinear analyses, an increase of strain values was seen in the results from nonlinear analysis. This was because the skin of the center crown started to buckle at 0.347-g up-bending load (or 22 kips of actuator load), which had resulted in more axial loads being taken by the crown T-caps instead of the crown skin. This prediction of 0.347-g up-bending load when the crown skin would start to buckle was derived from the results of the linear buckling analysis presented in Section 4.3.6.2. Because this effect of stiffness reduction from the crown skin buckling was included in the nonlinear analysis, strains of the crown T-cap from the nonlinear calculation would be higher than those produced by the linear solution, resembling a softening effect to a panel in post-buckling phase.

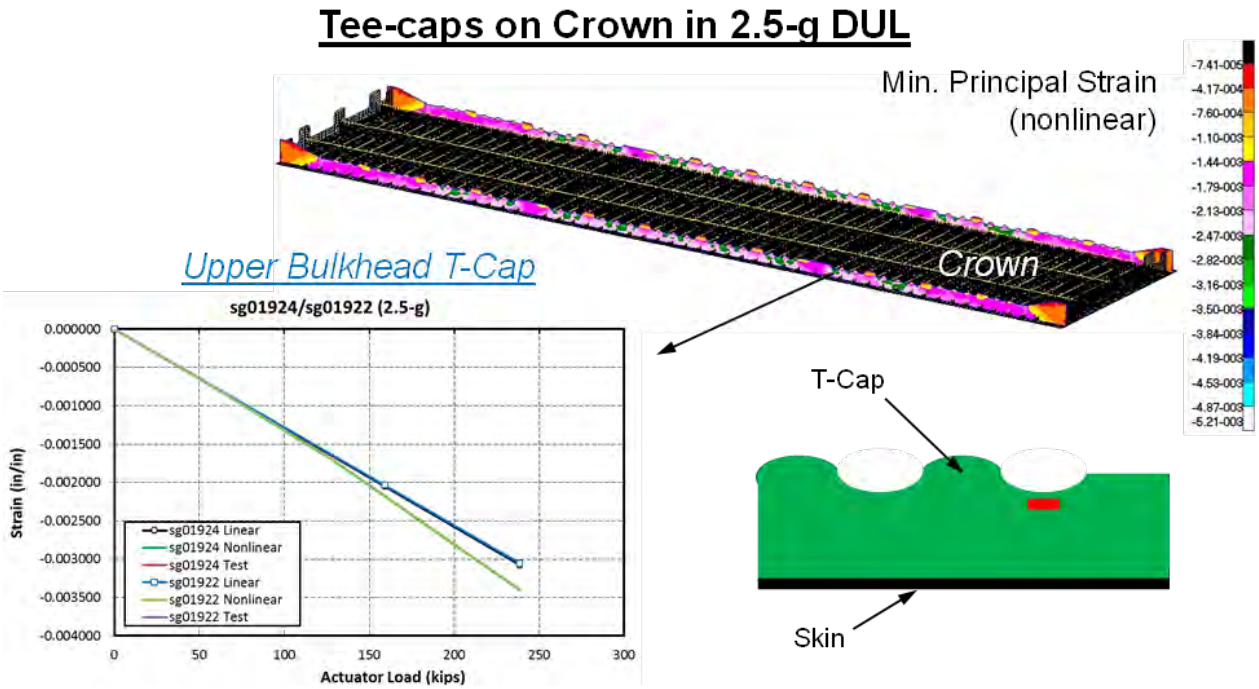

Figure 4-127. Strains on Crown T-caps in 2.5-g DUL Condition

Figure 4-128 shows a plot of minimum principal strains on the crown skin and charts of strain versus actuator load of rosette strain gage locations sg01288B/sg01291B (on the interior skin to measure principal strains) and back-to-back strain gage locations sg01106/sg01206 (on the exterior and interior skin). A critical minimum principal strain of -5,850 micro-in./.in on the skin was seen in the 2.5-g DUL maneuver condition. This critical strain was within the un-notched design strain value of -8,000 micro-in./in. for the skin. The calculated margin of safety was 37%, which indicated that a failure of the crown skin on the MBB was unlikely to occur at 2.5-g DUL. When comparing strain gage results calculated from linear and nonlinear analyses, an increase of strain values from the rosette strain gages and an increase of bending strain values from the back-to-back strain gages were seen from nonlinear analysis. This was because the skin of the center crown started to buckle at 0.347-g up-bending load (or 22 kips of actuator load), which had resulted in higher minimum principal strains and bending strains extracted from a buckled skin. This prediction of 0.347-g up-bending load when the crown skin would start to buckle was derived from the results of the linear buckling analysis presented in Section 4.3.6.2. Because this effect of the crown skin buckling was included in the nonlinear analysis, minimum principal strains and bending strains of the crown skin from the nonlinear calculation would be higher than those produced by the linear solution, resembling a softening effect to a panel in post-buckling phase.

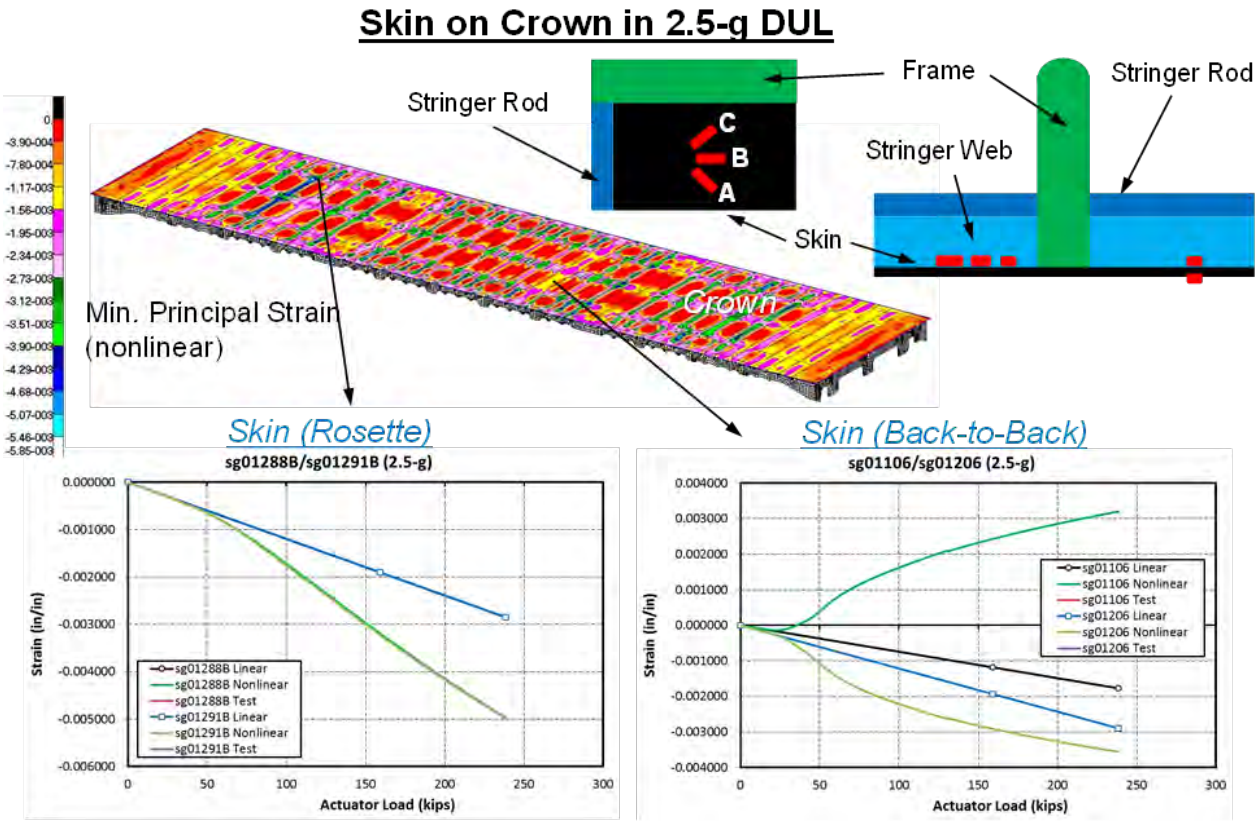

Figure 4-128. Strain on Crown Skin in 2.5-g DUL Condition

Figure 4-129 shows a plot of minimum principal strain on the upper bulkhead skin and charts of strain versus actuator load of rosette strain gage locations sg03108A/sg05108A and sg03109B/sg05109B (on the exterior skin to measure principal strains). A critical minimum principal strain of -6,030 micro-in./in. on the skin was seen in the 2.5-g DUL maneuver condition. This critical strain was within the un-notched design strain value of -8,000 micro-in./in. for the skin. The calculated margin of safety was 33%, which indicated that a failure of upper bulkhead skin on the MBB was unlikely to occur at 2.5-g DUL. When comparing strain gage results calculated from linear and nonlinear analyses, a sudden increase of strain rate occurred at approximately 2.0-g (or 130 kips of actuator load), showing that a local skin buckling of the upper bulkhead skin had occurred. As actuator load continued to increase, the same high strain rate remained until at approximately 2.5-g (or 159 kips of actuator load) when the strain rate was back to a slower rate again. This upper bulkhead skin buckling at 2.0-g was not discovered in the linear buckling analysis, as presented in Section 4.3.6.2. This 2.0-g up-bending load was much higher than the first buckling load of the crown skin at 0.347 g, and the linear buckling analysis was not performed up to this buckling load. Because this effect of the skin buckling was included in the nonlinear analysis, strains of the upper bulkhead skin from the nonlinear calculation would be higher than those produced by the linear solution, resembling a softening effect to a panel in post-buckling phase.

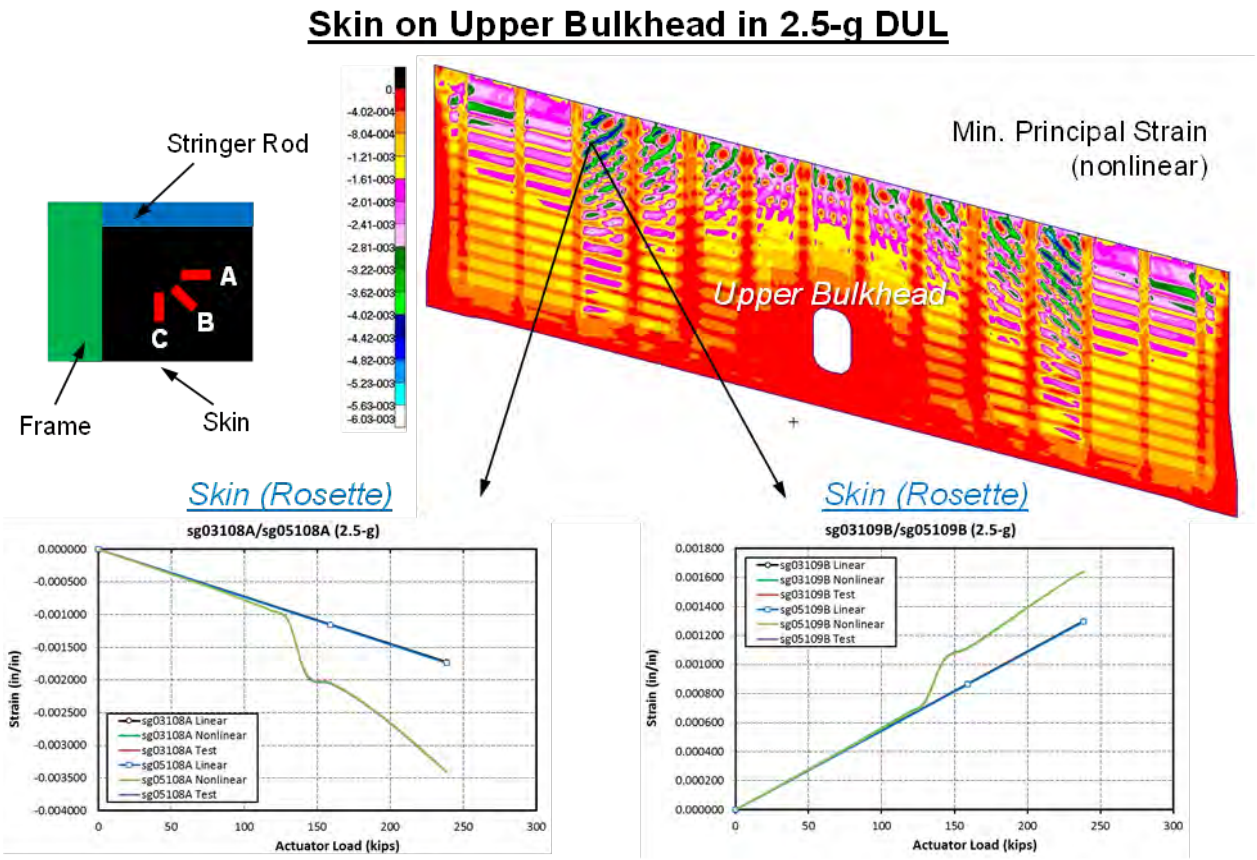

Figure 4-129. Rosette Strains on Upper Bulkhead Skin in 2.5-g DUL Condition

Figure 4-130 shows a plot of maximum principal strain on the side keel frames and a chart of strain versus actuator load of strain gage locations sg08810/sg09810 (on the frame top). A critical maximum principal strain of 3,790 micro-in./in. on the frame was seen in the 2.5-g DUL maneuver condition. This critical strain was within the un-notched design strain value of 10,000 micro-in./in. for the frame web. The calculated margin of safety was 164%, which indicated that a failure of the side keel frame on the MBB was unlikely to occur at 2.5-g DUL. When comparing strain gage results calculated from linear and nonlinear analyses, only a slight increase of strain values was seen in the results from nonlinear analysis. In the 2.5-g DUL maneuver condition, the side keel frames would be loaded in tension. No buckling was expected to occur for the side keel. This is why the strain results of the side keel were almost identical from linear and nonlinear analyses at 2.5-g DUL. The slight increase of strain values on the side keel frames was likely caused by buckling of the crown skin in the 2.5-g DUL maneuver condition, which resulted in a shift of the bending center at the up-bending load to the MBB.

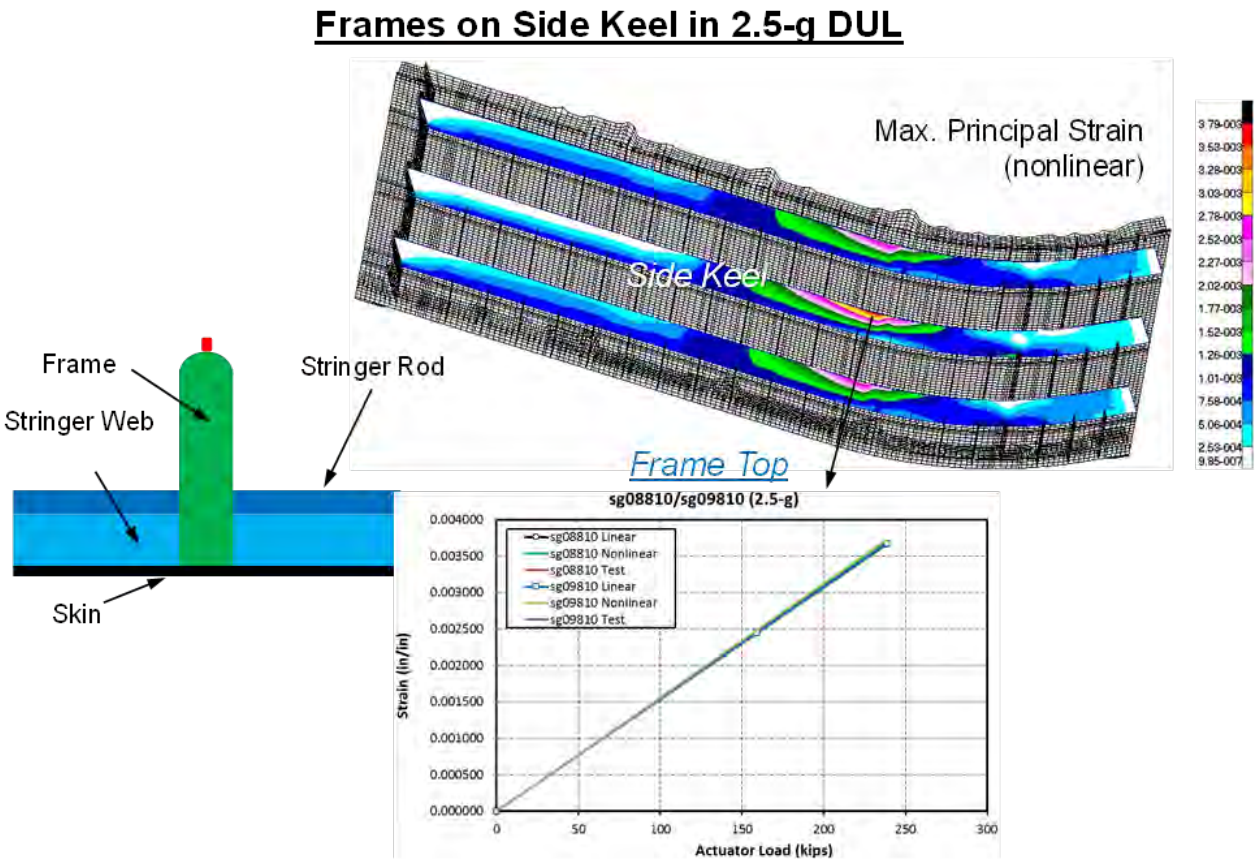

Figure 4-130. Strains on Side Keel Frames in 2.5-g DUL Condition

Figure 4-131 shows a plot of von Mises strain of the Lower External Side Load Introduction Fitting (ZJ153654-1) and a chart of strain versus actuator load of strain gage locations sg16017/sg16018 (on the fitting lower flange). A critical strain of 5,470 micro-in./in. located at the fitting web was seen in the 2.5-g DUL maneuver condition. Using Young's modulus of 10.3 Msi for aluminum alloy 7050-T7451, this strain was equivalent to a stress of 56.3 ksi. Compared to the yielding allowable of 65 ksi for the Lower External Side Load Introduction Fitting (ZJ153654-1), this critical stress was within the yielding allowable of the fitting. The calculated margin of safety was 15%, which indicated that a failure of the Lower External Side Load Introduction Fitting on the MBB was unlikely to occur at 2.5-g DUL. When comparing strain gage results, strain values calculated from linear and nonlinear analyses were almost identical, which meant that stress/strain results of metallic fittings on the MBB were mostly linear. Linear analysis was sufficient for the failure predictions for metallic fittings in the 2.5-g DUL maneuver condition.

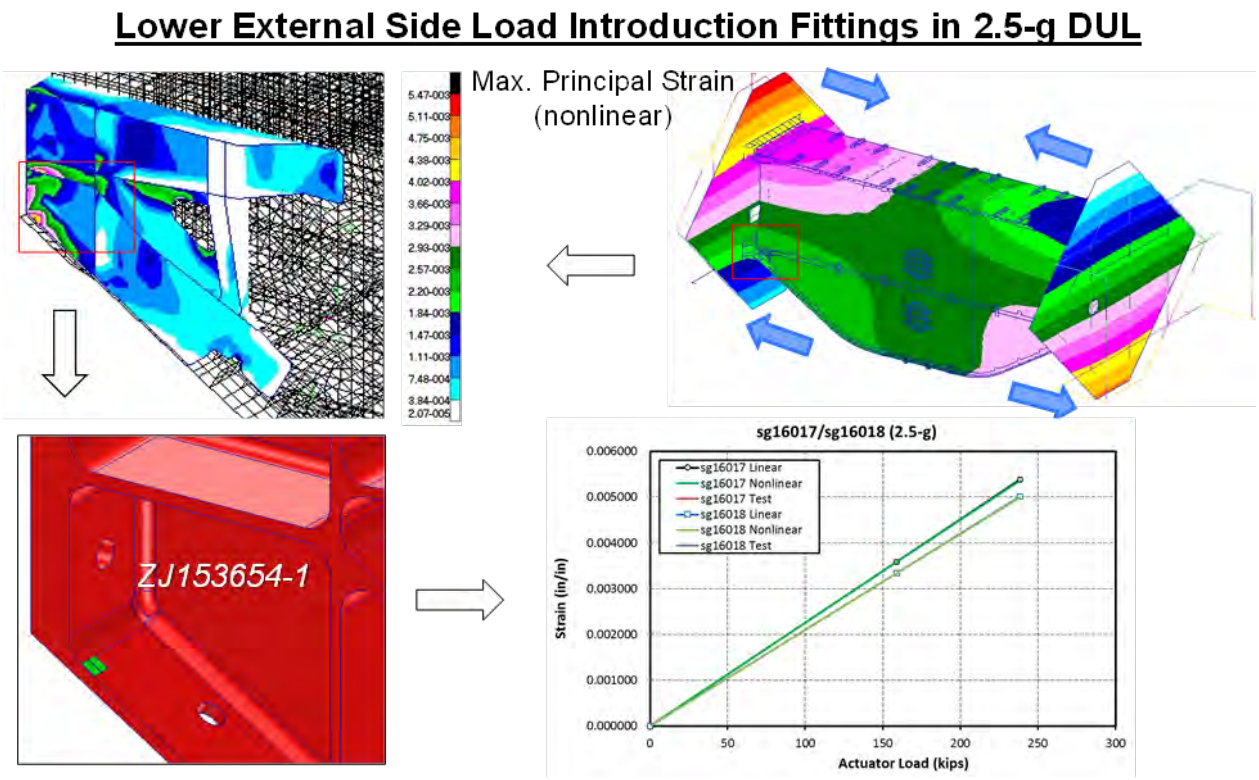

Figure 4-131. Strains on Fittings Connected to Lower Load-Introduction Fittings in 2.5-g DUL Condition

For tests of the MBB after impact damage, the following two critical locations were identified near the impact damage for possible failure locations that warranted evaluation:

1. On the exterior impact site no. 2, which was on the stringer flange of the center keel.
2. On the exterior impact site no. 3, which was on the mid-bay skin of the center keel.

Strain gages were placed near these impact-damaged locations to monitor the behavior of structure with impact damage during tests. Strain versus internal pressure of the critical strain gages are shown in Figure 4-132 and Figure 4-133. Strain gage predictions from linear and nonlinear analyses were compared to evaluate the extent of geometric nonlinearity of the MBB

in the 2.5-g DUL maneuver condition. Failure predictions were made by comparing the maximum and minimum principal strain values of the MBB from nonlinear analysis to the notched strain design values (in impact-damaged condition) of the composites shown in Table 4-7.

Figure 4-132 shows charts of strain versus actuator load of back-to-back strain gage locations sg18103/sg18303 (located 0.5-in. forward from the impact site) and sg18104/sg18304 (located 0.5-inch aft from the impact site) near exterior impact site no. 2 on the stringer flange of the center keel. When comparing strain results of these back-to-back strain gages, it was found that tension strain derived from nonlinear analysis was only slightly higher than the tension strain from linear analysis, whereas the bending strain derived from nonlinear analysis was lower than the bending strain from linear analysis. This was because some bending strains were suppressed and replaced with an in-plane tensioning on the panel skin/stringer/frame in tension loading. As a result, lower strains were detected on the panel skin/stringer/frame from nonlinear analysis, resembling a softening effect to a panel in axial load. Results from nonlinear analysis showed that the critical tension strain was 1,100 micro-in./in. near the impact damage site in the 2.5-g DUL maneuver condition. These strains were within the notched design strain values of 5,900 micro-in./in. for the stringer flange. The calculated margin of safety was 436%, which indicated that a failure of the stringer flange at exterior impact site no. 2 of the center keel on the MBB was unlikely to occur at 2.5-g DUL.

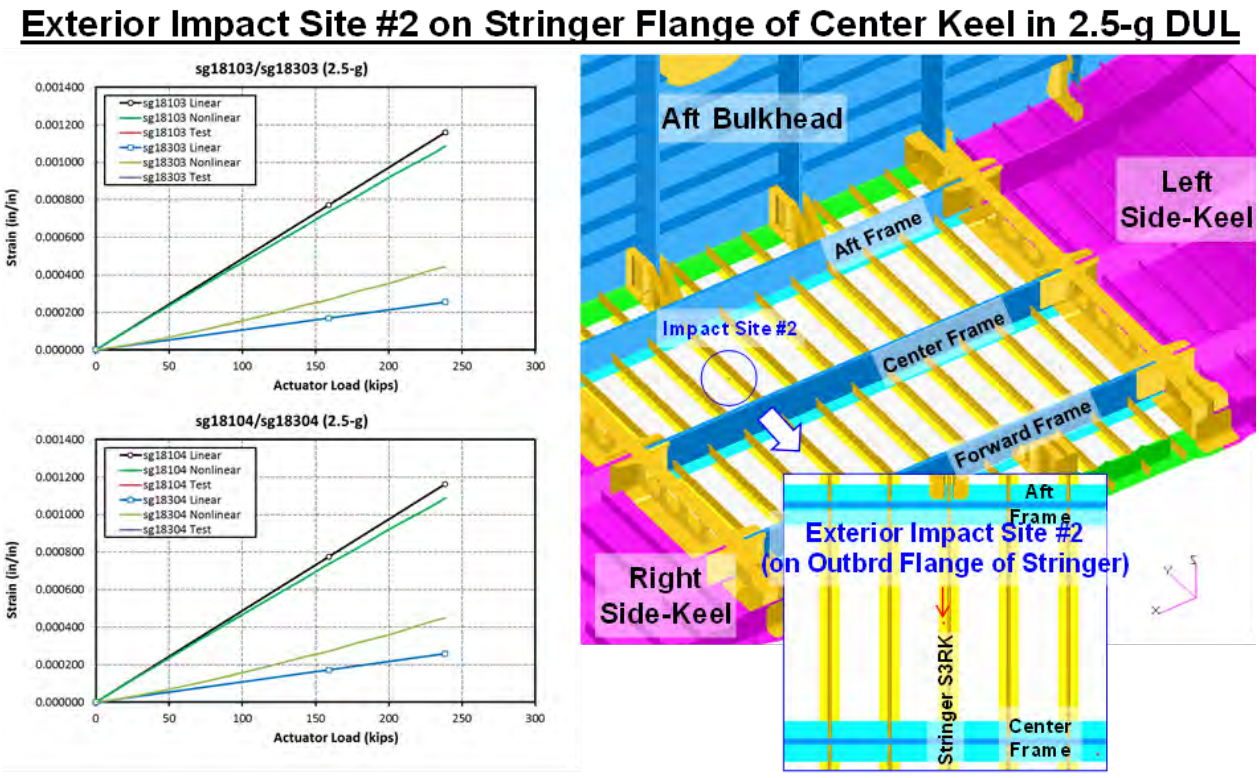

Figure 4-132. Strains on Exterior Impact Site no. 2 in 2.5-g DUL Condition

Figure 4-133 shows charts of strain versus actuator load of back-to-back strain gage locations sg18105/sg18205 (located 1.0-in. left of the impact site) and sg18106/sg18206 (located 1.0-in. right of the impact site) near exterior impact site no. 3 on the mid-bay skin of the center keel. When comparing strain results of these back-to-back strain gages, it was found that tension strain derived from nonlinear analysis was higher than the tension strain from linear analysis, whereas the bending strain derived from nonlinear analysis was significantly lower than the bending strain from linear analysis. This was because some bending strains were suppressed and replaced with an in-plane tensioning on the panel skin/stringer/frame in tension loading. As a result, lower strains were detected on the panel skin/stringer/frame from nonlinear analysis, resembling a softening effect to a panel in axial load. Results from nonlinear analysis showed that the critical tension strain was 1,318 micro-in./in. near the impact damage site in the 2.5-g DUL maneuver condition. This strain was within the notched design strain value of 5,900 micro-in./in. for the skin. The calculated margin of safety was 348%, which indicated that a failure of the skin at exterior impact site no. 3 of the center keel on the MBB was unlikely to occur at 2.5-g DUL.

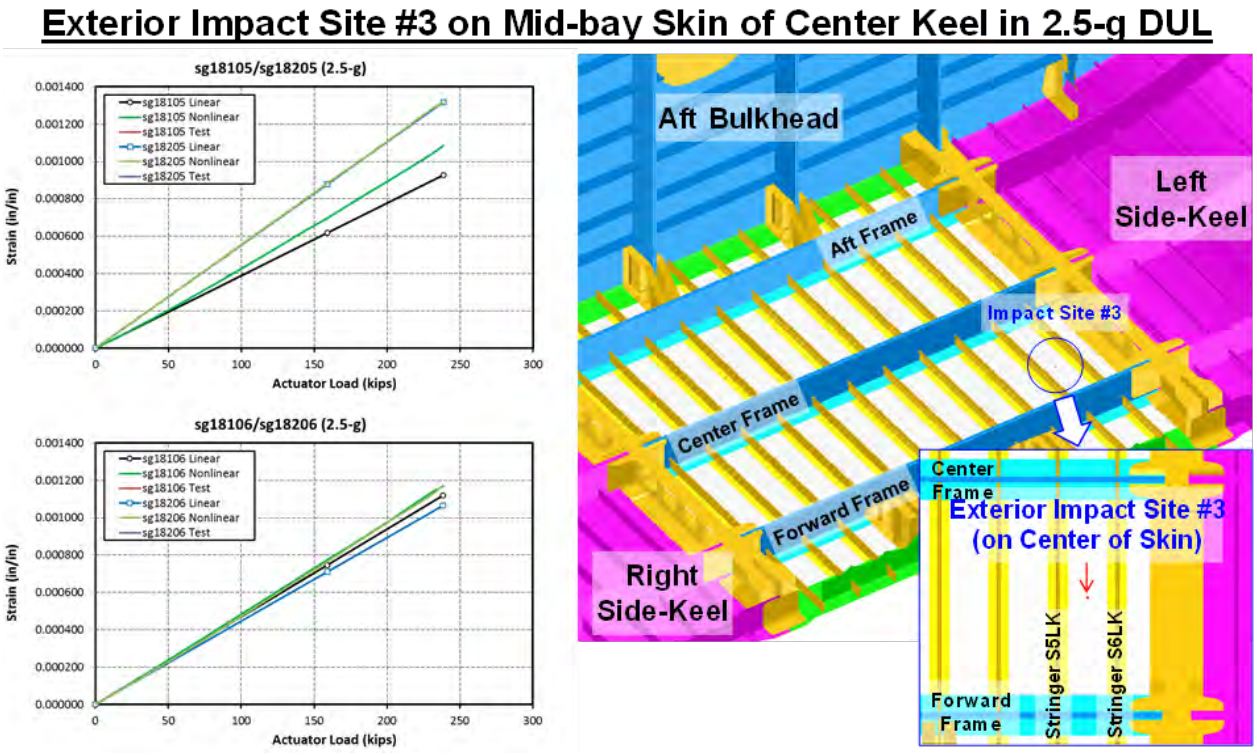

Figure 4-133. Strains on Exterior Impact Site no. 3 in 2.5-g DUL Condition

4.4.3 2.5-g + 1P DUL Combined Loading Condition

Failure predictions for the MBB were made based on results from nonlinear analysis of the global FEM in the 2.5-g + 1P DUL combined loading condition. In this condition, concentrated loads were applied on the COLTS fixture to simulate a 2.5-g DUL (3.75-g) up-bending load plus a 1P DUL (1.5P, or 13.8 psi) pressure, creating a force normal to the internal skin surface that would deform the crown, bulkhead, and keel panels outward. To understand the structural behavior of the MBB and the crown panel in 2.5-g + 1P DUL combined loads, displacement plots from nonlinear and linear analyses were compared and are shown in Figure 4-134 and Figure 4-135.

For the MBB, the maximum displacement at the upper edge of the COLTS loading platen was 0.824 in. from the nonlinear analysis and 0.823 in. from the linear analysis. For the crown panel, the maximum displacement at the right end of the crown was 0.445 in. from the nonlinear analysis and 0.387 in. from the linear analysis. Although deformations of the platens were almost identical, the deformations of the crown panel were completely different from linear and nonlinear analyses in the 2.5-g + 1P DUL combined loading condition. It appeared that structures of the MBB behaved with influences from both 2.5-g maneuver and pressure loads. The internal pressure seemed to delay early skin buckling of composite panel in compressive load. While examining the results of strain gages on the crown skin, it was found that the skin of the crown started to buckle at 1.8-g + 0.7P (116 kips + 6.7 psi), which was much higher than the 0.347-g up-bending load seen in the maneuver only load (Section 4.3.6.2).

These results from linear buckling and nonlinear analyses of the MBB confirmed that a cabin pressure would greatly increase the buckling initiation load of a composite panel in compression. (Details of the crown skin results are presented later in this section.) The interactive effect between maneuver and pressure loads to a structure made predicting structural behaviors of the MBB difficult using only linear analysis. Nonlinear analysis was able to capture both structural stiffening in the pressure load and structural softening in the compressive load on the crown panel of the MBB. Therefore, results from the nonlinear analysis were used in making failure predictions for the MBB in the 2.5-g + 1P DUL combined loading condition.

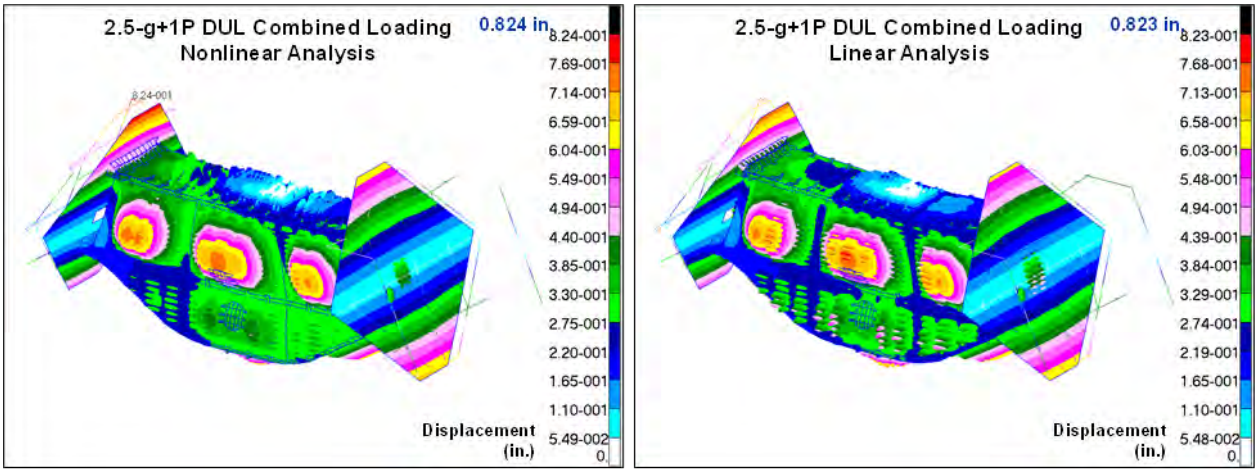

Figure 4-134. Displacements of the MBB From Linear and Nonlinear Analyses in 2.5-g + 1P DUL Condition

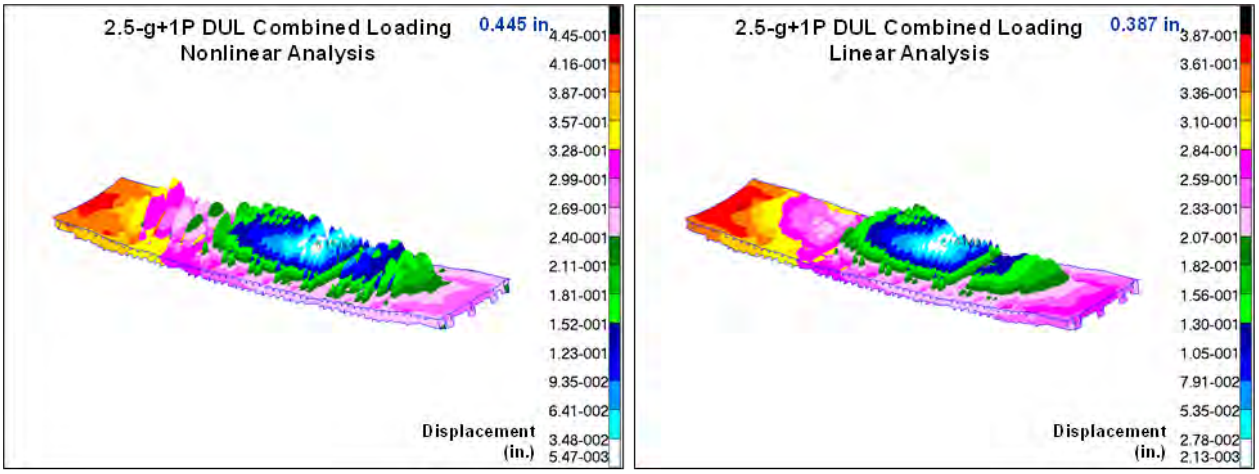

Figure 4-135. Displacements of the Crown From Linear and Nonlinear Analyses in 2.5-g + 1P DUL Condition

In testing of the 2.5-g + 1P DUL combined loading condition, the MBB was loaded up to 2.5-g + 1P DUL (3.75-g). During the test, in-plane strains and out-of-plane deformations were measured by VIC-3D, LVDT, and strain gages. Locations of the VIC-3D, LVDT, and strain gages are shown in the HWB MBB Test Specification (Ref. 4-9). Predictions of VIC-3D plots from nonlinear analysis are shown in Figure 4-136, and displacement prediction charts of the LVDT are shown in Figure 4-136 for the upper bulkhead and in Figure 4-137 for the reacting platen. Results from linear and nonlinear analyses are plotted and compared. Results from the LVDT charts showed that normal displacements of the upper bulkhead were slightly lower and rotation of the reacting platen was slightly higher from the nonlinear analysis than displacements from the linear analysis in the 2.5-g + 1P DUL combined loading condition.

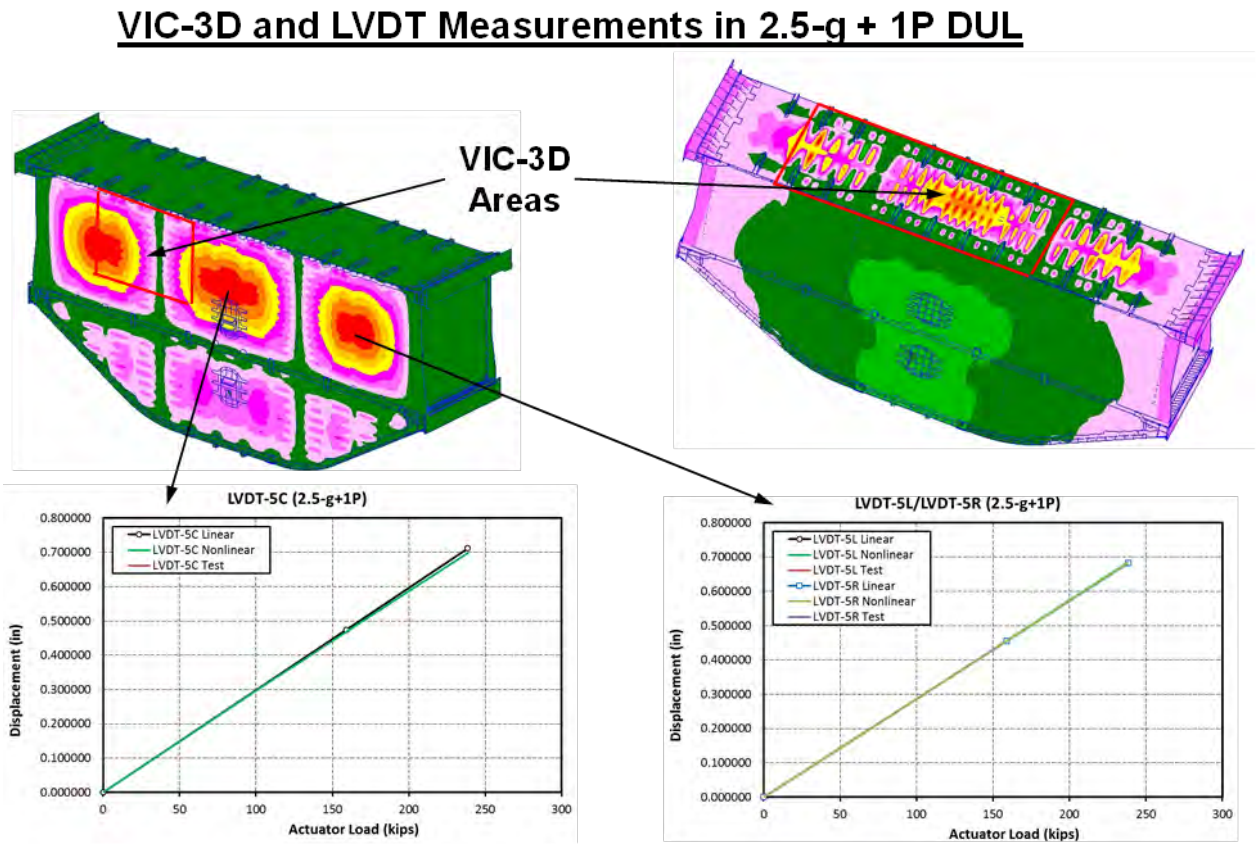

Figure 4-136. VIC-3D Measurements of the MBB in 2.5-g + 1P DUL Condition

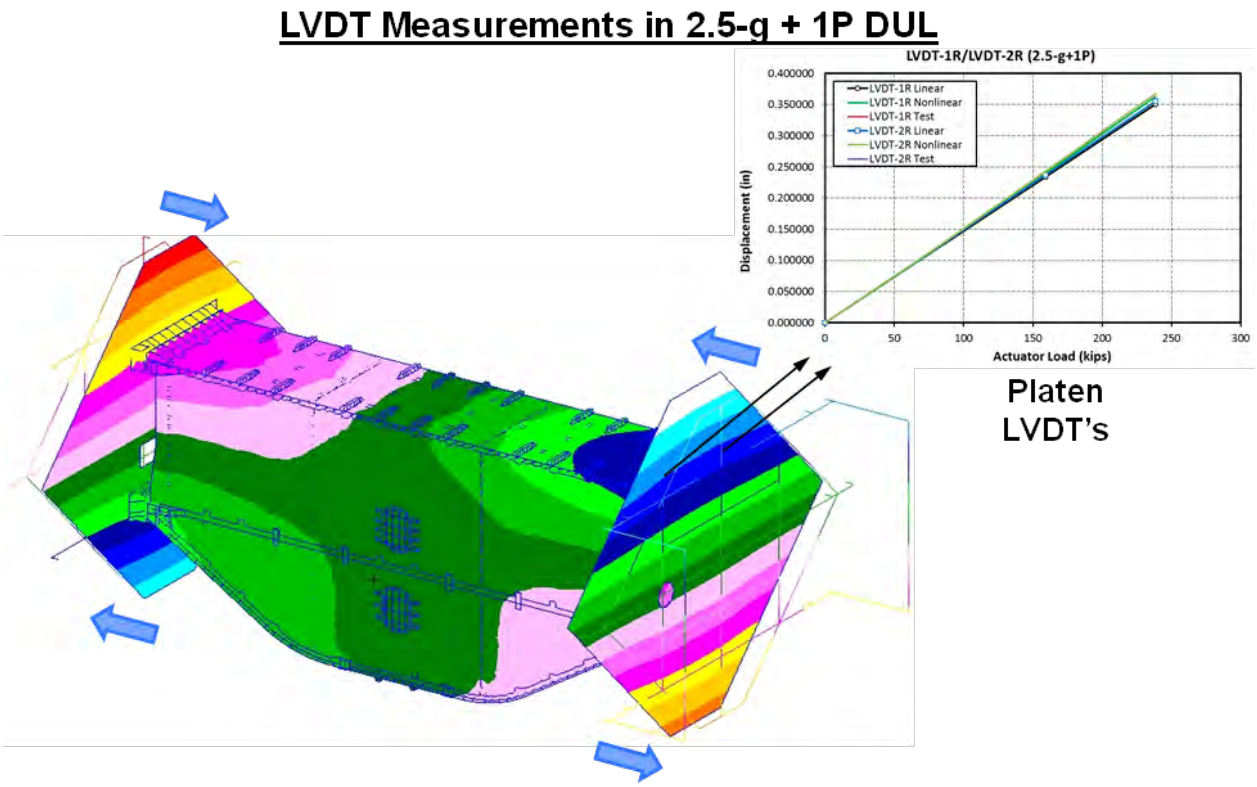

Figure 4-137. LVDT Measurements of the MBB in 2.5-g + 1P DUL Condition

In addition to the VIC-3D and LVDT instruments, strain gages were placed on the MBB where high strains and stresses were expected during tests. As shown in Figure 4-138, for the MBB structures that were considered to be pristine (not impact damaged), the following seven critical locations were identified for possible failure locations that warranted evaluation:

1. On the crown frames.
2. On the crown T-caps.
3. On the crown stringer webs and stringer rods near the frames.
4. On the crown skin.
5. On the upper bulkhead skin.
6. On the side keel frames.
7. On the metallic fittings connected to the lower load-introduction fittings.

Strain gages were placed at these critical locations to monitor the structural behavior and integrity of the MBB during tests. Maximum or minimum principal strain distribution plots from nonlinear analysis and strain gage predictions from linear and nonlinear analyses are shown in Figure 4-139 through Figure 4-145. Strain gage predictions from linear and nonlinear analyses were compared to evaluate the extent of geometric nonlinearity of the MBB in the 2.5-g + 1P DUL combined loading condition. Failure predictions were made by comparing the maximum and minimum principal strain values of the MBB from nonlinear analysis to the un-notched strain design values (in the pristine condition) of the composites shown in Table 4-7, and by comparing von Mises stresses of the metallic fittings and bolts to the ultimate strengths of metals. In summary, failure prediction results showed that the MBB in its pristine condition

would not fail catastrophically at 2.5-g + 1P DUL. Detailed results for these critical locations are presented in the following discussion.

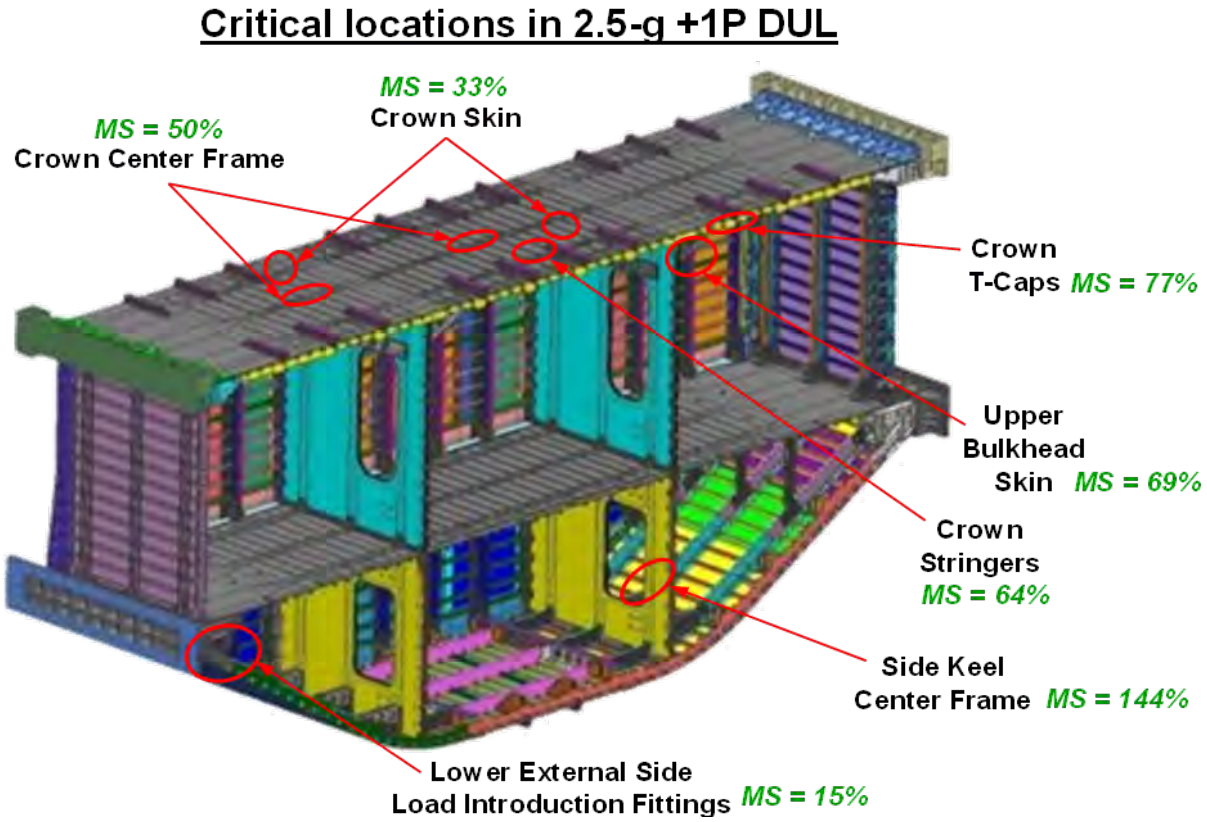

Figure 4-138. Critical Locations in Failure Predictions for the MBB in 2.5-g + 1P DUL Condition

Figure 4-139 shows a plot of minimum principal strain on the crown frames and charts of strain versus actuator load of strain gage locations sg01875/sg01876 and sg01874 (on the frame top). A critical minimum principal strain of -5,320 micro-in./in. on the frame was seen in the 2.5-g + 1P DUL combined loading condition. This critical strain was within the un-notched design strain value of -8,000 micro-in./in. for the frame web. The calculated margin of safety was 50%, which indicated that a failure of crown frame on the MBB was unlikely to occur at 2.5-g + 1P DUL. When comparing strain gage results calculated from linear and nonlinear analyses, an increase of strain values was seen in the results from nonlinear analysis. This was because the skin of the center crown started to buckle at 1.8-g + 0.7P (116 kips + 6.7 psi), which resulted in more axial loads being taken by the crown frames instead of the crown skin. (Details of the crown skin results are presented later in this section.) Because this effect of stiffness reduction from the crown skin buckling was included in the nonlinear analysis, strains of the crown frame from the nonlinear calculation would be higher than those produced by the linear solution, resembling a softening effect to a panel in post-buckling phase.

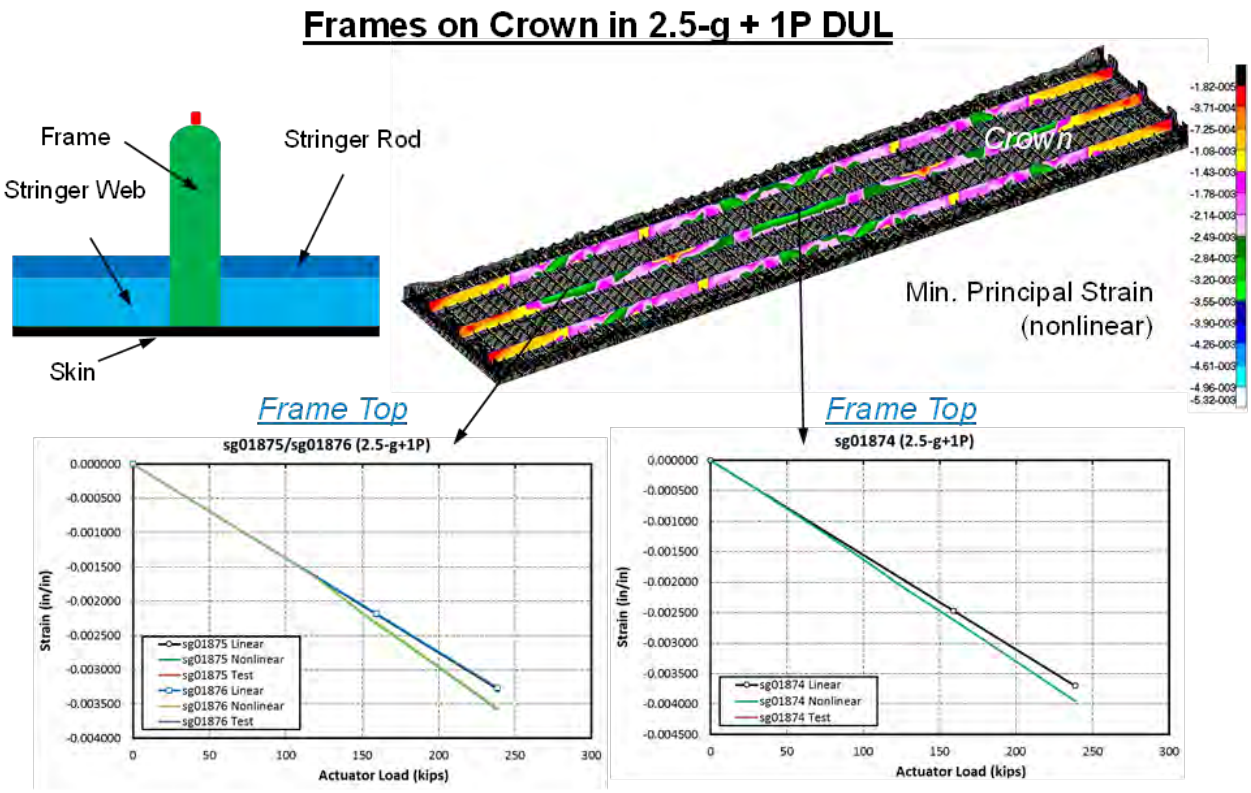

Figure 4-139. Strains on Crown Frames in 2.5-g + 1P DUL Condition

Figure 4-140 shows a plot of minimum principal strain on the crown T-caps and a chart of strain versus actuator load of strain gage locations sg01924/sg01922 (on the T-cap web). A critical minimum principal strain of -4,510 micro-in./in. on T-caps was seen in the 2.5-g + 1P DUL combined loading condition. This critical strain was within the un-notched design strain value of -8,000 micro-in./in. for the T-cap web. The calculated margin of safety was 77%, which indicated that a failure of the crown T-cap on the MBB was unlikely to occur at 2.5-g + 1P DUL. When comparing strain gage results calculated from linear and nonlinear analyses, an increase of strain values was seen in the results from nonlinear analysis. This was because the skin of the center crown started to buckle at 1.8-g + 0.7P (116 kips + 6.7 psi), which resulted in more axial loads being taken by the crown T-caps instead of the crown skin. (Details of the crown skin results are presented later in this section.) Because this effect of stiffness reduction from the crown skin buckling was included in the nonlinear analysis, strains of the crown T-cap from the nonlinear calculation would be higher than those produced by the linear solution, resembling a softening effect to a panel in post-buckling phase.

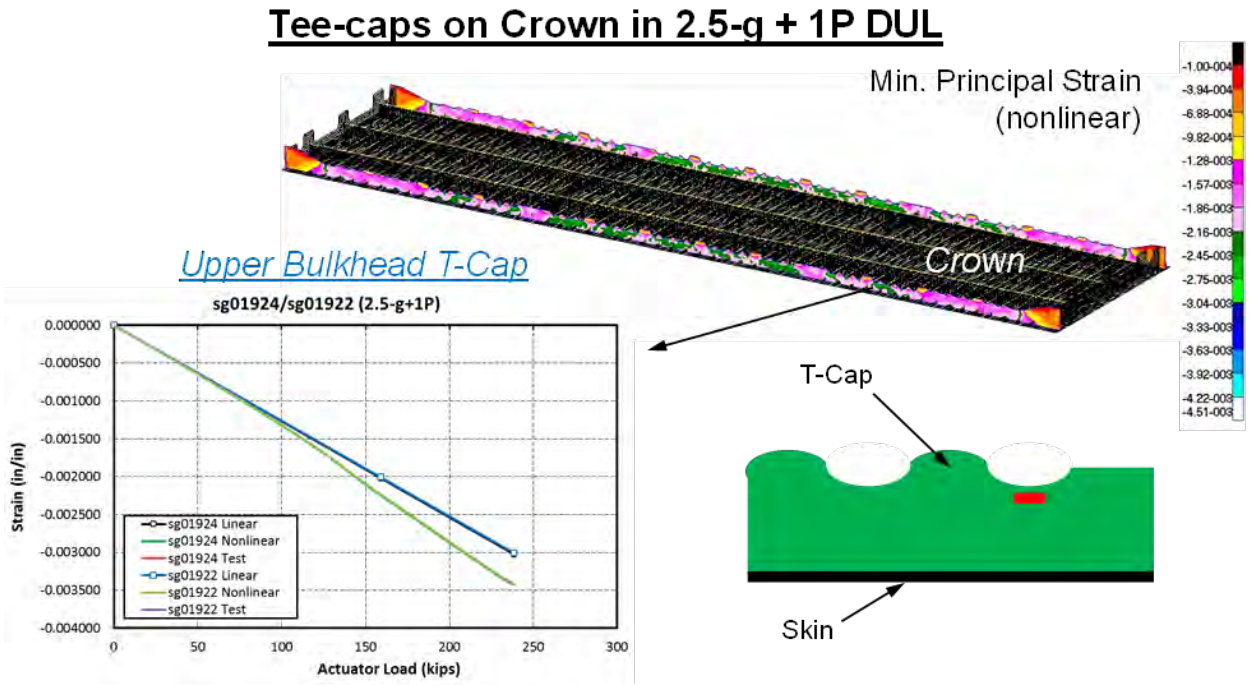

Figure 4-140. Strains on Crown T-caps in 2.5-g + 1P DUL Condition

Figure 4-141 shows a plot of maximum principal strain on the crown stringer web near the frames and charts of strain versus actuator load of rosette strain gage locations sg01436C/sg01440C (on the stringer web to measure principal strains) and sg01525/sg01529 (on the stringer rod). A critical maximum principal strain of 6,090 micro-in./in. on the stringer web/rod was seen in the 2.5-g + 1P DUL combined loading condition. This critical strain was within the un-notched design strain value of 10,000 micro-in./in. for the stringer web. The calculated margin of safety was 64%, which indicated that a failure of the crown stringer web and stringer rod on the test article was unlikely to occur at 2.5-g + 1P DUL. When comparing strain gage results calculated from linear and nonlinear analyses, the strain of the stringer rod was slightly lower and the strain of the stringer web was slightly higher from the nonlinear analysis than those from the linear analysis in the 2.5-g + 1P DUL combined loading condition. This was because an appreciable out-of-plane deformation was suppressed and replaced with an in-plane tensioning on the panel skin/stringer/frame in pressure loading. As a result, lower strains were detected on the panel skin/stringer/frame from nonlinear analysis, resembling a stiffening effect to a panel in pressure load.

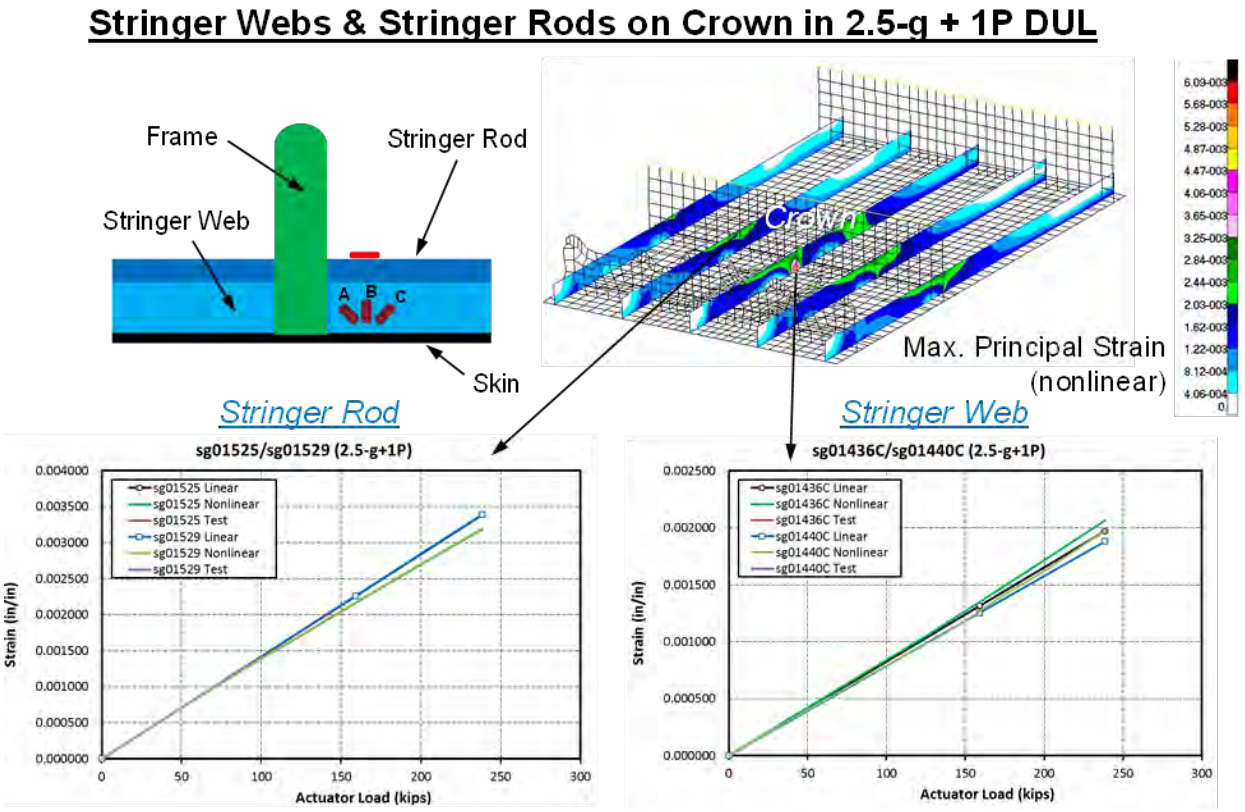

Figure 4-141. Strains on Crown Stringer Webs in 2.5-g + 1P DUL Condition

Figure 4-142 shows a plot of minimum principal strains on the crown skin and charts of strain versus actuator load of rosette strain gage locations sg01288B/sg01291B (on the interior skin to measure principal strains) and back-to-back strain gage locations sg01106/sg01206 (on the exterior and interior skin). A critical minimum principal strain of -6,020 micro-in./in. on the skin was seen in the 2.5-g + 1P DUL combined loading condition. This critical strain was within the un-notched design strain value of -8,000 micro-in./in. for the skin. The calculated margin of safety was 33%, which indicated that a failure of the crown skin on the MBB was unlikely to occur at 2.5-g + 1P DUL. When comparing strain gage results calculated from linear and nonlinear analyses, an increase of strain values from the rosette strain gages and an increase of bending strain values from the back-to-back strain gages were seen from nonlinear analysis. This was because the skin of the center crown started to buckle at 1.8-g + 0.7P (116 kips + 6.7 psi), which was much higher than the 0.347-g up-bending load seen in the maneuver only load (see Section 4.3.6.2). These results from linear buckling and nonlinear analyses of the MBB confirmed that a cabin pressure would greatly increase the buckling initiation load of a composite panel in compression. Because this effect of the crown skin buckling was included in the nonlinear analysis, minimum principal strains and bending strains of the crown skin from the nonlinear calculation would be higher than those produced by the linear solution, resembling a softening effect to a panel in post-buckling phase.

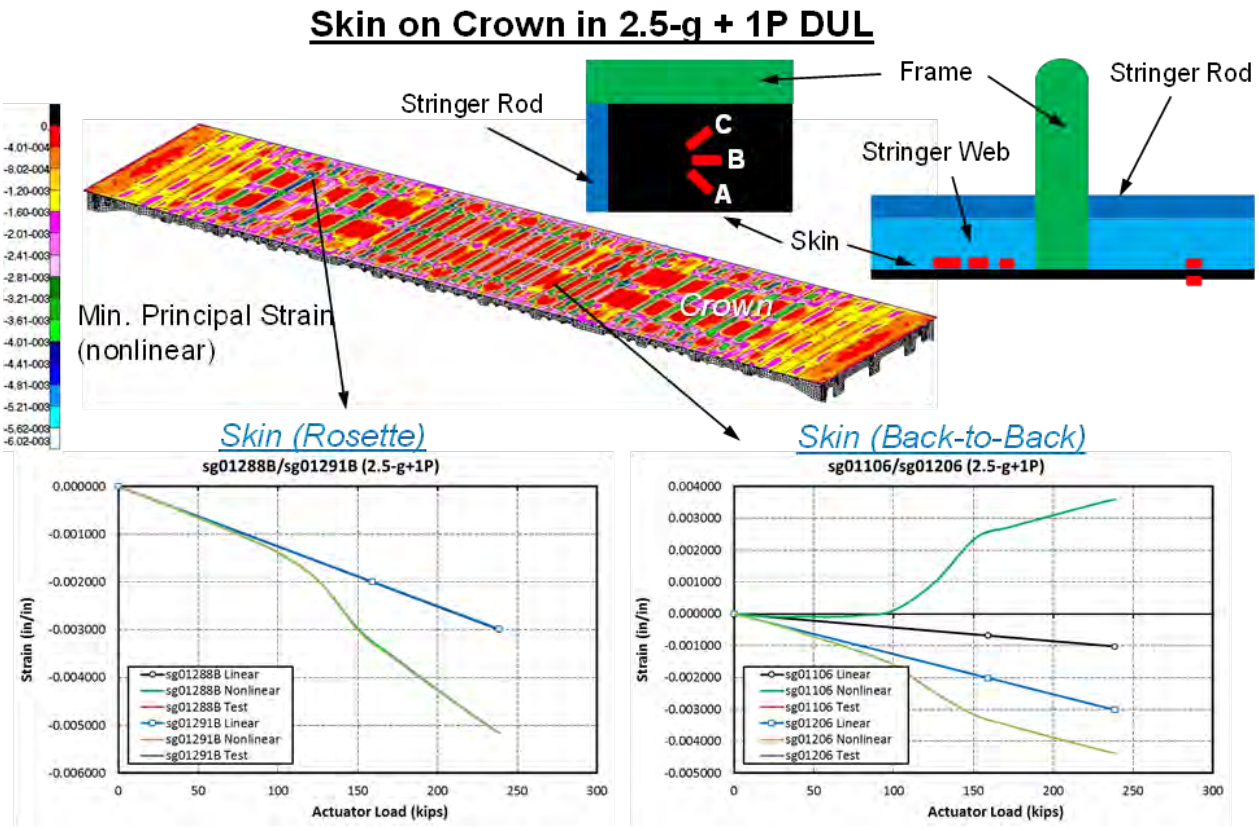

Figure 4-142. Strain on Crown Skin in 2.5-g + 1P DUL Condition

Figure 4-143 shows a plot of minimum principal strain on the upper bulkhead skin and charts of strain versus actuator load of rosette strain gage locations sg03111A/sg05111A and sg03112B/sg05112B (on the exterior skin to measure principal strains). A critical minimum principal strain of -4,720 micro-in./in. on the skin was seen in the 2.5-g + 1P DUL combined loading condition. This critical strain was within the un-notched design strain value of -8,000 micro-in./in. for the skin. The calculated margin of safety was 69%, which indicated that a failure of the upper bulkhead skin on the MBB was unlikely to occur at 2.5-g + 1P DUL. When comparing exterior strain gage results calculated from linear and nonlinear analyses, a gradual increase of strain rate as actuator load increased. This was similar to the strain gage results in the 2.5-g DUL maneuver condition, except that a local skin buckling of the upper bulkhead skin did not occur at roughly 2.5-g (or 159 kips of actuator load). It was believed that the cabin pressure in the 2.5-g + 1P DUL combined loading condition had prevented the buckling of upper bulkhead skin below 2.5-g DUL up-bending load. Because the effects of the upper bulkhead skin in pressure and compressive load were included in the nonlinear analysis, strains of the upper bulkhead skin from the nonlinear calculation were found to be higher than those produced by the linear solution, resembling a softening effect to a panel in combined pressure and maneuver load.

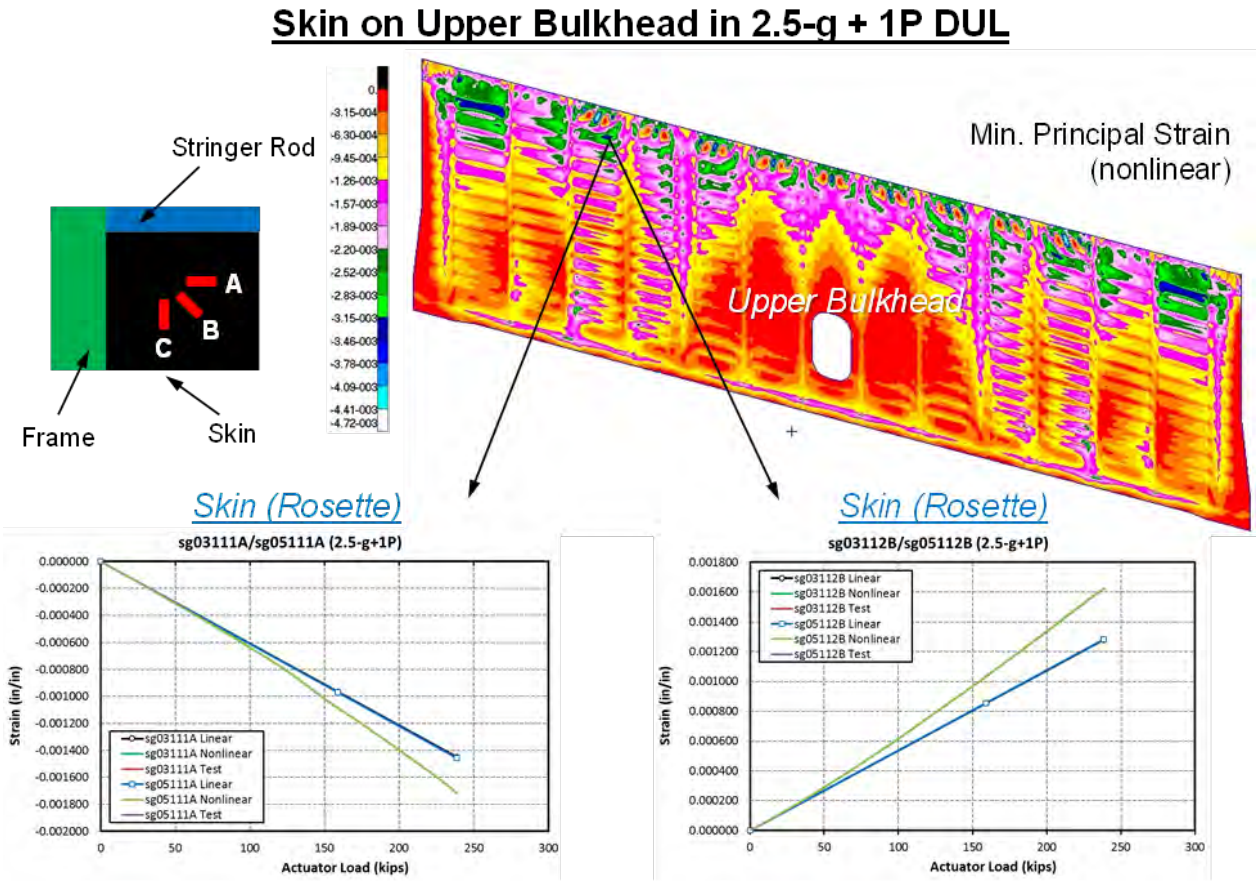

Figure 4-143. Rosette Strains on Upper Bulkhead Skin in 2.5-g + 1P DUL Condition

Figure 4-144 shows a plot of maximum principal strain on the side keel frames and a chart of strain versus actuator load of strain gage locations sg08810/sg09810 (on the frame top). A critical maximum principal strain of 4,090 micro-in./in. on the frame was seen in the 2.5-g + 1P DUL combined loading condition. This critical strain was within the un-notched design strain value of 10,000 micro-in./in. for the frame web. The calculated margin of safety was 144%, which indicated that a failure of the side keel frame on the MBB was unlikely to occur at 2.5-g + 1P DUL. When comparing strain gage results of strain gage locations sg08810/sg09810 (on the frame top) calculated from linear and nonlinear analyses, only a slight decrease of strain values was seen on results from the nonlinear analysis. In the 2.5-g + 1P DUL combined loading condition, the side keel frames would be loaded in tension from up-bending load (2.5-g DUL) and also in tension from pressure (1.5P). No buckling was expected to occur for the side keel. This was why the strain results of the side keel were almost identical from linear and nonlinear analyses at 2.5-g + 1P DUL. The slight decrease of strain values on the side keel frames was likely caused by an appreciable out-of-plane deformation that was suppressed and replaced with an in-plane tensioning on the panel skin/stringer/frame in pressure loading. As a result, lower strains were detected on the panel skin/stringer/frame from nonlinear analysis, resembling a stiffening effect to a panel in pressure load.

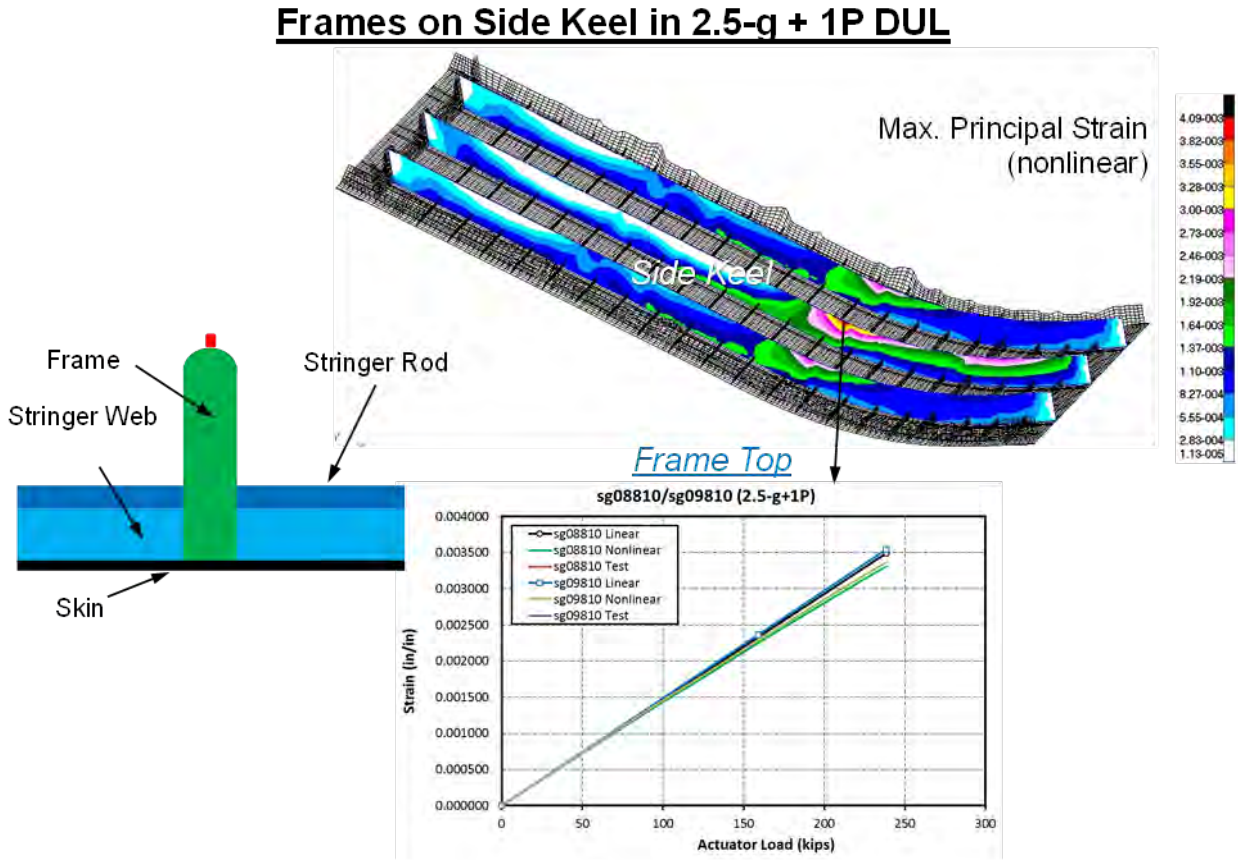

Figure 4-144. Strains on Side Keel Frames in 2.5-g + 1P DUL Condition

Figure 4-145 shows a plot of von Mises strain of the Lower External Side Load Introduction Fitting (ZJ153654-1) and a chart of strain versus actuator load of strain gage locations sg16017/sg16018 (on the fitting lower flange). A critical strain of 5,470 micro-in./in. located at the fitting web was seen in the 2.5-g + 1P DUL combined loading condition. Using Young's modulus of 10.3 Msi for aluminum alloy 7050-T7451, this strain was equivalent to a stress of 56.3 ksi. Compared to the yielding allowable of 65 ksi for the Lower External Side Load Introduction Fitting (ZJ153654-1), this critical stress was within the yielding allowable of the fitting. The calculated margin of safety was 15%, which indicated that a failure of the Lower External Side Load Introduction Fitting on the MBB was unlikely to occur at 2.5-g + 1P DUL. When comparing strain gage results, strain values calculated from linear and nonlinear analyses were almost identical, which meant that stress/strain results of the metallic fittings on the MBB were mostly linear. Linear analysis was sufficient for the failure predictions for metallic fittings in the 2.5-g + 1P DUL combined loading condition.

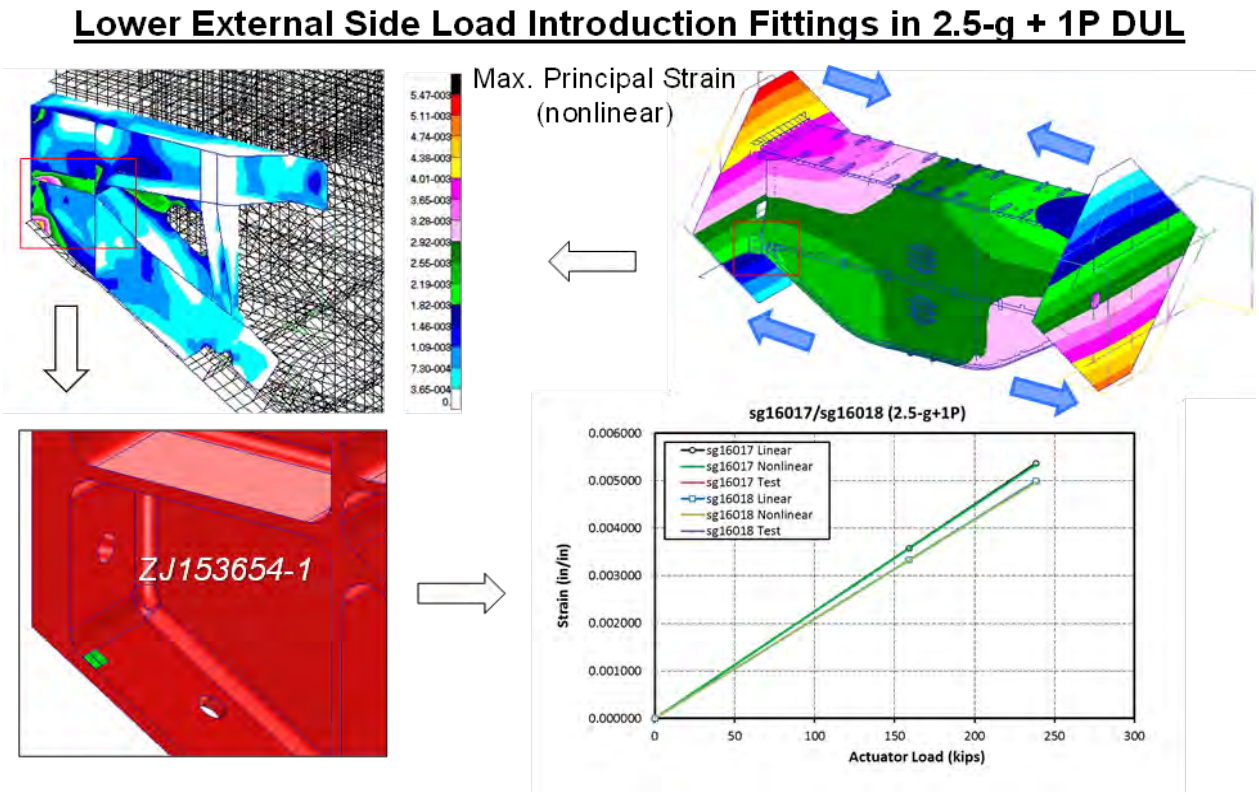

Figure 4-145. Strains on Fittings Connected to Lower Load-Introduction Fittings in 2.5-g + 1P DUL Condition

For tests of the MBB after impact damage, the following four critical locations were identified near the impact damage for possible failure locations that warranted evaluation:

1. On the exterior impact site no. 2, which was on the stringer flange of the center keel.
2. On the exterior impact site no. 3, which was on the mid-bay skin of the center keel.
3. On the interior impact site no. 1, which was on the frame top of the upper bulkhead.
4. On the interior impact site no. 3, which was on the mid-bay skin of the upper bulkhead.

Strain gages were placed near these impact-damaged locations to monitor the behavior of structure with impact damage during tests. Strain versus internal pressure of the critical strain

gages are shown in Figure 4-146 through Figure 4-149. Strain gage predictions from linear and nonlinear analyses were compared to evaluate the extent of geometric nonlinearity of the MBB in the 2.5-g + 1P DUL combined loading condition. Failure predictions were made by comparing the maximum and minimum principal strain values of the MBB from nonlinear analysis to the notched strain design values (in impact-damaged condition) of the composites shown in Table 4-7.

Figure 4-146 shows charts of strain versus actuator load of back-to-back strain gage locations sg18103/sg18303 (located 0.5-in. forward from the impact site) and sg18104/sg18304 (located 0.5-in. aft from the impact site) near exterior impact site no. 2 on the stringer flange of the center keel. When comparing strain results of these back-to-back strain gages, it was found that tension strain derived from nonlinear analysis was similar to the tension strain from linear analysis, whereas the bending strain derived from nonlinear analysis was significantly lower than the bending strain from linear analysis. This was because some bending strains were suppressed and replaced with an in-plane tensioning on the panel skin/stringer/frame in tension loading. As a result, lower strains were detected on the panel skin/stringer/frame from nonlinear analysis, resembling a stiffening effect to a panel in pressure load. Results from nonlinear analysis showed that the critical tension strain was 1,493 micro-in./in. near the impact damage site in the 2.5-g + 1P DUL combined loading condition. These strains were within the notched design strain values of 5,900 micro-in./in. for the stringer flange. The calculated margin of safety was 295%, which indicated that a failure of the stringer flange at exterior impact site no. 2 of the center keel on the MBB was unlikely to occur at 2.5-g + 1P DUL.

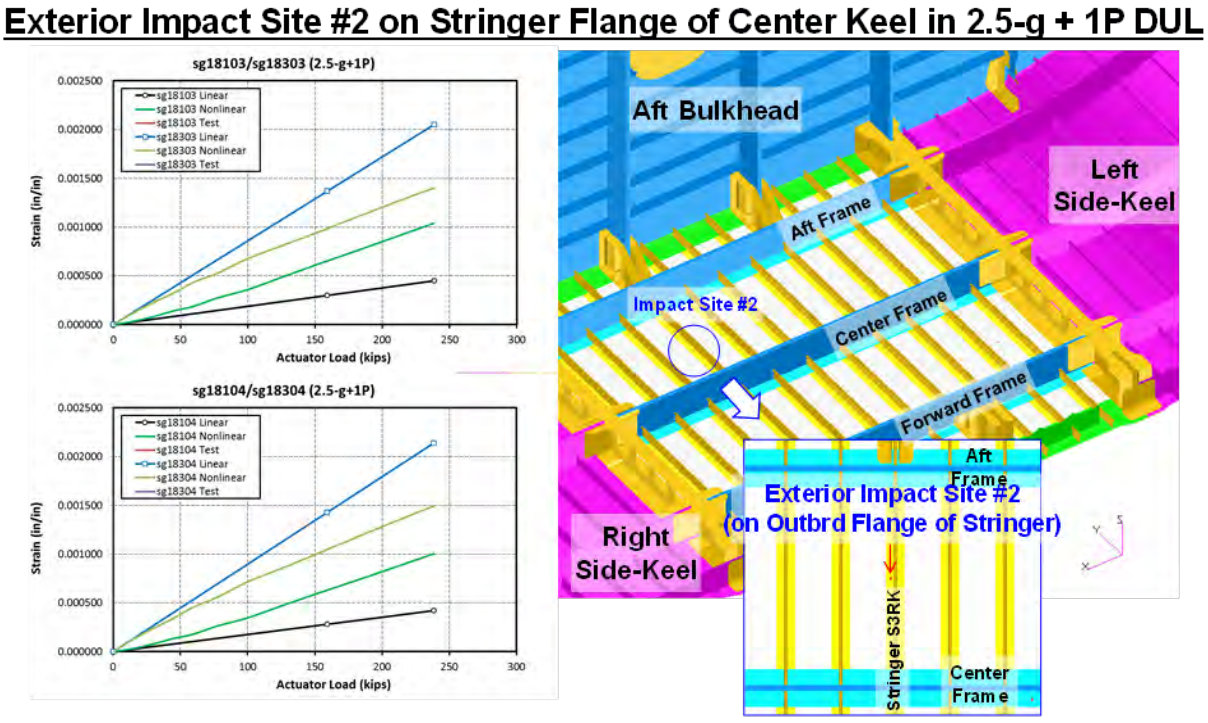

Figure 4-146. Strains on Exterior Impact Site no. 2 in 2.5-g + 1P DUL Condition

Figure 4-147 shows charts of strain versus actuator load of back-to-back strain gage locations sg18105/sg18205 (located 1.0-in. left of the impact site) and sg18106/sg18206 (located 1.0-in. right of the impact site) near exterior impact site no. 3 on the mid-bay skin of the center keel. When comparing strain results of these back-to-back strain gages, it was found that tension strain derived from nonlinear analysis was higher than the tension strain from linear analysis, whereas the bending strain derived from nonlinear analysis was significantly lower than the bending strain from linear analysis. This was because some bending strains were suppressed and replaced with an in-plane tensioning on the panel skin/stringer/frame in tension loading. As a result, lower strains were detected on the panel skin/stringer/frame from nonlinear analysis, resembling a stiffening effect to a panel in pressure load. Results from nonlinear analysis showed that the critical tension strain was 2,034 micro-in./in. near the impact damage site in the 2.5-g + 1P DUL combined loading condition. This strain was within the notched design strain value of 5,900 micro-in./in. for the skin. The calculated margin of safety was 190%, which indicated that a failure of the skin at exterior impact site no. 3 of the center keel on the MBB was unlikely to occur at 2.5-g + 1P DUL.

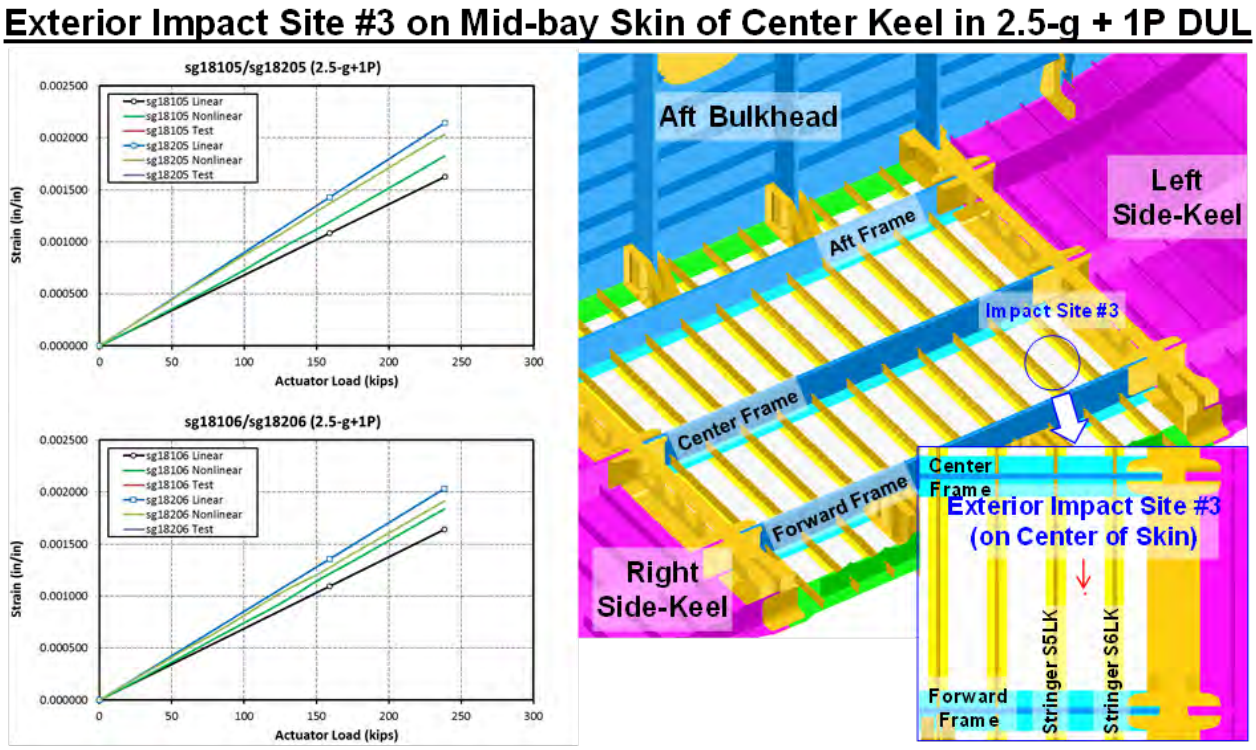

Figure 4-147. Strains on Exterior Impact Site no. 3 in 2.5-g + 1P DUL Condition

Figure 4-148 shows a chart of strain versus actuator load of strain gage locations sg18807 (located 1.0-in. up from the impact site) and sg18808 (located 1.0-in. down from the impact site) near interior impact site no. 1 on top of the frame-cap of the forward upper bulkhead. When comparing strain results of these strain gages, it was found that strain derived from nonlinear analysis was slightly higher than the strain from linear analysis. This was caused by combined effects of the upper bulkhead in pressure and compressive load. As a result, slightly higher strains were detected on the panel skin/stringer/frame from nonlinear analysis, resembling a softening effect to a panel in pressure load. Results from nonlinear analysis showed that the critical compression strain was -3,696 micro-in./in. near the impact damage site in the 2.5-g + 1P DUL combined loading condition. This strain was within the notched design strain values of -5,800 micro-in./in. for the frame web/cap. The calculated margin of safety was 57%, which indicated that a failure of the frame web/cap at interior impact site no. 1 of the forward upper bulkhead on the MBB was unlikely to occur at 2.5-g + 1P DUL.

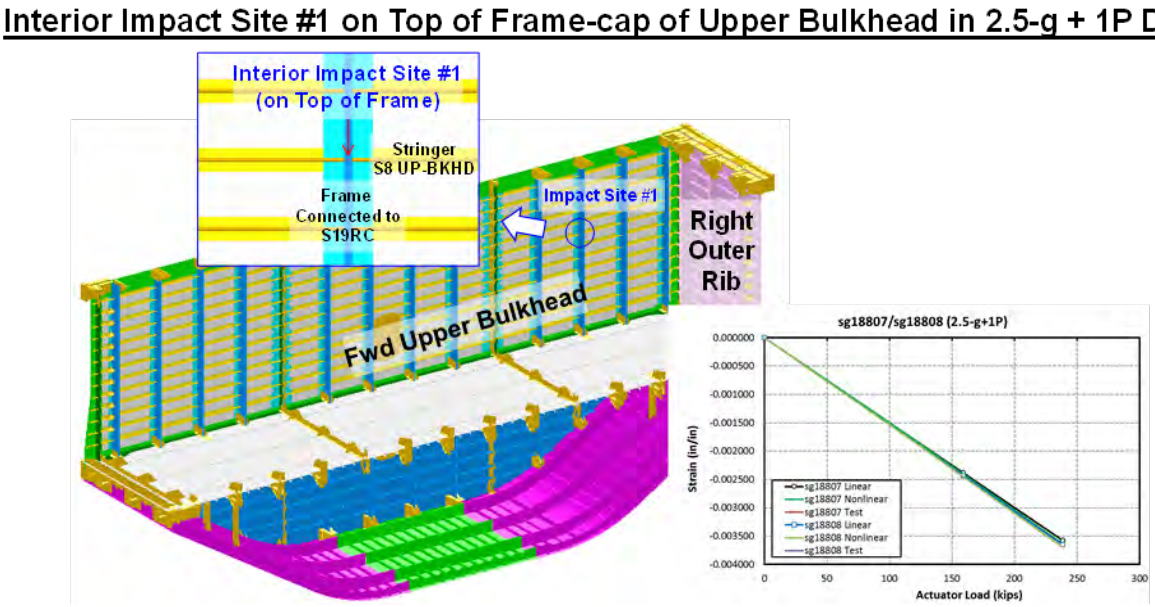

Figure 4-148. Strains on Interior Impact Site no. 1 in 2.5-g + 1P DUL Condition

Figure 4-149 shows charts of strain versus actuator load of back-to-back strain gage locations sg18107/sg18211 (located 1.0-in. up from the impact site) and sg18108/sg18212 (located 1.0-in. down from the impact site) near interior impact site no. 3 on the mid-bay skin of forward upper bulkhead. When comparing strain results of these back-to-back strain gages, it was found that tension strain derived from nonlinear analysis was only slightly higher than the tension strain from linear analysis, whereas the bending strain derived from nonlinear analysis was significantly lower than the bending strain from linear analysis. This was because an appreciable out-of-plane deformation was suppressed and replaced with an in-plane tensioning on the panel skin/stringer/frame in pressure loading. As a result, lower strains were detected on the panel skin/stringer/frame from nonlinear analysis, resembling a stiffening effect to a panel in pressure load. Results from nonlinear analysis showed that the critical tension strain was 1,225 micro-in./in. near the impact damage site in the 2.5-g + 1P DUL combined loading condition. This strain was within the notched design strain value of 5,900 micro-in./in. for the skin. The calculated margin of safety was 382%, which indicated that a failure of the skin at interior impact site no. 3 of the forward upper bulkhead on the MBB was unlikely to occur at 2.5-g + 1P DUL.

Interior Impact Site #3 on Mid-bay Skin of Upper Bulkhead in 2.5-g + 1P DUL

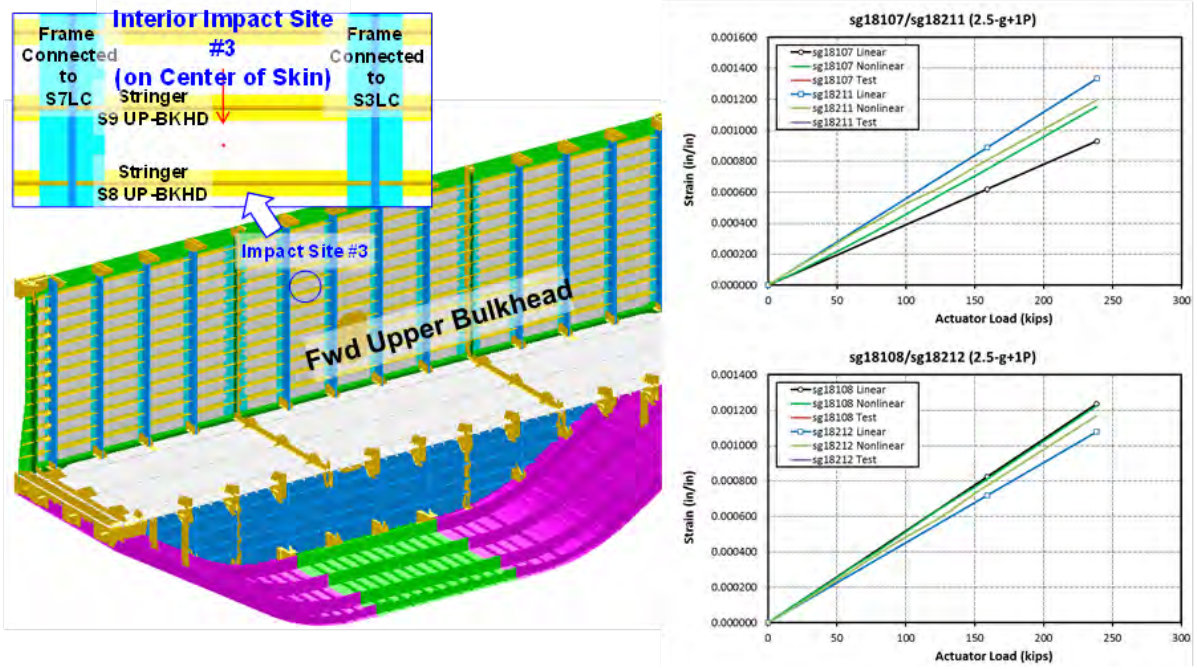

Figure 4-149. Strains on Interior Impact Site no. 3 in 2.5-g + 1P DUL Condition

4.4.4 -1.0-g DUL Maneuver Condition

Failure predictions for the MBB were made based on results from nonlinear analysis of the global FEM in the -1.0-g DUL maneuver condition. In this condition, concentrated loads were applied on the COLTS fixture to simulate a -1.0-g DUL (-1.5-g) down-bending load. To understand the structural behavior of the MBB and the center and side keels in -1.0-g DUL down-bending load, displacement plots from nonlinear and linear analyses were compared and are shown in Figure 4-150 and Figure 4-151.

For the MBB, the maximum displacement at the upper edge of the COLTS loading platen was 0.320 in. from the nonlinear analysis and 0.323 in. from the linear analysis. Different from the results of the 2.5-g DUL maneuver condition, displacements of the loading platen from the nonlinear analysis were slightly lower than those from the linear analysis in the -1.0-g DUL maneuver condition. According to the results from linear analysis (see Section 4.3.6.3), the skin of the center keel started to buckle at -0.754-g, and the skin of the floor started to buckle at -0.840-g down-bending load. The buckled skin on the center keel and floor would soften the stiffness of the center keel and floor and cause a rotational center shift on the MBB, resulting in a slight reduction of the displacements of the loading platen in the -1.0-g DUL down-bending load.

When checking the displacements on the center and side keels from nonlinear analysis, a maximum displacement of 0.212 in. occurred at the center keel due to post-buckling of the skin on the center keel. Conversely, from linear analysis (wherein post-buckling of the skin on the center keel was not included in the calculation), a maximum displacement of 0.140 in. was found at the side keel instead. Results from nonlinear analysis were considered to be more accurate than the results from linear analysis; therefore, they would be used in failure predictions for the MBB.

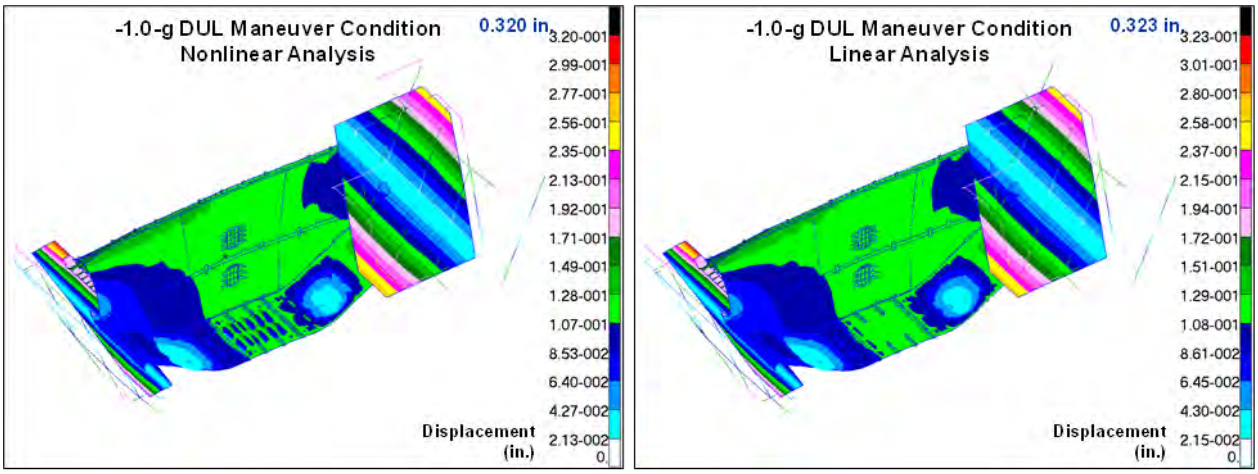

Figure 4-150. Displacements of the MBB From Linear and Nonlinear Analyses in -1.0-g DUL Condition

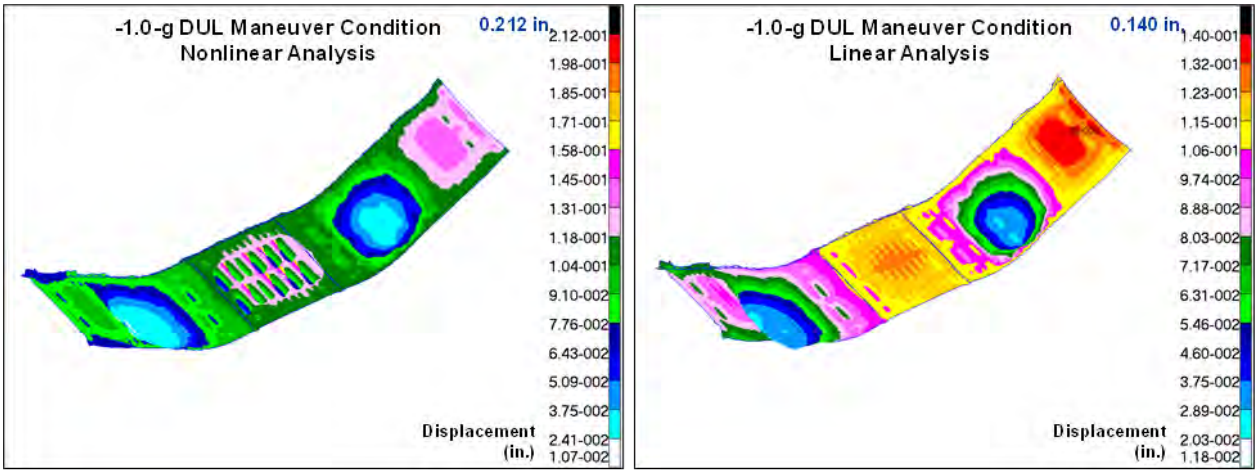

Figure 4-151. Displacements of the Center and Side Keels From Linear and Nonlinear Analyses in -1.0-g DUL Cond

In testing of the -1.0-g DUL maneuver condition, the MBB was loaded up to -1.0-g DUL (-1.5-g). During the test, in-plane strains and out-of-plane deformations were measured by VIC-3D, LVDT, and strain gages. Locations of the VIC-3D, LVDT, and strain gages are shown in the HWB MBB Test Specification (Ref. 4-9). Predictions of VIC-3D plots from nonlinear analysis are shown in Figure 4-152, and a displacement prediction chart of the LVDT is shown in Figure 4-153 for the reacting platen. Results from linear and nonlinear analyses are plotted and compared. Results from the LVDT chart showed that rotation of the reacting platen was slightly higher from the nonlinear analysis than from the linear analysis in the -1.0-g DUL maneuver condition.

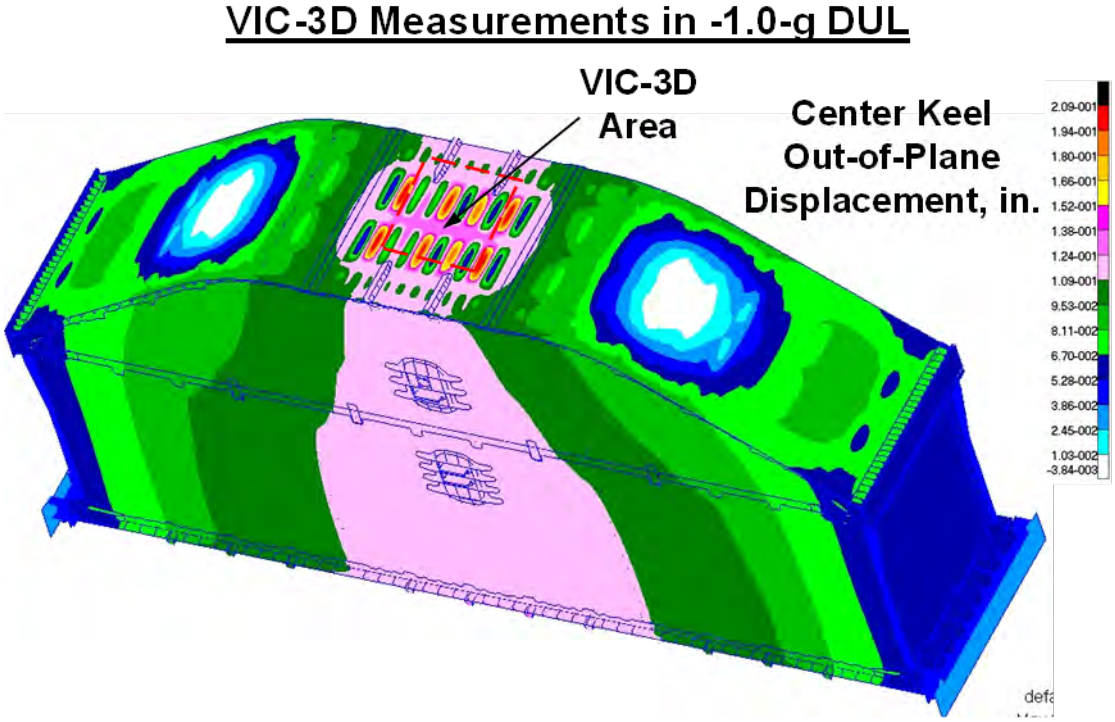

Figure 4-152. VIC-3D Measurements of the MBB in -1.0-g DUL Condition

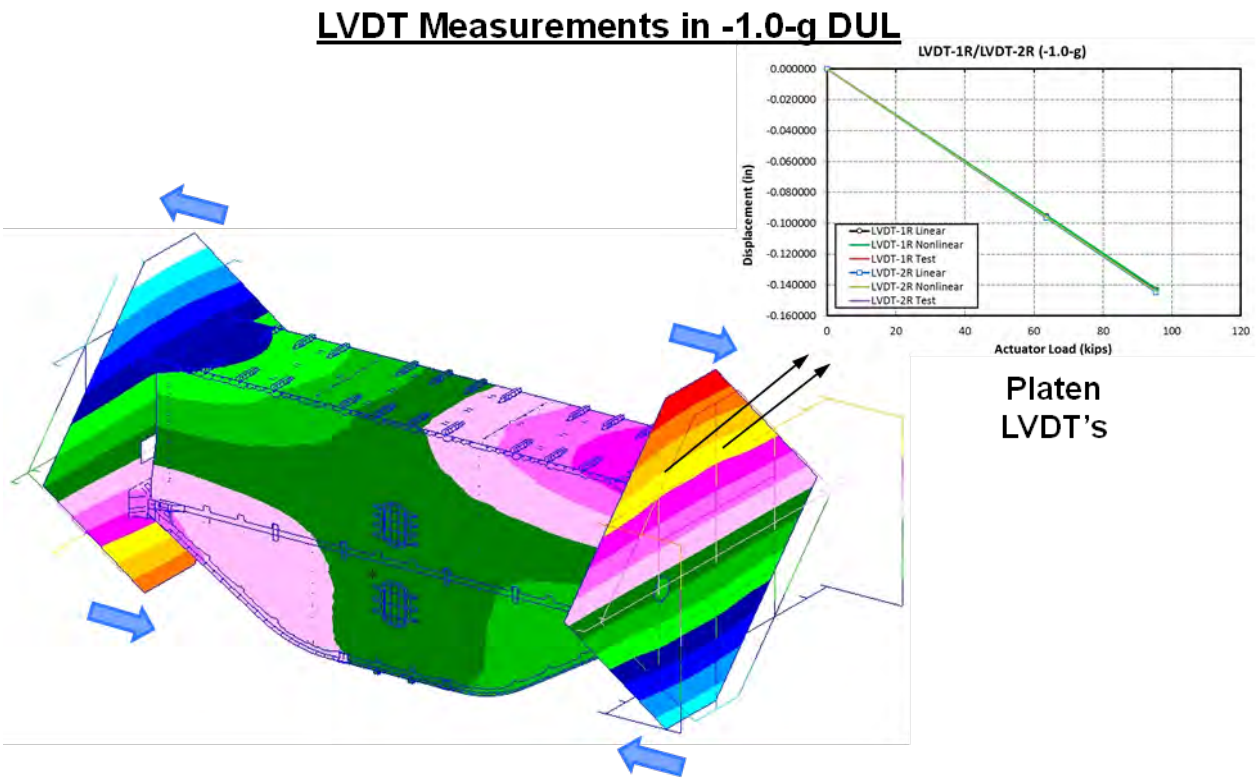

Figure 4-153. LVDT Measurements of the MBB in -1.0-g DUL Condition

In addition to the VIC-3D and LVDT instruments, strain gages were placed on the MBB where high strains and stresses were expected during tests. As shown in Figure 4-154, for the MBB structures that were considered to be pristine (not impact damaged), the following three critical locations were identified for possible failure locations that warranted evaluation:

1. On the crown frames and skin.
2. On the center keel skin.
3. On the side keel frames.

Strain gages were placed at these critical locations to monitor the structural behavior and integrity of the MBB during tests. Maximum or minimum principal strain distribution plots from nonlinear analysis and strain gage predictions from linear and nonlinear analyses are shown in Figure 4-155 through Figure 4-157. Strain gage predictions from linear and nonlinear analyses were compared to evaluate the extent of geometric nonlinearity of the MBB in the -1.0-g DUL maneuver condition. Failure predictions were made by comparing the maximum and minimum principal strain values of the MBB from nonlinear analysis to the un-notched strain design values (in pristine condition) of the composites shown in Table 4-7, and by comparing von Mises stresses of metallic fittings and bolts to the ultimate strengths of metals. In summary, failure prediction results showed that the MBB in its pristine condition would not fail catastrophically at -1.0-g DUL. Detailed results for these critical locations are presented in the following discussion.

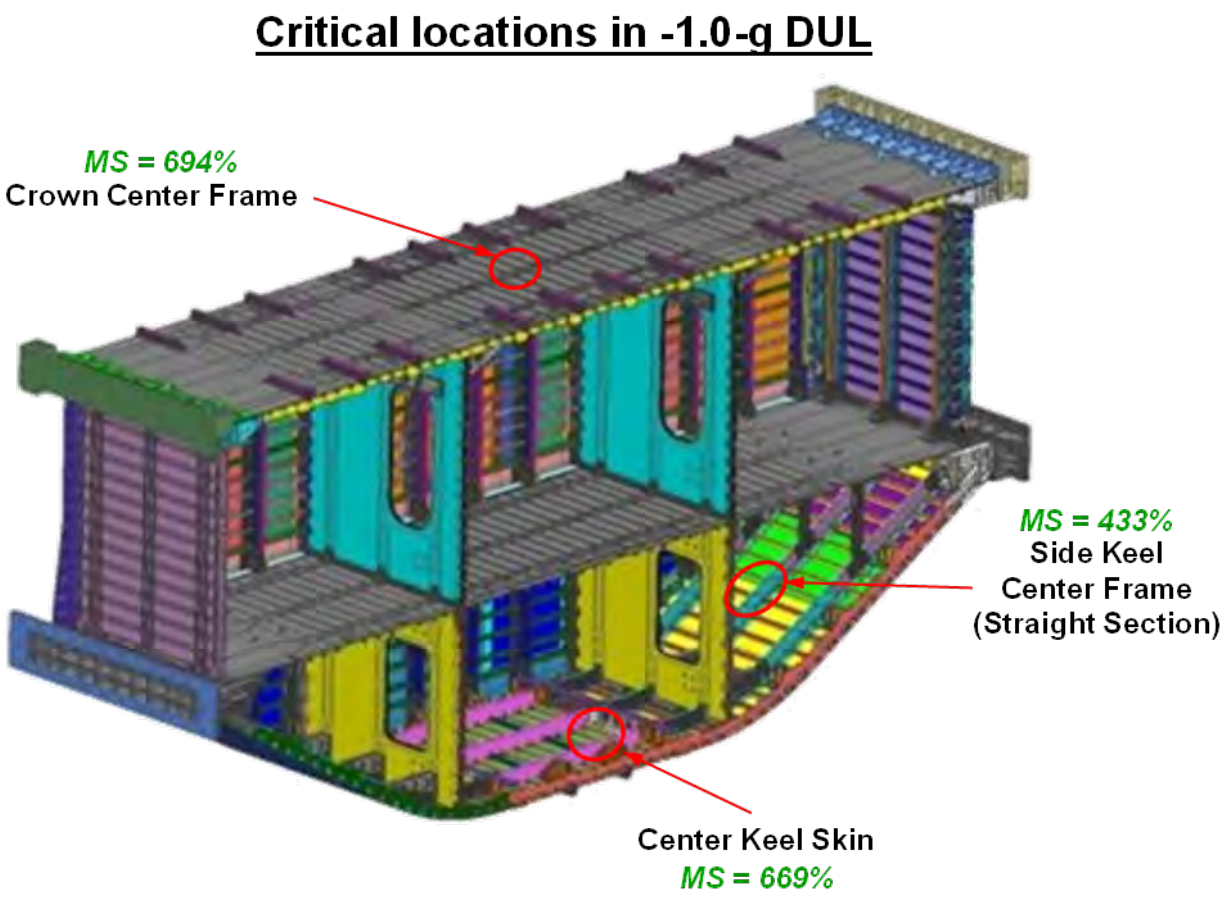

Figure 4-154. Critical Locations in Failure Predictions for the MBB in -1.0-g DUL Condition

Figure 4-155 shows a plot of maximum principal strain on the crown frames and charts of strain versus actuator load of strain gage location sg01874 (on the frame top) and back-to-back strain gage locations sg01107/sg01207 (on the exterior and interior skin). A critical maximum principal strain of 1,260 micro-in./in. on the frame was seen in the -1.0-g DUL maneuver condition. This critical strain was within the un-notched design strain value of 10,000 micro-in./in. for the frame web. The calculated margin of safety was 694%, which indicated that a failure of the crown frame on the MBB was unlikely to occur at -1.0-g DUL. When comparing strain gage results calculated from linear and nonlinear analyses, a slight increase of skin in-plane tension strains was seen in the results from nonlinear analysis. Also, a slight decrease of the frame top strains and an apparent reduction of skin bending strains were seen from the nonlinear analysis results. It appeared that the strains on the crown frame and skin were calculated more accurately in the nonlinear analysis with the nonlinear geometric effects between in-plane and bending strains. As a result, more skin in-plane tension strains and fewer skin bending strains on the crown were seen from the results of nonlinear analysis.

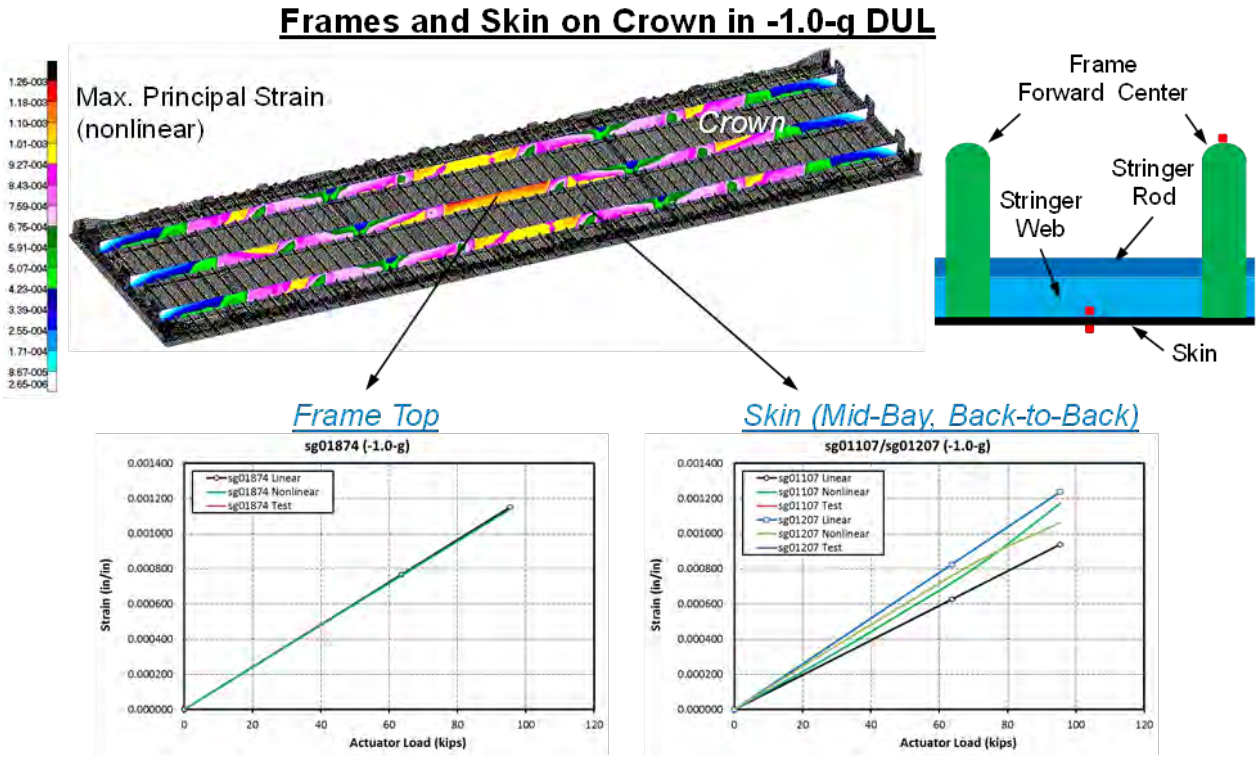

Figure 4-155. Strains on Crown Frames in -1.0-g DUL Condition

Figure 4-156 shows a plot of minimum principal strains on the center keel skin and charts of strain versus actuator load of back-to-back strain gage locations sg07107/sg07207 (on the exterior and interior skin). A critical minimum principal strain of -1,040 micro-in./in. on the skin was seen in the -1.0-g DUL maneuver condition. This critical strain was within the un-notched design strain value of -8,000 micro-in./in. for the skin. The calculated margin of safety was 669%, which indicated that a failure of the center keel skin on the MBB was unlikely to occur at -1.0-g DUL. When comparing strain gage results calculated from linear and nonlinear analyses, an apparent increase of bending strain values from the back-to-back strain gages was seen from the nonlinear analysis. This was because the skin of the center keel started to buckle at -0.754-g down-bending load (or -48 kips of actuator load), which resulted in higher minimum principal strains and bending strains extracted from a buckled skin. This prediction of -0.754-g down-bending load when the center keel skin started to buckle was derived from the results of linear buckling analysis presented in Section 4.3.6.3. Because this effect of the crown skin buckling was included in the nonlinear analysis, minimum principal strains and bending strains of the center keel skin from the nonlinear calculation would be higher than those produced by the linear solution, resembling a softening effect to a panel in post-buckling phase.

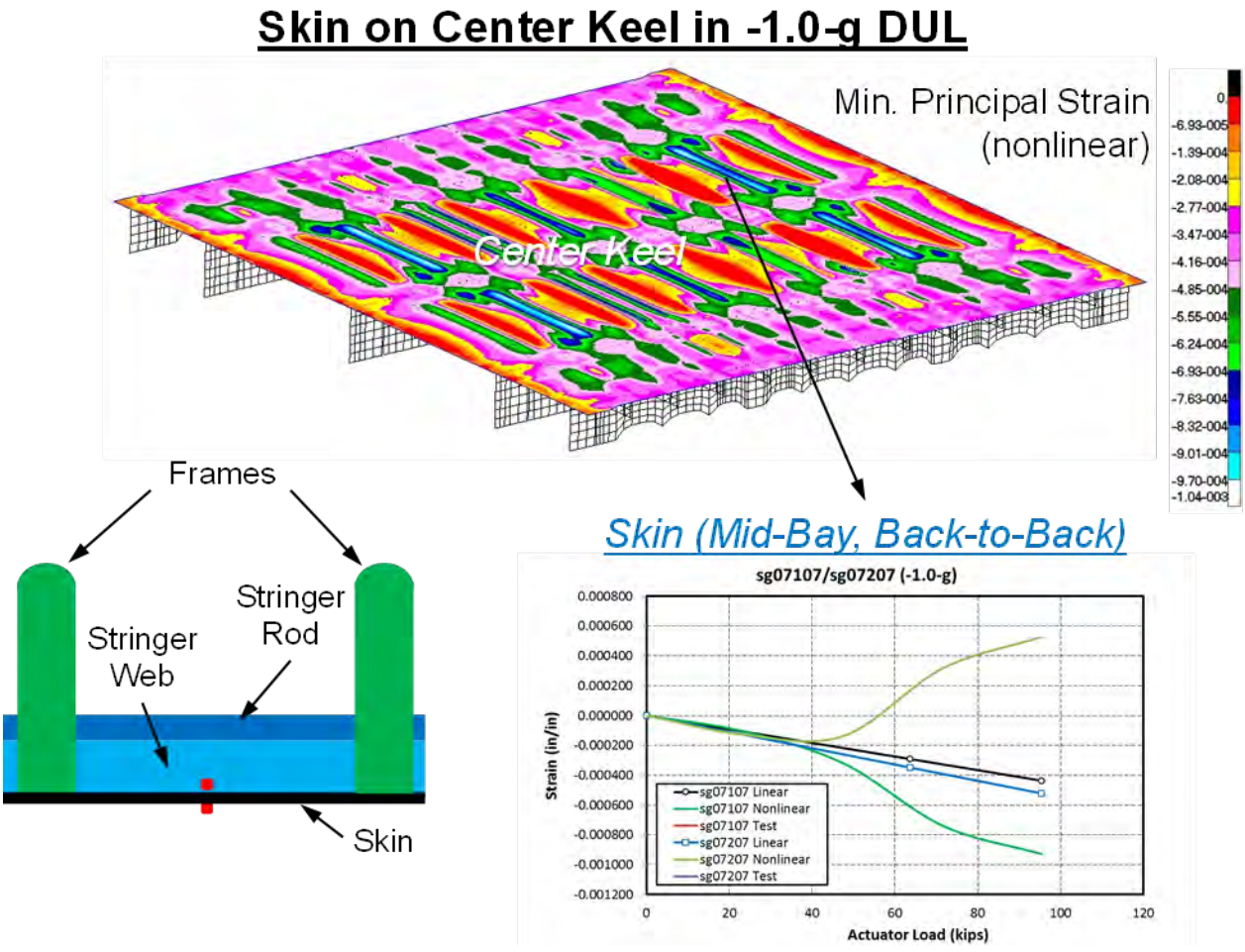

Figure 4-156. Strain on Center Keel Skin in -1.0-g DUL Condition

Figure 4-157 shows a plot of minimum principal strain on the side keel frames and a chart of strain versus actuator load of strain gage locations sg08810/sg09810 (on the frame top). A critical minimum principal strain of -1,500 micro-in./in. on the frame was seen in the -1.0-g DUL maneuver condition. This critical strain was within the un-notched design strain value of -8,000 micro-in./in. for the frame web. The calculated margin of safety was 433%, which indicated that a failure of the side keel frame on the MBB was unlikely to occur at -1.0-g DUL. When comparing strain gage results calculated from linear and nonlinear analyses, only a slight increase of strain values was seen in the results from nonlinear analysis. In the -1.0-g DUL maneuver condition, the side keel frames would be loaded in compression. However, the compressive loads on the side keels were small in -1.0-g DUL, and no buckling was expected to occur for the side keel. This is why the strain results of the side keel were almost identical from linear and nonlinear analyses at -1.0-g DUL. The slight increase of strain values on the side keel frames was likely caused by buckling of the center keel skin in the -1.0-g DUL maneuver condition, which resulted in a shift of the bending center at down-bending load to the MBB.

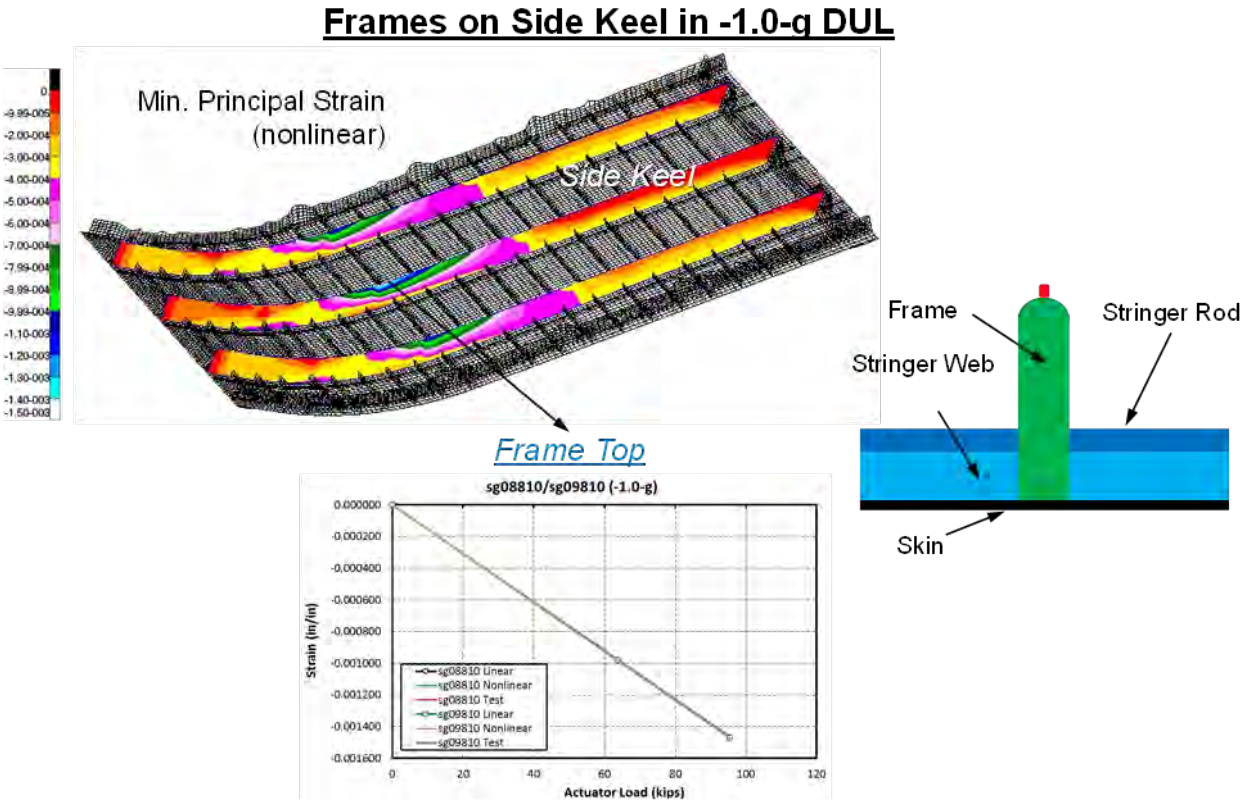

Figure 4-157. Strains on Side Keel Frames in -1.0-g DUL Condition

For tests of the MBB after impact damage, the following critical location was identified near the impact damage for possible failure location that warranted evaluation:

1. On the exterior impact site no. 3, which was on the mid-bay skin of the center keel.

Strain gages were placed near this impact-damaged location to monitor the behavior of structure with impact damage during tests. Strain versus internal pressure of the critical strain gages are shown in Figure 4-158. Strain gage predictions from linear and nonlinear analyses were compared to evaluate the extent of geometric nonlinearity of the MBB in the -1.0-g DUL

maneuver condition. Failure predictions were made by comparing the maximum and minimum principal strain values of the MBB from nonlinear analysis to the notched strain design values (in impact-damaged condition) of the composites shown in Table 4-7.

Figure 4-158 shows charts of strain versus actuator load of back-to-back strain gage locations sg18105/sg18205 (located 1.0-in. left of the impact site) and sg18106/sg18206 (located 1.0-in. right of the impact site) near exterior impact site no. 3 on the mid-bay skin of the center keel. When comparing strain results of these back-to-back strain gages, it was found that in-plane compression strains of the center keel skin derived from nonlinear analysis were almost identical to the results from linear analysis until -0.754-g down-bending load (or -48 kips of actuator load), when an apparent skin buckling appeared on the center keel. This skin buckling of the center keel at -0.754-g down-bending load matched the results of the linear buckling analysis presented in Section 4.3.6.3. After the skin of the center keel started to buckle (from the nonlinear analysis results), the in-plane compression strains started to increase at slower rates, and the skin bending strains started to increase at a much higher rate due to the post-buckling of the skin on the center keel. Results from nonlinear analysis showed that the critical tension strain was -816 micro-in./in. near the impact damage site in the -1.0-g DUL maneuver condition. This strain was within the notched design strain value of -4,800 micro-in./in. for the skin. The calculated margin of safety was 488%, which indicated that a failure of the skin at exterior impact site no. 3 of the center keel on the MBB was unlikely to occur at -1.0-g DUL.

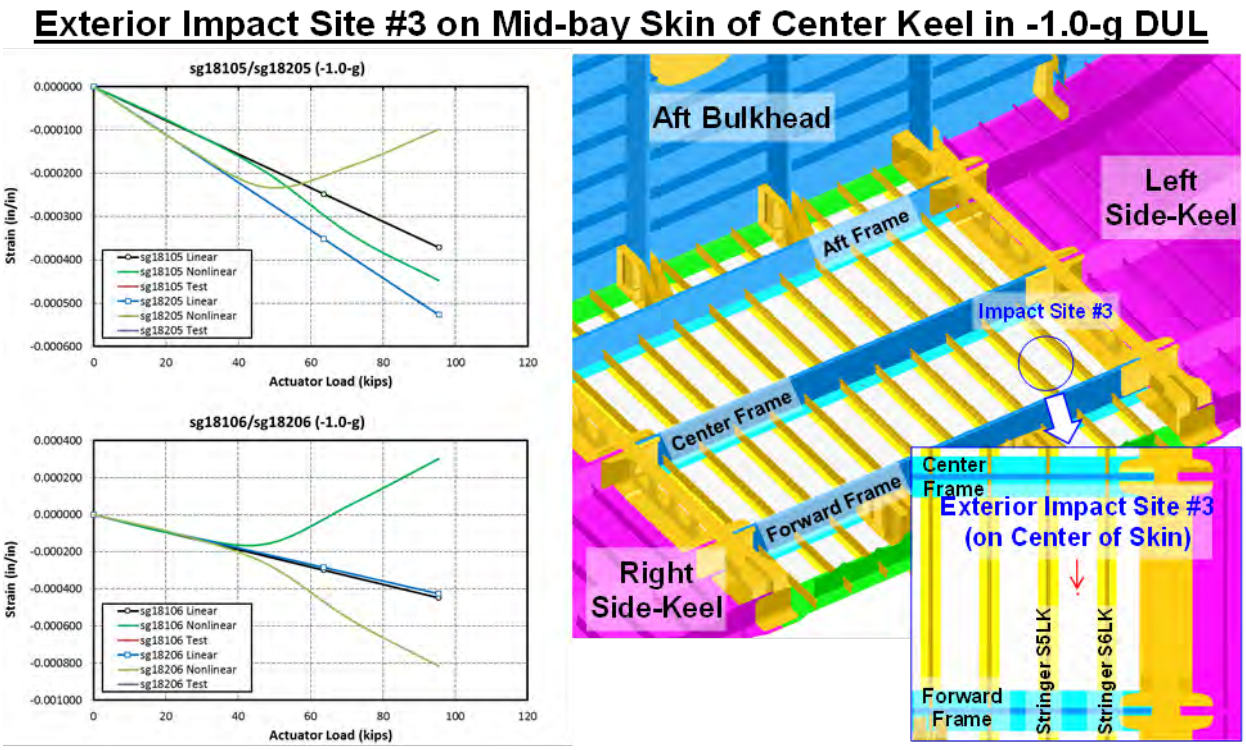

Figure 4-158. Strains on Exterior Impact Site no. 3 in -1.0-g DUL Condition

4.4.5 -1.0-g + 1P DUL Combined Loading Condition

Failure predictions for the MBB were made based on results from nonlinear analysis of the global FEM in the -1.0-g + 1P DUL combined loading condition. In this condition, concentrated loads were applied on the COLTS fixture to simulate a -1.0-g DUL (3.75-g) down-bending load plus a 1P DUL (1.5P, or 13.8 psi) pressure, creating a force normal to the internal skin surface that deformed the crown, bulkhead, and keel panels outward. To understand the structural behavior of the MBB and the crown panel in -1.0-g + 1P DUL combined loads, displacement plots from nonlinear and linear analyses were compared and are shown in Figure 4-159 and Figure 4-160.

For the MBB, the maximum displacement at the center of the forward upper bulkhead was 0.747 in. from the nonlinear analysis and 0.843 in. from the linear analysis. For the center and side keels, the maximum displacement at the side keel was 0.474 in. from the nonlinear analysis and 0.516 in. from the linear analysis. When loaded with both maneuver and pressure loads in the -1.0-g + 1P DUL combined loading condition, it appeared that structures of the MBB were influenced more from pressure load. Consequently, similar to the 2P pressure condition, the results showed that displacements from the nonlinear analysis were smaller than those from the linear analysis in the -1.0-g + 1P DUL combined loading condition. No buckling on the skin of the composite panels was seen in the -1.0-g + 1P DUL combined loading condition, which confirmed that a cabin pressure would greatly increase the buckling initiation load of a composite panel in compression. Details of the crown, center keel, and side keel results are presented later in this section. This interactive effect between maneuver and pressure loads to a structure made predicting structural behaviors of the MBB difficult using only linear analysis. The nonlinear analysis was able to capture both structural stiffening in pressure load and structural softening in compressive load on the composite panels of the MBB if buckling occurred. Therefore, results from the nonlinear analysis were used in making failure predictions for the MBB in the -1.0-g + 1P DUL combined loading condition.

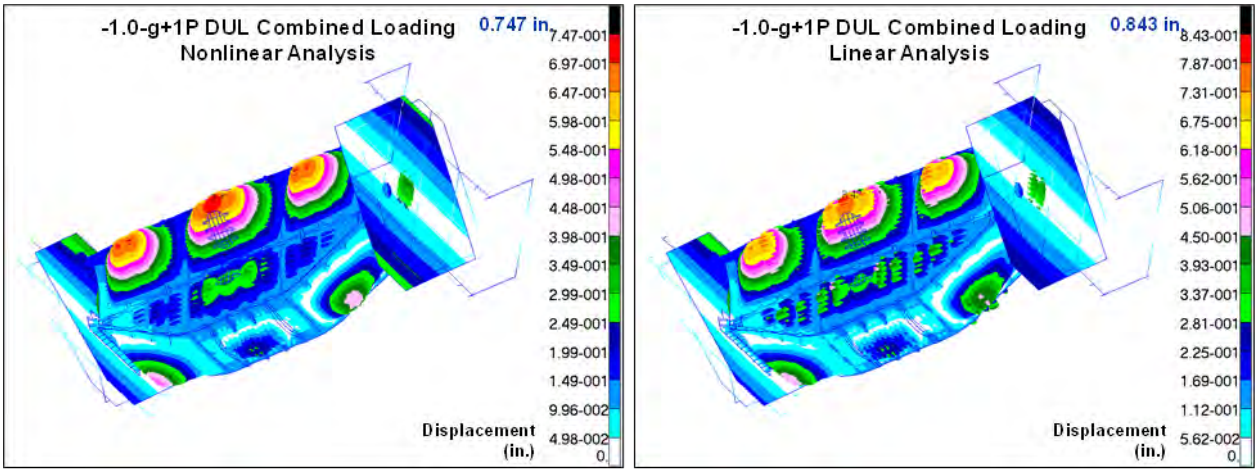

Figure 4-159. Displacements of the MBB From Linear and Nonlinear Analyses in -1.0-g + 1P DUL Condition

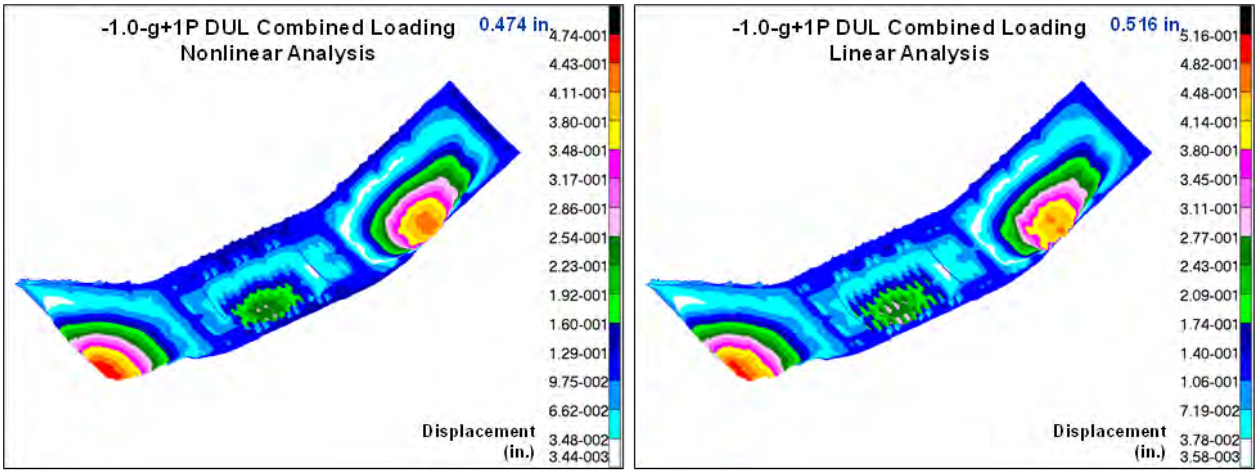

Figure 4-160. Displacements of the Crown From Linear and Nonlinear Analyses in -1.0-g + 1P DUL Condition

In testing of the -1.0-g + 1P DUL combined loading condition, the MBB was loaded up to -1.0-g + 1P DUL (-1.5-g). During the test, in-plane strains and out-of-plane deformations were measured by VIC-3D, LVDT, and strain gages. Locations of the VIC-3D, LVDT, and strain gages are shown in the HWB MBB Test Specification (Ref. 4-9). Predictions of VIC-3D plots from nonlinear analysis are shown in Figure 4-161, and displacement prediction charts of the LVDT are shown in Figure 4-161 for the upper bulkhead and side keel and in Figure 4-162 for the reacting platen. Results from linear and nonlinear analyses are plotted and compared. Results from the LVDT charts showed that normal displacements of the upper bulkhead and side keel were slightly lower, and rotation of the reacting platen was also slightly lower from the nonlinear analysis than those from the linear analysis in the -1.0-g + 1P DUL combined loading condition.

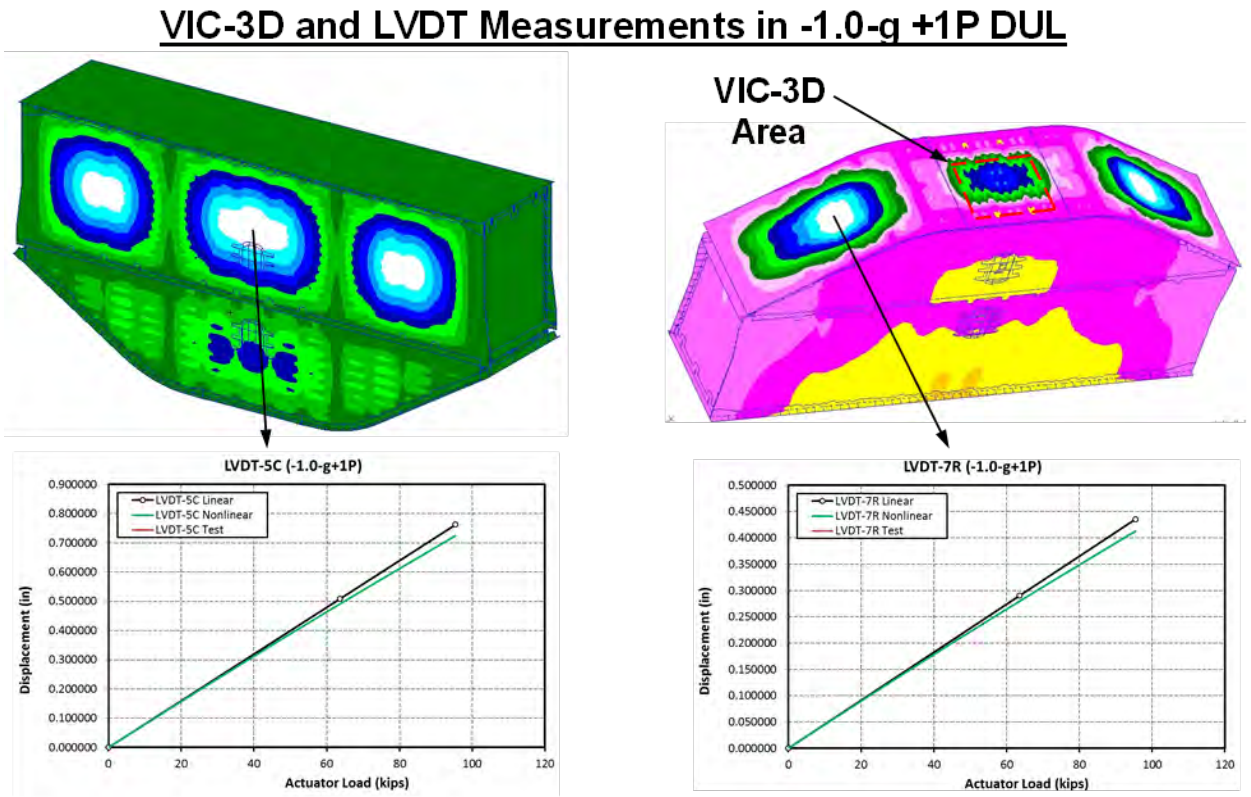

Figure 4-161. VIC-3D Measurements of the MBB in -1.0-g + 1P DUL Condition

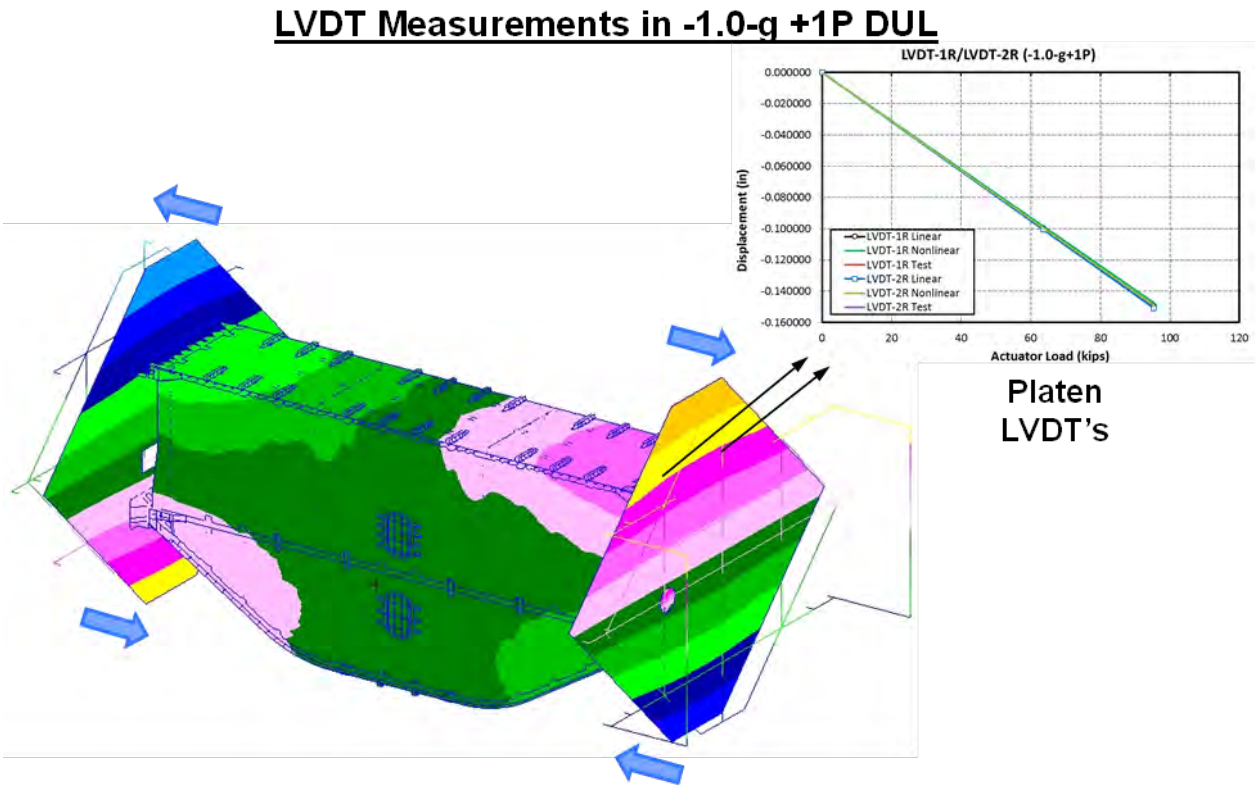

Figure 4-162. LVDT Measurements of the MBB in -1.0-g + 1P DUL Condition

In addition to the VIC-3D and LVDT instruments, strain gages were placed on the MBB where high strains and stresses were expected during tests. As shown in Figure 4-163, for the MBB structures that were considered to be pristine (not impact damaged), the following four critical locations were identified for possible failure locations that warranted evaluation:

1. On the crown stringer webs.
2. On the center keel frames.
3. On the side keel straight frames.
4. On the side keel curved frames.

Strain gages were placed at these critical locations to monitor the structural behavior and integrity of the MBB during tests. Maximum or minimum principal strain distribution plots from nonlinear analysis and strain gage predictions from linear and nonlinear analyses are shown in Figure 4-164 through Figure 4-167. Strain gage predictions from linear and nonlinear analyses were compared to evaluate the extent of geometric nonlinearity of the MBB in the -1.0-g + 1P DUL combined loading condition. Failure predictions were made by comparing the maximum and minimum principal strain values of the MBB from nonlinear analysis to the un-notched strain design values (in pristine condition) of the composites shown in Table 4-7, and by comparing von Mises stresses of metallic fittings and bolts to the ultimate strengths of metals. In summary, failure prediction results showed that the MBB in its pristine condition would not fail catastrophically at -1.0-g + 1P DUL. Detailed results for these critical locations are presented in the following discussion.

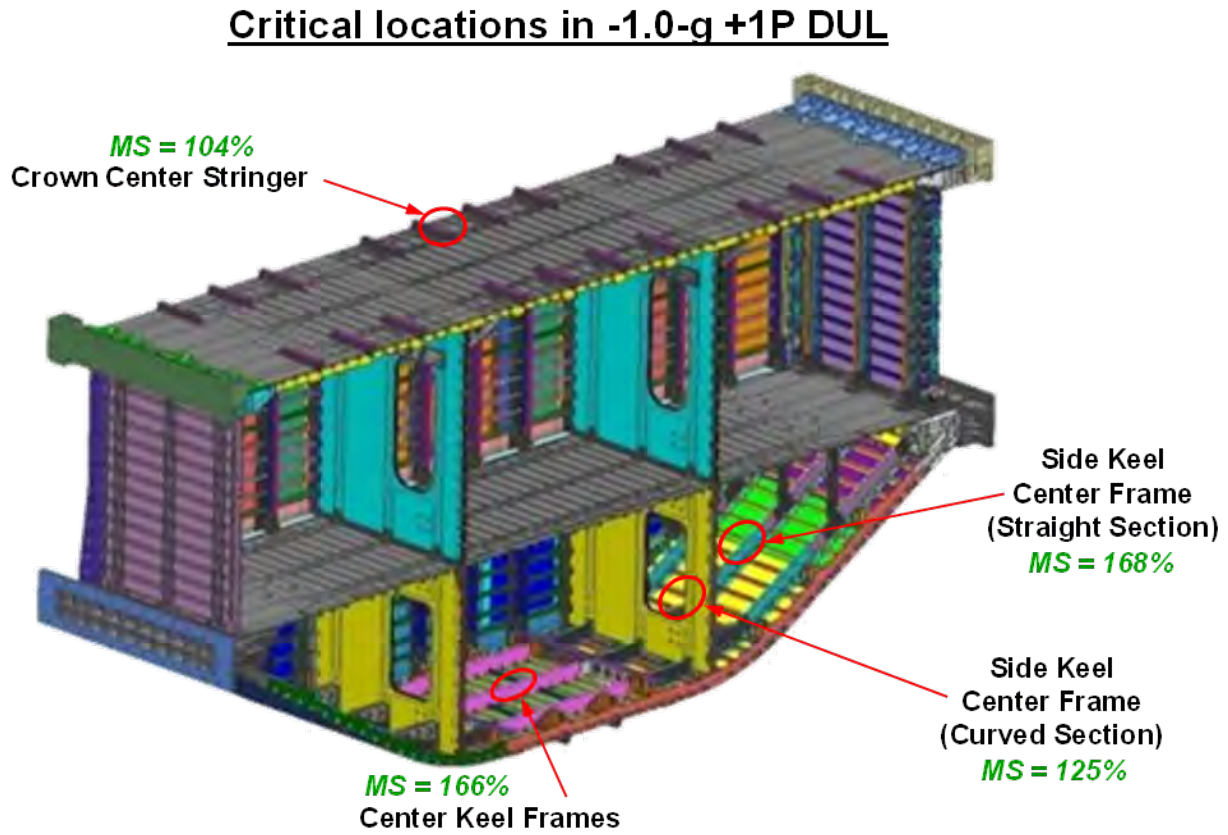

Figure 4-163. Critical Locations in Failure Predictions for the MBB in -1.0-g + 1P DUL Cond.

Figure 4-164 shows a plot of minimum principal strain on the crown stringer web and charts of strain versus actuator load of rosette strain gage locations sg01428C/sg01432C (on the stringer web to measure principal strains) and back-to-back strain gage locations sg01105/sg01205 (on the exterior and interior skin). A critical minimum principal strain of -3,920 micro-in./in. on the stringer web/rod was seen in the -1.0-g + 1P DUL combined loading condition. This critical strain was within the un-notched design strain value of -8,000 micro-in./in. for the stringer web. The calculated margin of safety was 104%, which indicated that a failure of the crown stringer web and stringer rod on the MBB was unlikely to occur at -1.0-g + 1P DUL. When comparing strain gage results calculated from linear and nonlinear analyses, the strains of the stringer web were slightly lower from the nonlinear analysis than those from the linear analysis in the -1.0-g + 1P DUL combined loading condition. When comparing back-to-back skin strain gage results, it was found that in-plane tension strain derived from nonlinear analysis was only slightly higher than the in-plane tension strain from linear analysis, whereas the bending strain derived from nonlinear analysis was significantly lower than the bending strain from linear analysis. This was because an appreciable out-of-plane deformation was suppressed and replaced with an in-plane tensioning on the panel skin/stringer/frame in pressure loading. As a result, lower strains were detected on the panel skin/stringer/frame from nonlinear analysis, resembling a stiffening effect to a panel in pressure load.

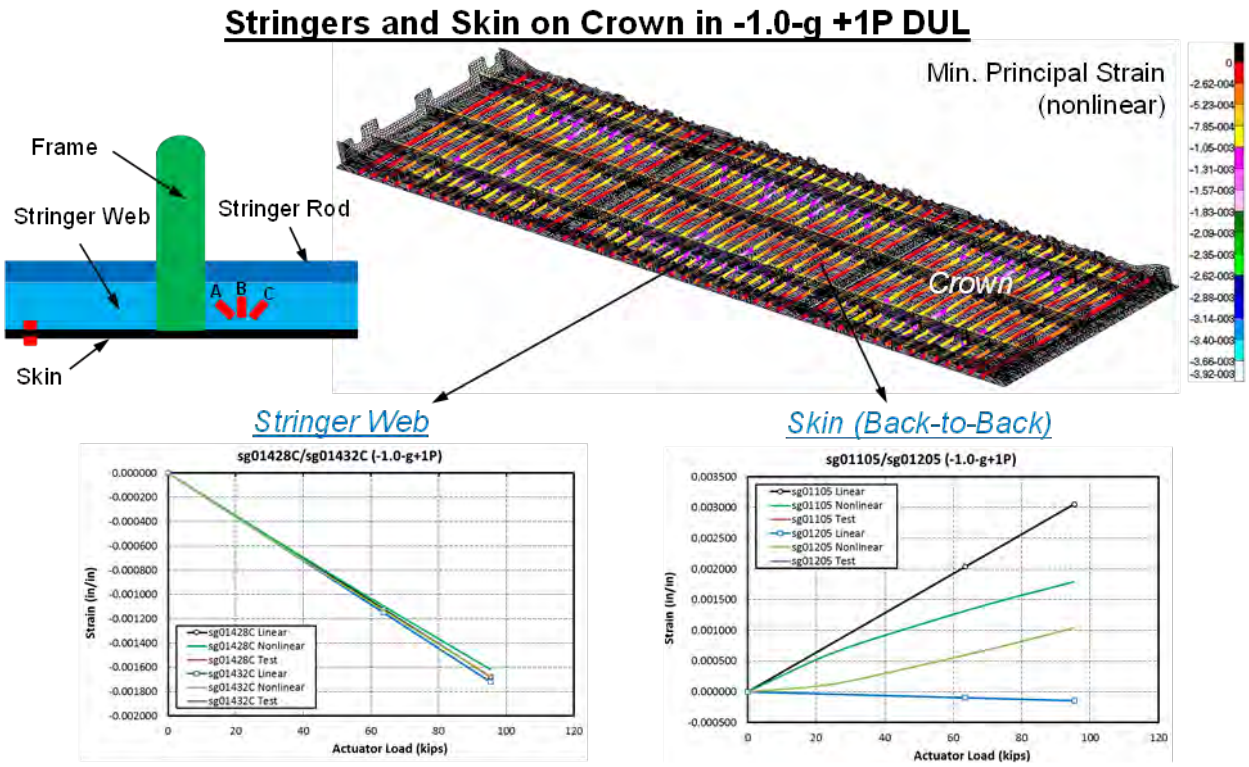

Figure 4-164. Strains on Crown Stringer Webs in -1.0-g + 1P DUL Condition

Figure 4-165 shows a plot of minimum principal strain on the center keel frames and charts of strain versus actuator load of strain gage location sg07874 (on the frame top) and back-to-back strain gage locations sg07105/sg07205 (on the exterior and interior skin). A critical minimum principal strain of -3,010 micro-in./in. on the frame was seen in the -1.0-g + 1P DUL combined loading condition. This critical strain was within the un-notched design strain value of -8,000 micro-in./in. for the frame web. The calculated margin of safety was 166%, which indicated that a failure of the center keel frame on the MBB was unlikely to occur at -1.0-g + 1P DUL. In the -1.0-g + 1P DUL combined loading condition, the center keel frames would be in compression from down-bending load (-1.0-g DUL). However, unlike the center keel frames, the center keel skin was in tension in the -1.0-g + 1P DUL combined loading condition because the tension from pressure (1.5P) predominated the compression from down-bending load (-1.0-g DUL). In addition, frames, stringers, and skin on the center keel were bending from the pressure load. The bending strains of the center keel frames, stringer, and skin from nonlinear analysis were lower than those from linear analysis. This was why the results of strain gages on the frame top were slightly lower from the nonlinear analysis than those from the linear analysis in the -1.0-g + 1P DUL combined loading condition. When comparing back-to-back skin strain gage results, it was found that in-plane tension strain derived from nonlinear analysis was only slightly higher than the in-plane tension strain from linear analysis, whereas the bending strain derived from nonlinear analysis was significantly lower than the bending strain from linear analysis. It appeared that an appreciable out-of-plane deformation was suppressed and replaced with an in-plane tensioning on the panel skin/stringer/frame in pressure loading. As a result, lower strains were detected from nonlinear analysis, resembling a stiffening effect to a panel in pressure load.

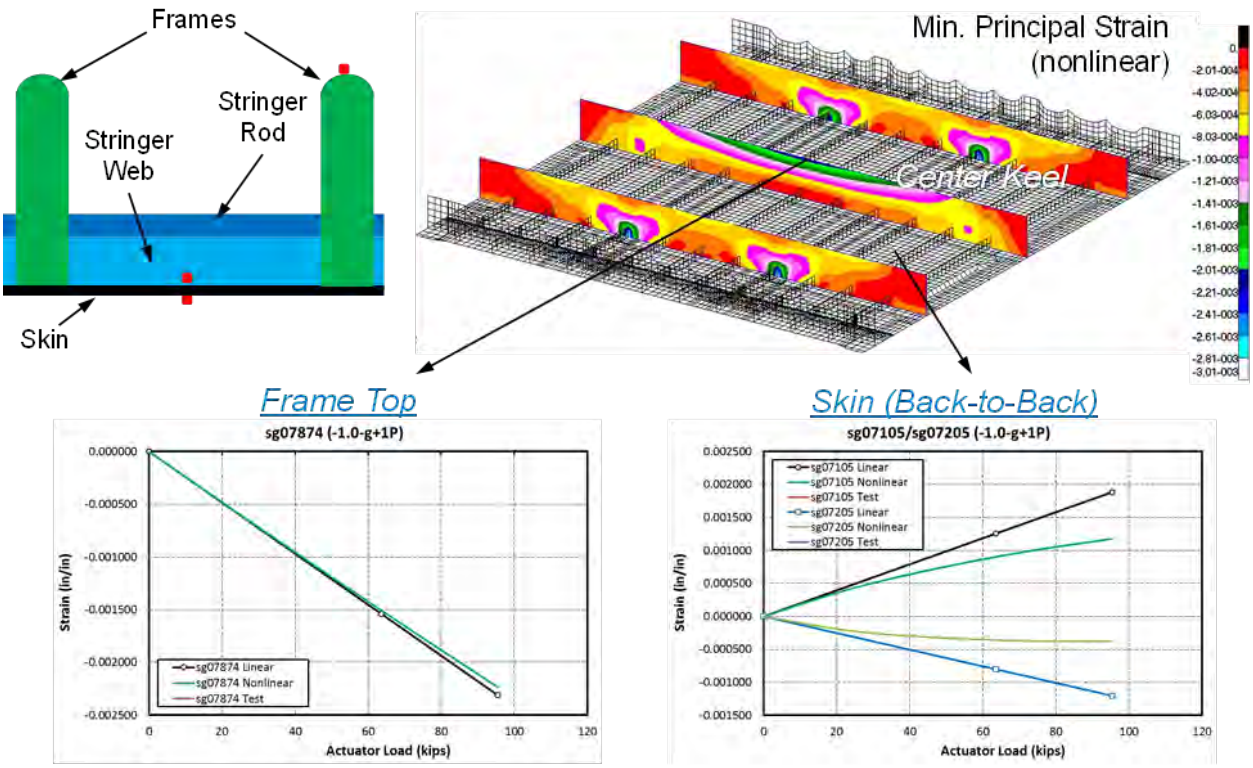

Figure 4-165. Strains on Center Keel Frames in -1.0-g + 1P DUL Condition

Figure 4-166 shows a plot of minimum principal strain on the side keel frames and a chart of strain versus actuator load of strain gage locations sg08811/sg09811 (on the frame top). A critical minimum principal strain of -2,990 micro-in./in. on the frame was seen in the -1.0-g + 1P DUL combined loading condition. This critical strain was within the un-notched design strain value of -8,000 micro-in./in. for the frame web. The calculated margin of safety was 168%, which indicated that a failure of the side keel frame on the MBB was unlikely to occur at -1.0-g + 1P DUL. In the -1.0-g + 1P DUL combined loading condition, the side keel frames would be in compression from down-bending load (-1.0-g DUL). However, unlike the side keel frames, the side keel skin was in tension in the -1.0-g + 1P DUL combined loading condition because the tension from pressure (1.5P) predominated the compression from down-bending load (-1.0-g DUL). In addition, frames, stringers, and skin on the side keel were bending from pressure load. The bending strains of the side keel frames, stringer, and skin from nonlinear analysis were lower than those from linear analysis. This was why the results of strain gage locations sg08811/sg09811 (on the frame top) from nonlinear analysis were slightly lower than those from linear analysis in the -1.0-g + 1P DUL combined loading condition. It appeared that an appreciable out-of-plane deformation was suppressed and replaced with an in-plane tensioning on the panel skin/stringer/frame in pressure loading. As a result, lower strains were detected from nonlinear analysis, resembling a stiffening effect to a panel in pressure load.

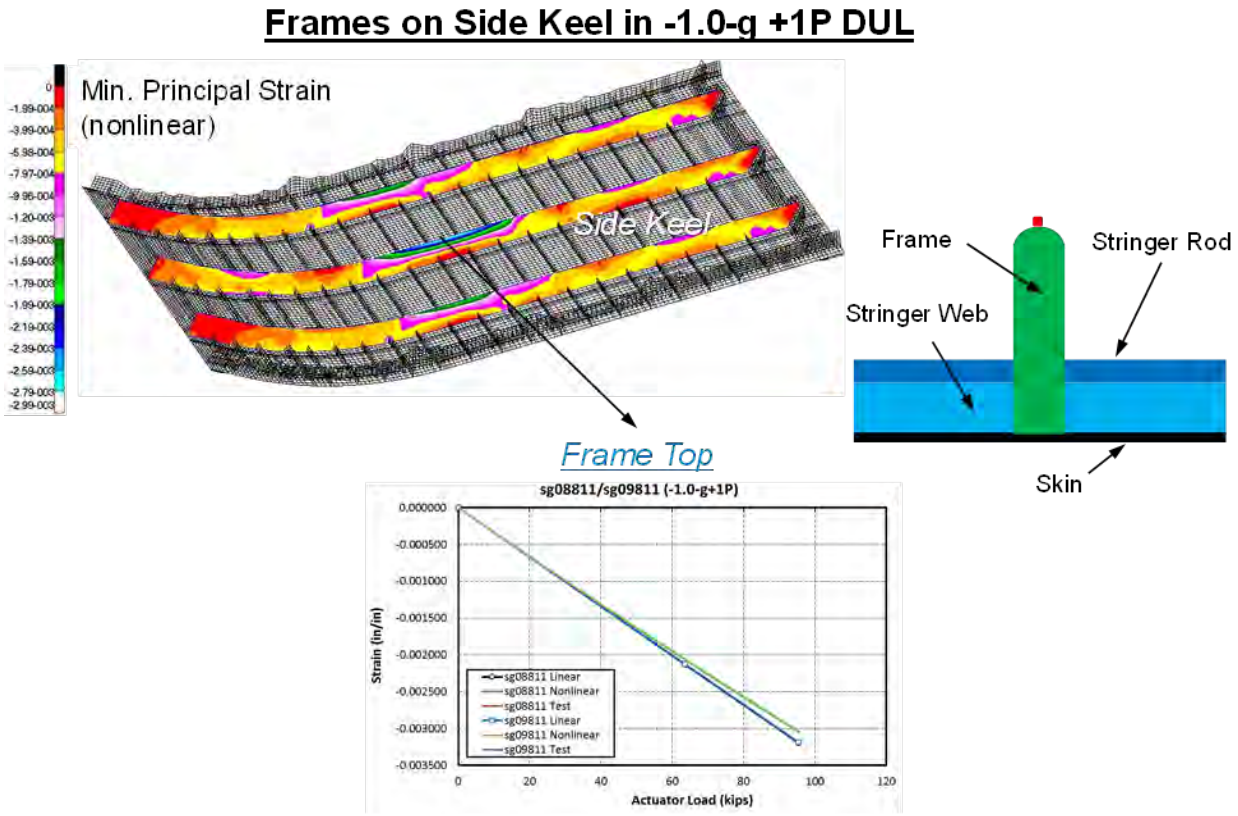

Figure 4-166. Strains on Side Keel Frames in -1.0-g + 1P DUL Condition

Figure 4-167 shows a plot of maximum principal strain on the side keel frames and a chart of strain versus actuator load of strain gage locations sg08809/sg09809 (on the frame top) and sg08503/sg08504 (on the stringer rod). A critical maximum principal strain of 4,450 micro-in./in. on the frame was seen in the -1.0-g + 1P DUL combined loading condition. This critical strain was within the un-notched design strain value of 10,000 micro-in./in. for the frame web. The calculated margin of safety was 125%, which indicated that a failure of the side keel frame on the MBB was unlikely to occur at -1.0-g + 1P DUL. In the -1.0-g + 1P DUL combined loading condition, the side keel frames would be in compression from down-bending load (-1.0-g DUL). However, unlike the side keel frames, the side keel skin was in tension in the -1.0-g + 1P DUL combined loading condition because the tension from pressure (1.5P) predominated the compression from down-bending load (-1.0-g DUL). In addition, the frames, stringers, and skin on the side keel were bending from pressure load. The bending strains of the side keel frames, stringer, and skin from nonlinear analysis were lower than those from linear analysis. At locations where the center keel frames connected to the lower center ribs, high bending moments were seen on the frames, which resulted in high tension strains on the frame top in pressure load. This was why the results of strain gage locations sg08811/sg09811 (on the frame top) were in tension, and the tension strains from nonlinear analysis were slightly lower than those from linear analysis in the -1.0-g + 1P DUL combined loading condition. Similarly, the results of strain gage locations sg08503/sg08504 (on the stringer rod) from nonlinear analysis were also slightly lower than those from linear analysis. It appeared that an appreciable out-of-plane deformation was suppressed and replaced with an in-plane tensioning on the panel skin/stringer/frame in pressure loading. As a result, lower strains were detected from nonlinear analysis, resembling a stiffening effect to a panel in pressure load.

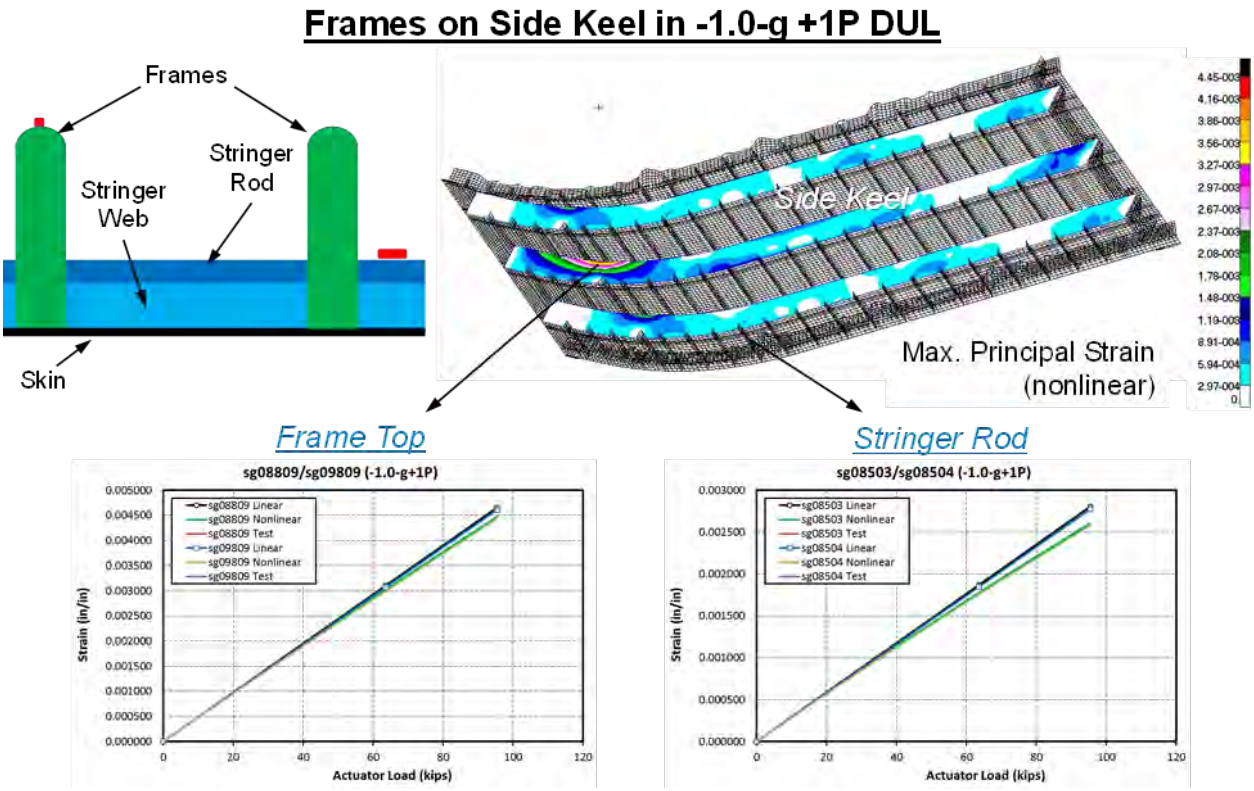

Figure 4-167. Strains on Side Keel Frames in -1.0-g + 1P DUL Condition

For tests of the MBB after impact damage, the following three critical locations were identified near the impact damage for possible failure locations that warranted evaluation:

1. On the exterior impact site no. 2, which was on the stringer flange of the center keel.
2. On the interior impact site no. 1, which was on the frame top of the upper bulkhead.
3. On the interior impact site no. 3, which was on the mid-bay skin of the upper bulkhead.

Strain gages were placed near these impact-damaged locations to monitor the behavior of structure with impact damage during tests. Strain versus internal pressure of the critical strain gages are shown in Figure 4-168 through Figure 4-170. Strain gage predictions from linear and nonlinear analyses were compared to evaluate the extent of geometric nonlinearity of the MBB in the -1.0-g + 1P DUL combined loading condition. Failure predictions were made by comparing the maximum and minimum principal strain values of the MBB from nonlinear analysis to the notched strain design values (in impact-damaged condition) of the composites shown in Table 4-7.

Figure 4-168 shows charts of strain versus actuator load of back-to-back strain gage locations sg18103/sg18303 (located 0.5-in. forward from the impact site) and sg18104/sg18304 (located 0.5-in. aft from the impact site) near exterior impact site no. 2 on the stringer flange of the center keel. When comparing strain results of these back-to-back strain gages, it was found that tension strain derived from nonlinear analysis was similar to the tension strain from linear analysis, whereas the bending strain derived from nonlinear analysis was significantly lower than the bending strain from linear analysis. This was because some bending strains were suppressed and replaced with an in-plane tensioning on the panel skin/stringer/frame in tension loading. As a result, lower strains were detected on the panel skin/stringer/frame from nonlinear analysis, resembling a stiffening effect to a panel in pressure load. Results from nonlinear analysis showed that the critical tension strain was 1,202 micro-in./in. near the impact damage site in the -1.0-g + 1P DUL combined loading condition. These strains were within the notched design strain values of 5,900 micro-in./in. for the stringer flange. The calculated margin of safety was 391%, which indicated that a failure of stringer flange at exterior impact site no. 2 of the center keel on the MBB was unlikely to occur at -1.0-g + 1P DUL.

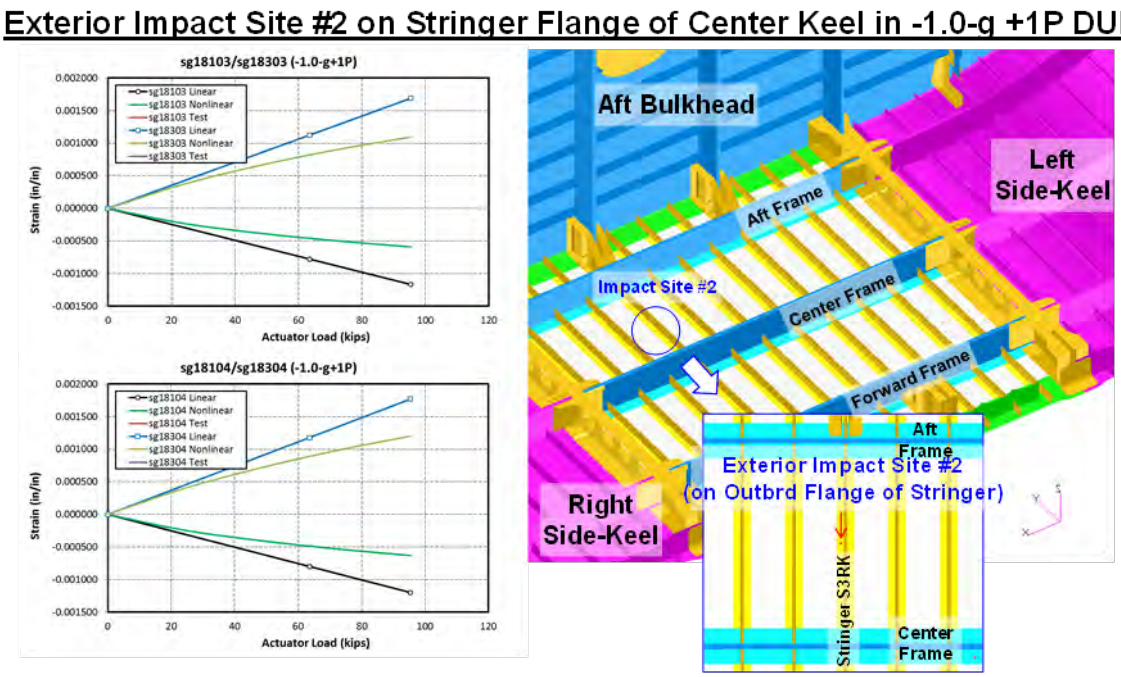

Figure 4-168. Strains on Exterior Impact Site no. 2 in -1.0-g + 1P DUL Condition

Figure 4-169 shows a chart of strain versus actuator load of strain gage locations sg18807 (located 1.0-in. up from the impact site) and sg18808 (located 1.0-in. down from the impact site) near the interior impact site no. 1 on top of the frame cap of the forward upper bulkhead. When comparing strain results of these strain gages, it was found that strain derived from nonlinear analysis was slightly lower than the strain from linear analysis. This was caused by combined effects of upper bulkhead in pressure and compressive load. As a result, slightly lower strains were detected on the panel skin/stringer/frame from nonlinear analysis, resembling a stiffening effect to a panel in pressure load. Results from nonlinear analysis showed that the critical compression strain was -3,527 micro-in./in. near the impact damage site in the -1.0-g + 1P DUL combined loading condition. This strain was within the notched design strain values of -5,800 micro-in./in. for the frame web/cap. The calculated margin of safety was 64%, which indicated that a failure of the frame web/cap at interior impact site no. 1 of the forward upper bulkhead on the MBB was unlikely to occur at -1.0-g + 1P DUL.

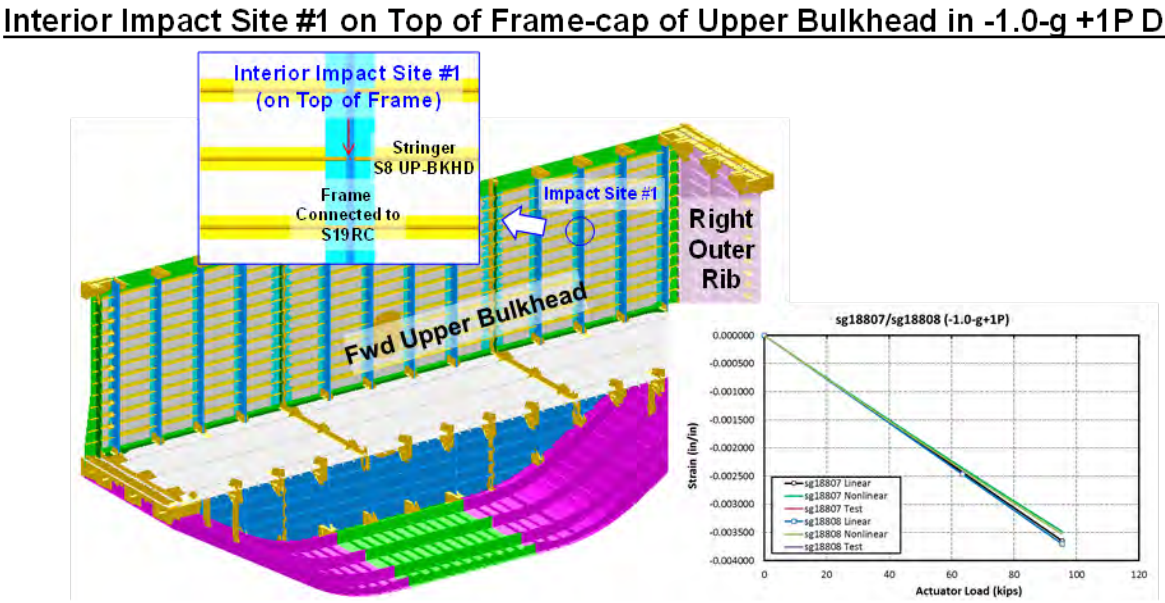

Figure 4-169. Strains on Interior Impact Site no. 1 in -1.0-g + 1P DUL Condition

Figure 4-170 shows charts of strain versus actuator load of back-to-back strain gage locations sg18107/sg18211 (located 1.0-in. up from the impact site) and sg18108/sg18212 (located 1.0-in. down from the impact site) near interior impact site no. 3 on the mid-bay skin of the forward upper bulkhead. When comparing strain results of these back-to-back strain gages, it was found that tension strain derived from nonlinear analysis was only slightly higher than the tension strain from linear analysis, whereas the bending strain derived from nonlinear analysis was significantly lower than the bending strain from linear analysis. This was because an appreciable out-of-plane deformation was suppressed and replaced with an in-plane tensioning on the panel skin/stringer/frame in pressure loading. As a result, lower strains were detected on the panel skin/stringer/frame from nonlinear analysis, resembling a stiffening effect to a panel in pressure load. Results from nonlinear analysis showed that the critical tension strain was 1,333 micro-in./in. near the impact damage site in the -1.0-g + 1P DUL combined loading condition. This strain was within the notched design strain value of 5,900 micro-in./in. for the skin. The calculated margin of safety was 343%, which indicated that a failure of the skin at interior impact site no. 3 of the forward upper bulkhead on the MBB was unlikely to occur at -1.0-g + 1P DUL.

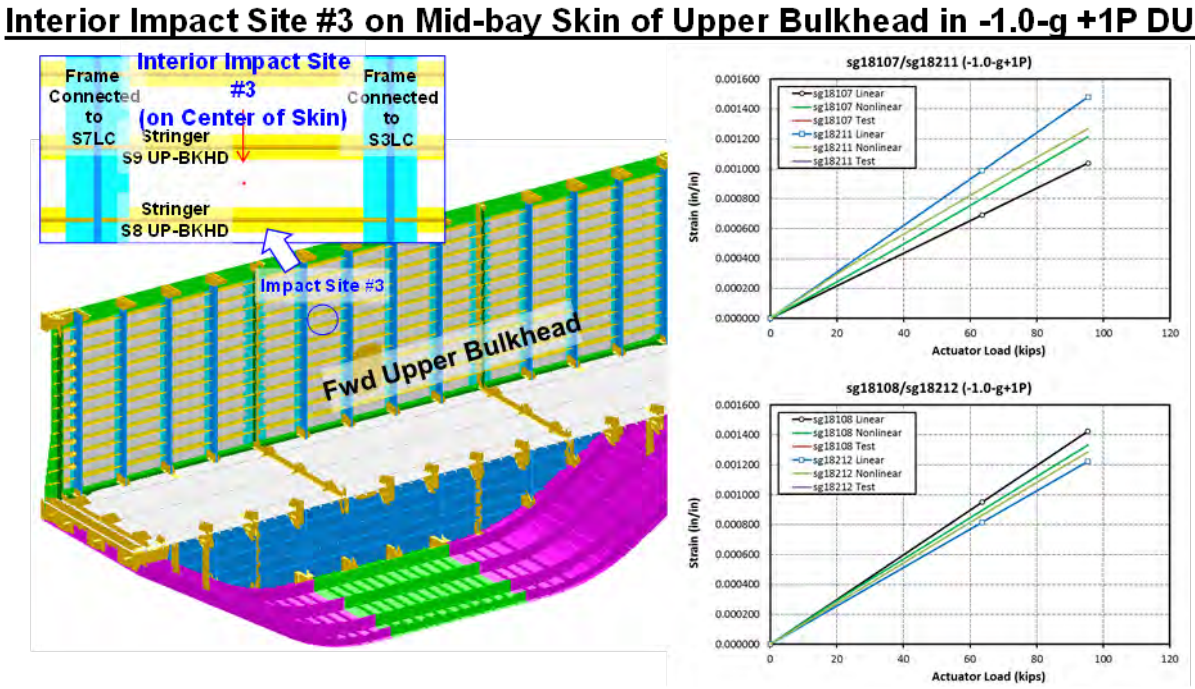

Figure 4-170. Strains on Interior Impact Site no. 3 in -1.0-g + 1P DUL Condition

4.4.6 Final Failure Testing Condition

Failure predictions for the MBB in the final failure testing condition were made based on results from nonlinear analysis of the global FEM. The final failure testing condition was planned to be the last test case for the MBB, and in this test case, the impact-damaged MBB would be tested to catastrophic failure, or until it reached a maximum mechanical load of 200% DLL. Several loading steps, as shown in Figure 4-171, were performed in sequence on the MBB in the final failure testing condition.

To demonstrate the load-carrying capability of the MBB beyond the ultimate loads before final failure of the MBB occurred, in Load Sequence 1 the MBB would first be tested to 150% of the 2.5-g limit load and 1.5P (13.8 psi) pressure, which was the same as the 2.5-g + 1P DUL combined loading condition. In other words, the 2.5-g + 1P DUL case became Load Sequence 1 of the final failure testing condition.

Then, in Load Sequence 2, the mechanical load was increased to 10% above the 2.5-g ultimate load while holding pressure at 1.5P (13.8 psi). With a factor of safety of 1.5, 110% of the ultimate load was equivalent to 165% of the limit loads. Next, in Load Sequence 3, the mechanical load was reduced to 2.5-g DUL while holding pressure at 1.5P (13.8 psi). In Load Sequence 4, the pressure was reduced to zero while keeping the mechanical load at 2.5-g DUL. Then, in Load Sequence 5, the mechanical load would be increased to 165% of 2.5-g DLL and then to 200% of 2.5-g DLL, or until a catastrophic failure of the MBB occurred. Failure predictions were made at the end of Load Sequence 2, which was at 4.125-g + 1.5P combined loads, and at the end of Load Sequence 5, which was at 5.0-g maneuver load.

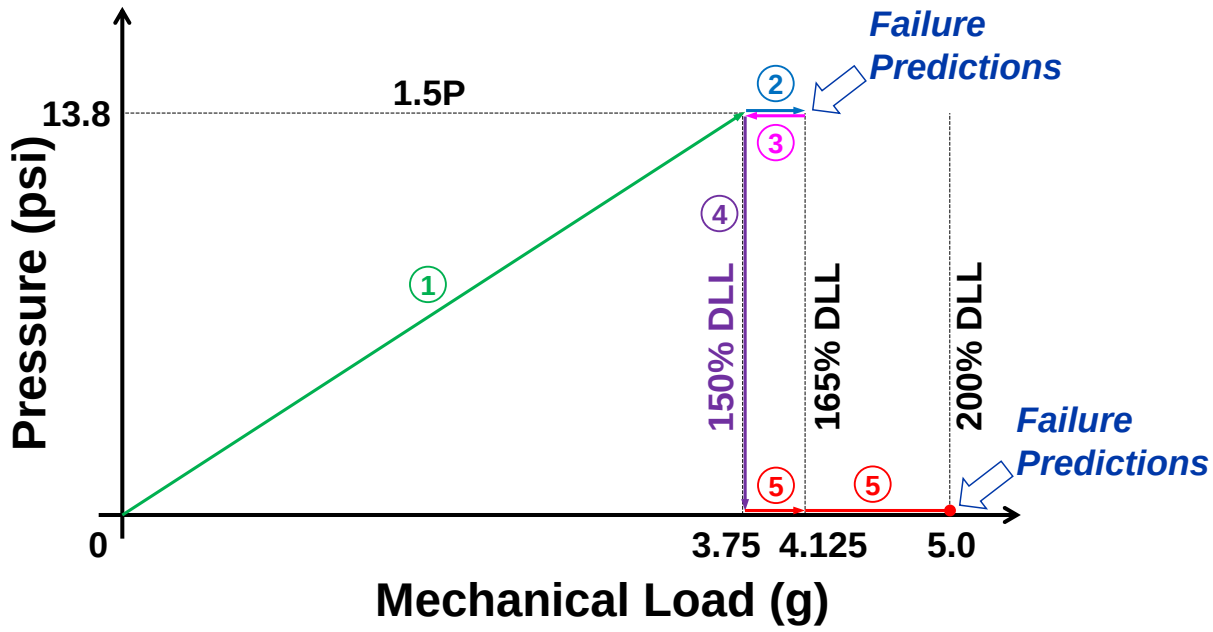

Figure 4-171. Loading Sequence Chart of Final Failure Testing

In the failure analysis of the MBB in the 2P pressure, 2.5-g and -1.0-g DUL maneuver, and 2.5-g + 1P and -1.0-g + 1P DUL combined loading conditions, un-notched (pristine) composite strength values were used for failure predictions for composites, except at locations of impact damage where notched strength values were used. As shown in Table 4-7, un-notched composite strength values for the MBB were -8,000 micro-in./in. for compression and 10,000 micro-in./in. for tension.

Differing from the failure analysis presented above, in the failure analysis of the MBB loaded beyond 2.5-g DUL and 2.5-g + 1P DUL, a more conservative approach was used. This was done because more uncertainties appear in the failure predictions when the applied loads exceed DUL. Instead of using -8,000 micro-in./in. for compression and 10,000 micro-in./in. for tension, ranges of design values were used for failure predictions for composites, except at locations of impact damage where notched strength values were used. To calculate the ranges of design values, assuming the failure strain values were 5% above the un-notched composite strength values, the failure strength values became -8,400 micro-in./in. for compression and 10,500 micro-in./in. for tension. To be conservative, a biased range of 15% below to 5% above the failure strength values was used, and the ranges of -7,140 to -8,820 micro-in./in. for compression and 8,925 to 11,025 micro-in./in. for tension were derived. Margins of safety on the composites at locations without impact damage were calculated as ranges using these biased design values.

For metallic fittings and fasteners, instead of using tensile yield strengths for design and in margin-of-safety calculations, tensile ultimate strengths of metals were used in failure predictions. In Table 4-7, only tensile yield strengths of metals were listed; however, the ultimate strengths of metals were derived from these yield strength values. For instance, strength values of 15% above the yield strengths shown in Table 4-7 were used as the ultimate strengths of metals. This is because ultimate strengths of metals are generally 15% greater than their yielding strengths.

4.4.6.1 4.125-g + 1.5P

Failure predictions for the MBB were made based on results from nonlinear analysis of the global FEM in the 4.125-g + 1.5P (or 165% of 2.5-g DLL + 1.5P) combined loading condition. In this condition, concentrated loads were applied on the COLTS fixture to simulate 165% of the 2.5-g DLL (4.125-g) up-bending load plus a 1P DUL (1.5P, or 13.8 psi) pressure, creating a force normal to the internal skin surface that deformed the crown, bulkhead, and keel panels outward. The structural behavior of the MBB at 4.125-g + 1.5P combined loads was similar to the results at 2.5-g + 1P DUL combined loads discussed in Section 4.4.3. During the test, in-plane strains and out-of-plane deformations were measured by VIC-3D, LVDT, and strain gages. Locations of the VIC-3D, LVDT, and strain gages are shown in the HWB MBB Test Specification (Ref. 4-9).

Predictions of VIC-3D plots from nonlinear analysis are shown in Figure 4-172, and displacement prediction charts of the LVDT are shown in Figure 4-172 for the upper bulkhead and in Figure 4-173 for the reacting platen. Results beyond DUL from nonlinear analysis are also included in these plots. Results from the LVDT charts in Figure 4-172 showed that normal displacements of the upper bulkhead stopped growing after reaching DUL because the internal pressure to the MBB was kept constant at 1.5P beyond DUL. Conversely (as shown in Figure 4-173), displacements of the reacting platen continued to grow after DUL because the up-bending load applied to the MBB continued to grow past DUL.

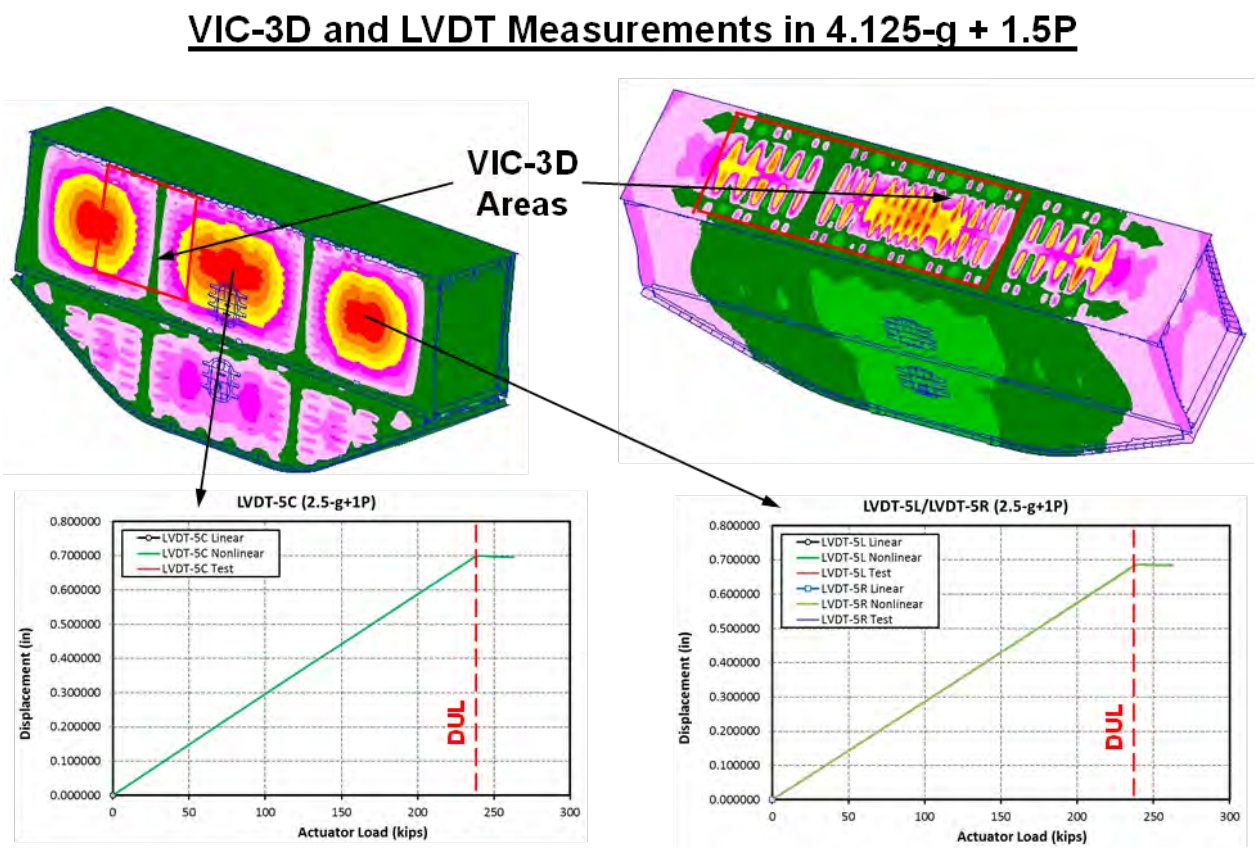

Figure 4-172. VIC-3D and LVDT Measurements of the MBB in 4.125-g + 1.5P Condition

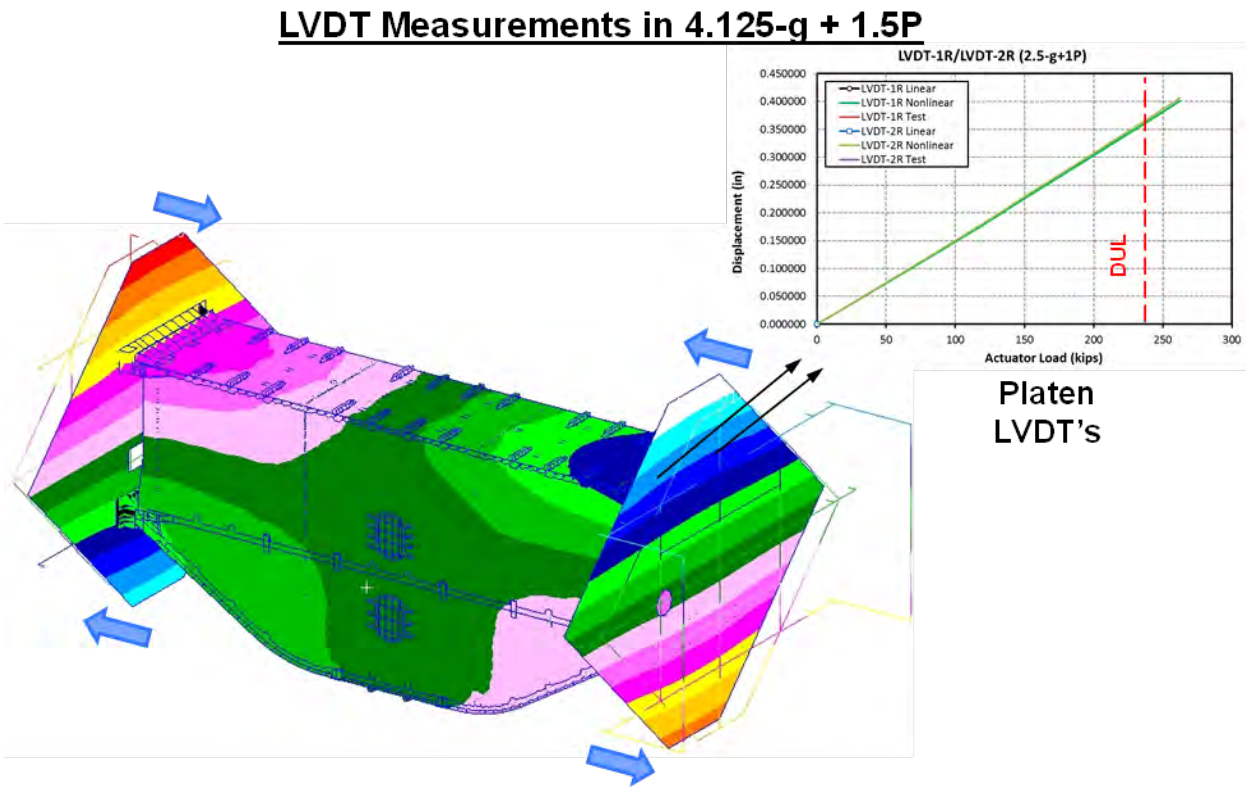

Figure 4-173. LVDT Measurements of the MBB in 4.125-g + 1.5P Condition

In addition to the VIC-3D and LVDT instruments, strain gages were placed on the MBB where high strains and stresses were expected during tests. As shown in Figure 4-174, for the MBB structures that were considered to be pristine (not impact damaged), the following seven critical locations were identified for possible failure locations that warranted evaluation:

1. On the crown frames.
2. On the crown T-caps.
3. On the crown stringer webs and stringer rods near the frames.
4. On the crown skin.
5. On the upper bulkhead skin.
6. On the side keel frames.
7. On the metallic fittings connected to the lower load-introduction fittings.

Strain gages were placed at these critical locations to monitor the structural behavior and integrity of the MBB during tests. Maximum or minimum principal strain distribution plots from nonlinear analysis and strain gage predictions from nonlinear analysis are shown in Figure 4-175 through Figure 4-181. As discussed earlier, for composite structures, failure predictions were made by comparing the maximum and minimum principal strain values from nonlinear analysis to failure strength ranges of -7,140 to -8,820 micro-in./in. for compression and 8,925 to 11,025 micro-in./in. for tension (in pristine condition).

For metallic structures, failure predictions were made by comparing von Mises stresses of metallic fittings and bolts to the ultimate strengths of metals. In Table 4-7, only tensile yield strengths of metals were listed; however, the ultimate strengths of metals were derived from

these yield strength values. For instance, strength values of 15% above the yield strengths shown in Table 4-7 were used as the ultimate strengths of metals. This is because ultimate strengths of metals are generally 15% greater than their yielding strengths. In summary, failure prediction results showed that the MBB in its pristine condition would not fail catastrophically at 4.125-g + 1.5P combined loads. Detailed results for these critical locations are presented in the following discussion.

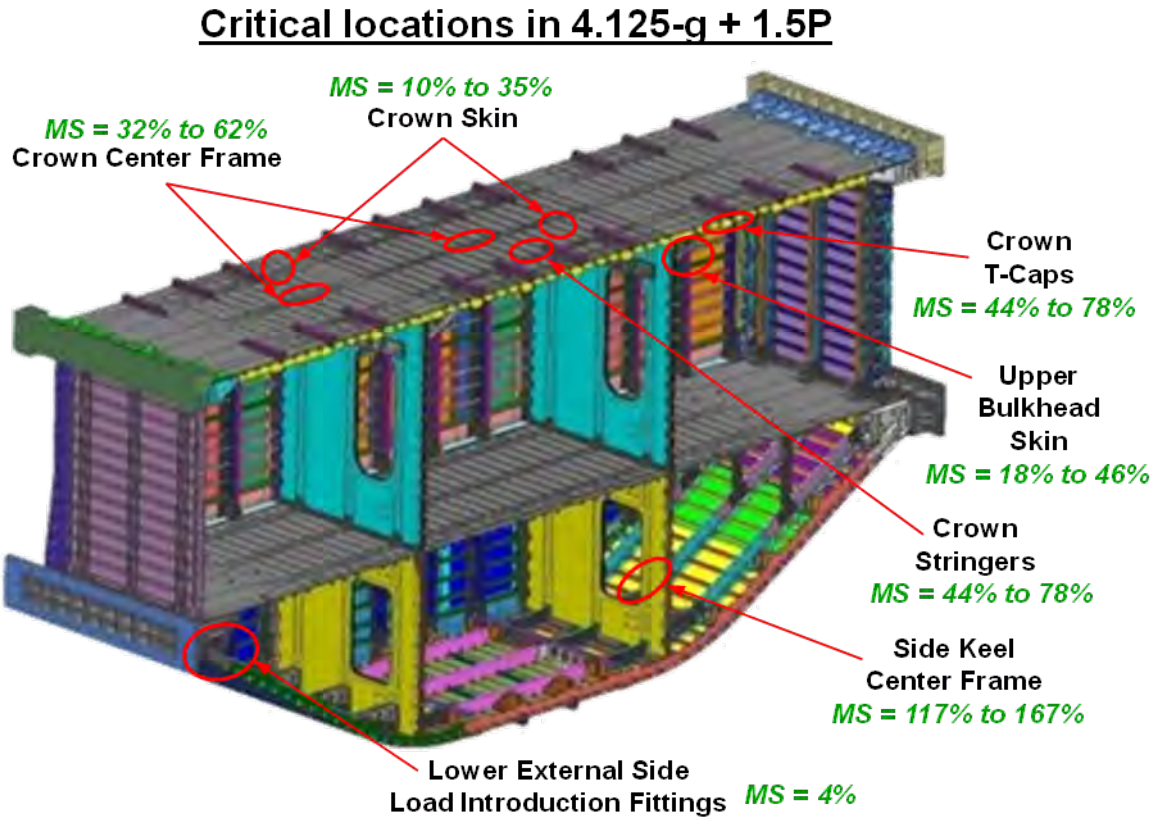

Figure 4-174. Critical Locations in Failure Predictions for the MBB in 4.125-g + 1.5P Condition

Figure 4-175 shows a plot of minimum principal strain on the crown frames and charts of strain versus actuator load of strain gage locations sg01875/sg01876 and sg01874 (on the frame top). A critical minimum principal strain of -5,429 micro-in./in. on the frame was seen in the 4.125-g + 1.5P combined loading condition. This critical strain was within the failure strength ranges of -7,140 to -8,820 micro-in./in. in compression for the frame web. The calculated margin of safety range was from 32% to 62%, which indicated that a failure of the crown frame on the MBB was unlikely to occur at 4.125-g + 1.5P combined loads.

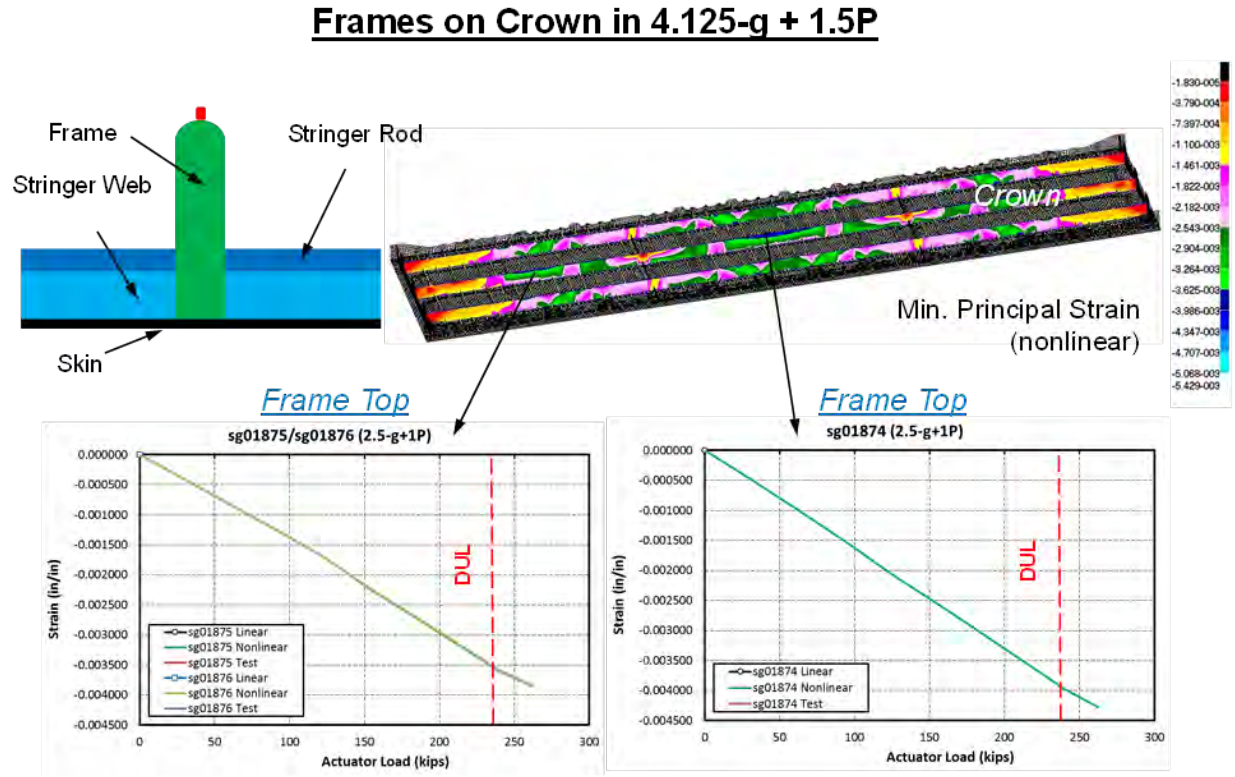

Figure 4-175. Strains on Crown Frames in 4.125-g + 1.5P Condition

Figure 4-176 shows a plot of minimum principal strain on the crown T-caps and a chart of strain versus actuator load of strain gage locations sg01924/sg01922 (on the T-cap web). A critical minimum principal strain of -4,948 micro-in./in. on the T-caps was seen in the 4.125-g + 1.5P combined loading condition. This critical strain was within the failure strength ranges of -7,140 to -8,820 micro-in./in. in compression for the T-cap web. The calculated margin-of-safety range was from 44% to 78%, which indicated that a failure of the crown T-cap on the MBB was unlikely to occur at 4.125-g + 1.5P combined loads.

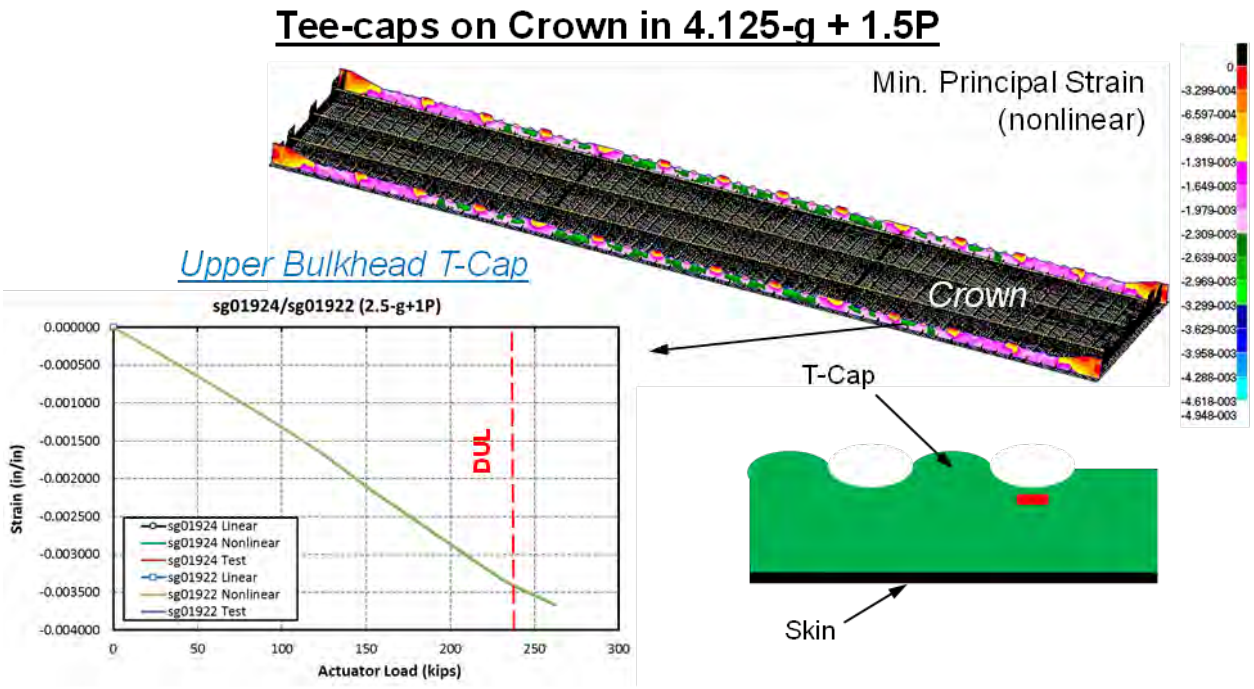

Figure 4-176. Strains on Crown T-caps in 4.125-g + 1.5P Condition

Figure 4-177 shows a plot of maximum principal strain on the crown stringer web near the frames and charts of strain versus actuator load of rosette strain gage locations sg01436C/sg01440C (on the stringer web to measure principal strains) and sg01525/sg01529 (on the stringer rod). A critical maximum principal strain of 6,211 micro-in./in. on the stringer web/rod was seen in the 4.125-g + 1.5P combined loading condition. This critical strain was within the failure strength ranges of 8,925 to 11,025 micro-in./in. in tension for the stringer web. The calculated margin-of-safety range was from 44% to 78%, which indicated that a failure of the crown stringer web and stringer rod on the MBB was unlikely to occur at 4.125-g + 1.5P combined loads.

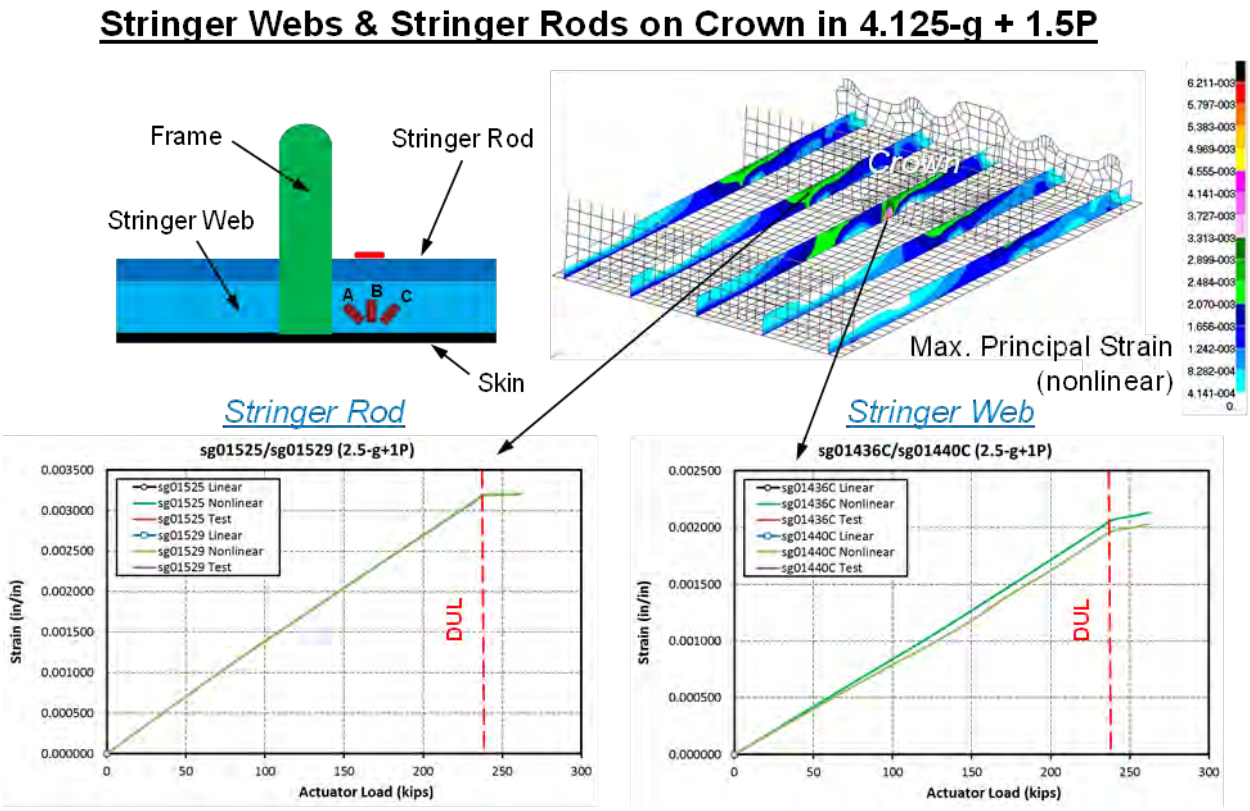

Figure 4-177. Strains on Crown Stringer Webs in 4.125-g + 1.5P Condition

Figure 4-178 shows a plot of minimum principal strains on the crown skin and charts of strain versus actuator load of rosette strain gage locations sg01288B/sg01291B (on the interior skin to measure principal strains) and back-to-back strain gage locations sg01106/sg01206 (on the exterior and interior skin). A critical minimum principal strain of -6,514 micro-in./in. on the skin was seen in the 4.125-g + 1.5P combined loading condition. This critical strain was within the failure strength ranges of -7,140 to -8,820 micro-in./in. in compression for the skin. The calculated margin-of-safety range was from 10% to 32%, which indicated that a failure of the crown skin on the MBB was unlikely to occur at 4.125-g + 1.5P combined loads.

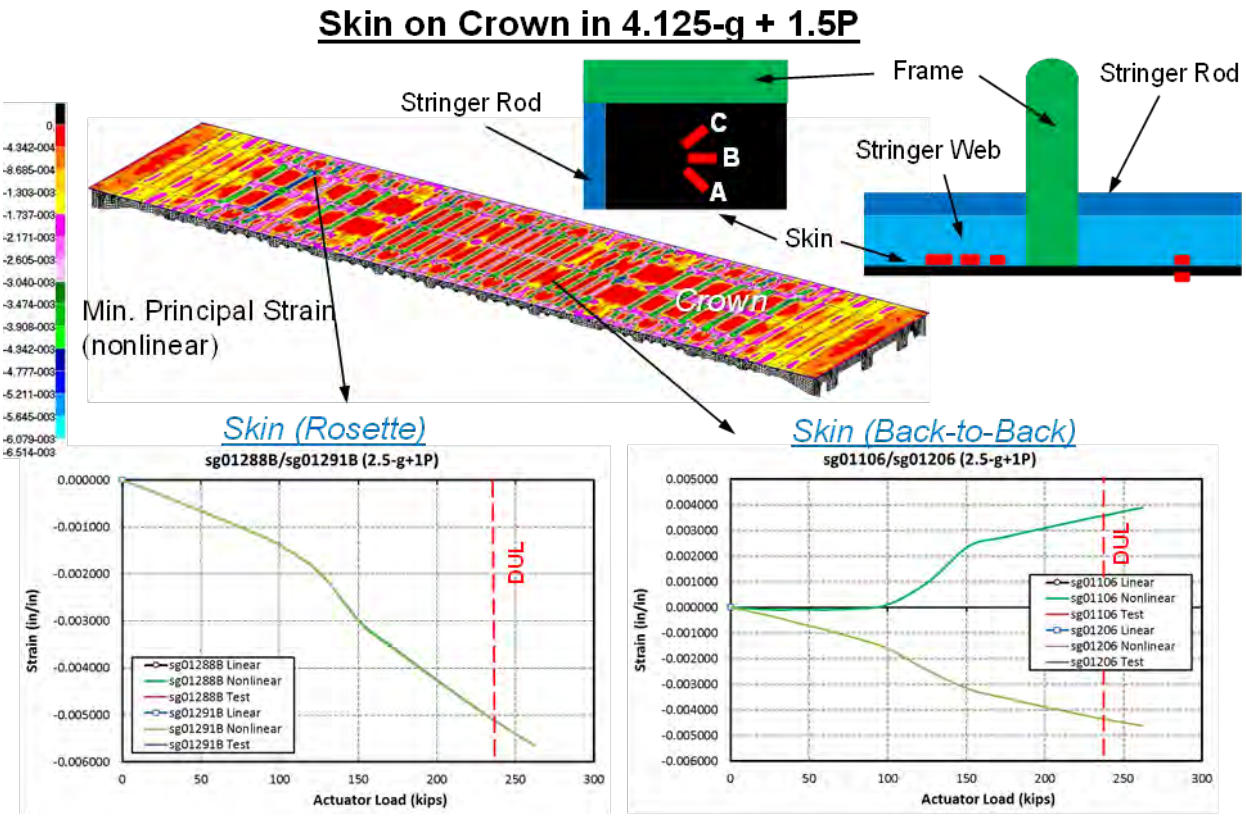

Figure 4-178. Strain on Crown Skin in 4.125-g + 1.5P Condition

Figure 4-179 shows a plot of minimum principal strain on the upper bulkhead skin and charts of strain versus actuator load of rosette strain gage locations sg03111A/sg05111A and sg03112B/sg05112B (on the exterior skin to measure principal strains). A critical minimum principal strain of -6,042 micro-in./in. on the skin was seen in the 4.125-g + 1.5P combined loading condition. This critical strain was within the failure strength ranges of -7,140 to -8,820 micro-in./in. in compression for the skin. The calculated margin-of-safety range was from 18% to 46%, which indicated that a failure of the upper bulkhead skin on the MBB was unlikely to occur at 4.125-g + 1.5P combined loads.

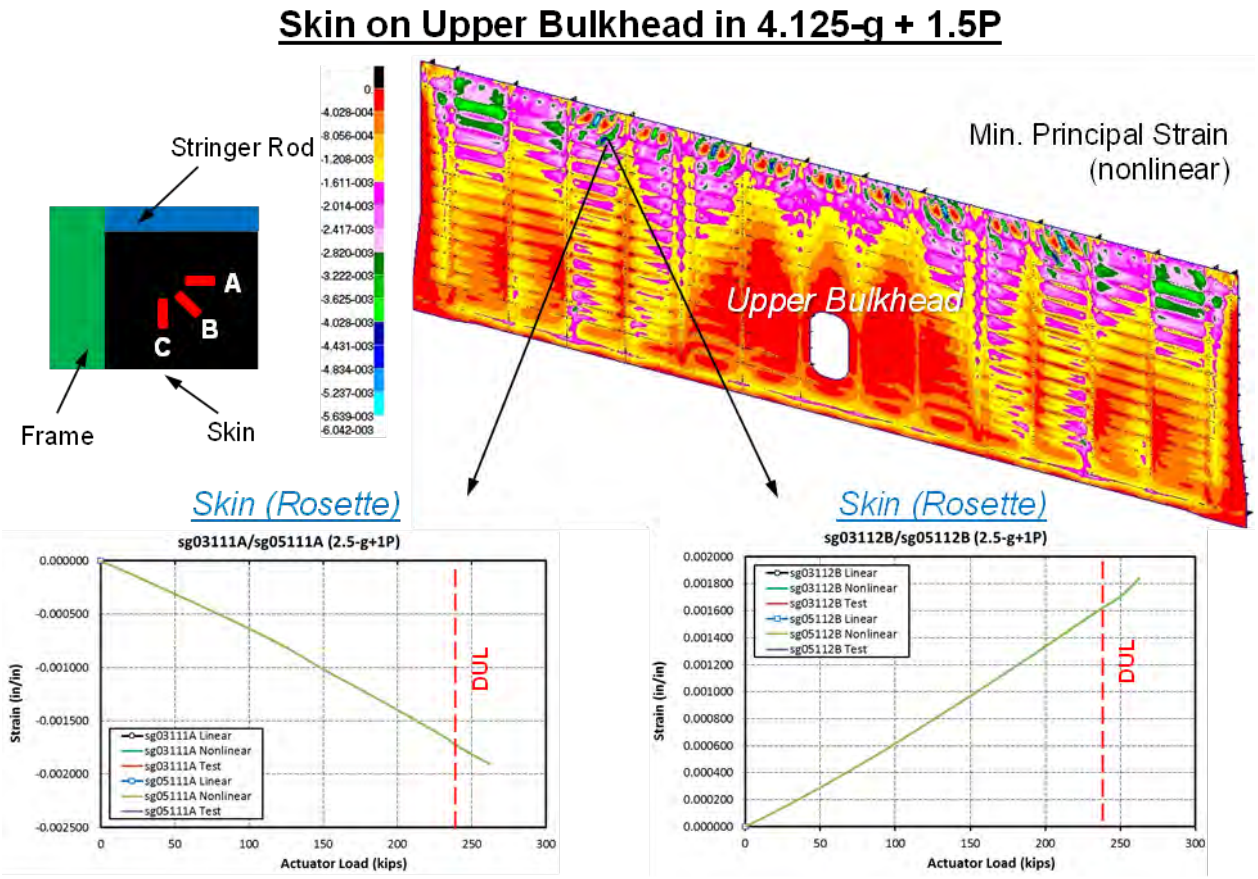

Figure 4-179. Rosette Strains on Upper Bulkhead Skin in 4.125-g + 1.5P Condition

Figure 4-180 shows a plot of maximum principal strain on the side keel frames and a chart of strain versus actuator load of strain gage locations sg08810/sg09810 (on the frame top). A critical maximum principal strain of 4,122 micro-in./in. on the frame was seen in the 4.125-g + 1.5P combined loading condition. This critical strain was within the failure strength ranges of 8,925 to 11,025 micro-in./in. in tension for the frame web. The calculated margin-of-safety range was from 117% to 167%, which indicated that a failure of the side keel frame on the MBB was unlikely to occur at 4.125-g + 1.5P combined loads.

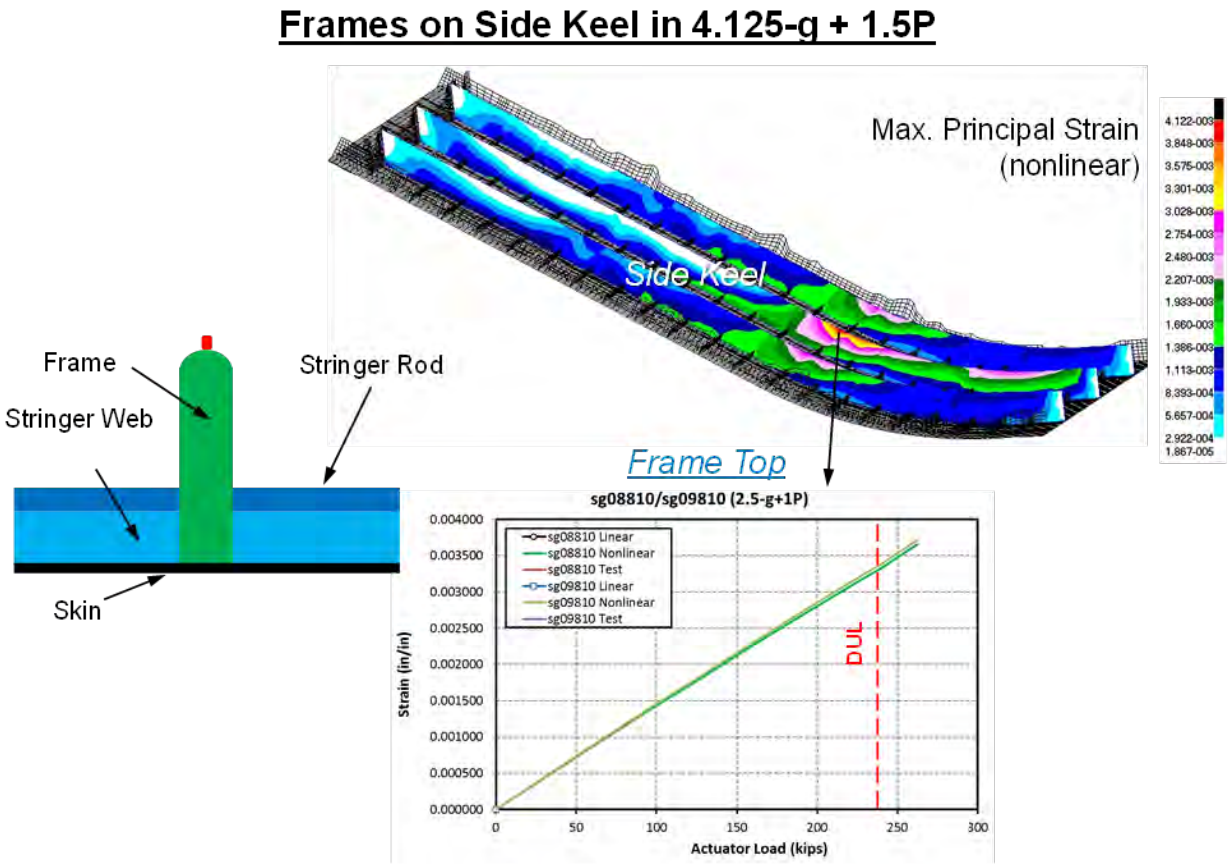

Figure 4-180. Strains on Side Keel Frames in 4.125-g + 1.5P Condition

Figure 4-181 shows a plot of von Mises strain of the Lower External Side Load Introduction Fitting (ZJ153654-1) and a chart of strain versus actuator load of strain gage locations sg16017/sg16018 (on the fitting lower flange). A critical strain of 6,064 micro-in./in. located at the fitting web was seen in the 4.125-g + 1.5P combined loading condition. Using Young's modulus of 10.3 Msi for aluminum alloy 7050-T7451, this strain was equivalent to a stress of 62.5 ksi. Compared to the yielding allowable of 65 ksi for the Lower External Side Load Introduction Fitting (ZJ153654-1), this critical stress was within the yielding allowable of the fitting. The calculated margin of safety was 4%, which indicated that a failure of the Lower External Side Load Introduction Fitting on the MBB was unlikely to occur at 4.125-g + 1.5P combined loads.

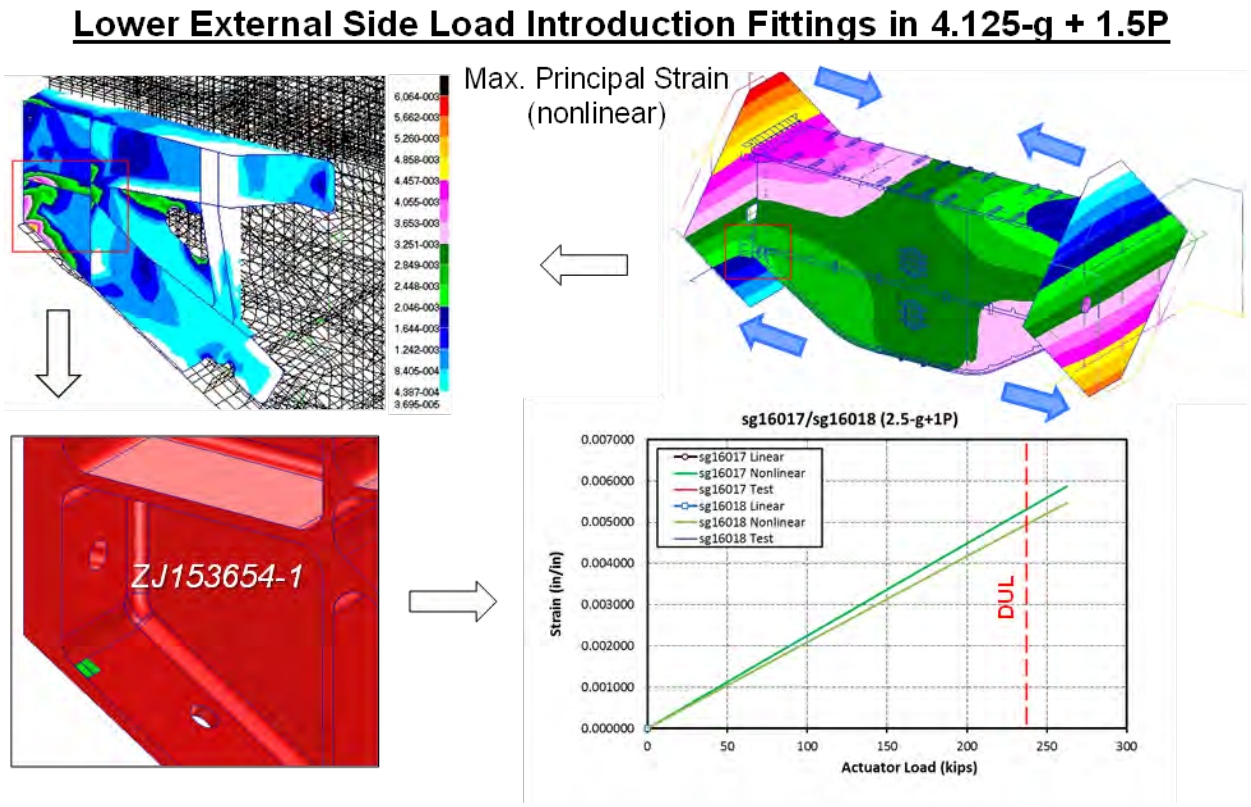

Figure 4-181. Strains on Fittings Connected to Lower Load-Introduction Fittings in 4.125-g + 1.5P Condition

For tests of the MBB after impact damage, the following four critical locations were identified near the impact damage for possible failure locations that warranted evaluation:

1. On the exterior impact site no. 2, which was on the stringer flange of the center keel.
2. On the exterior impact site no. 3, which was on the mid-bay skin of the center keel.
3. On the interior impact site no. 1, which was on the frame top of the upper bulkhead.
4. On the interior impact site no. 3, which was on the mid-bay skin of the upper bulkhead.

Strain gages were placed near these impact-damaged locations to monitor the behavior of structure with impact damage during tests. Strain versus internal pressure of the critical strain gages are shown in Figure 4-182 through Figure 4-185. Strain gage predictions from linear and nonlinear analyses were compared to evaluate the extent of geometric nonlinearity of the MBB

in the 4.125-g + 1.5P combined loading condition. Failure predictions were made by comparing the maximum and minimum principal strain values of the MBB from nonlinear analysis to the notched strain design values (in impact-damaged condition) of the composites shown in Table 4-7.

Figure 4-182 shows charts of strain versus actuator load of back-to-back strain gage locations sg18103/sg18303 (located 0.5-in. forward from the impact site) and sg18104/sg18304 (located 0.5-inch aft from the impact site) near exterior impact site no. 2 on the stringer flange of the center keel. Results from nonlinear analysis showed that the critical tension strain was 1,530 micro-in./in. near the impact damage site in the 4.125-g + 1.5P combined loading condition. These strains were within the notched design strain values of 5,900 micro-in./in. for the stringer flange. The calculated margin of safety was 286%, which indicated that a failure of the stringer flange at exterior impact site no. 2 of the center keel on the MBB was unlikely to occur at 4.125-g + 1.5P combined loads.

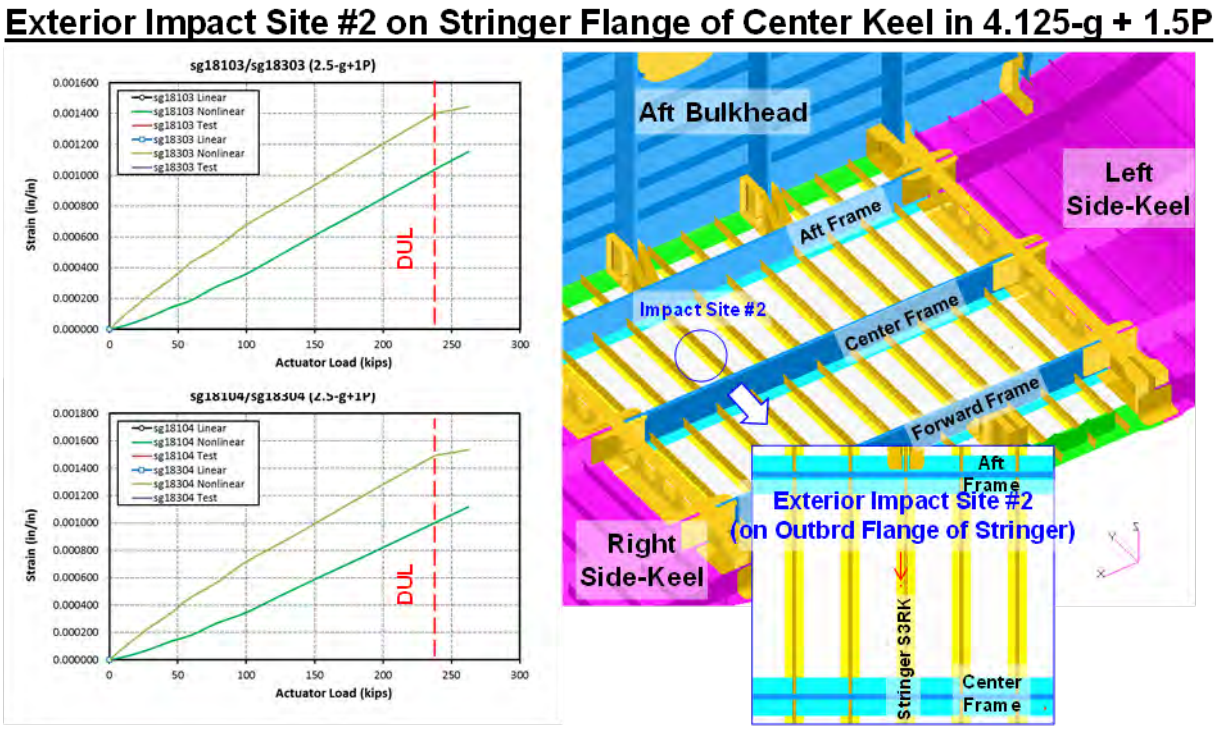

Figure 4-182. Strains on Exterior Impact Site no. 2 in 4.125-g + 1.5P Condition

Figure 4-183 shows charts of strain versus actuator load of back-to-back strain gage locations sg18105/sg18205 (located 1.0-in. left of the impact site) and sg18106/sg18206 (located 1.0-in. right of the impact site) near exterior impact site no. 3 on the mid-bay skin of the center keel. Results from nonlinear analysis showed that the critical tension strain was 2,200 micro-in./in. near the impact damage site in the 4.125-g + 1.5P combined loading condition. This strain was within the notched design strain value of 5,900 micro-in./in. for the skin. The calculated margin of safety was 168%, which indicated that a failure of the skin at exterior impact site no. 3 of the center keel on the MBB was unlikely to occur at 4.125-g + 1.5P combined loads.

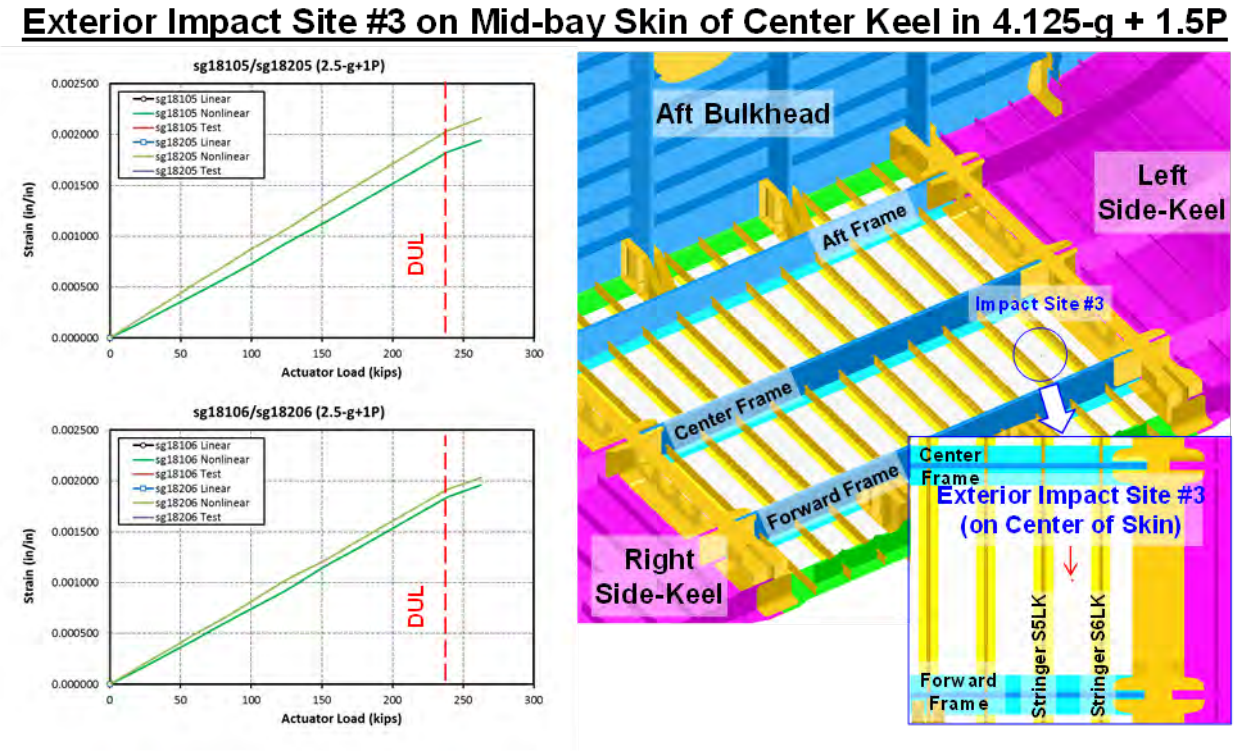

Figure 4-183. Strains on Exterior Impact Site no. 3 in 4.125-g + 1.5P Condition

Figure 4-184 shows a chart of strain versus actuator load of strain gage locations sg18807 (located 1.0-in. up from the impact site) and sg18808 (located 1.0-in. down from the impact site) near interior impact site no. 1 on top of the frame cap of the forward upper bulkhead. Results from nonlinear analysis showed that the critical compression strain was -3,750 micro-in./in. near the impact damage site in the 4.125-g + 1.5P combined loading condition. This strain was within the notched design strain values of -5,800 micro-in./in. for the frame web/cap. The calculated margin of safety was 55%, which indicated that a failure of the frame web/cap at interior impact site no. 1 of the forward upper bulkhead on the MBB was unlikely to occur at 4.125-g + 1.5P combined loads.

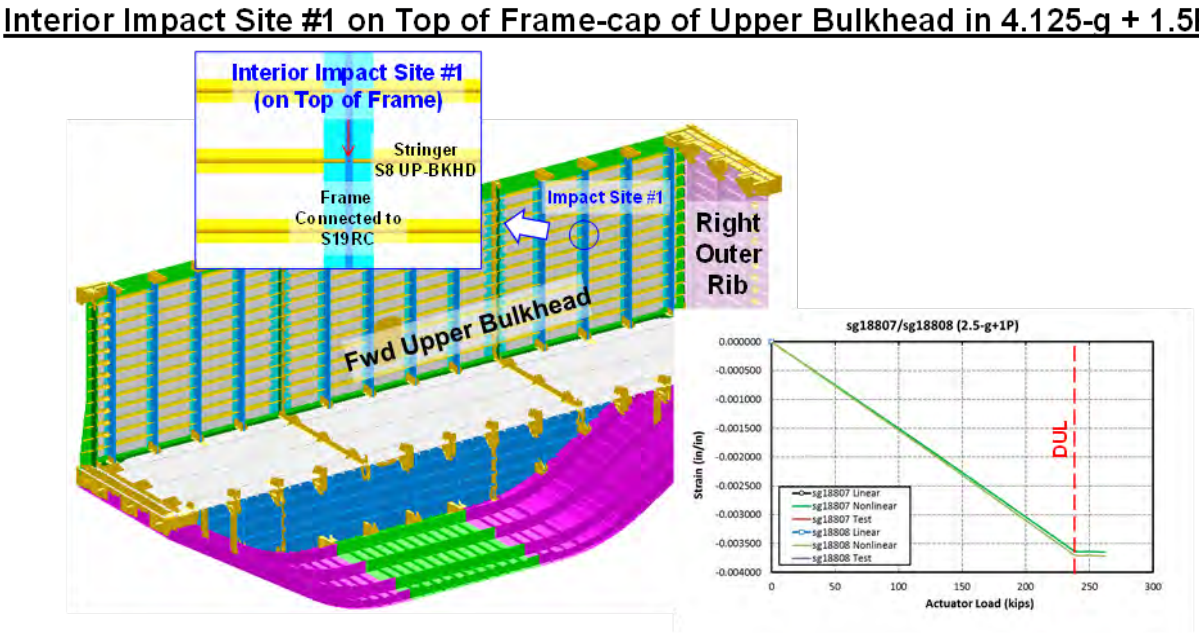

Figure 4-184. Strains on Interior Impact Site no. 1 in 4.125-g + 1.5P Condition

Figure 4-185 shows charts of strain versus actuator load of back-to-back strain gage locations sg18107/sg18211 (located 1.0-in. up from the impact site) and sg18108/sg18212 (located 1.0-in. down from the impact site) near interior impact site no. 3 on the mid-bay skin of the forward upper bulkhead. Results from nonlinear analysis showed that the critical tension strain was 1,225 micro-in./in. near the impact damage site in the 4.125-g + 1.5P combined loading condition. This strain was within the notched design strain value of 5,900 micro-in./in. for the skin. The calculated margin of safety was 382%, which indicated that a failure of the skin at interior impact site no. 3 of the forward upper bulkhead on the MBB was unlikely to occur at 4.125-g + 1.5P combined loads.

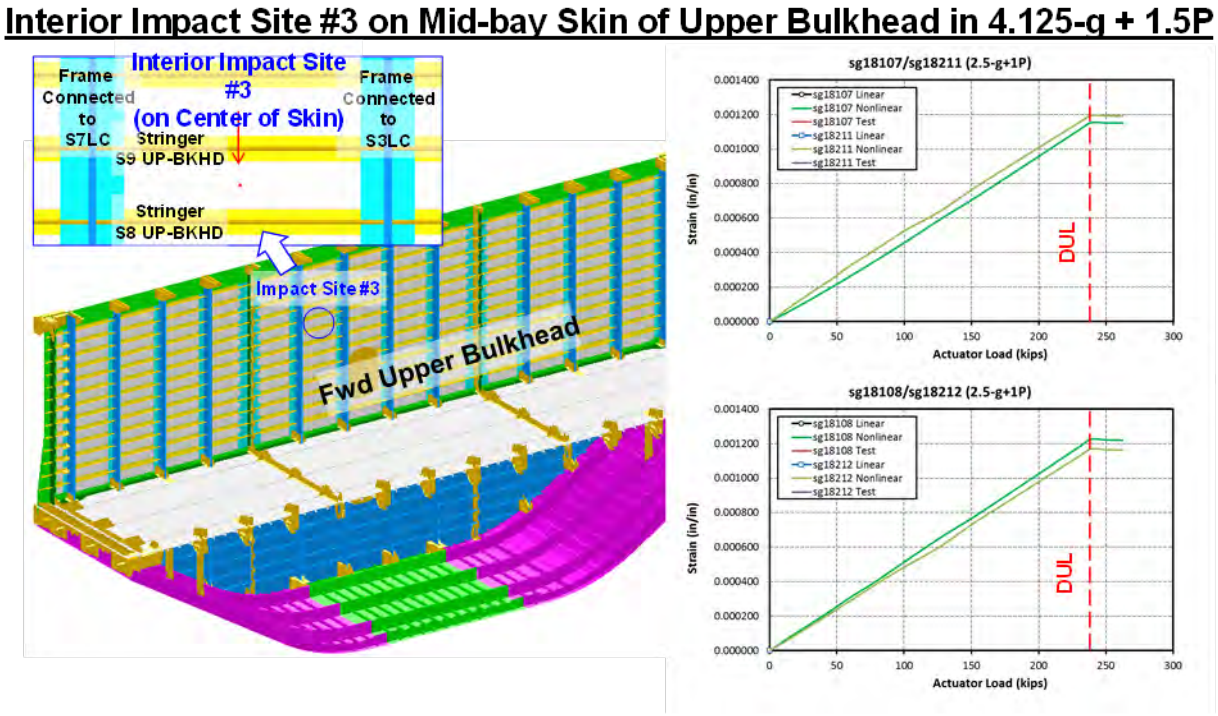

Figure 4-185. Strains on Interior Impact Site no. 3 in 4.125-g + 1.5P Condition

4.4.6.2 200% of 2.5-g DLL

Failure predictions for the MBB were made in the 5.0-g (or 200% of 2.5-g DLL) maneuver condition. In this condition, concentrated loads were applied on the COLTS fixture to simulate 200% of the 2.5-g DLL (5.0-g) up-bending load. In the nonlinear analysis of the global FEM in the 5.0-g (or 200% of 2.5-g DLL) maneuver condition, due to numerical issues, convergent results were achieved only up to 4.66-g (or 186.3% of 2.5-g DLL) maneuver load. Results were extrapolated to 5.0-g maneuver load for margin-of-safety calculations. The structural behavior of the MBB at 5.0-g maneuver load was similar to the results at the 2.5-g maneuver load discussed in Section 4.4.2.

During the test, in-plane strains and out-of-plane deformations were measured by VIC-3D, LVDT, and strain gages. Locations of the VIC-3D, LVDT, and strain gages are shown in the HWB MBB Test Specification (Ref. 4-9). Predictions of VIC-3D plots from nonlinear analysis are shown in Figure 4-186, and a displacement prediction chart of the LVDT is shown in Figure 4-187 for the reacting platen. Results beyond DUL from nonlinear analysis are also included in these plots. Results from the LVDT chart in Figure 4-187 showed that the displacements of the reacting platen continued to increase beyond DUL because the up-bending load applied to the MBB continued to increase beyond DUL.

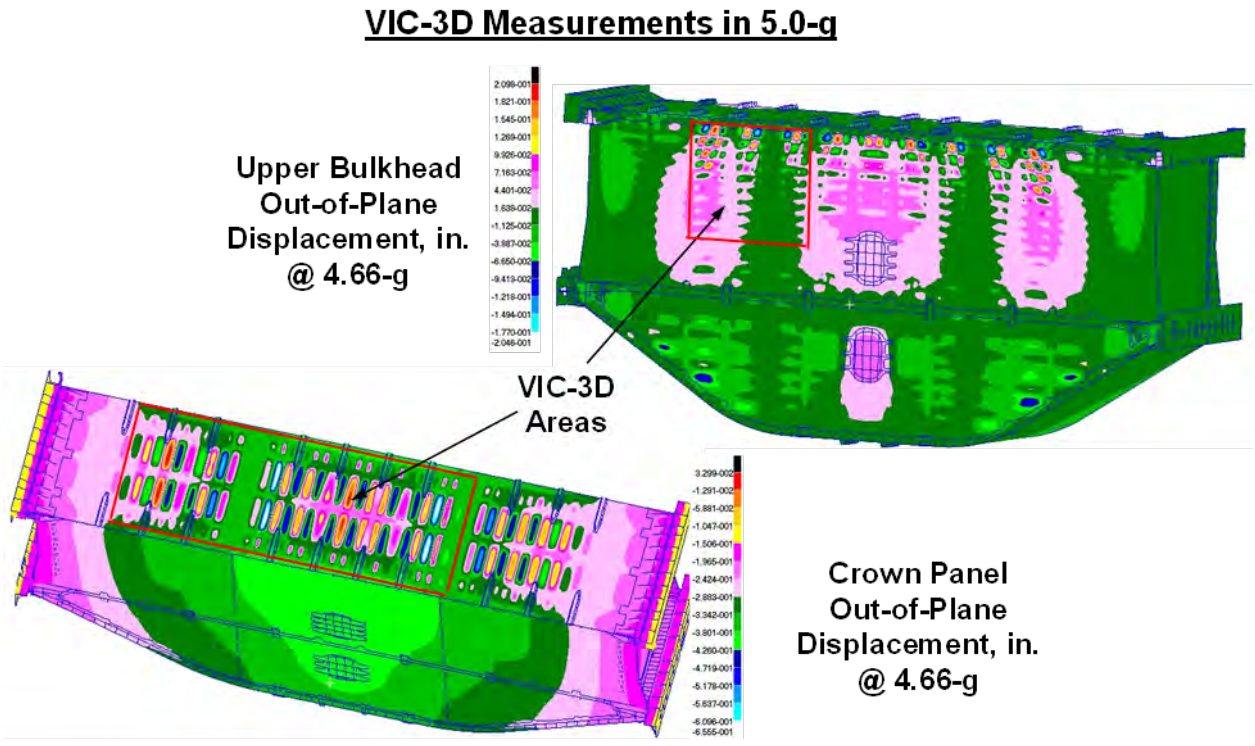

Figure 4-186. VIC-3D Measurements of the MBB in 5.0-g Condition

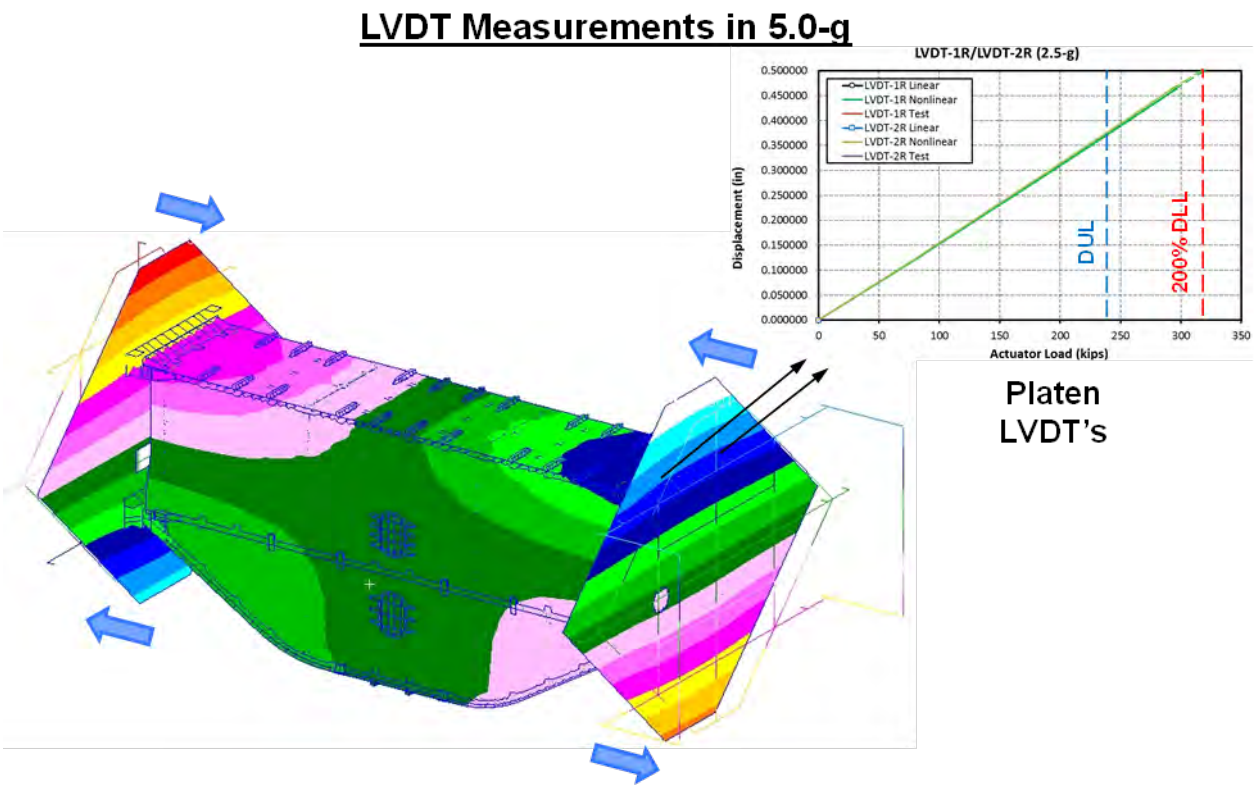

Figure 4-187. LVDT Measurements of the MBB in 5.0-g Condition

In addition to the VIC-3D and LVDT instruments, strain gages were placed on the MBB where high strains and stresses were expected during tests. As shown in Figure 4-188, for the MBB structures that were considered to be pristine (not impact damaged), the following four critical locations were identified for possible failure locations that warranted evaluation:

1. On the crown frames.
2. On the crown T-caps.
3. On the upper bulkhead skin.
4. On the metallic fittings connected to the lower load-introduction fittings.

Strain gages were placed at these critical locations to monitor the structural behavior and integrity of the MBB during tests. Maximum or minimum principal strain distribution plots from nonlinear analysis and strain gage predictions from nonlinear analysis are shown in Figure 4-189 through Figure 4-192. As discussed earlier, for composite structures, failure predictions were made by comparing the maximum and minimum principal strain values from nonlinear analysis to failure strength ranges of -7,140 to -8,820 micro-in./in. for compression and 8,925 to 11,025 micro-in./in. for tension (in pristine condition). For metallic structures, failure predictions were made by comparing von Mises stresses of metallic fittings and bolts to the ultimate strengths of metals. In Table 4-7, only tensile yield strengths of metals were listed; however, the ultimate strengths of metals were derived from these yield strength values. For instance, strength values of 15% above the yield strengths shown in Table 4-7 were used as the ultimate strengths of metals. This is because ultimate strengths of metals are generally 15% greater than their yielding strengths. In summary, failure prediction results showed that the MBB in its pristine condition

would not fail catastrophically at 5.0-g maneuver load. Detailed results for these critical locations are presented in the following discussion.

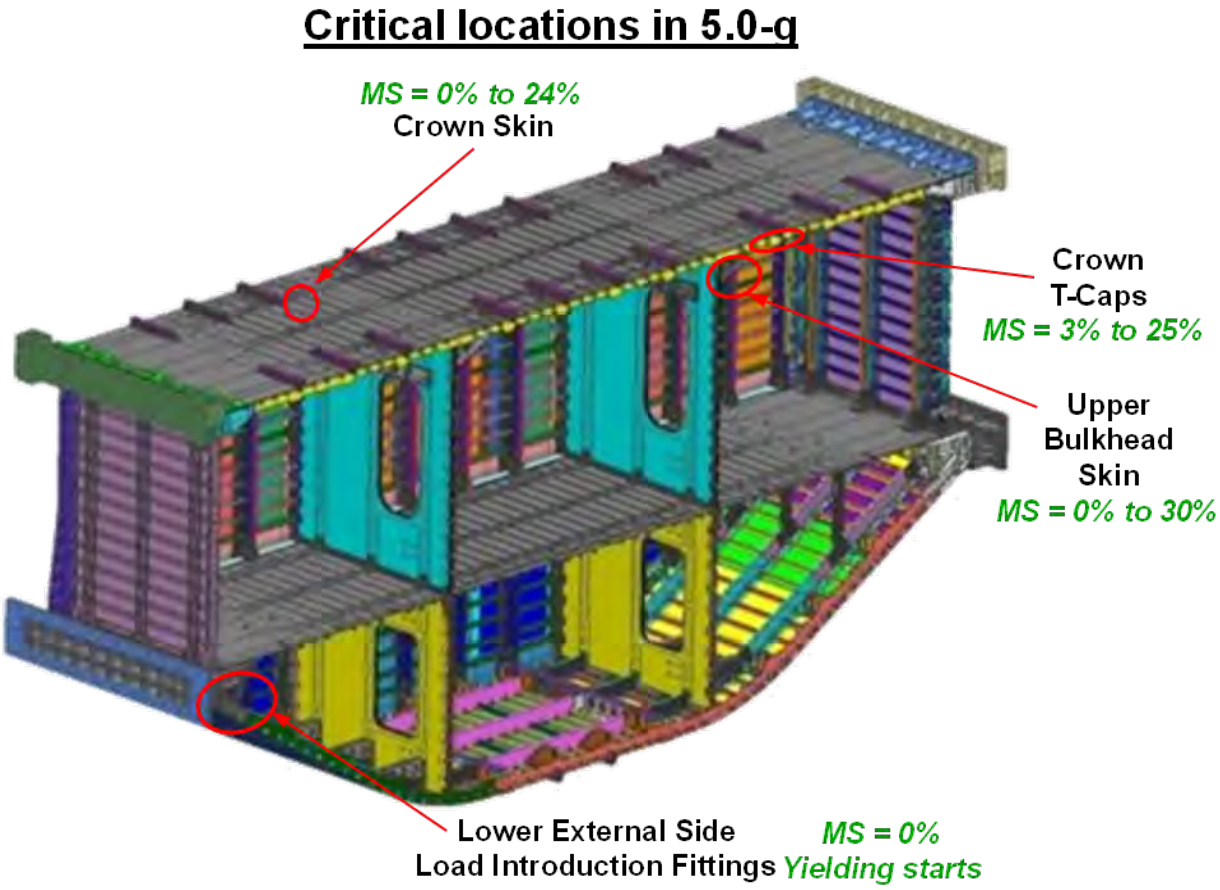

Figure 4-188. Critical Locations in Failure Predictions for the MBB in 5.0-g Condition

In Figure 4-189, minimum principal, rosette principal, and rosette B-gage strains versus actuator load at the critical location of the crown frame are plotted. As discussed earlier, strain values beyond 4.66-g were extrapolated from nonlinear analysis results and compared to the composite failure strain range of -7,140 to -8,820 micro-in./in. for compression (in pristine condition). The maximum and minimum principal strains for rectangular rosette strain gages were calculated from the formula shown in Figure 4-189. As shown, the minimum principal strain at the critical location of the crown frame reached -7,140 micro-in./in. at 5.0-g and -8,820 micro-in./in. at the 6.2-g up-bending load. This was equivalent to a margin of safety ranging from 0% to 24% at 5.0-g maneuver load, which indicated that a failure of the crown frame on the MBB could occur at 5.0-g maneuver load.

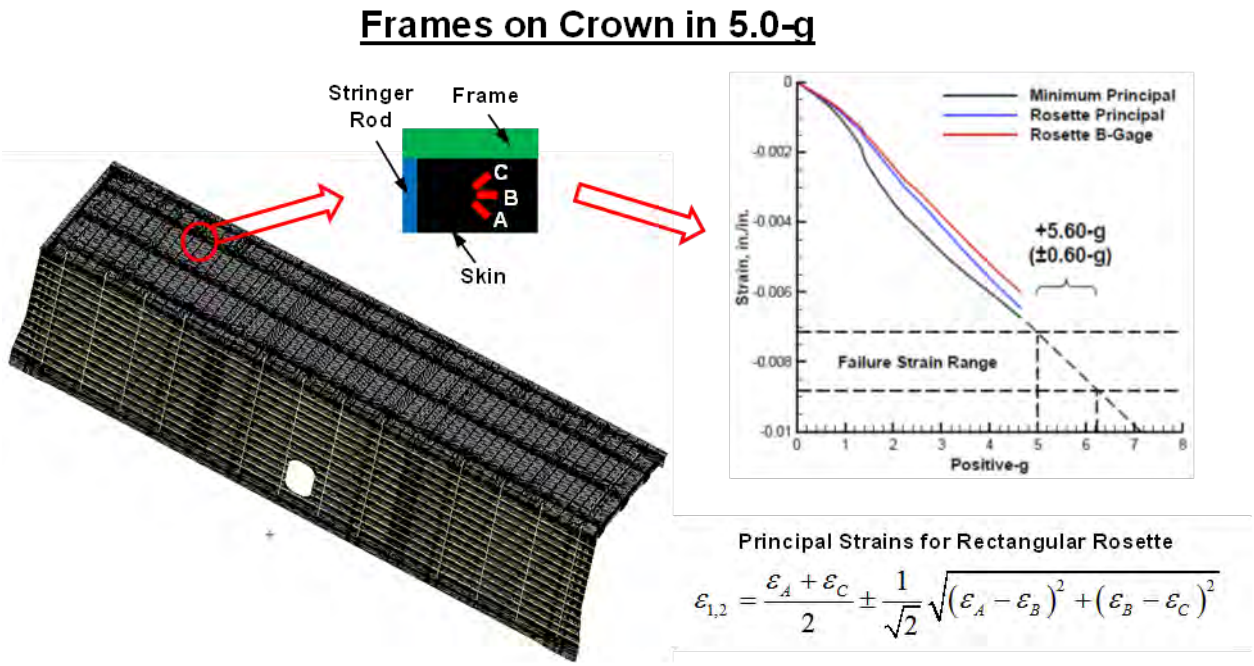

Figure 4-189. Strains on Crown Frames in 5.0-g Condition

In Figure 4-190, minimum principal and linear strains versus actuator load at the critical location of the crown T-cap are plotted. As discussed earlier, strain values beyond 4.66-g were extrapolated from nonlinear analysis results and compared to the composite failure strain range of -7,140 to -8,820 micro-in./in. for compression (in pristine condition). The maximum and minimum principal strains for rectangular rosette strain gages were calculated from the formula shown in Figure 4-190. As shown, the minimum principal strain at the critical location of the crown T-cap reached -7,140 micro-in./in. at 5.15-g and -8,820 micro-in./in. at 6.25-g up-bending load. This was equivalent to a margin of safety ranging from 3% to 25% at 5.0-g maneuver load, which indicated that a failure of the crown T-cap on the MBB was unlikely to occur at 5.0-g maneuver load.

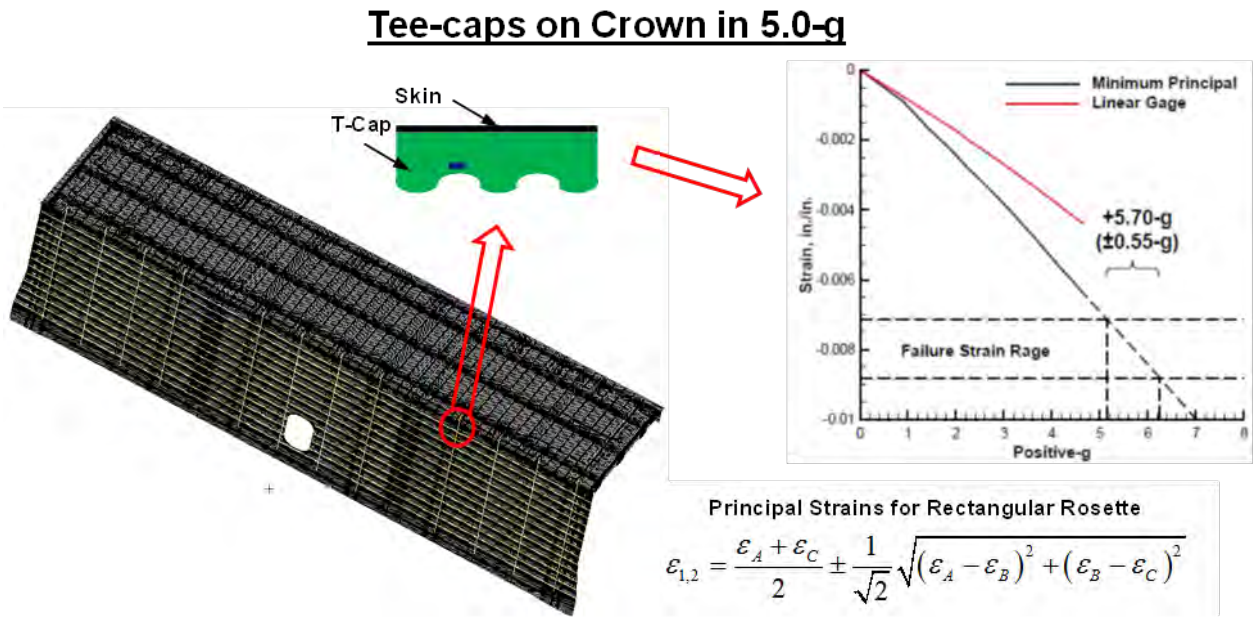

Figure 4-190. Strains on Crown T-caps in 5.0-g Condition

In Figure 4-191, minimum principal, rosette principal, and rosette A-gage strains versus actuator load at the critical location of upper bulkhead skin are plotted. As discussed earlier, strain values beyond 4.66-g were extrapolated from nonlinear analysis results and compared to the composite failure strain range of -7,140 to -8,820 micro-in./in. for compression (in pristine condition). The maximum and minimum principal strains for rectangular rosette strain gages were calculated from the formula shown in Figure 4-191. As shown, the minimum principal strain at the critical location of the upper bulkhead skin reached -7,140 micro-in./in. at 5.0-g and -8,820 micro-in./in. at 6.5-g up-bending load. This was equivalent to a margin of safety ranging from 0% to 30% at 5.0-g maneuver load, which indicated that a failure of the upper bulkhead skin on the MBB could occur at 5.0-g maneuver load.

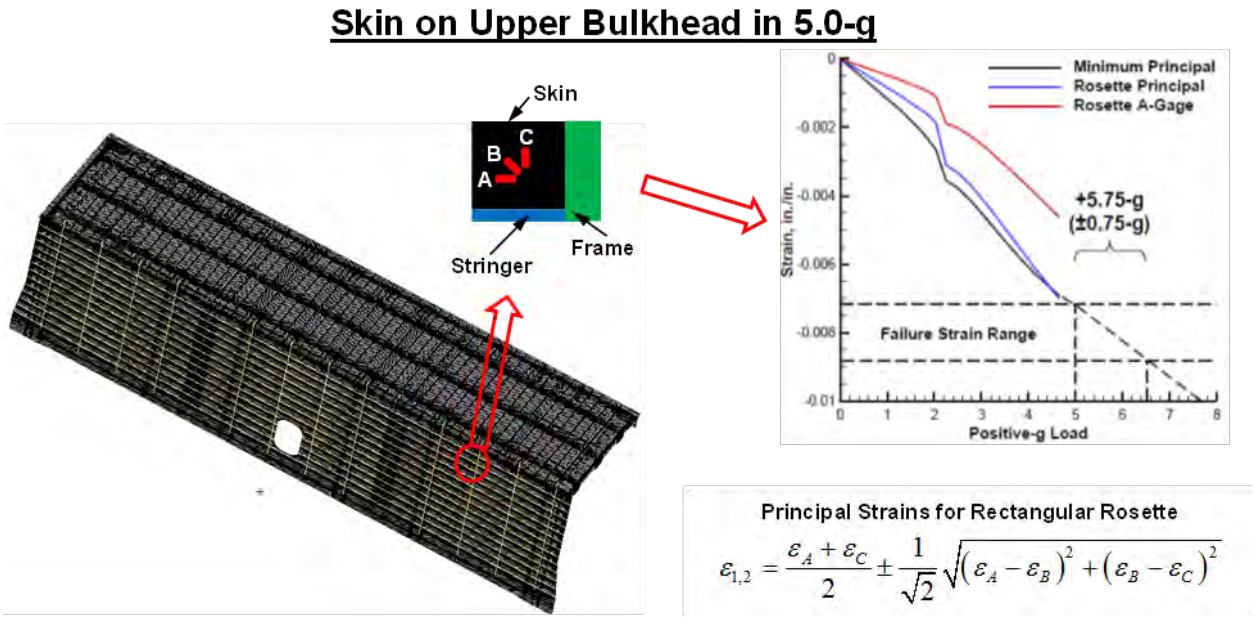

Figure 4-191. Strains on Upper Bulkhead Skin in 5.0-g Condition

Figure 4-192 shows a plot of von Mises strain of the Lower External Side Load Introduction Fitting (ZJ153654-1) and a chart of strain versus actuator load of strain gage locations sg16017/sg16018 (on the fitting lower flange). As shown in Figure 4-192, strains on gages sg16017/sg16018 reached the metallic yielding strain of the Lower External Side Load Introduction Fitting before the 5.0-g (or 200% of 2.5-g DLL) maneuver load. This high strain appeared to be localized in a small area of the fitting flange. Therefore, it was believed that the flange of the metallic fitting would yield and continue to carry tension load up to the 5.0-g maneuver load. A failure of this metallic fitting on the MBB was unlikely to occur at 5.0-g maneuver load.

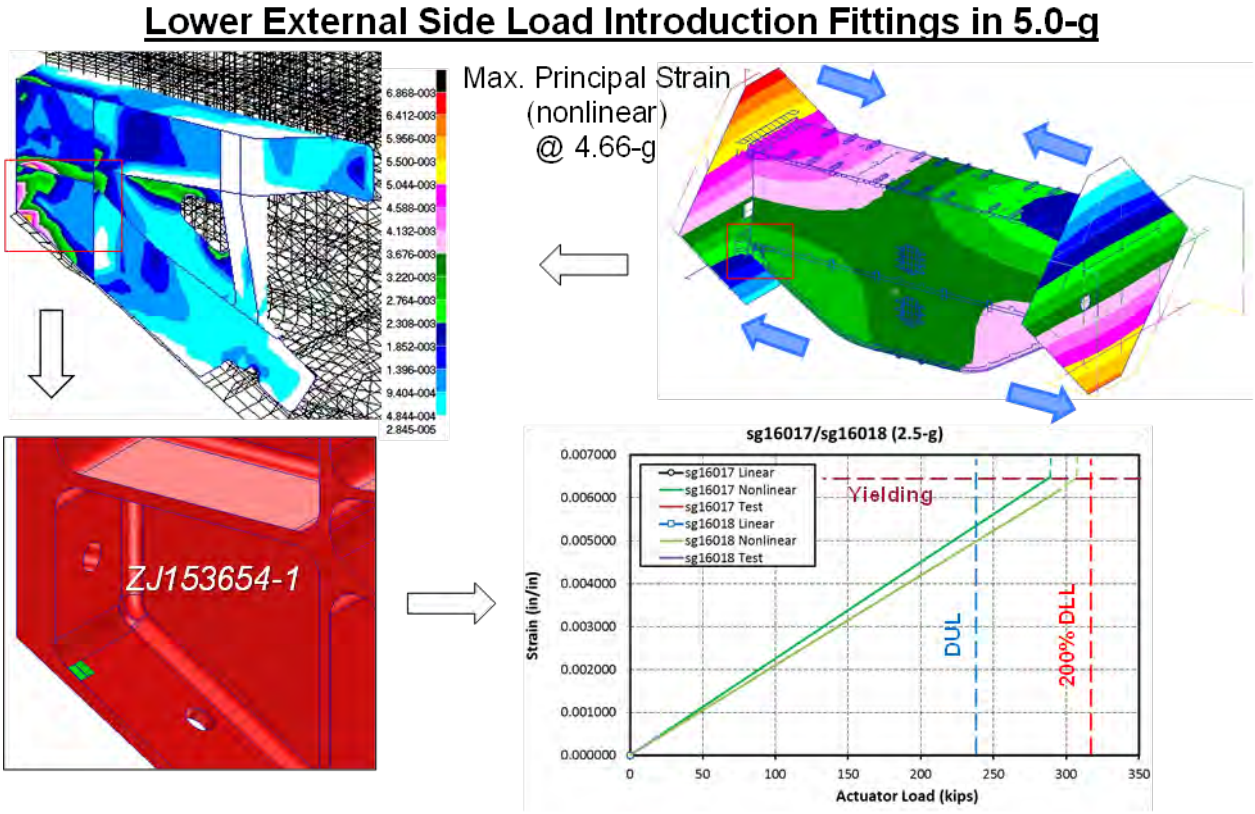

Figure 4-192. Strains on Fittings Connected to Lower Load-Introduction Fittings in 5.0-g Condition

For tests of the MBB after impact damage, the following two critical locations were identified near the impact damage for possible failure locations that warranted evaluation:

1. On the exterior impact site no. 2, which was on the stringer flange of the center keel.
2. On the exterior impact site no. 3, which was on the mid-bay skin of the center keel.

Strain gages were placed near these impact-damaged locations to monitor the behavior of structure with impact damage during tests. Strain versus internal pressure of the critical strain gages are shown in Figure 4-193 and Figure 4-194. Strain gage predictions from linear and nonlinear analyses were compared to evaluate the extent of geometric nonlinearity of the MBB in the 5.0-g maneuver condition. Failure predictions were made by comparing the maximum and minimum principal strain values of the MBB from nonlinear analysis to the notched strain design values (in impact-damaged condition) of the composites shown in Table 4-7.

Figure 4-193 shows charts of strain versus actuator load of back-to-back strain gage locations sg18103/sg18303 (located 0.5-in. forward from the impact site) and sg18104/sg18304 (located 0.5-in. aft from the impact site) near exterior impact site no. 2 on the stringer flange of the center keel. When comparing strain results of these back-to-back strain gages, it was found that tension strain derived from nonlinear analysis was only slightly higher than the tension strain from linear analysis, whereas the bending strain derived from nonlinear analysis was lower than the bending strain from linear analysis. This was because some bending strains were suppressed and replaced with an in-plane tensioning on the panel skin/stringer/frame in tension loading. As a result, lower strains were detected on the panel skin/stringer/frame from nonlinear analysis, resembling a softening effect to a panel in axial load. Results from nonlinear analysis showed that the critical tension strain was 1,350 micro-in./in. near the impact damage site in the 5.0-g maneuver condition. These strains were within the notched design strain values of 5,900 micro-in./in. for the stringer flange. The calculated margin of safety was 337%, which indicated that a failure of the stringer flange at exterior impact site no. 2 of the center keel on the MBB was unlikely to occur at 5.0-g maneuver load.

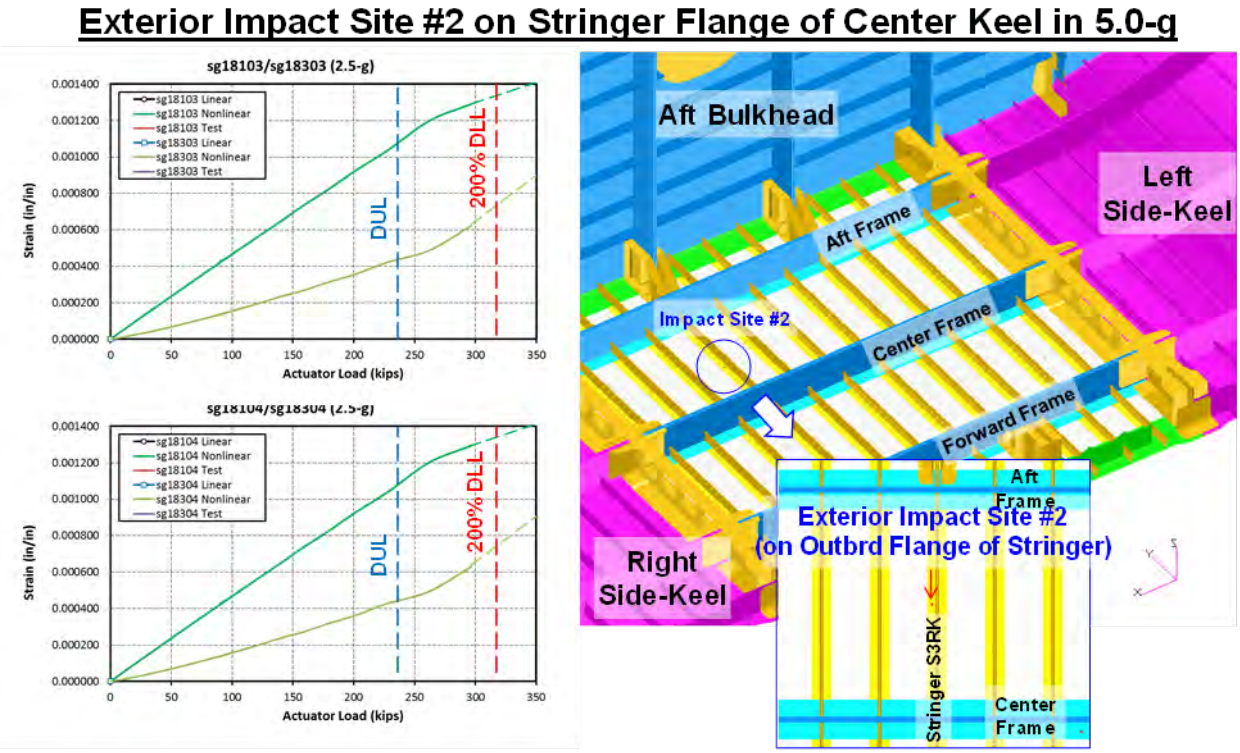

Figure 4-193. Strains on Exterior Impact Site no. 2 in 5.0-g Condition

Figure 4-194 shows charts of strain versus actuator load of back-to-back strain gage locations sg18105/sg18205 (located 1.0-in. left of the impact site) and sg18106/sg18206 (located 1.0-in. right of the impact site) near exterior impact site no. 3 on the mid-bay skin of the center keel. When comparing strain results of these back-to-back strain gages, it was found that tension strain derived from nonlinear analysis was higher than the tension strain from linear analysis, whereas the bending strain derived from nonlinear analysis was significantly lower than the bending strain from linear analysis. This was because some bending strains were suppressed and replaced with an in-plane tensioning on the panel skin/stringer/frame in tension loading. As a result, lower strains were detected on the panel skin/stringer/frame from nonlinear analysis, resembling a softening effect to a panel in axial load. Results from nonlinear analysis showed that the critical tension strain was 2,250 micro-in./in. near the impact damage site in the 5.0-g maneuver condition. This strain was within the notched design strain value of 5,900 micro-in./in. for the skin. The calculated margin of safety was 162%, which indicated that a failure of the skin at exterior impact site no. 3 of the center keel on the MBB was unlikely to occur at 5.0-g maneuver load.

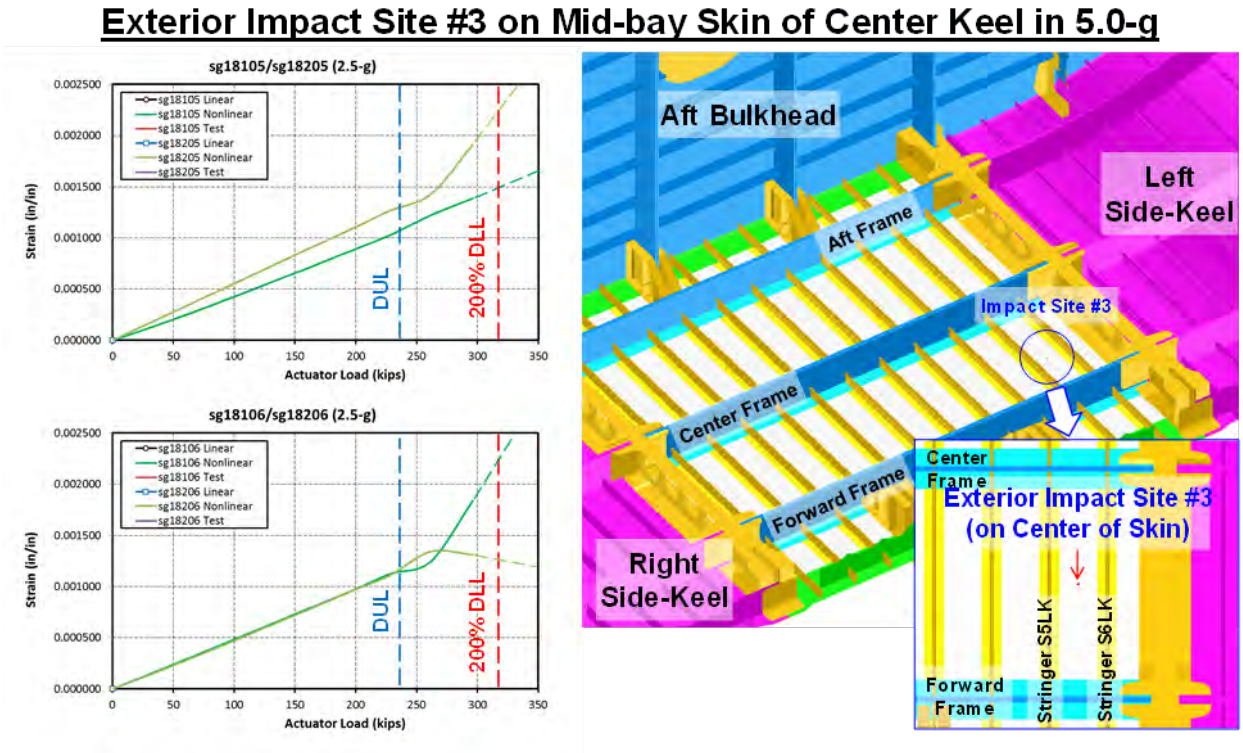

Figure 4-194. Strains on Exterior Impact Site no. 3 in 5.0-g Condition

5.0 TOOL DESIGN AND FABRICATION

The tool design effort represented one of the most challenging aspects of the MBB program because it not only required the fabrication of larger and more dimensionally accurate toolsets than previously built, it also needed to accommodate the higher levels of panel complexity that continued to evolve as novel composite joining techniques were engineered for the first time. This, in turn, required a continuous flow of new tooling ideas and feature incorporation, which took place as the toolsets were being designed, fabricated, and eventually assembled to support first-article fabrication. As changes rippled through the design cycle, punishing cost growth and schedule slips were experienced because the initial tools had to be reworked numerous times before they could finally be used to build parts.

Fortunately, once these tooling issues were resolved, the tools performed exactly as expected and capably produced high-quality integrated PRSEUS structures. These panels demonstrated the production-like processing schemes and design tolerances necessary to meet the respective Technology Readiness Level (TRL) and Manufacturing Readiness Level (MRL) goals established for the program. This was one of the most important aspects of the project because it demonstrated that high-quality parts could be built with lower recurring fabrication costs. This critical discriminator is vital for any new composite technology implementation decision, and even more so for an unconventional airplane geometry such as the HWB.

5.1 Tooling Commonality Design Scheme

Two primary toolsets were used to construct the PRSEUS panels. First, a stitching fixture was used to hold the dry fabric in position during the stitching operation, and then a rigid mold tool was used to support the dry stitched preform during the resin-infusion and cure operations. Key steps in building a PRSEUS panel are shown in Figure 5-1. The photographs on the left side of the figure show the preform assembly and stitching steps, and the photographs on the right show the key resin-infusion and cure tool steps.

Figure 5-1. Preform Assembly and Cure Tooling Are Primary Toolsets for Panel Fabrication

Because each unique panel configuration required an individual stitching and cure tool setup to locate and form detail shapes, it quickly became apparent that any large stiffened panel geometry would have a relatively high tooling cost associated with it, and especially so for a single-unit test article. Although this situation may be acceptable for a nominal production run, wherein nonrecurring costs can be amortized over many units, these high initial tooling costs are difficult to accept for single-unit research programs. To help address this problem, a decision was made to use flat surfaces that would approximate the slightly contoured loft surfaces of the

HWB airplane configuration to reduce machining costs for the tools. Additionally, these flat surfaces would also enable a commonality design scheme. This approach enabled multiple panels to be fabricated from common toolsets that incorporated interchangeable sets of tooling details, which would accommodate the unique aspects of each panel's configuration. Although this commonality scheme reduced the upfront tooling costs for the program, it nevertheless also exacerbated schedule delays during the tool checkout and setup phases. The shared details reduced the flexibility to rework parts because the linked details forced the rework efforts to be done sequentially rather than in a more efficient parallel manner.

Once the decision to use a flat loft was made, a common stitching table and common cure table were designed and fabricated with a series of interchangeable tooling details for each panel. All PRSEUS panels were fabricated using this basic approach, just as it was conceptually described in the original proposal (Figure 5-2). Although this approach worked relatively well, the overall level of tool reuse originally envisioned at program outset was not completely realized in practice. Primarily, the problem was due to the difficulty of maintaining configuration control over each tooling package from one panel to the next. This resulted in less reuse and, ultimately, higher tooling costs as the tool designers unknowingly designed identical tooling details for subsequent panels. Although it was physically possible to attain such a level of configuration control, a lesson learned from this effort was that the means to manage such a complex tool design scheme within an R&D organization was likely not entirely feasible and should be avoided in the future.

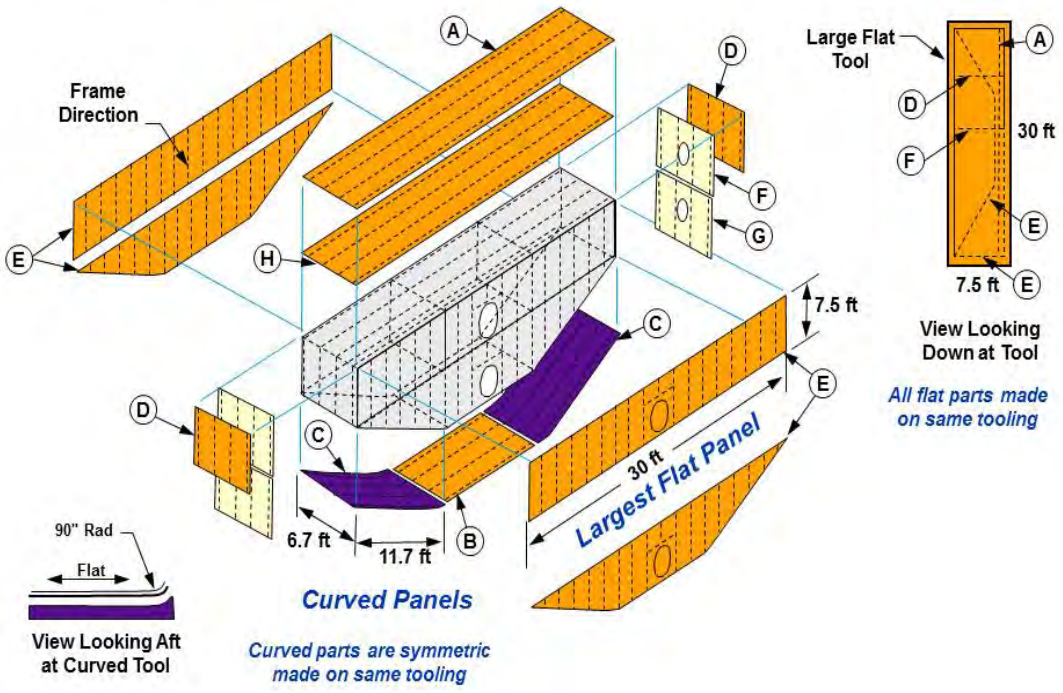

Figure 5-2. Tooling Commonality Was Emphasized to Reduce Overall Program Cost

In addition to the model design and configuration-control aspects of the effort, there were two primary technical challenges in building the 11 PRSEUS panels on a common toolset: (1) the first was the changing orientation of the frames and stringers, which alternated between the longitudinal and transverse panel directions, and (2) the second was molding the curved ends of the keel panels. In both cases, these design challenges were easily accommodated by the modular tooling techniques planned at the outset of the program. Ultimately, this approach demonstrated how the versatility and dimensional accuracy could be achieved by indexing part features to a common OML tool, which resulted in integrated composite panels that were easily assembled to one another using substantially fewer fasteners and fittings than conventional design practices.

5.2 Preform Assembly Tools

The preform assembly fixture, or stitching tool, consisted of two main elements: (1) a common support table with a series of precision-drilled holes that were used for indexing the foam blocks, and (2) the actual sets of foam blocks that support, shape, and locate the dry fabric details that hold the skin, stringers, frames, and cap elements for the preform stitching operations. The common support table (Figure 5-3) was a conventional welded steel construction with indexing features positioned at the corners. This enabled the table to be accurately repositioned relative to the stitching head rail system each time it was moved to deliver the preform to the cure tool. Additionally, the table was relatively rigid to limit deflections during the preform rotation step (pictured in the upper left corner of Figure 5-3) to ensure that the preform did not deform or change position as it was being lowered onto the cure tool. Table design and fabrication were straightforward exercises, despite some minor rework required to increase the table bending stiffness. (The only major challenge was to ensure that the numerous locating holes through the flat surface would not interfere with one another for each different panel configuration.)

Figure 5-3. Common Stitching Table Used to Support Different Foam Block Configurations

Conversely, design of the foam blocks turned out to be much more difficult than originally anticipated. Unlike the smaller test panels that were used on prior projects, the complexity of the airplane-like geometry of the MBB included numerous skin buildups and corner joints that converged in the corners to create complex 3D modeling problems for the tool designers to surmount. This problem was further complicated by the difference between the as-cured part model (defined by design engineering) and the thicker dry fabric bulk preform model (defined by the tool design engineer). Making the transformation between these two model geometries proved to be too difficult, and it resulted in foam block modeling efforts that were in excess of four times the original estimates included in the program plan. However, once the models were completed and the data released to a local machining vendor, the blocks were readily machined and delivered to Boeing, where they were placed in storage until needed to assemble the panel preforms (Figure 5-4).

Figure 5-4. Foam Block Fabrication and End Use on Stitching Table

A key feature of the improved block design was the new one-piece, wooden “picture-frame” element (Figure 5-5). Unlike previous block designs, wherein individual dropout rail members were used to ensure the release of the stringer bulb feature during tool removal, the new unified picture-frame design was used instead to reduce the number of tool pieces that would have to be tracked and located for the large number of preforms. Ultimately, this approach worked well as it properly supported the preforms during stitching, as well as when the blocks were removed after the preform was laid onto the cure tool. The inherent flexibility of the stitched preform assembly, coupled with the satin finish (or absence of tack) of the dry fabric, easily permitted the slightly larger one-piece frame member to be withdrawn from the slightly smaller preform opening, as illustrated in the lower right corner of Figure 5-5.

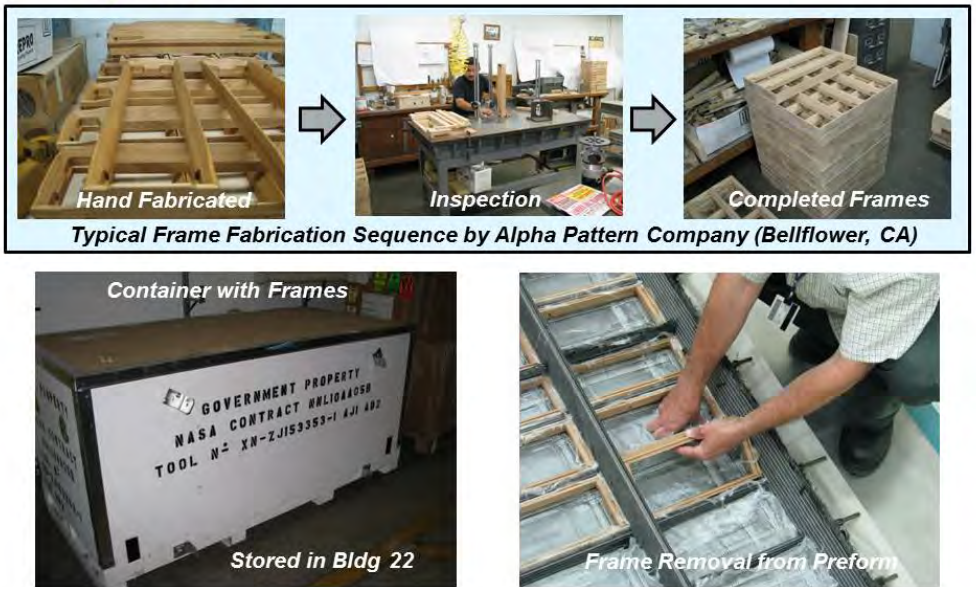

Figure 5-5. Wooden Stitching Frame Fabrication and End Use Removal from Preform

The ease with which the wooden picture frames could be removed from the stitched preform was unexpected, and it ultimately led to further improvements in the block design that were thought to be physically impossible at the outset of the program. With a newfound appreciation of the preform flexibility, and the ability to easily slide rod members in and out to increase the side-to-side clearance, it was discovered that the two-piece block design was not necessary and that a one-piece foam block design (as depicted by the red outline shape shown in Figure 5-6) would be sufficient. This change was made to the final stitching tool that was used for the center keel panel, and it resulted in a one-piece foam block design that worked well during the stitching operations and yet also easily released from the trapped position within the preform.

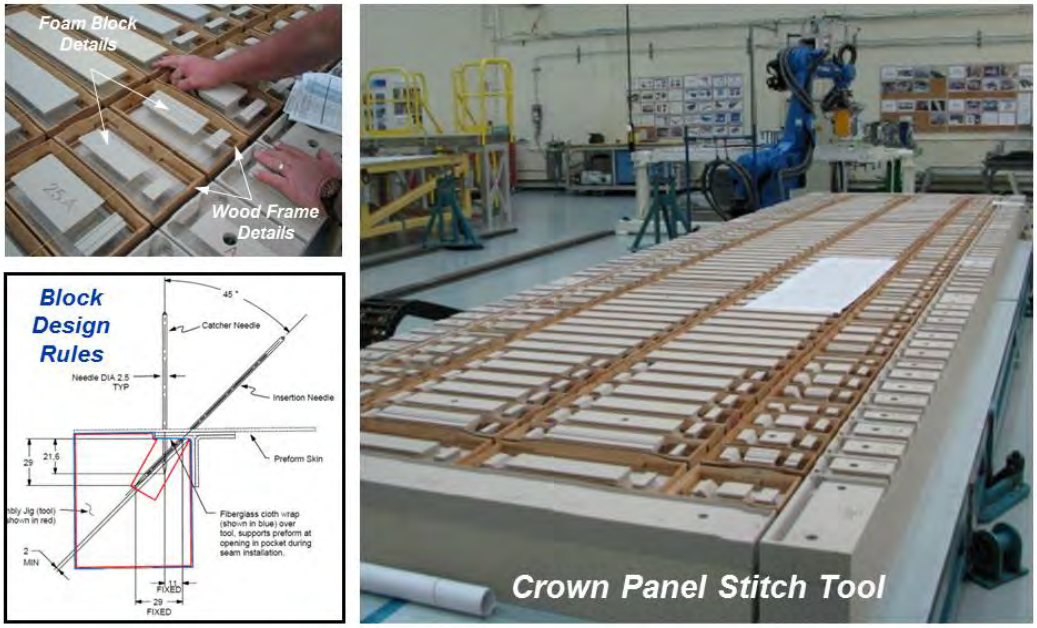

Figure 5-6. Crown Panel Stitch Tool Design Approach and Checkout

Once the stitching tools were checked out and reworked to eliminate the block design errors, the tools performed trouble free. This was particularly noteworthy in build sequences involving multiple panels being fabricated on the same tool setup (one for the left-hand and right-hand units) because it clearly demonstrated how rapidly the tool could be reassembled and readied for the next preform. From the first panel stitched (the crown panel shown in Figure 5-7) to the final lower keel panel, all preform assembly and stitching operations went as expected without any further complications introduced by the stitching tools.

This basic tooling arrangement was repeated six times for each of the unique PRSEUS panel configurations (not counting left-hand and right-hand panels twice). Compared to the initial crown panel design, the differences for subsequent tools (Figure 8) primarily involved changes to frame and stringer orientations, as well as the addition of the curved segment on the outboard keel panels. All of these changes were planned from the beginning to be accommodated by the reconfigured sets of foam blocks indexed to the common hole pattern drilled in the support table. In general, this approach worked well and accomplished its primary objective of reducing the upfront tooling acquisition costs. The only negative aspect of this approach was that the sharing of common tooling details undeniably limited the flexibility to uncover tool design problems during setup. This was because it forced each toolset to be inspected sequentially rather than in a more efficient parallel manner.

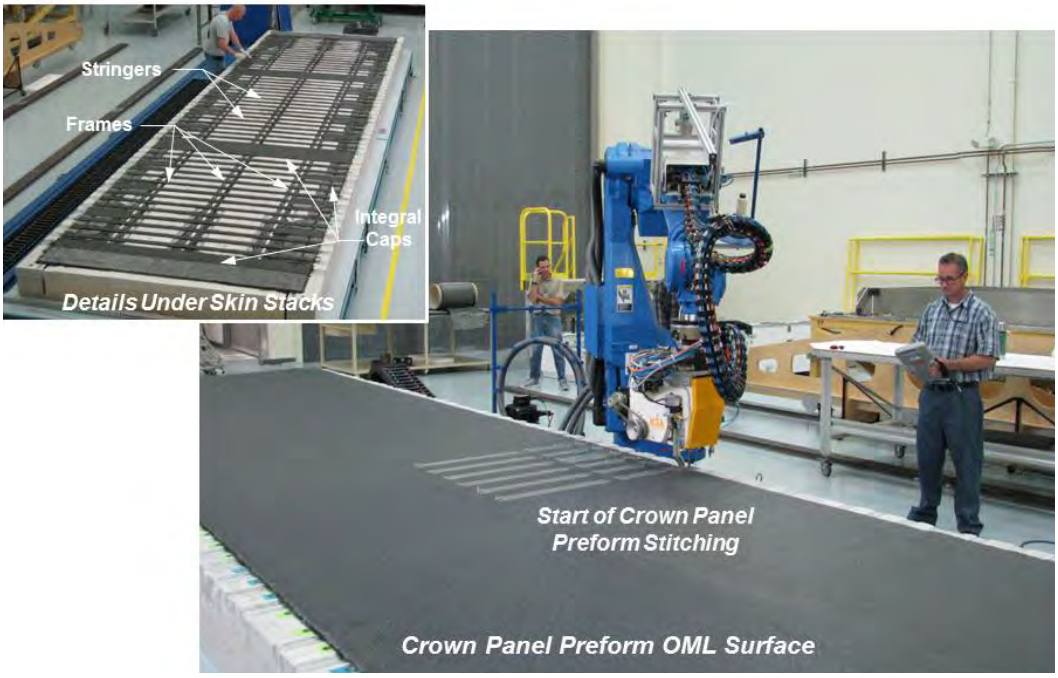

Figure 5-7. Initial Seam Laydown on First Panel Stitched (Crown Panel)

Figure 5-8. Multiple Block Configurations Shown on Common Stitching Table

5.3 Panel Cure Tools

Cure tooling also used the same commonality approach as that used for the stitching tools; however, because the toolset was constructed of Invar material, the overall cost savings to program was even greater. The justification for procuring the more expensive but highly thermally compliant Invar tooling was based on the fact that 11 panels would be fabricated on the common cure table. Another benefit of the Invar tooling was that the dimensional stability enabled more accurate control of the integral cap station planes, which would ultimately define the tolerances between the adjacent panels during final assembly.

The common cure table (Figure 5-9) was fabricated by a local tooling vendor using a conventional welded Invar steel construction approach. The table consisted of a nominal 0.50-in.-thick plate supported by a rolling 4- by 4-in.-square tube-welded support structure. A shallow grid system was machined into the plate surface to deliver resin to the preform OML, which would be fed by a collection of disposable Teflon lines and brass quick-disconnect valves that were secured to the edges as well as underneath the table.

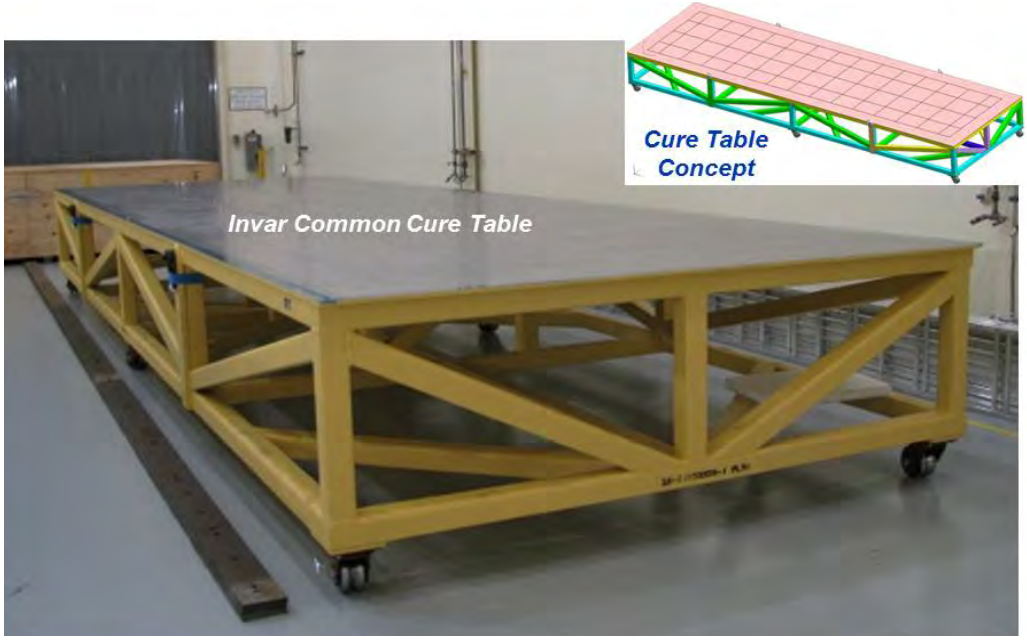

Figure 5-9. Common Cure Table Used to Support Different IML Tooling Arrangements

The dimensionally critical features of the panels were molded by under-bag tooling details that were indexed to the common hole pattern drilled into the cure table surface (Figure 5-10). Although this same basic tooling approach was used successfully to build the 4-ft-long cube specimen panels, the scale-up to 30-ft-long panels was expected to be challenging. Those concerns were quickly realized during the plate rigging and inspection signoff on the first cure tool at the vendor's site. During the dimensional checks, it was evident that the large end-supported plate members were sagging and bowing out-of-plane due to their mass, which had not occurred on the smaller cure tools. To resolve this problem, the end supports were changed and a stiffener member (as shown in the lower right photograph in Figure 5-10) was added to each of the longer plate members. These changes resolved the problems, and the tools could then be assembled to meet the stringent dimensional tolerances required for the rib station plane surfaces that would be molded by the plates.

Figure 5-10. IML Details Rigged and Checked Out on Common Cure Table

Some of the critical interfaces established by the IML tooling are shown in Figure 5-11. Generally, all frames and stringers at panel edges that would interface with an adjacent panel had to be molded by a rigid tooling detail, which was indexed to the cure tool mold surface.

Figure 5-11. IML Tooling Details Assembled Onto Preform

The other key features that were molded by a hard-tooled surface were the up-standing integral cap stacks that formed the cap leg for adjacent bulkhead and/or rib panels to attach to. These plates are clearly visible in Figure 5-12 as they extend beyond the preform edges to provide room for bolting on the end support details. In the photograph, the fully tooled crown panel preform is shown before installation of the vacuum bag.

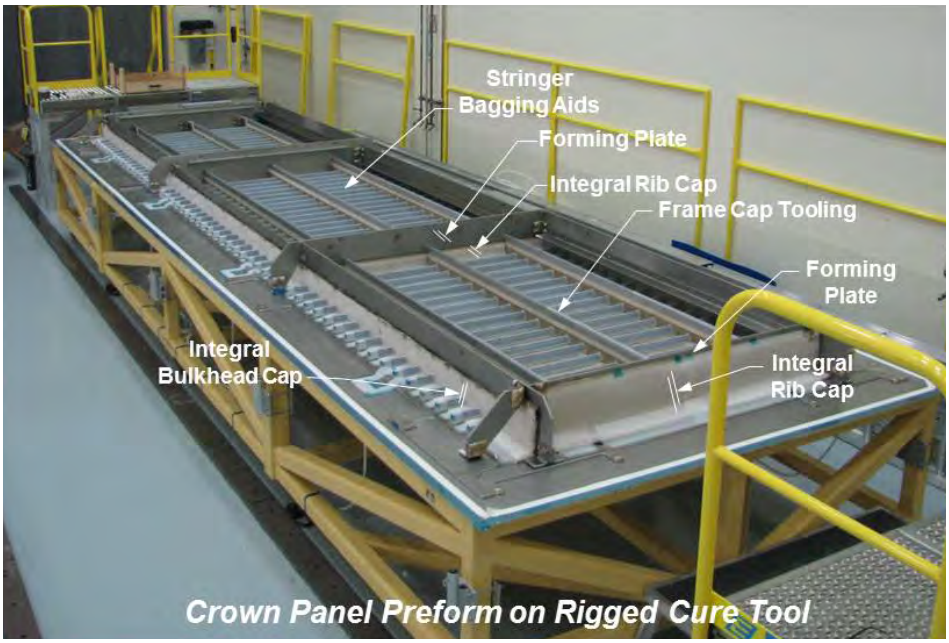

Figure 5-12. IML Tooling Details Positioned Over Preform

Although the crown panel tooling was the most complex, this basic tooling approach was repeated five more times for each of the unique PRSEUS panel configurations (not counting left-hand and right-hand panels twice). Once the initial scale-up issues were resolved, the challenges of changing stiffener orientations and panel curvature were easily overcome (Figure 5-13).

Figure 5-13. Multiple Panel Configurations Built on the Common Cure Tool

Figure 5-14 shows the pleated vacuum bag placed over the rib panel tools on the left, and the completed panel is shown on the right after resin infusion and cure. Although under-bag tooling seems to be relatively complex, the capability to remove a near-finished, fastener-less, and integrally stiffened panel geometry from the oven justified the added investment in tooling and panel preparation to eliminate downstream drill-and-fill operations, which are typical of conventionally built-up panel constructions.

Figure 5-14. Rib Panel Shown Under Vacuum Before Infusion and After Cure

5.4 Multi-bay Box Assembly Tool

Although a determinant self-tooling method of joining panels was planned from the outset, there were initial concerns that the large weight and panel size might adversely affect the overall dimensional stability of the assembly process. To address this concern, a rigid steel tool fixture (Figure 5-15) was designed and fabricated with locating features that would positively position the majority of the panels. The design also encompassed translating rails to facilitate panel repositioning, which enabled drill chips and debris to be easily cleaned from the interfaces before final fastener installation.

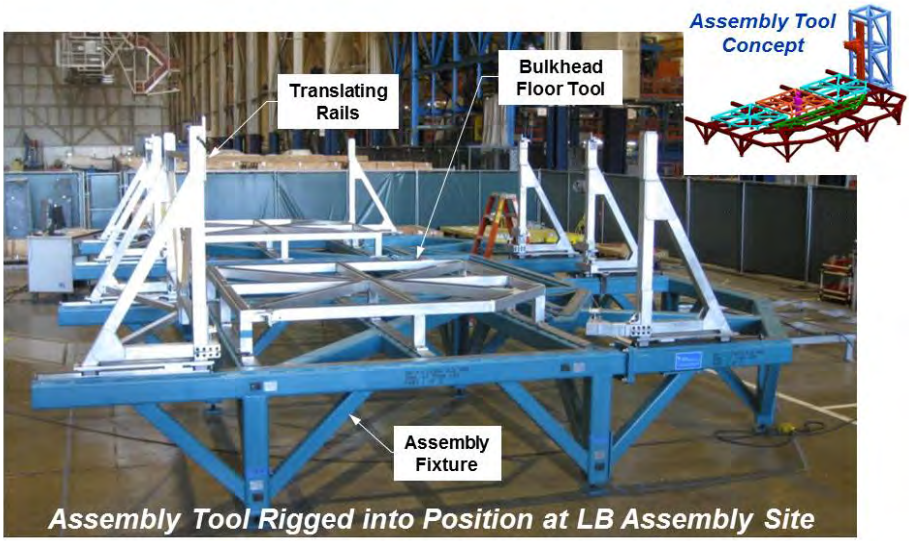

Figure 5-15. Multi-bay Box Assembly Tool Before Panel Installation

Another key aspect of the design was placing the MBB on its side, which expedited entering and exiting the two-deck arrangement until after the lower keel panel was permanently attached. This approach also helped improve hole-drilling ergonomics for the mechanics by lowering the overall height of the structure during assembly. Once all panels were securely fastened, the entire structure was then rotated into the vertical position where more limited access was gained through holes in the bulkheads. The other prominent feature of the assembly jig was the incorporation of a milling tower structure that was designed to support a portable milling machine apparatus. This device would be used to machine tight-tolerance parallel end planes on the fully assembled structure.

All aspects of the assembly tool worked as planned, and only a few minor adjustments were needed as the panels came together. By far, the biggest challenge for the assembly tooling was the final step when the end machining took place to create the finished planar surfaces that would slide in between the COLTS loading platens. Once the milling tower was secured to the shop floor and dimensionally inspected with laser tracking equipment, the actual material removal was started. The tower structure was a rigid, vibration-free restraint system that worked well as multiple machining passes were made. Each pass was checked using the laser tracking system to ensure that final tolerances were being achieved (Figure 5-16). After the final length and planar dimensions were achieved on each end, the leased portable milling system was returned to the vendor and the milling tower was returned to storage.

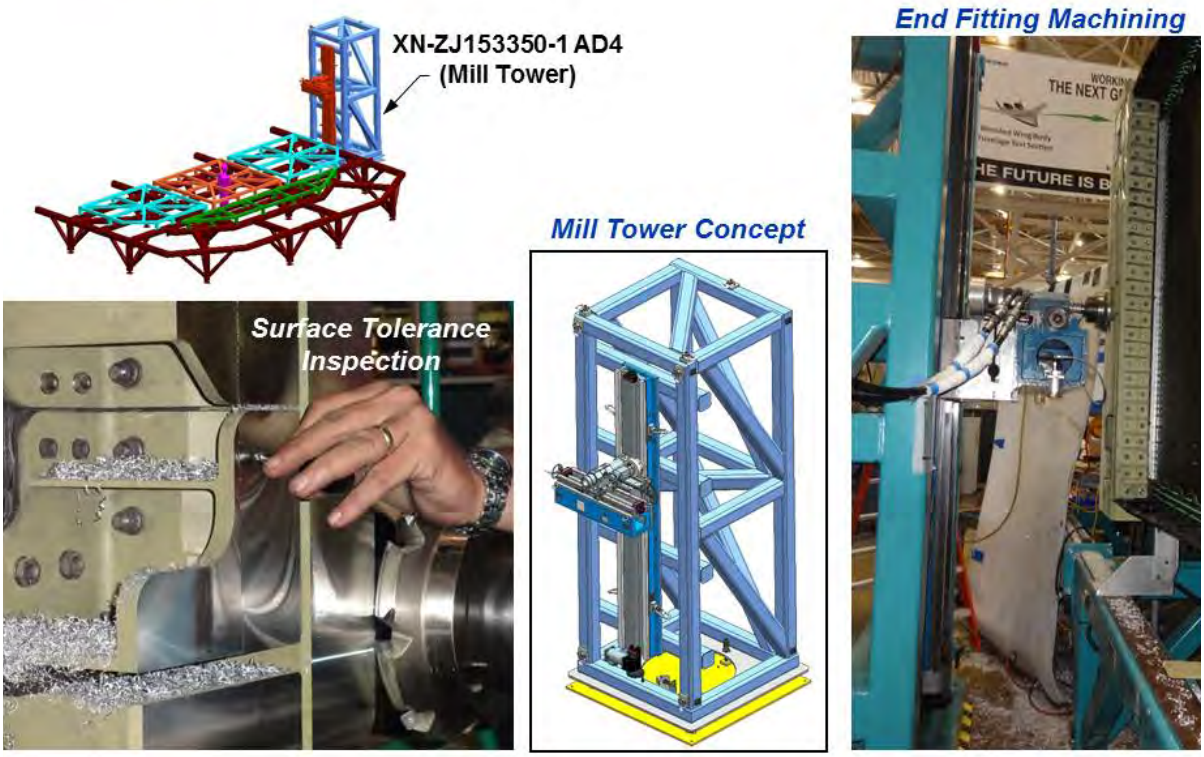

Figure 5-16. Milling Tower Concept and Machining Approach

Smaller ancillary toolsets were also required to support panel assembly operations. Adjustable struts (Figure 5-17) were fabricated to help position rib members, a multi-element floor-protection system (Figure 5-18) was used to provide protection from tool drops and foot traffic during assembly, and a lift-beam assembly (Figure 5-19) was designed that could move anything from an individual panel to the entire completed MBB.

Figure 5-17. Holding Aids Used to Support Internal Ribs During Assembly

Figure 5-18. Floor Protection Pads Used During Box Assembly

Figure 5-19. Custom Lift Beams Fabricated to Support MBB and Panel Transfer

6.0 TEST ARTICLE FABRICATION

6.1 Panel Fabrication

This section describes the innovative manufacturing approach that was used to build PRSEUS panel assemblies. The description is included in this report for completeness, although most of the panel fabrication work was done under contract NNL13AA11C and TO NNL13AB38T (Refs. 6-1 and 6-2).Dry, near-net-shape, 3D preforms for these highly integrated panels were produced from carbon-fiber multi-axial warp-knit fabric. Flat patterns of material were cut, folded, formed, stitched, and/or stapled to create separate preform details. Rigid closed-cell foam core material and pultruded carbon-fiber epoxy rods, utilized for frame and stringer structural elements, also served as tooling to support the soft dry fabric construction during subsequent resin-infusion processing. Final assembly of the panel preform occurred on a jig, whereby a robotic stitching system was used to structurally join stringer, frame, and cap components to the base skin. Infusion of the preform with an amine-cured epoxy-resin system produced a unitized monolithic structure, which was cured in an oven using the Boeing Controlled Atmospheric Pressure Resin Infusion (CAPRI) process.

6.1.1 Materials

Multi-Axial Warp-Knit Carbon-Fiber Fabric

The PRSEUS concept arose from the need to significantly improve the structural efficiency and lower the manufacturing cost of a composite primary structure for large transport aircraft. To achieve these objectives, a departure from conventional prepreg materials and the associated manufacturing processes developed for those materials during the last 40 years was required. The fundamental idea behind the PRSEUS concept is that non-impregnated dry fabric can be cut, formed, shaped, and assembled into a complete structure with less effort, and with a higher level of structural integration than would otherwise be possible with pre-impregnated materials. This approach begins with the use of multi-axial carbon-fiber warp-knit fabric, also known as Non-Crimp Fabric (NCF). This material form was conceived in the 1970s to automate the layup of carbon-fiber tow into a preassembled stack consisting of individual material layers orientated in the 0, +45, -45, and 90-deg conventional directions typically used in composite laminates. As shown in Figure 6-1, the layers are straight in-plane, stacked on top of one another, and not woven. They are held together with stitching to provide the performance of a tape product with the benefit of reduced layup time in the factory. For the HWB fuselage section, an NCF equivalent to nine layers of tape with a total fiber areal weight of 1,425 gsm was used. The fabric was produced by Saertex in Germany using standard modulus carbon fiber and delivered in roll widths of 55-in. and 99-in.

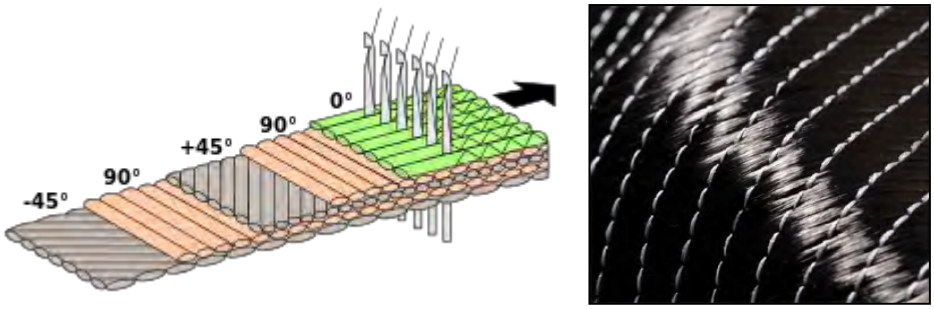

Figure 6-1. Multi-Axial Warp-Knit Fabric Construction

Closed-Cell Foam Core

Rohacell WF110 closed-cell foam was used as a core material in the fuselage frames. The 6.6-lb/ft^3 density foam was furnished by Evonik Foams, Inc. in blanks measuring 1.0 in. thick by 8.0 in. wide by 8 ft long. Because the foam has a propensity to grow with a change in moisture content, Boeing established a strict handling procedure for it. The blanks were first conditioned for several weeks in the relative humidity environment of the clean room where fabrication of the dry fiber preforms for the structural panels occurred. Once saturated, the foam was then hermetically sealed in foil vacuum bags and shipped back to the supplier for Numerical Control (NC) machining to final-net-shape dimensions. After machining was completed, the foam was then placed back inside the foil vacuum bag, sealed, and returned to Boeing for incorporation into the fuselage frames. This procedure proved successful on prior applications with core sections measuring up to 28 ft long.

Unfortunately, the proper handling and machining procedures were not adequately followed on this project. Dimensional changes in the core assembly up to 6 mm in length were discovered after several days of exposure to the relative humidity environment of the clean room. Root cause analysis determined that the core was not fully saturated prior to NC machining. To bring the core assembly back into dimensional compliance with the engineering tolerances, the core was sectioned at multiple locations and then bonded back together to adjust cutout feature spacing in the frame core assembly. NC-machined, solid fiberglass/epoxy laminate sections were used at highly loaded bolted joint locations. Small doublers cut from NCF material were positioned around the stringer keyhole features in the crown and center keel panels, as shown in Figure 6-2.

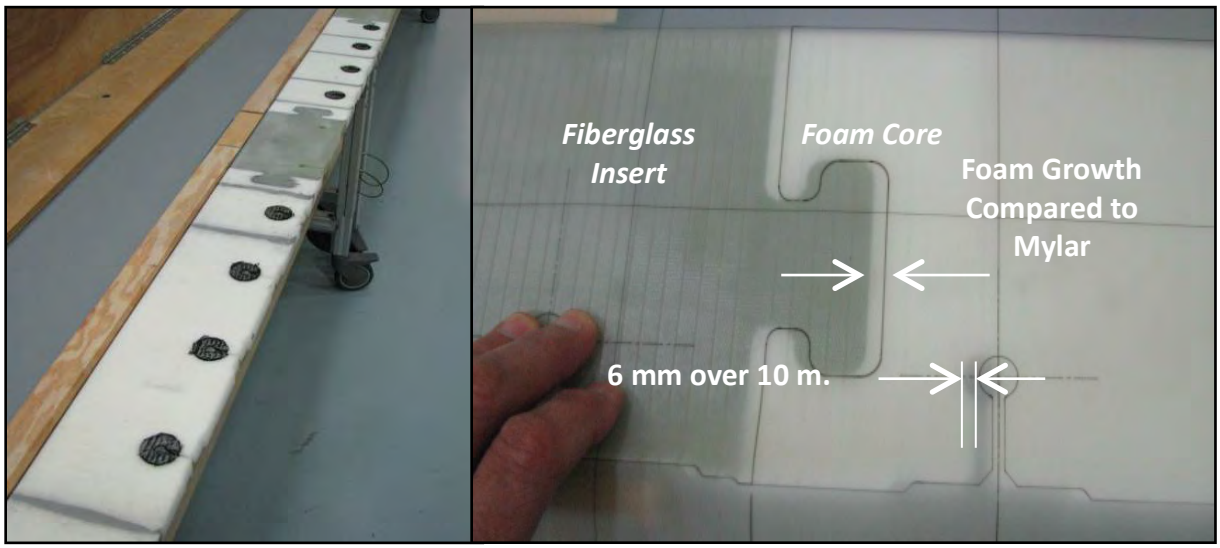

Figure 6-2. Frame Core Assembly and Associated Growth due to Change in Moisture Content

Pultruded Carbon-Fiber-Epoxy Rods

Pultruded rods for the bulb-shaped stringers were fabricated by Lawrie Technologies Inc. using standard modulus carbon fiber and Applied Poleramic, Inc. PUL6 amine-cured epoxy resin. A precision-ground steel mold die was used to produce the specified cross-section, which contained an integral fillet feature at the base of a primarily circular geometry, as shown in Figure 6-3. The rods were furnished in a cured condition and in lengths up to 30 ft. Once received, the rods were post-cured at 350°F for 2 hours and then cut to length. The fillet feature was ground off at the ends to accommodate installation of the rod into mold tool blocks during the resin-infusion process of the entire panel. One end of the rod was drilled and tapped to attach a leader wire, which was used during installation of the rod into the stringer preform. The outer surface of the rod was grit-blasted and rinsed with deionized water to prepare the surface for bonding with the epoxy resin during infusion processing of the panel. Water break testing was performed to verify that a bondable surface had been achieved, and the rods were then dried in an oven to remove any moisture uptake from the surface-preparation operation.

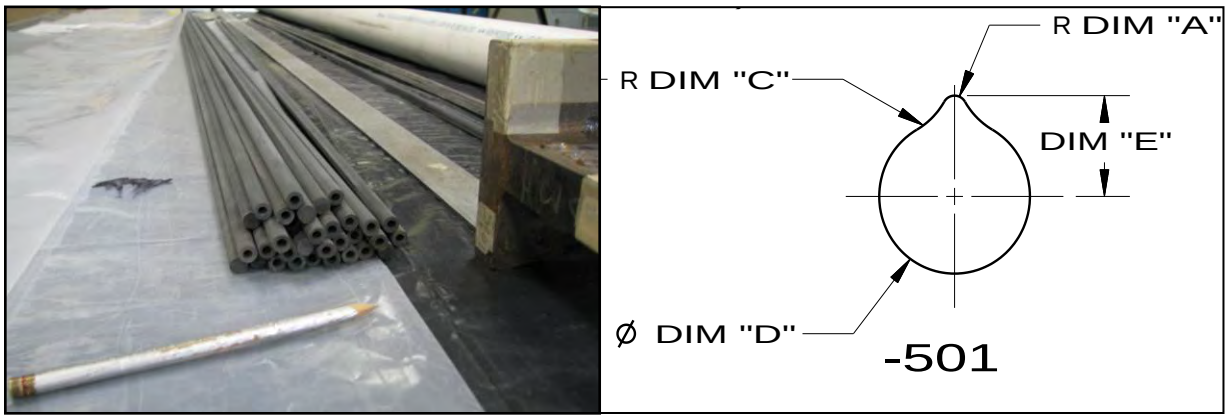

Figure 6-3. Prepared Pultruded Carbon-Fiber Epoxy Rods Shown With Section View

Sewing Thread

Vectran sewing thread was used for assembling the dry fiber preforms and to provide out-of-plane structural reinforcement at critical interfaces between the skin, stringer, frame, rib cap, and bulkhead cap elements of the panel. The sewing thread was manufactured by Saunders Thread Company in 1,200-denier and 1,600-denier sizes. The thread was constructed from multiple ends of twisted 400-denier yarn, which was brought together using a plied twist in the opposite direction. A nylon resin was then applied and cured to bond the multi-filament twisted thread into a unified product. The sewing thread performed extremely well in both the lock-stitch gantry sewing machine and one-sided robotic stitching end effector used for panel preform fabrication.

Epoxy-Resin System and Associated Cure Cycle

A Hexcel Hexflow VRM34 resin system was used for resin-infusion processing of the dry fiber preform assembly. The system is a two-part amine-cured epoxy that is a liquid at room temperature. This particular resin system is currently used in production at Boeing and was supplied in 5-gal kits. The resin system was infused into the preform at 140°F and then cured at 200°F for 5 hr. Upon completion of initial cure, the part was cooled to room temperature, and the vacuum bag and inner mold line tooling were removed. The panel was then post-cured at 350°F for 2 hr in a freestanding condition.

6.1.2 Preform Component Fabrication

Stringer Preforms

The PRSEUS design utilized a bulb-shaped stringer cross-section with a varying flange width and localized buildups dependent on stringer location on the panel. Stringer preforms were fabricated using 55-in.-wide carbon-fiber multi-axial warp-knit fabric of a seven-layer construction and having a total fiber areal weight of 1,425 gsm. Net-sized flat patterns were created and nested to optimize material utilization. A Computer Numerically Controlled (CNC) ply-cutting table was used to cut the flat patterns from the wide fabric, as shown in Figure 6-4. Base stack material along with doubler plies were laid out flat onto a table surface. The doubler plies were secured to the base stack material using tack stitches inserted by hand. A stainless-steel twisted wire cable was placed down the centerline of the layup. The flat layup was then folded over upon itself along the centerline to capture the cable. The cable facilitated the installation of the pultruded rods to form the bulb feature of the stringer during final assembly of the entire panel preform.

Binder clips secured the folded material assembly as it was positioned by hand inside a holding jig. As shown in Figure 6-5, the jig was located inside a gantry-type stitching machine, wherein seams of stitching were inserted into the web of the stringer. A lock stitch was used with 1,200-denier Vectran sewing thread to meet engineering strength requirements. A single seam of stitching was inserted near the fold line to create the bulb feature of the stringer. A second seam was installed at the tangent point for the web-to-flange radius. With the bulb feature still in the collapsed position and the flanges yet to be formed, the stitched stringer preform was then placed inside a sealed polyethylene vacuum bag and forwarded to the panel preform assembly jig.

Figure 6-4. Stringer Nested Flat Patterns and Folding of Stringer Ply Stacks

Figure 6-5. Stitching of Stringer Preform Web Shown With Vacuum-Bagged Stringer Preforms

Rib and Bulkhead Cap Preforms

Structural panels for the MBB contained integrated rib and bulkhead cap elements of a "*T*" type cross-section (referred to as T-caps), with the flat web section oriented according to the mating rib or bulkhead panel direction. Bulkhead and rib cap preforms were fabricated using a similar approach to that used for the stringer preforms. One exception was that the NCF ply stacks for the cap were not folded over but rather laid up and stitched in the flat condition, as shown in Figure 6-6. As was the case with the stringer preforms, the flat patterns for the cap plies were cut on a CNC ply-cutting table to net size (i.e., no manufacturing trim), and they included stringer keyhole features. The web feature of the cap received multiple parallel rows of stitching over the entire surface, bound at the bottom by the tangent point of the web-to-flange radius. As shown in Figure 6-7, ply stacks for the flanges were typically extended at discrete locations for interleaving with the adjacent frame and/or cap flange ply stacks during final assembly of the entire panel preform.

Figure 6-6. Stitching of Bulkhead Cap Preform Shown With Net-Size Features

Figure 6-7. Complete Bulkhead Cap Preform for Crown Panel With Extended Flange Stacks

Frame Preforms

As noted in Section 6.1.1, frames for the PRSEUS panel were of a sandwich-type design, which utilized a closed-cell foam core. The core contained “keyhole” features to accept the bulb-shaped stringer components. Vertical grooves were machined into the face of the core to assist resin-infusion processing of the frame web. Once again, net-sized flat patterns were cut from NCF fabric and positioned over the core assembly, lining up the keyhole features in the fabric with the corresponding features in the core. A pneumatic gun was then used to insert thin wire stainless-steel staples into the NCF fabric, securing it to the foam core. The core with fabric attached was then flipped, placing the fabric down against the table surface with the foam core facing up. Next, the free edge of the fabric plies were wrapped over the top of the core and hand worked down into position while lining up the keyhole features in the fabric and core, as shown in Figure 6-8. Staples were inserted into the opposite face of the frame web, which completed the fabrication of the frame preform assembly. The completed frame preforms were then placed inside sealed polyethylene vacuum bags for installation into the panel preform assembly jig.

Figure 6-8. Layup and Subsequent Stapling of Fabric to Foam Core for Frame Component

6.1.3 Preform Assembly and Stitching

Preform Assembly Jig

A jig was used for assembling the stringer, frame, cap, and skin components into a complete near-net-shaped 3D preform for each panel. The jig consisted of Inner Mold Line (IML) tooling details pinned and bolted to a welded steel base platform that was located in the robotic stitching cell (shown in Figure 6-9). CNC-machined, 10-lb/ft^3 urethane foam blocks and small wooden "picture-frame" components supported and positioned the separate frame, cap, stringer, and skin details relative to one another. Cavities incorporated into the design of the IML tool enabled one-sided stitching of stringer, frame, and cap flanges to the base skin. The sewing needles penetrated through the thickness of the preform and exited the bottom surface of the material into the tool channel, where the sewing thread loop was formed and subsequently captured by the hook on the catcher needle. The foam blocks and wood picture frames were wrapped with a lightweight fiberglass cloth to support the soft carbon fabric during installation of the flange-to-skin seams of stitching. On subsequent panels, the jig was sized to accommodate the accumulative bulk of the preform with respect to the stitching plane. The wood stitching frames were incorporated into the design of the jig as a cost-reduction measure. It was originally believed that using wood frames would take less effort to design, fabricate, and use than would fully machined foam blocks; however, that assumption was incorrect. Future preform assembly jig designs will use the fully machined foam blocks exclusively (Figure 6-9).

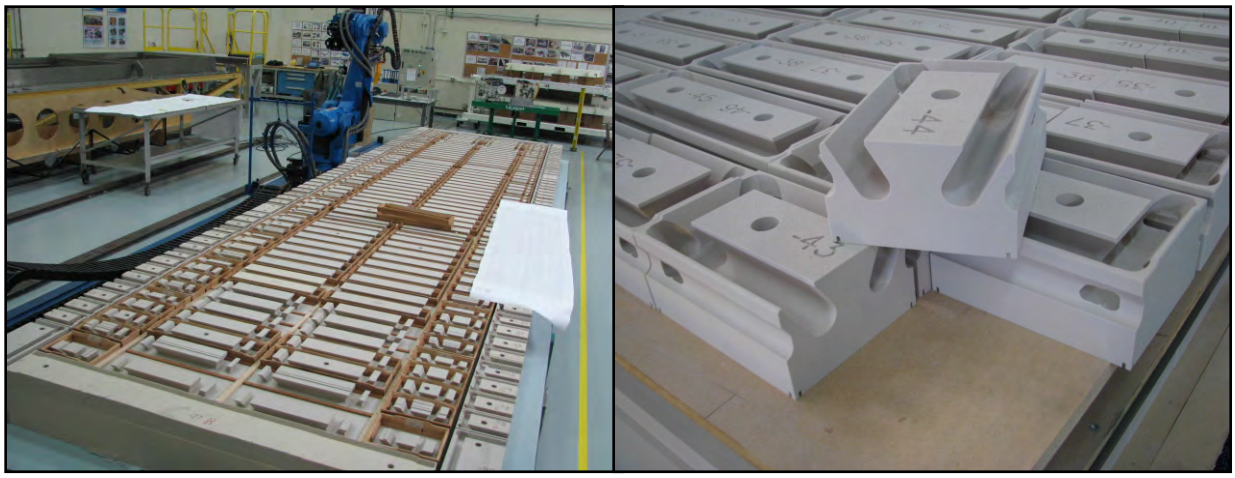

Figure 6-9. Preform Assembly Jig for Crown Panel Utilized Machined Foam IML Tool Blocks

Installation of Preform Components and Skin Layup

Assembly of the panel preform began with the installation of the frames. A vacuum was pulled on the preform details inside the sealed polyethylene bags to remove bulk before installation into the jig. The frame preforms were installed into the jig while still under vacuum inside the polyethylene bag and with the web of the frame pointing down, as shown in Figure 6-10. Once installed, the vacuum bag was then removed from the frame preform by slitting the bag open on one end and pulling it off from the other end. Rib and bulkhead cap performs were installed next, depending on the interleaving sequence of the respective flange stacks. The stringer preforms were installed using a similar approach, with the collapsed web being inserted into the keyhole feature of the frame foam core detail and bulkhead cap web, as shown in Figure 6-10, and the flanges of the frame and cap preforms were then folded down against the tool surface, as shown in Figure 6-11. Three-dimensional woven fillets were installed at the base of the cap web and tack-stitched down the length of the cap to hold them in place. Because the frame foam cores were machined with an integral fillet feature, a separate carbon-fiber fillet detail was not required.

The pultruded rod was then attached to the end of the twisted steel wire cable located inside the top of the stringer web using a specially designed adapter (Figure 6-11). Next, the rod was installed into the stringer by pulling on the steel cable and pushing on the rod. This subsequently formed the bulb feature of the stringer and locked the stringer into the frame foam core as the rod passed through the preform. The stringer flanges were then folded down against the tool and 3D woven fillets were installed at the base of the stringer web, as shown in Figure 6-12. Tear straps were laid up over the formed flanges of the frame and stringers. Skin ply stacks were then laid up over the tear straps and cap flanges (Figure 6-12.)

Figure 6-10. Installation of Frame (left) and Stringer (right) Preform Details Into Assembly Jig

Figure 6-11. Forming of Cap and Frame Flanges (left), Carbon Rod With Leader Wire Adapter (right)

Figure 6-12. Rod and Fillet Installation (left) and Skin Layup Under Progress (right)

Robotic Stitching

A KSL/KSA RS535 one-sided stitching end effector was used to install the modified 3D chain-stitch seams required for final panel preform assembly. The end effector was attached to a Motoman UP130 arm that was mounted on the base axis rail. A unique NC program was created offline for each seam of stitching. These programs were structured using multiple segments with stitching speed, stitch pitch, and material thickness information defined for each segment. Programming of the actual stitching seam path motion was performed using a Tool Center Point (TCP) probe attached to the end of the needle bar on the end effector, as shown in Figure 6-13. Go-to points were taught by touching the preform assembly fixture with the probe at discrete locations, which defined the start and end points for a given stitching seam segment. Stringer flange-to-skin seams were installed first, working from the center of the panel outward (Figure 6-13 and Figure 6-14.) Cap flange-to-skin seams were installed next followed by frame-to-skin seams. Due to the limited reach of the robotic arm, the assembly jig with panel preform had to be rotated 180 deg inside the robot cell to complete all required stitching.

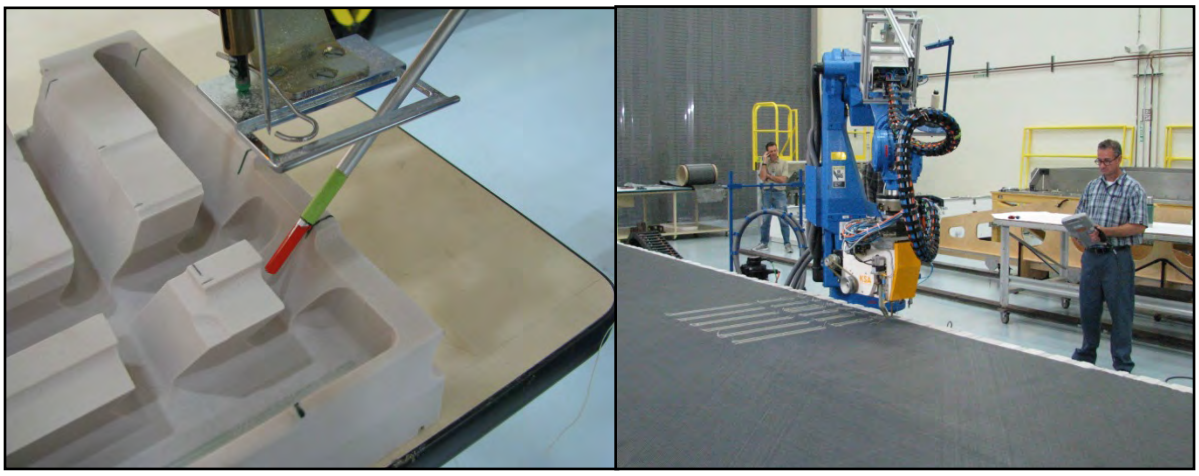

Figure 6-13. TCP Probe Used to Teach Seam Path (left) and Robotic Stitching Panel Preform (right)

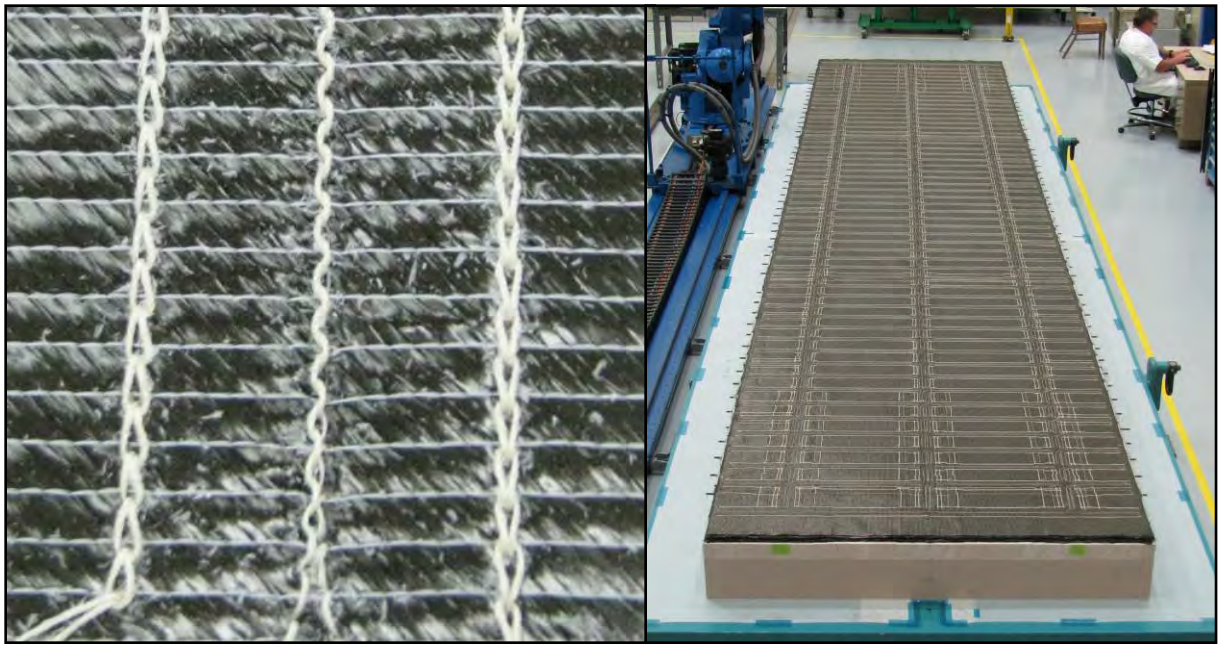

Figure 6-14. Modified 3D Chain-Stitch Seam (left) and Complete Crown Panel Stitching (right)

6.1.4 Preform Infusion and Cure

Resin-infusion processing of the panel dry fiber preform assembly was accomplished using the Boeing CAPRI process. Tooling consisted of a one-piece welded OML tool and multiple IML tooling details constructed of Invar steel. Silicone rubber mandrels were used over the bulb stiffeners to aid in installation of the vacuum bag. The OML tool contained integral ports welded to the bottom surface of the tool facesheet for mounting resin inlet valves and vacuum outlet valves. Grooves machined into the top surface of the facesheet intersected with the inlet ports and facilitated distribution of the resin across the tool surface. Once the mold tool was cleaned and a release agent applied, flow media was then allocated over the mold surface followed by perforated plate and release ply layers. The preform was then transferred from the assembly jig to the mold tool. This was accomplished by first banding the preform down against the assembly jig. The entire assembly was then raised using an overhead crane and rotated so that the skin was facing down when placed over the mold tool (Figure 6-15). The banding straps were then removed from around the preform, and the assembly jig was removed, leaving the preform resting on the mold surface, as shown in Figure 6-16. The IML tooling details were installed over the preform followed by the installation of the primary and secondary nylon vacuum bags (Figure 6-17 and Figure 6-18). The mold tool with part was then moved inside a walk-in oven for resin-infusion processing and cure.

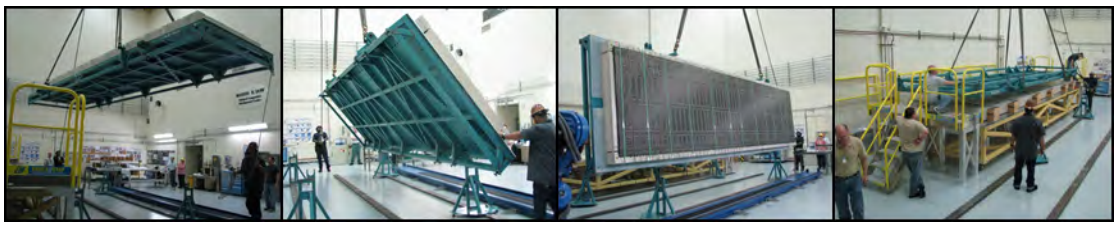

Figure 6-15. Transfer of Stitched Panel Preform From Assembly Jig to the OML Tool

Figure 6-16. Crown Panel Preform Positioned on OML Tool

Figure 6-17. Installation of IML Tooling Over Crown Panel Preform

Figure 6-18. Installation of Vacuum Bag Over Crown Panel Preform and IML Tooling

A Servo Rotary Dispensing (SRD) machine (Figure 6-19), manufactured by Advanced Process Technology (APT), was used to prepare the epoxy resin and infuse the preform. Resin and hardener were loaded into the respective holding tanks on the machine and thin-film degassed at elevated temperature. A single mold line connected the machine to the resin inlet manifold on the mold tool. With the mold at temperature and materials properly degassed, the preform was infused in an automated manner using the SRD machine, which metered, mixed, and delivered the resin at a specified pressure on demand. Infusion of the 28-ft-long by 7-ft-wide highly integrated panel (as shown in Figure 6-20) was completed in approximately 45 min. Once resin-infusion processing of the panel preform was completed, the machine was stopped, the mold lines were disconnected, and the temperature of the oven was raised to 200°F to complete the initial part cure. The part was cooled to room temperature, the vacuum bag system removed, and the IML tooling taken off (Figure 6-21). The panel was then lifted off the OML tool to enable the flow media to be removed from the bottom surface. The part was placed back down onto the OML tool and post-cured at 350°F inside the oven. Figure 6-22 shows the as-cured crown panel before periphery machining.

Figure 6-19. APT Servo Rotary Dispensing Machine for Automated Resin-Infusion Processing

Figure 6-20. Resin-Infusion Processing of Crown Panel Inside Oven

Figure 6-21. Removal of Vacuum Bag and IML Tooling From Infused and Cured Panel

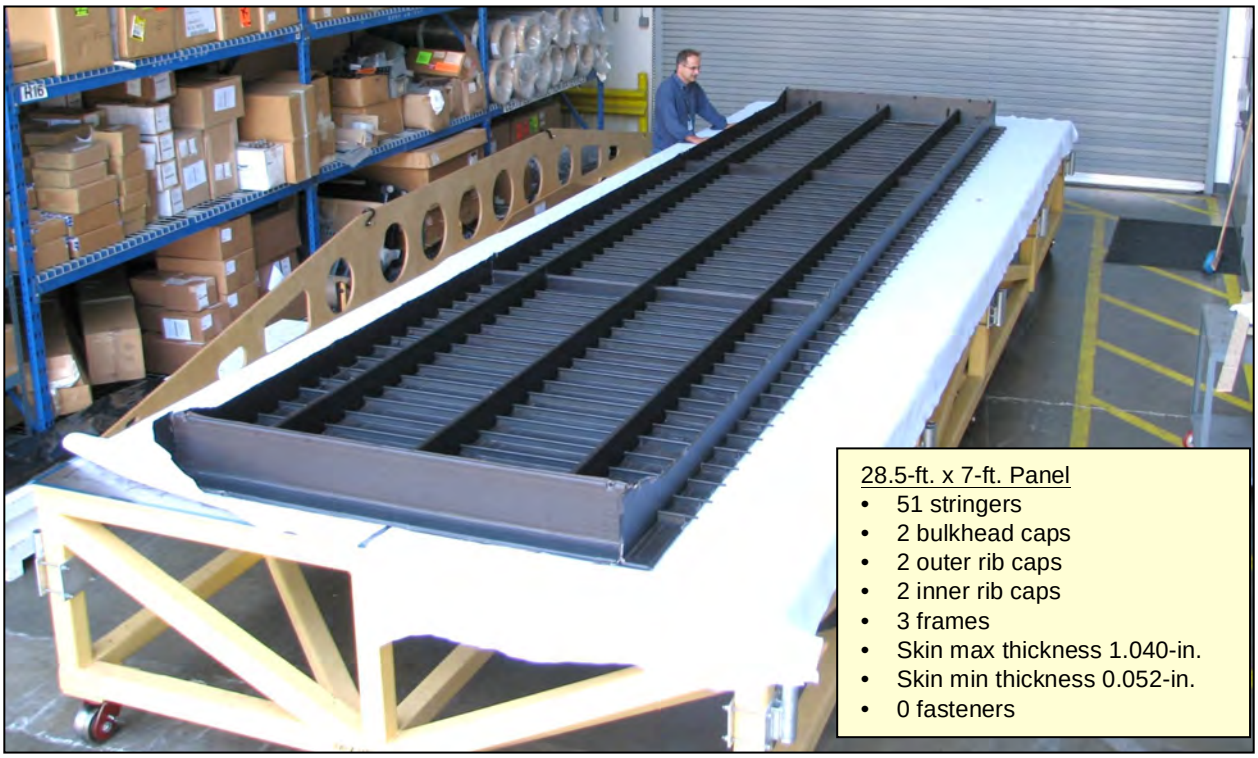

Figure 6-22. Resin-Infused and Cured Crown Panel Before Periphery Machining

Each panel was visually inspected after post-curing was complete to look for manufacturing defects. When a defect was found, a detailed inspection report was created documenting the type, the disposition required, and the action taken by engineering or manufacturing to address any findings. Typical panel quality was very high on both the IML and OML surfaces, as shown in Figure 6-23 and Figure 6-24. This was a significant achievement considering the fact that 7 of the 11 panels were “first-off-the-tool” articles, with the remaining 4 panels being identical replicates. There were no tool proof parts required or produced. The majority of the defects

found were related to either tooling markoff or bridging of vacuum bag materials (i.e., armalon release ply), which resulted in resin flash on the panel IML surface, as shown in Figure 6-25. Disposition of these types of defects consisted of sanding or grinding locally to remove the excess resin or high spot. This was done to eliminate any potential riding condition that might occur at panel-to-panel interfaces or at locations where aluminum fittings would be installed during assembly of the MBB.

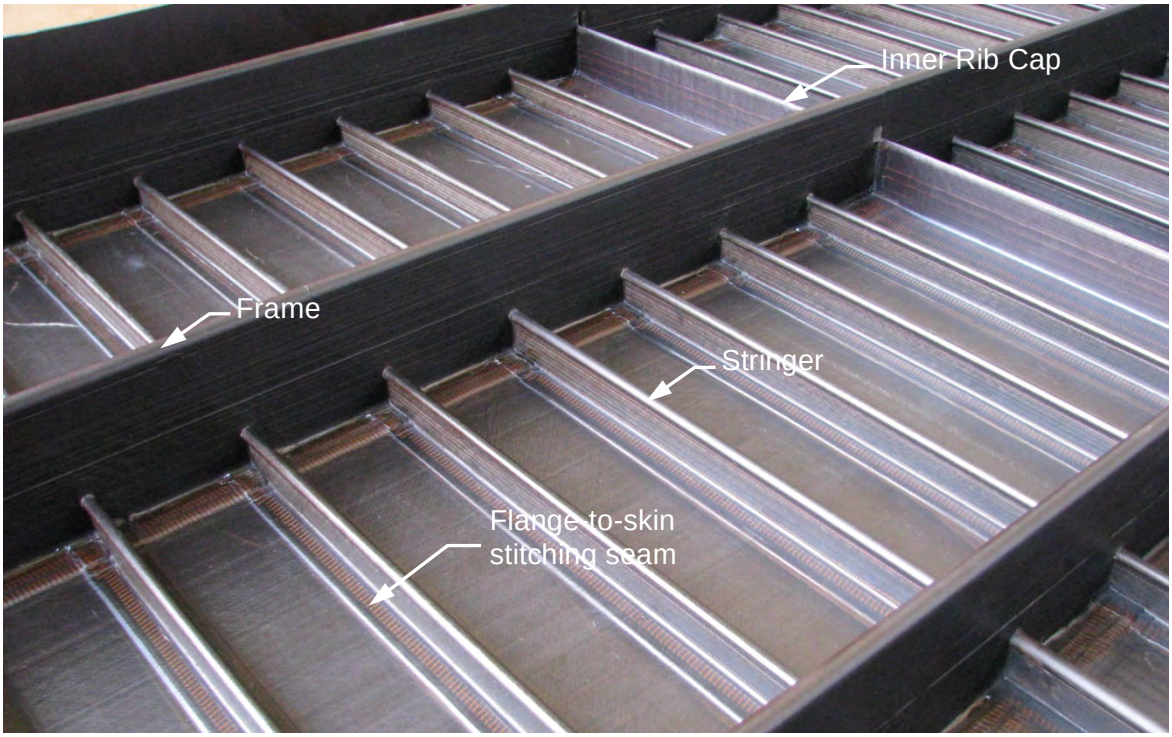

Figure 6-23. Typical IML Surface Quality of PRSEUS Panel

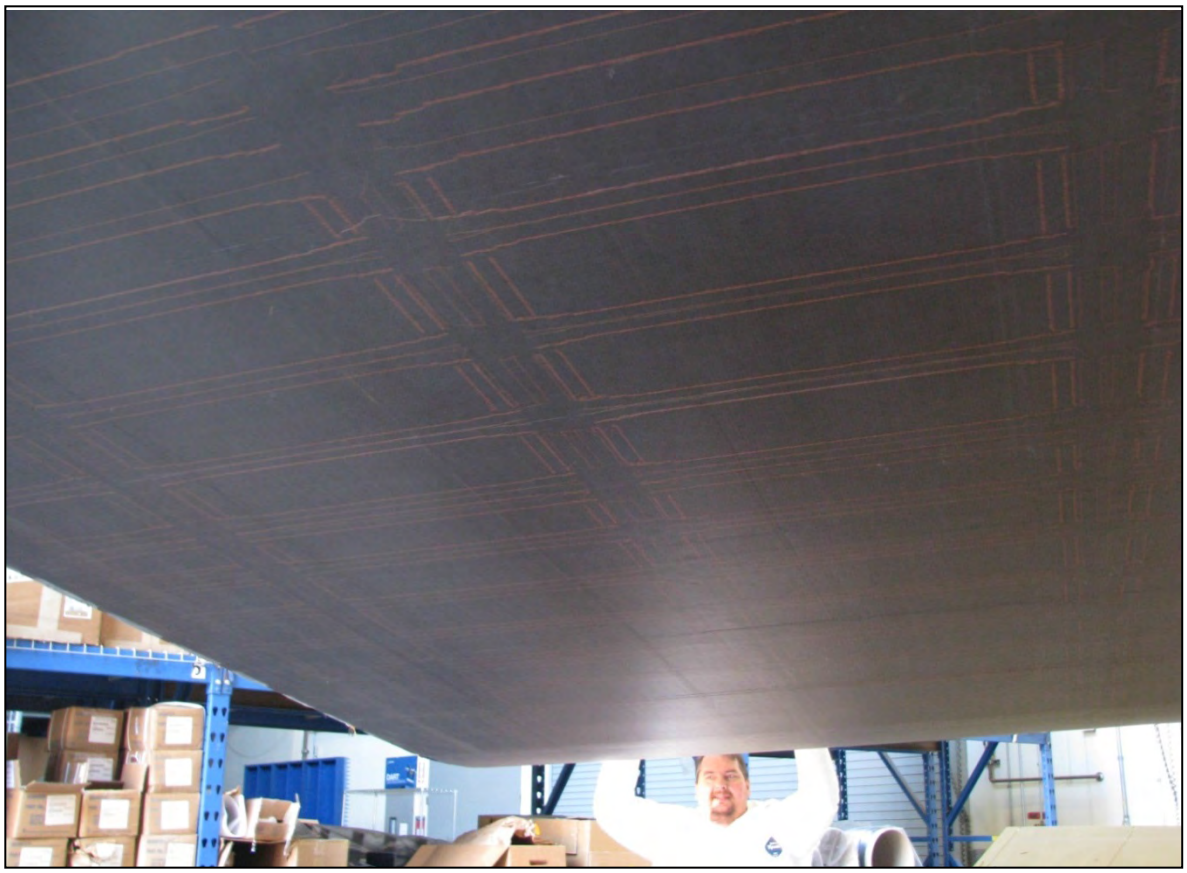

Figure 6-24. Typical Skin OML Surface Quality of PRSEUS Panel

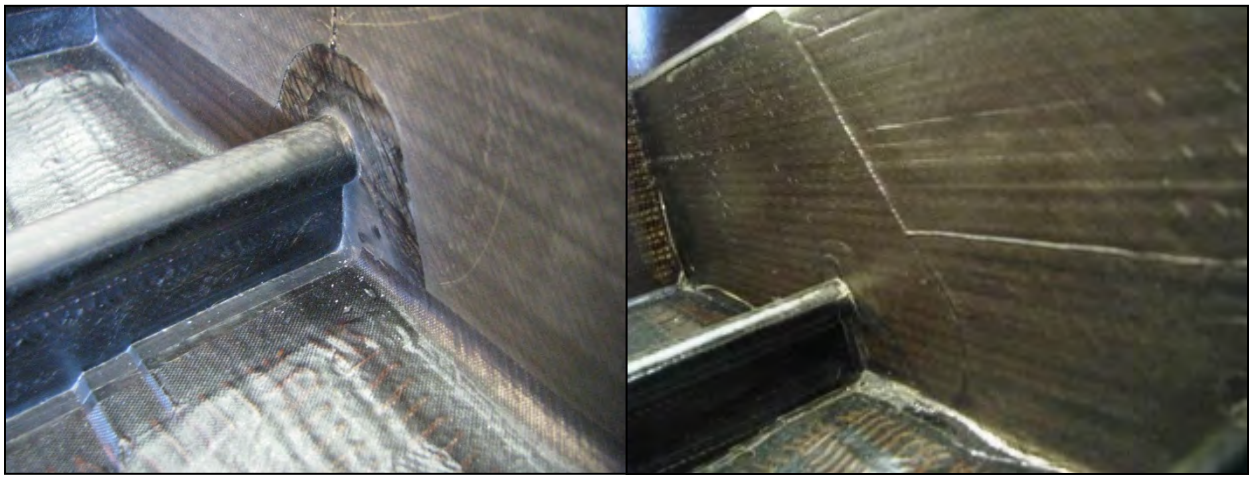

Figure 6-25. Typical Tooling Markoff on Face of Frame Required Sanding to Remove Resin Flash

The only manufacturing defects that required substantial rework or repair were the impressions found on the OML surface of the crown panel (Figure 6-26). As mentioned earlier, low-carbon steel perforated plates were used between the wire mesh flow distribution media and the preform during resin-infusion processing to produce a smooth part surface. With an insufficient gap between adjacent plates for thermal expansion, the steel plates crushed together (Figure 6-27) and protruded upward into the preform during initial cure of the part at 200°F. To address any potential compromise to the structural integrity of the skin and frame tear strap plies created by the deep impressions, thin repair patches were fabricated and secondarily bonded locally to the OML surface of the panel, as shown in Figure 6-28. Appendix B of this report contains a full description of this issue and the repair.

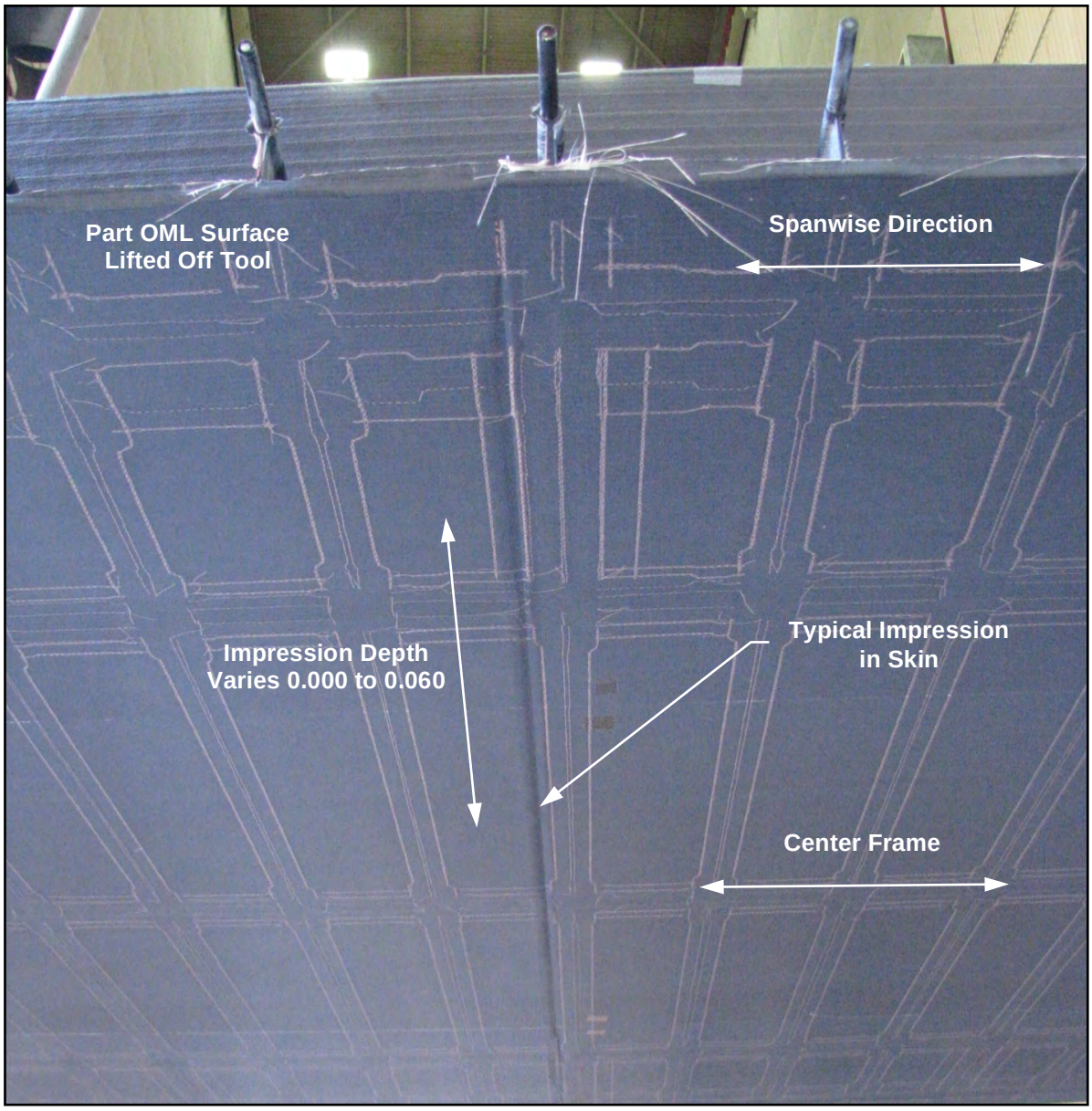

Figure 6-26. Impressions Formed in Skin of Panel due to Thermal Expansion of Perforated Plates

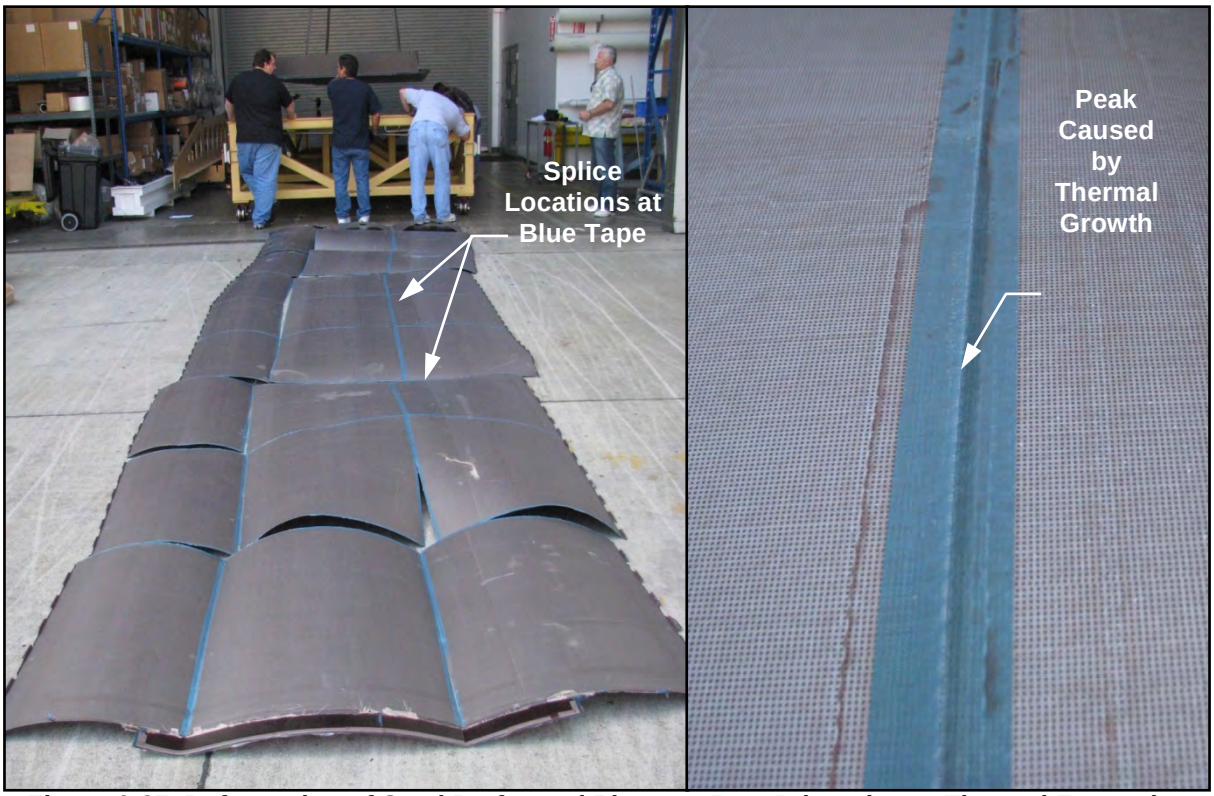

Figure 6-27. Deformation of Steel Perforated Plates at Butt Joints due to Thermal Expansion

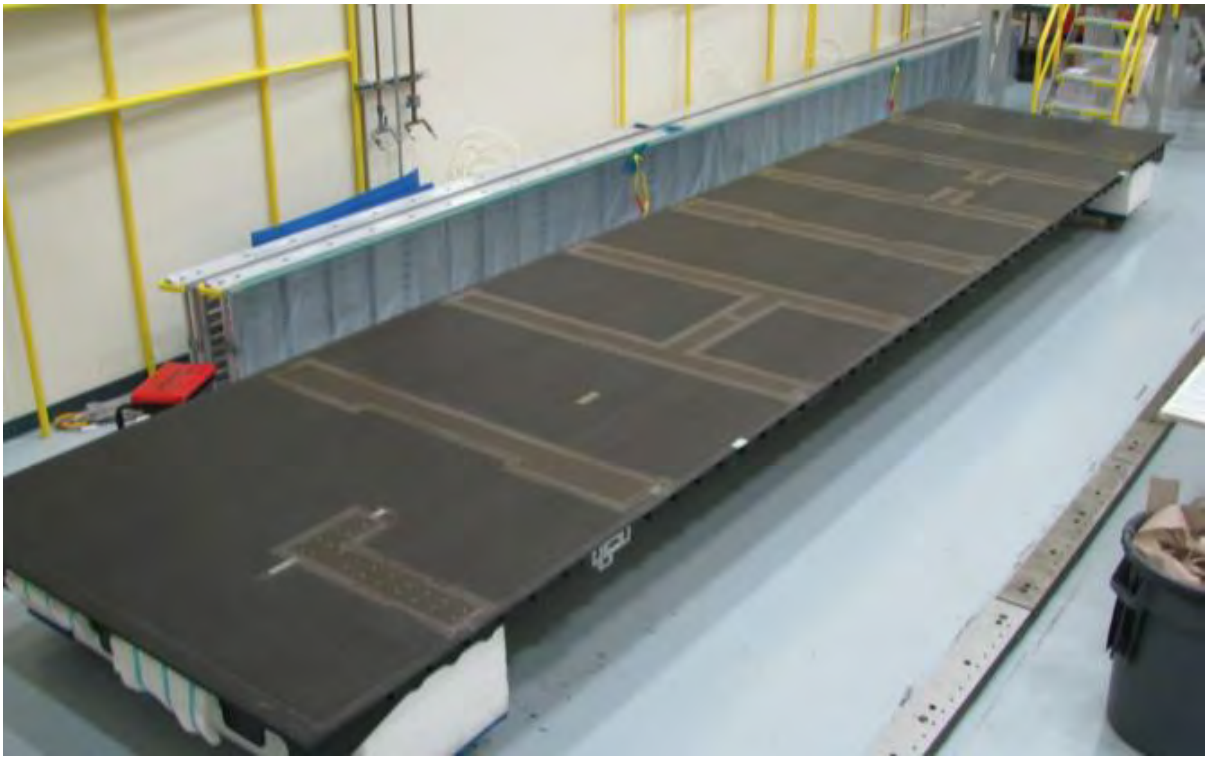

Figure 6-28. Repair Patches Positioned Over Impressions in Crown Panel Skin Outer Surface

6.1.5 Panel Machining

Panels were manufactured with excess material around the perimeter and along the top of the bulkhead/rib cap webs. The final profile of the skin and caps was achieved by machining at an outside supplier. To accomplish this, a cured panel was placed onto a large transport dolly (Figure 6-29), the dolly with panel was loaded inside a SEAVAN container (Figure 6-30), and the panel was then transported by truck to the machining supplier's facility.

Figure 6-29. Upper Bulkhead Panel Loaded Onto Transport Dolly for Shipment

Figure 6-30. Panel on Transportation Dolly Loaded Inside SEAVAN Container

The panels were installed onto a large CNC milling machine for final edge trim. Perimeter clamps and sandbags were used to hold the panel flat against the machine bed, as shown in Figure 6-31. Solid carbide rotary bits and small-diameter abrasive cutoff wheels were used to produce the detailed features in the periphery of the skin and scalloped profile of the cap web, as shown in Figure 6-32. Large access door openings were also cut out of the upper and lower bulkhead panels. Finally, pilot holes were drilled into each panel at discrete locations to support the Determinate Assembly (DA) approach being used for the MBB. The net-trimmed panels were then shipped to the Boeing C-17 facility in Long Beach, California, where assembly of the MBB was performed.

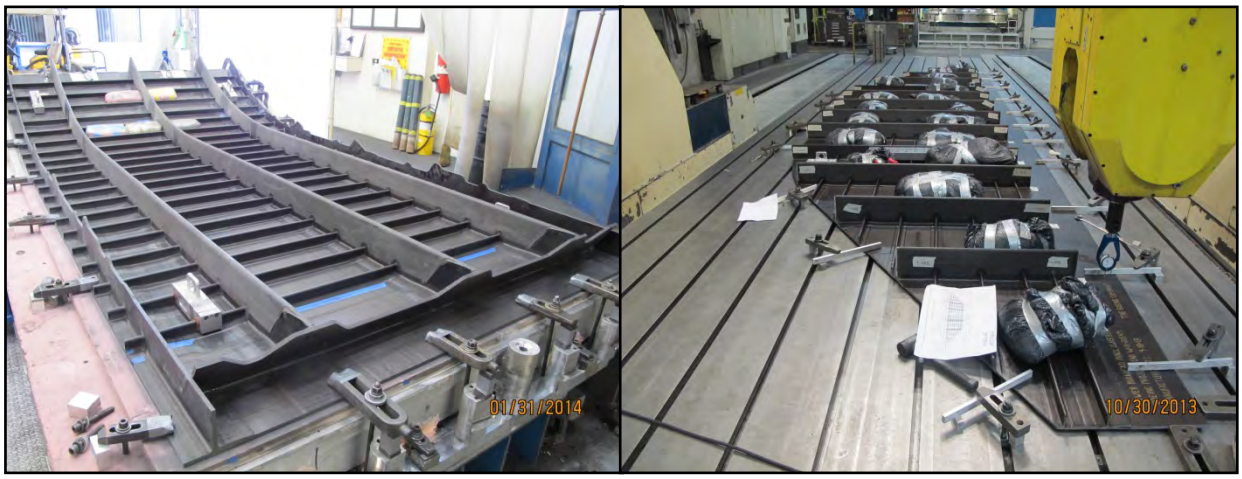

Figure 6-31. Periphery Machining of Lower Bulkhead Panel (left) and Side Keel Panel (right)

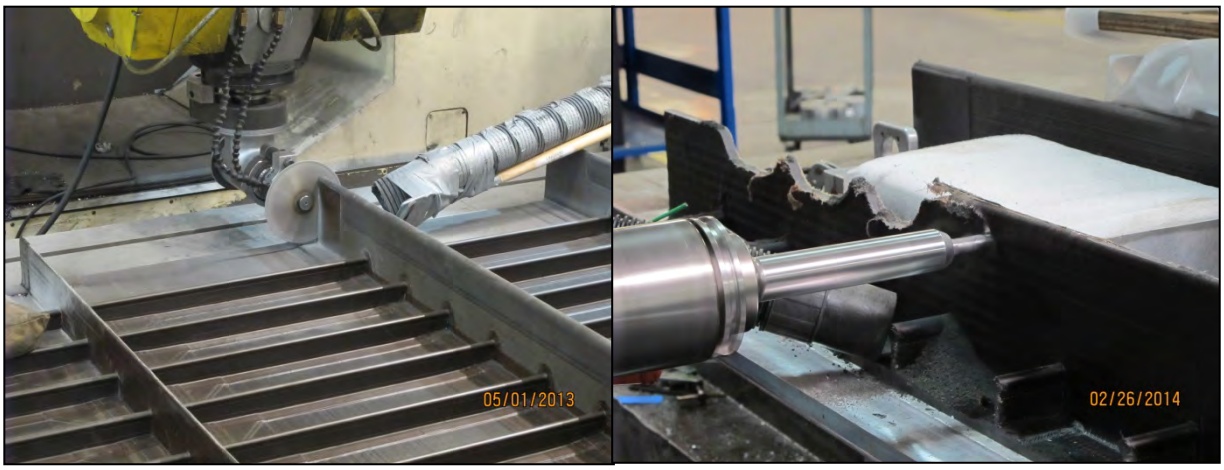

Figure 6-32. Machining of Center Keel Panel Periphery and Bulkhead Cap Web

A full dimensional inspection of the trim was performed on each panel before and after machining. The panels were placed on top of two large surface tables with the IML surface facing up (Figure 6-33). With the panel restrained, measurements were taken off the IML surface using a laser tracker. Inspection data was then compared against the CAD models to evaluate the machined surfacesand DA hole locations.

Figure 6-33. Upper Bulkhead Panel Positioned on Surface Table for Final Dimensional Inspection

6.1.6 Summary of Panels Fabricated

The manufacturing approach taken to fabricate the large and highly integrated composite panels and then assemble them into the MBB proved to be extremely successful. It was a significant step in demonstrating the scale-up capability of stitched resin-infusion technology for primary structures on transport aircraft. Foremost was the ability to efficiently integrate structure using dry NCF material and one-sided robotic stitching technology to produce near-net-shape 3D preform panels. Also demonstrated was the robustness of the resin-infusion process itself, as 500 lb of resin were metered, mixed, and dispensed to the mold automatically and continuously at proper temperatures and pressures, producing high-quality, high-fiber-volume-fraction, void-free laminates without an autoclave. Finally, also proven were the advantages of net-molding cap-type features into panels to produce simple flat plane interfaces, which enabled DA of the fuselage structure as opposed to the typical lofted interface for built-up structure, which inevitably requires shimming.

The next steps to advance this new composite structure and manufacturing technology will be to automate and industrialize the processes for handling and forming dry carbon-fiber fabrics to produce stringer and frame preforms at the high rates needed for commercial aircraft. New simplified mold tool designs are needed to reduce the amount of labor required to clean, install, and remove tools while still supporting the rapid installation of the vacuum bag system. New,

resin systems, next-generation NCF materials with toughened interlayers, and improved closed-cell foam core technologies beyond those used in this program should also be aggressively pursued. Finally, implementation of the technology onto an actual piece of flight hardware (as done for stitched composite main landing gear doors) is needed to obtain experience, build confidence, and gain acceptance by program management for broader use on future airframe applications.

6.2 Multi-bay Box Assembly

The MBB was composed of 15 highly integrated and stitched composite panels. These panels were fabricated in the Boeing Huntington Beach, California, facility. They were then sent to local vendors for final engineering profile machining and inspection before being shipped to the Boeing Long Beach, California, facility for final assembly. Figure 6-34 illustrates MBB major components.

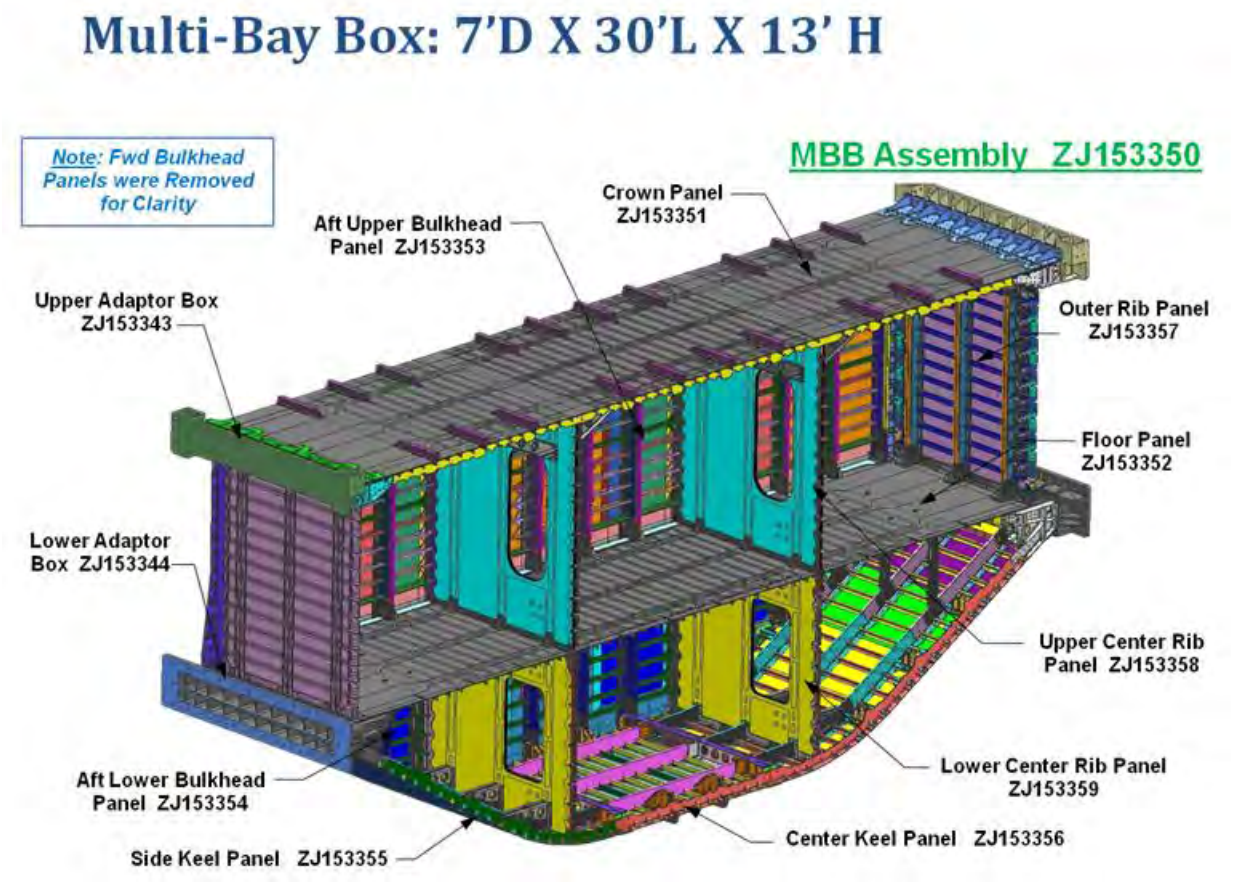

Figure 6-34. Multi-bay Box Assembly Major Components

The MBB final assembly staging area (Figure 6-35) was located in the same Boeing Long Beach, California, facility where the C-17 airlifter was assembled.

This site was chosen due to infrastructure advantages that the C-17 facility had to offer, including tools, lift cranes, space to assemble the 30-ft MBB, rapid turnaround of fastener inventory, a quick-fix shop for metal shims and fittings, and manpower experience with assembly of large structural components.

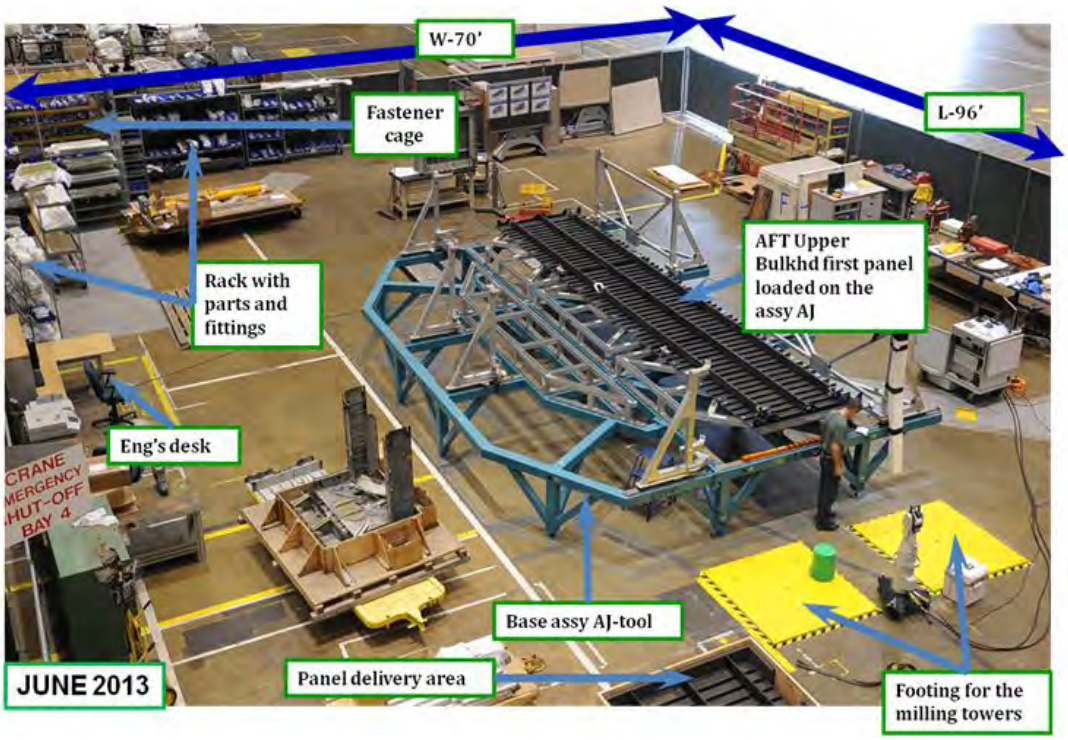

Figure 6-35. MBB Assembly Staging Area at Long Beach, California

6.2.1 Determinant Assembly Features

The assembly jig "AJ1" was established on the floor of the assembly staging area. Laser trackers shot designated tooling holes to establish the MBB coordinate system in relation to the AJ1. These laser inspection shots (Figure 6-36) ensured that the DA holes positioned the panels level and squared before the assembly began.

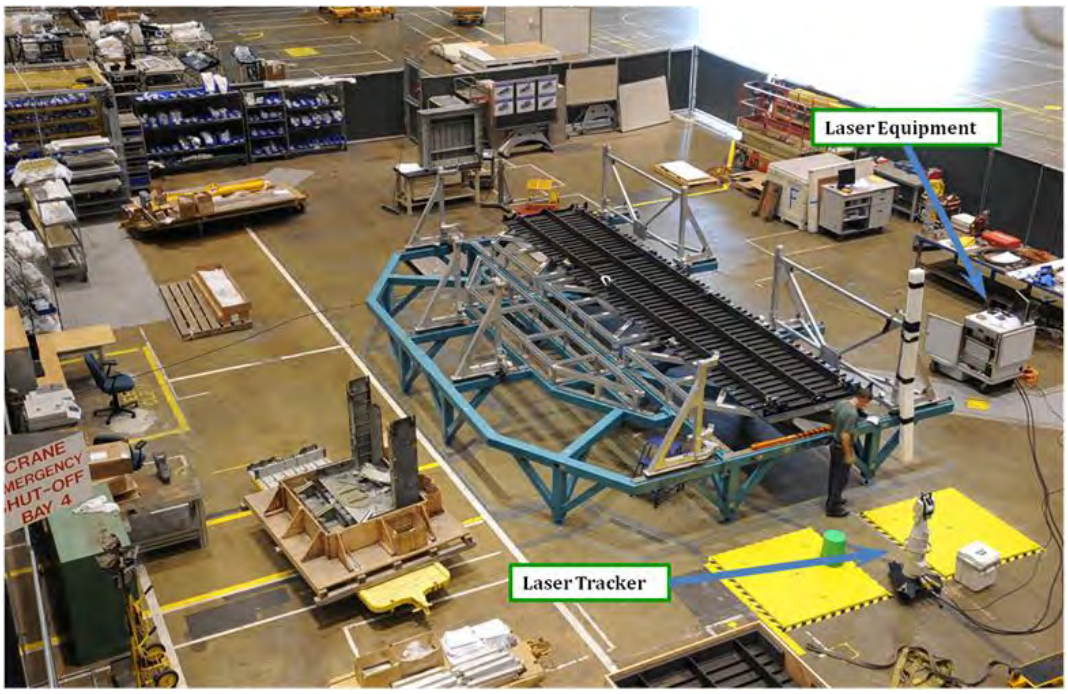

Figure 6-36. Laser Tracker Inspection on Assembly Jig AJ1

First, the aft upper bulkhead was loaded and located on the tool with coordinated tooling holes. This established the location of the MBB assembly on the AJ1 tool. Next, the inner and outer ribs were located to the aft upper bulkhead panels using the coordinated DA holes in the integral caps (Figure 6-37).

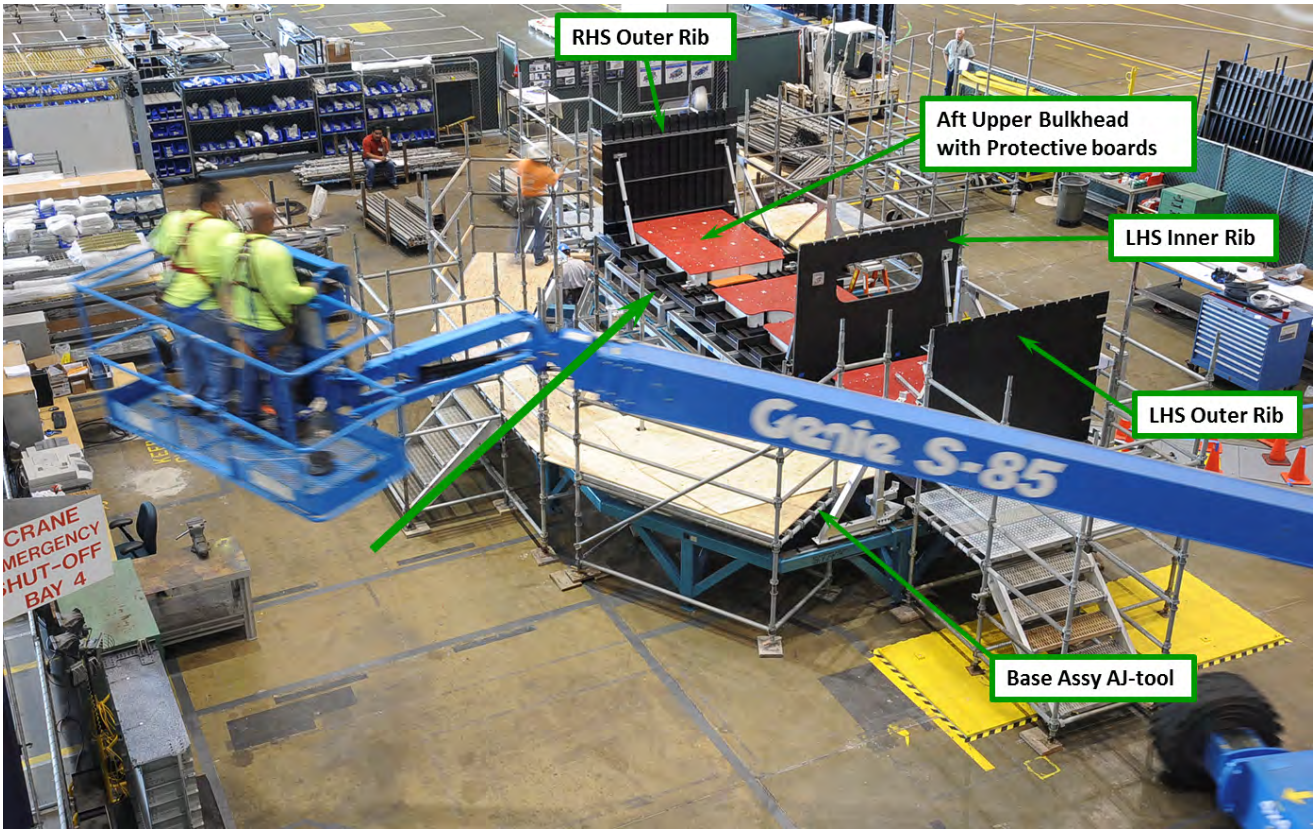

Figure 6-37. Upper Panels Being Loaded on the Assembly Jig

The DA holes used were 0.190/0.192 in. diameter. Each panel had DA holes to locate and align the panels together by placing clecos or temporary fasteners to hold the structure without assembly tooling. With fully integrated panels (skins with frames, stringers, and caps all cocured together), assembly tooling was minimized and was only required to support the MBB itself to allow access into the MMB during assembly. This significantly reduced the nonrecurring tooling costs (Figure 6-38).

The upper section panels were placed and held together with DA holes in a sequence that allowed mechanics to work safely inside the box as it was being assembled. The upper section, which consisted of the crown panel, upper forward and upper aft bulkhead, two end rib panels, and two inner rib panels, underwent a series of laser shots and alignment methods to ensure that the upper section was “squared” to engineering tolerances and not skewed or canted.

Once the upper section was squared and plumb, the first holes were drilled to locate and install the spider tool weldment at the floor level of the box, as shown in Figure 6-39.

These spider tools enabled safe entry into the upper section of the box to work details and maintain the box opening rigid until the upper section panel-to-panel fasteners and metal fittings were installed.

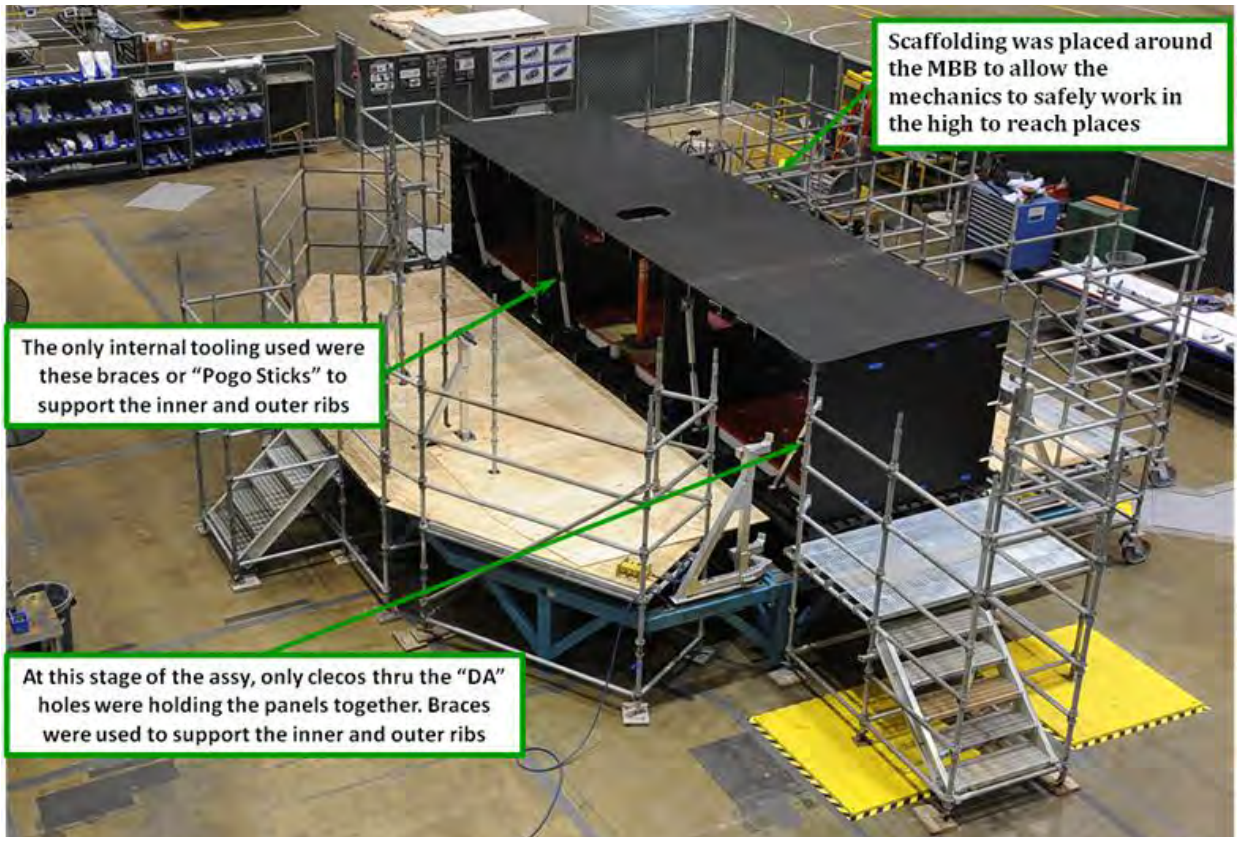

Figure 6-38. Determinate Assembly "DA" Holes Were Used to Reduce Tooling Costs

Figure 6-39. Upper Section With Spider Tools at the Floor Line of the MBB

6.2.2 Panel Installation

Panel-to-panel installation was done in sequence to account for any panel-to-panel deviations that resulted in gaps between the cap surfaces and the mating panel. This was an expected issue, and a shimming system had been developed before starting assembly to solve any gap problems that might arise (Figure 6-40).

Use of the GAPMAN hand-held measuring device was essential to determine the approximate tapers and contours of the shims that filled the gaps, especially at the crown panel to upper bulkhead cap interfaces and the end rib to upper bulkhead cap interfaces (Figure 6-41).

All gap readings were conducted while the panels were in position and pinned with clecos or temporary fasteners utilizing the DA holes only. Panels were not preloaded and were held in a relaxed state for measuring gaps with the GAPMAN device. Shims were fabricated at the C-17 quick-fix shop in Huntington Beach in accordance with the Unigraphics solid models that define the outer trimmed shape and the GAPMAN readings that define the thickness, as shown in Figure 6-42.

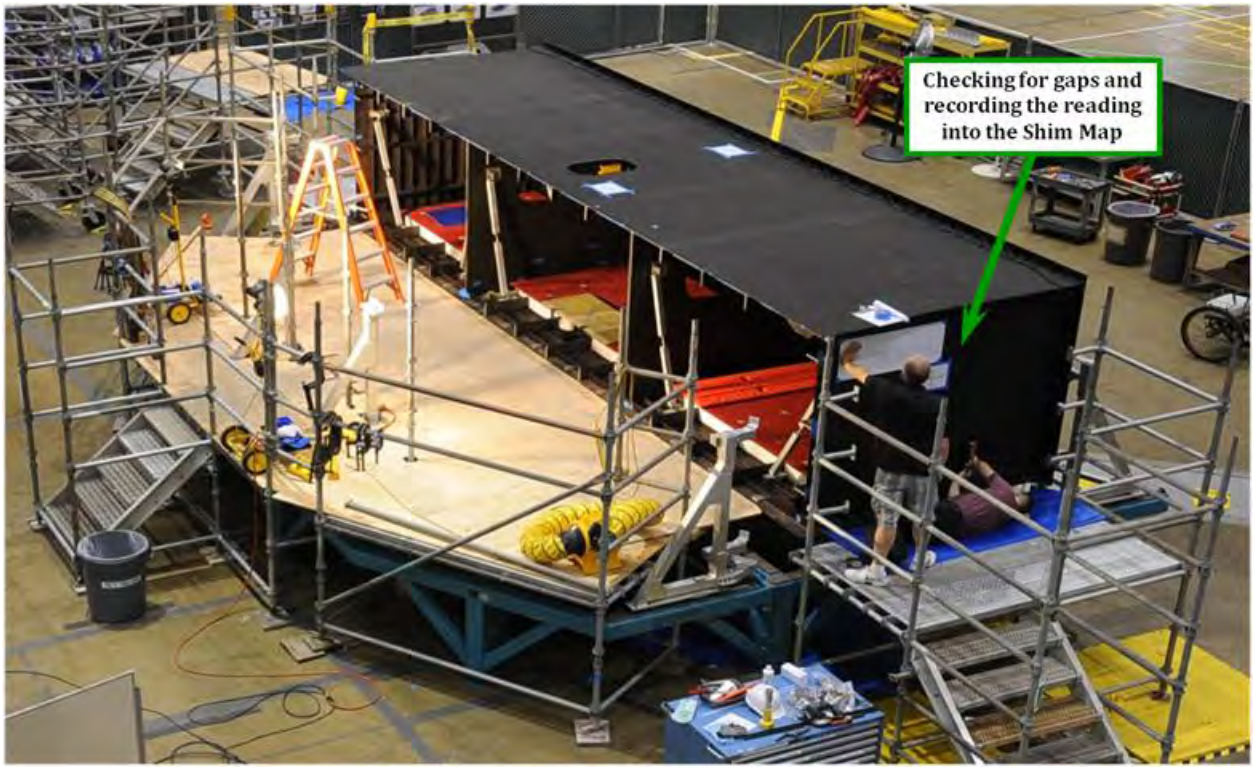

Figure 6-40. Upper Section—Checking for Gaps and Recording Them Into the Shim Map

Figure 6-41. Using the GAPMAN Device to Measure Gaps and Tapers

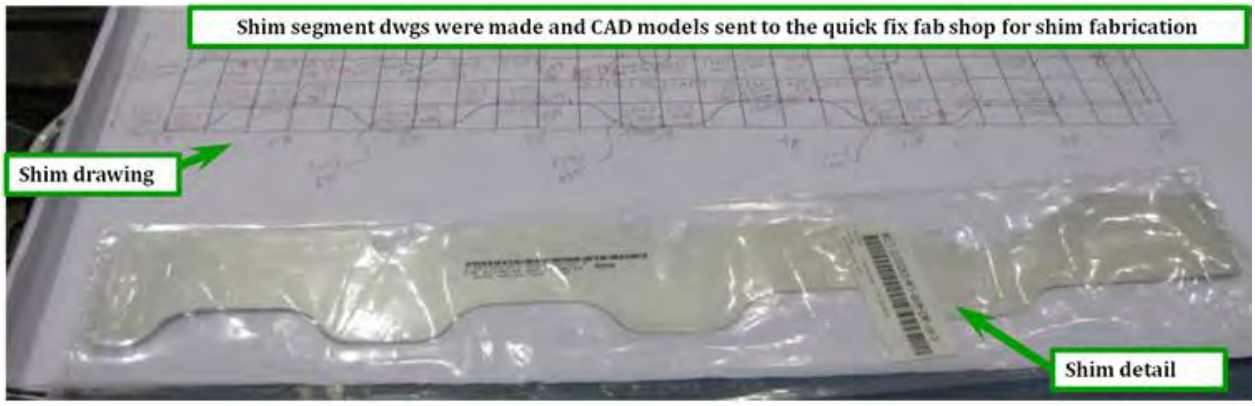

Figure 6-42. Typical Shim Drawing and Fabricated Shim Detail

Drilling with the aid of Drill-Ream Templates (DRT) and Quackenbush pneumatic power feed drill motors reduced drill times and increased hole quality (Figure 6-43). Improved efficiency examples included:

- Automated drilling allowed one-time drilling to a full-size hole (eliminating the need to "step" drill larger hole diameters).
- With cocured fiberglass ply located at fastener areas, use of special cutters, and constant feed drill motor, backside hole breakout was eliminated without needing to back up the backside of the hole. This further reduced the cost per hole drilled on the assembly.

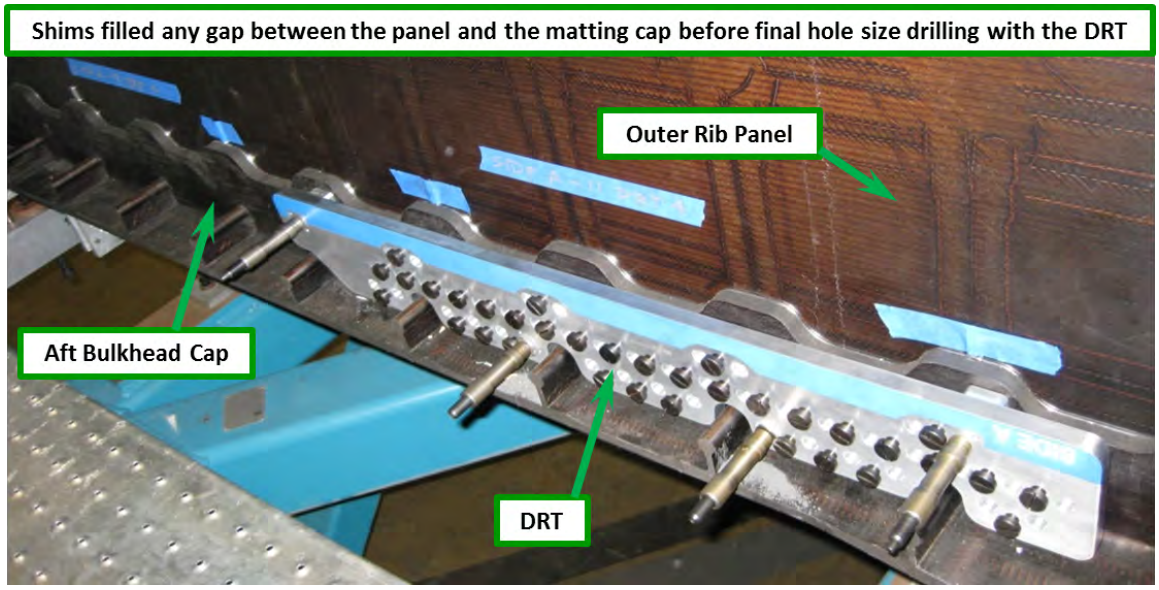

Figure 6-43. Typical Shim Detail Installation Between Composite Panel Interfaces

As shown in Figure 6-44, hole drilling was conducted with safety in mind using proper vacuums, ventilation, and safety gear for the mechanics performing the drill operation.

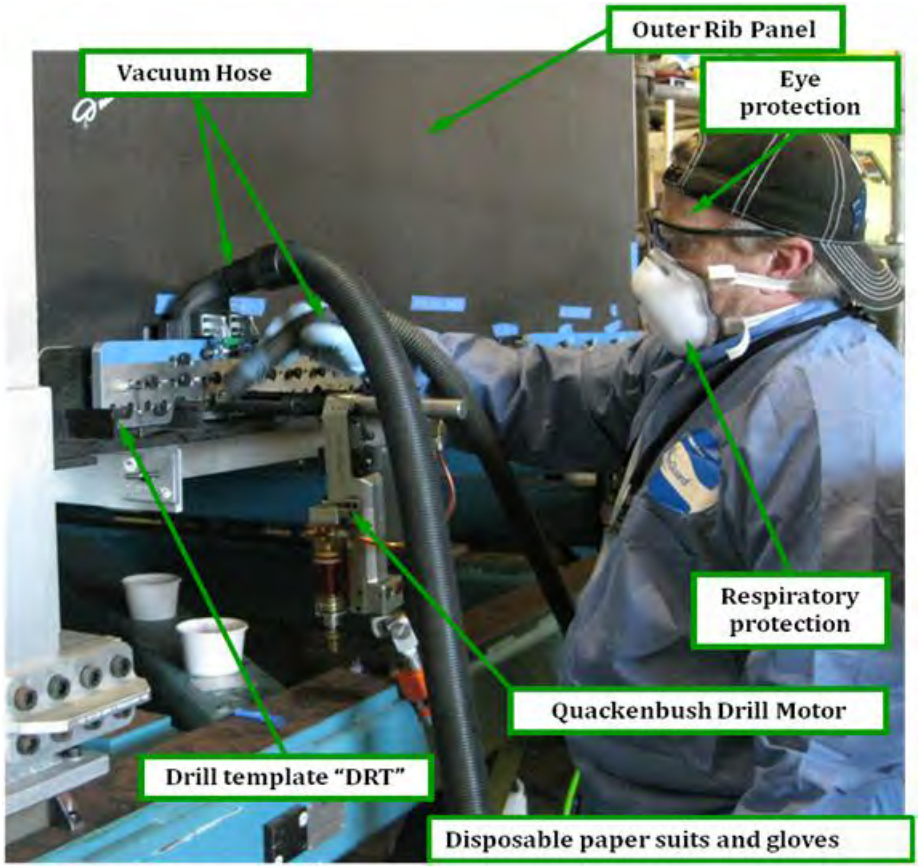

Figure 6-44. Typical Drilling Operation Setup and Preparedness

From drilling trials that were done on the bench, it was determined that each drill on the Quackenbush setup would be changed after 32 holes were drilled. Mechanics always had three Quackenbush drills set up and ready to go, which avoided slowing down the drilling operation. Figure 6-45 shows a typical drilling setup.

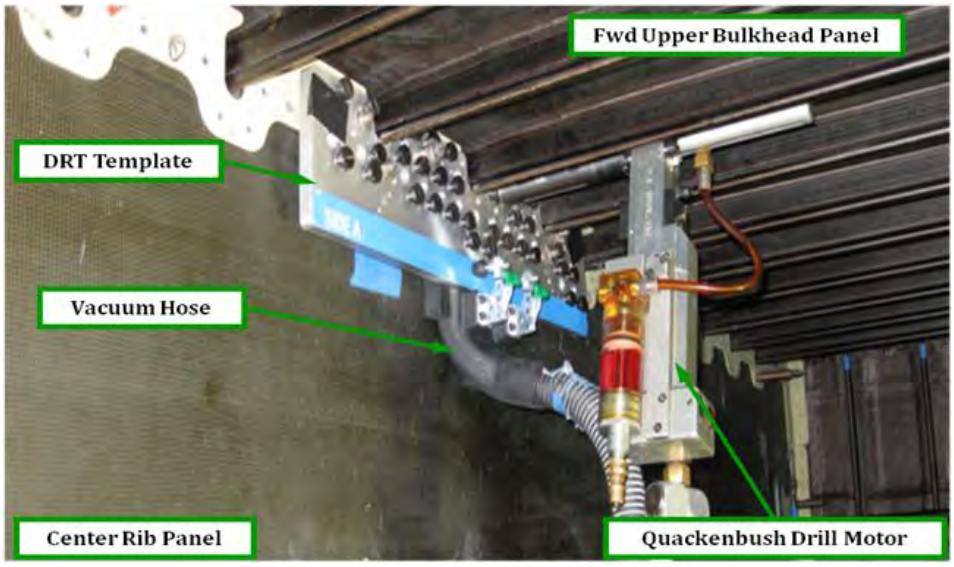

Figure 6-45. Typical Drilling Operation Setup

After all upper fittings were installed, the floor panel was located and installed (Figure 6-46). Next, the lower section panels were installed except for the center keel panel (Figure 6-47), which facilitated installation of the lower section fitting. No panel-to-panel shims were required when assembling the lower section panels (Figure 6-48). This accelerated the hole-drilling and fastener installment operation because it eliminated the need for shims to be modeled, fabricated, and placed, as was done in the upper section.

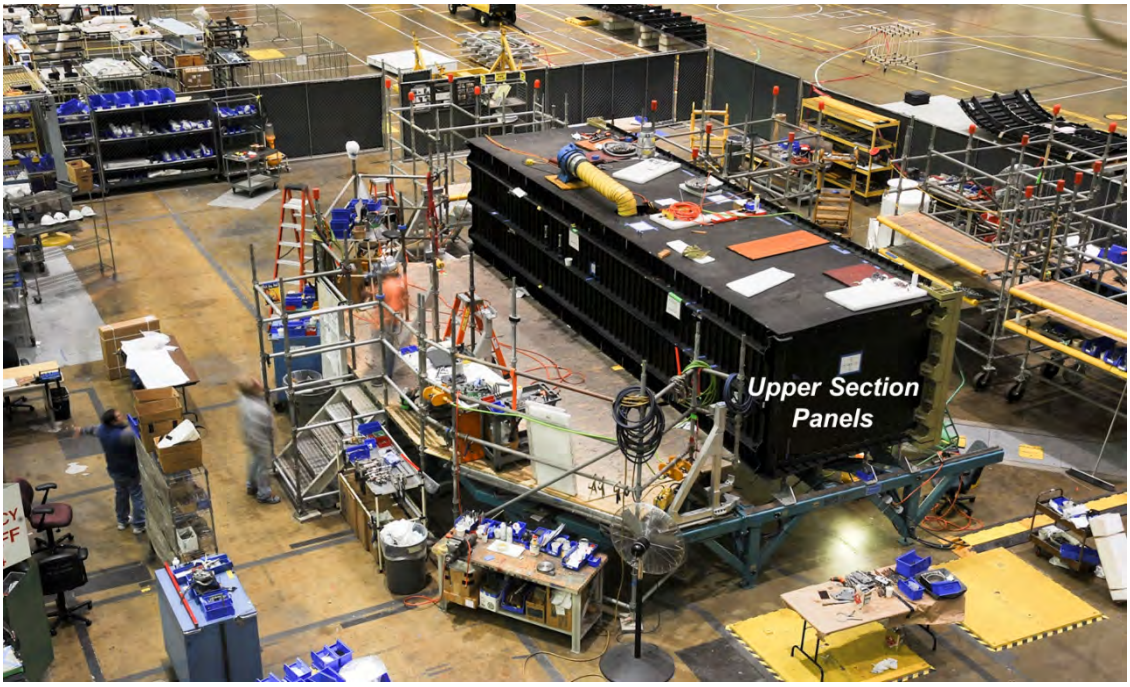

Figure 6-46. Upper Section Panel Assembled With Floor Panel Installed

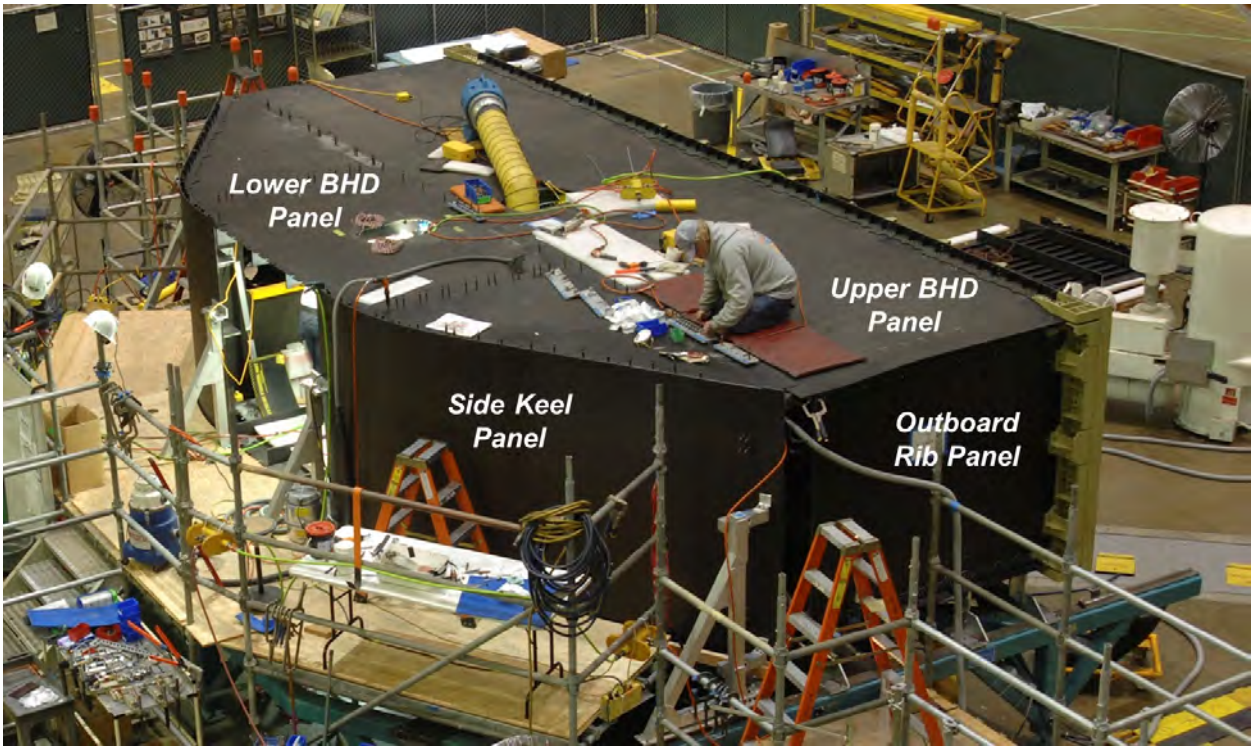

Figure 6-47. Lower Section Panel Assembly With Center Keel Panel Removed

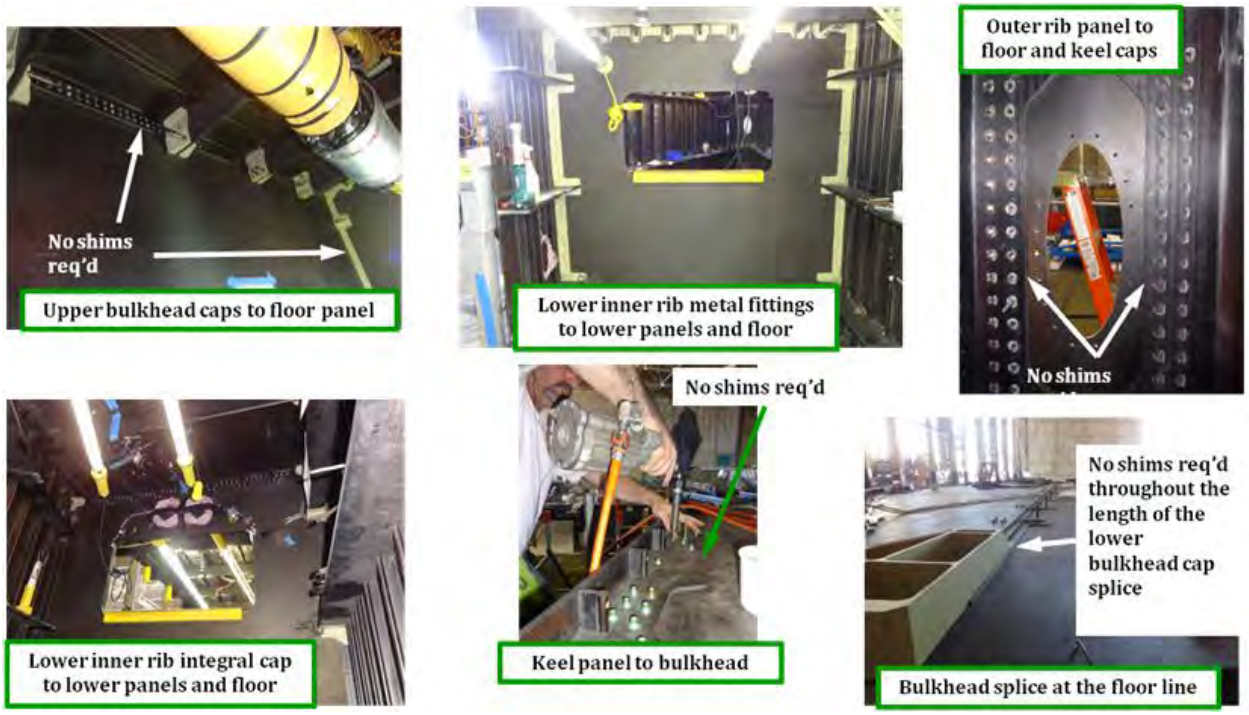

Figure 6-48. Lower Section Panels Assembled Without Shims

6.2.3 Panel Joining

As shown in Figure 6-49, the following panel-joining sequence of operations was employed. Panels were joined after all panel-to-panel hole drilling was complete. Spot facing of the holes was done on the holes where proud stitching would prevent the joining fastener head or washer from sitting flush on the composite surface (Figure 6-50). The panels were thoroughly cleaned of all drill dust and metallic chips on the shims using shop cloth rags and alcohol to eliminate any cooling lubricant oil that might have leaked from the Quackenbush drill. The panels were then reassembled with clecos, and permanent fasteners were installed in sequence, beginning at the center of the panel and then moving in the outboard direction. This sequence eliminated any "zipper" effect on the panel skins. The typical panel-to-panel fastener was a 0.25-in.-diameter lock-bolt, washer, and collar arrangement.

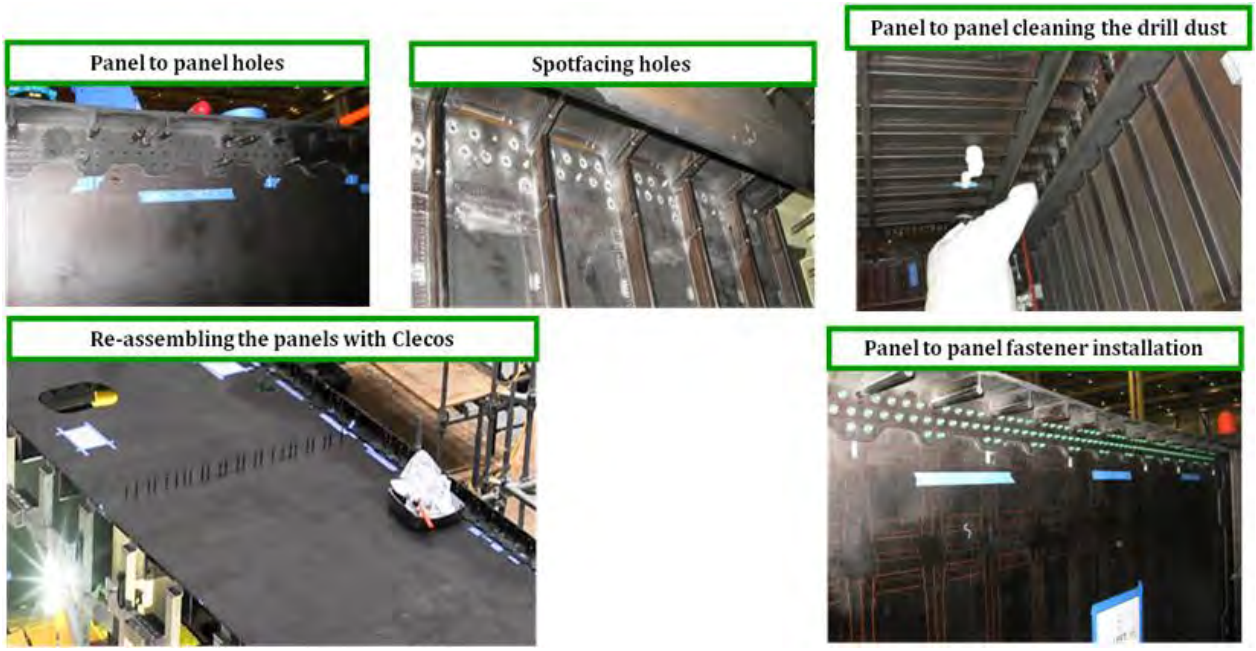

Figure 6-49. Typical Panel-Joining Sequence of Operations

When spot facing was performed, only the minimal material required was removed to get 100% surface cleanup for fastener head or washer bearing. In most cases, material depth removed was between 0.030 to 0.015 in.

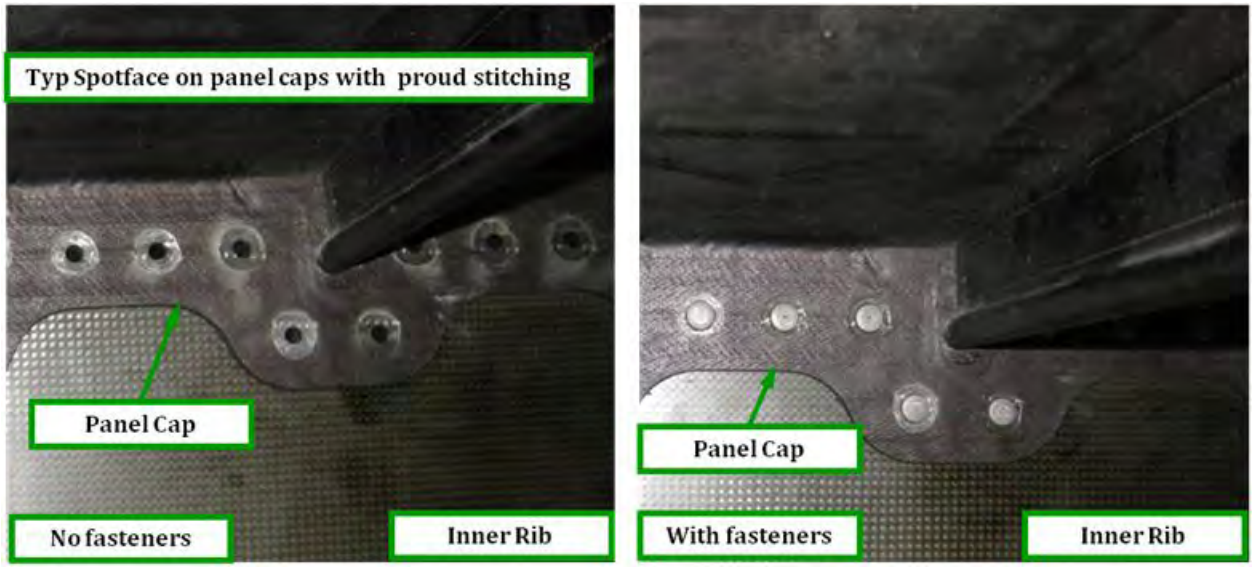

Figure 6-50. Typical Fastener Installation on Proud Stitching

6.2.4 Fitting Installation

Figure 6-51 shows all of the fittings that were installed in the MBB. These fittings were installed after the panel-to-panel fasteners were installed.

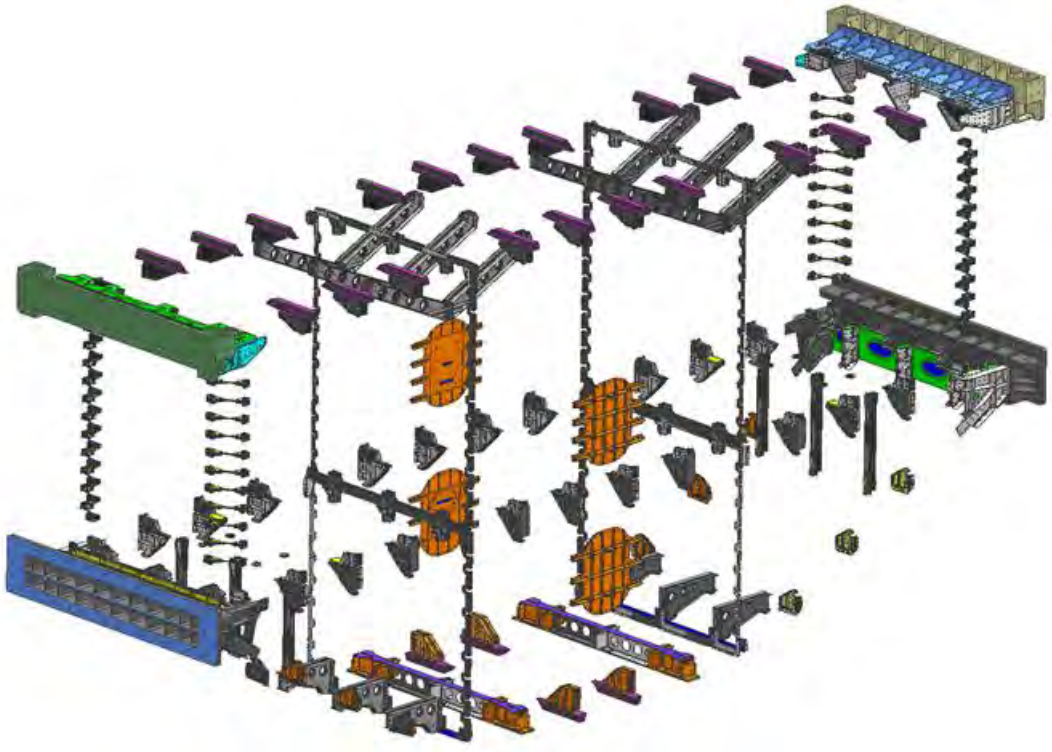

Figure 6-51. Fittings for the Multi-bay Box

MBB part count included the following:

- Number of metallic fittings: 735.
  - Load-introduction fittings: 108.
  - Standard fittings: 627.
- Number of fasteners: 12,500.
  - Panel-to-panel: 3,814.
  - Load-introduction fittings: 1,148.
  - Standard fittings: 6,954.
  - Miscellaneous (doors, covers, and gang channels): 584.

All of the fittings were machined from aluminum. To ensure that all possible air leak paths that might be found behind a fitting were accounted for, the area where the fitting was to be applied was thoroughly evaluated. All voids and leak paths were filled with PR1422, Class B2 sealant, as shown in Figure 6-52.

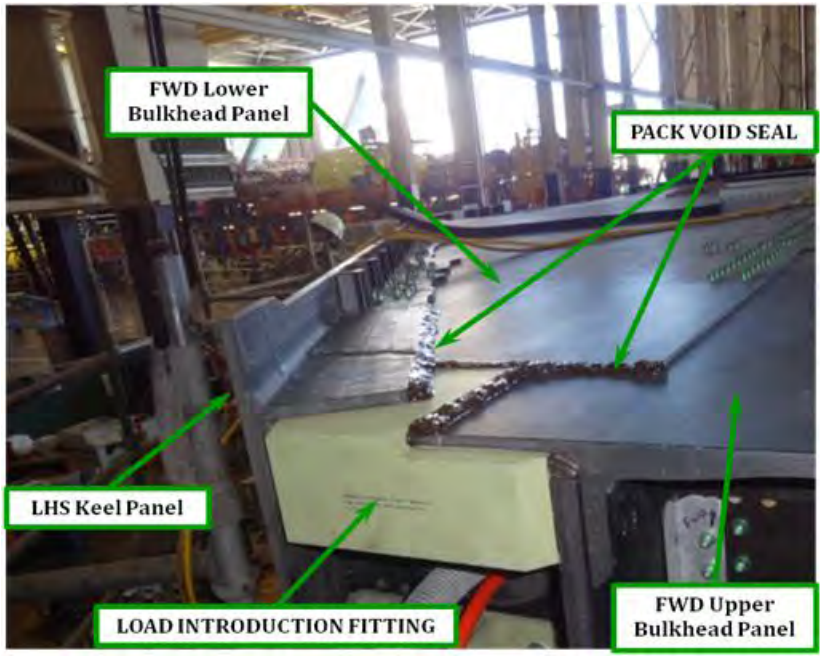

Figure 6-52. Typical Pack Void Sealant Application

Because the fittings interfaced with wavy panel surfaces, proud stitching, and panel imperfections, the fittings were first coated with Frekote Mold Release material and installed with liquid shim material DPM5535-2 (EA934) or DPM5535-4 (EA9394). Should the fitting need to be removed for any reason, the Frekote would release from the liquid shim and prevent any damage occurring to the composite panel. Clecos and temporary fasteners were also coated with Frekote so that they could be easily removed and not be bonded in the pilot hole that was used to clamp and hold the fitting in place.

The liquid shim compound came in two-part cans. Because the working life after mixing the compounds was less than 30 min, all affected parts and surfaces had to be ready for liquid shim

application and part clamp-up into the structure. Figure 6-53 shows the application of the liquid shim compound.

Figure 6-53. Liquid Shim Application

With the fitting firmly in place, full-size holes were drilled using DRTs and Quackenbush motors, or by hand with drill bars. Because the fitting was in intimate contact with the entire surface, which prevented carbon dust or aluminum chips from falling into the interface, the fitting did not need to be removed. Fasteners were simply installed and torqued to engineering specifications, as shown in Figure 6-54 and Figure 6-55.

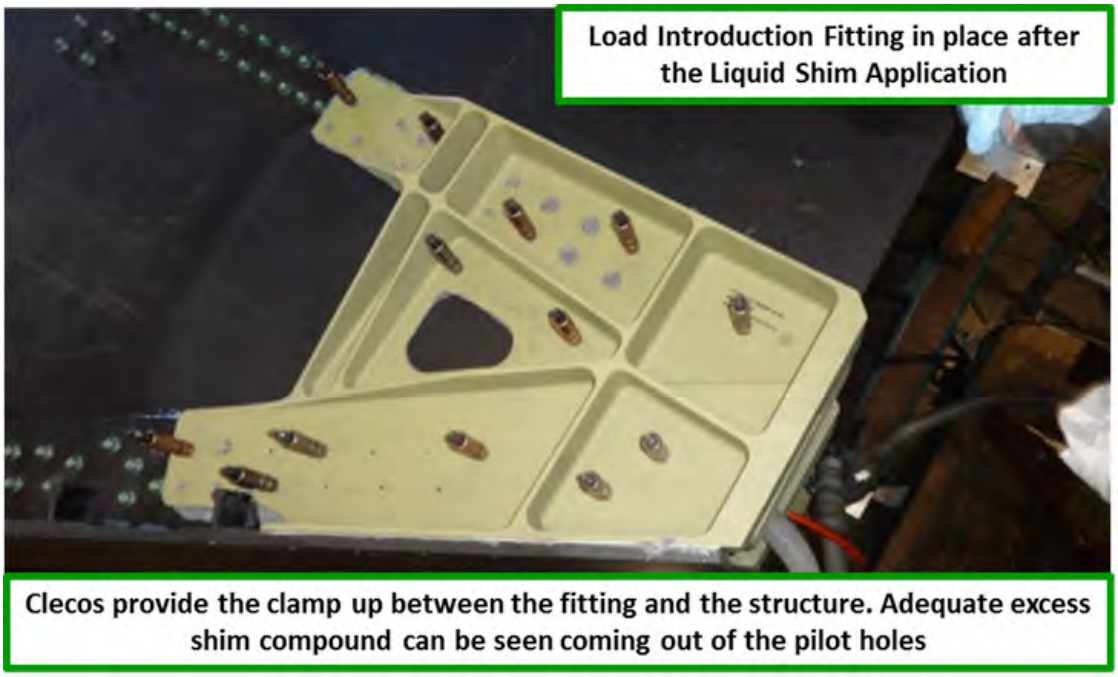

Figure 6-54. Typical Fitting in Place After Liquid Shimming

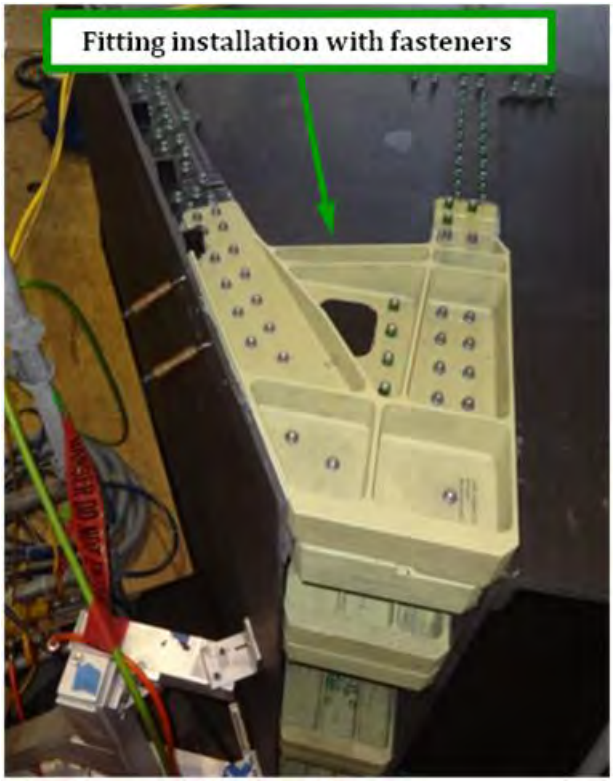

Figure 6-55. Typical Fitting With Completed Fastener Installation

6.2.5 Sealing and Fastener Encapsulation

Flight assemblies that are required to remain leak proof for 20 or more years seal a structure in four different ways: (1) faying surface seal between mating details, (2) fillet seals, (3) fastener encapsulation, and (4) all fasteners installed wet with sealant. Because the MBB was only required to be leak proof for about 6 months, and to reduce the assembly effort and save costs, only two of the four methods were used. Figure 6-56 depicts the fillet seal requirement for all joints. At discrete locations, sealant was applied on the non-pressure side of the MBB under the fitting to reduce leaks around large fittings.

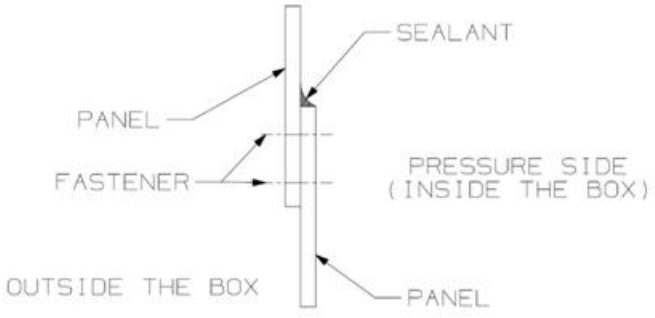

Figure 6-56. Typical Edge-Sealing Requirement Instructions

To eliminate any leaks at fastener locations, all fasteners were encapsulated on the pressure side, as shown in Figure 6-57.

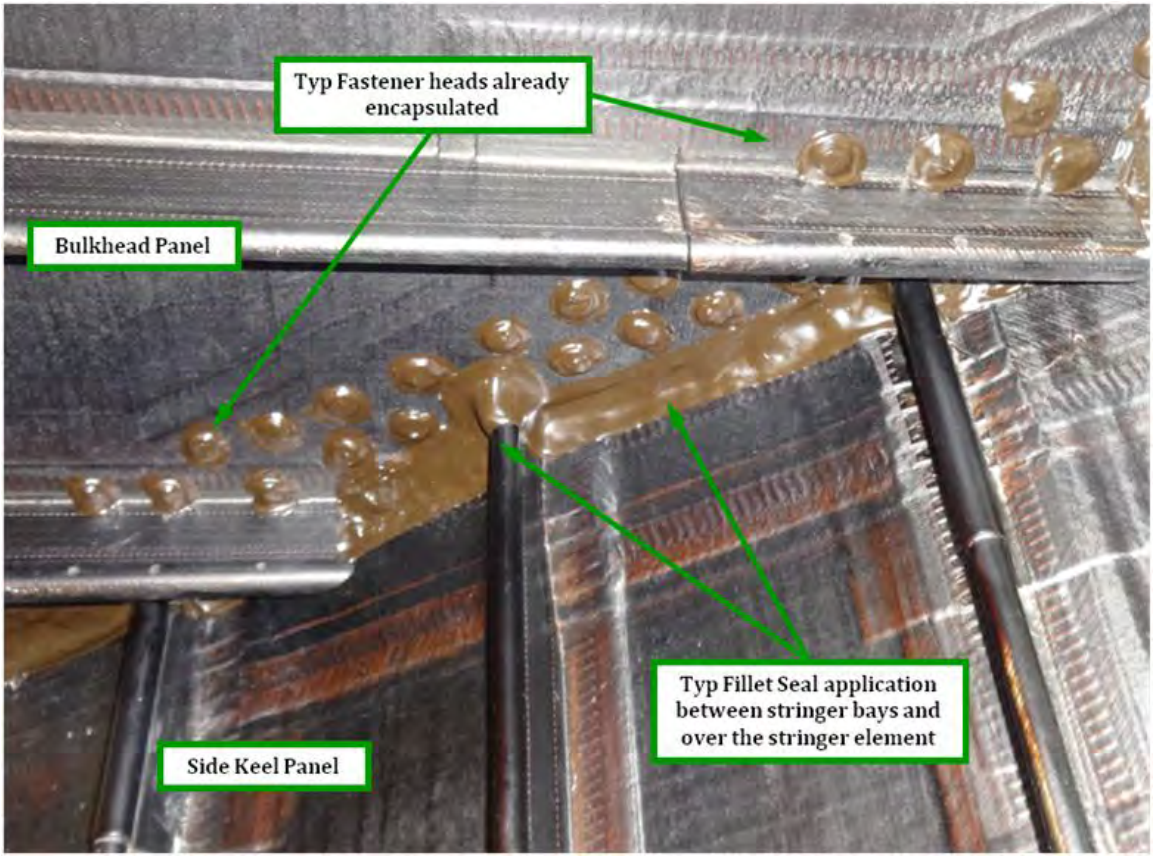

Figure 6-57. Typical Panel-to-Panel Edge Sealing

All sealing was done by wing tank mechanics. Fillet seal and fastener encapsulation was done by applying PR1422 sealant with a seal gun and then working it in by hand with a sealers spatula, as shown in Figure 6-58.

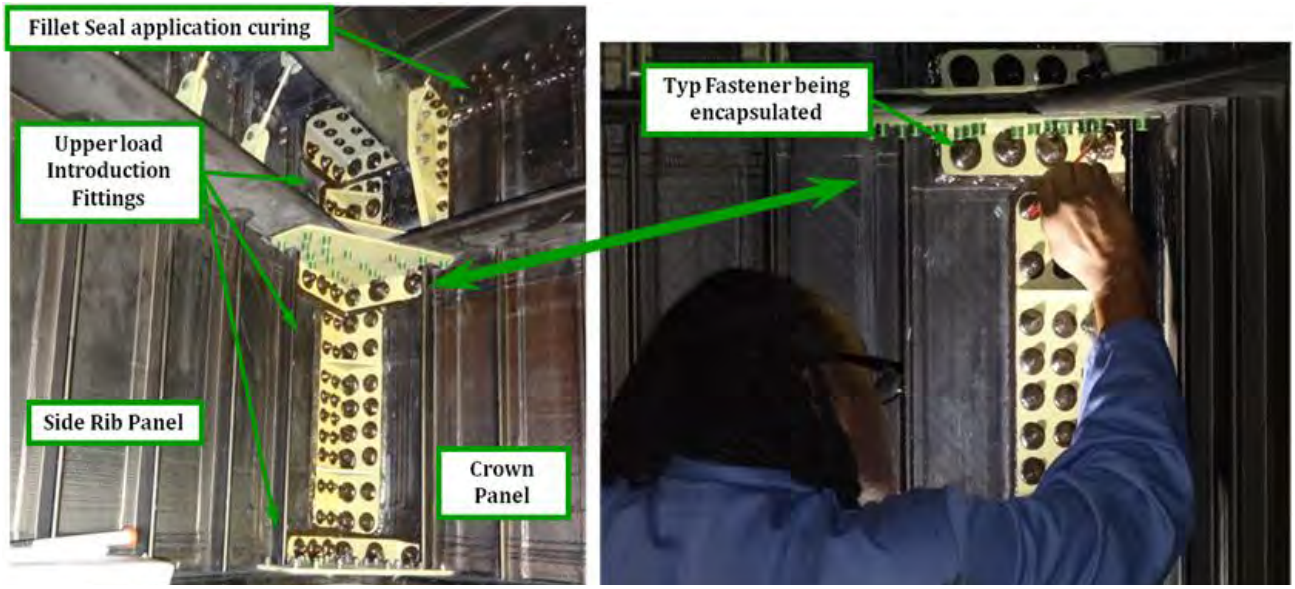

Figure 6-58. Typical Fastener Encapsulation Process

6.2.6 Milling Task for the Load-Introduction Fittings

The overall MBB assembly, with adapter fittings at each of the four corners, had to be within the parameters established to fit in between the platens at the NASA COLTS facility. This distance was held at 360 ±0.12 in., and all four corners were held in a parallel plane within 0.015 in., as shown in Figure 6-59. Because of this, load-introduction fittings were milled after they had been installed and all fasteners torqued.

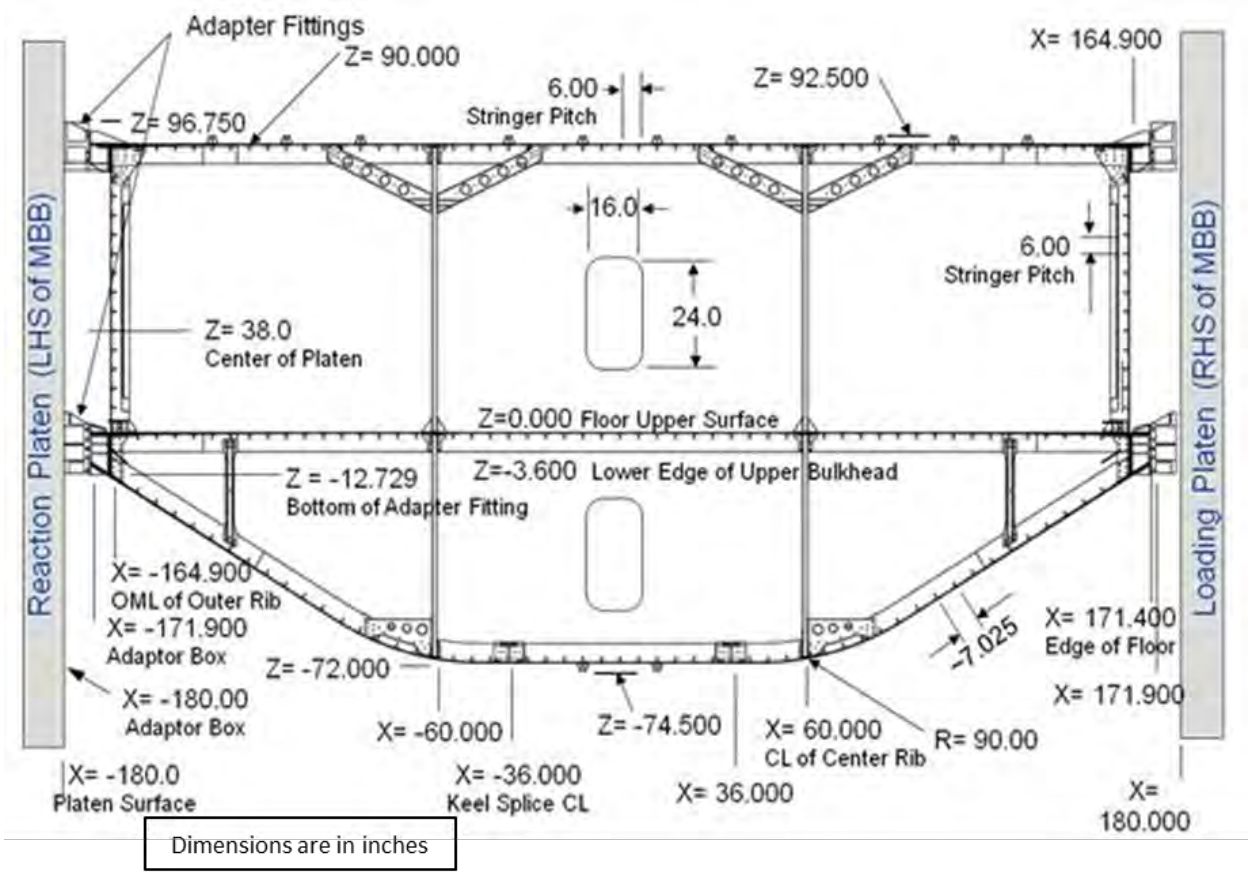

Figure 6-59. General Arrangement for the Multi-bay Box at the NASA COLTS Facility

To reduce the risk of damaging the MBB or delaying the assembly schedule, a mockup was built and a portable milling machine was tested (Figure 6-60). With the mockup, the cutter feed and speeds were determined, and final head alignment was also established at this time. This was important because the cutter was only 8 in. wide, so two passes were required at each cutter depth. Any out of alignment would create a ridge in the machined surface. Once the machined surface was smooth and flat, the milling tower was then moved back to the MBB assembly site.

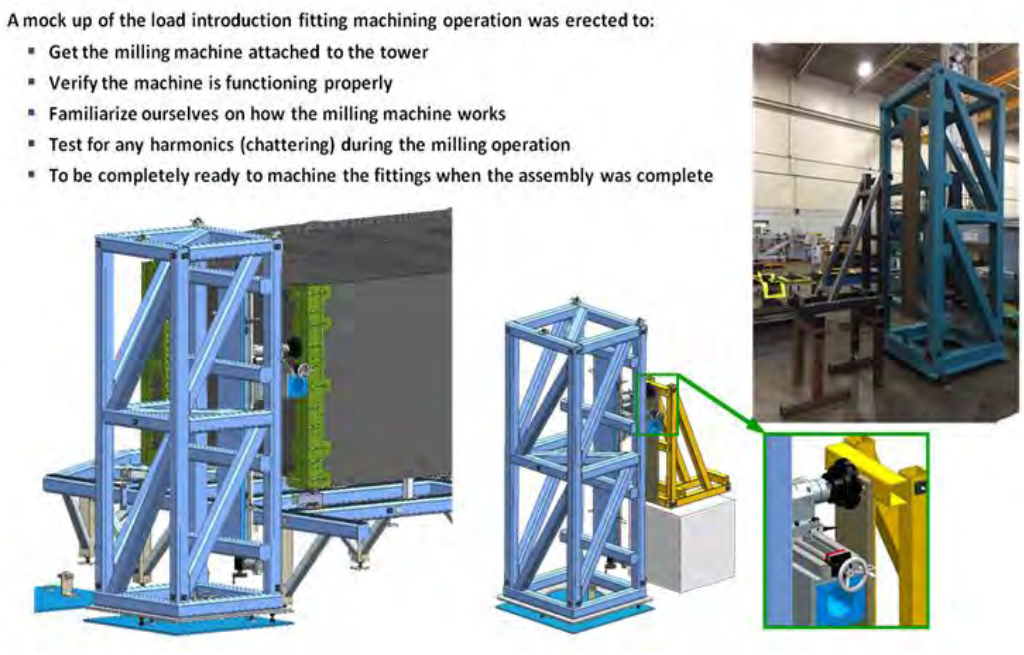

Figure 6-60. Milling Risk-Reduction Trial

Milling operations started on the upper right-hand corner fittings of the MBB. To eliminate any possible vibration and harmonics while cutting away material, milling was performed during the second shift and with no personnel inside the MBB assembly. After every pass of the cutter, spot checks were made and computed by tooling to ensure that the milling did not surpass the desired limits on the overall 30-ft, 0.120-in. span, as shown in Figure 6-61.

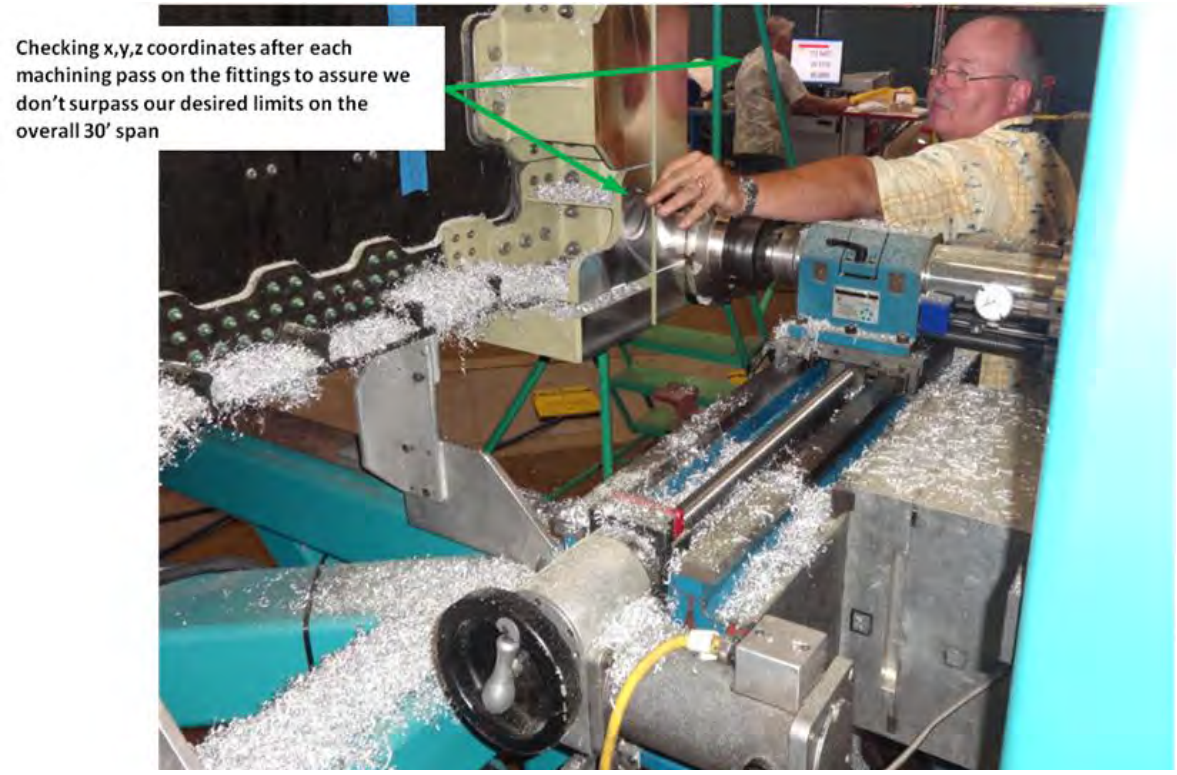

Figure 6-61. Milling the Load-Introduction Fittings—Checking X, Y, and Z Coordinates

All load-introduction fittings were designed with an extra 0.25-in. wall thickness that would be machined away on assembly. The milling tower was moved to each of the four corners and aligned to the coordinate system of the AJ1 at each location. There were no problems encountered with the milling operation, and using the mockup had proved to be time well spent. The surfaces were parallel within 0.010 in., and the overall width was 30 ft, 0.12 in. The decision was made to go to the maximum tolerance to eliminate any reduction of the nominal load-introduction fitting thicknesses. One fitting was slightly shifted when compared to the other fittings. Milling operations (Figure 6-62 and Figure 6-63) were completed in 4 days, which was much less than expected. The next major milestone was the MBB rotation to upright position and placement in the handling fixture.

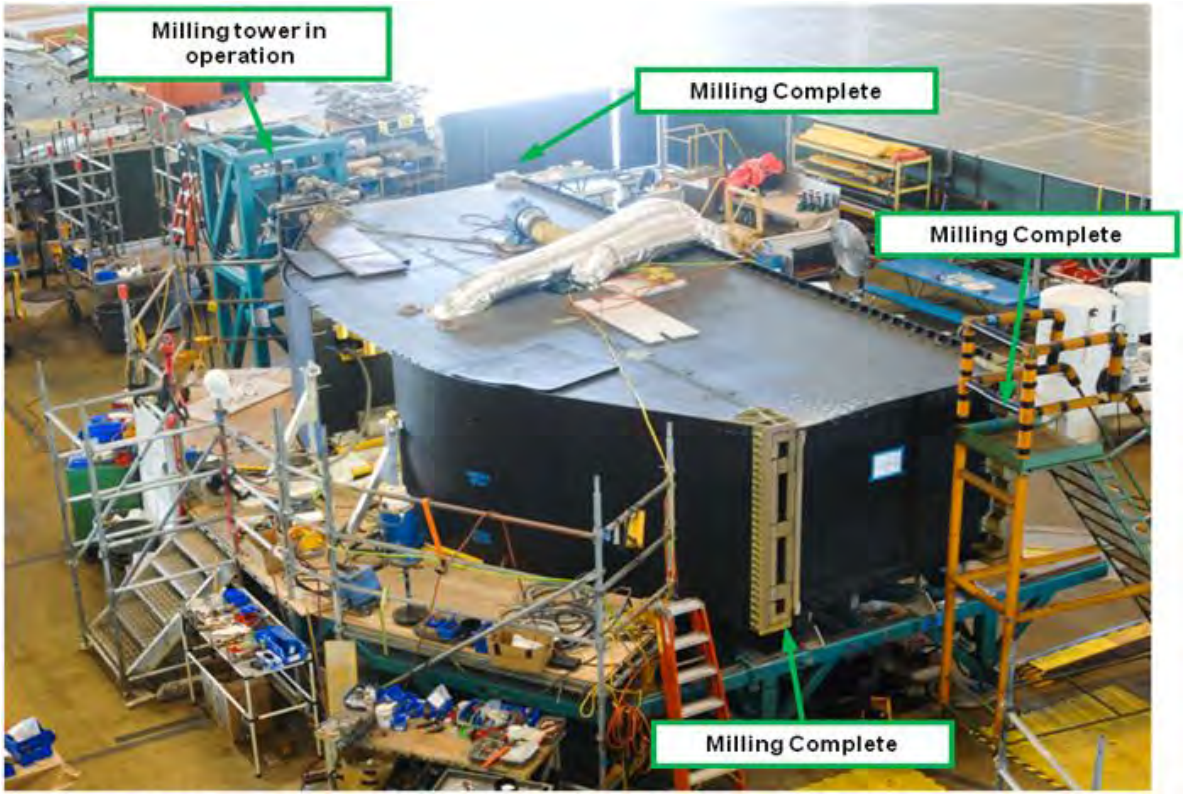

Figure 6-62. Milling Load-Introduction Fittings

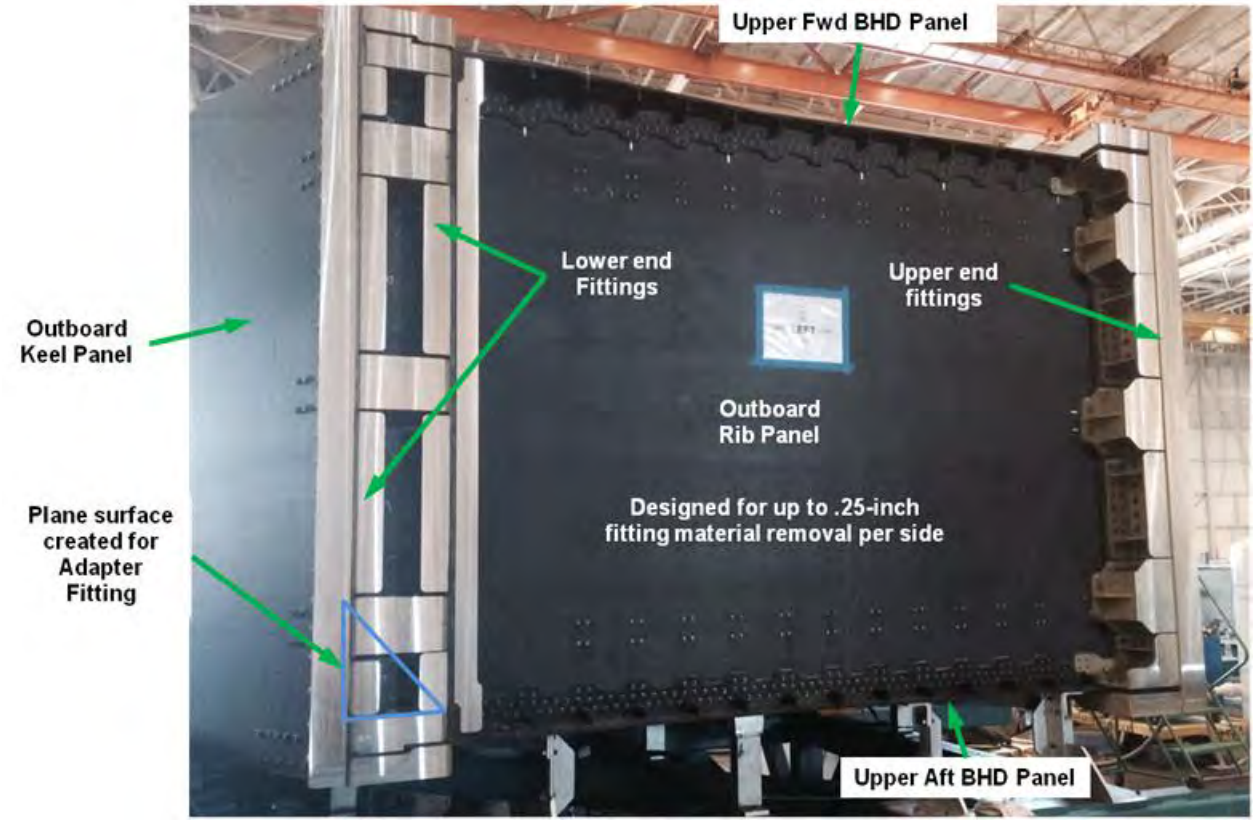

Figure 6-63. No Problems Arose With Milling the Load-Introduction Fittings

6.2.7 Multi-bay Box Rotation

As shown in Figure 6-64, the MBB was assembled on its aft side. In this position, no additional assembly tools were required to build the test article. The highly integrated panels were stiff enough to maintain their shape, and once DA-pinned together, the MBB rectangular shape was very rigid. With the bulkhead panel on the bottom acting as the base, the other panels were simply pinned together. Conversely, in an upright position, assembly jigs would have been required to support in position both the panels and the technicians standing on them. The approach taken also made it easier to assemble the side keel panels in the lower section. (In an upright position, the technicians would have had to climb up the slopped sides, making assembly much harder.)

As shown in Figure 6-65, the rotation process had been well prepared, and all equipment needed was ready and properly positioned on the scheduled day to lift the MBB.

Figure 6-64. Starting Position of the Multi-bay Box

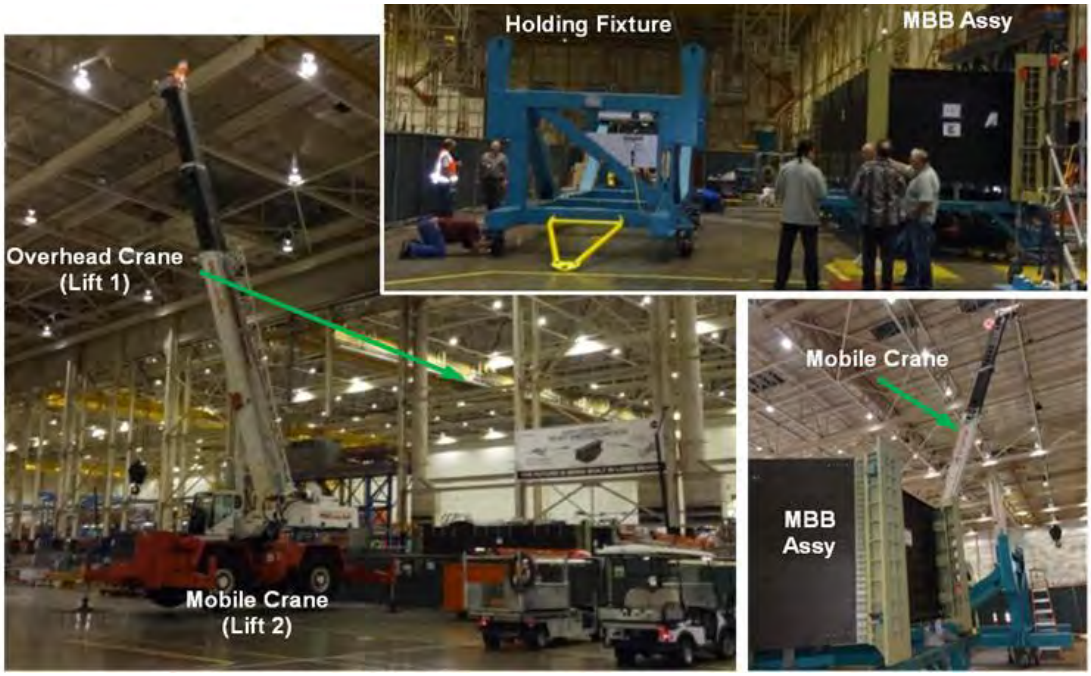

Figure 6-65. Preparing for the Move to the Holding Fixture

The holding fixture (a steel weldment assembly with casters) had arrived at the assembly site weeks before the move. This fixture was placed parallel to and approximately 8 ft away from the assembly, and in line to limit the moving distance once the MBB was rotated vertically. Two cranes were needed to lift the MBB, a mobile crane and an overhead crane. These two cranes operated simultaneously, lifting the MBB by four hoist points to rotate the structure. Other equipment such as spreader bars, cables, shackles, and hooks were already accounted for and on hand. The lift to the holding fixture began by lifting the MBB vertically straight up to clear the AJ1, as shown in Figure 6-66.

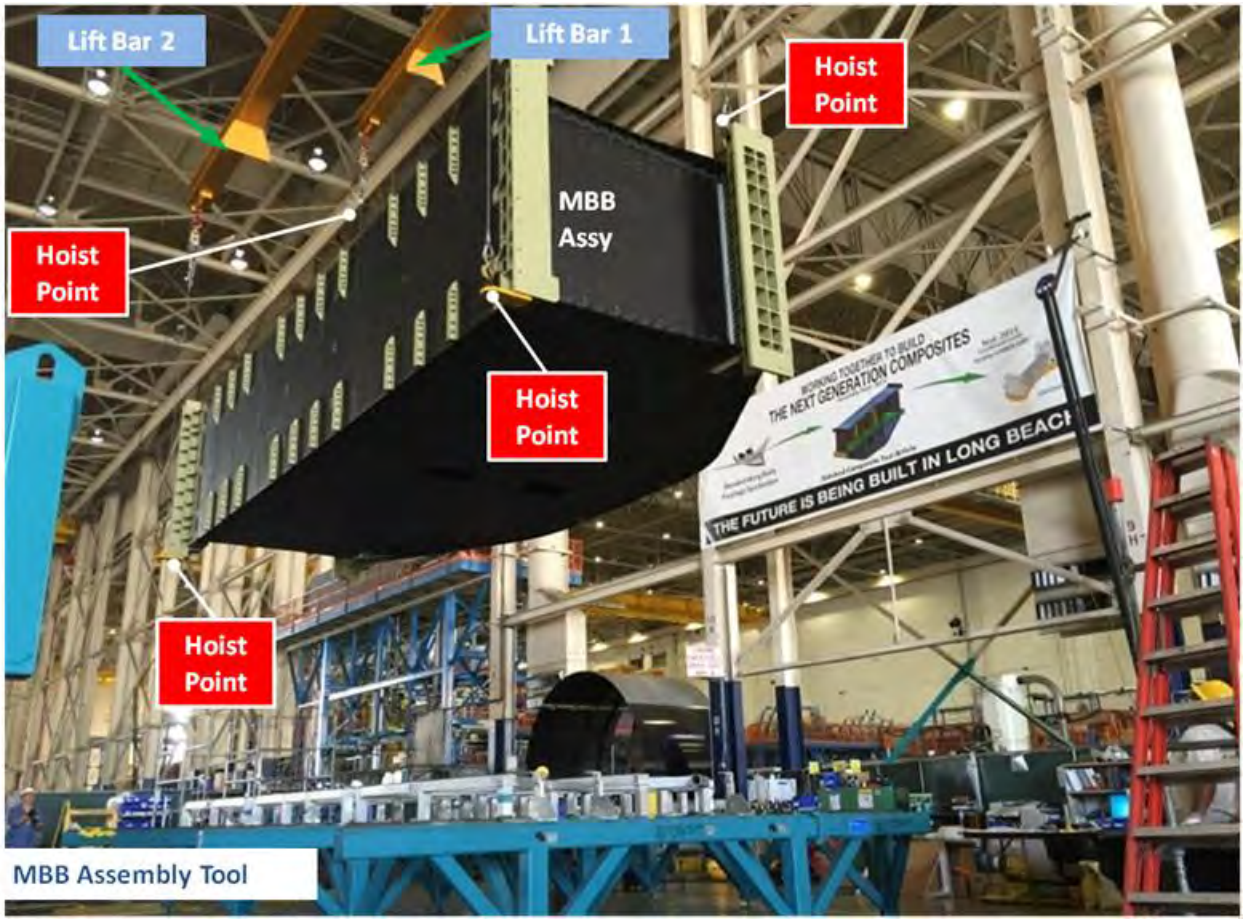

Figure 6-66. Starting the Move to the Holding Fixture

The lift, rotation, and turning the MBB into its vertical position went as planned and with no incidents, as shown in Figure 6-67, Figure 6-68, and Figure 6-69.

Figure 6-67. Rotation of the Multi-bay Box

Figure 6-68. Multi-bay Box Assembly in Vertical Position

Figure 6-69. Multi-bay Box Assembly Moving Into the Holding Fixture

Once the MBB was set and locked in the holding fixture (Figure 6-70), preparations began to restart work in the upper and lower bays and complete the work needed that had been inaccessible in the aft bulkheads due to the beams in the assembly jig AJ1 tool.

Figure 6-70. Multi-bay Box Assembly on the Holding Fixture

6.2.8 Strain Gages

Strain gages were placed on all composite panels and some fittings to record loads on the structure. This would enable engineering to monitor the structure during the test and compare it to the analysis that had been performed on the MBB. The upper section panels were strain-gaged during the mechanical assembly of the lower section of the box, as shown in Figure 6-71.

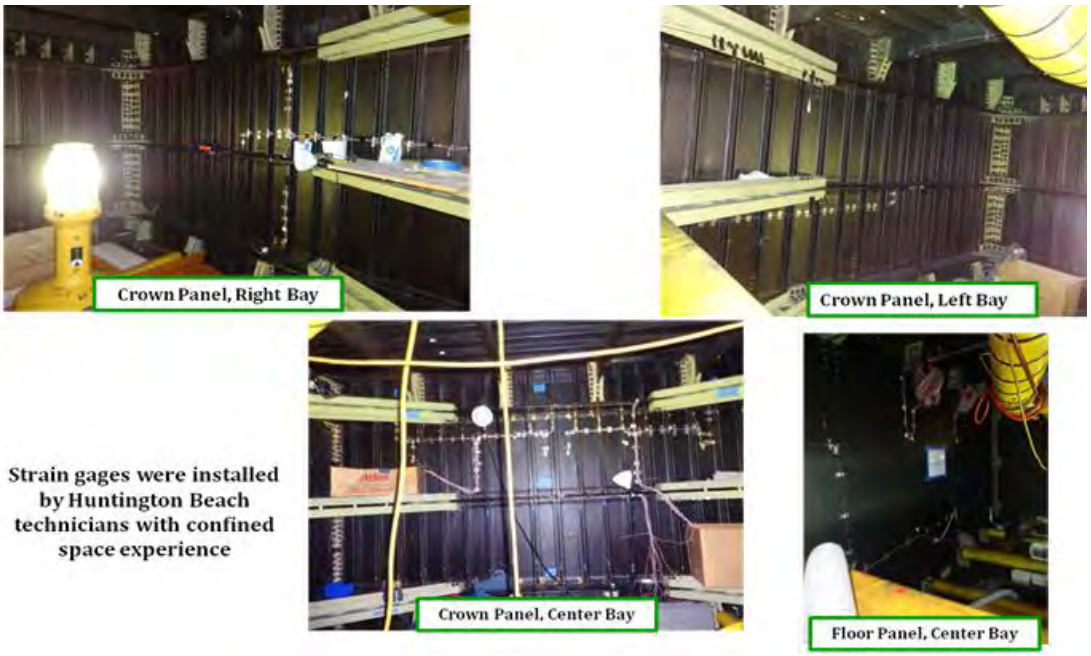

Figure 6-71. Upper Section Strain Gage Installation

Strain gages for the lower section panels had been installed at the Boeing Huntington Beach facility (Figure 6-72) before the panels were shipped for final assembly in Long Beach, which helped reduce the overall MBB assembly duration.

Figure 6-72. Lower Panels Were Strain-Gaged Before Assembly

To further reduce the overall assembly time span, both mechanical installations and strain gaging were done in parallel in the lower section of the MBB, as shown in Figure 6-73.

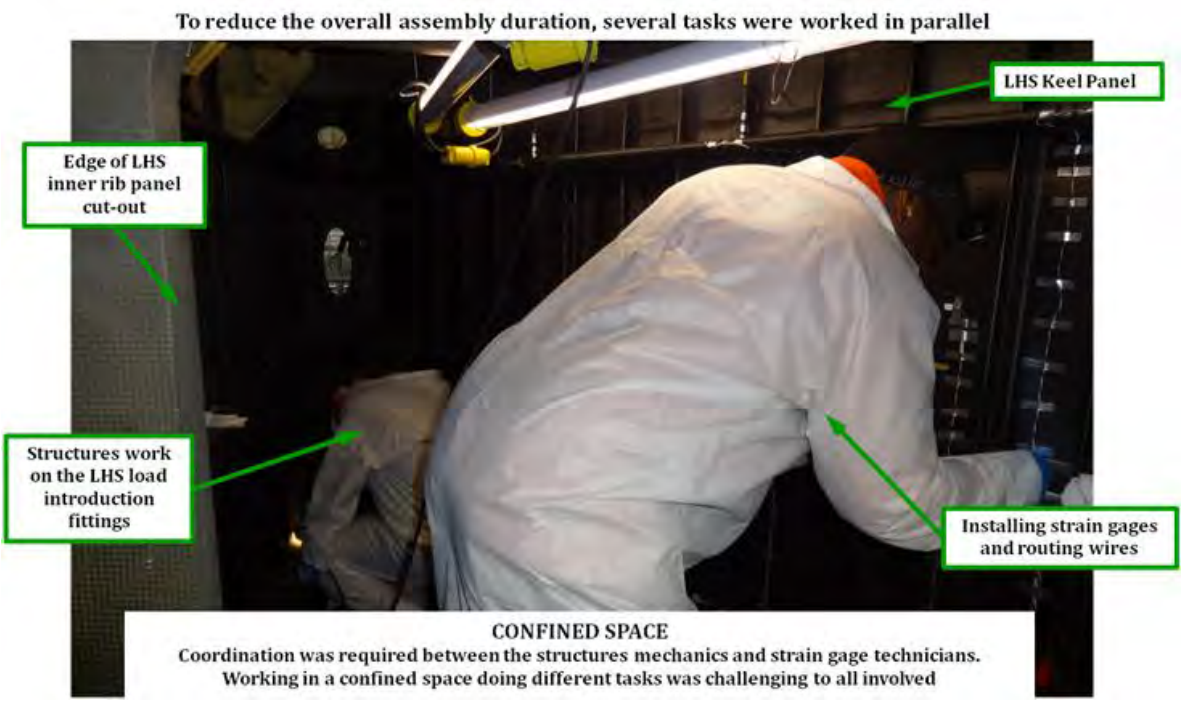

Figure 6-73. Mechanical Installations and Strain-Gaging Done in Parallel

Confined Space training facilitated strain-gaging work in this environment. For the comfort and safety of mechanics and technicians, there was always proper air ventilation and an air-conditioning unit to cool the air inside the box, especially during the hot summer months. Permits for soldering the gage wires inside the box were obtained, and every day during assembly the box was ‘sniffed” to make sure that air particle count was at the proper limits required by Boeing safety standards.

There were a total of 470 strain gage wires placed in the MBB structure. Of these, Boeing installed 352 gages during assembly, and NASA installed the remaining 118 gages at its COLTS facility.

6.2.9 Pressure Test

The MBB was to be tested under pressure conditions up to 18.4 psi. To verify that the MBB could hold pressure without leaking, a 6-psi pressure check was conducted, which was the maximum pressure that could be safely tested on the factory floor. Additionally, 6 psi would be sufficient pressure to determine if the MBB had any leaks. Although it was not required that the MBB be totally leak free, the intent was for it to be pressure tight as much as possible, and any large leaks would have made it harder to maintain pressure during testing.

Once MBB assembly had been completed, pressure test equipment was assembled and placed at the assembly site. The two remaining access doors were fastened on the forward upper and lower bulkhead panels, and air hoses were attached to the aft lower access door union fitting. Figure 6-74 shows preparations for the 6-psi pressure check.

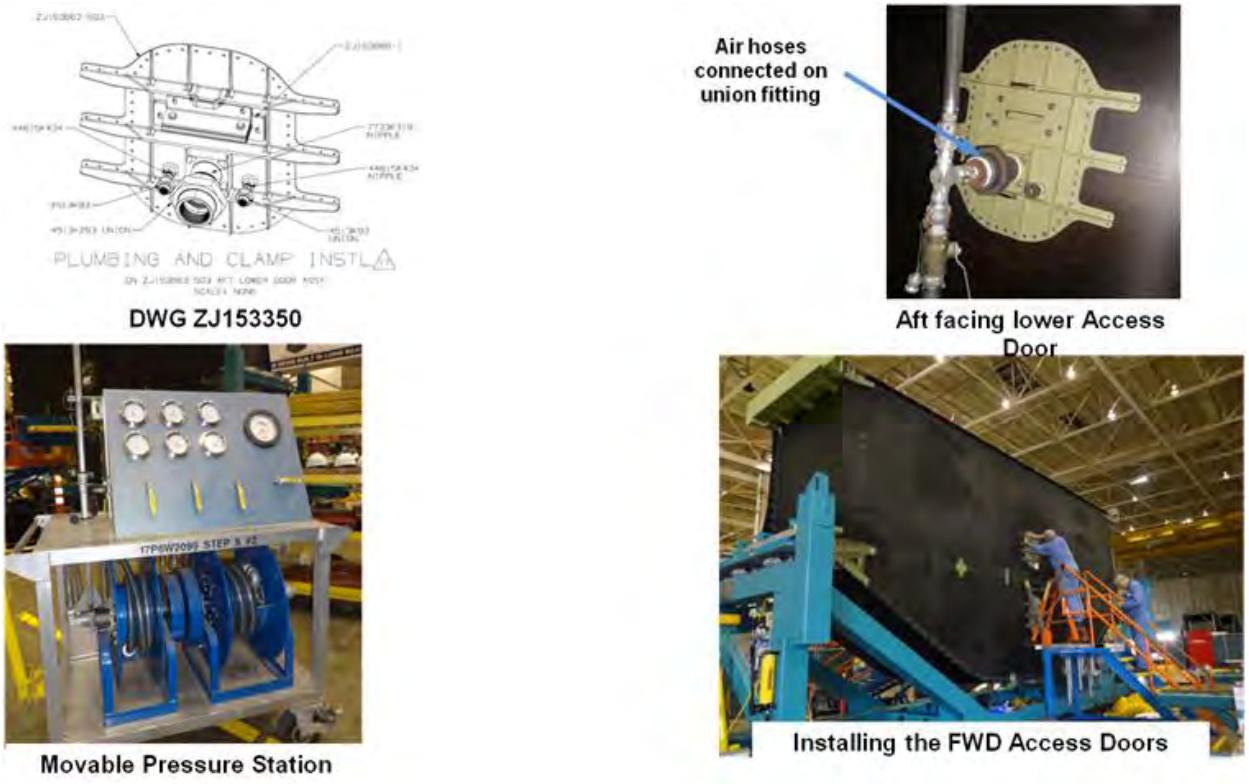

Figure 6-74. Preparations for Pressure Check at 6 psi

The 6-psi pressure test was conducted on the MBB at the Long Beach facility before delivery to NASA (Figure 6-75). Soapy water was used to enable detection of any air leaks in the structure. In Figure 6-75, the soapy water is shown running down the bulkhead surface after being sprayed along the crown panel cap joint at the top of the panel. Finding the actual source of air leaks was challenging, however, because only two of the four methods to seal the MBB had been used. Without the faying surface in the panel-to-panel joints, air was free to travel along the joint.

Figure 6-75 shows the soapy water bubbling up along the lower bulkhead to side keel joint. Once leak areas were marked for inspection, the forward face access doors were removed so that mechanics could reenter the MBB and reseal the leaks. To help determine actual leak sites, air was blown from the outside in (Figure 6-76) while mechanics sprayed soapy water along the joints on the inside Figure 6-77. The leaks for the bubbles shown in Figure 6-76 were two small pin holes. A similar situation occurred along the upper cap. Figure 6-78 shows an internal view of the leaky joint that had three small pin holes, both before and after the area was resealed. Any air leaks that were found were resealed with the same PR1422 sealant material that was used to fillet seal and encapsulate the fasteners on the MBB.

Figure 6-75. MBB Leak Check at 6 psi Using Soapy Water to Detect Leaks

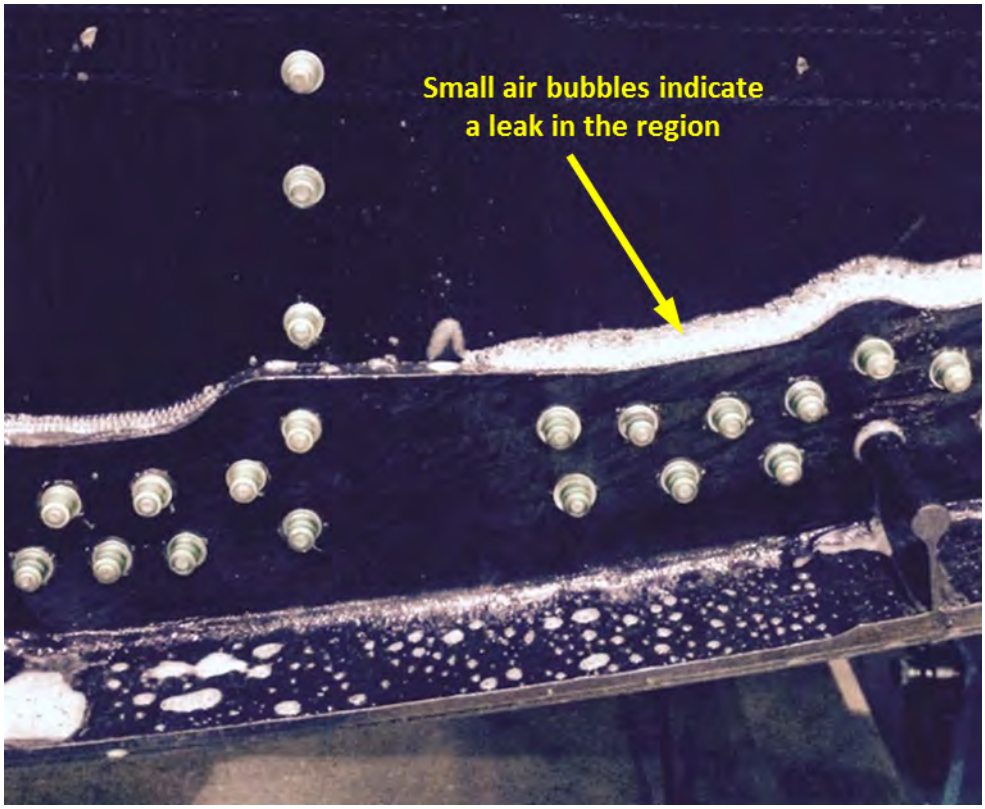

Figure 6-76. Soapy Water Exposed MBB Leaks at 6 psi

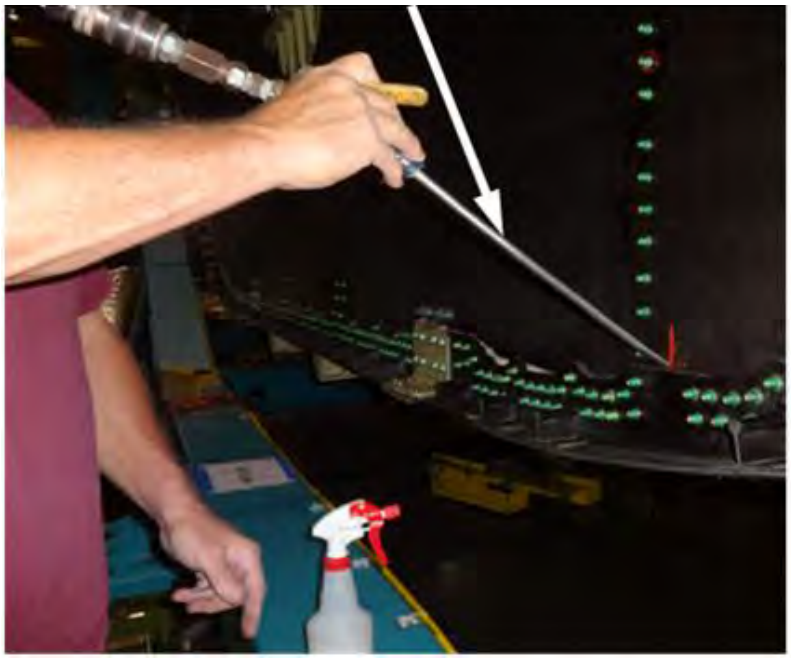

Figure 6-77. Technician Blows Air Back Into the Joint to Track the Source of the Leak Inside

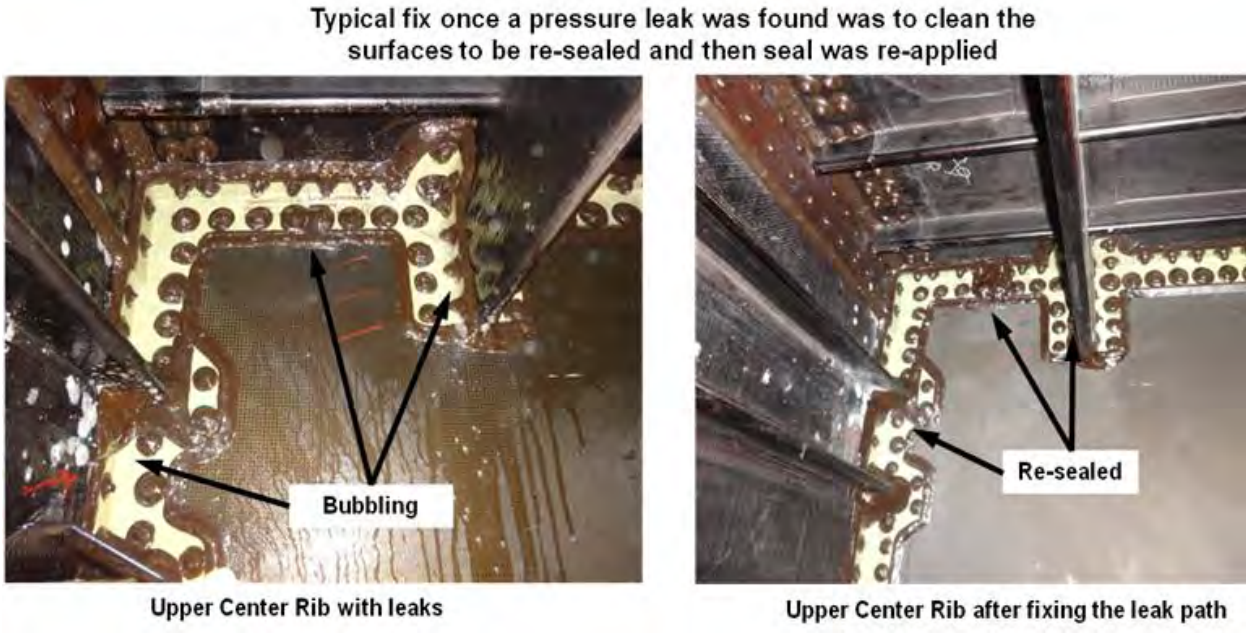

Figure 6-78. Typical Pressure Leaks, Checks, and Fixes

6.2.10 Painting the Multi-bay Box

After the MBB passed the pressure test required for delivery, the structure was transported to the paint hangar for painting, both inside and outside, as shown in Figure 6-79.

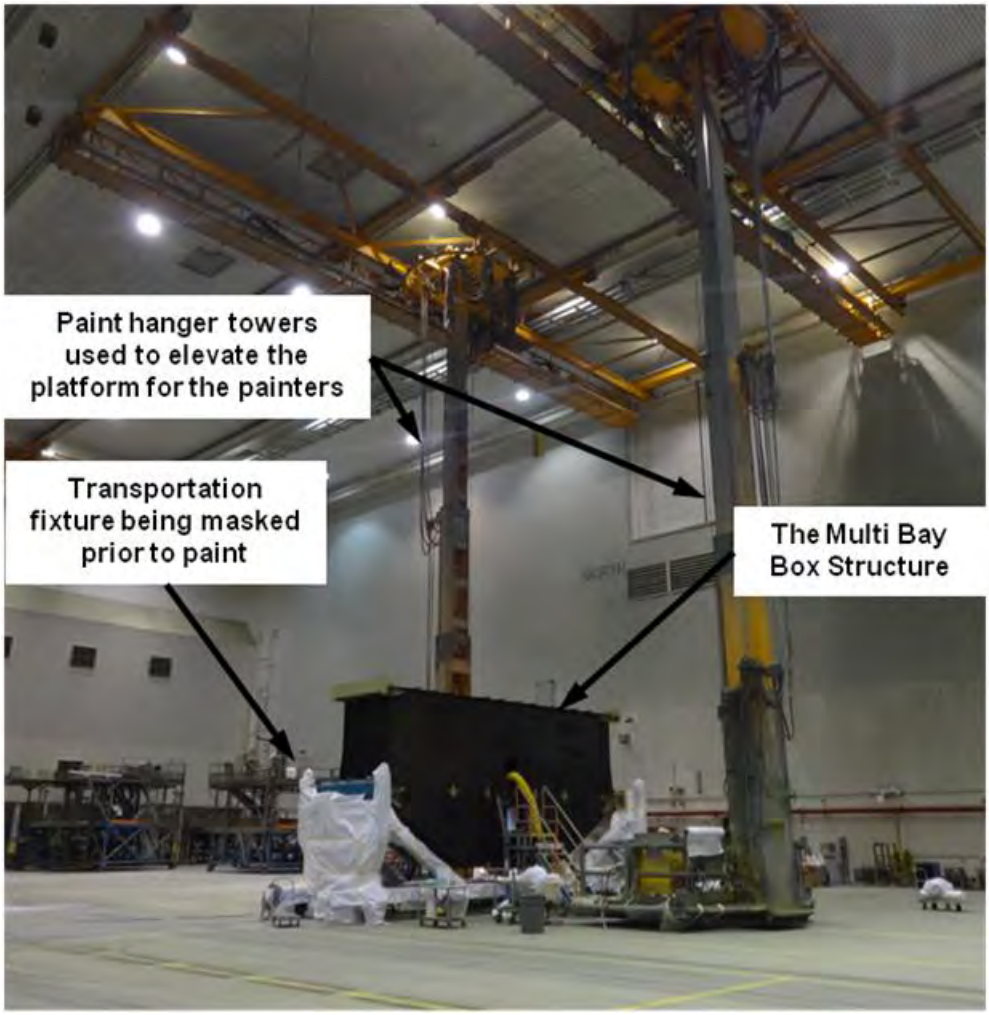

Figure 6-79. Multi-bay Box Inside the Long Beach Paint Hangar

Because the composite material was a dark color, it would be difficult to see where delamination or ply separation would start and end during testing. Therefore, the MBB was painted a tone of white both inside and outside to enable effects on the material during and after testing to be more readily seen.

All composite panels and interior metal fittings that held the structure were painted. However, the outside load-introduction fittings, adapter fittings, and the four access doors were not painted. Also not painted were some stay-out areas on the composite panels for the exterior instrumentation that NASA would install, as shown in Figure 6-80.

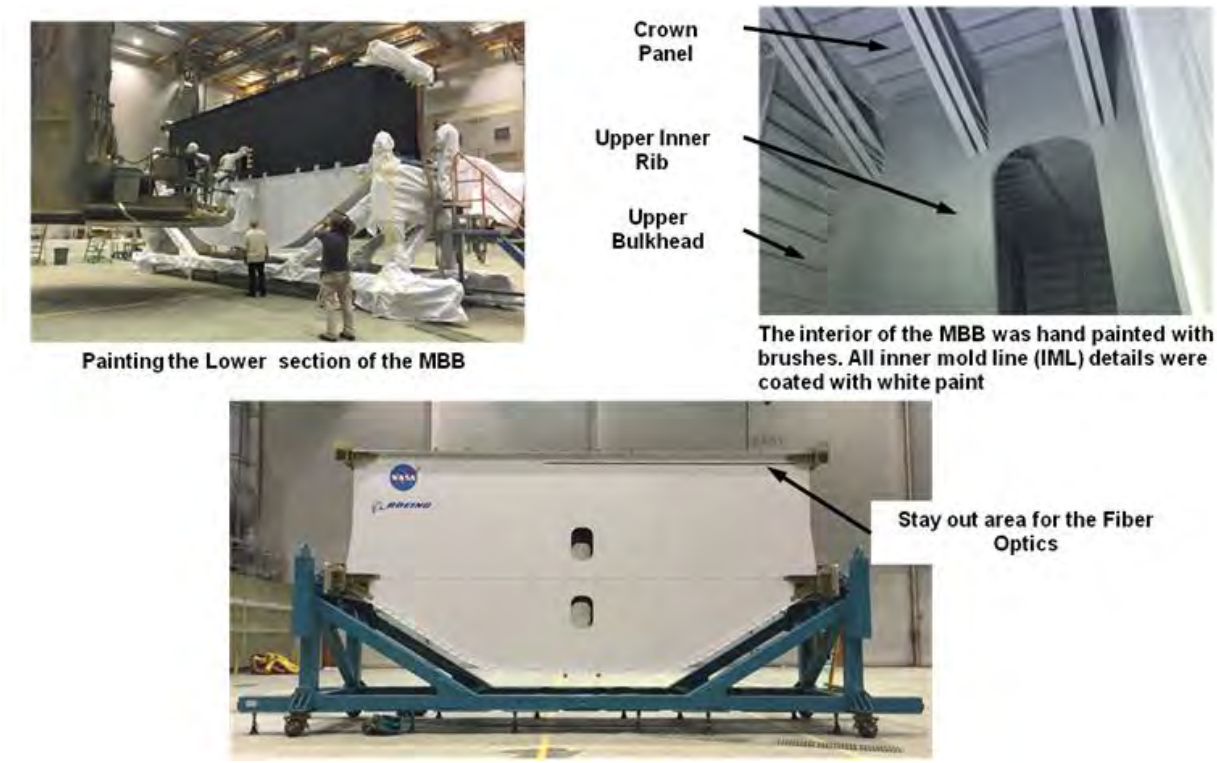

Figure 6-80. Painting the Multi-bay Box

With painting complete and NASA and Boeing logos placed on the structure (Figure 6-81), the MBB on the holding fixture was moved to the shop area adjacent to the delivery ramp. Once there, final preparation were made to get the MBB ready for shipping on the NASA Super Guppy aircraft for delivery to NASA LaRC.

Figure 6-81. Multi-bay Box Painting Complete

6.2.11 Weight

Weight measurements were taken at both the panel level and at the assembly level. Each individual panel was weighed, and a Center of Gravity (CG) was calculated and compared to the 3D computer model. The computer models for the panels were loaded with the density for each ply stack and every detail to generate model-based weight and CG location. After machining each panel, the panel was weighed using three scales to be able to calculate the CG. Figure 6-82, Figure 6-83, and Figure 6-84 show the model weight, actual weight, and an areal weight for each panel.

The MBB assembly was weighed when it was moved onto the handling fixture. At that time, the assembly was approximately 98% complete. Weight estimates were allocated to the items remaining to be installed, and they were added to the actual MBB weight to determine the final assembled MBB weight. Figure 6-85 shows the weight breakdown. By major component type, the weight breakdown is:

8,986 lb Overall MBB Weight
4,373 lb PRSEUS Panels (actuals)
641 lb Center and Aux Ribs (actuals)
3,049 lb Metallic Fittings (estimate based on 3D models)
417 lb Fasteners (estimate)
506 lb Miscellaneous (paint, sealant, shims, sealant, etc.)

Panel	Panel Area (ft2)	Actual Weight (lbs)	Estimated Weight (lbs)	% Weight Difference (Est-Act)	Areal Weight (lb/ft2)
Crown 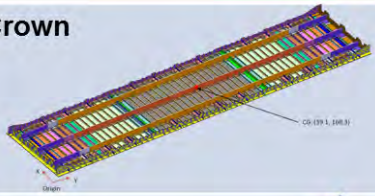	182.9	751.0	758.8	1.0%	4.11
Floor 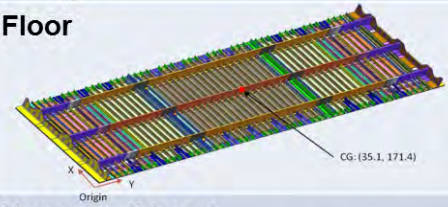	166.2	588.0	561.8	-4.5%	3.54
Upper Bulkhead 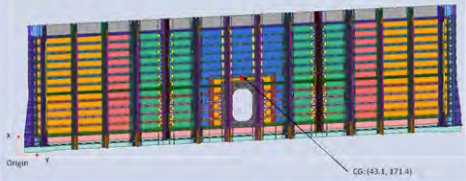	214.4	645.0	655.0	1.6%	3.01
	214.4	650.3	655.0	0.7%	3.03

Note: Panel weights include thick load introduction doublers that would not be present in an actual aircraft

Figure 6-82. Crown, Floor, and Upper Bulkhead Panel Weights

Panel	Panel Area (ft2)	Actual Weight (lbs)	Estimated Weight (lbs)	% Weight Difference (Est-Act)	Areal Weight (lb/ft2)
Lower Bulkhead 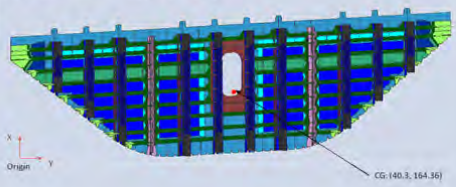	121.8	323.0	309.0	-4.3%	2.65
	121.8	320.0	309.0	-3.4%	2.63
Side Keel 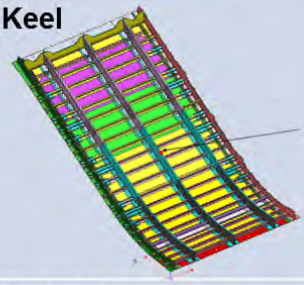	81.6	384.0	348.9	-9.1%	4.71
	81.6	N/A	348.9	N/A	N/A
Center Keel 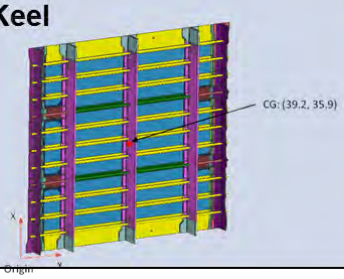	38.6	105.5	103.0	-2.4%	2.73

Figure 6-83. Lower Bulkhead, Side, and Center Keel Panel Weights

Panel	Panel Area (ft2)	Actual Weight (lbs)	Estimated Weight (lbs)	% Weight Difference (Est-Act)	Areal Weight (lb/ft2)
Outboard Rib 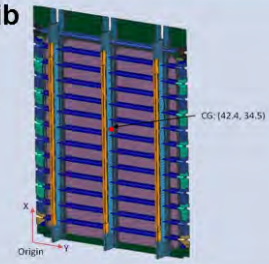	42.6	N/A	112.8	N/A	N/A
	42.6	111.3	112.8	1.3%	2.61
Upper Center Rib 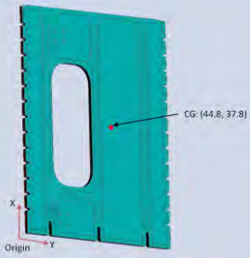	37.0	176.3	174.9	-0.8%	4.76
	37.0	N/A	174.9	N/A	N/A
Lower Center Rib 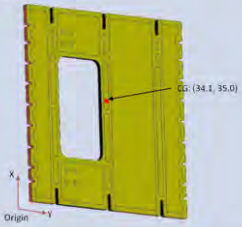	28.9	137.2	140.5	2.4%	4.75
	28.9	138.0	140.5	1.8%	4.78

Figure 6-84. Side Rib, and Upper and Lower Center Rib Panel Weights

Actuals for 98% Plus to Go Work	
Fasteners (Estimate)	2 lbs
Sealant (Estimate)	12 lbs
Strain Gage Wire (Estimate)	2 lbs
Paint (Estimate)	66 lbs
Aluminum Fittings (Model Based)	64 lbs
Actuals	8,840 lbs
Total Weight	**8,986 lbs**

Vertical Weighing Position

Figure 6-85. MBB Weight Based on 98% of the Assembly Being Completed

6.3 Final Preparation for Shipping

6.3.1 Handling Fixture Design

The MBB had to be moved from the horizontal assembly tool to gain access to install the remaining few fasteners and complete the final assembly tasks (shown in section 6.2.7). In addition, a fixture would also be required to ship the MBB to the COLTS facility for testing. Finally, a third fixture would be required to prepare the MBB for installation onto the COLTS platens. So a single handling fixture was designed that could accommodate the remaining activities. This approach saved tooling costs by eliminating the design and build of two additional tools. It also saved additional labor costs and reduced risk by eliminating transferring the MBB from tool to tool. It did, however, increase the complexity of the singe tool that was built, which had to meet requirements from Boeing, NASA JSC, and NASA LaRC.

The two main configurations of the fixture are shown in Figure 6-86. The final assembly configuration would be used at Boeing to complete the final assembly tasks and as a transportation dolly to move the MBB around the factory. The shipping configuration would be used to transport the MBB on the Super Guppy. The test integration configuration would be used by NASA LaRC to complete the final preparation steps to install the MBB onto the COLTS platens.

By far, the most difficult requirements to meet were the NASA JSC Super Guppy requirements. The Super Guppy had one pallet that interfaced with the aircraft. Figure 6-87 depicts the MBB positioned inside the aircraft for clearance checks. Because the cargo section of the aircraft was not temperature controlled, the fixture had to be designed to maintain its ductility in cold temperatures, including the welding. Figure 6-88 shows the different materials that were used to meet the cold-temperature ductility requirements.

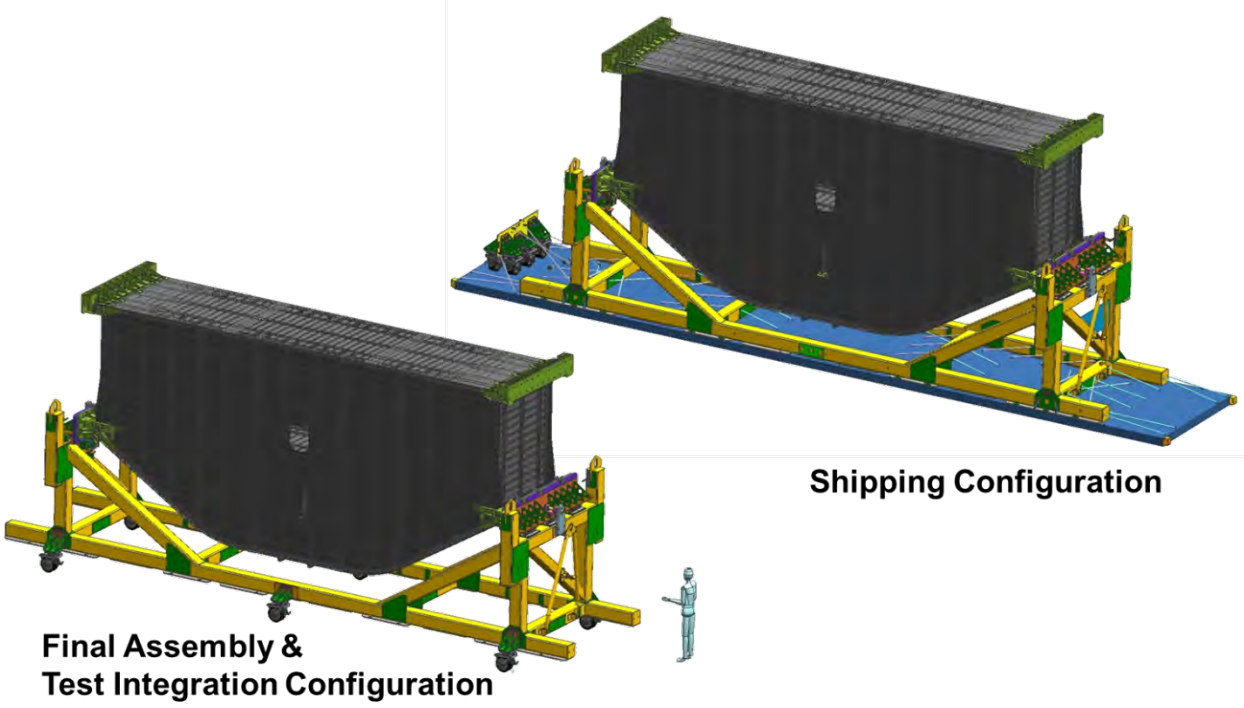

Figure 6-86. Holding Fixture Tool for the MBB

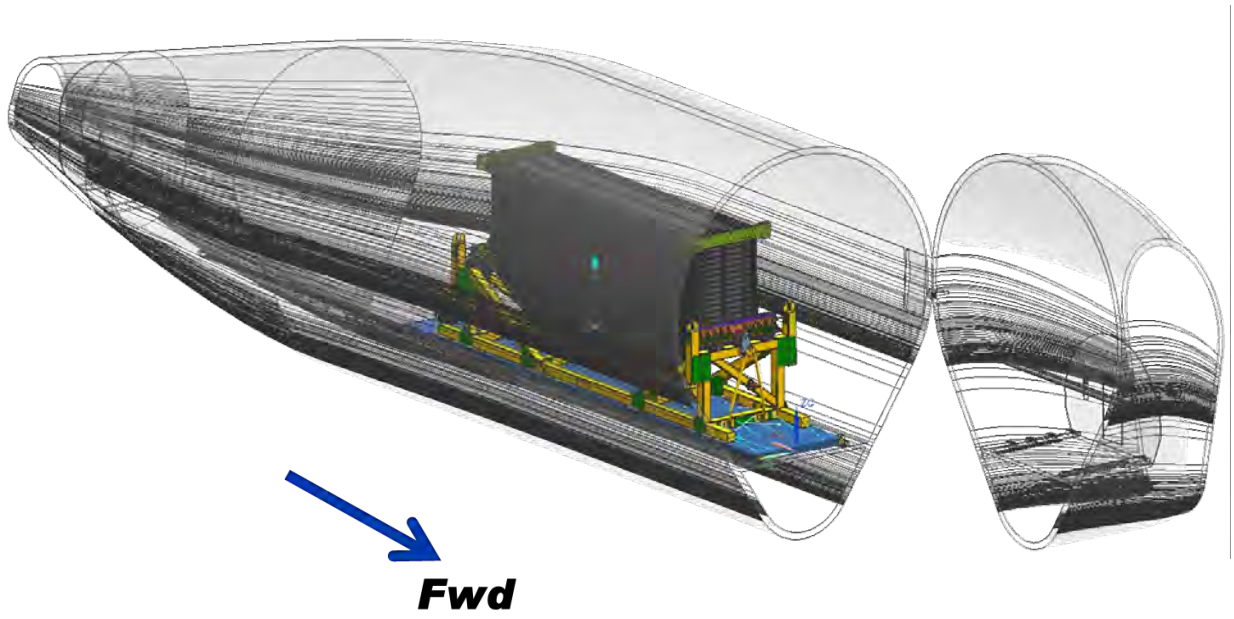

Figure 6-87. MBB Positioned Inside the Super Guppy

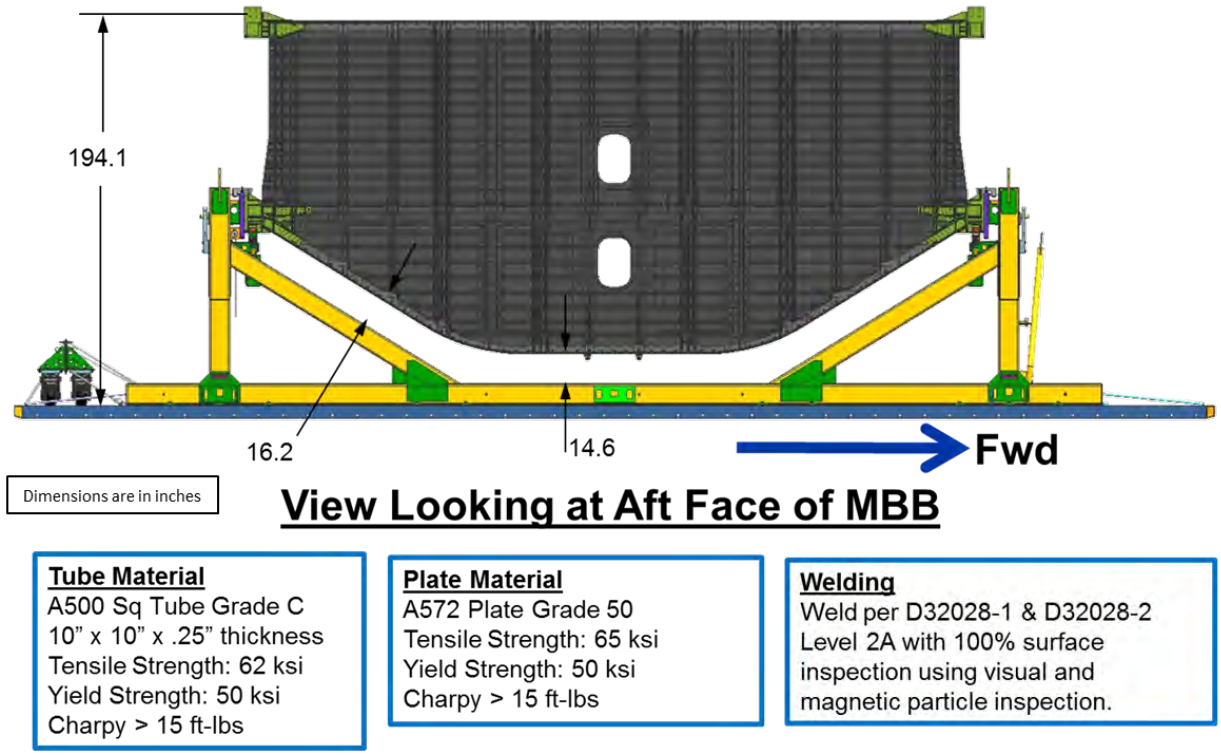

Figure 6-88. Material Used to Fabricate the Holding Fixture

The fixture had to fit within the pallet surface, which determined the maximum width of the fixture base. The pallet had several imbedded inserts with low pull-out allowables, and they were installed in a pattern that had very loose tolerances. A laser shoot of the pallet inserts was required to document their actual location. With a steel fixture and an aluminum pallet, the interface had to accommodate the cargo bay temperature range of 0 to 120°F. This was accomplished using a combination of bolts and chains. The slots were machined into the welded fixture assembly, maintaining very tight tolerance to ensure that it could be properly bolted to the pallet. The design used the chains to take the forward and aft loads (Figure 6-89) and the bolts to take the side-to-side and the up loads. Long slots at the bolt locations allowed the aluminum pallet to move relative to the steel tool along the length. However, it required 56 chains to reduce the load at each chain to an acceptable pallet insert load level and the amount of stretch at each chain to reduce the slots in the fixture to an acceptable length. The entire side load was supported by the 10 bolts on the left side of the fixture (Figure 6-90), allowing the pallet to move independently of the fixture at temperature in the Y direction. Figure 6-91 shows that the right-hand side slot was wider than the left-hand side. It also shows the gaps in the forward and aft directions. To ensure that there would always be adequate surface contact to react the up loads, a flanged bushing straddled the slotted hole (Figure 6-92). This bushing was sized to maintain a minimum of 0.50-in. surface contact around the entire slot.

During a weight-savings exercise to reduce the line loads exerted along the long edges of the pallet, the wheel assemblies were removed for shipping. These wheel assemblies were bolted to a flat plate to create a single assembly, which would be located at the aft end of the pallet and be easily chained into position during shipping. Figure 6-93 shows the position of the wheels on the pallet and the six additional tiedown chains required for shipping.

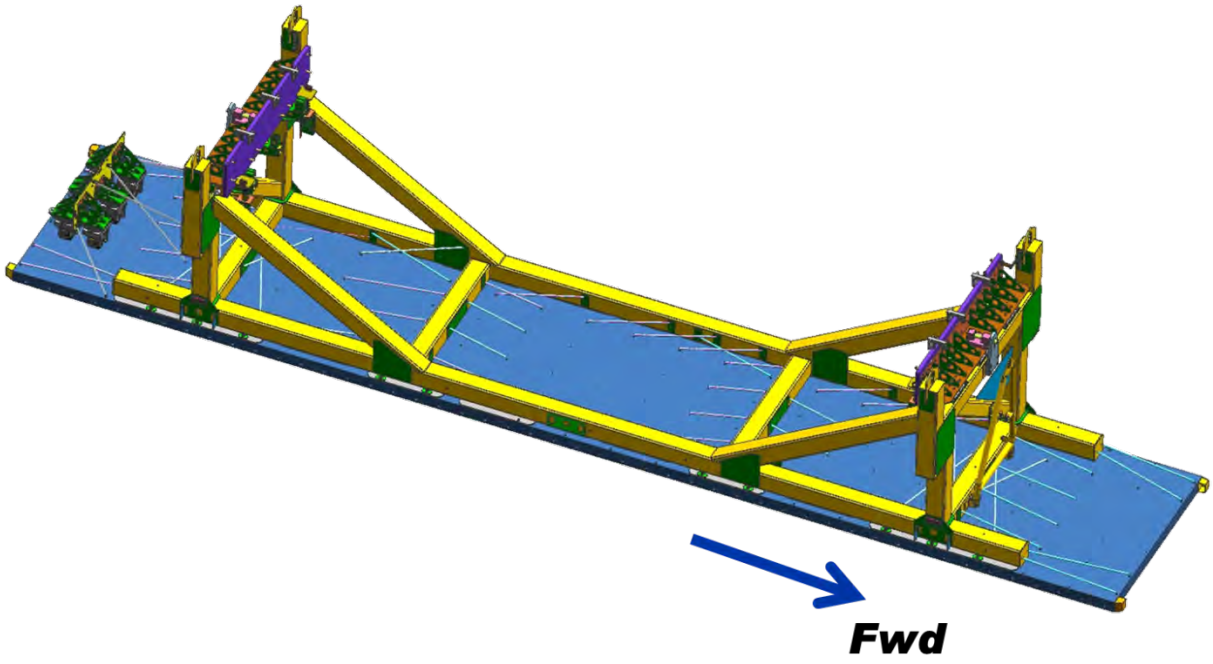

Figure 6-89. Chain Tiedown Arrangement

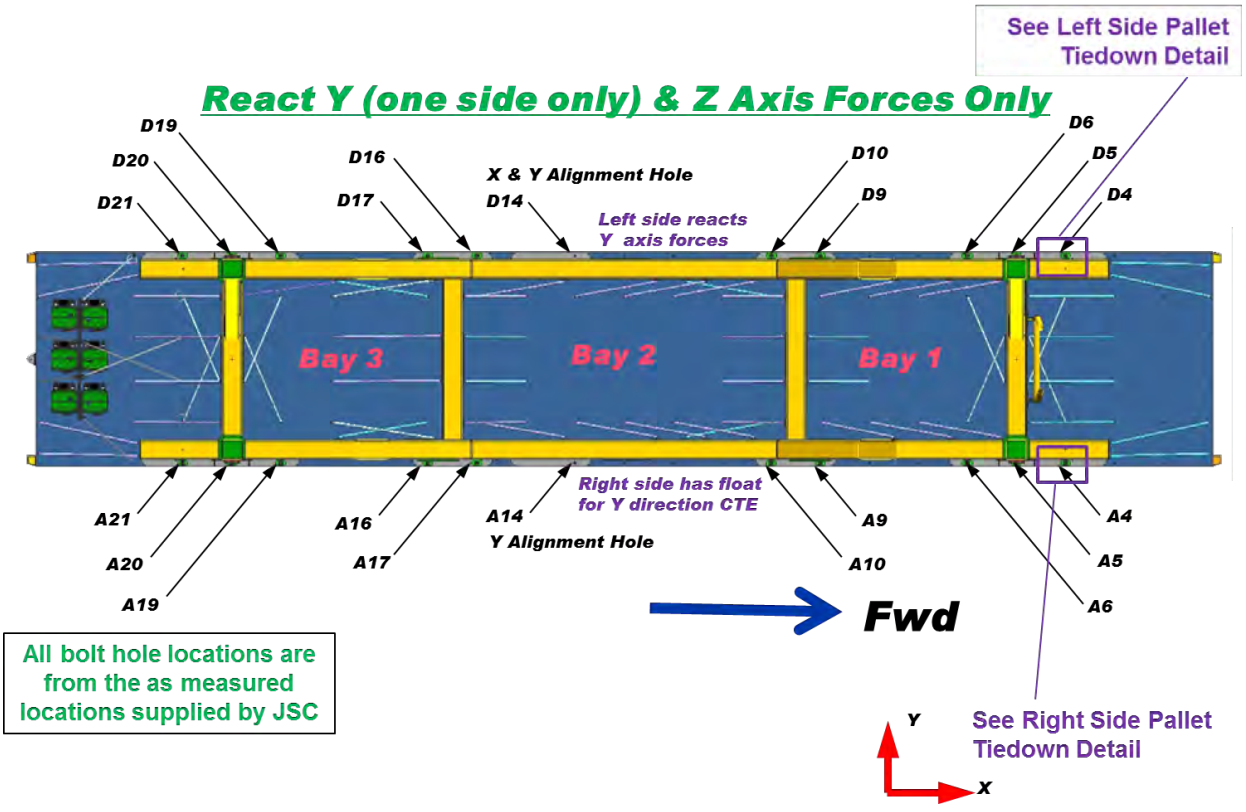

Figure 6-90. Fixture Tiedown Bolt Arrangement

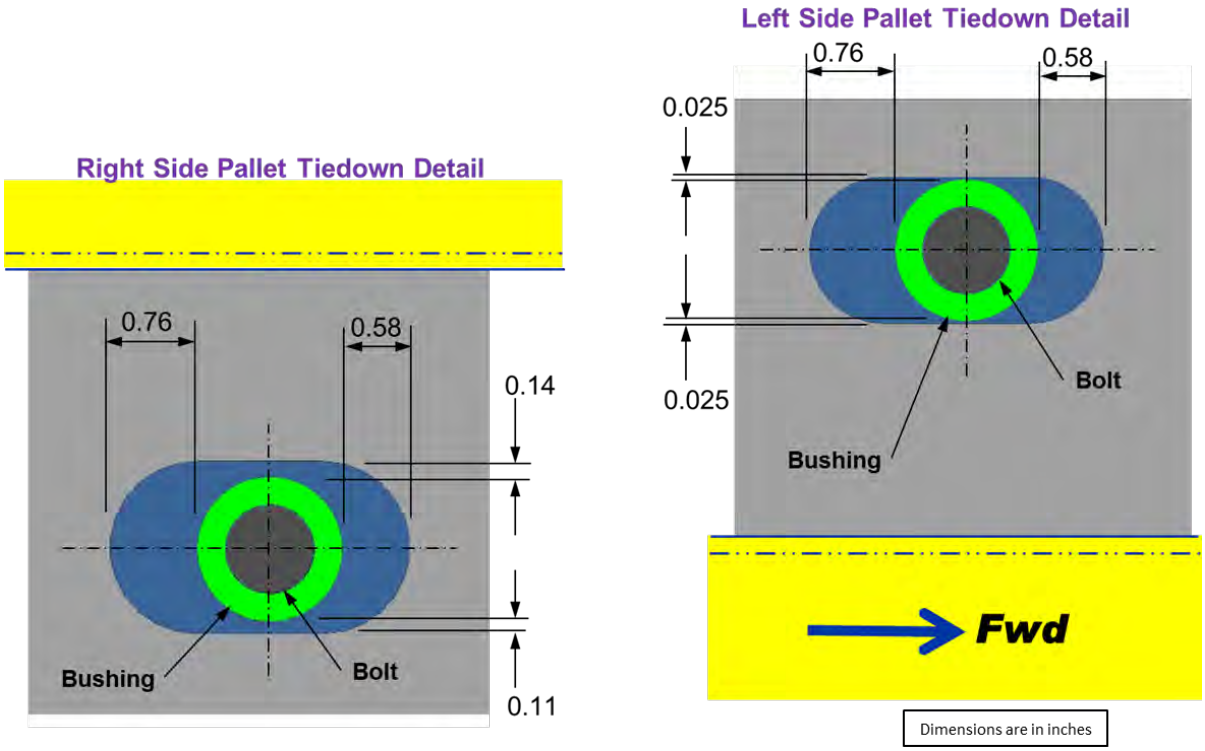

Figure 6-91. Bolt-Hole Slots in the Fixture Accommodated Thermal Expansion Differences

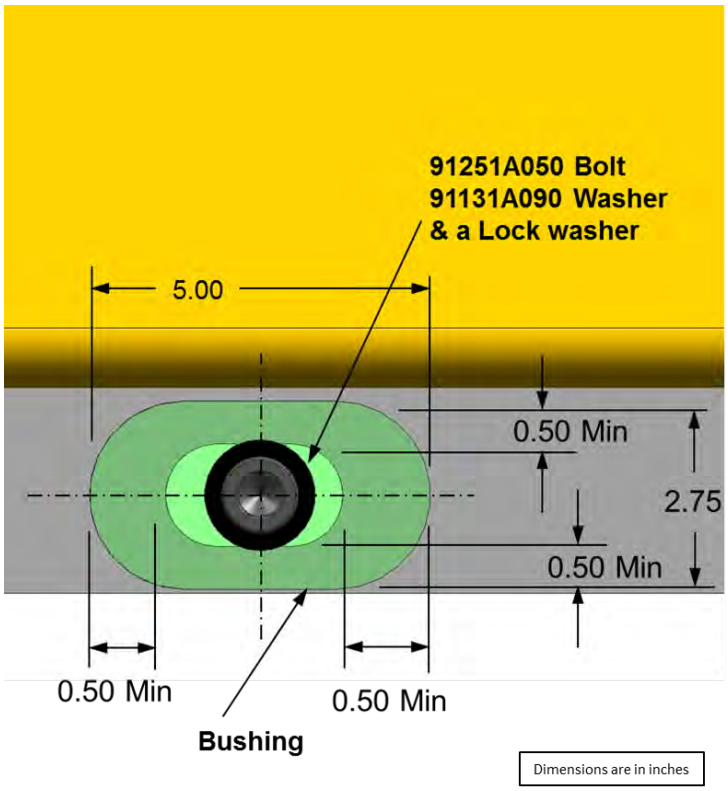

Figure 6-92. Flanged Bushing Maintained a Minimum of 0.50-in. Contact Around the Slot

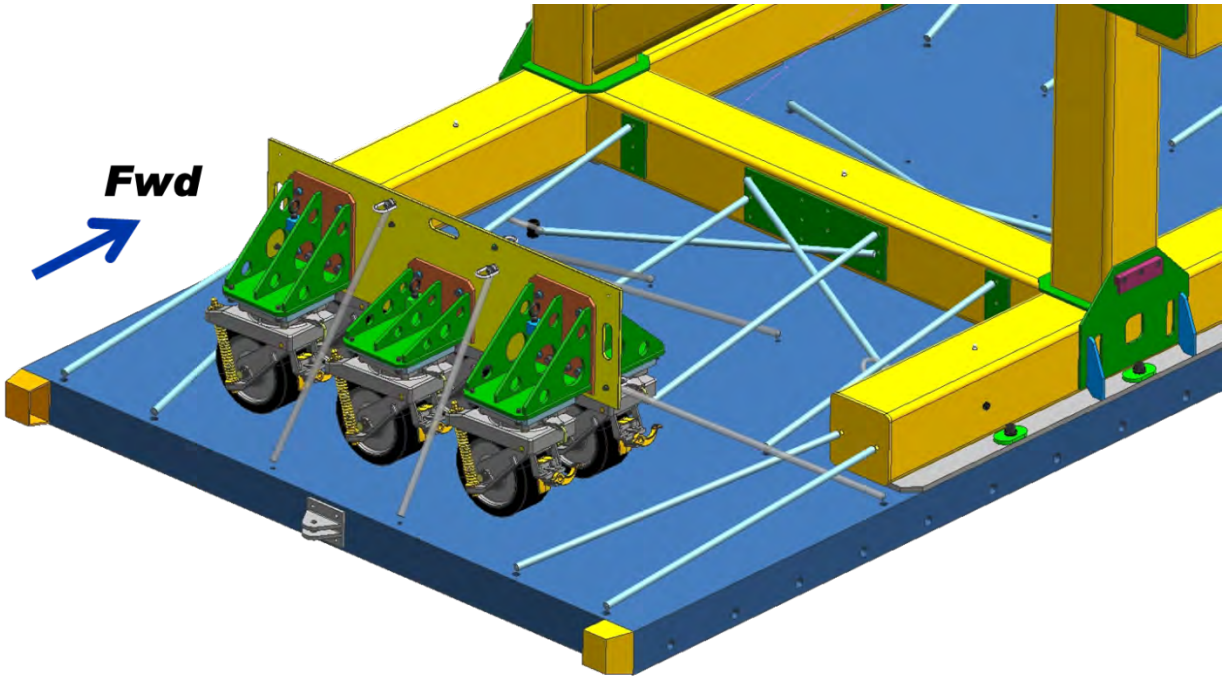

Figure 6-93. Wheel Assemblies Were Shipped Separately and Positioned on the Aft of the Pallet

A simple method was required to be able to properly locate the MBB within the handling fixture. It was also important to have the MBB free from all attachments before any crane-lifting loads were applied. This would guarantee that none of the handling fixture could be lifted inadvertently during the MBB removal process. The easiest way to accomplish this was to have the attachment bolts in tension (parallel to the lifting direction). As previously mentioned, part of the complexity of the tool were the many multi-use requirements. It would have been easy to design a detail that bolted to the adaptor fittings to orient the fixture attachment bolts vertically. However, during the test integration portion of the fixture use, the MBB adaptor fittings needed to be free of any bolted-on details after the MBB was lifted out of the fixture to allow it to be positioned in between the COLTS platens.

Trying to remove any fittings attached to the MBB adaptor fittings with the MBB suspended from a crane would have been unsafe. Therefore, a three-point loading pad was designed (Figure 6-94). These three points precisely located the MBB in the fixture every time and allowed it to be completely unbolted from the fixture before being attached to a crane for removal. This meant that shear bolts could be used to bolt an attachment plate onto the adaptor fittings. To compensate for the actual height of the MBB on the fixture, a hydraulic system was added. With the weight of the MBB riding on wire rope isolators, the MBB needed to be lifted to a neutral position to be able to remove the shear attachments. To accomplish this, four jacks were used, one in each corner, as shown in Figure 6-94. To ensure that the MBB was free to move on the isolators during shipping, the interface details swung out of the way, as shown in Figure 6-95.

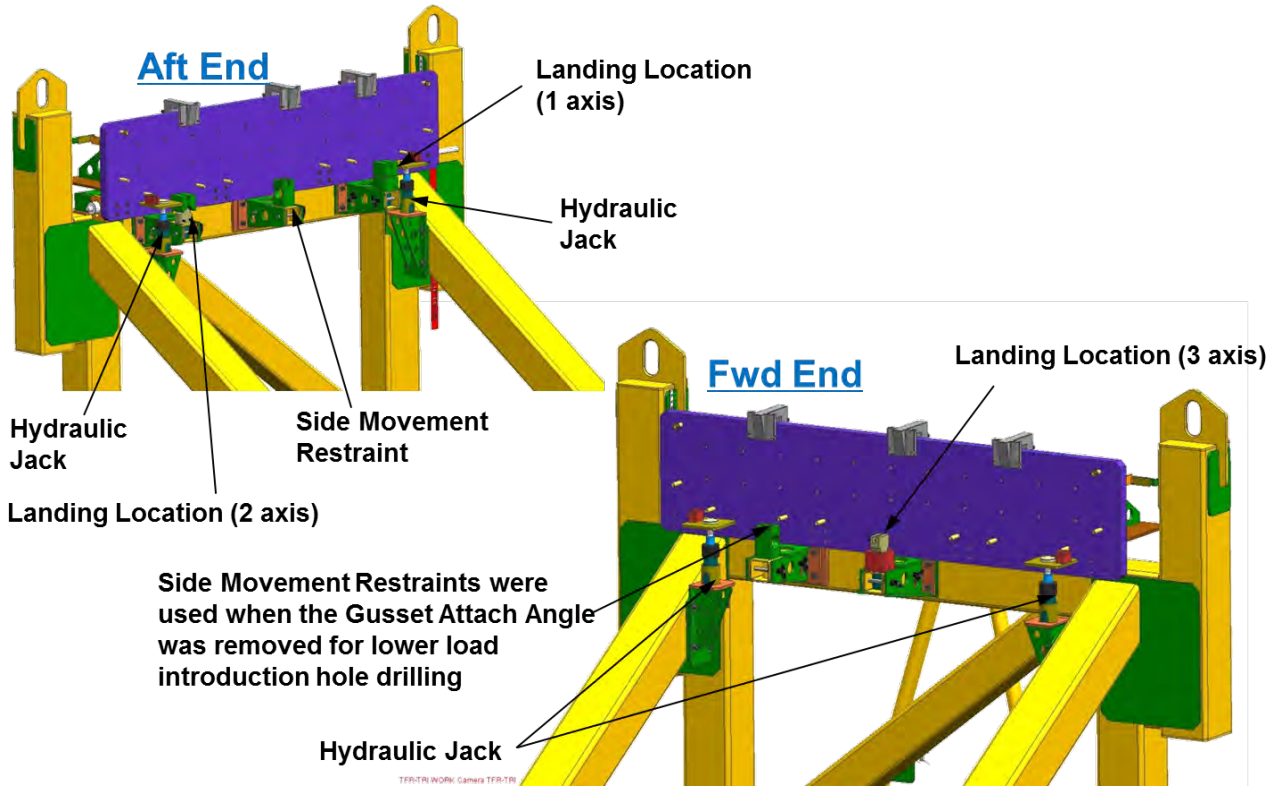

Figure 6-94. MBB-to-Holding Fixture Interface

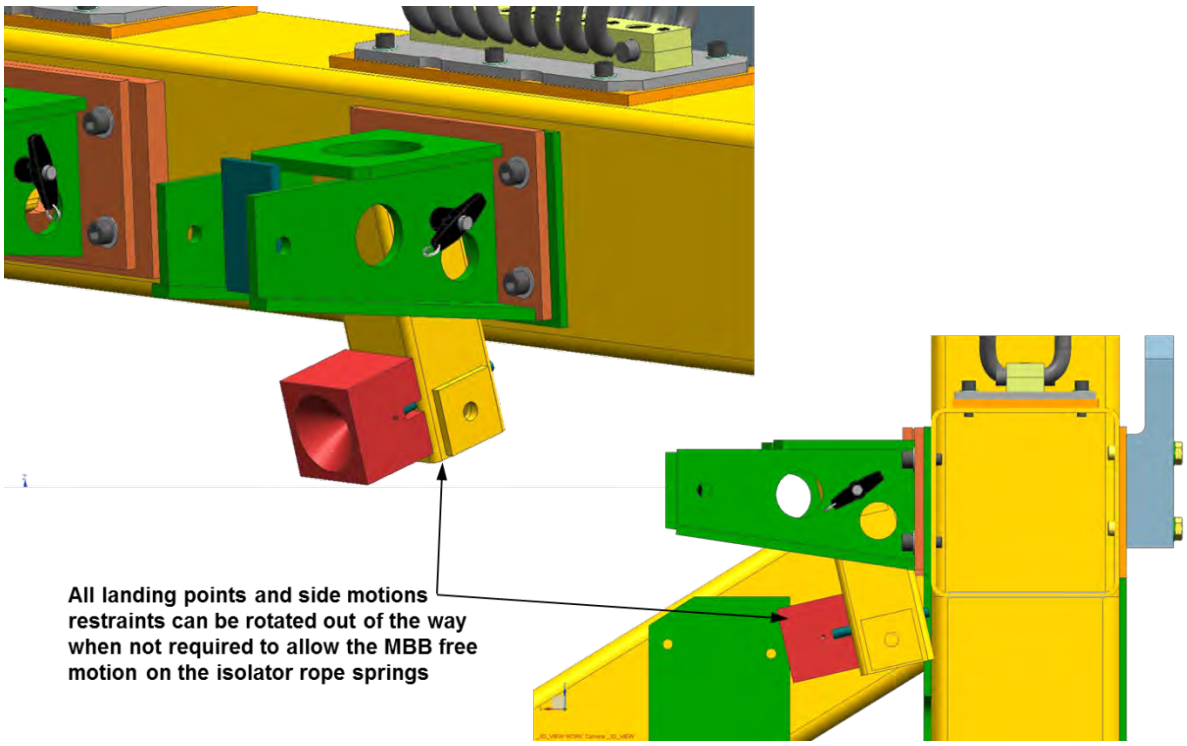

Figure 6-95. Interface Handing Fixture Swing-Down to Allow the MBB to "Float" on the Isolators

Wire rope isolator springs were added to the fixture to decouple the MBB from the fixture (Figure 6-96). With the composite MBB attached to a steel tool riding in an environment that could range from 0 to 120°F, thermal expansion differences needed to be considered. The isolator springs eliminated the unwanted thermal loading and softened the potentially high vertical loads imparted by the Super Guppy shipping requirements. Unfortunately, the isolators also allowed the MBB to oscillate in the side-to-side and forward and aft directions more than desired. To resolve this problem, side-to-side motion plates and bars were added to both ends of the fixture (Figure 6-96), and a forward and aft motion bar was also added to the aft end of the fixture. It used four finger fittings located between the isolators, as shown in Figure 6-97. These finger fittings and the side motion plates had vertical slots that did not restrain the up-and-down motion based on the stiffness of the isolators (Figure 6-98).

With a tall payload and the fixture width constrained by the width of the Super Guppy shipping pallet, outrigger wheel assemblies were used to increase stability of the fixture. A majority of the weight was supported by the end wheels located at the four corners. The center wheels were added mainly to reduce the fixture's flexing under its own weight (which would cause the vertical supports to bow inward) and to keep the center from bouncing during towing. Fail-safe angles were used to back up the four end wheel attachments. The wheel assemblies are shown in Figure 6-99.

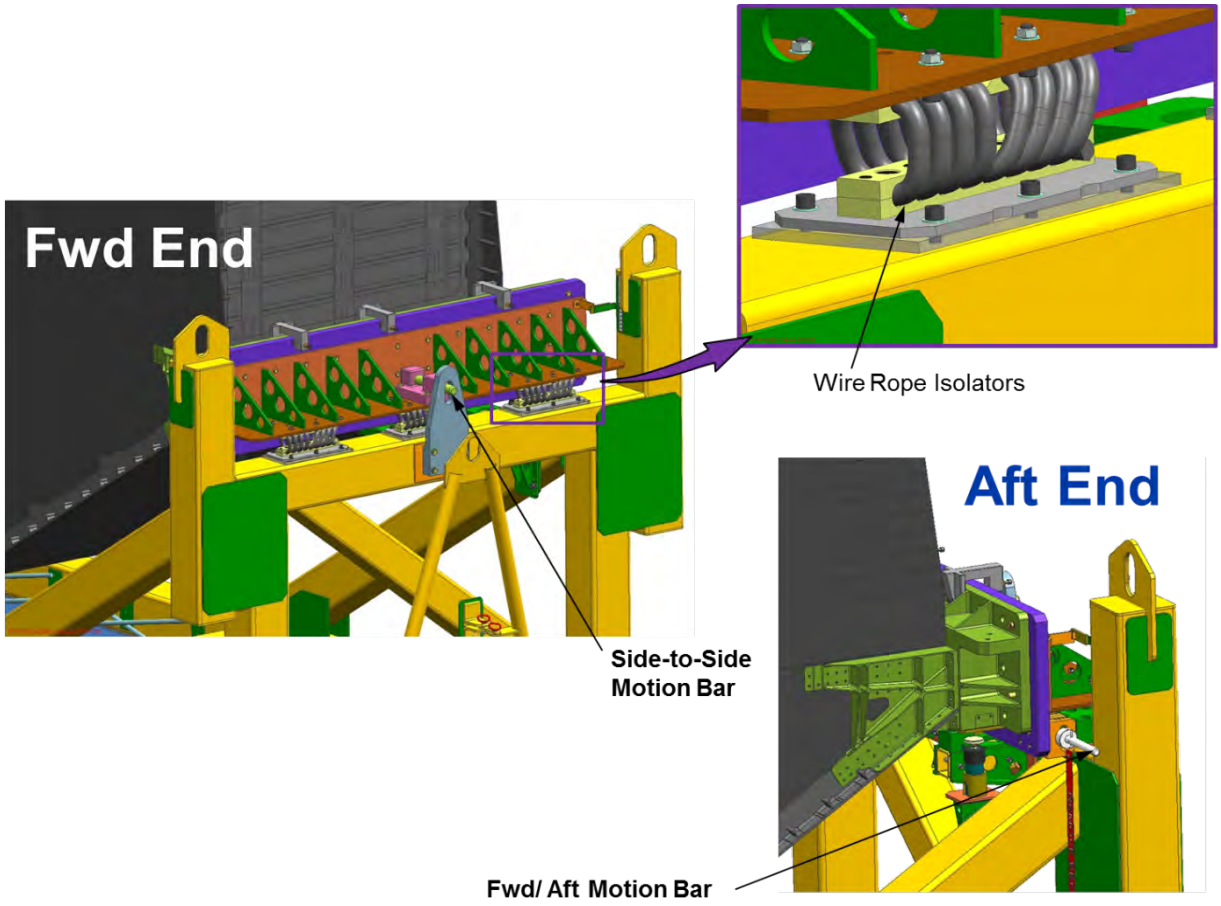

Figure 6-96. Holding Fixture Restraint System

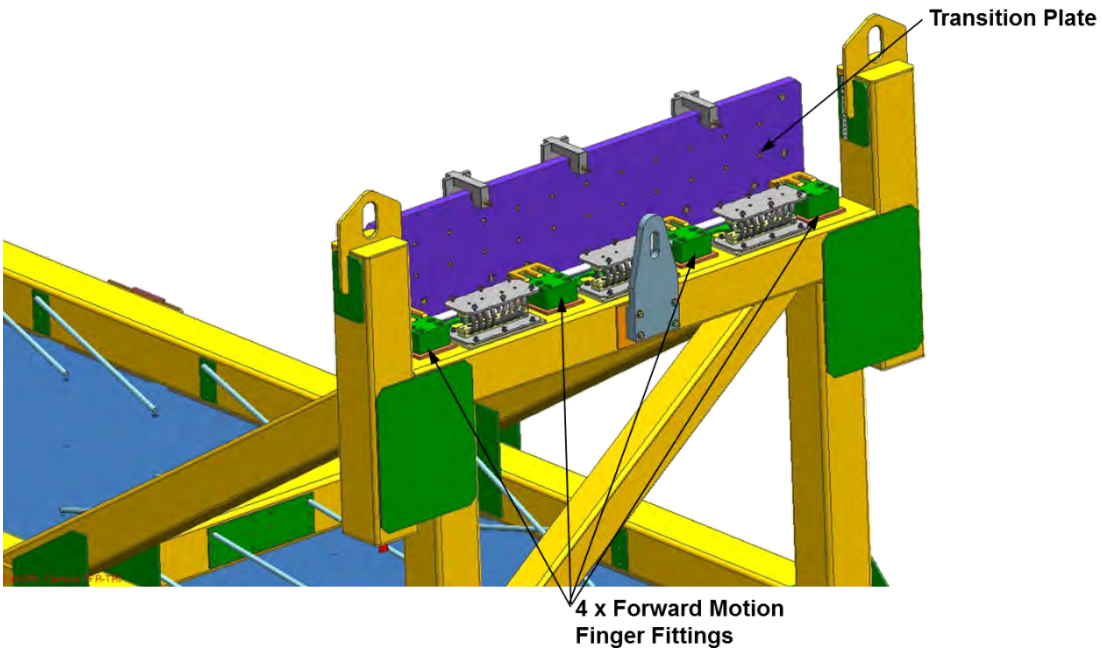

Figure 6-97. Forward/Aft Motion Finger Fittings Located Between the Isolators

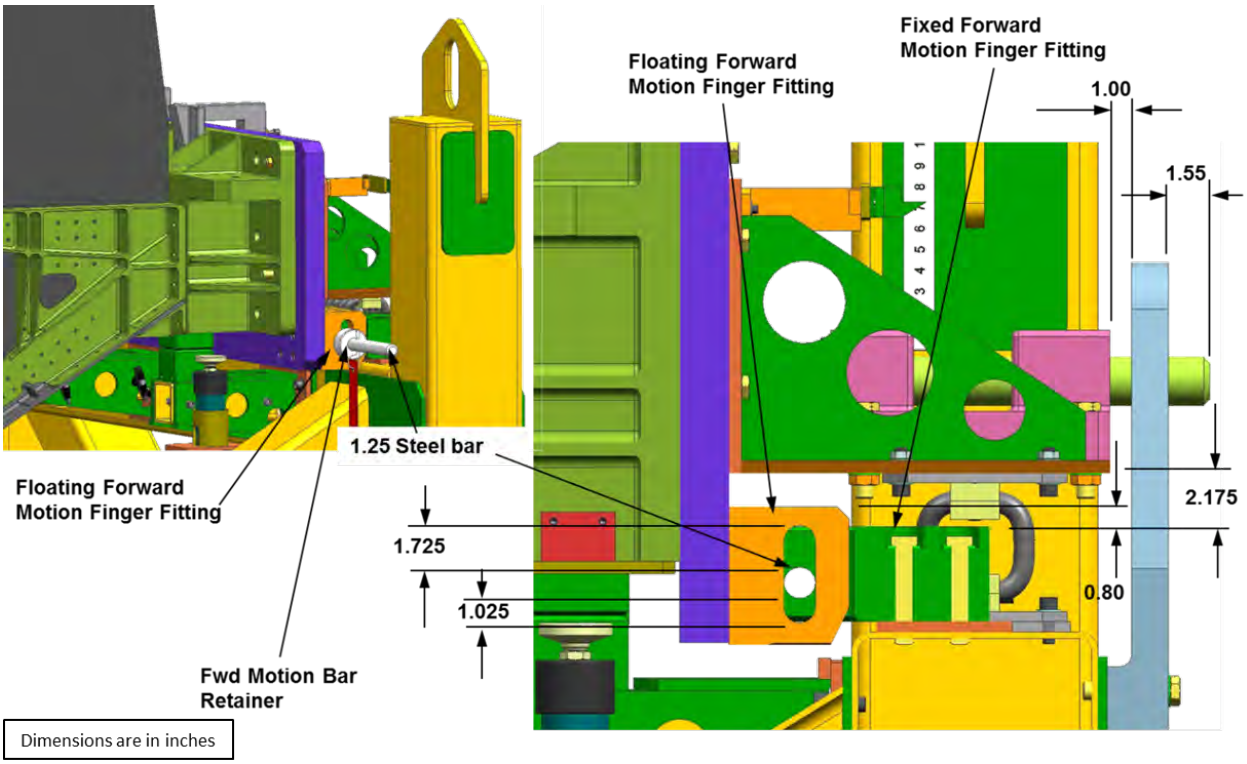

Figure 6-98. Motion Restraint Bar Clearances

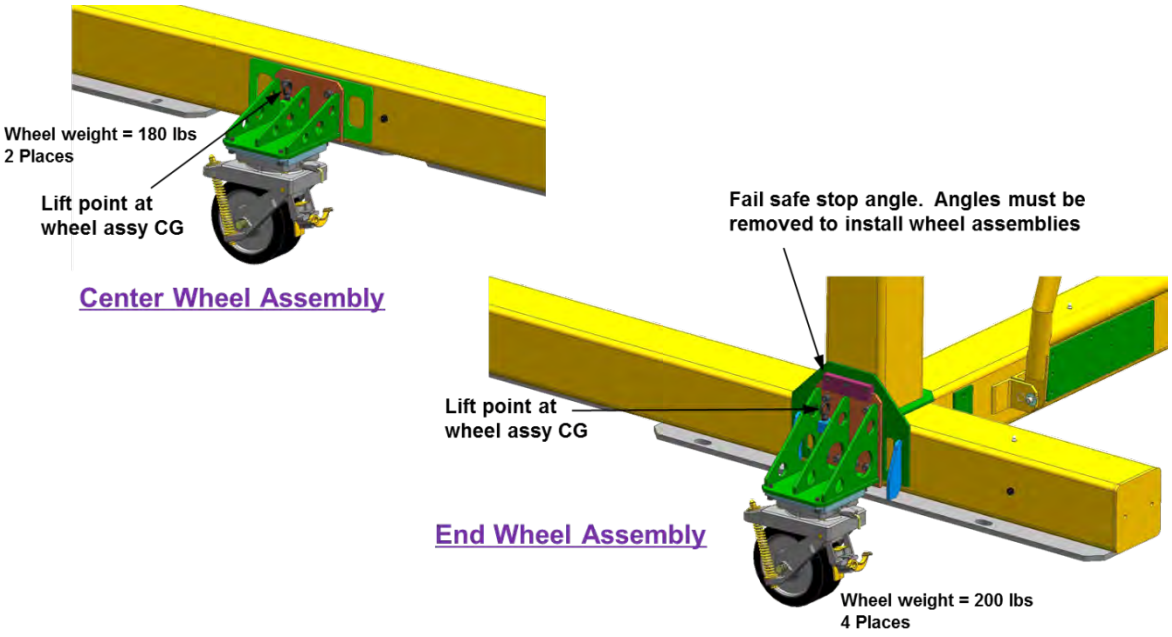

Figure 6-99. End and Center Wheel Assemblies

When the handling fixture was configured as a work stand, 12 additional jack stands were required (Figure 6-100). The wheels had a factor of safety greater than 2, which was required to tow the fixture around the factory. However, with mechanics and technicians working on or inside the MBB, a factor of safety of 5 was required. Therefore, jack stands positioned under the lower tubes to offload the wheels for loads greater than 1g were added at discrete locations. Counter-bore pockets were machined into the feet of the fixture to prevent the fixture from sliding off the jack stands. These pockets also marked the exact location for placing the jack stand under the lower tube (Figure 6-101).

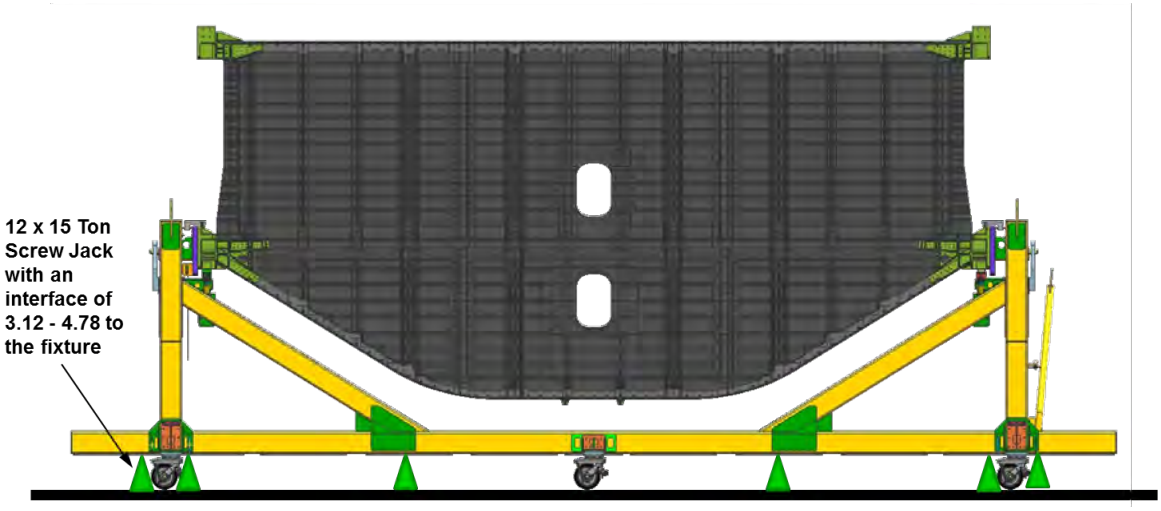

Figure 6-100. Additional Jack Stands Were Required for the Work-Stand Configuration

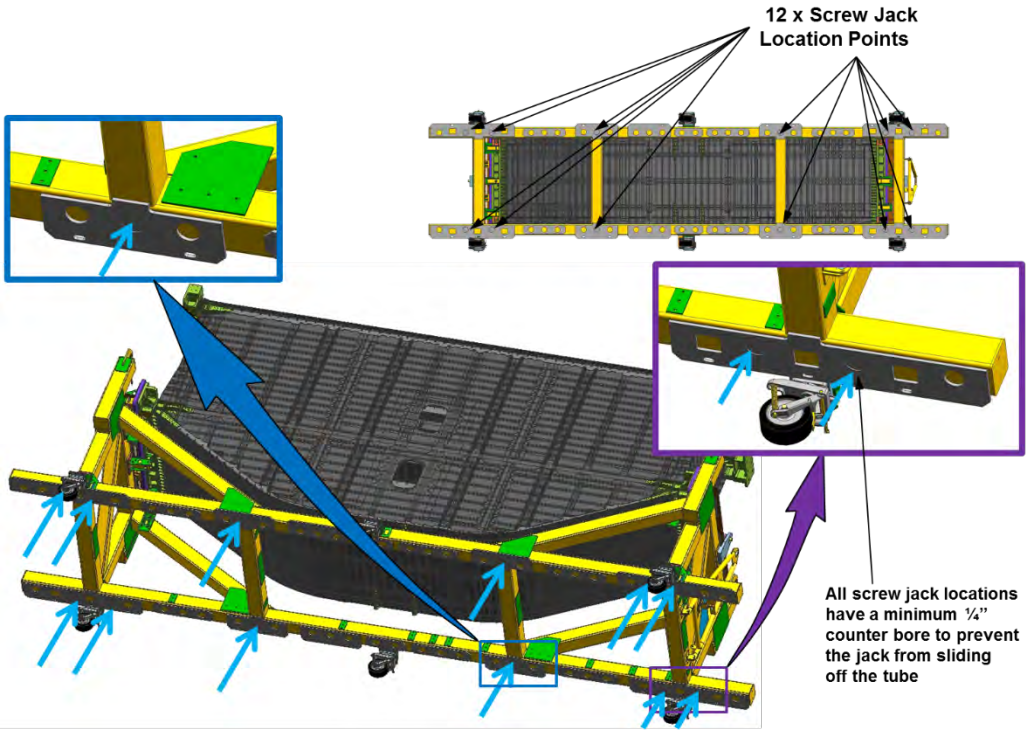

Figure 6-101. Counter-Bore Pockets Marked the Jack-Stand Locations

During the test integration phase, the COLTS platen interface holes would be drilled in the MBB adaptor fittings. This required the fitting that attached the MBB to the fixture to be removed to gain access to the adaptor fitting. Two hydraulic jacks would hold the MBB in position so that the attachment fitting could be removed. However, the jacks interfaced to a flat plate; so for added safety, side movement restraint details were added, one on each end (Figure 6-102). They would be rotated into position when the attachment fitting was removed and then rotated back out of the way once the attachment plate was reinstalled.

The fixture had to be designed to allow adequate clearances around the adaptor fitting for the drilling operation. The horizontal cross bar and vertical posts were located down and outward to create working space around the fitting (Figure 6-103). The vertical posts raised the lift attachment points well above the combined MBB/fixture Center of Gravity (CG) to preclude any rotation tendency during lifting (Figure 6-104). Once the MBB was delivered to the NASA COLTS facility, the fixture would be rolled into the staging area. This meant that the height of the rollup door and the overall working area in the staging area had to be considered. The low-profile fixture cleared the bottom of the rollup door by 19 in., and the overall length left 2.5 ft of clearance on each end to get around the fixture once it was positioned inside the staging area (Figure 6-105).

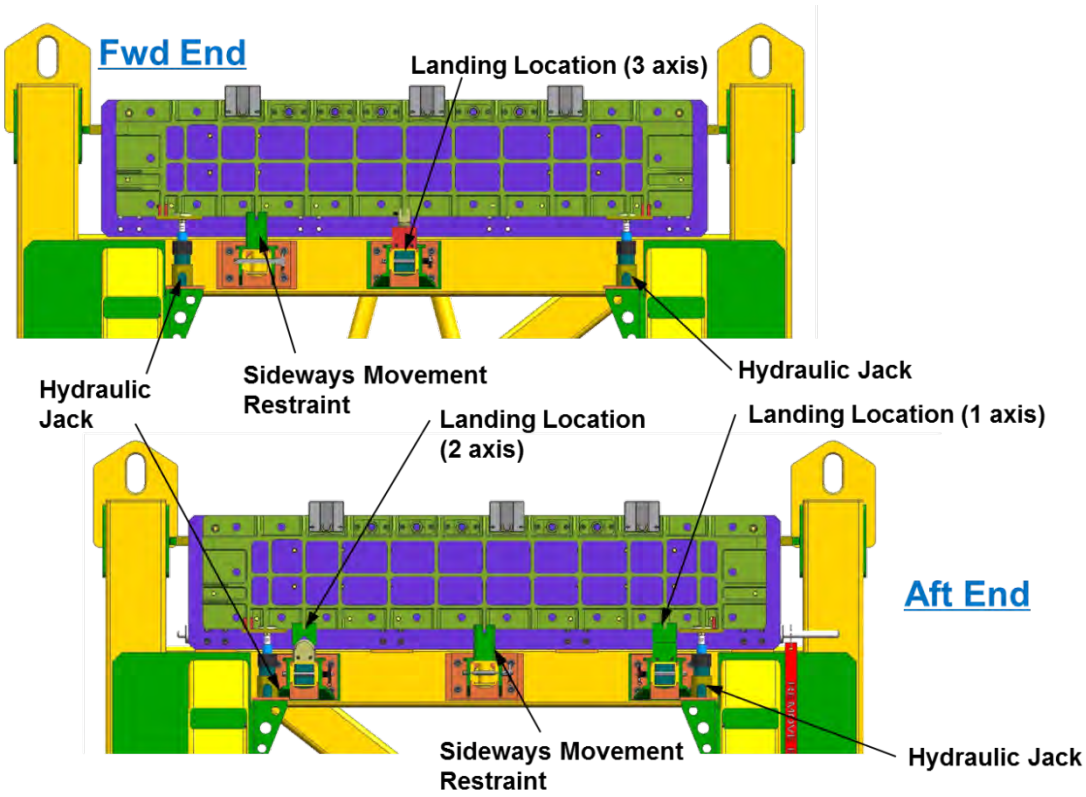

Figure 6-102. Side Movement Restraints Added for Increased Safety

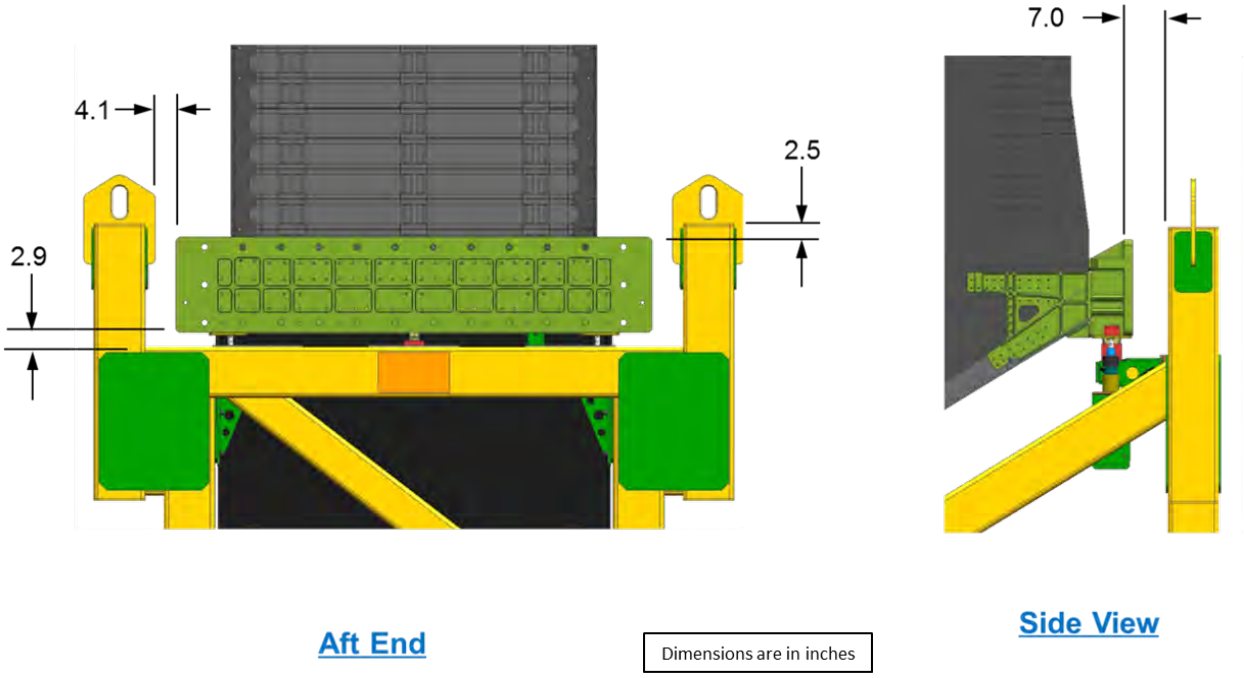

Figure 6-103. Clearances to the Fixture for Platen Hole-Drilling Operation

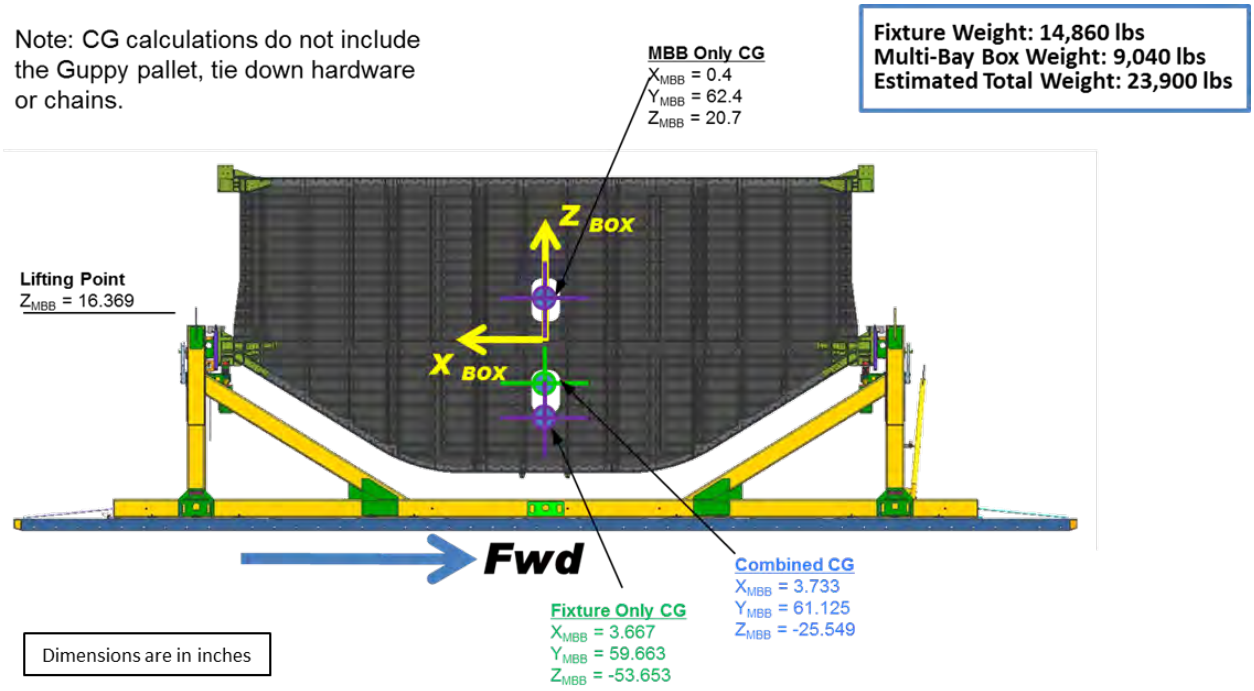

Figure 6-104. Lift Point Was Positioned Well Above the Combined CG Location

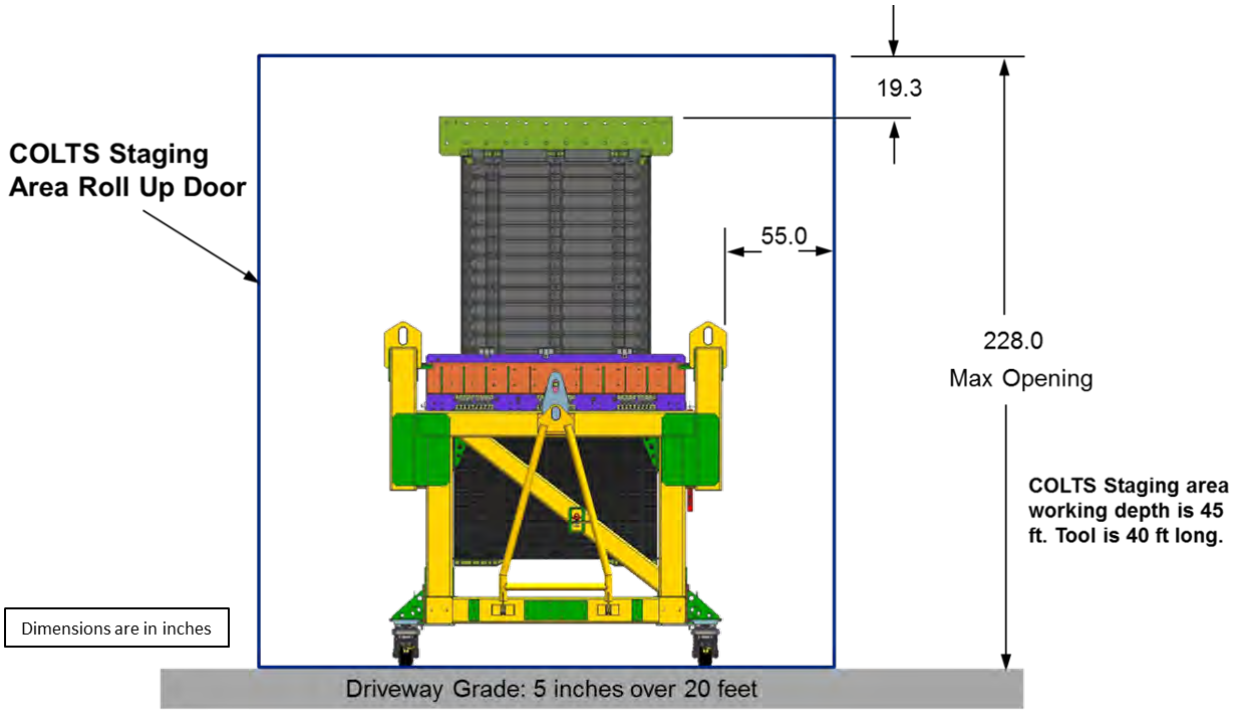

Figure 6-105. Low-Profile Fixture to Fit in the Rollup Door and Staging Area

6.3.2 Handling Fixture Analysis

In the handling fixture analysis, seven design scenarios were included in the study. They were the Guppy Maneuver, Guppy Crash, Final Assembly, Moving, Hoisting, MBB Setup for Landing, and MBB Setup for Jacking design scenarios. Different factor-of-safety values, as shown in Figure 6-106, were used for analyses of welding, hoisting lug and load alignment structures, composites, metallic fittings, bolts/beams/plates of the fixture, reaction forces between the floor beam and pallet, and structural deflection tolerance. Analyses were performed on a global FEM and several detailed FEMs of the handling fixture. Material design values of the fixture were obtained from Military Handbook (MIL-HDBK) and vendors' data. Design ultimate loads were derived from multiplying the design limit loads with the factors of safety shown in Figure 6-106. Margins of safety were calculated by comparing the calculated stress and displacement values with the material design values and Super Guppy requirements at the design ultimate loads.

Load Cases	Factors of Safety on Welding	Factors of Safety on Hoisting Lug and Load Alignment Structures	Factors of Safety on Composites, Metallic Fittings, Bolts, Beams, Plates of Fixture	Reaction Forces Between Floor Beam and Pallet	Factors of Safety on Structural Deflection Tolerance
Guppy Maneuver	2.0	N.A.	2.0	1.0	1.0
Guppy Crash	2.0	N.A.	1.0	1.0	1.0
Final Assembly	5.0	N.A.	5.0	N.A.	1.0
Moving	2.0	N.A.	2.0	N.A.	1.0
Hoisting	5.0	5.0	2.0	N.A.	1.0
MBB Setup Landing	2.0	2.0	2.0	N.A.	1.0
MBB Setup Jacking	5.0	5.0	2.0	N.A.	1.0

Figure 6-106. Design Regimes and Factors of Safety of the Handling Fixture

Each design scenario contained one or more load cases with different values of g-load in forward/aft, left/right, and down/up directions. In total, 27 load cases were used to calculate the margins of safety for the holding fixture. Details of these load cases and their corresponding g-load values are shown in Figure 6-107. Also, depending on the design scenario, FEM of the handling fixture was modified slightly, and appropriate boundary conditions were applied to simulate the actual loading conditions. Details of the handling fixture and the MBB are depicted in Figure 6-108 and Figure 6-109 for the seven design scenarios studied.

ID	Guppy Maneuver Load Cases	Fwd(+)/Aft(-) (G)	Left(+)/Right(-) (G)	Down(+)/Up(-) (G)
0	1G	0	0	+1
1	Symmetric 1	+1	0	+2.5
2	Symmetric 2	+1	0	-1
3	Symmetric 3	-1	0	+2.5
4	Symmetric 4	-1	0	-1
5	Rudder Kick 1	0	+1	+1
6	Rudder Kick 2	0	-1	+1
7	Rolling Pullout 1	+0.75	+1	+1.67
8	Rolling Pullout 2	+0.75	-1	+1.67
9	Rolling Pullout 3	-0.75	+1	+1.67
10	Rolling Pullout 4	-0.75	-1	+1.67

ID	Guppy Crash Load Cases	Fwd(+)/Aft(-) (G)	Left(+)/Right(-) (G)	Down(+)/Up(-) (G)
11	Crash 1	+3	0	0
12	Crash 2	-1.5	0	0
13	Crash 3	0	+1.5	0
14	Crash 4	0	-1.5	0
15	Crash 5	0	0	+4.5
16	Crash 6	0	0	-2.0

ID	Final Assembly Load Case	Fwd(+)/Aft(-) (G)	Left(+)/Right(-) (G)	Down(+)/Up(-) (G)
21	1G	0	0	+1.2

ID	Moving Load Cases	Fwd(+)/Aft(-) (G)	Left(+)/Right(-) (G)	Down(+)/Up(-) (G)
31	Moving 1	-0.2	0	+1.1
32	Moving 2	+0.2	0	+1.1
33	Moving 3	0	-0.1	+1.1
34	Moving 4	0	+0.1	+1.1

ID	Hoisting Load Cases	Fwd(+)/Aft(-) (G)	Left(+)/Right(-) (G)	Down(+)/Up(-) (G)
41	MBB-Long Beach	0	0	+1.2
42	Holding Fixture	0	0	+1.2
43	MBB-Langley	0	0	+1.2

ID	MBB Landing Load Case	Fwd(+)/Aft(-) (G)	Left(+)/Right(-) (G)	Down(+)/Up(-) (G)
51	Setup-Landing Pt	0	0	+1.2

ID	MBB Jacking Load Case	Fwd(+)/Aft(-) (G)	Left(+)/Right(-) (G)	Down(+)/Up(-) (G)
52	Setup-Jack Pt	0	0	+1.2

Figure 6-107. G-Load Requirements for the Different Load Cases

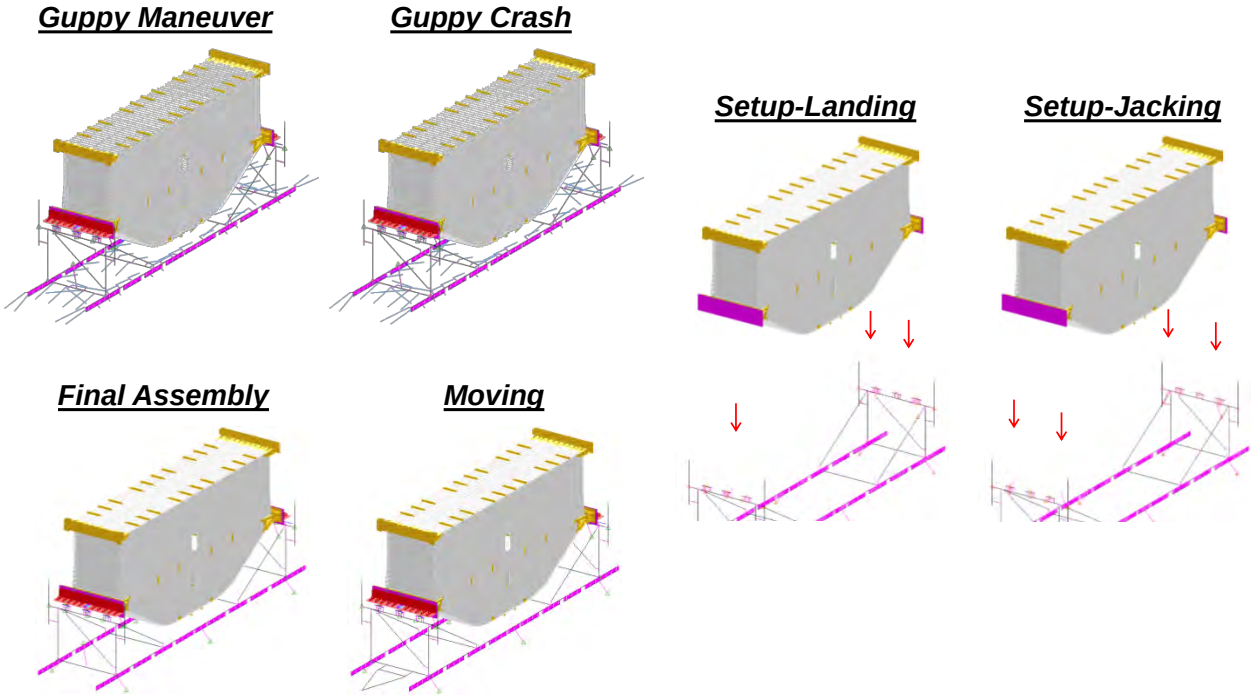

Figure 6-108. Design Scenarios Studied (1/2)

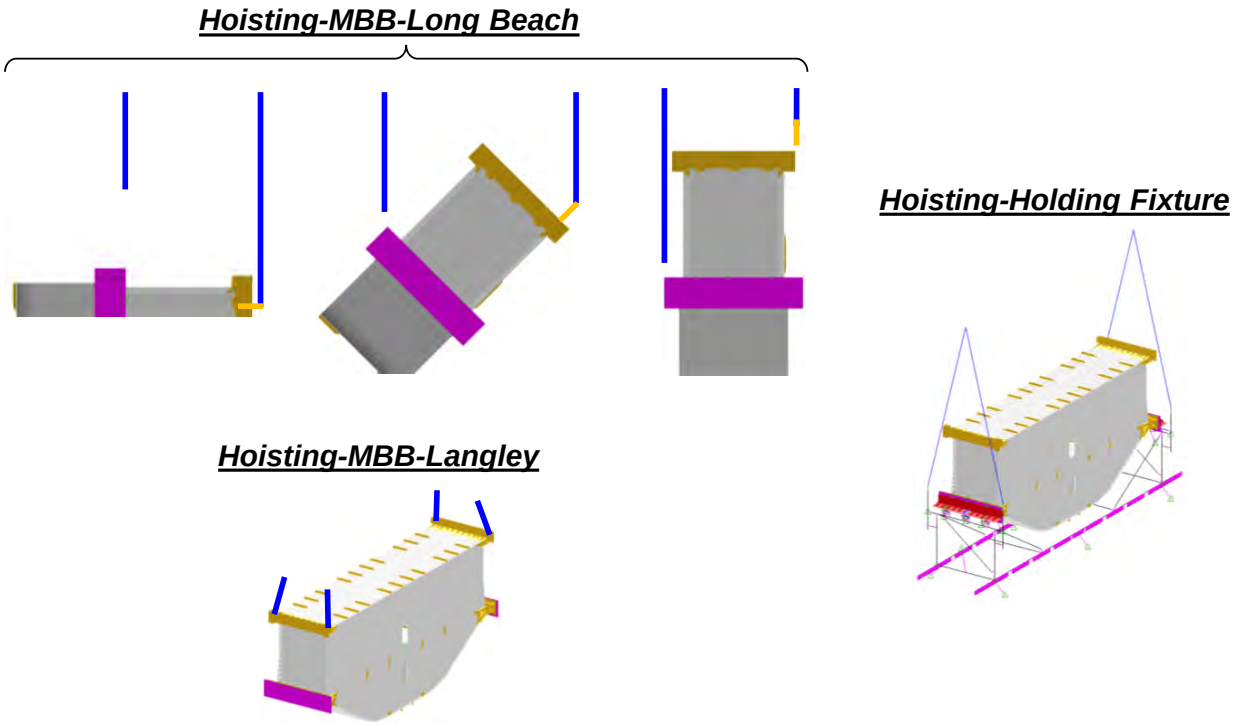

Figure 6-109. Design Scenarios Studied (2/2)

From the analysis, it appeared that the most critical cases were the ones that were dictated by the Super Guppy requirements in the Guppy Maneuver and Crash scenarios. For example, the maximum contact loads allowed from handling fixture floor beams to the pallet surface were 60.5 lb/in. for the 1-g condition and 272.3 lb/in. for the dynamic condition per side. The chain tension force limit was 10,000 lb in columns A and B and 5,000 lb in column C for tiedowns on the pallet. The floor pad bolt-down force limit was 10,000 lb in column A on the pallet. In terms of the fixture movements inside the Super Guppy, the static/dynamic clearance was 12 in. between the handling fixture and the aircraft's fuselage interior. A comparison between the handling fixture and MBB actual geometry and the FEM is shown in Figure 6-110. The results of the Guppy Maneuver design scenario were selected to be shown in this report. The margins of safety are summarized in Figure 6-111 through Figure 6-113. As shown in Figure 6-113, all margins of safety were positive in the Guppy Maneuver design scenario. Although the margins of safety in other design scenarios were also positive, they are not shown.

Load Cases	Factors of Safety on Welding	Factors of Safety on Hoisting Lug and Load Alignment Structures	Factors of Safety on Composites, Metallic Fittings, Bolts, Beams, Plates of Fixture	Reaction Forces Between Floor Beam and Pallet	Factors of Safety on Structural Deflection Tolerance
Guppy Maneuver	2.0	N.A.	2.0	1.0	1.0

ID	Guppy Maneuver Load Cases	Fwd(+)/Aft(-) (G)	Left(+)/Right(-) (G)	Down(+)/Up(-) (G)
0 to 10	various maneuver cases	from -1 to +1	from -1 to +1	from -1 to +2.5

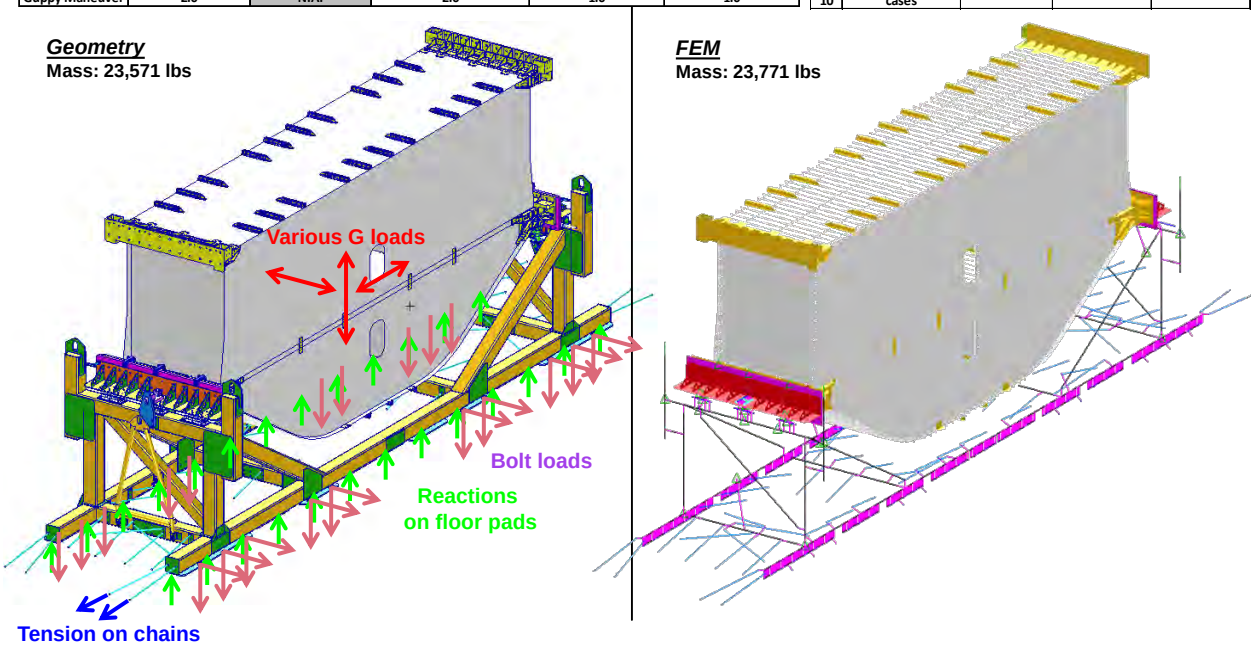

Figure 6-110. Guppy Maneuver Scenario—Cases 0 to 10

"M.S. = High" Means M.S. > 200%

	Critical Case	Calc. Result	F.S.	Design Value	M.S.	Comments
Floor Pad Reaction Force on Pallet - Static (lbs/in)	1G	58.4 (G6)	1.0	60.5 (C5)	3.6%	JSC Spec.
Floor Pad Reaction Force on Pallet - Dynamic (lbs/in)	Rolling Pull out 3	223.7 (G15)	1.0	272.25 (C5)	21.7%	JSC Spec.
Chain Force - Col. A&B (lbs)	Symmetric 3	1,972 (G9)	2.0	10,000 (C6)	153.5%	JSC Spec.
Chain Force - Col. C (lbs)	Symmetric 3	1,248 (G9)	2.0	5,000 (C6)	100.3%	JSC Spec.
Max. Bolt Tension Load on Floor Pad in Z-Dir (lbs)	Symmetric 2	3,575 (G45)	2.0	10,000 (C6)	39.9%	JSC Spec.
Max. Bolt Shear Load on Floor Pad in Y-Dir (lbs)	Rudder Kick 1	2,983 (G48)	2.0	10,000 (C6)	67.6%	JSC Spec.
Lateral Deformation (in.) @ Top of MBB	Rolling Pull out 4	1.216 (G16)	1.0	75.7 (C4)	High	JSC Spec.
Lateral Deformation (in.) @ Top of Fixture Post	Rolling Pull out 4	0.125 (G16)	1.0	65.4 (C4)	High	JSC Spec.
Lateral Deformation (in.) @ Bottom of Fixture Post	Rolling Pull out 4	0.070 (G16)	1.0	41.9 (C4)	High	JSC Spec.

	Critical Case	Calc. Result	F.S.	Design Value	M.S.	Comments
Lateral Displacement Tolerance of Fwd/Aft-Stop Fitting (in.)	Rolling Pull out 1	0.074 (G30)	1.0	0.162 (C9)	PASS	Fitting Design
Max. Forward (X-) Movement of Fixture (in.)	Symmetric 1	0.074 (G44)	1.0	0.580 (C8)	PASS	Fixture Design
Max. Thermal Forward (X-) Movement of Fixture (in.)	T = 0F	0.091 (calc.)	1.0			
Max. Aft (X-) Movement of Fixture (in.)	Symmetric 3	0.116 (G46)	1.0	0.760 (C8)	PASS	Fixture Design
Max. Thermal Aft (X-) Movement of Fixture (in.)	T = 0F	0.091 (calc.)	1.0			
Max. LHS (Y-) Movement of Fixture (in.)	Rudder Kick 1	0.020 (G48)	1.0	0.140 (C8)	PASS	Fixture Design
Max. Thermal LHS (Y-) Movement of Fixture (in.)	T = 120F	0.031 (calc.)	1.0			
Max. RHS (Y-) Movement of Fixture (in.)	Rolling Pull out 4	0.022 (G53)	1.0	0.110 (C8)	PASS	Fixture Design
Max. Thermal RHS (Y-) Movement of Fixture (in.)	T = 0F	0.043 (calc.)	1.0			
Max. Upward (Z-) Movement of Isolator (in.)	Symmetric 4	0.302 (G47)	1.0	2.000 (C7)	PASS	Vendor's Data
Max. Downward (Z-) Movement of Isolator (in.)	Rolling Pull out 2	0.731 (G51)	1.0	2.000 (C7)	PASS	Vendor's Data

Figure 6-111. Margins of Safety—Guppy Maneuver Scenario (1/3)

"M.S. = High" Means M.S. > 200%

	Critical Case	Calc. Result	F.S.	Design Value	M.S.	Comments
Max. Isolator Force (lbs) Fwd/Aft (X-) Direction	Symmetric 3	244 (G21)	2.0	10,000 (C7)	High	Vendor's Data
Max. Isolator Force (lbs) Laterial (Y-) Direction	Rolling Pull out 4	203 (G28)	2.0	10,000 (C7)	High	Vendor's Data
Max. Isolator Force (lbs) Vertical (Z-) Tension	Symmetric 2	2,286 (G20)	2.0	15,000 (C7)	High	Vendor's Data
Max. Isolator Force (lbs) Vertical (Z-) Compression	Rolling Pull out 4	5,569 (G28)	2.0	15,000 (C7)	34.7%	Vendor's Data
Max. Force (lbs) on Lateral-Stop Fitting	Rolling Pull out 4	6,493 (G41)	2.0	141,600 (C10)	High	Lug Analysis
Max. Force (lbs) on Fwd/Aft-Stop Fitting	Symmetric 1	4,478 (G32)	2.0	47,600 (C11)	High	Lug Analysis
MBB Composite Max. Principal Strain (μ-ε)	Symmetric 3	540 (G154)	2.0	5,900 (C3)	High	Notched Design Value
MBB Composite Min. Principal Strain (μ-ε)	Symmetric 3	-451 (G154)	2.0	-4,800 (C3)	High	Notched Design Value
MBB Metallic Fittings (ksi)	Symmetric 1	11.2 (G152)	2.0	55.4 (C2)	147.3%	Reduced Allow @ 120F

	Critical Case	Calc. Result	F.S.	Design Value	M.S.	Comments
Max von Mises Stress (ksi) Thick Aluminum Plate	Rolling Pull out 2	2.0 (G63)	2.0	74.3 (C2)	High	Reduced Allow @ 120F
Max von Mises Stress (ksi) Gusset Plate	Rolling Pull out 1	16.0 (G62)	2.0	62.7 (C2)	95.9%	Reduced Allow @ 120F
Max von Mises Stress (ksi) Isolate Mounting Plate	Symmetric 3	15.9 (G58)	2.0	62.7 (C2)	97.2%	Reduced Allow @ 120F
Max Combined Bar Stress 10x10 and 8x8 Tube (ksi)	Rolling Pull out 3	5.81 (G76)	2.0	59.8 (C2)	High	Reduced Allow @ 120F
Min Combined Bar Stress 10x10 and 8x8 Tube (ksi)	Rolling Pull out 3	-6.83 (G76)	2.0	-59.8 (C2)	High	Reduced Allow @ 120F
Max Combined Bar Stress Fwd/Aft-Stop Pin (ksi)	Symmetric 1	13.8 (G80)	2.0	62.7 (C2)	127.2%	Reduced Allow @ 120F
Min Combined Bar Stress Fwd/Aft-Stop Pin (ksi)	Symmetric 1	-13.8 (G80)	2.0	-62.7 (C2)	127.2%	Reduced Allow @ 120F
Max Combined Bar Stress Lateral-Stop Pin (ksi)	Rolling Pull out 4	16.1 (G101)	2.0	62.7 (C2)	94.7%	Reduced Allow @ 120F
Min Combined Bar Stress Lateral-Stop Pin (ksi)	Rolling Pull out 4	-16.1 (G101)	2.0	-62.7 (C2)	94.7%	Reduced Allow @ 120F

Figure 6-112. Margins of Safety—Guppy Maneuver Scenario (2/3)

"M.S. = High" Means M.S. > 200%

	Critical Case	Calc. Result	F.S.	Design Value	M.S.	Comments
Fastener Tensile Force (lbs) Between Thick Aluminum Plate & Gusset Plate	Rolling Pull out 4	4,145 (G113)	2.0	46,900 (C13)	High	Calculated Design Value
Fastener Shear Force (lbs) Between Thick Aluminum Plate & Gusset Plate	Rolling Pull out 2	1,607 (G111)	2.0	28,100 (C13)	High	Calculated Design Value
Fastener Tensile Force (lbs) Between Gusset Plate & Isolator Plate	Symmetric 3	1,250 (G118)	2.0	32,100 (C15)	High	Calculated Design Value
Fastener Shear Force (lbs) Between Gusset Plate & Isolator Plate	Symmetric 1	1,711 (G116)	2.0	19,300 (C15)	High	Calculated Design Value
Fastener Tensile Force (lbs) Between Gusset Plate & Lateral-Stop Fitting	Rolling Pull out 3	2,448 (G136)	2.0	67,700 (C16)	High	Calculated Design Value
Fastener Shear Force (lbs) Between Gusset Plate & Lateral-Stop Fitting	Rolling Pull out 3	3,894 (G136)	2.0	40,600 (C16)	High	Calculated Design Value
Fastener Tensile Force (lbs) Between Load Intro Fitting & Thick Aluminum Plate	Symmetric 1	4,376 (G140)	2.0	67,700 (C14)	High	Calculated Design Value
Fastener Shear Force (lbs) Between Load Intro Fitting & Thick Aluminum Plate	Symmetric 1	2,315 (G140)	2.0	40,600 (C14)	High	Calculated Design Value
Fastener Tensile Force (lbs) Between Isolator Bars	Symmetric 2	571.5 (=2,286 /4)	2.0	13,600 (C23)	High	Calculated Design Value

	Critical Case	Calc. Result	F.S.	Design Value	M.S.	Comments
Max. von Mises Stress on Lateral-Stop Fitting & Weld Plate (ksi)	Rolling Pull out 4	20.1 (D5)	2.0	62.7 (C2)	56.0%	Detail Analysis
Max. von Mises Stress on Floor Pad from Bolt-Down Bolt Load (ksi)	Symmetric 2	27.2 (D11)	2.0	59.8 (C2)	9.9%	Detail Analysis
Fastener Tensile Force (lbs) Between Lateral-Stop Fitting and Weld Plate	Rolling Pull out 4	703 (D5)	2.0	67,700 (C16)	High	Detail Analysis
Fastener Shear Force (lbs) Between Lateral-Stop Fitting and Weld Plate	Rolling Pull out 4	6,084 (D5)	2.0	40,600 (C16)	High	Detail Analysis
C-Clamp Tensile Force (lbs) Between Load Intro Fitting & Thick Aluminum Plate	Symmetric 1	3,581 (G140)	2.0	11,260 (D3)	57.2%	Calculated Design Value

Figure 6-113. Margins of Safety—Guppy Maneuver Scenario (3/3)

In addition to the analysis of the global FEM of the handling fixture, detailed FEMs were also built and analyzed at critical locations where high stress concentrations were expected. The locations of these detailed FEMs are shown in Figure 6-114. Results such as stresses and bolt loads were extracted and compared with the material design values for margins-of-safety calculations.

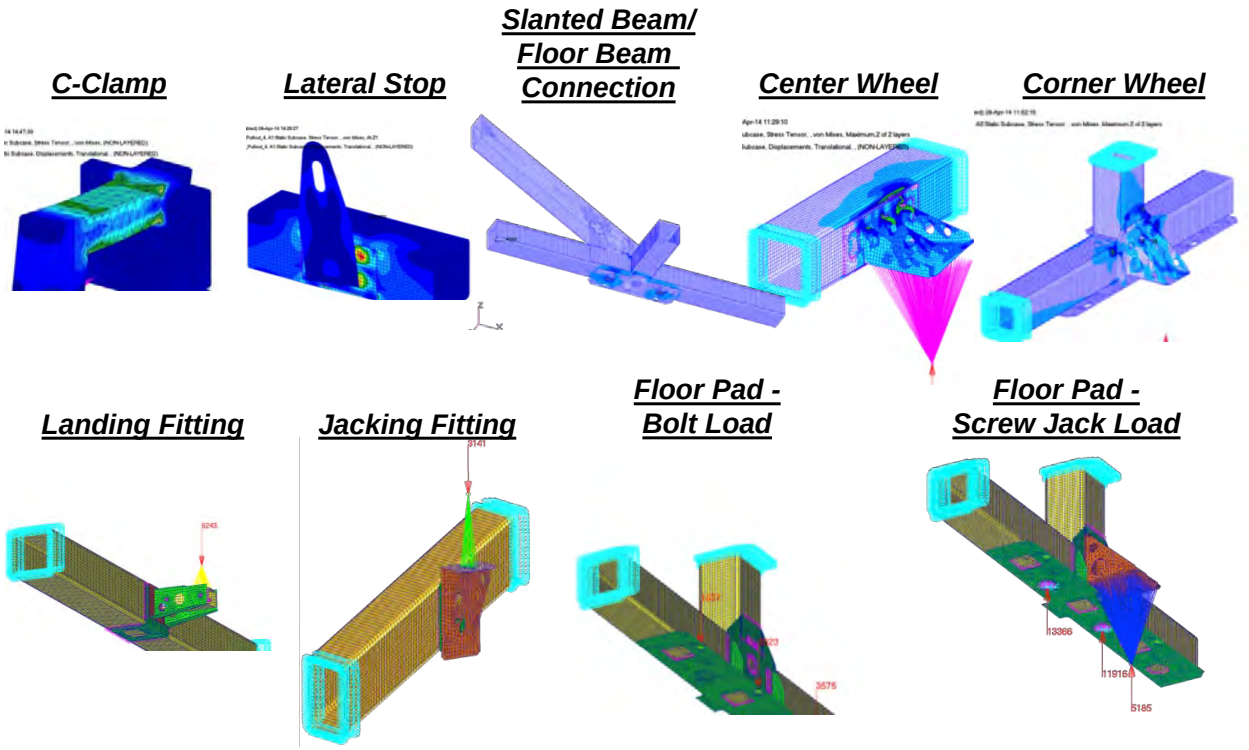

Figure 6-114. Detailed FEMs of the Handling Fixture

From the analyses of the handling fixture, the four most critical margins of safety and their locations are shown in Figure 6-115. In the load cases of the Guppy Maneuver design scenario, the lowest margin of safety was 3.6% for static reaction force between the floor pad and pallet. In the load cases of the Guppy Crash design scenario, the lowest margin of safety was also 3.6% for dynamic reaction force between the floor pad and pallet. In the load cases of the Moving design scenario, the lowest margin of safety was 6.5% for welding between the floor beam and angle plates of tow bars. In the load cases of the Hoisting design scenario, the lowest margin of safety was 0.04% for welding between the 8-by-8 side beams and 10-by-10 vertical beams, whereas a conservative factor of safety of 5 was used. In conclusion, all margins of safety were positive in all design cases from the analyses of the handling fixture.

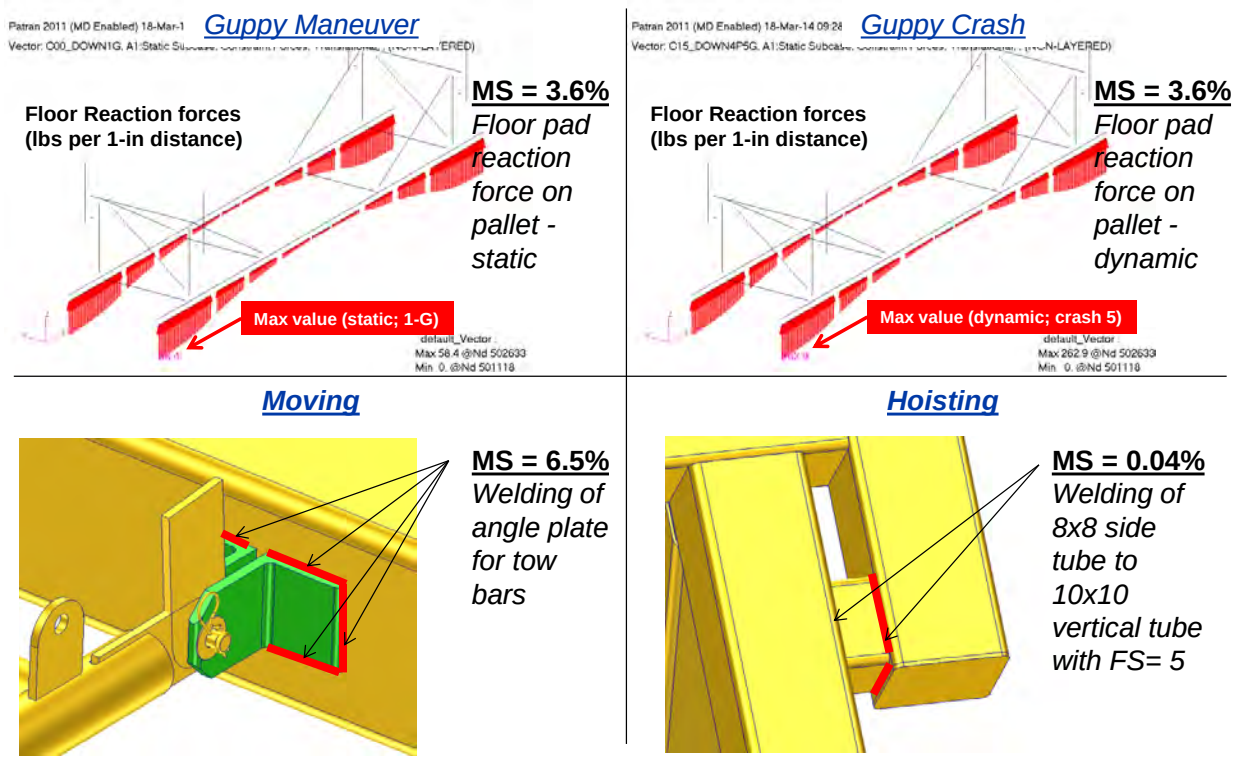

Figure 6-115. Critical Margins of Safety From the Handling Fixture Analysis

6.3.2 Final Preparation

A final combined X axis and Y axis CG positions along with a final weight were taken during the installation of the fixture onto the Super Guppy pallet. Scales were located at the four corners of the fixture (Figure 6-116). Based on the weight and exact scale location, the final CG and weight were calculated and given to the Super Guppy team to determine the final pallet location. In preparation for shipping, the fixture was loaded onto the pallet prior to the arrival of the aircraft (Figure 6-117), and the tiedown bolts were installed at the 20 locations. Each flanged bushing was shimmed to maintain a 0.002- to 0.50-in. gap between the flange bushing and the foot of the fixture (Figure 6-118). This ensured that the pallet could grow and shrink during the flight due to temperatures swings in the cargo bay of the aircraft and not bind up. Once the pallet was loaded into the floor track system of the aircraft, the shims were readjusted to account for the uneven floor tracks. Any gap between the foot of the fixture and the pallet was also shimmed out using simple sheet stock.

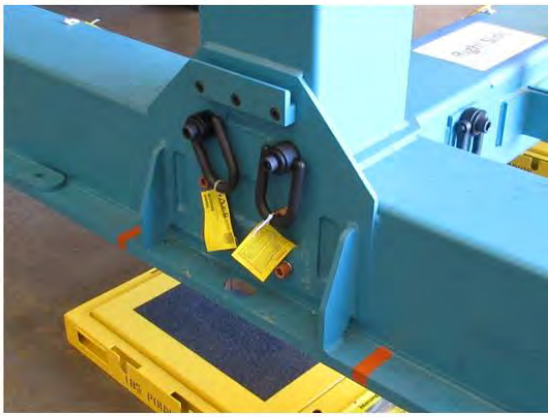

	Actual	Model*	Delta
Weight	23,741 lbs	23,955 lbs	214 lbs
X_{Pallet}	283.00 in	286.73 in	-3.73 in
Y_{Pallet}	0.78 in	1.12 in	-0.33 in
Z_{Pallet}		77.96 in	------

Figure 6-116. Combined Weight and CG Location Determined for X and Y Directions

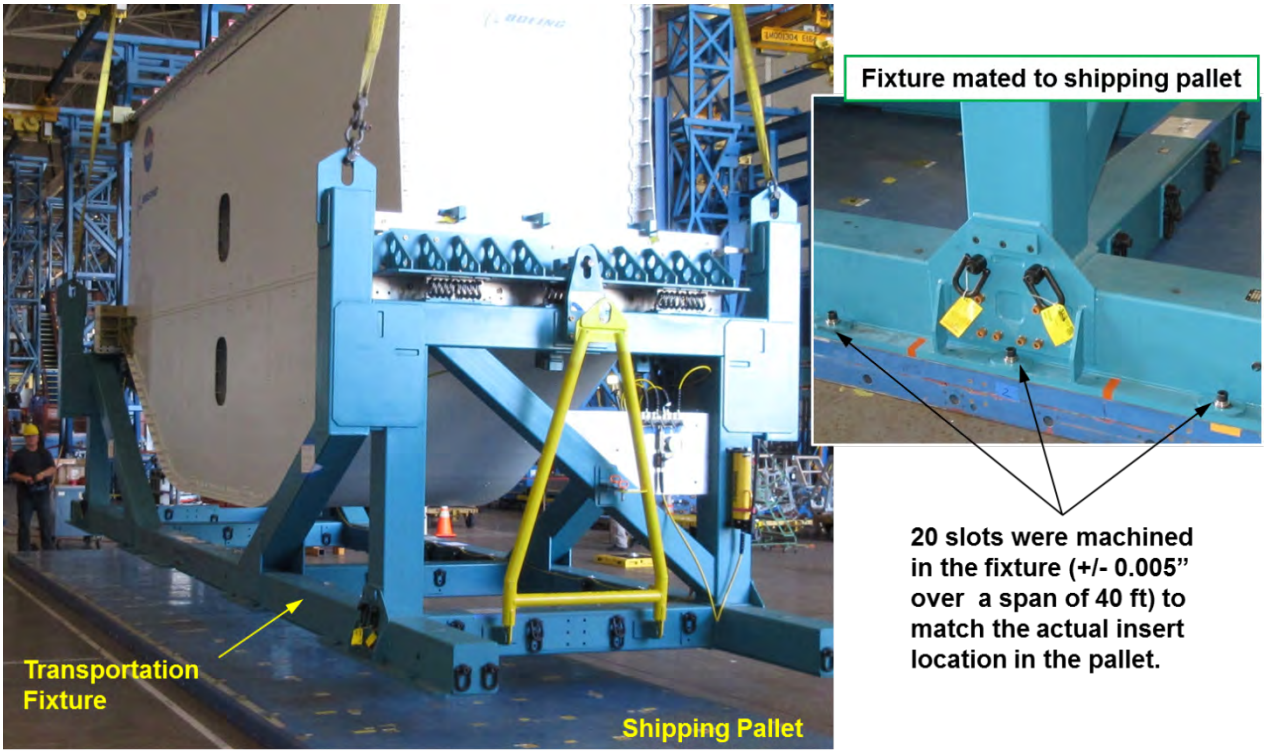

Figure 6-117. Placing the Fixture on the Super Guppy Pallet

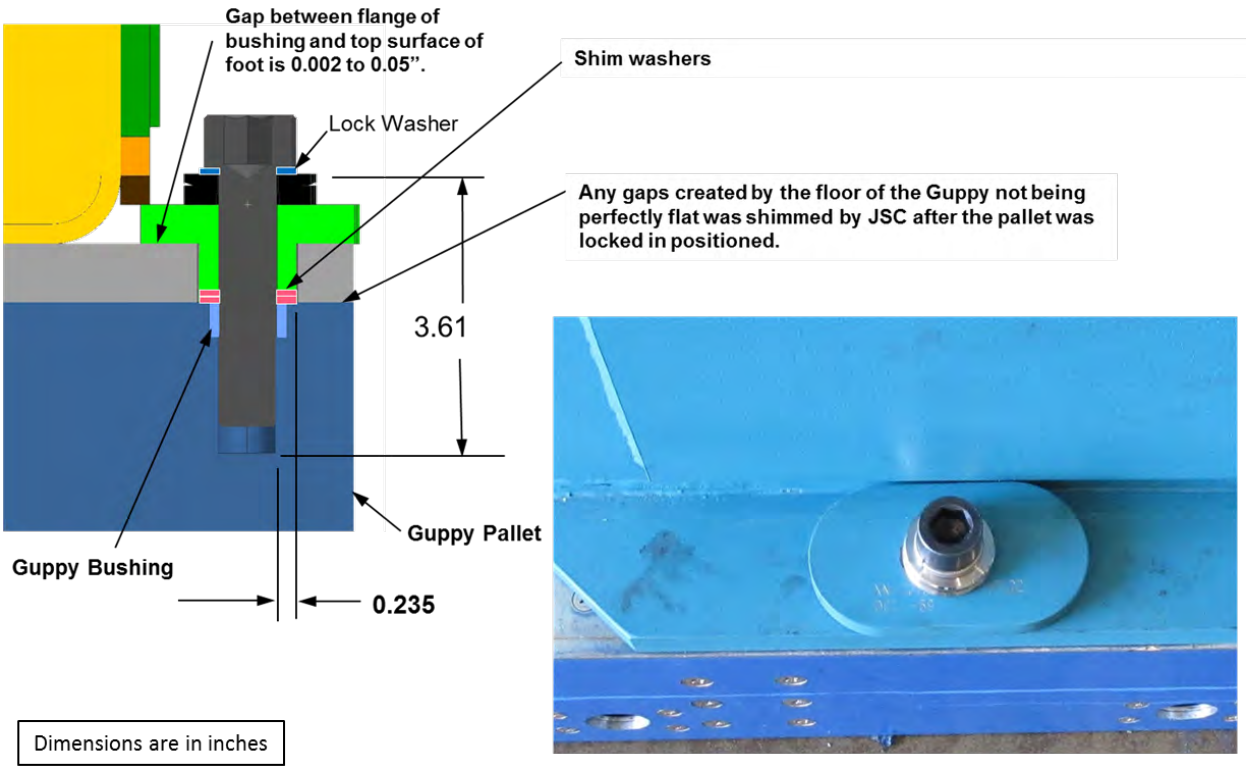

Figure 6-118. Z-Axis Restraints

6.4 Shipping

There were several possible ways to ship the MBB from Long Beach, California, to Hampton, Virginia. Shipping by truck would have required the MBB to be shipped on its side. Nevertheless, this would still have been a "tall" load, requiring separate permits in every state that the truck passed through along with two police escorts from each state. A route could have been developed that bypassed all low bridges, but it may have required trees to be trimmed or power lines or traffic lights to be moved along the route. Weather could also have been a factor inasmuch as the schedule for shipping was December 1, and the load was headed east. The feasibility of using trains and boats was also evaluated.

The final solution was to ship by air using the NASA Super Guppy. The cargo bay for the aircraft was large enough to ship the MBB in an upright position, eliminating the need to perform a second MBB rotation at the COLTS facility. Both assembly of the MBB at the Boeing Long Beach factory (Figure 6-119) and testing at the NASA LaRC facility (Figure 6-120) were in ideal locations because they were both adjacent to an airport. In addition, an enclosed shipping fixture would not be required to protect the MBB from the weather.

Figure 6-119. MBB Assembly Site at the Boeing Facility in Long Beach, California

Figure 6-120. MBB Test Site at the NASA LaRC Facility in Hampton, Virginia

The fixture (with the pallet attached) was loaded onto a K-Loader using two cranes, one overhead and one mobile, and it was secured to the K-Loader using eight chains. Then all 56 chains that secured the fixture to the pallet were installed (Figure 6-121). The Super Guppy arrived at the Boeing Long Beach facility and was parked on the C-17 flight ramp (Figure 6-122). Preparations were made to the aircraft for loading the MBB, and once the forward supports were lowered, the nose of the aircraft was opened. The K-Loader transported the MBB to the aircraft and raised it to align with the aircraft cargo track system (Figure 6-123 and Figure 6-

124). The pallet was positioned to align the CG of the payload with the CG of the aircraft. Large pins in the track system locked the pallet in position.

Two (one overhead and one mobile) cranes were used to load the MBB on the K-loader.

Once loaded, the fixture was chained to the pallet and the pallet was chained to the K-Loader.

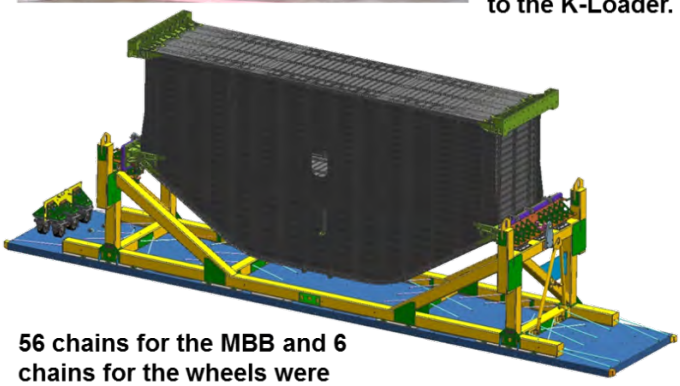

56 chains for the MBB and 6 chains for the wheels were used for fwd and aft restraint.

Figure 6-121. Loading the MBB on the K-Loader for Loading Onto the Super Guppy

NASA Super Guppy is parked on the C-17 flight ramp to pick up the MBB 12-8-2014

Figure 6-122. Supper Guppy Arrives at the Boeing Long Beach Facility

Figure 6-123. K-Loader Loading the MBB Into the Aircraft

Figure 6-124. MBB Loaded in the Super Guppy

An accelerometer was bolted onto the aft end of the fixture attachment fitting to measure the shock loading that the MBB would undergo during shipment (Figure 6-125). The accelerometer recorded all g-loading events in all three directions above 0.3 g's. Figure 6-126 shows the g-level plot for all 69 events that were recorded. The unit also recorded the temperature and relative humidity throughout the duration of the flight (Figure 6-127). The maximum g-loading event shown in Figure 6-128 occurred during the unloading of the fixture from the K-Loader at the COLTS facility. The maximum g-loading during takeoff or landing is shown in Figure 6-129 and was 0.92 g's (side to side). This was below the design requirement of 1.0 g or a maximum of 1.5 g's.

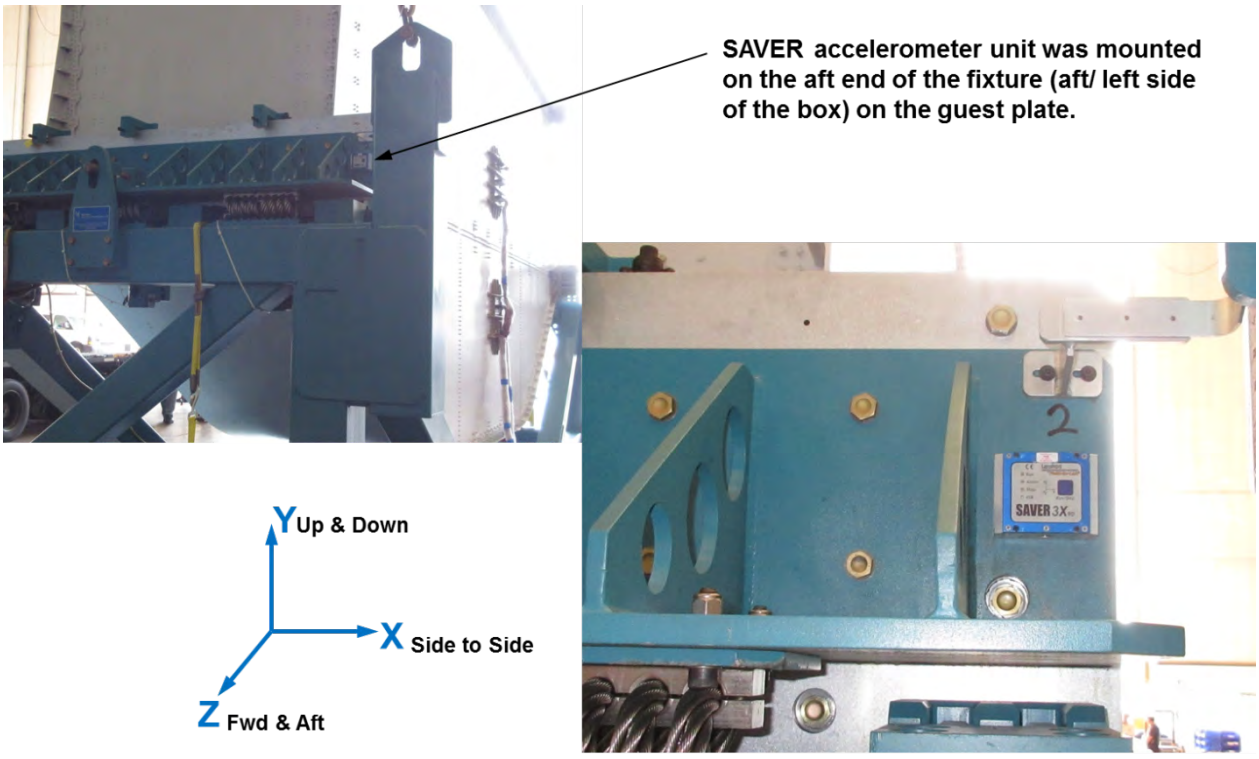

Figure 6-125. Accelerometer Mounted on the Aft End of the Fixture to Measure g-Loading

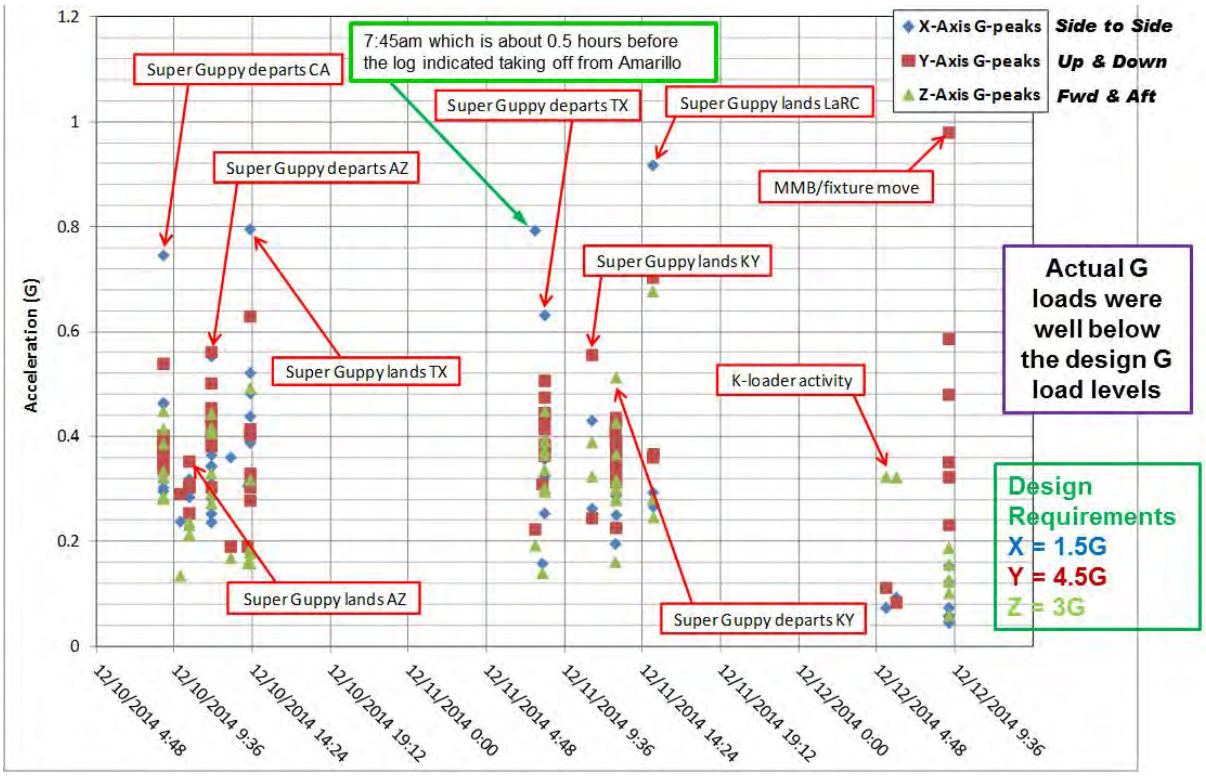

Figure 6-126. Maximum g-Peaks Recorded During Shipment (69 g-Triggered Events)

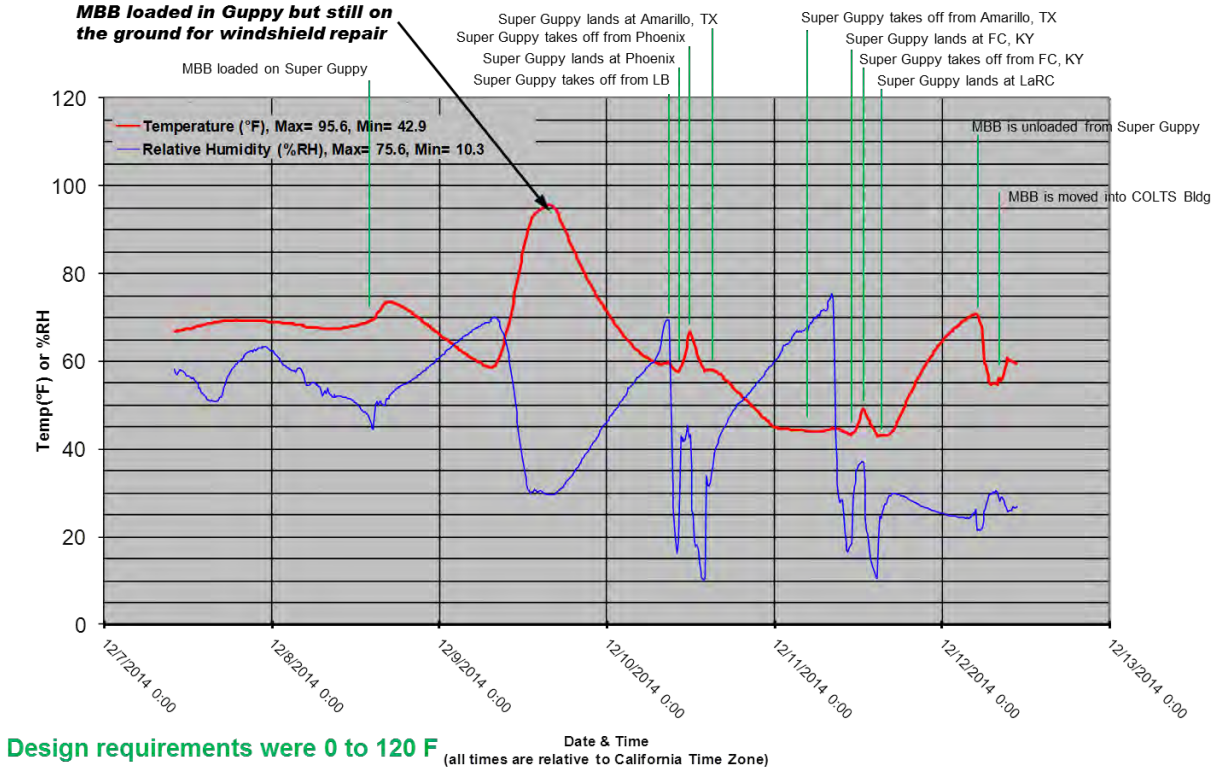

Figure 6-127. Temperature and Humidity Chart for the Duration of Shipping

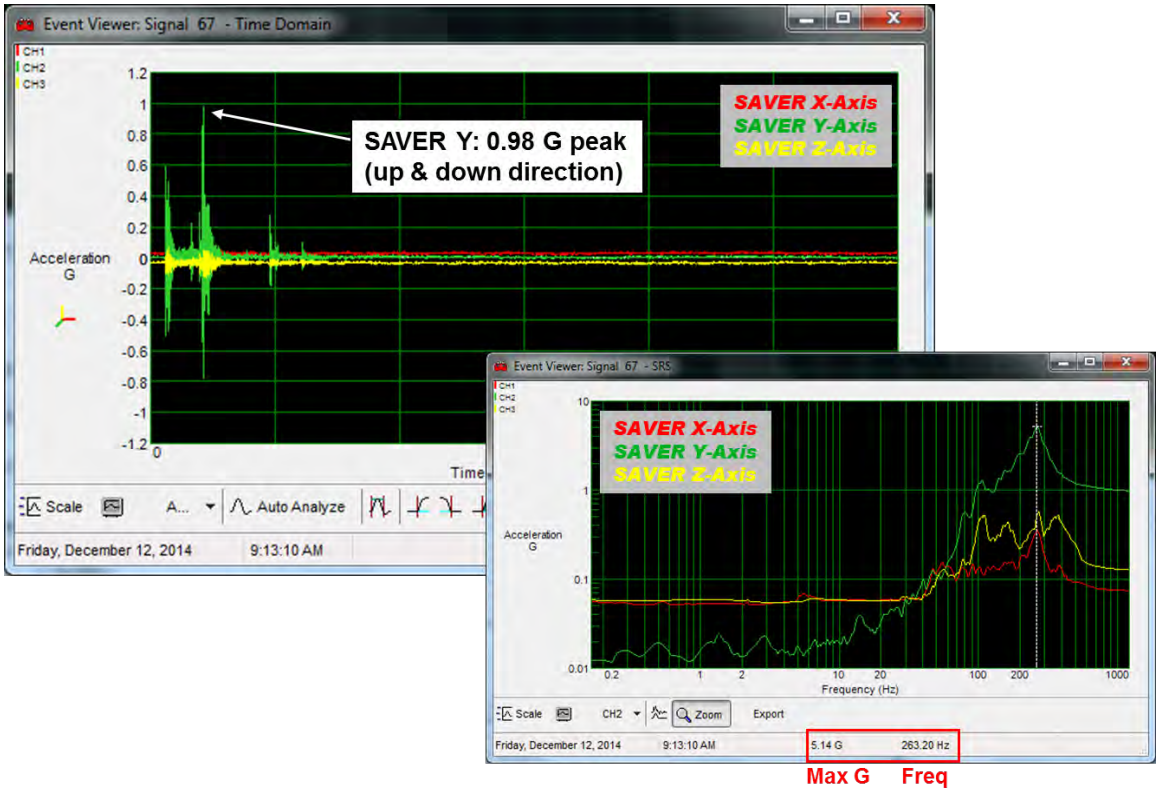

Figure 6-128. Maximum Event (no. 67) Occurred During Unloading at NASA COLTS Facility

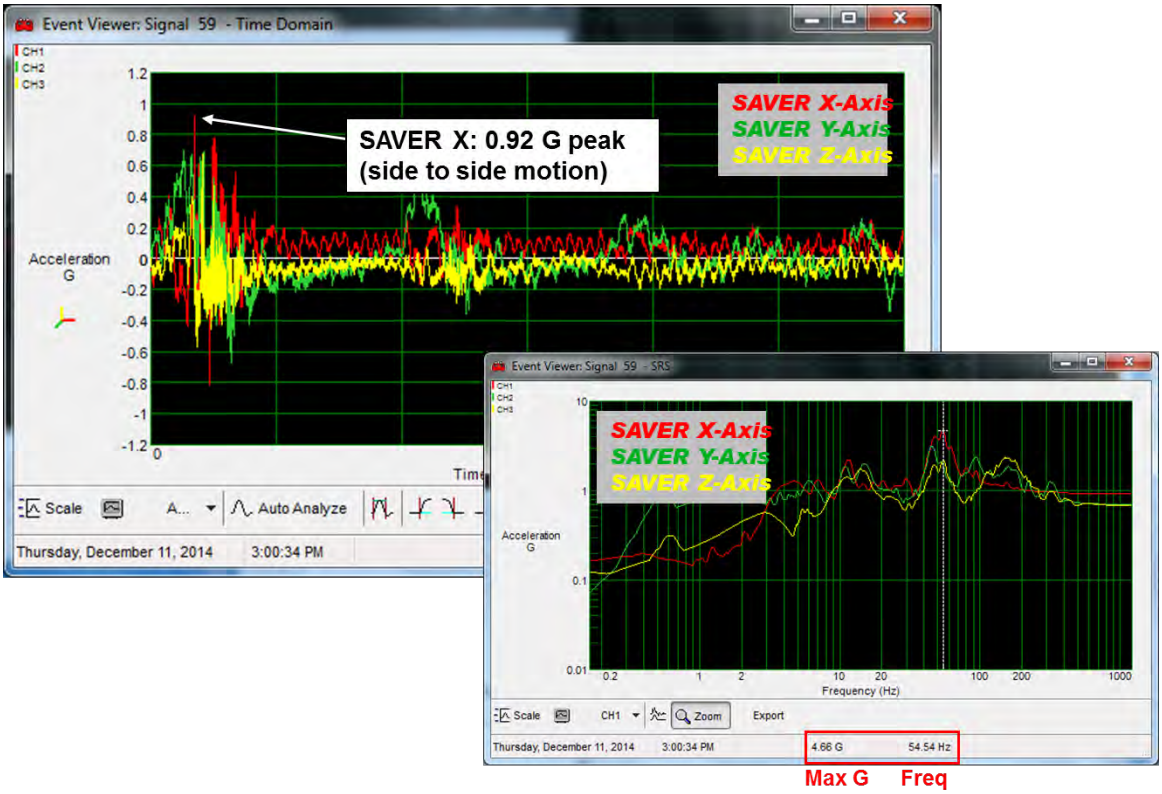

Figure 6-129. Maximum Landing Event (no. 59) at NASA LaRC on 11 December 2014

Thirty hours after the Super Guppy took off from Long Beach, it touched down in Hampton at NASA LaRC. The next day, the MBB was unloaded (Figure 6-130) onto a K-Loader. Alignment scribe lines that were marked on the fixture and pallet in Long Beach were checked to determine if the fixture had moved relative to the pallet. The lines were still perfectly aligned, indicating that the fixture had not moved during shipping. The K-Loader was driven to the COLTS facility where the MBB was unloaded. After the wheel assemblies were installed onto the fixture, the fixture was then pushed into the COLTS staging area (Figure 6-131).

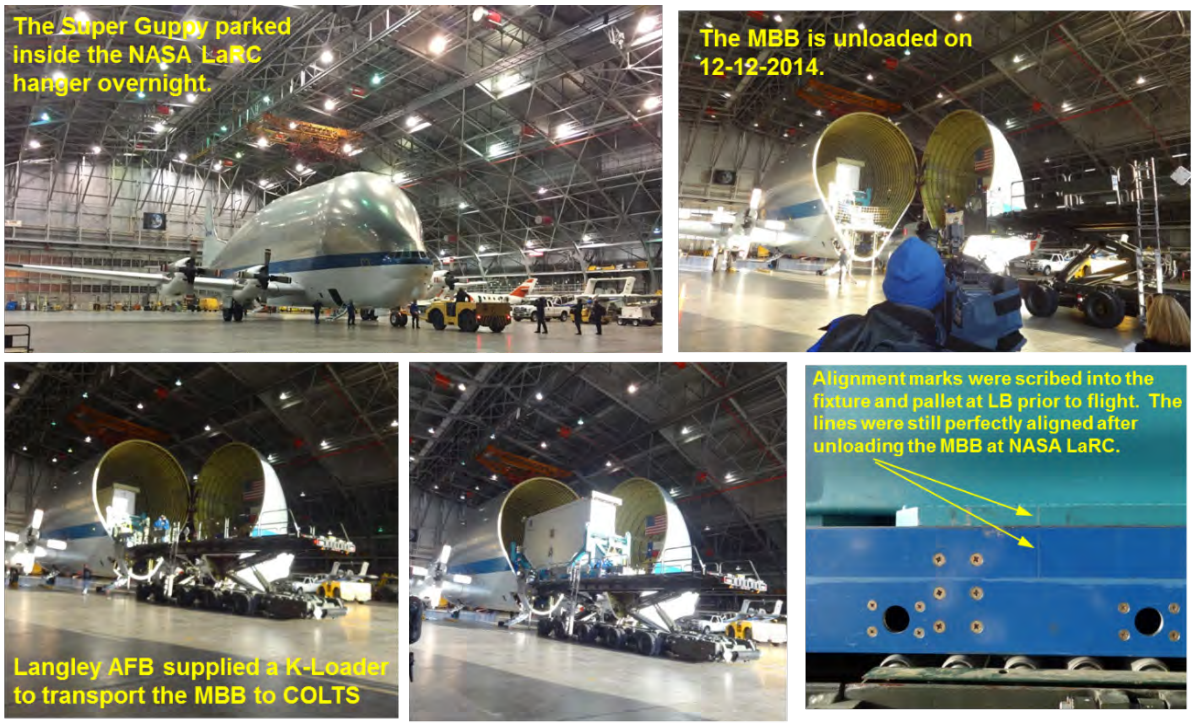

Figure 6-130. MBB Arrived at NASA LaRC on 11 December 2014 and Was Unloaded the Next Day

The low profile fixture design allows ample clearance under the top of the roll up door.

Figure 6-131. MBB Pushed Into COLTS Staging Area

7.0 TESTING PREPARATION

Before the MBB was delivered to the COLTS facility, a thorough assessment was conducted to determine how the MBB would be loaded into the COLTS and how it would be tested. Once the MBB was delivered to NASA LaRC, the contracted work statement for this project was essentially complete. From this point forward, NASA was responsible for attaching the MBB to the platens, completing the remaining instrumentation package, conducting system checkouts, and then completing testing. However, all of the work effort to load the MBB into the COLTS facility was planned and coordinated under the contract and is discussed in this section. The final plan was to test the MBB under combined loading that would represent wing bending loads applied to a pressurized passenger cabin. The load cases tested were negative 1.0 g's with and without pressure, positive 2.5 g's with and without pressure, and pressure alone.

7.1 Specimen Installation at the COLTS Facility

After the MBB had been delivered to the COLTS facility, the next step was to attach it to the platens. Before the MBB was removed from the assembly fixture, the exact position of the adaptor fittings was defined to ensure that the MBB would be correctly positioned into the COLTS. Once the assembly was complete, the position of each adaptor fitting was measured in the MBB coordinate system established by the coordinate system stamped on the assembly tool (Figure 7-1). The mating surface of each platen as well as the entire perimeter of all four adaptor fittings were recorded and analyzed.

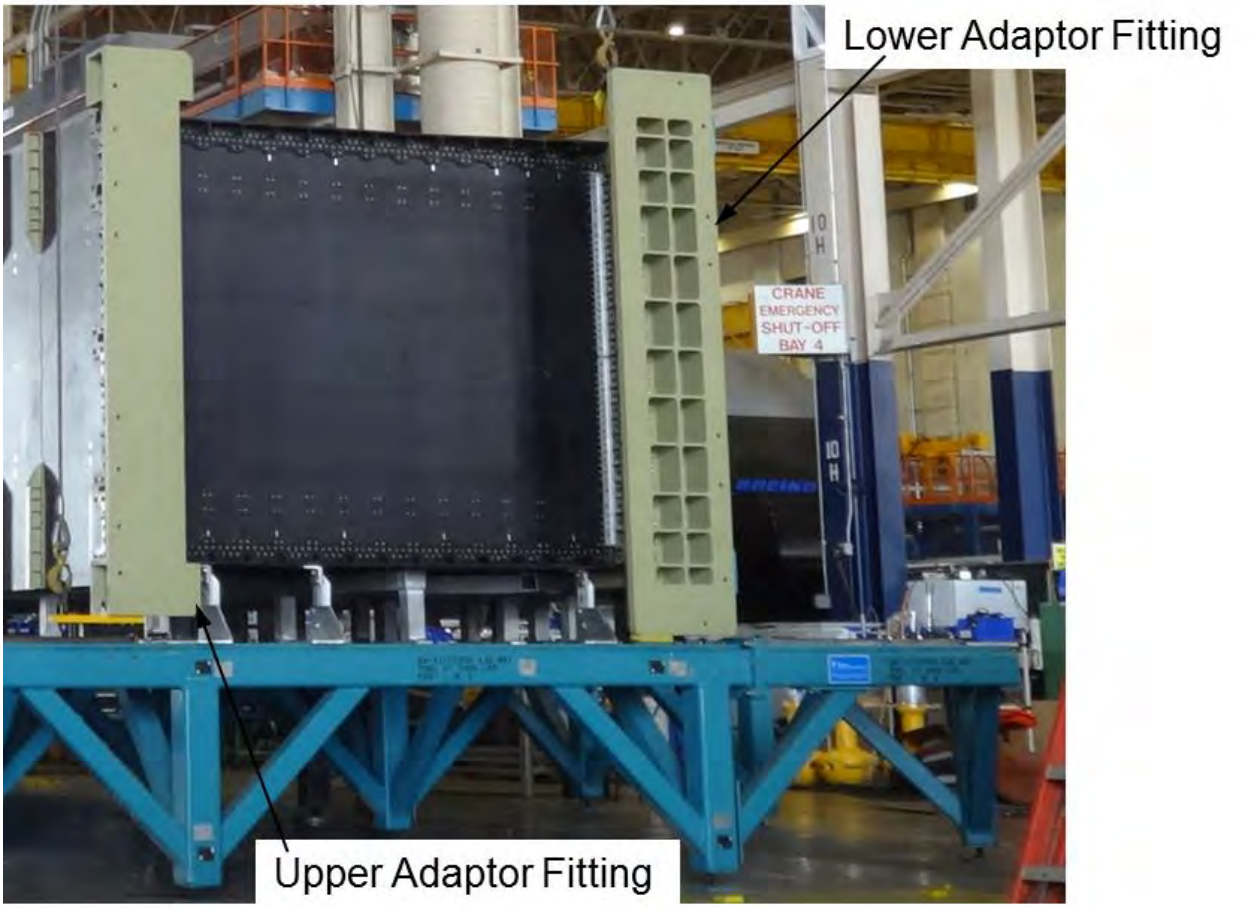

Figure 7-1. Adaptor Fittings Installed on the Completed MBB

To ensure that the MBB could be accurately located on the platens, a clevis was designed to mate with the lower surface of the lower adaptor fittings (Figure 7-2). Using the alignments' targets on each clevis and the actual orientation of the lower adaptor fitting interface surface, the clevis plates were optically aligned and attached to each platen (Figure 7-3 and Figure 7-4). This ensured that the MBB would be positioned correctly on the platens' surface. The slopped surfaces on each side of the clevis and radius corners on the lower adaptor fitting allowed the MBB to slide easily into a repeatable position (Figure 7-5). Figure 7-6 shows the MBB positioned on the platens.

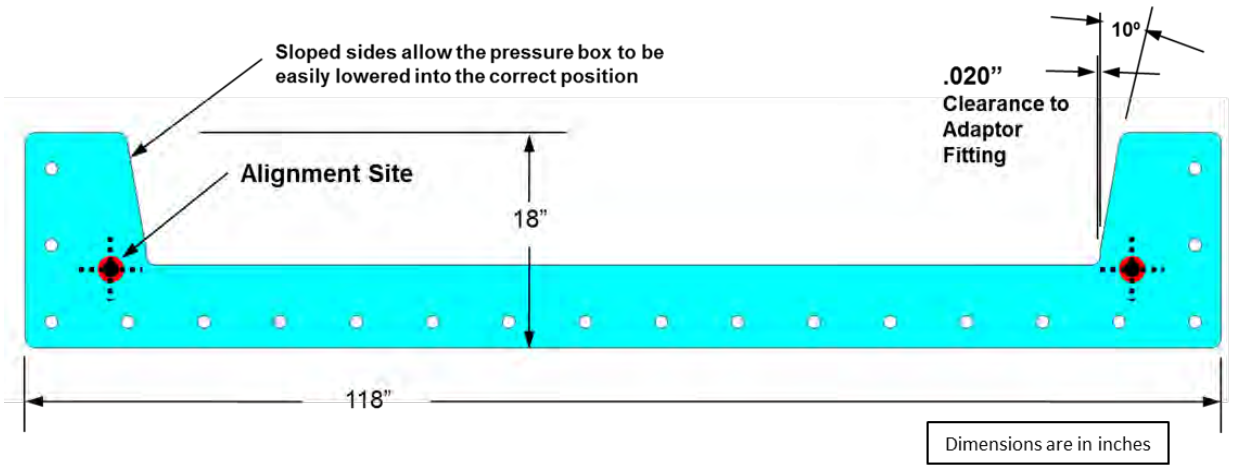

Figure 7-2. Alignment Clevis Used to Locate the MBB on the Platens

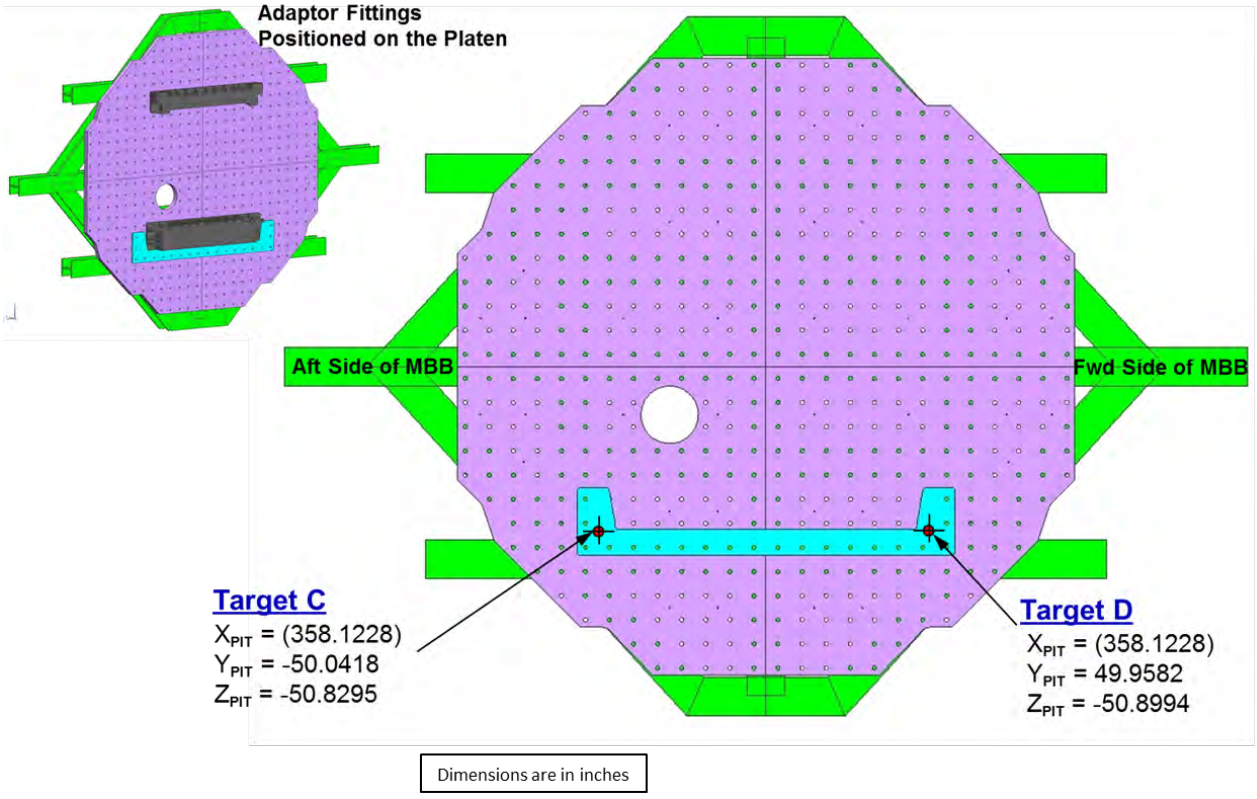

Figure 7-3. Reaction Platen Clevis "As-Built" Target Locations

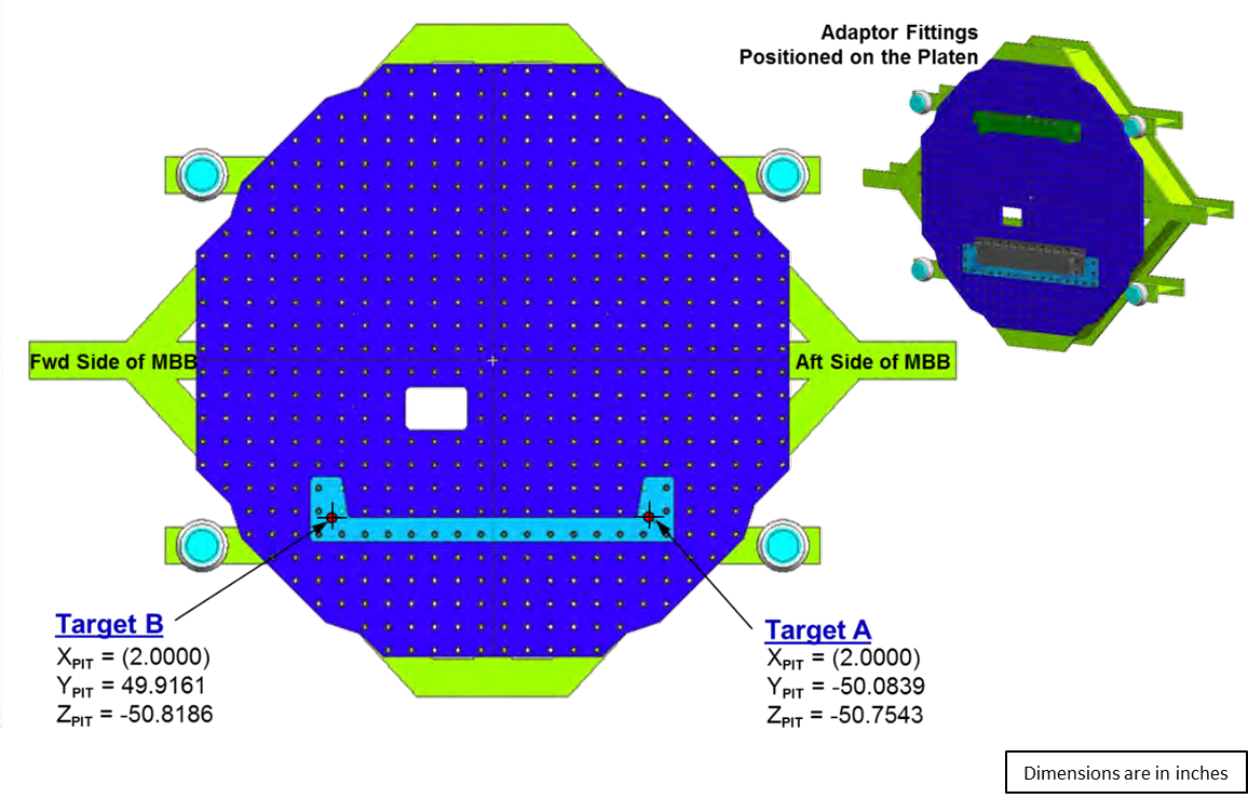

Figure 7-4. Loading Platen Clevis "As-Built" Target Locations

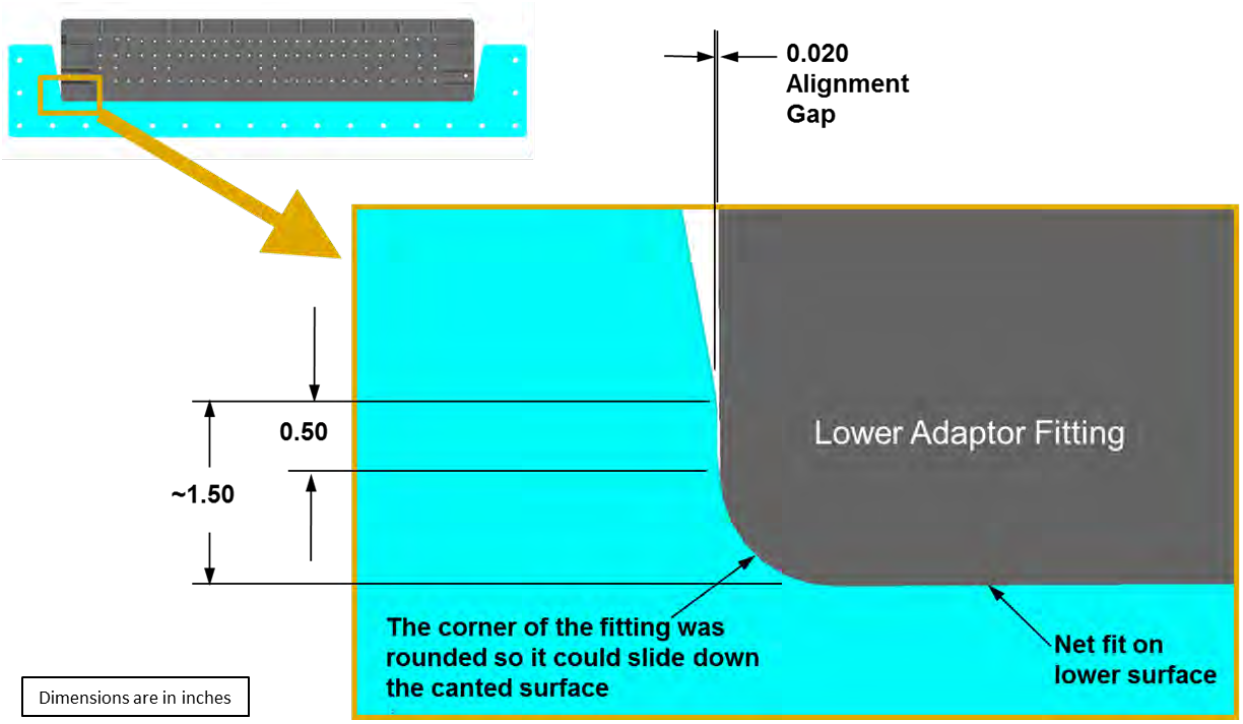

Figure 7-5. Close-Tolerance Fit Between the Clevises and the MBB Adaptor Fitting

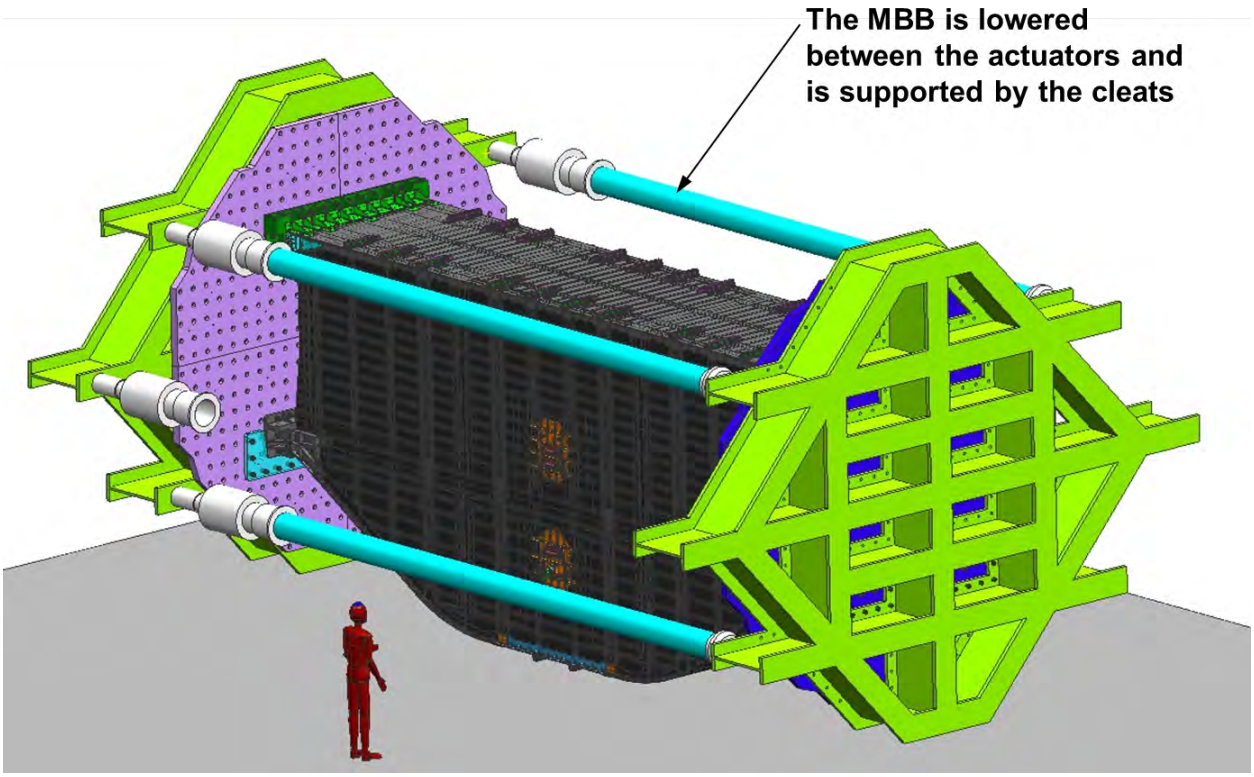

Figure 7-6. MBB Positioned on the Platens

Because the MBB would be removed and reinstalled on the platens, it was important that the MBB's position be repeatable. The adaptor fittings were assembled on the MBB without the platen holes because, at the time of assembly, the platens' exact hole locations and positional tolerances were still unknown. Since there were only a few small holes in the fittings that were used for shipping, this meant that the first time the MBB was located on the platens there would be no bolts to hold it in place.

With the MBB resting on the clevises, the 1.25-in.-diameter platen hole patterns were transferred (center-punched) to the adaptor fittings. The MBB was then removed to enable access for drilling all of the platen attachment holes. The MBB was again positioned on the platens using the clevises and then bolted to the platens. Access holes were designed into the upper adaptor fitting to ensure free access to tighten the lower row of bolts on the upper fitting (Figure 7-7). The lower adaptor fitting used specially designed nut retainers to allow sufficient float to accommodate the maximum tolerance buildup for the hole locations (Figure 7-8 and Figure 7-9) to eliminate access issues for the upper row of bolts.

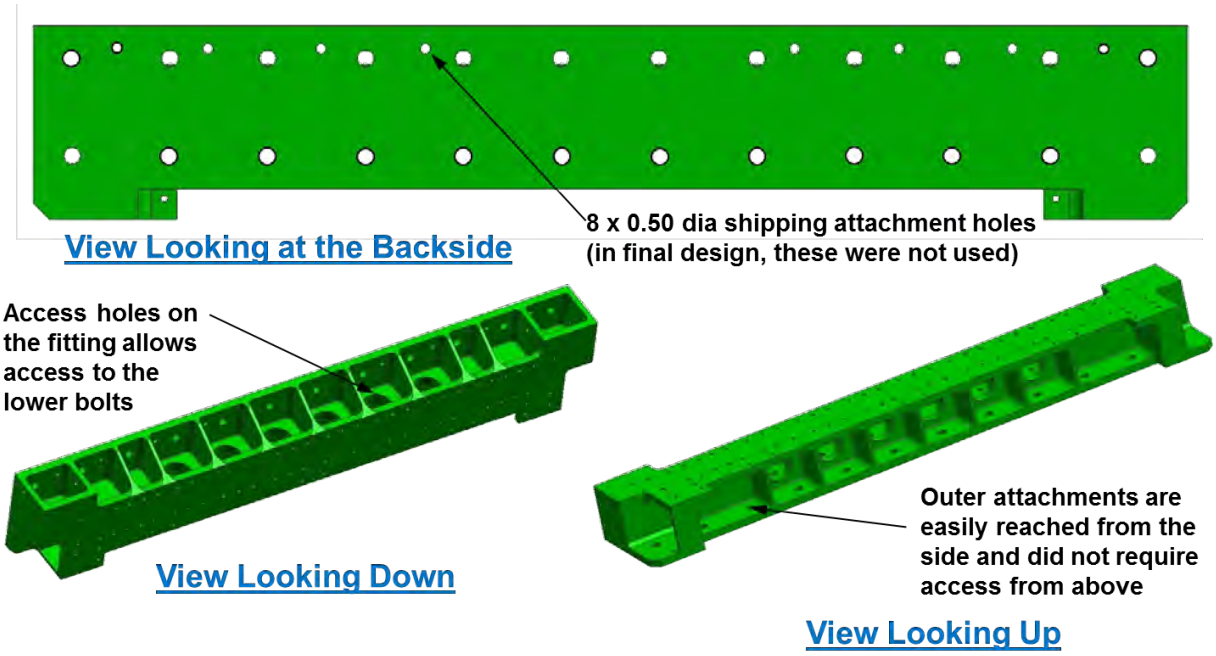

Figure 7-7. Upper Adaptor Fitting

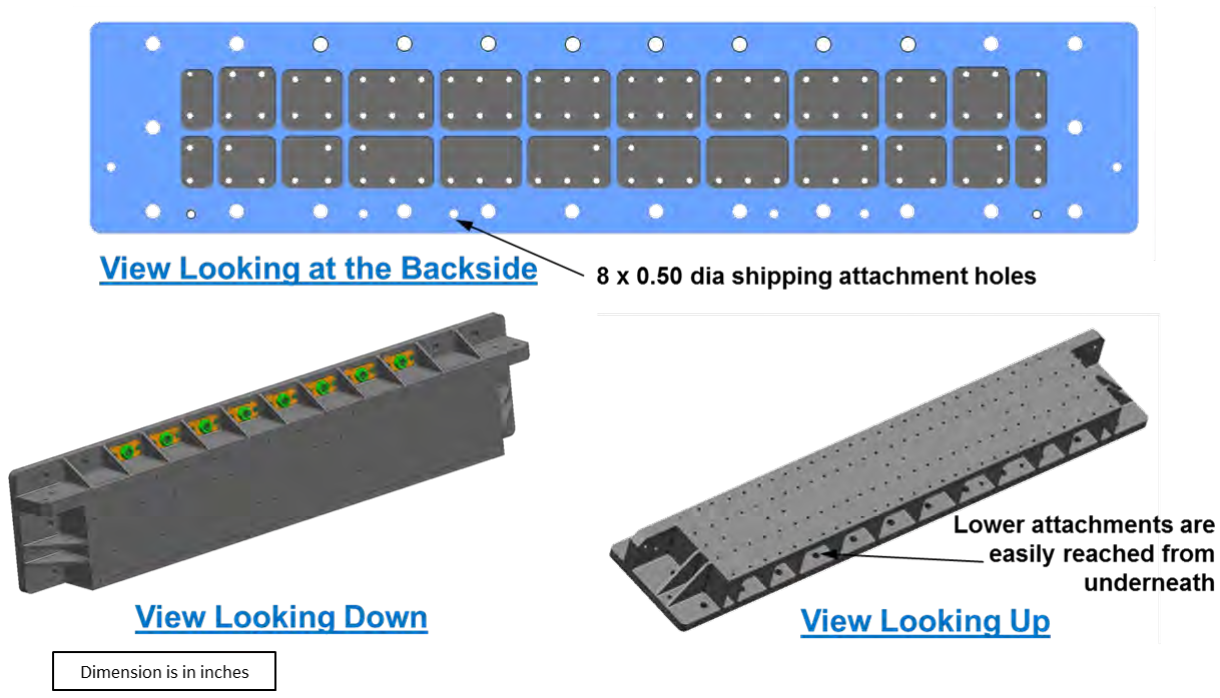

Figure 7-8. Lower Adaptor Fitting

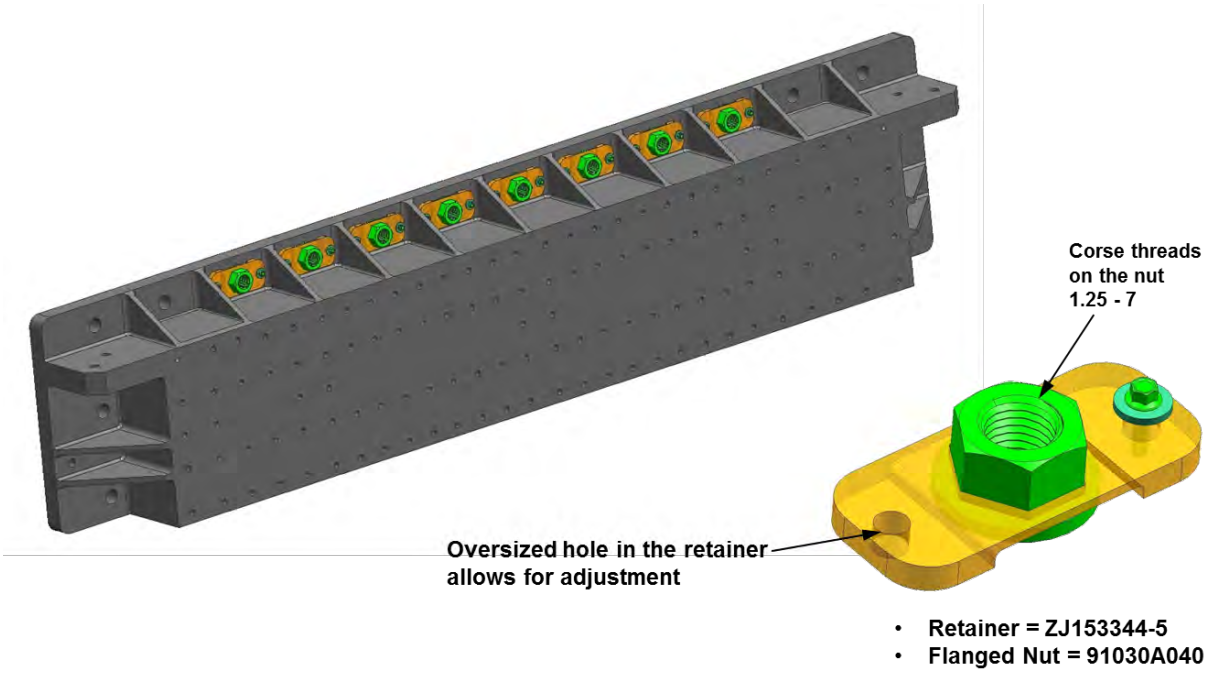

Figure 7-9. Floating Nut Retainer for the Lower Adaptor Fittings

At the COLTS facility, all preparation work on the MBB was performed in the staging area located on the right-hand side of the facility, as shown in Figure 7-10. To get the MBB into the COLTS test area, the MBB had to be crane-lifted over a wall and through the test area lids located in the roof of the test area. Figure 7-11 shows the COLTS test area from above looking through the opening at the top (roof lids removed). The yellow temporary fence located around the perimeter of the opening would be removed before making the move. Special low-profile lifting hardware was designed to maintain clearance between the MBB and the facility. Figure 7-10 shows the minimum clearance of 15.5 in. as the MBB was lifted over the wall. Detailed parts of the lifting hardware are shown in Figure 7-12. Once the MBB cleared the handling fixture, it was rotated 90 deg and then translated across the room to clear an unrelated test fixture being stored on the roof (Figure 7-13). The 90-deg rotation would not have been required with a clear path but was done to eliminate an additional crane move. The MBB was then rotated back to the longitudinal direction, aligned with the loading platens, and lowered into position between the two platens (Figure 7-14). The main spreader bar also had to be custom designed to fit between the platens. With the lower profile requirements to get the MBB over the wall, the main spreader bar would need to fit between the platens. Figure 7-15 shows the 3.0-in. minimum clearance between the platens and the spreader bar. The final MBB position was then verified one more time by the laser tracker before NASA started transferring the 1.25-inch-diameter platen hole positions referenced earlier. Figure 7-16 shows the MBB reinstalled on the clevises after the platens holes were drilled in the adaptor fittings.

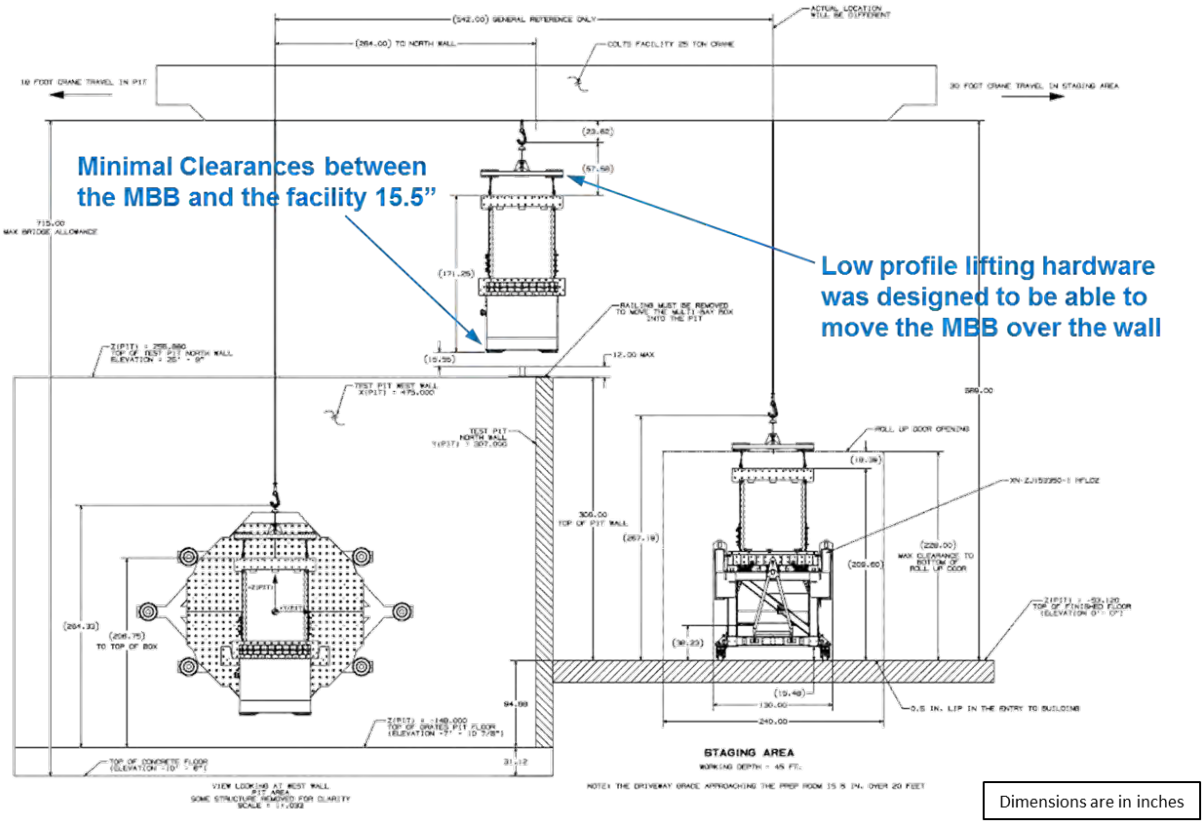

Figure 7-10. COLTS Facility Layout

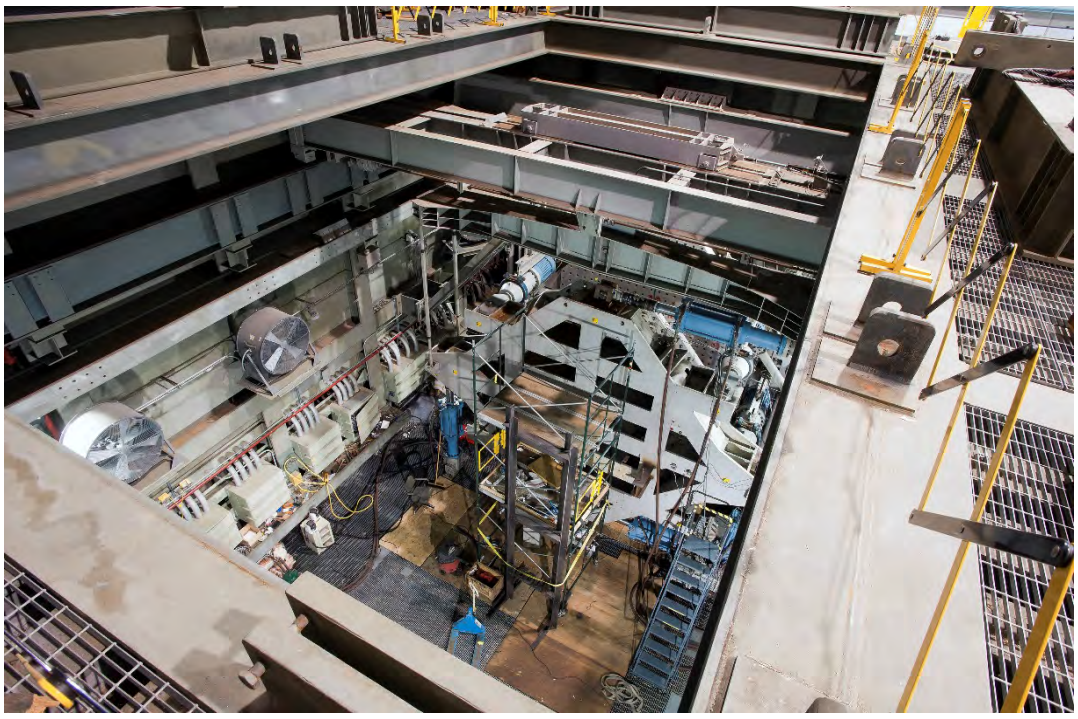

Figure 7-11. Final Preparation of the Test Cell for MBB Installation

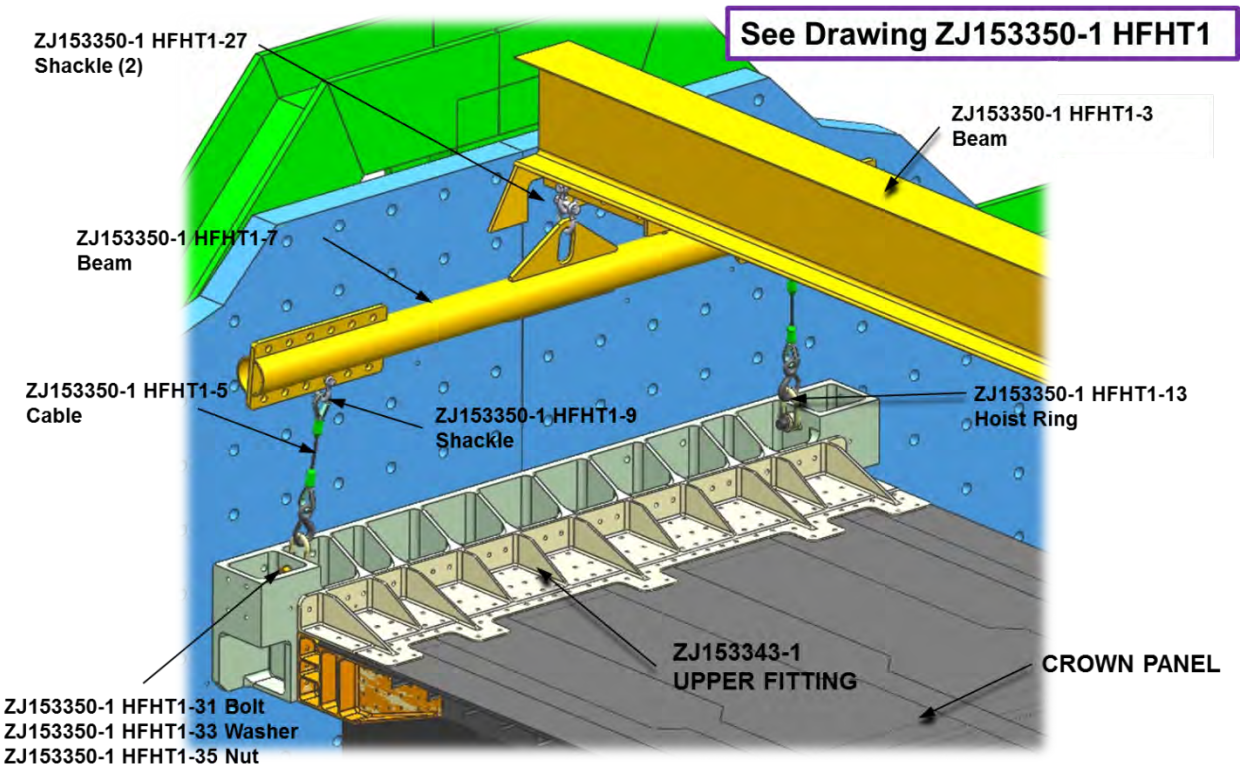

Figure 7-12. Low-Profile Lifting Hardware for the MBB

Figure 7-13. Lifting the MBB into the COLTS Test Cell

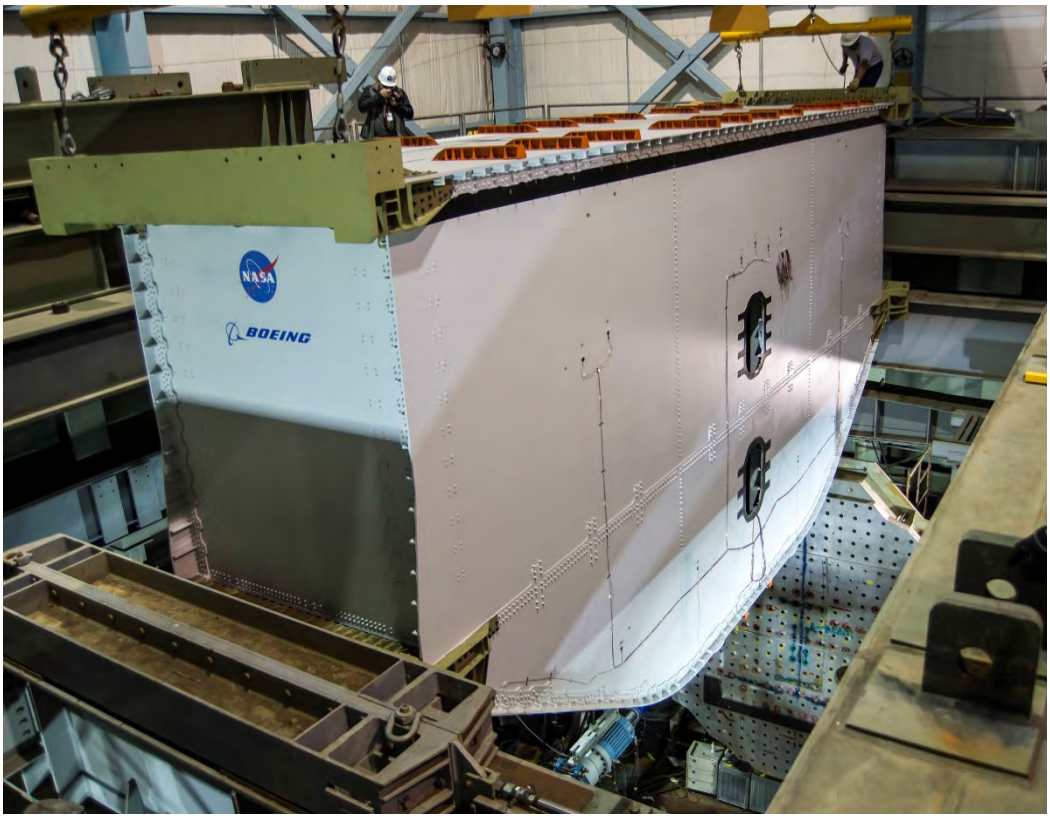

Figure 7-14. Lowering the MBB Into Position Between the Platens

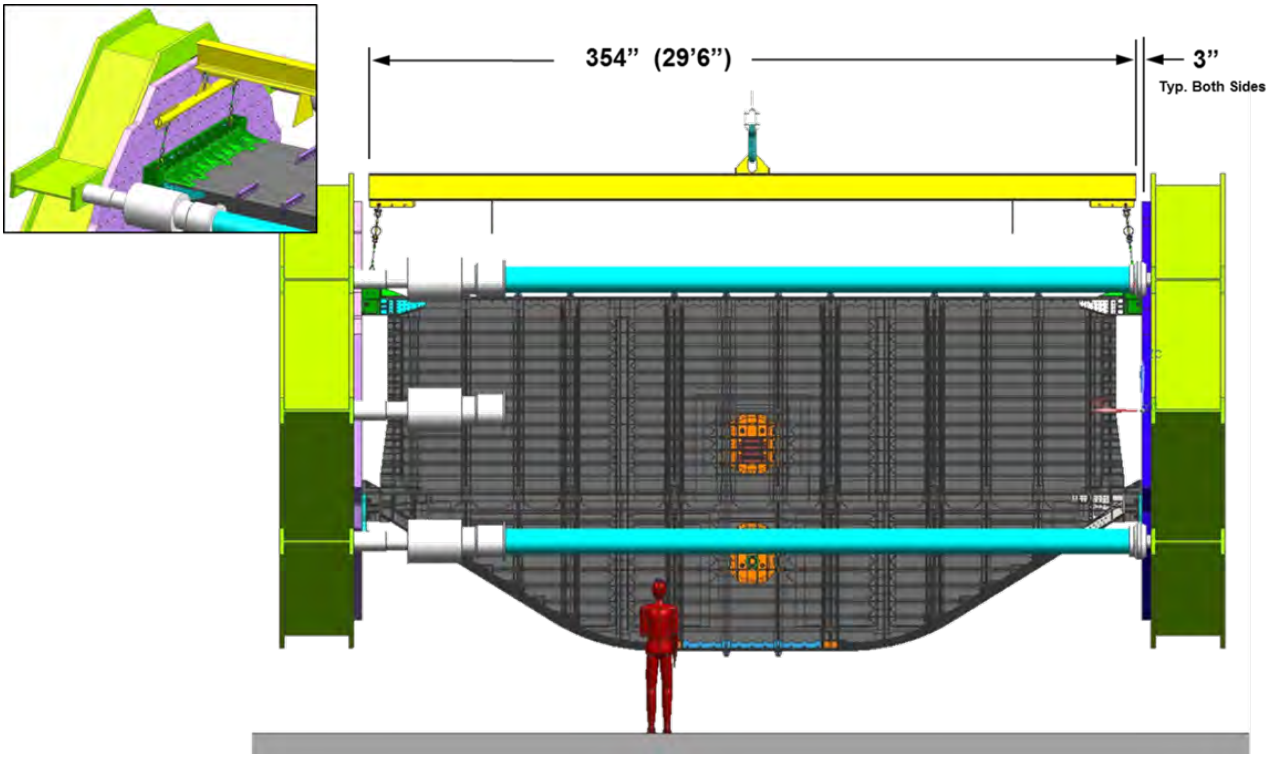

Figure 7-15. Main Spreader Bar Clearances Between the Platens

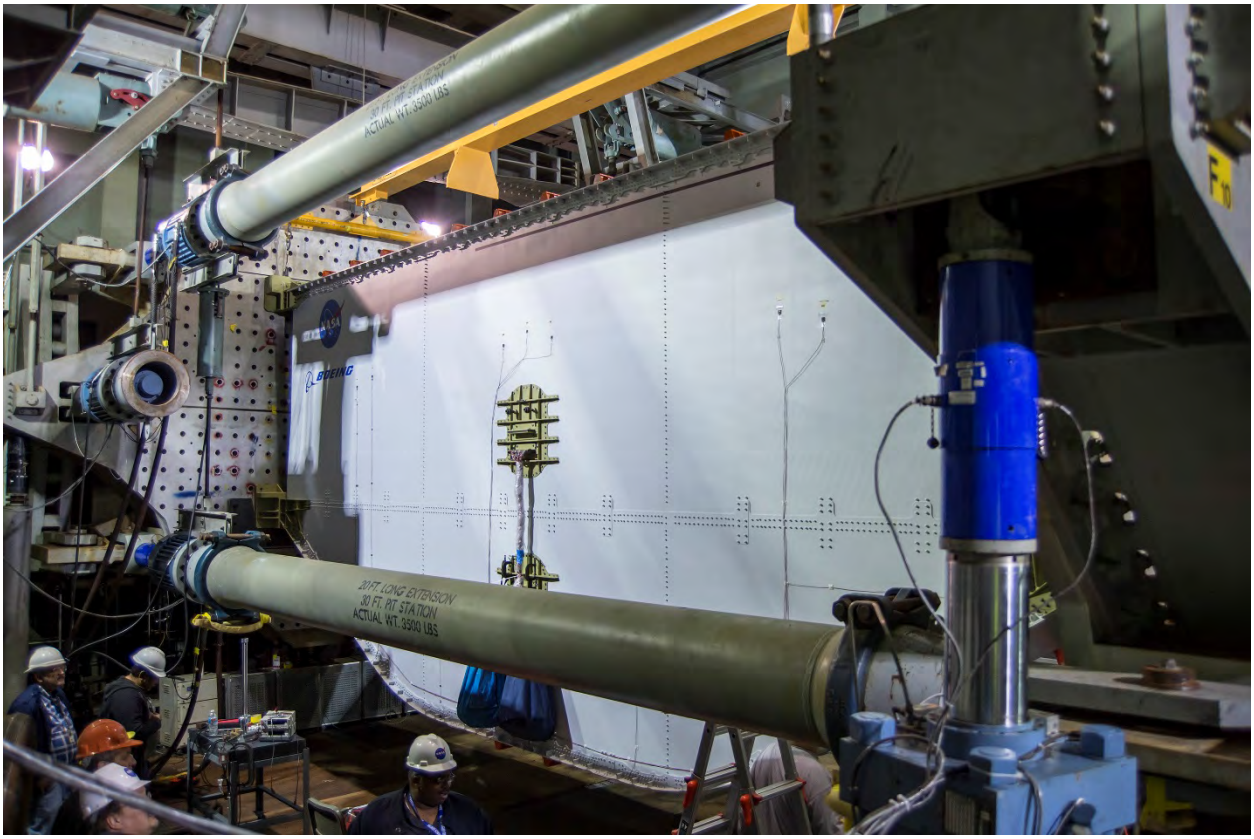

Figure 7-16. MBB Resting on Clevises Prior to Final Fastener Installation

All plumbing required for the MBB was located on the upper and lower doors on the aft side (Figure 7-17). Two pressure transducer ports were located in each door, for a total of four ports. The upper door had two wire pass-through ports. All upper interior strain gage wires exited the MBB through the lower port and were sealed at Boeing before being shipped. The upper wire pass-through port on the upper door was used by NASA to get the internal camera and light wires out of the MBB.

The lower door also had a wire pass-through port. All lower strain gage wires exited the MBB through this port, which was also sealed at Boeing before shipment. Figure 7-18 shows the elevation of the MBB plumbing.

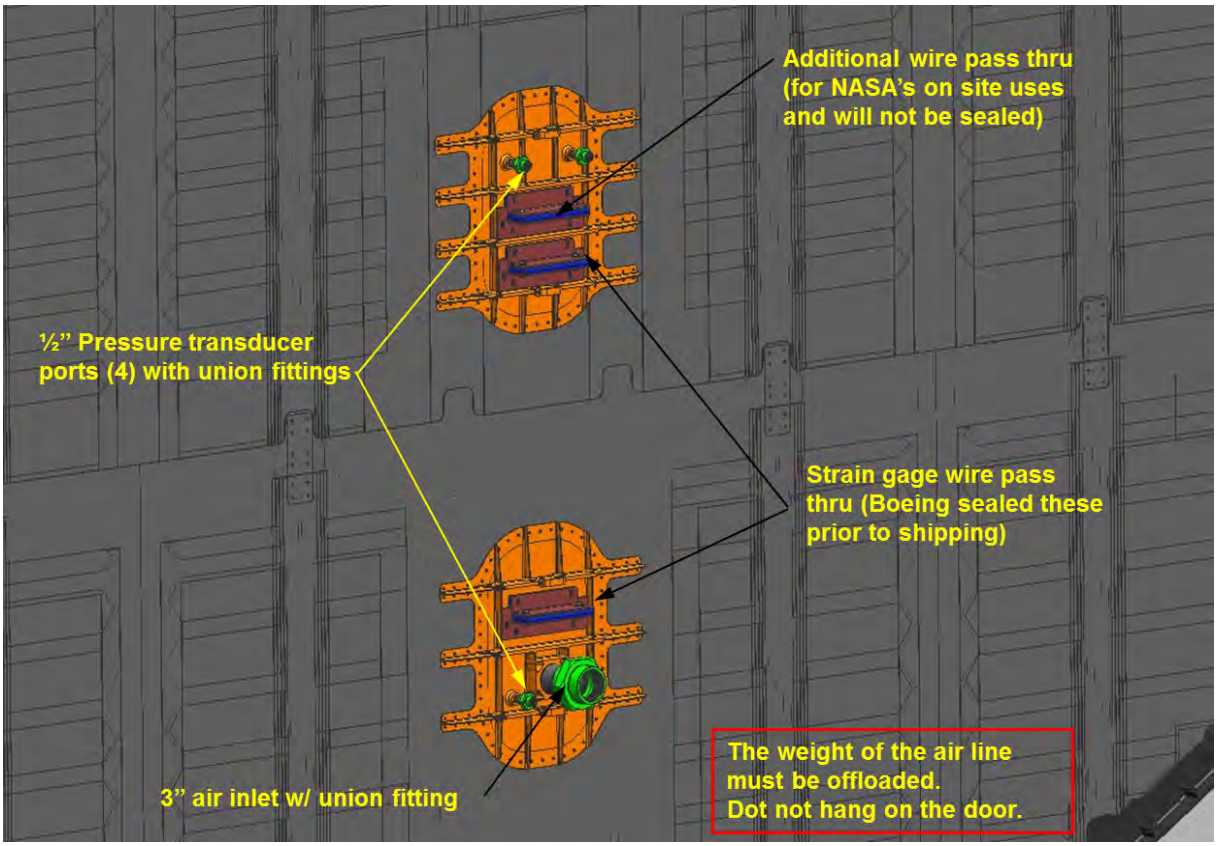

Figure 7-17. MBB Plumbing Located in the Aft Side Doors

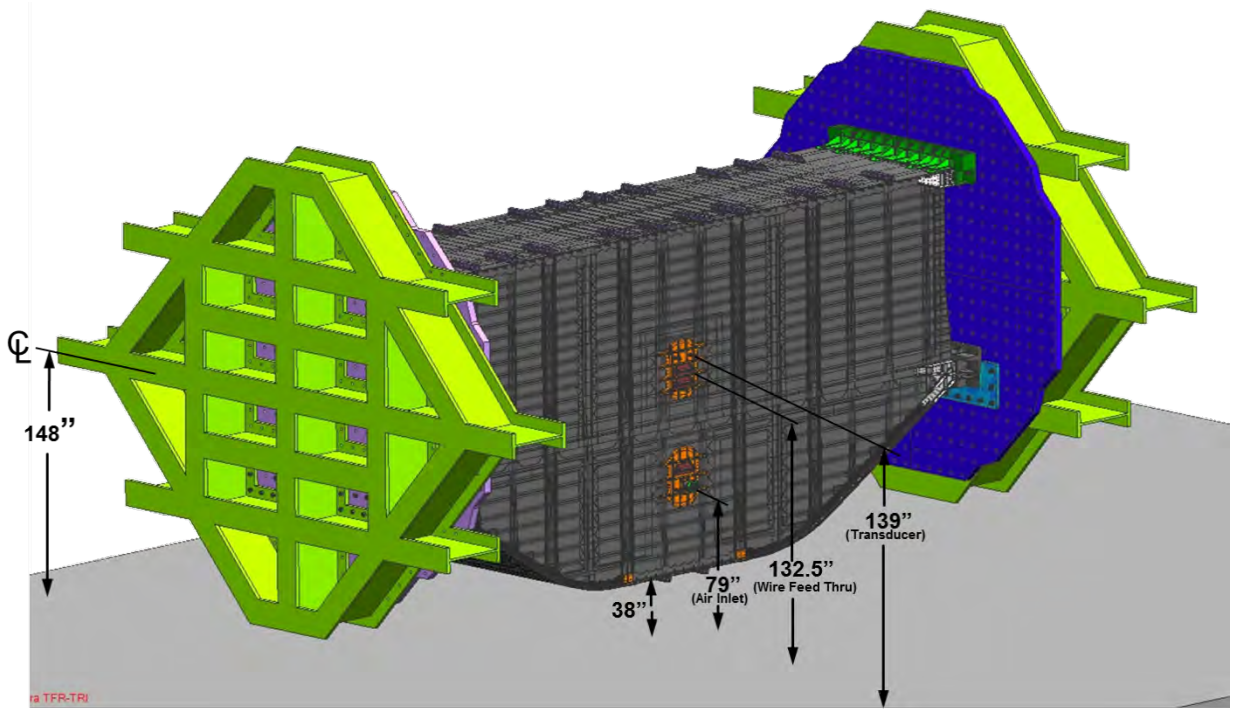

Figure 7-18. Location of MBB Plumbing

7.2 Test Loads and Conditions

To validate the structural integrity of the MBB, a series of tests was performed under the most critical Hybrid Wing Body (HWB) loading conditions. In accordance with vehicle sizing trade results, as stated in the Phase I and Phase II final reports for contract NNL07AA48C (Refs. 2-1 and 2-2), five load cases were determined to be the most critical to the HWB airplane pressure cabin. These five critical load cases were the 2P pressure condition, the 2.5-g and -1.0-g maneuver conditions, and the 2.5-g + 1P and -1.0-g + 1P combined loading conditions.

To verify structural load-carrying capability, the MBB was tested in its pristine condition (without impact damage) to Design Limit Load (DLL) and Design Ultimate Load (DUL) levels of these five load cases. After completion of these tests in pristine condition, the MBB was subjected to Barely Visible Impact Damage (BVID) on its interior and exterior surfaces. Next, these DLL and DUL cases were repeated on the impact-damaged MBB. Upon completing all DLL and DUL tests in the pristine and impact-damaged conditions, the MBB was subjected to final failure load testing. The purpose of this testing was to demonstrate the load-carrying capability of the MBB beyond ultimate loads. A catastrophic failure could occur at any time during the final failure load testing, with the result being that the MBB would not be capable of carrying load. All tests performed on the MBB are depicted in the flowchart shown in Figure 7-19.

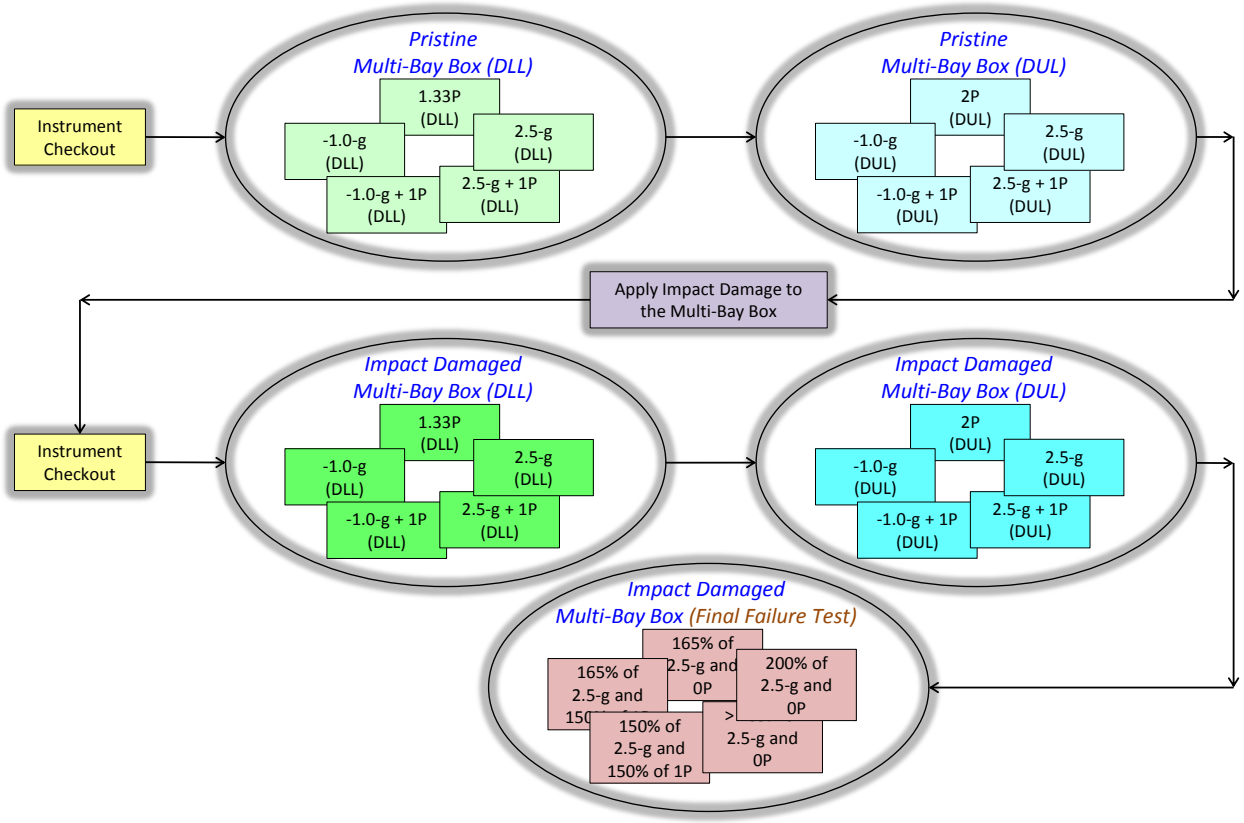

Figure 7-19. Flowchart of the MBB Structural Tests

The MBB was built to undergo structural loading for aircraft maneuvers in conjunction with internal pressurization. In addition to internal pressure loads, -1.0-g down-bending and 2.5-g up-bending loads were applied at the cabin corners to simulate HWB wing loads. These combined loading conditions were designed to satisfy FAR 25.305 and FAR 25.371, which require that limit and ultimate structural loads be applied with and without pressure loading to capture the worst case conditions.

The following four critical test cases were derived by combining structural and pressure loadings: -1.0-g, -1.0-g + 1P, 2.5-g, and 2.5-g + 1P. To deliver the -1.0-g down-bending and 2.5-g up-bending mechanical loads to the MBB, loads were applied to the actuators on the COLTS fixture. To determine the actuator loads needed for the tests, the center frame of the crown was loaded at 80 kips at 2.5-g DUL, as shown in Figure 7-20. This was based on the vehicle sizing trade results contained in the Phase I and Phase II final reports for contract NNL07AA48C (Refs. 2-1 and2-2).

The linear static analysis of the global FEM presented in Section 4 was used to determine amount of platen rotation required to generate the approate wing bending load levels. It was found that by applying 238.5 kips, positive load to the two upper actuators and negative load to the two lower actuators on the COLTS fixture, it would simulate a 2.5-g DUL wing bending load case for the MBB. With a factor of safety of 1.5, the actuator loads were 159 kips for the 2.5-g DLL case. For the -1.0-g down-bending cases, a 0.4 factor was applied and the directions were reversed to the actuator loads for the 2.5-g up-bending cases. Consequently, the actuator loads were -63.6 kips for the -1.0-g DLL case and were -95.4 kips for the -1.0-g DUL case. Details of the actuator loads for the -1.0-g DLL, -1.0-g DUL, 2.5-g DLL, and 2.5-g DUL test cases are shown in Figure 7-21.

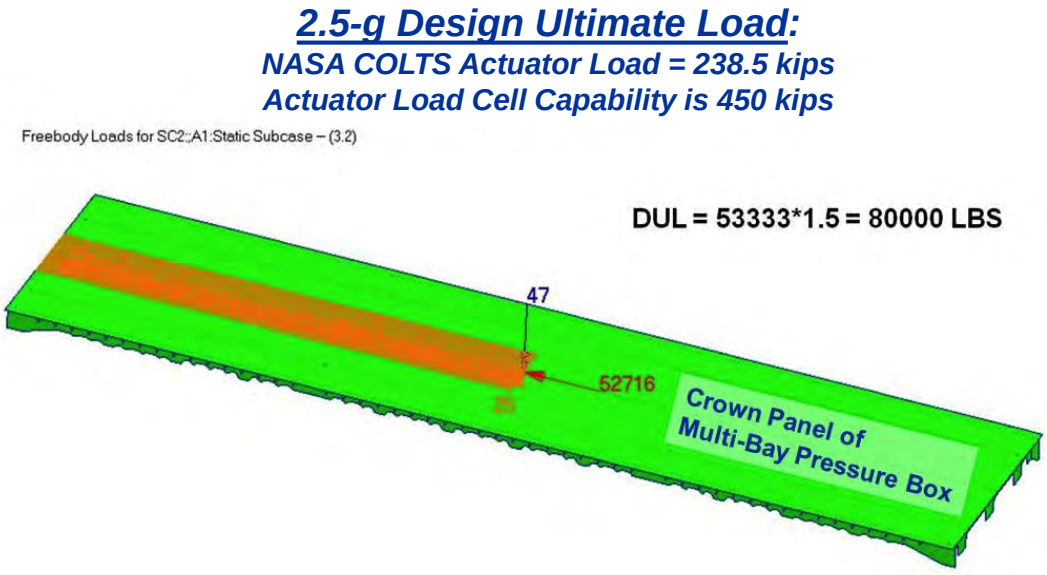

Figure 7-20. Derivation of 80 kips on One Frame/Skin on the Center Crown Panel for 2.5-g DUL

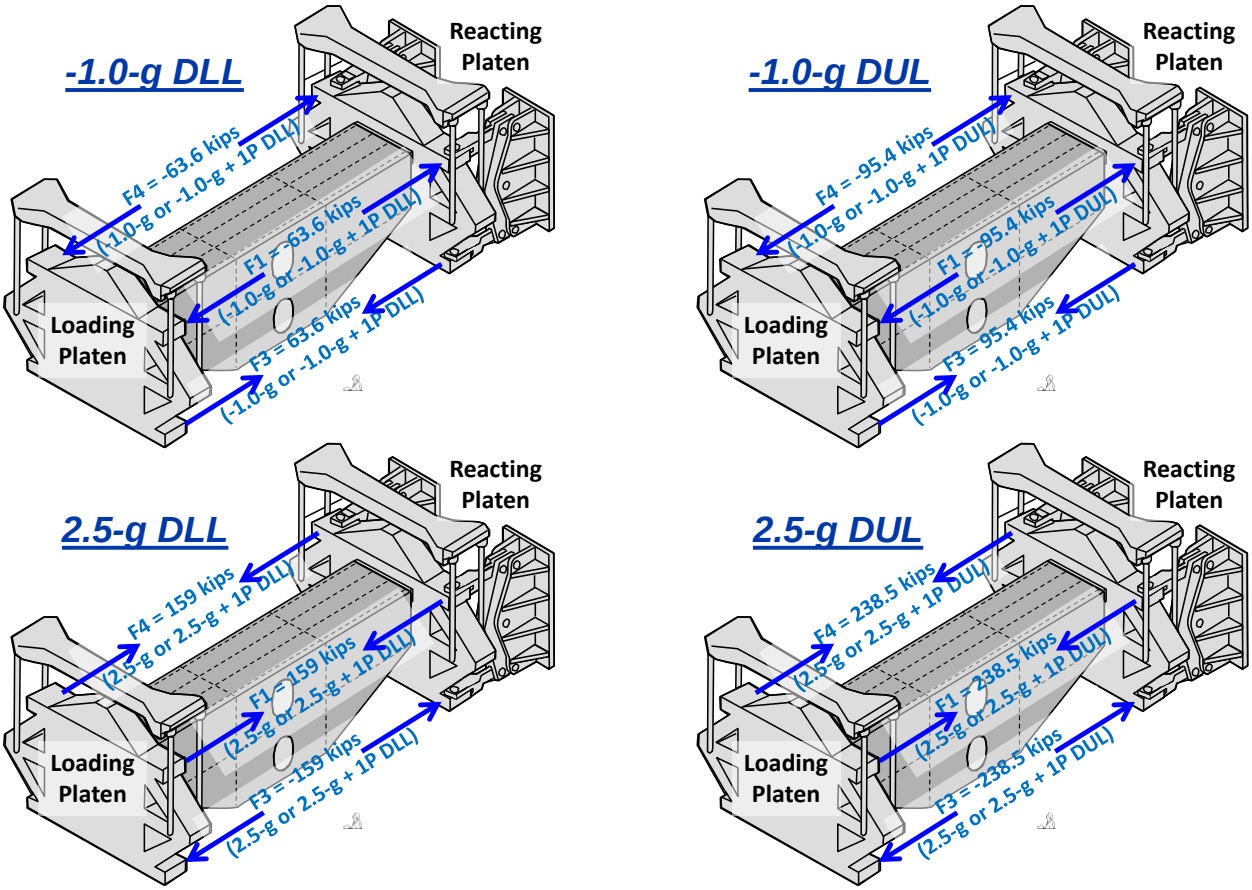

Figure 7-21. COLTS Actuator Test Loads

In addition to the four maneuver-induced test cases described above, the MBB was also proof loaded using only pressure. In these pressure-only tests, the MBB was internally pressurized to 1.33P (12.2 psi) DLL and 2P (18.4 psi) DUL. No mechanical loads were applied for these pressure-only cases. (The 2P internal pressure is an ultimate design condition that satisfies the requirements of FAR 25.365(d).)

As discussed earlier, the MBB was tested initially in the pristine structural condition (without impact damage imposed) at DLL, and then again at DUL. Upon completion of these DLL and DUL test cases, the MBB was subjected to impact damage on its exterior and interior surfaces in accordance with BVID requirements. Detailed locations of the impact damage sites are shown in drawing ZJ153986 for exterior impacts on the center keel, and in drawing ZJ153983 for interior impacts on the forward upper bulkhead.

Impactors with 1.0-in.-diameter hemispherical steel heads were used to simulate the impact incidents. To attain the desired impact energy for BVID more accurately, three impactor masses were used. For exterior impacts, an impactor of 5-lb mass was used for the skin impact, and a 15-lb mass impactor was used for the stringer and frame impacts. For interior impacts, a 3.708-lb mass impactor was used for the skin, stringer, and frame impacts. All impacts were applied normal to the composite surface (direct hit).

In accordance with FAR requirements (PART 25–Airworthiness Standards: Transport Category Airplanes), composite structures with Category 1 damage, including BVID, are required to demonstrate a reliable service life while retaining ultimate load capability. For the MBB, the BVID to a composite surface is limited to 100 ft-lb of impact energy or a 0.04-in. indent depth (visible indentation) from an exterior impact, and 20 ft-lb of impact energy or a 0.04-in. indent depth (visible indentation) from an interior impact. A BVID also includes any observable fiber breakages or matrix cracking on the composite surface of impact. It is noted that the impact energy required to cause a BVID on a composite is greatly influenced by the structural geometry and stiffness of the composite at the impact site, whether exterior or interior.

To determine the minimum impact energy for a BVID on the exterior and interior sides of the MBB, trial impact tests were performed on discarded PRSEUS panels. From the results of these impact trials, impactor masses and impact energies that would be used at various impact sites on the MBB for BVID were determined. These masses and energies are summarized in Table 7-1 for exterior impacts on the center keel and in Table 7-2 for interior impacts on the forward upper bulkhead of the MBB. These impact sites are also shown graphically for exterior impacts on the exterior side of the center keel in Figure 7-22 and for interior impacts on the interior side of the forward upper bulkhead in Figure 7-23.

Table 7-1. Exterior Impacts Applied to the Exterior Side of the Center Keel

Exterior Impact Site	Location	Impactor Mass	Impact Energy
No. 1	Flange of frame	15 lb	60 ft-lb
No. 2	Flange of stringer	15 lb	50 ft-lb
No. 3	Center of skin	5 lb	15 ft-lb

Table 7-2. Interior Impacts Applied to the Interior Side of the Forward Upper Bulkhead

Interior Impact Site	Location	Impactor Mass	Impact Energy
No. 1	Top of frame cap	3.708 lb	20 ft-lb
No. 2	Top of stringer rod	3.708 lb	20 ft-lb
No. 3	Center of skin	3.708 lb	15 ft-lb

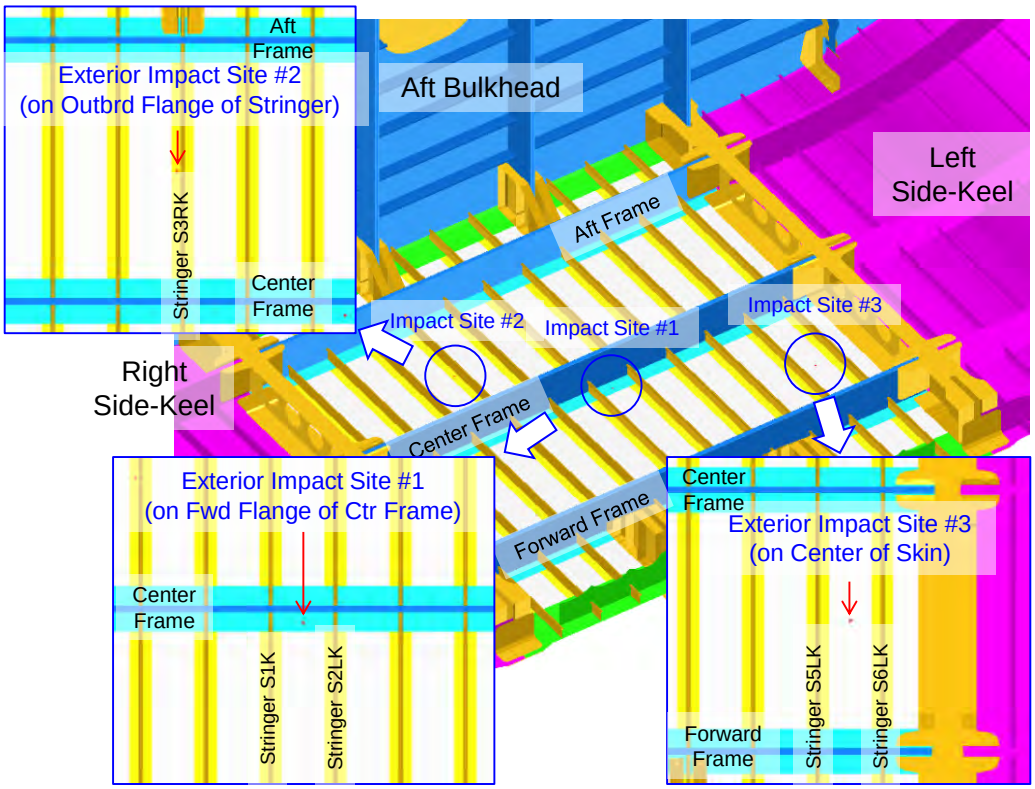

Figure 7-22. Locations of the Exterior Impacts to the Center Keel

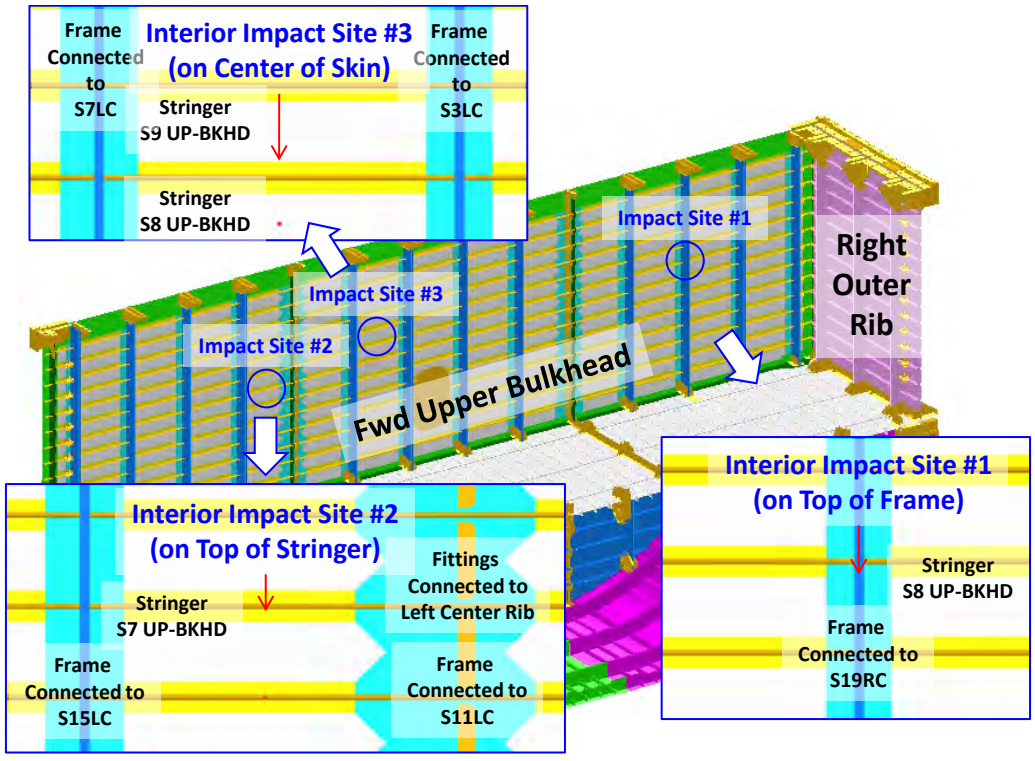

Figure 7-23. Locations of the Interior Impacts to the Forward Upper Bulkhead

Impacting devices developed by NASA were used to inflict impact damages to the MBB. For exterior impacts to the exterior side of the center keel, a roller-coaster type of impactor, as shown in Figure 7-24, was used. For interior impacts to the interior side of the forward upper bulkhead, a spring-loaded type of impactor, as shown in Figure 7-25, was used. Only one impact incident was permitted on each site, and no multiple impacts were performed on the same site even if there was no visible damage observed after the impact.

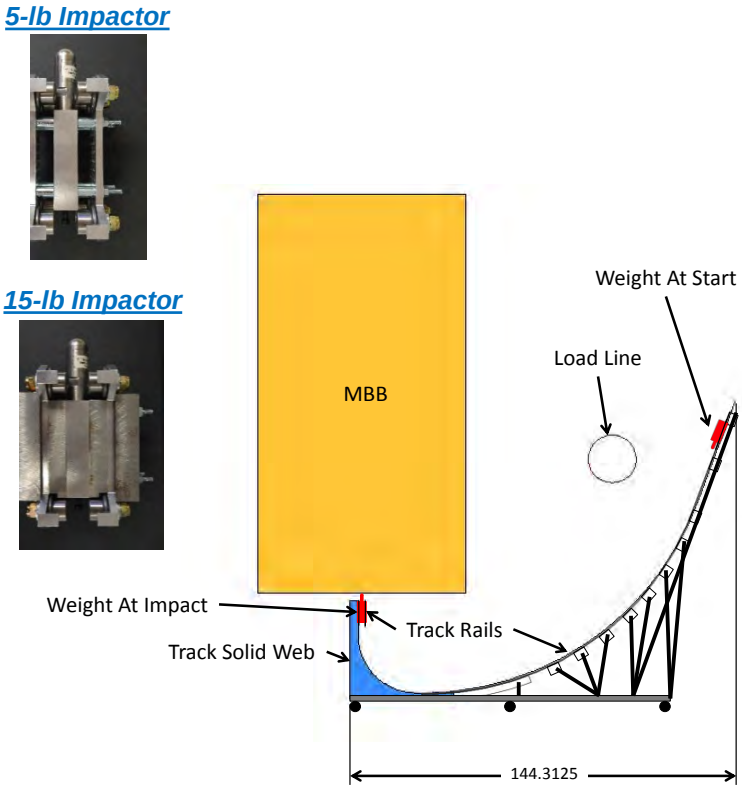

Figure 7-24. NASA Roller-Coaster Impactor

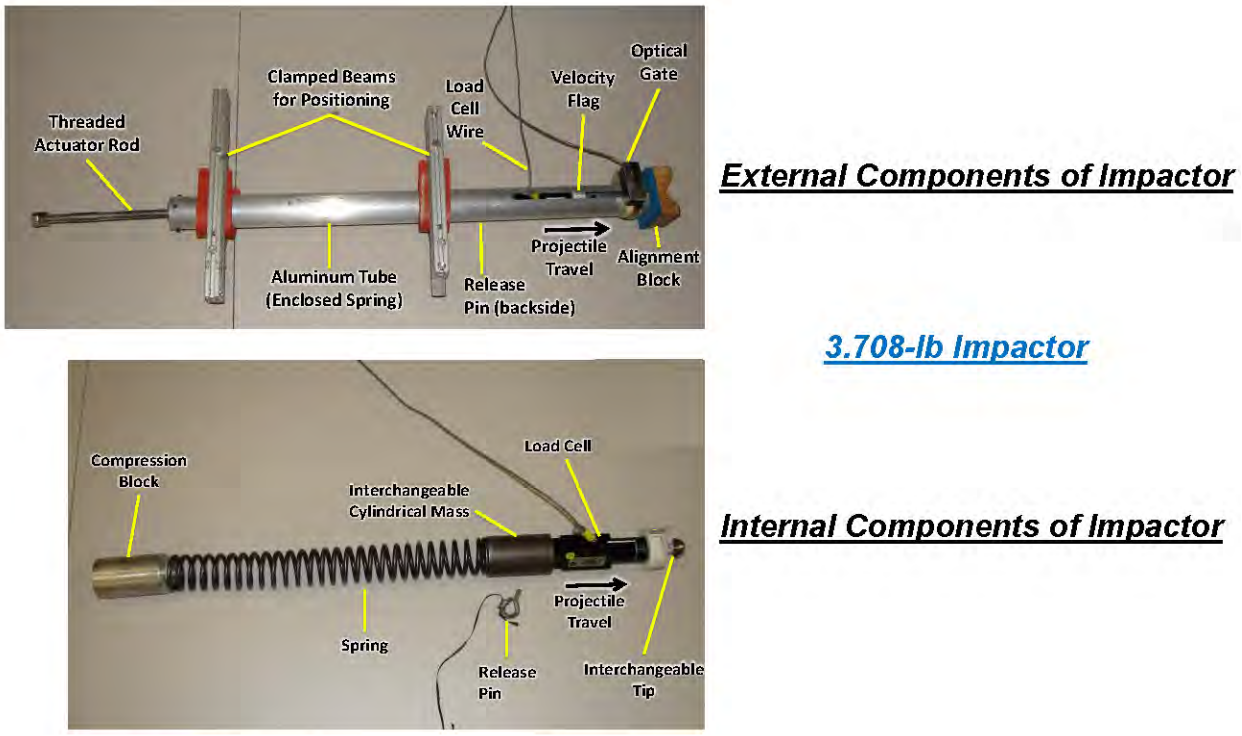

Figure 7-25. NASA Spring-Loaded Impactor

7.3 Testing Sequence

As discussed previously, the MBB was tested in two (pristine and impact-damaged) conditions, two design load (DLL and DUL) conditions, five load cases (-1.0-g, -1.0-g + 1P, 2.5-g, 2.5-g + 1P, 2P or 1.33P), and several testing sequences in final failure testing. As shown previously in Figure 7-19, the MBB was first tested in its pristine condition (without impact damage) to DLL and DUL levels of the five load cases. After completion of these tests in pristine condition, the MBB was subjected to BVID on its interior and exterior surfaces. Next, these DLL and DUL cases were repeated on the impact-damaged MBB. Upon completing all DLL and DUL tests in pristine and impact-damaged conditions, the MBB was tested for the final failure load testing.

The exact testing sequence of all these tests was based on the rationale that the least critical load case should be tested first and the most critical load case tested last. In other words, the load case with the potential to cause the most damage should be tested last to minimize risk to the test article for subsequent testing.

When determining an optimal testing sequence, two probable types of damage to the MBB needed to be evaluated, nondetrimental and detrimental. With regard to nondetrimental damage, typical examples include composite delamination failures between plies (however, these failures are arrested/contained by stitching); or metallic fittings/fasteners yielding but not yet reaching ultimate failure; or reaching failure but with their internal loads redistributed to other structures without failure to the entire structure. In general, these types of nondetrimental damage do not cause a catastrophic failure to the entire structure.

In terms of detrimental damage, typical examples include composite strength failures, which cause a final failure of the entire structure; or a global buckling of primary structural members (such as frames or T-caps in the MBB) due to local failures on metallic fittings, which causes a loss of boundary constraints to these primary structural members. In contrast to nondetrimental damage, detrimental damage results in a catastrophic failure of the entire structure.

The final testing sequence of the MBB was decided based on (1) the results from linear and nonlinear analyses, such as local skin buckling, margins of safety for composite structures, metallic fittings, and fasteners, and (2) failure predictions of nondetrimental and detrimental damage. Clearly, the MBB should be tested in pristine condition first and in impact-damaged condition afterward, and DLL cases should be tested before DUL cases. Additionally, the down-bending cases of -1.0-g and -1.0-g + 1P should be tested before the up-bending cases of 2.5-g and 2.5-g + 1P because less mechanical load is applied to the MBB in the down-bending cases. Finally, the -1.0-g + 1P case should be tested after the -1.0-g case, and the 2.5-g + 1P case should be tested after the 2.5-g case because an addition of 1P pressure represents a higher strain energy stored in the MBB, causing greater likelihood of failure.

To determine whether the 1.33P (or 2P) case should be tested before the 2.5-g case or after the 2.5-g + 1P case, more analytical result comparisons were needed. For the DLL cases, testing order was determined from the following result comparisons.

a. From results of the linear buckling analyses, no buckling was expected at 1.33P pressure-only load (Section 4.3.6.1), whereas local skin buckling was expected on the crown at 0.347-g (or 13.9% of 2.5-g DLL) maneuver-only load (Section 4.3.6.2).

b. From nonlinear analysis, the critical composite strains were -3,627 micro-in./in. on the crown stringer web and -3,087 micro-in./in. on the upper bulkhead frame cap in the 1.33P case (Section 4.4.1), whereas the critical composite strains were -4,300 micro-in./in. on the crown skin and -3,600 micro-in./in. on the upper bulkhead skin in the 2.5-g DLL case (Section 4.4.2).

c. Also derived from nonlinear analysis, the lowest margin of safety for metallic fittings was 54% on the “External Center Keel Stringer Support Fitting” (ZJ153666-1) in the 1.33P case, whereas the lowest margin of safety for metallic fittings was 72% on the “Upper Load Introduction Fitting” (ZJ153345-1) in the 2.5-g DLL case.

Based on the result comparison above, it was apparent that the 1.33P test case should be tested before the 2.5-g DLL test case.

For the DUL cases, testing order was determined from the following result comparisons.

a. From nonlinear analysis, critical composite strains were -5,440 micro-in./in. on the crown stringer web and -4,630 micro-in./in. on the upper bulkhead frame cap in the 2P case (Section 4.4.1), whereas critical composite strains were -5,850 micro-in./in. on the crown skin and -6,030 micro-in./in. on the upper bulkhead skin in the 2.5-g DUL case (Section 4.4.2).

b. Also derived from nonlinear analysis, the lowest margin of safety for metallic fittings was 2.5% on the “External Center Keel Stringer Support Fitting” (ZJ153666-1) in the 2P case, whereas the lowest margin of safety for metallic fittings was 15% on the “Upper Load Introduction Fitting” (ZJ153345-1) in the 2.5-g DUL case.

Based on the result comparison above, it was concluded that the 2P test case could be tested either before the 2.5-g DUL test case or after the 2.5-g + 1P DUL test case. Taking into

consideration final failure testing, it was decided that the 2P case would be tested after the 2.5-g + 1P DUL test case in pristine condition, and the 2P case would be tested before the 2.5-g DUL test case in impact-damaged condition.

As described earlier, the final failure testing condition was the last test case for the MBB, and it was completed after all DLL and DUL tests (in pristine and impact-damaged conditions) had been performed. The purpose of the final failure load testing was to demonstrate the load-carrying capability of the MBB beyond the ultimate loads. In this case, the impact-damaged MBB would be tested to catastrophic failure, or until a maximum mechanical load of 200% DLL was reached. Several loading steps, as shown in Figure 7-26, were performed in sequence to the MBB.

To demonstrate the load-carrying capability of the MBB beyond the ultimate loads before final failure of the MBB occurred, in Load Sequence 1 the MBB would first be tested to 150% of the 2.5-g limit load and 1.5P (13.8 psi) pressure, which is the same as the 2.5-g + 1P DUL combined loading condition. In other words, the 2.5-g + 1P DUL case became Load Sequence 1 of the final failure testing condition.

Then, in Load Sequence 2, the mechanical load was increased to 10% above the 2.5-g ultimate load while holding pressure at 1.5P (13.8 psi). With a factor of safety of 1.5, 110% of the ultimate load is equivalent to 165% of the limit loads. Next, in Load Sequence 3, the mechanical load was reduced to 2.5-g DUL while holding pressure at 1.5P (13.8 psi). In Load Sequence 4, the pressure was reduced to zero while keeping the mechanical loads at 2.5-g DUL. Then, in Load Sequence 5, the mechanical load would be increased to 165% of 2.5-g DLL and then to 200% of 2.5-g DLL, or until a catastrophic failure of the MBB occurred. Failure predictions were made at the end of Load Sequence 2, which was at 4.125-g + 1.5P combined loads, and at the end of Load Sequence 5, which was at 5.0-g maneuver load.

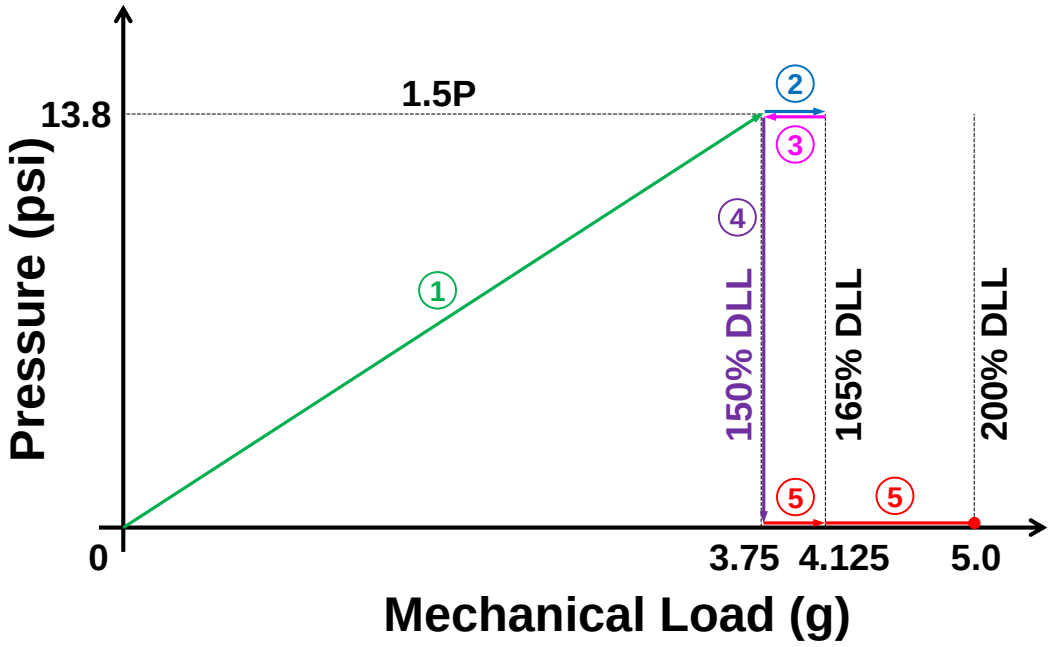

Figure 7-26. Loading Sequence Chart of Final Failure Testing

In summary, the sequence of the MBB structural tests is depicted graphically in Figure 7-27. Instrument checkout was performed before limit load tests for the MBB in pristine and impact-damaged conditions. Detailed procedures of each test case are contained in the HWB Multi-bay Test Article Test Specification (Ref. 4-9).

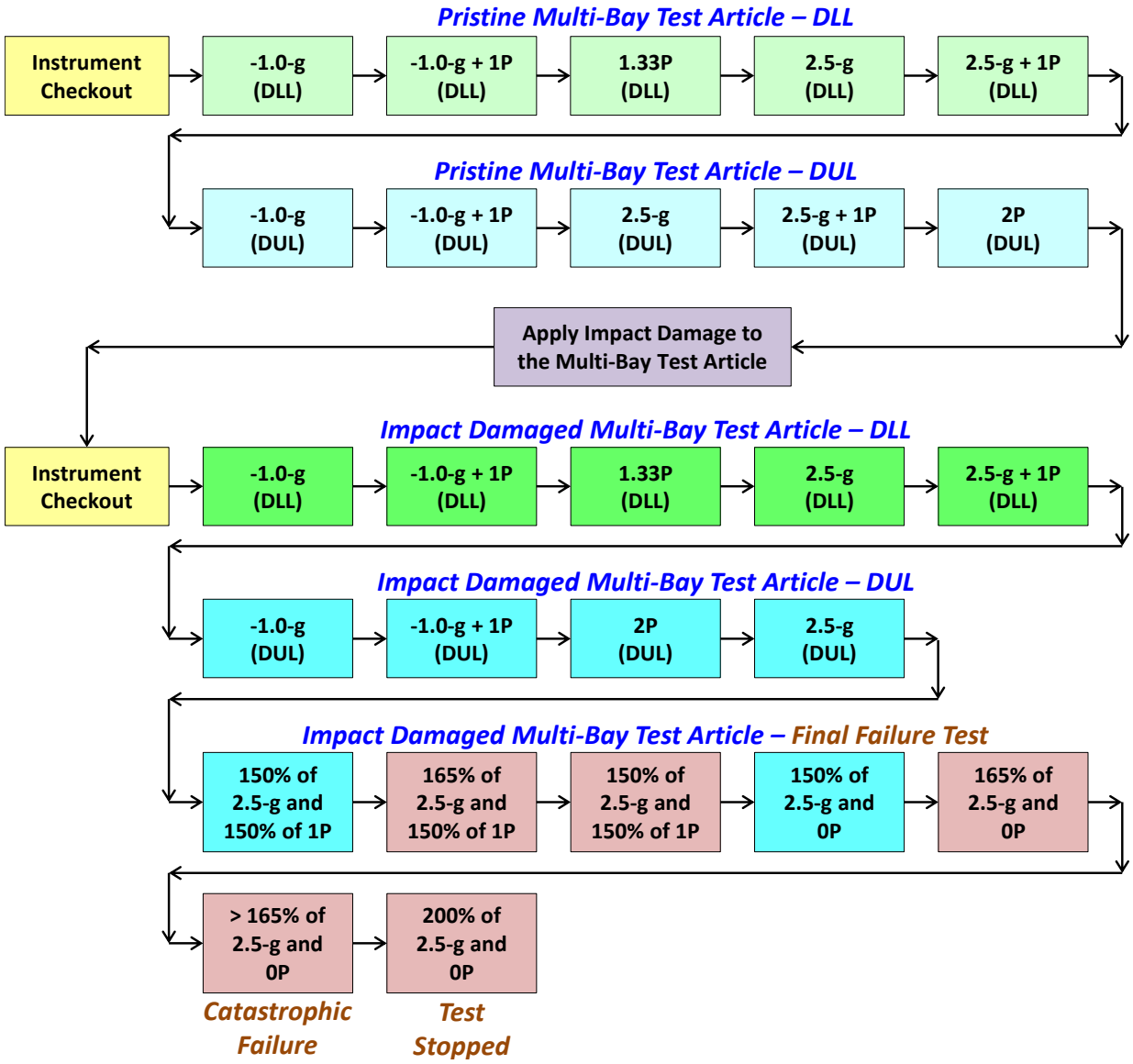

Figure 7-27. Sequence of the MBB Structural Tests

7.4 Test Documents and References

Test documents and references were created to support MBB testing at the COLTS facility at NASA Langley Research Center. These documents and references include the HWB Multi-bay Test Article Test Specification (Ref. 4-9), the Installation Drawing of the Multi-bay Box to COLTS Test Fixture (as shown Figure 7-28), and drawings for Strain Gage Installation, MBB Holding Fixture, MBB Lifting Hardware, and Locating Cleat (as shown in Table 7-3).

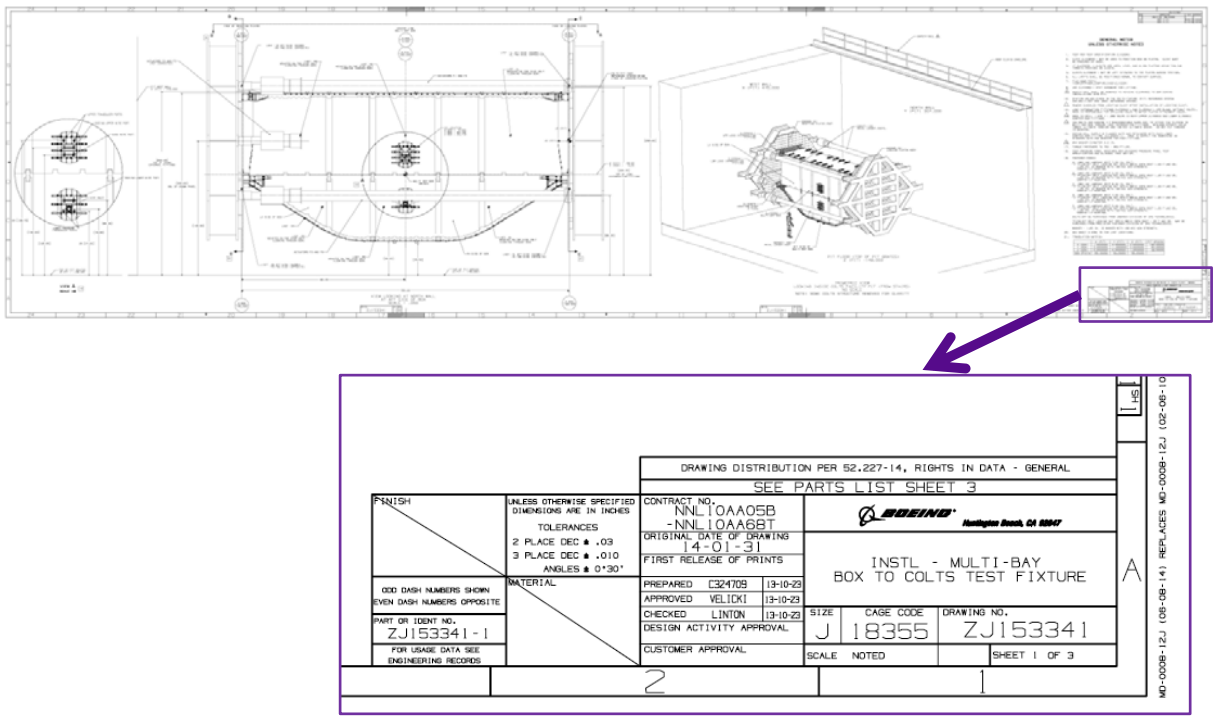

Figure 7-28. Installation Drawing of the MBB–to-COLTS Test Fixture

Table 7-3. Strain Gage and Tooling Drawing Numbers

Drawing Number	Description	Rev Letter
ZJ153981	Strain Gage Installation – Crown Panel	B
ZJ153982	Strain Gage Installation – Floor Panel Assembly	New
ZJ153983	Strain Gage Installation – Upper Bulkhead Panel	C
ZJ153984	Strain Gage Installation – Lower Bulkhead Panel	New
ZJ153985	Strain Gage Installation – Side Keel Panel	B
ZJ153986	Strain Gage Installation – Center Keel Panel	B
ZJ153987	Strain Gage Installation – Outer Rib Panel	A
ZJ153988	Strain Gage Installation – Upper enter Rib Panel	A
ZJ153989	Strain Gage Installation – Lower Center Rib Panel	New

Drawing Number	Description	Rev Letter
ZJ153350-1 HFLD2	MBB-Holding Fixture	T1D
ZJ153350-1 HFHT2	MBB Lifting Hardware	T3
ZJ153978	Locating Cleat	New

8.0 SUMMARY AND CONCLUSIONS

The Multi-bay Box (MBB) was the final test article in a building-block test program, which was designed to assess the overall feasibility of meeting the pressure cabin design requirements for the flat-sided shell structure of the Hybrid Wing Body (HWB) airframe. Delivery of the MBB to NASA culminated a multi-year effort involving multiple contracts. The final task was the testing of the MBB performed by NASA, with Boeing providing support under Boeing funding and not under NASA contract. The summary and conclusions presented in this section pertain to the work completed through MBB delivery and before testing by NASA.

8.1 Summary

The goals of the NASA Environmentally Responsible Aviation (ERA) project included reducing fuel burn, noise, and emissions. The MBB effort contributed to these goals by developing a lighter, more robust airframe structure using the Pultruded Rod Stitched Efficient Unitized Structure (PRSEUS) concept. PRSEUS was identified as an enabling technology for the HWB aircraft configuration, which reduces drag and fuel consumption. It was uniquely capable of meeting the combined pressure and mechanical loading requirements of the flat-sided pressure cabin of the HWB aircraft while maintaining a weight-efficient structure. The MBB effort advanced the Manufacturing Readiness Level (MRL) and the Technology Readiness Level (TRL) of PRSEUS specifically, and damage-arresting composites in general. Although aimed at the HWB aircraft, the advancements would benefit conventionally shaped vehicles as well, including tube-and-wing aircraft.

The concept for the MBB had been developed during prior efforts. The MBB design requirements were derived from vehicle-level analyses, and they were supported by testing of PRSEUS structural coupons and elements. A multi-year effort was conceived to design, fabricate, and test the MBB. Testing of the MBB would demonstrate, at relevant scale and load levels, nonlinear behavior and damage tolerance that could not be captured at the panel level or shown by analysis. Initial concept development was followed by a risk-reduction effort involving fabrication and testing of a small pressure cube specimen. This cube was built by Boeing and tested by NASA. The success of the pressure cube test validated design concepts for joints between PRSEUS panels and provided design values for MBB analysis and test.

For the MBB, the majority of the initial design, linear analyses, and fabrication work was performed by Boeing, and the activities related to nonlinear analysis and testing were completed by NASA at the Langley Research Center (LaRC). The PRSEUS panels for the MBB were fabricated at the Boeing Huntington Beach, California, facility, and the MBB was assembled at the Boeing Long Beach, California, facility. The structure was delivered to NASA in December 2014 for testing in the Combined Loads Test System (COLTS) facility during 2015.

The design of the MBB was developed to a highly detailed level. For each structural panel, every layer of fabric and every stitch row were modeled and defined. The assembly drawings were similarly thorough. Boeing performed linear analyses for designing and sizing the MBB, and the Finite Element Model (FEM) of the MBB developed by Boeing was of such high quality that NASA could directly use it for nonlinear analyses. The FEM was an excellent balance between efficiency and fidelity, and provided a foundation for refinements and adjustments by NASA to get accurate results to support testing. Margins of safety were checked for all critical features in the panels, and for all fittings and fasteners with both linear and nonlinear analysis

results. The designs were updated based on analysis results to help ensure that the MBB would perform as expected during testing.

Successful performance of panel fabrication and on-time completion of MBB assembly tasks were critical to meeting the required schedule for delivering the MBB to NASA. One result of the focus on maintaining schedule while reducing remaining program risks was the development and implementation of an extensive risk-management effort. Many of the ensuing risk mitigations proved to be highly beneficial. In addition, timely reporting of risks avoided surprises among stakeholders, and risk documentation captured many lessons learned, which will help in similar future efforts. Ultimately, the MBB was delivered to NASA on time for testing.

Throughout the MBB effort, the damage-arresting stitched composites technology performed well. The fabrication effort produced the largest and most integrated stitched composites panels ever built, and it demonstrated the technology's scalability and robustness. The panels integrated skins, stringers, frames, rib caps, bulkhead caps, and pad ups, thereby eliminating large numbers of detail parts. The integration also eliminated the fasteners, shimming, and labor that otherwise would have been required to join the parts. The 11 integrated panels for the MBB would have required 165 detail parts and 17,000 fasteners for an equivalent state-of-the art composite design.

Many new features were included in the MBB panels. For example, near-edge stitching was used for the first time, for more robust stiffener flanges, and higher strength stitching thread was used to increase pull-off strength. Despite featuring many firsts in design and fabrication, all panels were eventually good to use, and none were scrapped. The integrated features enabled panels to be simply pinned together at Determinate Assembly (DA) holes. This approach virtually eliminated all assembly tooling, except for the tool needed to raise the MBB off the ground to enable access. A variety of lessons were learned, including methods to improve to the fabrication and assembly processes, and they were documented in monthly technical progress reports and other presentations to NASA. Thus, even before NASA's testing of the MBB, many significant accomplishments had been achieved.

Additionally, Boeing designed and built a single holding fixture that was used for final assembly, transport of the MBB to NASA LaRC, and test integration at the NASA COLTS facility. In addition, detailed instructions for moving and handling the MBB during each phase were included. Boeing also provided a detailed test specification document, based on analysis work by Boeing and NASA, defining the load conditions and test sequence for the MBB.

Finally, the MBB was linked to NASA ERA goals by key structural performance metrics that would, in turn, affect airframe weight reduction and fuel burn for the HWB aircraft. The tests by NASA would establish values for these metrics. Conclusions related to these metrics are discussed next.

8.2 Conclusions Prior to NASA Testing

Over the course of the NASA-sponsored development effort, increasing levels of structural design and testing complexity were achieved, which exceeded the initial design metrics established by the configuration sizing exercise. Although each element and subcomponent-level specimen validated a specific uniaxial-loaded design condition for the pressure cabin, the MBB was the only test article that was capable of replicating the combined pressure-plus-axial loading envelope that is distinctive of the HWB blended wing planform.

As such, success could not be fully claimed until (1) the MBB had successfully performed under this unique loading environment (wherein the basic structural concept would be simultaneously exercised in all three loading directions), (2) the joints/transitions were loaded in

a representative fashion, and (3) the influence of the damage-arresting design approach was demonstrated. Because these final test results would have a profound effect on the airframe weight calculation, the three metrics listed in Figure 8-1 as M1A (10% lighter than sandwich), M2A (minimum gauge meets 2P), and M2D (frame buckling at 80 kips) had the potential to dramatically change based on the load magnitudes and/or failure modes that were achieved during the MBB test.

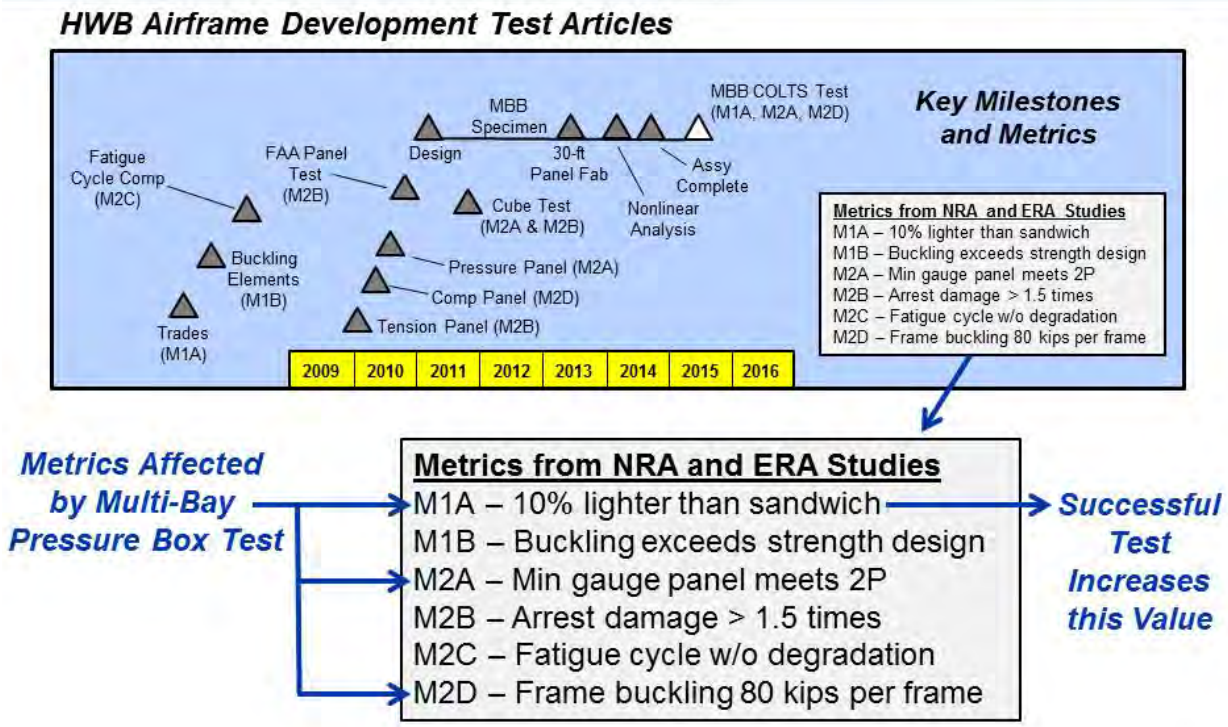

Figure 8-1. Summary of Development Testing Leading to MBB COLTS Test

If testing proceeded as planned and the entire spectrum of design loads and failure constraints were met, then the following three top-level design objectives would be achieved:

1. Validate the Basic Design and Loading Requirements for the HWB Pressure Cabin:
   a. Replace the old baseline sandwich-panel design with a damage-tolerant, fail-safe, multi-load path stiffened-panel design concept that meets primary structure design requirements.
   b. Validate minimum gage panel design (2.1 lb/ft^2) for the Two Times Maximum Internal Pressure (2P) load case (Metric M2A).
   c. Demonstrate advanced integral construction joining techniques by test (Metric M1A).
   d. Demonstrate combined loading capability for the HWB crown panel (Metric M2D).
   e. Quantify vehicle-level weight calculation and verified savings by test (Metric M1A).
2. Advance the Technical Readiness Level to 5 for the HWB Pressure Cabin:
   a. Demonstrate structural benefits of integral PRSEUS construction (Metric M1A).
   b. Demonstrate damage-arrest and fail-safety of stitched interfaces (Metric M2B).
3. Advance the Manufacturing Readiness Level to 4 for the HWB Pressure Cabin:
   a. Scale up fabrication and tooling techniques to build multiple 30-ft panels.
   b. Demonstrate robust nature and process repeatability of stitching/resin-infusion.

c. Demonstrate large-scale assembly methods to reduce future implementation risk.

Under such a scenario, all performance metrics listed in Figure 8-1 would be achieved. At that point, some of the initial conservative analytical assumptions used in the original vehicle-level sizing trade studies could be revisited with a new set of higher design allowables to resize the pressure cabin panels based on the success of the MBB testing. Ultimately, this would reduce the analytical risk of the airframe weight calculation based on the new test data. Conversely, not achieving the anticipated load levels or predicted failure modes, which were predicated on arresting damage propagation and maintaining residual part strength, would generally have an adverse effect on the current HWB airframe weight calculation.

Although novel configurations such as the HWB offer better aerodynamic performance as compared to traditional tube-and-wing aircraft, their blended wing shapes also pose significant new design challenges that cannot be resolved using conventional materials and structures. Developing an improved structural concept that is capable of meeting the structural weight fraction for these noncircular pressurized cabins remains the primary obstacle in implementing large lifting body designs such as the HWB. The MBB test would thus become an important milestone in assessing whether the novel PRSEUS structural concept would be capable of operating within this harsh design regime, making it uniquely capable of satisfying the structural fractions established for the HWB cabin design.

8.3 Post-Test Assessment Notes

Although testing of the MBB was not part of this contract, it is noted that, as of this writing, NASA has completed all MBB testing. The pristine structure was subjected to five critical load cases, which included pressure only, bending only, and combined bending and pressure conditions. The MBB was tested at Design Limit Load (DLL) and Design Ultimate Load (DUL) levels without experiencing any structural failures. Next, impact damage was deliberately inflicted in multiple locations, and the load cases were repeated. In the final test, on 8 May 2015, the MBB was tested to 10% beyond ultimate load (165% DLL), once again without structural failure. To preserve the MBB for a “bonus” test, the decision was made to stop the test at 165% DLL rather than find out if the MBB could reach 200% DLL. This concluded the test plan, and it achieved the full success criteria for this NASA ERA technology demonstration.

Because the MBB was still intact, a final bonus test was possible—a discrete source damage test to failure. The central frame of the crown panel was severed with a two-bay saw cut before this test. On 3 June 2015, this test was successfully completed, exceeding technical objectives. Quoting the lead engineer for the tests, “…the box performed beautifully.”

As such, the MBB tests were a welcome culmination of several years of dedicated effort. NASA’s next steps will be to evaluate both the wealth of data obtained and the MBB itself. Based on the successful tests, the ERA project can now assess the HWB aircraft using realistic estimates of structural weight savings.

9.0 REFERENCES

1-1 Velicki, A., Thrash, P. J., and Jegley, D., "Airframe Development for the Hybrid Wing Body Aircraft," 47th AIAA Aerospace Sciences Meeting, 2009, http://enu.kz/repository/2009/AIAA-2009-932.pdf.

2-1 Velicki, A. et al., "Damage Arresting Composites for Shaped Vehicles—Phase I Final Report," NASA/CR 2009 215932, Contract NNL07AA48C Project No. 4200208122, September 2008.

2-2 Velicki, A. et al., "Damage Arresting Composites for Shaped Vehicles—Phase II Final Report," NASA/CR 2011-216880, Contract NNL07AA48C, Project No. 4200208122, January 2011.

4-1 Mirsamadi, S., "Advanced Subsonic Technology (AST) Composite Wing Material Stiffness and Allowable Strength Properties for Stitched Composite Laminates," 98K0318, Rev. C, September 1998.

4-2 Hawley, A., BWB Material Stiffness and Allowable Strength Properties, March 2005.

4-3 Boeing Laboratory Report No. M&PE-3-1378 R-1, "Qualification of Class 75 and Class 78 Carbon Fiber Preforms to DMS 2436," 14 April 2003.

4-4 Velicki, A. and Thrash, P. J., "Advanced Structural Concept Development Using Stitched Composites," 49th AIAA/ASME/ASCE/AHS/ASC Structures, Structural Dynamics, and Materials Conference, 7 – 10 April 2008, Schaumburg, IL, AIAA paper 2008-2329.

4-5 Velicki, A. and Hansen, D., "Novel Blended Wing Body Structural Concepts Phase I Final Report," Final Report for NNL04AA36C, CLIN 0001, 13 July 2004.

4-6 Yovanof, N., Baraja, J., Lovejoy, A., and Gould, K., "Design, Analysis, and Testing of a PRSEUS Pressure Cube to Investigate Assembly Joints," 2012 Aircraft Airworthiness & Sustainment Conference, paper no. TP5431, 1 –5 April 2012, Baltimore, MD.

4-7 Yovanof, N. and Jegley, D., "Compressive Behavior of Frame-Stiffened Composite Panels," 52th AIAA Structures Dynamics and Materials Conference, AIAA-2011-1913, Denver, CO, 5 April 2011.

4-8 Johnston, P., "Ultrasonic Nondestructive Evaluation of PRSEUS Pressure Cube Article in Support of Load Test to Failure," NASA-TM-2013-217799, 2013.

4-9 Wu, H. T., "HWB Multi-Bay Test Article Test Specification," Rev B, ZA153342, November 2014.

6-1 Linton, K., et al, "PRSEUS Panel Fabrication Final Report," NASA/CR 2014 218149, Contract NNL13AA11C, January 2014.

6-2 Velicki, A., Linton, K., and Hoffman, K., "Fabrication of Lower Section and Upper Forward Bulkhead Panels of the Multi-bay Box and Panel Preparation," Final Report for Contract NNL10AA05B Task Order NNL13AB38T, March 2015.

APPENDIX A—HYPERSIZER ENHANCEMENTS

The Technology Support subtask (WBS 4.2) included an effort to enhance the local panel sizing software, the HyperSizer analysis computer code. The enhancements consisted of code improvements for better usability and accuracy of the PRSEUS module within HyperSizer. The work was performed by Collier Research Corporation under a subcontract from Boeing. This appendix presents the final report from Collier Research Corporation describing the enhancements.

HyperSizer PRSEUS Panel Sizing Enhancements

Submitted to Boeing Corporation
by Collier Research Corporation

Final Report
March 31, 2013

Table of Contents

1 Executive Summary

1.1 Introduction

This report describes HyperSizer code improvements beyond those already completed in NASA contract NNL07AA48C (Collier, 2010), which have been identified, incorporated, and verified against the previous HyperSizer version and independent FEA. Boeing, NASA, and Collier Research Corporation have jointly developed a list of improvements that will make local panel sizing code improvements to enhance the usability/accuracy of the PRSEUS module within the HyperSizer analysis computer code.

The agreed-to coding improvements have been implemented by Collier Research Corporation and delivered to Boeing for evaluation (March 2013). The final released version of the code will be delivered to NASA and Boeing, and then made commercially available to industry as an add-on module within HyperSizer.

There were two principal enhancements to HyperSizer under this contract. First, all graphics describing sizing variables associated with the PRSEUS panel concept have been recreated from scratch. The purpose of this effort was to clear up the variable definition for the user and to correct some inconsistencies in variable definition and sign convention. Several housekeeping items (changes to variable names, etc.) identified by Boeing were also implemented in the new version.

The second effort involved adding two independent material and thickness variables to the PRSEUS panel configuration to account for separate tear straps for the stringer and frame. In previous HyperSizer versions, tear straps could be included, but they were lumped together with the stringer flange and frame flange variables respectively. This prevented users from sizing the tear straps independently and also led to small discrepancies in the panel stiffness formulation in the overlap region between the stringer and frame flanges.

The new HyperSizer version has separated the stringer and frame tear straps into independent variables, however it is still possible to model the structure by lumping the tear straps with the flanges. This is so that results from previous HyperSizer databases can be imported into the new software and analyzed without the user needing to modify his previous set up.

The updated code (6.5) has been verified against the previous HyperSizer version (6.4).For cases where the tear strap is still lumped with the flanges, the results are identical. When the two variables are separated, there are some expected discrepancies, but they are fairly small and should not greatly affect sizing results.

1.2 Development Status

The PRSEUS panel concept with enhancements has been implemented into HyperSizer Version 6.5. All HyperSizer database infrastructure, thermoelastic formulation and failure analysis methods have been developed and verified against the previous HyperSizer version and against independent FEM analysis.

1.3 Statement of Work

4.0 SUPPLIER REQUIREMENTS

The supplier shall:

4.1 Write up an initial set of software changes and analytical enhancements that will be for HyperSizer analysis code by Collier Research. The proposed changes will be negotiated by telecon with Boeing and NASA-LaRC present until a final agreement is reached.

4.2 Modify PRSEUS input screens and properties as required in HyperSizer code.

4.3 Rewrite software code within HyperSizer to incorporate agreed to changes.

4.4 Modify existing PRSEUS user instructions which will be included as a chapter in the final written report.

4.5 Decouple tear strap optimization variable from flange.

1.4 Summary of Enhancements

1.4.1 Task 4.1: Write up of software changes and analytical enhancements

> *Write up an initial set of software changes and analytical enhancements that will be for HyperSizer analysis code by Collier Research. The proposed changes will be negotiated by telecon with Boeing and NASA-LaRC present until a final agreement is reached.*

This task was satisfied at the PRSEUS Enhancements kickoff meeting at NASA Langley on 2012-04-21.

See related powerpoint presentation, "6651_HyperSizer_PRSEUS NASA Boeing contract kick off (py) 2012-04-19.pdf" delivered to Boeing on 2012-05-09 and is included with this report.

1.4.2 Task 4.2: Modify PRSEUS input screens

> *Modify PRSEUS input screens and properties as required in HyperSizer code.*

The HyperSizer interface for PRSEUS has been updated based on the Excel file, "PRSEUS_HyperSizer_Issues_120315" delivered from Boeing to Collier Research on 2012-03-15 and negotiated at the kickoff meeting in April.

The images that illustrate the sizing variables have been recreated from scratch to clear up ambiguities in nomenclature and sign convention. Several of the variables were renamed according to suggestions in the Excel file.

1.4.3 Task 4.3: Modify PRSEUS input screens

> *Rewrite software code within HyperSizer as required to incorporate agreed to changes.*

The modified interface and analytical changes are included in HyperSizer Version 6.5.3 delivered to Boeing on 2013-03-15.

1.4.4 Task 4.4: Modify PRSEUS user instructions

Modify existing PRSEUS user instructions which will be included as a chapter in the final written report.

The modified user instructions are included as a chapter in this report.

1.4.5 Task 4.5: Decouple tear strap optimization variables from flanges

Decouple tear strap optimization variables from flanges.

In previous versions of HyperSizer, the stringer and frame tear straps were lumped together with the stringer and frame attached flanges into a single laminate variable. This somewhat limited the flexibility of the sizing especially when using effective laminates where the 0/45/90 ply percentages of the tear straps could not be specified separately between the flanges and tear straps.

In HyperSizer Version 6.5, the tear straps have been separated into separate variables with individual materials and thicknesses.

2 Description of PRSEUS Enhancements

2.1 Interface Enhancements

The principal purpose of this task was to update the input variables with more appropriate names and clear up the sign conventions to make user input more clear. For example, the variable previously named "Stringer Height" was actually the distance from the skin IML to the center of the rod. The variable has been renamed to "Stringer Rod Centerline Height".

The figures illustrating the variables have also been completely regenerated to make them more consistent (some of the sign conventions were wrong in the older figures) and more visually appealing.

The following figures for PRSEUS sizing are in the Version 6.5 software.

Skin Thickness and Material

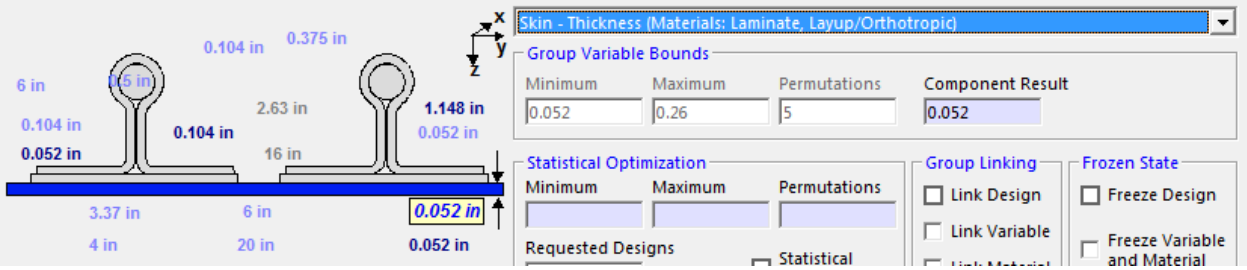

For reference, a screenshot from the previous software including the inconsistent sign convention is shown below.

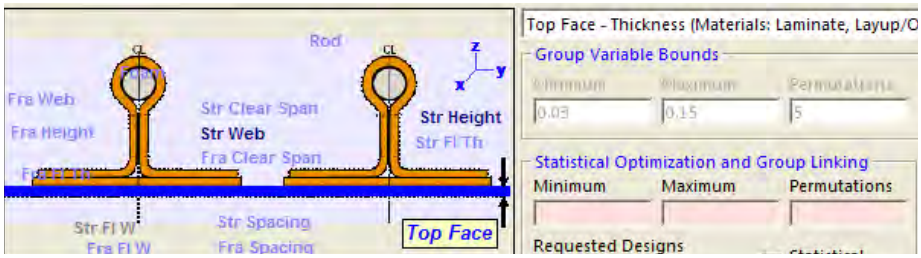

Stringer Web Thickness and Material

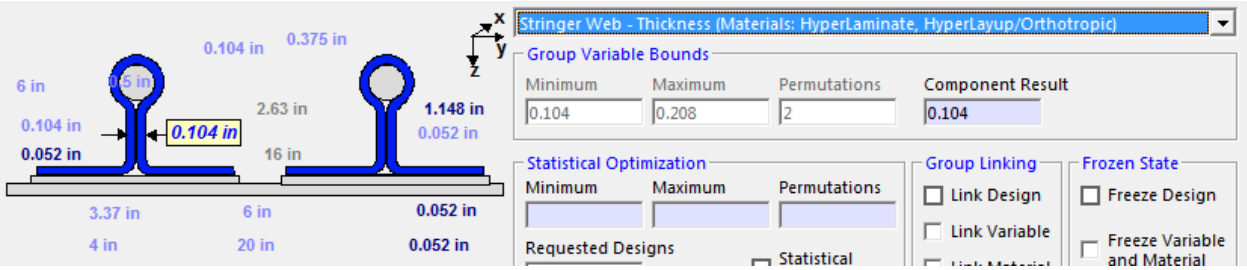

Stringer Rod Centerline Height

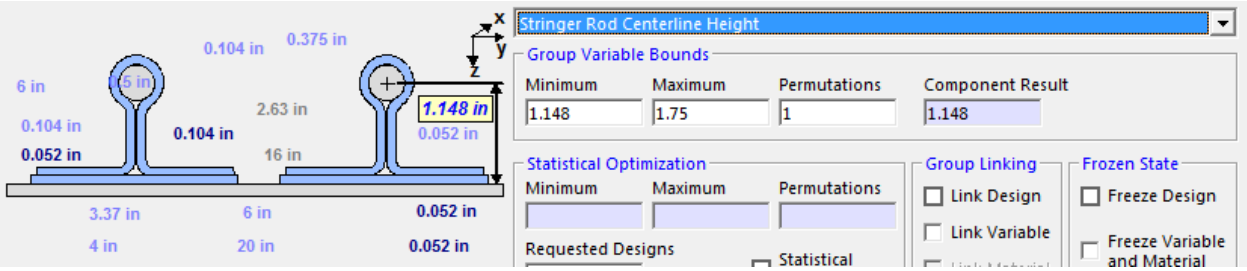

Stringer Spacing

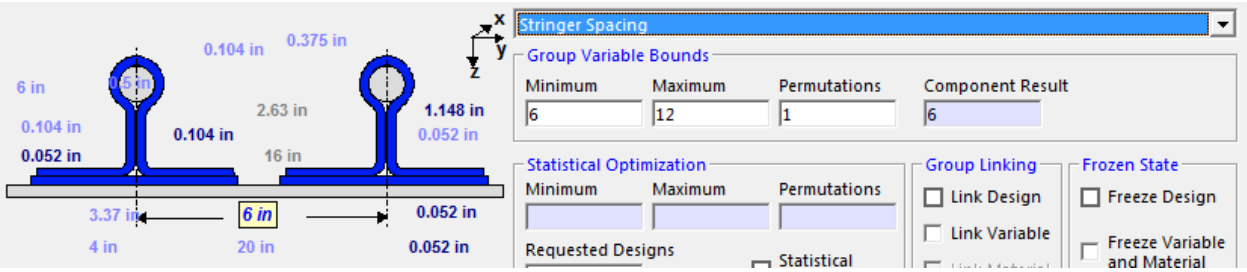

Frame Web Thickness and Material

Note the updated sign convention axis (frames are oriented in the global *y*-axis where stringers are oriented in the global *x*-axis).

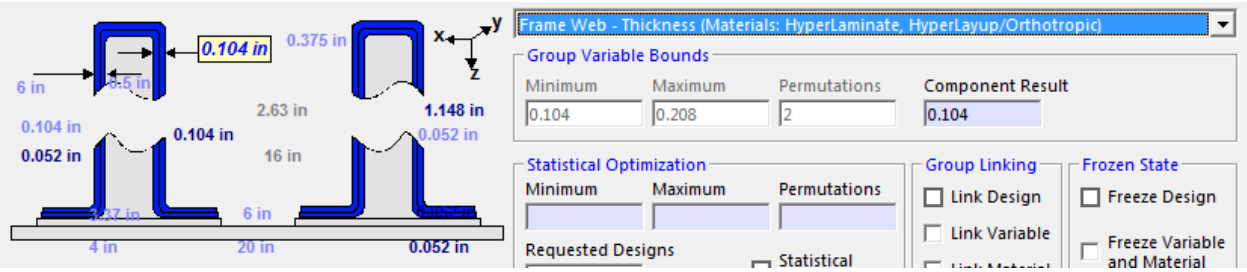

Frame Height

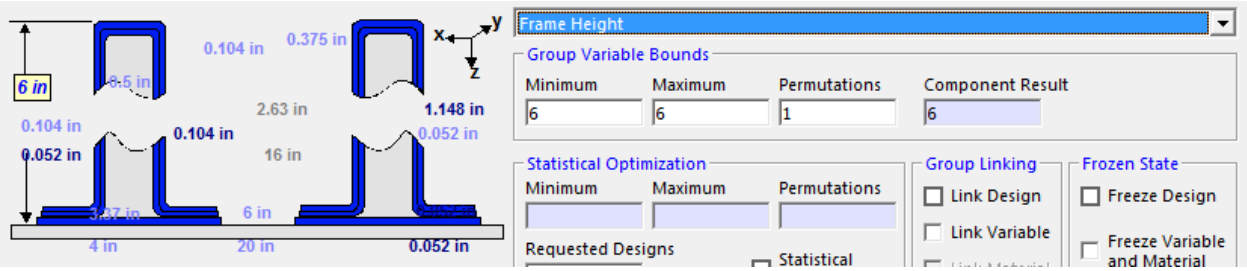

Frame Spacing

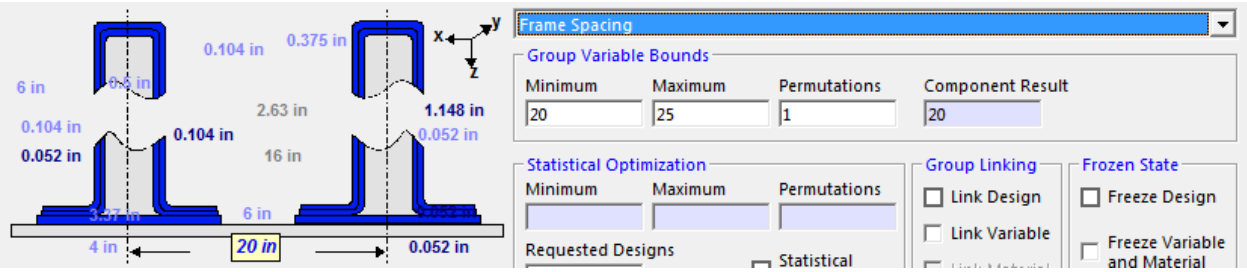

Frame Foam Thickness and Material

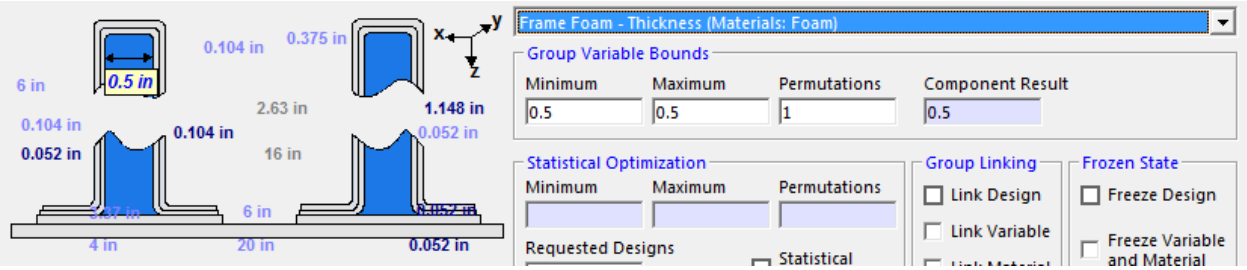

Stiffener Flange Width

Note: Variable encompasses both the stringer flange and tear strap widths.

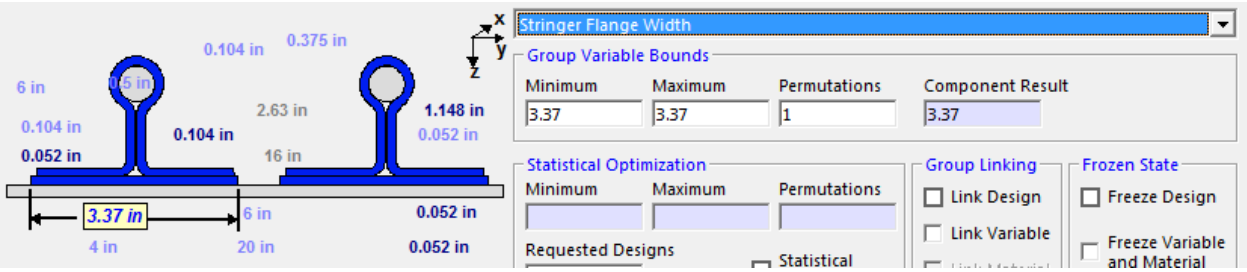

Stringer Flange Thickness

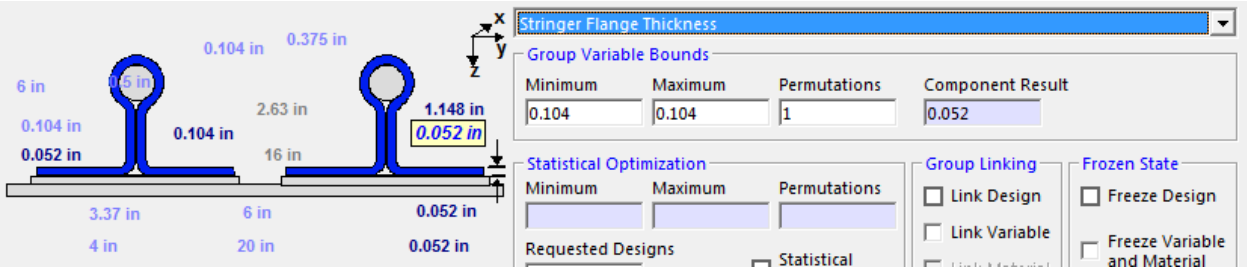

Frame Flange Width

Note: Variable encompasses both the frame flange and tear strap widths.

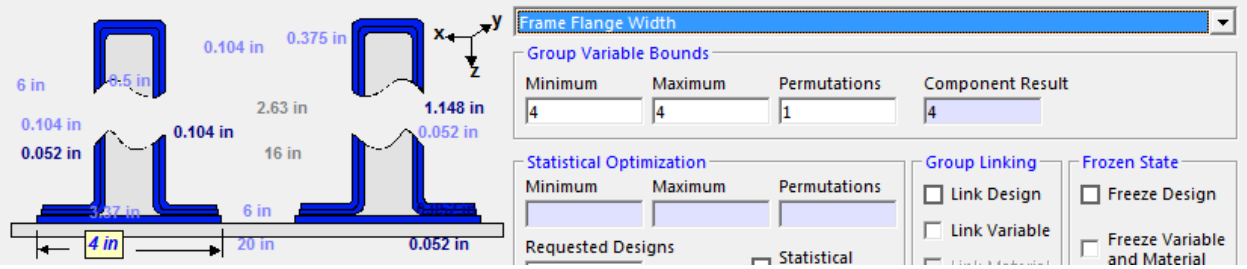

Frame Flange Thickness

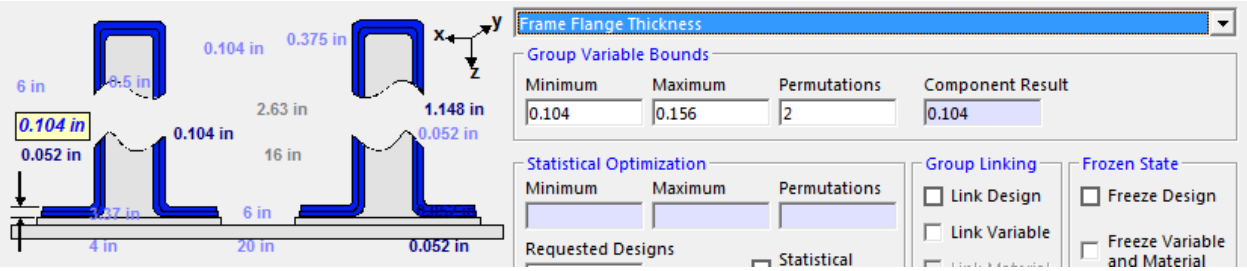

Rod Diameter and Material

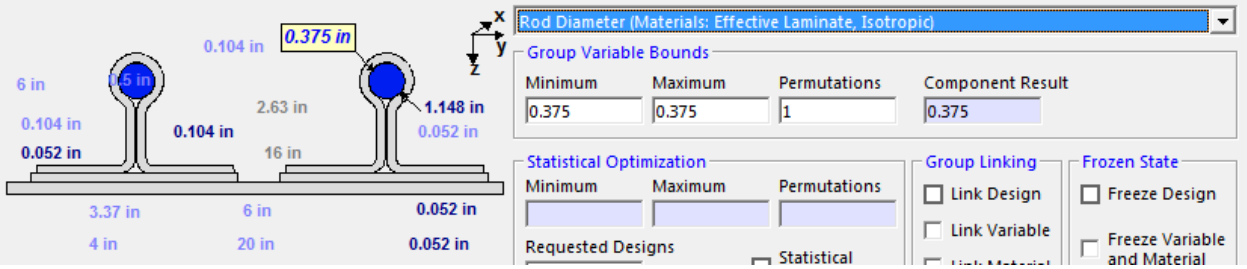

Stringer Clear Span (Dependent)

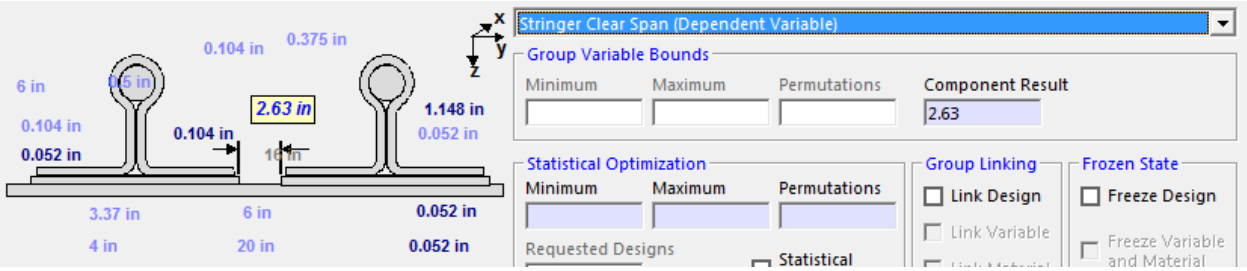

Frame Clear Span (Dependent)

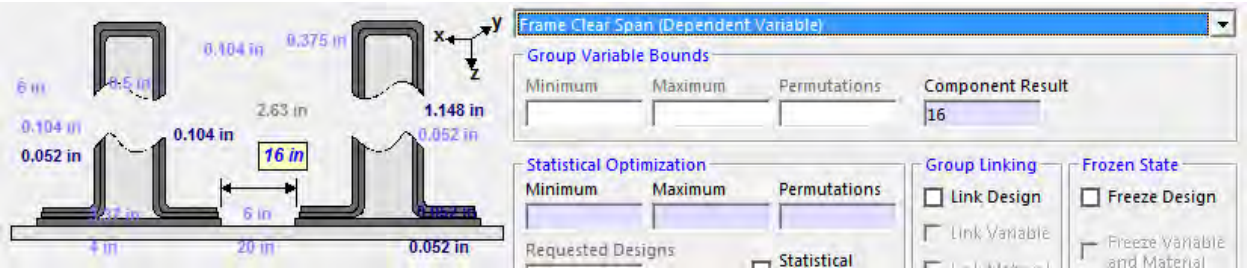

Stringer Tear Strap Thickness and Material

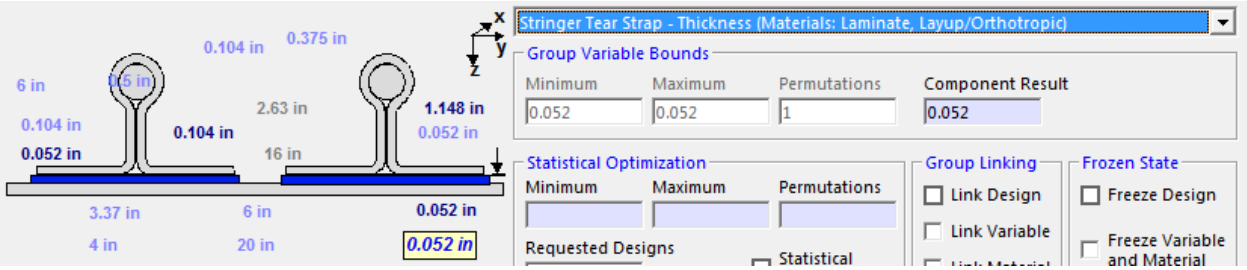

Frame Tear Strap and Material

2.2 Decoupling of stringer and frame tear straps from flange variables

2.2.1 Changes to Variable Layout

Stringer Variables (before update)

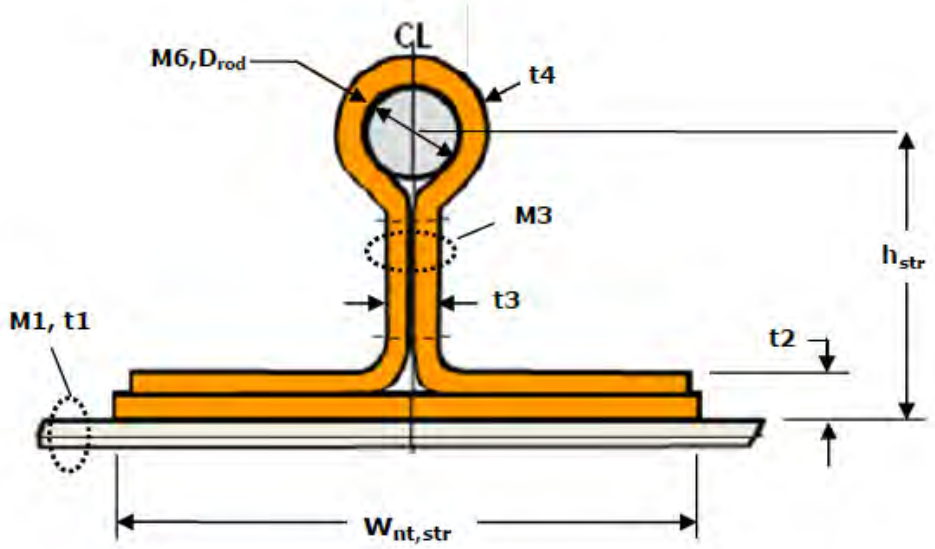

Geometric Variables

Sizing Variable	Symbol
Top Face - Thickness	t_1
Stringer Web - Thickness	t_3
Stringer Height	h_{str}
Stringer Spacing	S_{str}
Stringer Flange Width	$w_{nt,str}$
Stringer Flange Thickness	t_2
Stiffening Rod - Diameter	D_{rod}
Stringer Clear Span*	$F_{w,str}$

* Dependent Variable

Notes:
- If M3 is a HyperLaminate, the layup and thickness of the stringer flange (t_2) is a function of the thickness and layup of the stringer web variable (t_3).
- If M3 is an Effective Laminate, then the stringer flange thickness (t_2) is an independently sized variable with the same material as M3.
- The Rod overwrap is always assumed to be ½ the thickness of the stringer web.

Material Variables

Sizing Variable	Symbol	Material Type
Top Face - Material	M_1	Metal, Layup, Effective or Discrete Laminate
Stringer Web - Material	M_3	Metal, Layup, Effective or Discrete Laminate (HyperLaminate)
Stiffening Rod - Material	M_6	Metal, Effective Laminate

Stringer Variables (After Update)

The principal differences in the new software is the addition of the tear strap variable (t_6 and M_6). Some of the nomenclature has been changed (h changed to h_{rodCL}). Also, some of the variable "numbers" have changed to be consistent with updates to the analysis code. The differences in numbers are not exposed to the user running HyperSizer, therefore these changes should be benign.

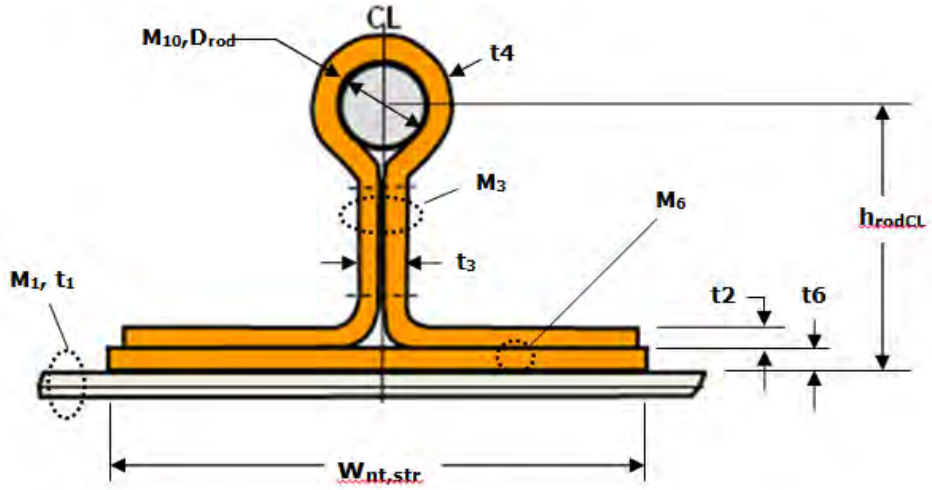

Geometric Variables

Sizing Variable	Symbol
Skin - Thickness	t_1
Stringer Web - Thickness	t_3
Stringer Tear Strap - Thickness	t_6
Stringer Rod Centerline Height	h_{rodCL}
Stringer Spacing	S_{str}
Stringer Flange Width	$W_{nt,str}$
Stringer Flange Thickness	t_2
Stiffening Rod - Diameter	D_{rod}
Stringer Clear Span*	$F_{wt,str}$

* Dependent Variable

Notes:
- If M3 is a HyperLaminate, the layup and thickness of the stringer flange (t_2) is a function of the thickness and layup of the stringer web variable (t_3).
- If M3 is an Effective Laminate, then the stringer flange thickness (t_2) is an independently sized variable with the same material as M3.
- The Rod overwrap is always assumed to be ½ the thickness of the stringer web.

Material Variables

Sizing Variable	Symbol	Material Type
Top Face - Material	M_1	Metal, Effective or Discrete Laminate
Stringer Web - Material	M_3	Metal, Effective or Discrete Laminate (HyperLaminate)
Stringer Tear Strap	M_6	Metal, Effective or Discrete Laminate
Stiffening Rod - Material	M_{10}	Effective Laminate

Frame Variables (before update)

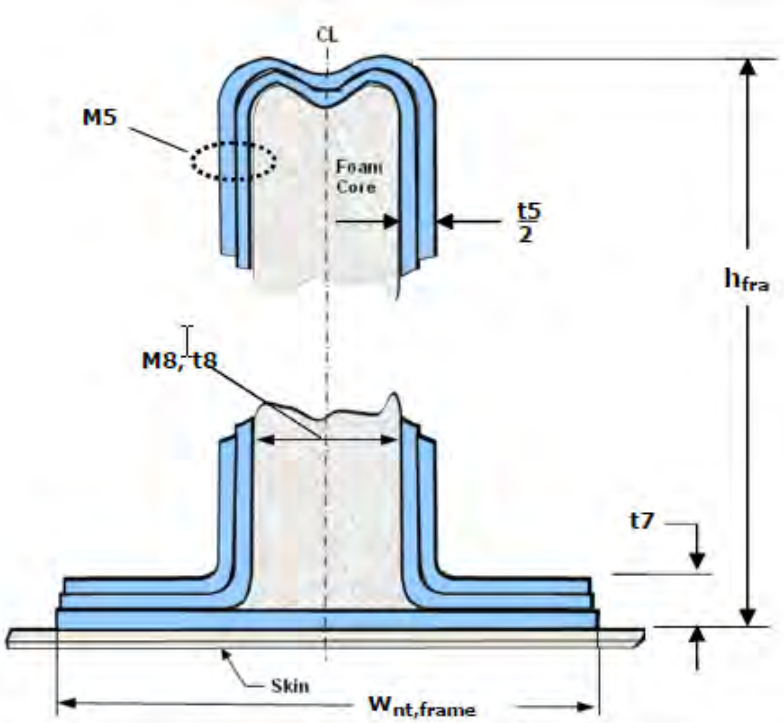

Geometric Variables

Sizing Variable	Symbol
Frame Web - Thickness	t_5
Frame Height	h_{fra}
Frame Spacing	S_{fra}
Frame Flange Width	$w_{nt,fra}$
Frame Flange Thickness	t_7
Frame Foam - Thickness	t_8
Stiffening Rod - Diameter	D_{rod}
Frame Clear Span*	$F_{w,fra}$

* Dependent Variable

Notes:
- Layup and thickness of the frame web (t_5) includes material on both sides of the foam core, each wall has thickness = $t_5/2$.
- If M5 is a HyperLaminate, the layup and thickness of the frame flange (t_7) is a function of the thickness and layup of the frame web variable (t_5).
- If M5 is an Effective Laminate, then the flange thickness (t_7) is an independently sized variable with the same material as M5.

Material Variables

Sizing Variable	Symbol	Material Type
Frame Web - Material	M_5	Metal, Layup, Effective or Discrete Laminate (HyperLaminate)
Frame Foam - Material	M_8	Foam

Frame Variables (after update)

The principal differences in the new software is the addition of the tear strap variable (t_7 and M_7). Also, some of the variable "numbers" have changed to be consistent with updates to the analysis code. The differences in numbers are not exposed to the user running HyperSizer, therefore these changes should be benign.

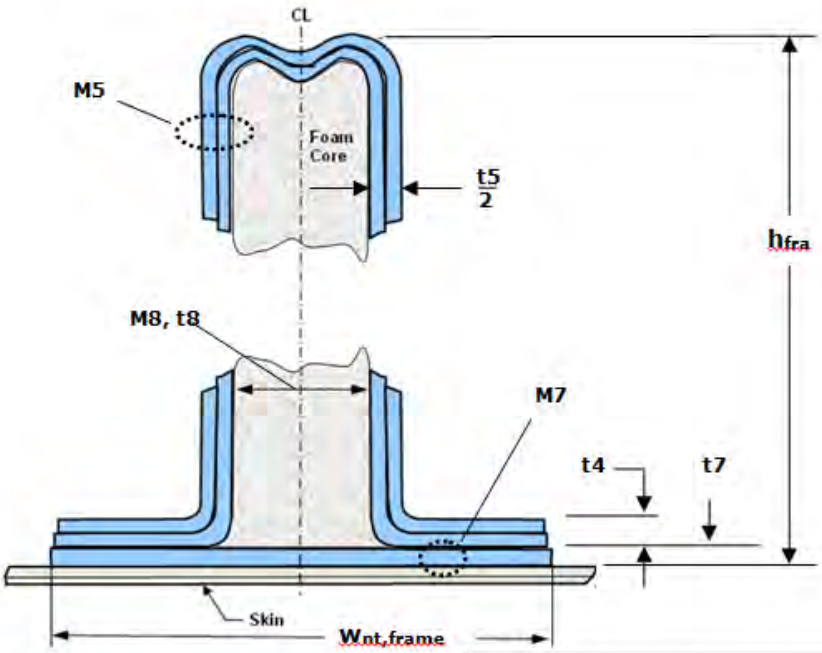

Geometric Variables

Sizing Variable	Symbol
Frame Web - Thickness	t_5
Frame Height	h_{fra}
Frame Spacing	S_{fra}
Frame Flange Width	$W_{nt,fra}$
Frame Flange Thickness	t_7
Frame Foam - Thickness	t_8
Stiffening Rod - Diameter	D_{rod}
Frame Clear Span*	$F_{vt,fra}$

* Dependent Variable

Notes:
- Layup and thickness of the frame web (t_5) includes material on both sides of the foam core, each wall has thickness = $t_5/2$.
- If M5 is a HyperLaminate, the layup and thickness of the frame flange (t_4) is a function of the thickness and layup of the frame web variable (t_5).
- If M5 is an Effective Laminate, then the flange thickness (t_4) is an independently sized variable with the same material as M5.

Material Variables

Sizing Variable	Symbol	Material Type
Frame Web - Material	M_5	Metal, Effective or Discrete Laminate (HyperLaminate)
Frame Foam - Material	M_8	Foam
Frame Tear Strap	M_7	Metal, Effective or Discrete Laminate

2.2.2 Changes in Weights/Stiffness Formulation

The present formulation corrects two issues that were noted in the "Assumptions and Limitations" section of the previous PRSEUS panel implementation report (Collier, 2010).

First, because the previous formulation lumped the tear straps with the flanges, in the overlap region between the frame and stringer flanges, the laminates were built out-of-order. In the as-built panel, the sequence is skin - frame tear strap (cap) - stringer tear strap - stringer flange - frame flange. In the previous software because the frame tear strap and frame flange were lumped together, they could not be separated and the sequence was implemented as: skin - stringer tear strap - stringer flange - frame tear strap (cap) - frame flange. In the updated HyperSizer Version 6.5, the proper sequence is now implemented.

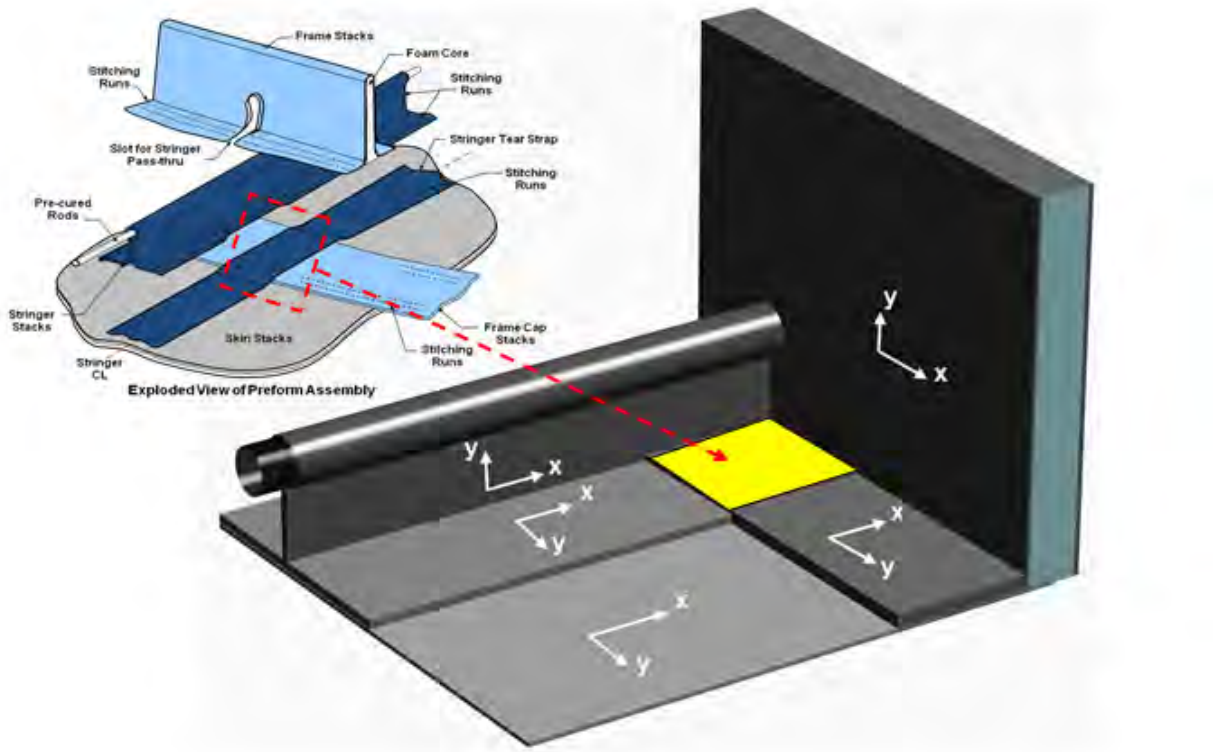

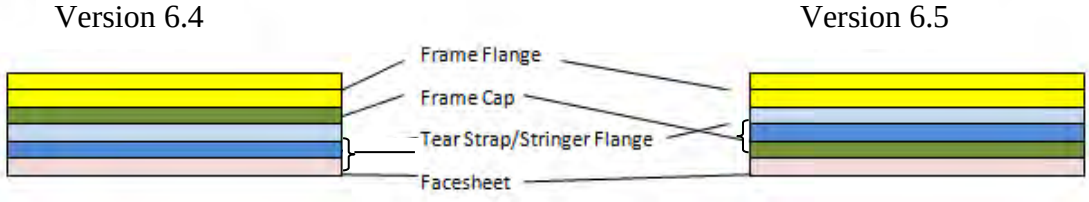

As noted in the previous report, the incorrect sequence caused 0-4% discrepancy in object stresses and strains, which is consistent with the findings in the updated formulation.

The second issue that is corrected in the updated code is that in the previous version the frame flange was assumed to be continuous across the frame foam. This causes a slight difference both in weight reporting and stiffness formulation between the previous and current software versions.

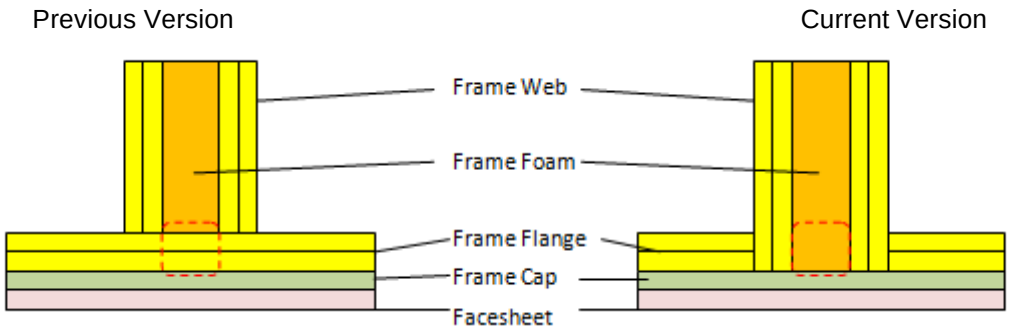

In the case of the as-fabricated PRSEUS test panel (2010) with single stack skin, the two differences in stiffness formulation and weight results in a 1% and 0.5% difference in overall panel stiffness and weight respectively. These differences will be dependent on the specific dimensions of the panel being analyzed.

As-Fabricated PRSEUS Test Panel	Stiffness A11 (lb/in)	Unit Weight (lb/ft^2)
HyperSizer Version 6.4 (Lumped flanges and tear straps)	1450000	2.128
HyperSizer Version 6.5 (Separate flanges and tear straps)	1434000	2.117
Difference	1.1%	0.5%

3 Verification of PRSEUS Enhancements

Several verifications of the updated formulation were carried out by comparing the updated Version 6.5 software with the previous Version 6.4 software. This verification serves two purposes. First, to make sure that projects from previous databases can be imported and analyzed without error and second to compare any expected differences in the analysis results.

A second type of verification was performed by comparing results within Version 6.5 where results where the tear strap is lumped with the flanges is compared to results with no tear strap.

3.1 Comparison with HyperSizer Version 6.4

The first verification presented here is a comparison between the updated Version 6.5 software with the previous Version 6.4 software.

The process begins by importing an established verification example from the original PRSEUS report into both the Version 6.4 and 6.5 software. The example chosen was the 2009/2010 as-fabricated 7-stringer test article with single stack facesheets. The load was entered as a 100 kip applied load (this equates to 2381 lb/in for the 42 in. wide test panel).

The comparisons between the two versions is performed both for linear (non-postbuckled) and postbuckled analysis. In this example, the software returns identical results between these two versions.

3.1.1 Linear (Non-Post Buckled Analysis)

Panel Strain and Bending Moment Response

Version 6.4

Free Body Diagram Output (Controlling Factored Loadcase)

Controlling Analysis Load: STRENGTH	Nx, εx	Ny, εy	Nxy, γxy	Mx, κx	My, κy	Mxy, κxy
Virtual Loads	0	0	0	-1076.25	322.499	3.83666E-03
Design-to Loads	-2381	0	0	-1076.25	322.499	3.83666E-03
Design-to Deformation	-1.661814E-03	1.832915E-04	0	0	0	0

Version 6.5

Free Body Diagram Output (Controlling Factored Loadcase)

Controlling Analysis Load: STRENGTH	Nx, εx	Ny, εy	Nxy, γxy	Mx, κx	My, κy	Mxy, κxy
Virtual Loads	0	0	0	-1076.25	322.499	3.83666E-03
Design-to Loads	-2381	0	0	-1076.25	322.499	3.83666E-03
Design-to Deformation	-1.661814E-03	1.832915E-04	0	0	0	0

Object Loads

Version 6.4

Load Results

Object	Nx (lb / in)	Ny (lb / in)	Nxy (lb / in)	Mx (lb-in / in)	My (lb-in / in)	Mxy (lb-in /...
Open Span	-429.083	-104.604	0	-0.378544	-0.691209	0.0836797
Bonded Combo, Stringer	-2175.45	-104.604	0	-137.15	-0.691209	0.034758
Bonded Combo, Frame	-1104.13	-98.4073	0	-57.0852	11.0444	-0.31194
Bonded Combo, Str+Frame	-1648.63	-98.4073	0	-92.8952	11.0444	-0.122654
Stringer Web	-1603.62	0	0	0	0	0
Stringer Rod and Laminate	-4452.76	0	0	0	0	0
Frame Web	353.745	0	0	0	0	0

Version 6.5

Load Results

Object	Nx (lb / in)	Ny (lb / in)	Nxy (lb / in)	Mx (lb-in / in)	My (lb-in / in)	Mxy (lb-in /...
Open Span	-429.083	-104.604	0	-0.378544	-0.691209	0.0836797
Bonded Combo, Stringer	-2175.45	-104.604	0	-137.15	-0.691209	0.034758
Bonded Combo, Frame	-1104.13	-98.4073	0	-57.0852	11.0444	-0.31194
Bonded Combo, Str+Frame	-1648.63	-98.4073	0	-92.8952	11.0444	-0.122654
Stringer Web	-1603.62	0	0	0	0	0
Stringer Rod and Laminate	-4452.76	0	0	0	0	0
Frame Web	353.745	0	0	0	0	0

Failure Modes

Version 6.4

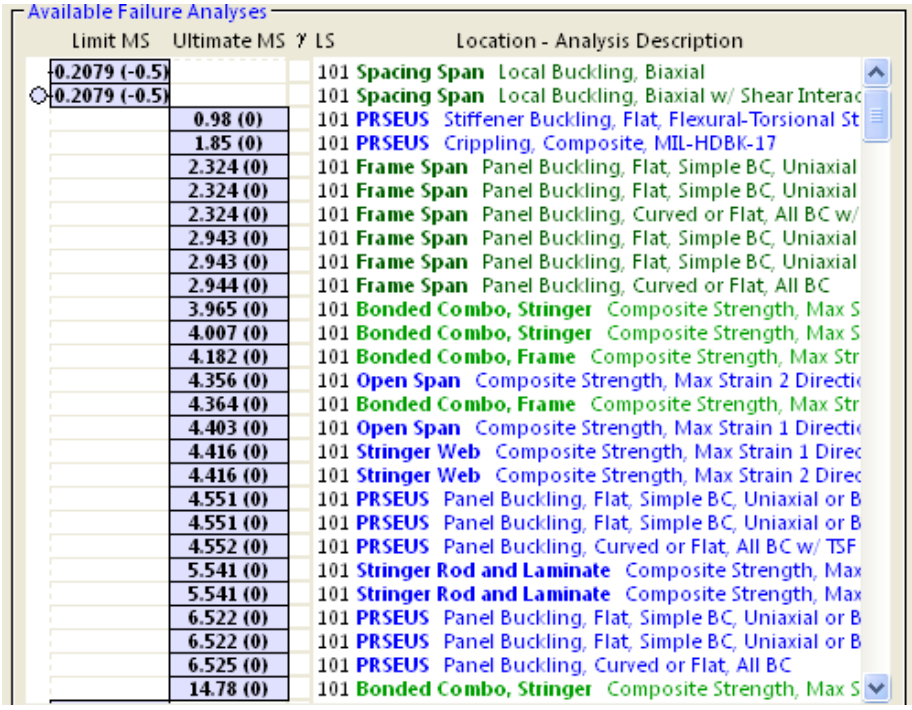

Version 6.5

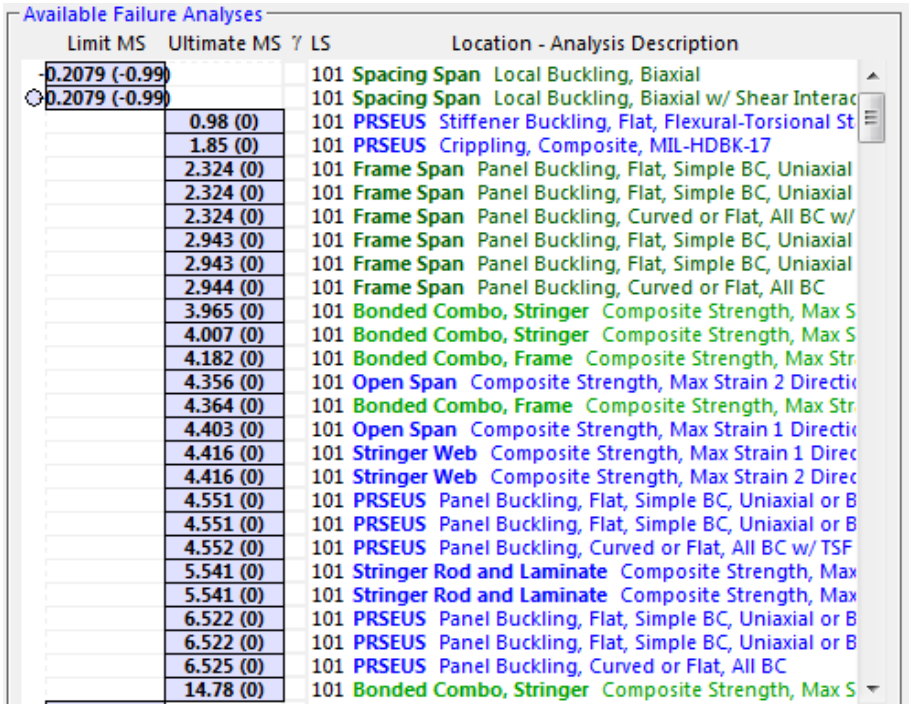

HyperFEMGen Local FEM Export

The final check between the two versions is on export of local FEM. The local FEM exported for the example problem along with eigenvalue and static object load results are shown below. The FEM and results for Version 6.4 and 6.5 are identical.

FEA Local Buckling Eigenvalue = 0.814

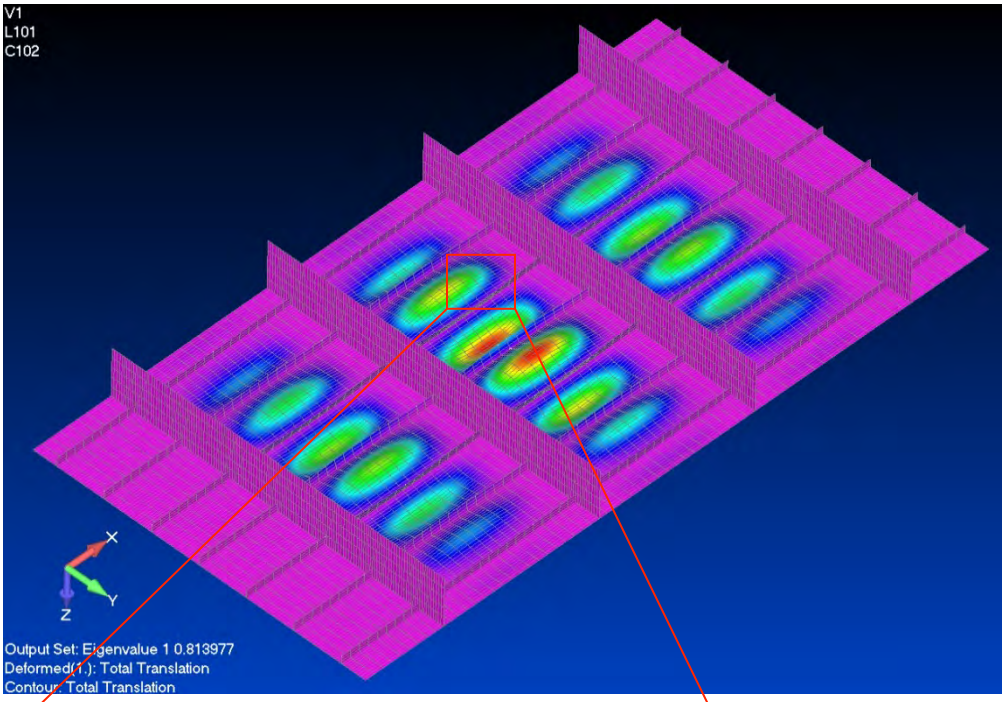

Object Loads (Nx)

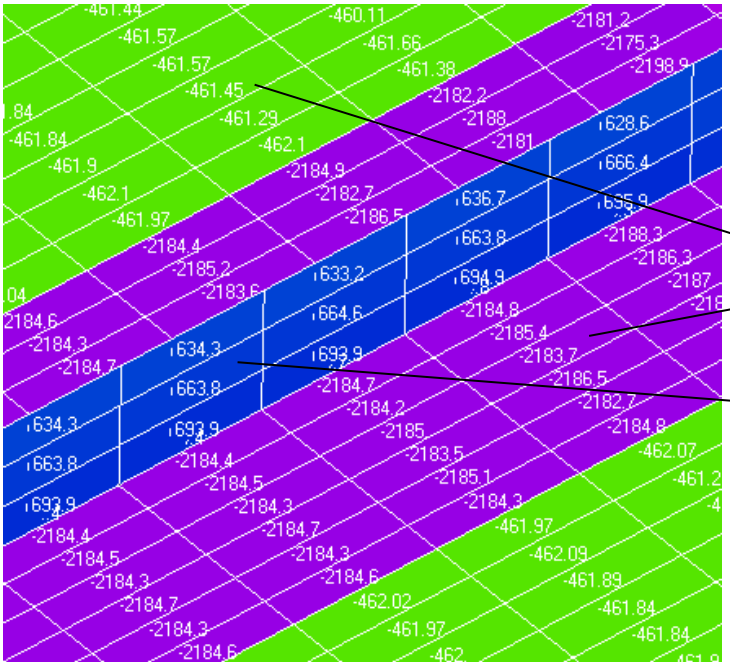

Load Results

Object	Nx (lb / in)
Open Span	-429.083
Bonded Combo, Stringer	-2175.45
Bonded Combo, Frame	-1104.13
Bonded Combo, Str+Frame	-1648.63
Stringer Web	-1603.62
Stringer Rod and Laminate	-4452.76
Frame Web	353.745

3.1.2 Postbuckling Analysis

Panel Strain and Bending Moment Response

Version 6.4

Free Body Diagram Output (Controlling Factored Loadcase)

Controlling Analysis Load: STRENGTH	Nx, εx	Ny, εy	Nxy, γxy	Mx, κx	My, κy	Mxy, κxy
Virtual Loads	0	0	0	-1148.94	360.131	0.0107785
Design-to Loads	-2381	0	0	-1148.94	360.131	0.0107785
Design-to Deformation	-1.775823E-03	2.056839E-04	0	0	0	0

Version 6.5

Free Body Diagram Output (Controlling Factored Loadcase)

Controlling Analysis Load: STRENGTH	Nx, εx	Ny, εy	Nxy, γxy	Mx, κx	My, κy	Mxy, κxy
Virtual Loads	0	0	0	-1148.94	360.131	0.0107785
Design-to Loads	-2381	0	0	-1148.94	360.131	0.0107785
Design-to Deformation	-1.775823E-03	2.056839E-04	0	0	0	0

Both methods show a 7% increase in overall panel strain vs the linear analysis.

Object Loads

Version 6.4

Load Results

Object	Nx (lb / in)	Ny (lb / in)	Nxy (lb / in)	Mx (lb-in / in)	My (lb-in / in)	Mxy (lb-in /...
Open Span	-456.183	-105.509	0	-0.370655	-0.695167	0.0828175
Bonded Combo, Stringer	-2290.55	-105.509	0	-143.782	-0.695167	0.0382071
Bonded Combo, Frame	-1319.1	-157.925	0	-77.9092	3.23354	-0.26654
Bonded Combo, Str+Frame	-2142.51	-157.925	0	-163.587	3.23354	-0.107393
Stringer Web	-1713.63	0	0	0	0	0
Stringer Rod and Laminate	-4758.24	0	0	0	0	0
Frame Web	396.962	0	0	0	0	0

Version 6.5

Load Results

Object	Nx (lb / in)	Ny (lb / in)	Nxy (lb / in)	Mx (lb-in / in)	My (lb-in / in)	Mxy (lb-in /...
Open Span	-456.183	-105.509	0	-0.370655	-0.695167	0.0828175
Bonded Combo, Stringer	-2290.55	-105.509	0	-143.782	-0.695167	0.0382071
Bonded Combo, Frame	-1319.1	-157.925	0	-77.9092	3.23354	-0.26654
Bonded Combo, Str+Frame	-2142.51	-157.925	0	-163.587	3.23354	-0.107393
Stringer Web	-1713.63	0	0	0	0	0
Stringer Rod and Laminate	-4758.24	0	0	0	0	0
Frame Web	396.962	0	0	0	0	0

Failure Modes

Version 6.4

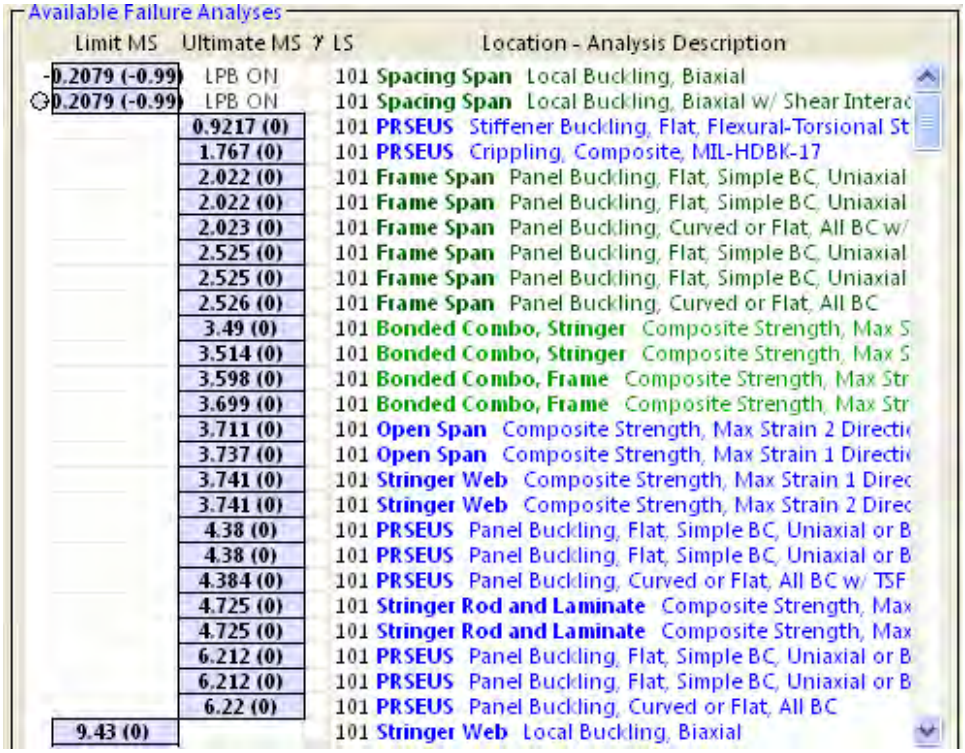

Version 6.5

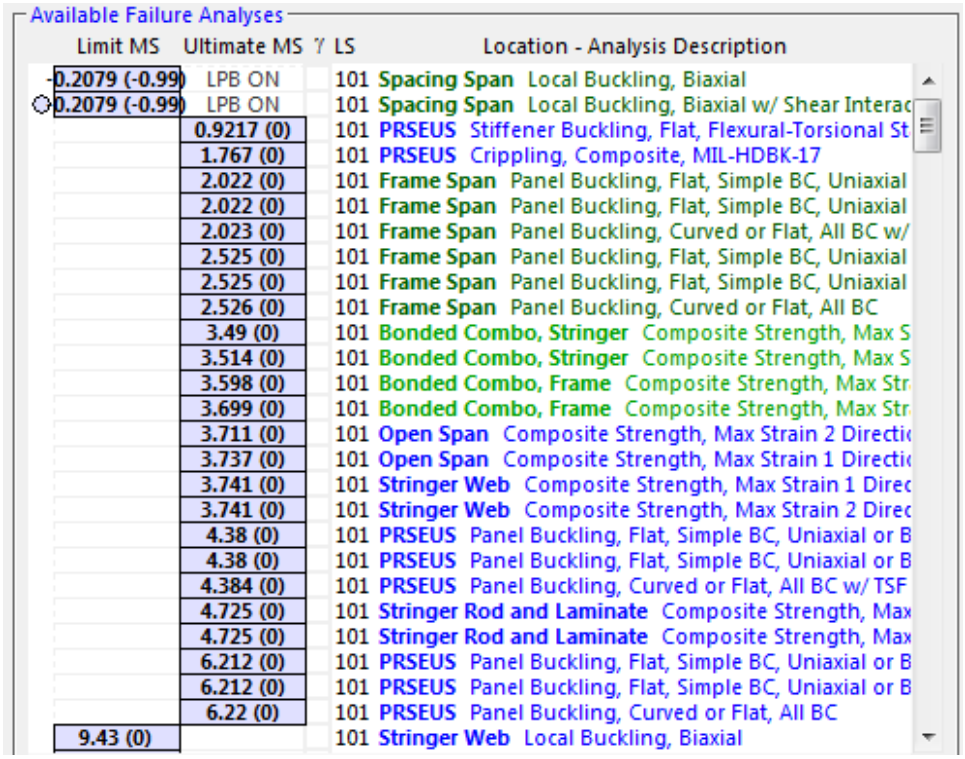

Post Buckling Effective Width

Version 6.4

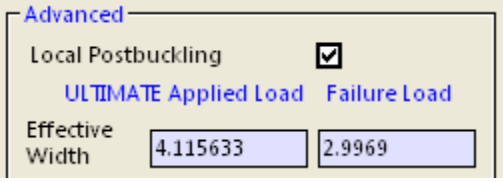

Version 6.5

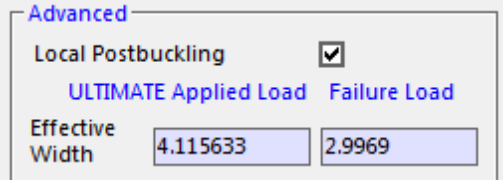

3.2 Comparison between original method and separate tear strap model

As noted, the updated code can be used either with the tear straps as independent variables or lumped together with the corresponding object flanges. If the tear straps are independent variables, then some inconsistencies between the physical model and the HyperSizer model are resolved which slightly changes the results.

The purpose of this section is to compare the two methods of modeling for stiffness, stress and strain analysis, failure analysis and FEM verification.

The same 7-stringer test panel will be used in this verification.

3.2.1 Linear (Non-Postbuckled) Analysis

Panel Stiffness

Method 1 (Lumped Tear Straps and Flanges)

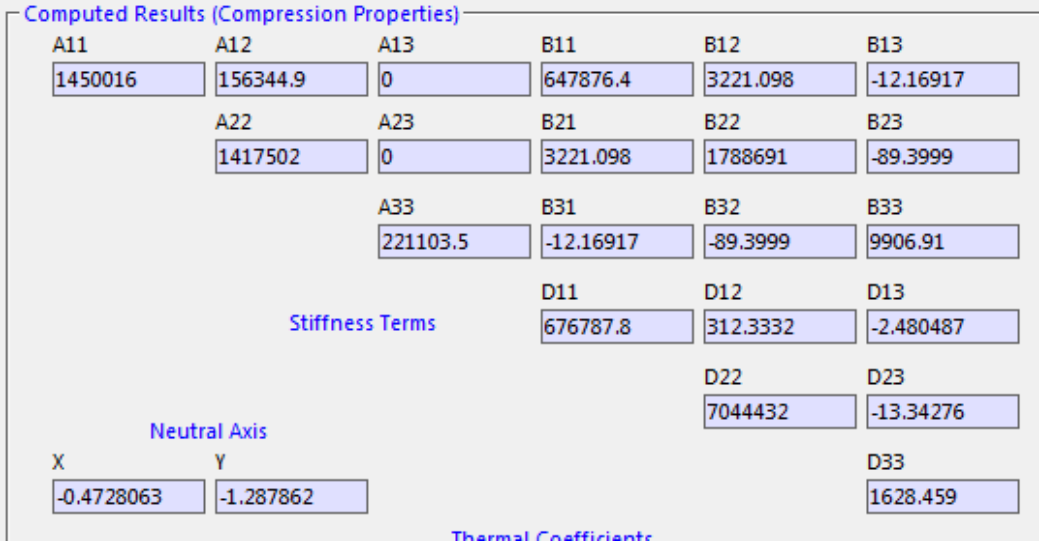

Method 2 (Separate Tear Straps and Flanges)

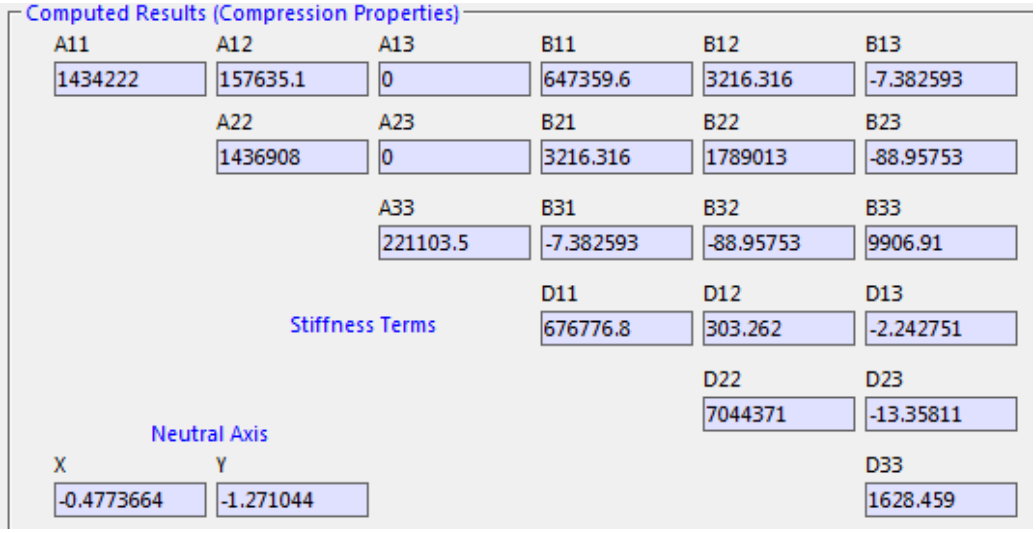

The A_{11} stiffness term is 1.1% lower for method 2 and the A_{22} stiffness term is 1.4% higher. This apparent difference in stiffness comes principally from the different eccentricity of the overlap region. In method 1, more 0° plies are concentrated on one side of the laminate and in method 2, because the tear straps are separated from the flanges, the 0° and 90° plies are more evenly distributed. When HyperSizer forms the combined **A** matrix from the skin, flange, and overlap region it takes into account the eccentricity which results in a different membrane stiffness for the two methods.

The membrane-bending coupling (**B**) and bending (**D**) stiffnesses appear to be almost identical between the two methods.

Panel Load/ Strain

Method 1 (Lumped Tear Straps and Flanges)

Free Body Diagram Output (Controlling Factored Loadcase)

Controlling Analysis Load: STRENGTH	Nx,εx	Ny,εy	Nxy,γxy	Mx,κx	My,κy	Mxy,κxy
Virtual Loads	0	0	0	-1076.25	322.499	3.83666E-03
Design-to Loads	-2381	0	0	-1076.25	322.499	3.83666E-03
Design-to Deformation	-1.661814E-03	1.832915E-04	0	0	0	0

Method 2 (Separate Tear Straps and Flanges)

Free Body Diagram Output (Controlling Factored Loadcase)

Controlling Analysis Load: STRENGTH	Nx,εx	Ny,εy	Nxy,γxy	Mx,κx	My,κy	Mxy,κxy
Virtual Loads	0	0	0	-1087.42	324.394	-3.99335E-03
Design-to Loads	-2381	0	0	-1087.42	324.394	-3.99335E-03
Design-to Deformation	-1.680395E-03	1.843467E-04	0	0	0	0

The difference in stiffness noted above results in a 1.2% difference in axial strain between the two methods for the same applied loads.

Object Loads

Method 1 (Lumped Tear Straps and Flanges)

Load Results

Object	Nx (lb / in)	Ny (lb / in)
Open Span	-429.083	-104.604
Bonded Combo, Stringer	-2175.45	-104.604
Bonded Combo, Frame	-1104.13	-98.4073
Bonded Combo, Str+Frame	-1648.63	-98.4073
Stringer Web	-1603.62	0
Stringer Rod and Laminate	-4452.76	0
Frame Web	353.745	0

Method 2 (Separate Tear Straps and Flanges)

Load Results

Object	Nx (lb / in)	Ny (lb / in)
Open Span	-420.602	-100.198
Bonded Combo, Stringer	-2162.73	-100.198
Bonded Combo, Frame	-1215.96	-119.005
Bonded Combo, Str+Frame	-1542.03	-119.005
Stringer Web	-1621.55	0
Stringer Rod and Laminate	-4502.55	0
Frame Web	355.782	0

As expected, there are also slight differences in the object loads between the two methods.

The largest differences between the N_x object loads are 10% higher load in the frame bonded combo (this is the laminate formed by the skin, frame tear strap and frame flange). This difference is most likely do to the removal of material over the frame tear strap between the two frame web laminates which has been removed for this implementation.

Failure Analysis

Method 1 (Lumped Tear Straps and Flanges)

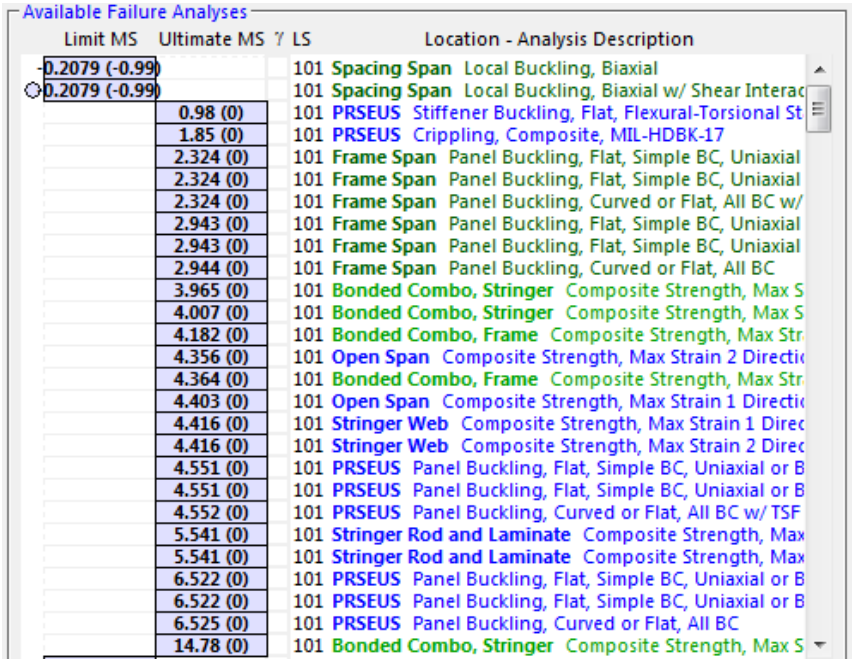

Method 2 (Separate Tear Straps and Flanges)

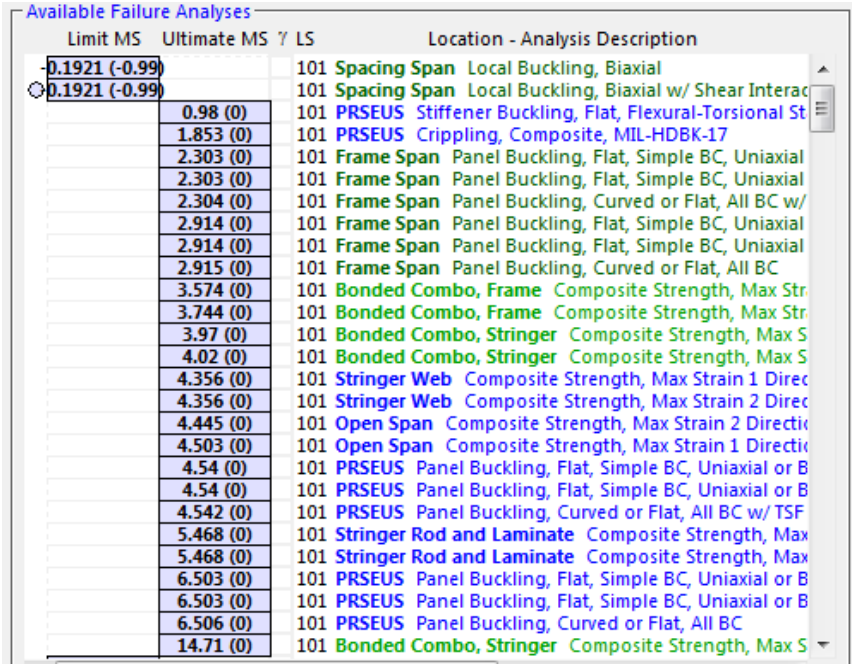

The differences in stiffness formulation results in a 2% increase in local buckling margin between the two methods. This is consistent with the 2% reduction in N_x load seen in the object loads. The other failure analysis differences are comparable. In this case, the "critical" failure mode, which is flexural-torsional buckling is identical between the two methods.

Finite Element Verification

The same FEA verification is performed for Method 2 that was performed for Method 1in Section 3.1.1 by exporting a mesh using HyperFEMGen from HyperSizer for both methods and then performing a FEA Eigenvalue analysis.

Local Buckling Eigenvalue

Method 1 (Lumped Tear Straps and Flanges)
Eigenvalue = 0.8140

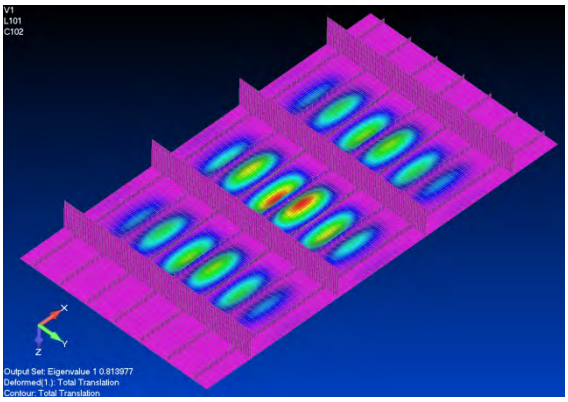

Method 2 (Separate Tear Straps and Flanges)
Eigenvalue = 0.8139

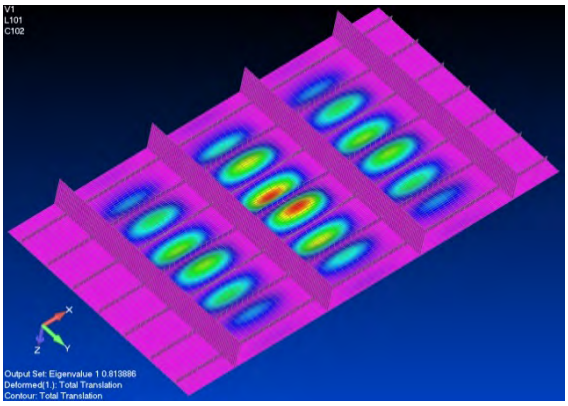

Object Loads

Method 1 (Lumped Tear Straps and Flanges)

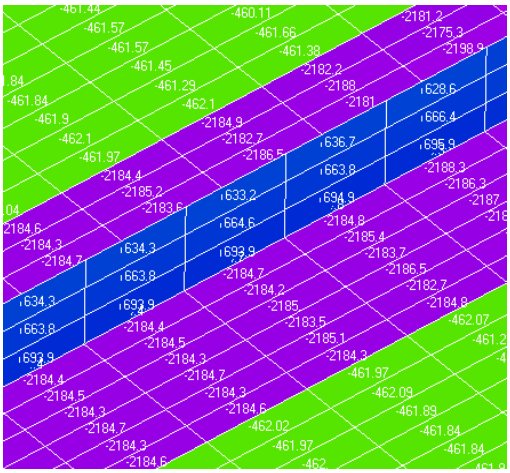

Method 2 (Separate Tear Straps and Flanges)

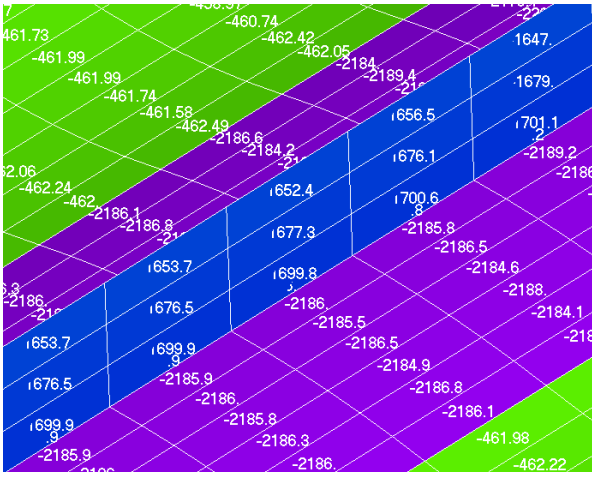

The overall FEM mesh and results are very similar between the two methods.

The snapshots below of the NASTRAN PCOMP cards for the overlap region confirm that the ply ordering has been corrected in the Verification FEM exported by the updated HyperSizer version.

Method 1 (Lumped Tear Straps and Flanges) Method 2 (Separate Tear Straps and Flanges)

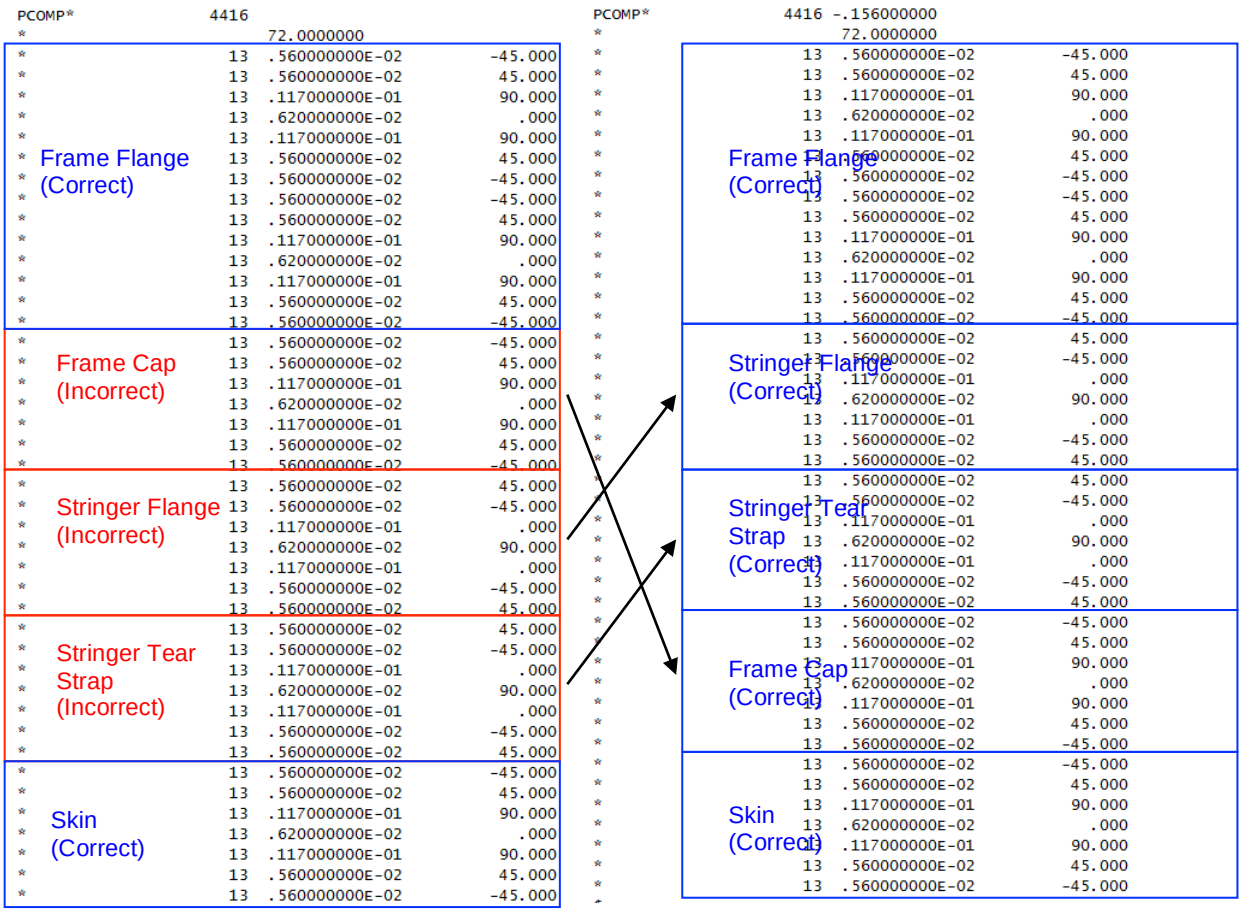

3.2.2 Linear (Non-Postbuckled) Analysis

Panel Strain and Bending Moment Response

Method 1 (Lumped Tear Straps and Flanges)

Free Body Diagram Output (Controlling Factored Loadcase)

Controlling Analysis Load: STRENGTH	Nx,εx	Ny,εy	Nxy,γxy	Mx,κx	My,κy	Mxy,κxy
Virtual Loads	0	0	0	-1148.94	360.131	0.0107785
Design-to Loads	-2381	0	0	-1148.94	360.131	0.0107785
Design-to Deformation	-1.775823E-03	2.056839E-04	0	0	0	0

Method 2 (Separate Tear Straps and Flanges)

Free Body Diagram Output (Controlling Factored Loadcase)

Controlling Analysis Load: STRENGTH	Nx,εx	Ny,εy	Nxy,γxy	Mx,κx	My,κy	Mxy,κxy
Virtual Loads	0	0	0	-1162.56	364.492	1.45515E-03
Design-to Loads	-2381	0	0	-1162.56	364.492	1.45515E-03
Design-to Deformation	-1.798628E-03	2.082217E-04	0	0	0	0

Both methods show a 7% increase in overall panel strain vs the linear analysis, and just as with the linear analysis, method 2 shows approximately 1.2% higher strain results from the same 100 kip test panel load.

Object Loads

Method 1 (Lumped Tear Straps and Flanges)

Load Results

Object	Nx (lb / in)	Ny (lb / in)	Nxy (lb / in)	Mx (lb-in / in)	My (lb-in / in)	Mxy (lb-in /...
Open Span	-456.183	-105.509	0	-0.370655	-0.695167	0.0828175
Bonded Combo, Stringer	-2290.55	-105.509	0	-143.782	-0.695167	0.0382071
Bonded Combo, Frame	-1319.1	-157.925	0	-77.9092	3.23354	-0.26654
Bonded Combo, Str+Frame	-2142.51	-157.925	0	-163.587	3.23354	-0.107393
Stringer Web	-1713.63	0	0	0	0	0
Stringer Rod and Laminate	-4758.24	0	0	0	0	0
Frame Web	396.962	0	0	0	0	0

Method 2 (Separate Tear Straps and Flanges)

Load Results

Object	Nx (lb / in)	Ny (lb / in)	Nxy (lb / in)	Mx (lb-in / in)	My (lb-in / in)	Mxy (lb-in /...
Open Span	-445.527	-99.3374	0	-0.392637	-0.708572	0.0863932
Bonded Combo, Stringer	-2272.83	-99.3374	0	-143.595	-0.708572	0.0341492
Bonded Combo, Frame	-1465.17	-189.767	0	-83.2359	2.8814	-0.325844
Bonded Combo, Str+Frame	-2103.56	-189.767	0	-171.975	2.8814	-0.13904
Stringer Web	-1735.64	0	0	0	0	0
Stringer Rod and Laminate	-4819.35	0	0	0	0	0
Frame Web	401.86	0	0	0	0	0

The relative differences in object loads between the two methods is consistent with the linear results. As expected, both methods show a substantial increase in load in the stringer web and stringer rod and laminate objects over the linear results.

Failure Modes

Method 1 (Lumped Tear Straps and Flanges)

Available Failure Analyses

Limit MS	Ultimate MS	Y	LS	Location - Analysis Description
-0.2079 (-0.99)	LPB ON		101	**Spacing Span** Local Buckling, Biaxial
-0.2079 (-0.99)	LPB ON		101	**Spacing Span** Local Buckling, Biaxial w/ Shear Interac
	0.9217 (0)		101	**PRSEUS** Stiffener Buckling, Flat, Flexural-Torsional St
	1.767 (0)		101	**PRSEUS** Crippling, Composite, MIL-HDBK-17
	2.022 (0)		101	**Frame Span** Panel Buckling, Flat, Simple BC, Uniaxial
	2.022 (0)		101	**Frame Span** Panel Buckling, Flat, Simple BC, Uniaxial
	2.023 (0)		101	**Frame Span** Panel Buckling, Curved or Flat, All BC w/
	2.525 (0)		101	**Frame Span** Panel Buckling, Flat, Simple BC, Uniaxial
	2.525 (0)		101	**Frame Span** Panel Buckling, Flat, Simple BC, Uniaxial
	2.526 (0)		101	**Frame Span** Panel Buckling, Curved or Flat, All BC
	3.49 (0)		101	**Bonded Combo, Stringer** Composite Strength, Max S
	3.514 (0)		101	**Bonded Combo, Stringer** Composite Strength, Max S
	3.598 (0)		101	**Bonded Combo, Frame** Composite Strength, Max Str
	3.699 (0)		101	**Bonded Combo, Frame** Composite Strength, Max Str
	3.711 (0)		101	**Open Span** Composite Strength, Max Strain 2 Directi
	3.737 (0)		101	**Open Span** Composite Strength, Max Strain 1 Directi
	3.741 (0)		101	**Stringer Web** Composite Strength, Max Strain 1 Direc
	3.741 (0)		101	**Stringer Web** Composite Strength, Max Strain 2 Direc
	4.38 (0)		101	**PRSEUS** Panel Buckling, Flat, Simple BC, Uniaxial or B
	4.38 (0)		101	**PRSEUS** Panel Buckling, Flat, Simple BC, Uniaxial or B
	4.384 (0)		101	**PRSEUS** Panel Buckling, Curved or Flat, All BC w/ TSF
	4.725 (0)		101	**Stringer Rod and Laminate** Composite Strength, Max
	4.725 (0)		101	**Stringer Rod and Laminate** Composite Strength, Max
	6.212 (0)		101	**PRSEUS** Panel Buckling, Flat, Simple BC, Uniaxial or B
	6.212 (0)		101	**PRSEUS** Panel Buckling, Flat, Simple BC, Uniaxial or B
	6.22 (0)		101	**PRSEUS** Panel Buckling, Curved or Flat, All BC
9.43 (0)			101	**Stringer Web** Local Buckling, Biaxial

Method 2 (Separate Tear Straps and Flanges)

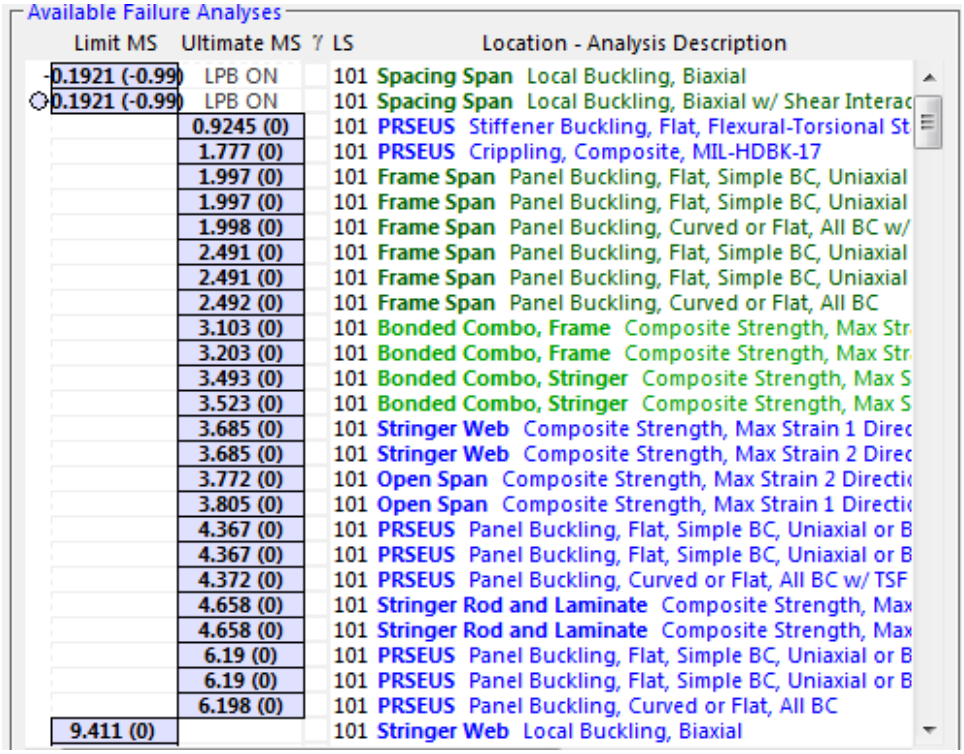

Post Buckling Effective Width

Method 1 (Lumped Tear Straps and Flanges)

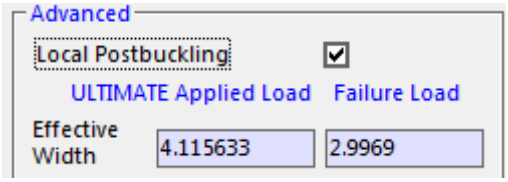

Method 2 (Separate Tear Straps and Flanges)

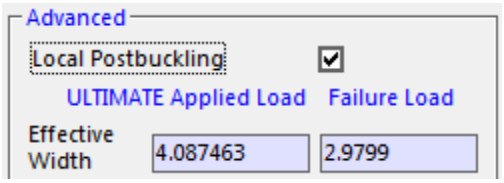

3.3 Sizing Verification

The final verification compares sizing results between the previous version (flange and tear straps lumped together, Method 1) and the current version (flange and tear straps as separate independent variables, Method 2).

The example chosen for comparison is the Cylindrical Space Structure described in the PRSEUS User Instructions. The cylinder is described below.

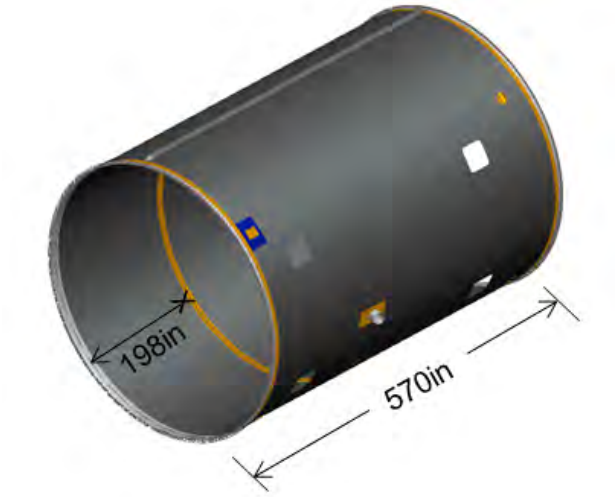

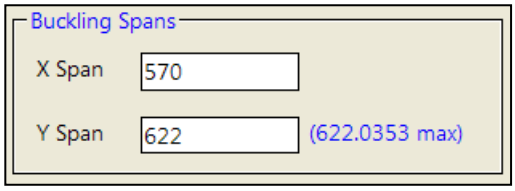

The loading for the non-FEA approach is based on the assumption that the maximum axial load from the flight conditions is to be clocked around the circumference of the structure and at preliminary stages of design the structure should be uniform from top to bottom. The derivation of the axial line load from the flight loads is shown below:

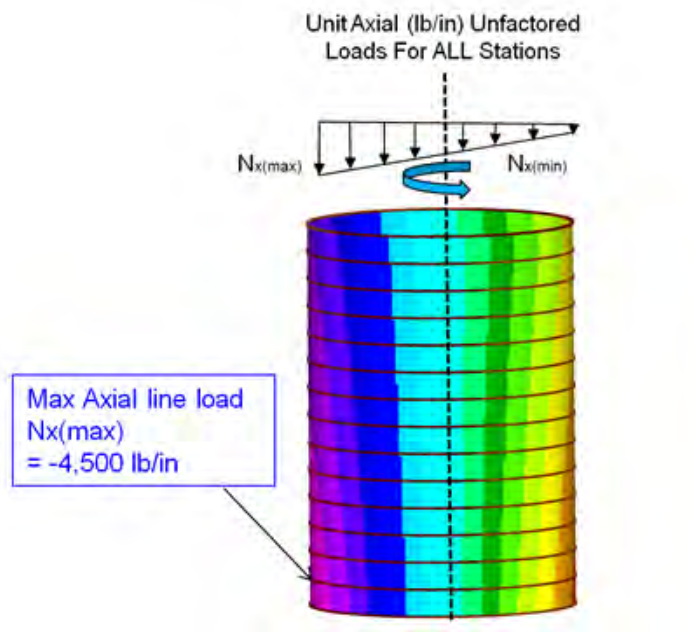

The critical load cases for this structure are identified as:

Load Case	Nx	Ny	Load Description
1	-4500	990	Axial Compression + Internal Pressure
2	-4500	-495	Axial Compression + Crush Pressure

The sizing results from the two methods are shown below.

	Lumped Tear Straps	Separate Tear Straps
Skin Thickness (in.)	0.114	0.114
Stringer Web Thickness (in.)	0.0798	0.0798
Rod CL Height (in.)	2	2
Stringer Spacing (in.)	7	7
Frame Web Thickness (in.)	0.1026	0.1026
Frame Height (in.)	7.25	7.25
Frame Spacing (in.)	38	38
Foam Thickness (in.)	0.5	0.5
Stringer Flange Width (in.)	3.5	3.5
Stringer Flange Thickness (in.)	0.0798	0.0399
Frame Flange Width (in.)	4	4
Frame Flange Thickness (in.)	0.1026	0.0513
Rod Diameter (in.)	0.6	0.6
Stringer Tear Strap Thickness (in.)	N/A	0.0399
Frame Tear Strap Thickness (in.)	N/A	0.0399
Stringer Tear Strap + Flange (in.)	0.0798	0.0798

Frame Tear Strap + Flange (in.)	0.1026	0.0912
Unit Weight (lb/ft^2)	2.138	2.134
Margin of Safety	.0058	.0042
Post-buckling effective width (in.)	4.96	4.97

The results between the two cases are very similar. The red items in the above table show that in method 1, the tear straps are lumped in with the flange variable meaning the flange variable is much thicker than in method 2. However, method 2 includes plies for the tear strap which are not included in method 1. The overall thickness of flange plus tear straps are very close between the two cases. In the case of the method 2, the sizing was able to find a solution with 1 fewer ply than with method 1. The difference in unit weight between the two methods is 0.1%.

4 References

Collier Research Corporation (2010). PRSEUS Implementation in HyperSizer - Final Report.

Collier Research Corporation (2010). HyperSizer User Manual, Rod/Bulb Stiffened Panel Family, Version 5.9.

APPENDIX B—CROWN PANEL REPAIR

Although no rework was required on the IML features of the crown panel, there was a problem encountered on the OML side of the panel. Once the peel layer was removed, it was immediately apparent that a rectangular pattern of grooves had been molded into the OML surface of the panel. Because the grid pattern matched the splice locations of the perforated plates, the problem was quickly diagnosed as an interference problem at the perforated plate splices. (A layer of perforated plates was inserted between the cure tool and preform to prevent the carbon fabric from imprinting into the flow media, which resulted in a roughly textured OML surface.)

Unlike the tooling used for prior PRSEUS panel infusions, this was the first time an Invar cure tool was used. With panels almost 30 ft long, the mismatch in thermal growth between a steel cure tool and a carbon-fiber part would have created out-of-tolerance panels. During fabrication of the crown panel, a mark-off pattern occurred on the OML surface of the part during the infusion and cure cycle. This was caused by the edges of the perforated caul sheets that were placed between the preform and cure tool. Driven by thermal expansion, the sheets pressed together and then dug into the preform during the cure cycle, molding a permanent groove in the OML surface of the part (Figure B-1). The relative locations and groove depths are depicted in Figure B-2.

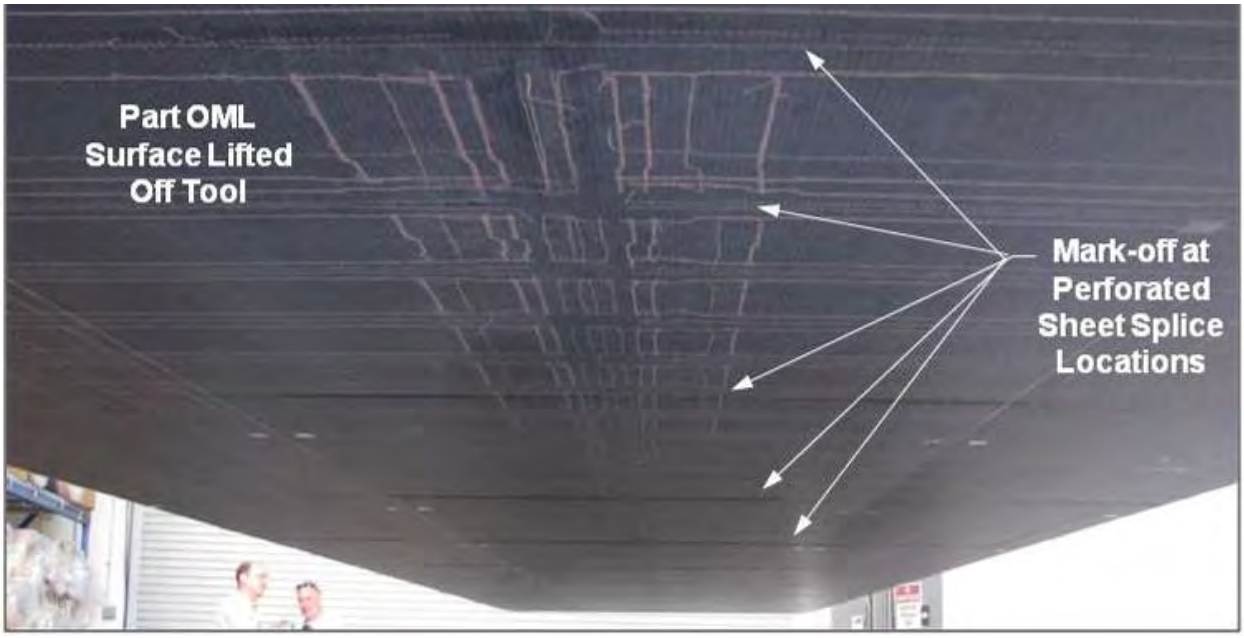

Figure B-1. Thermal Expansion of Caul Sheets Caused Mark-off on the Crown Panel OML

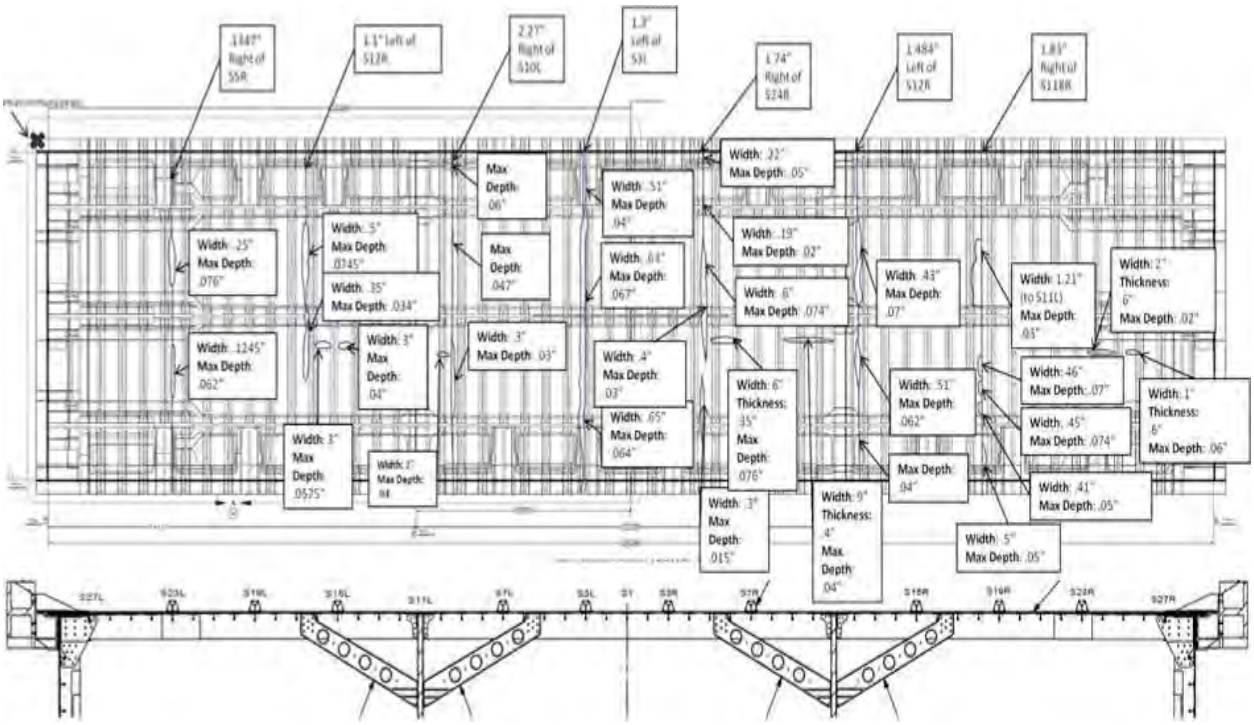

Figure B-2. Schematic of Groove Location and Depth Measurements

Because the resulting pattern matched the edges of the individual caul sheets, it was quickly determined that the difference in thermal expansion between the low-carbon steel perforated sheets and the Invar cure tool caused the interference. In addition to the mark-off, permanently buckled regions occurred in the caul sheets themselves along the spliced edges. This indicated that the sheets had grown during the cure cycle and caused permanent deformations in the regions with the smallest gaps between the sheets (Figure B-3). On subsequent panel infusions, the problem was resolved by increasing the spacing between the caul sheets, which eliminated the at-temperature interference condition that led to the grooves in the first panel.

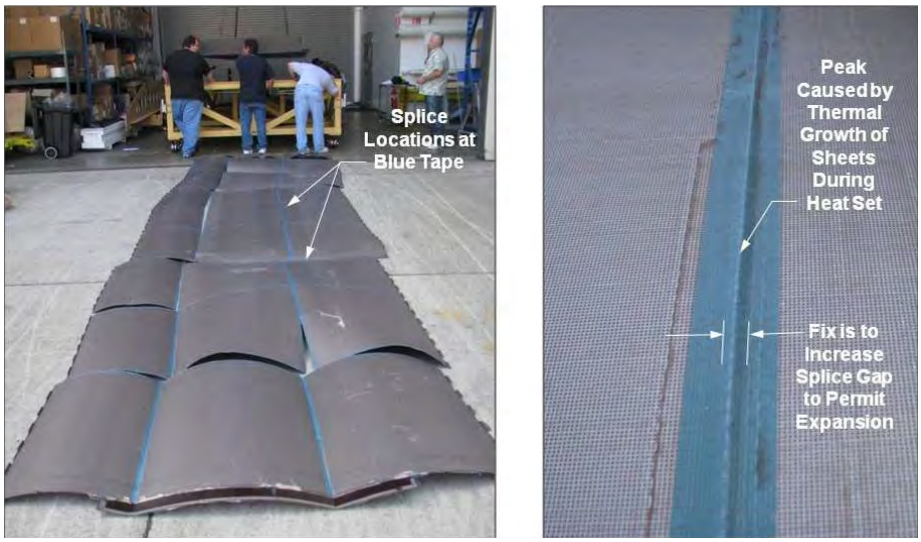

Figure B-3. Perforated Caul Sheets from Crown Panel Infusion (Revised for Subsequent Panels)

Rather than build an entirely new crown panel, a decision was made to repair the existing one. To accomplish this, the grooves were filled in with a rigid adhesive/filler and then sanded flush, while the repair technique and validation approach outlined in Figure B-4 was developed. This basic repair methodology and process control was first developed and tested at the coupon level. In addition to validating the repair approach, the testing also generated repair allowables that were used to write margins for the repaired panel condition on the MBB.

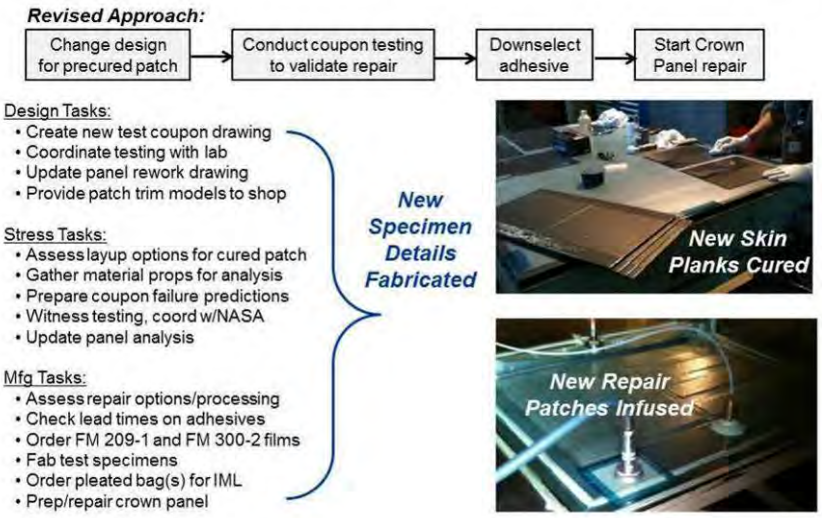

Figure B-4. Repair Technique and Validation Approach

Initially, two different repair approaches were considered before down-selecting a pre-cured bonded patch approach. In this approach, the patches would be built up using thinner two-ply warp-knit fabric stacks to replace the missing load path across the grooves. The "equivalent" stack architecture used to replicate the basic Class 72 skin stack is depicted in Figure B-5. This basic four-stack layup of DMS 2436 Class 75/76 stacks was used in the skin regions of the repair, and then it was locally doubled to eight layers at the frame intersections.

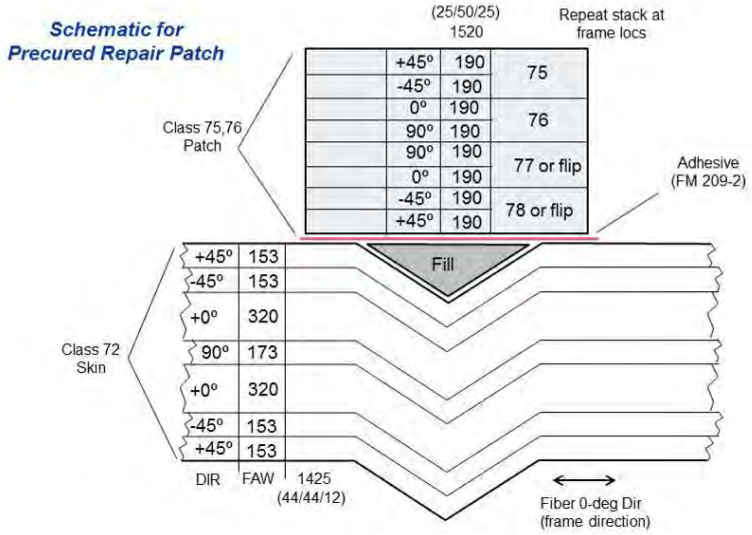

Figure B-5. Repair Patch Laminate Architecture Created Using Warp-Knit Fabrics

The primary design objective of the repair patch was to maintain a minimum taper ratio while providing an adequate overlap across the groove. Based on an FEM investigation of the load transfer across the patch, it was determined that a minimum patch width of at least 4 in. would be needed. This result drove the specimen cross-section design depicted in Figure B-6.

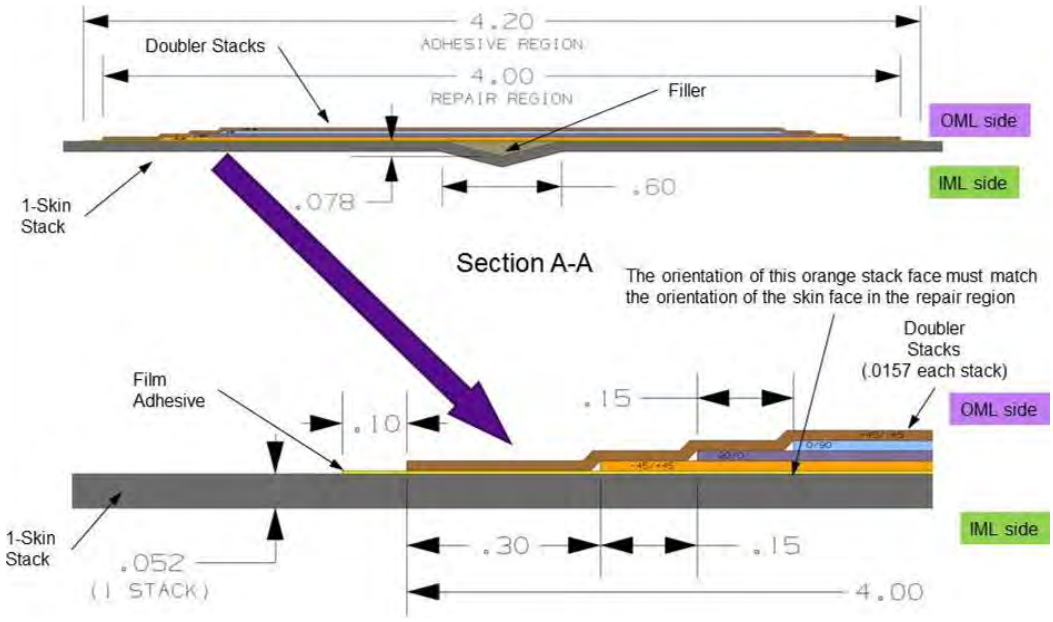

Figure B-6. Pre-cured Patch Overlap and Edge Taper Dimensions

The coupon specimens were fabricated and tested under tension and four-point bending loads to simulate the critical conditions for the crown panel (Figure B-7). In both cases, as expected, a classic first-ply failure separation occurred between the outer ±45-deg layers of the skin stack at a far-field strain averaging 0.0085 in./in., which exceeded the notched tension design allowable used to design the crown panel.

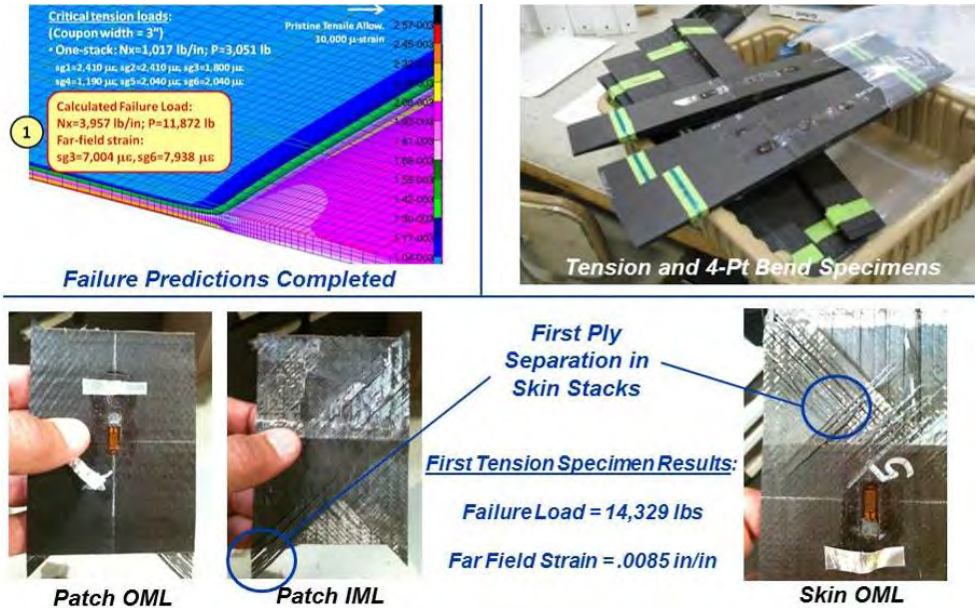

Figure B-7. Coupon Testing Was Used to Validate Repair Design and Processes

With the repair design validated by analysis and test, the approach was scaled up for the crown panel repair. In addition to being larger than the coupons, the minimum width of the patches was also increased to 6 in. to match the stringer spacing on the crown panel. This facilitated maintaining a minimum 2-in. overlap (measured from the groove centerline to the patch edge), while still enabling positioning the patch edges over skin buildups in the stringer flange and tear strap regions. The in-process layup of the repair patch dry fabric is shown in Figure B-8.

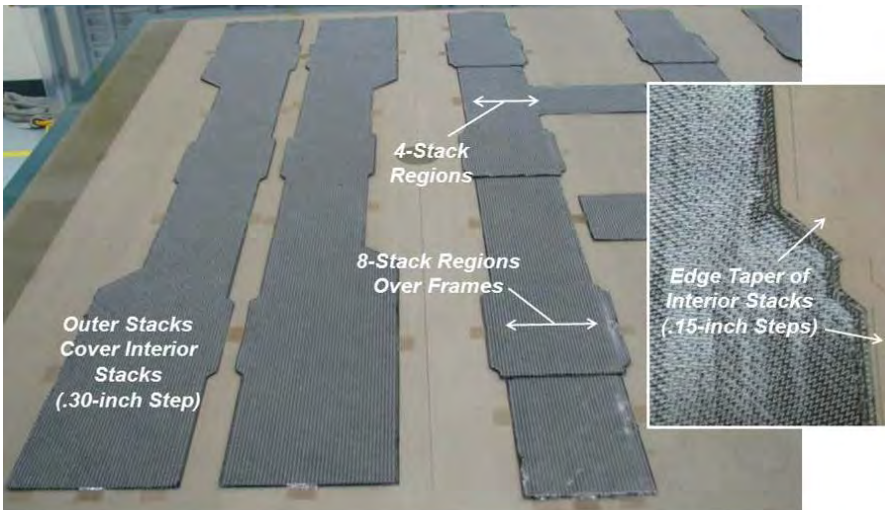

Figure B-8. Dry Fabric Layup Used to Create Pre-cured Patches

Once the patches were infused and cured in the oven, small bleed holes were mechanically drilled approximately 2 in. apart (to vent trapped air during bonding), and then an FM-209 film adhesive was applied to the back side of the patch (Figure B-9).

Figure B-9. Patches Were Infused and Cured in an Oven and then Secondarily Bonded

Simultaneously, the crown panel OML surface was being prepared by filling in the grooves, sanding them flush, grit-blasting the bonding regions, and then conducting water-break tests to verify the prepared surface condition (Figure B-10 and Figure B-11).

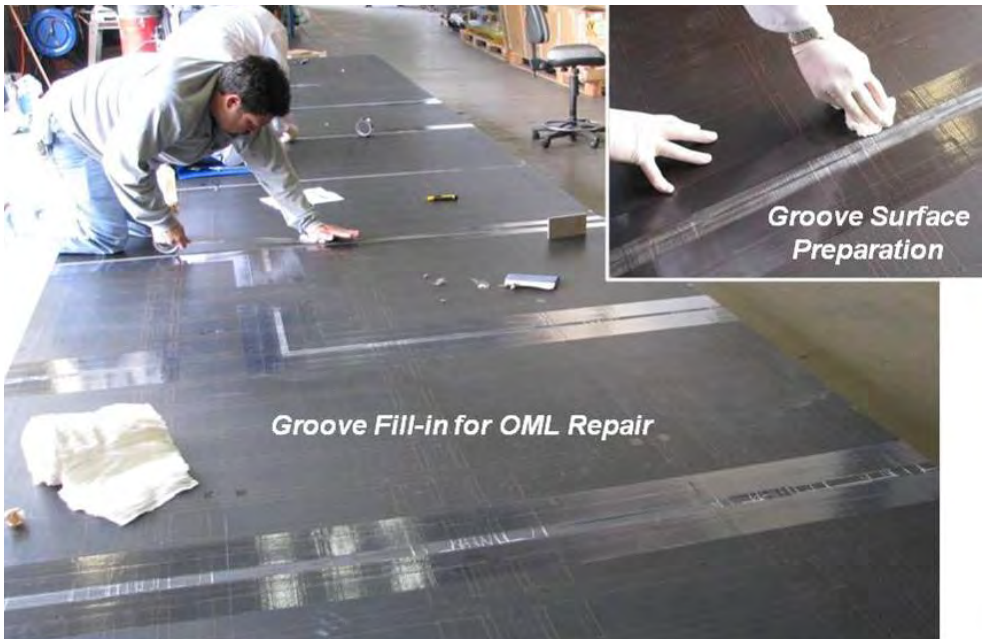

Figure B-10. Crown Panel OML Surface Prepared for Repair

Figure B-11. Bonding Surfaces Were Prepared for Repair Patches

The prepared patches were then located into position, taped along the edges to secure them, and marked to aid in finding the bleed holes after the bonding cycle (Figure B-12). The panel was then flipped over onto the cure tool and vacuum bagged (Figure B-13).

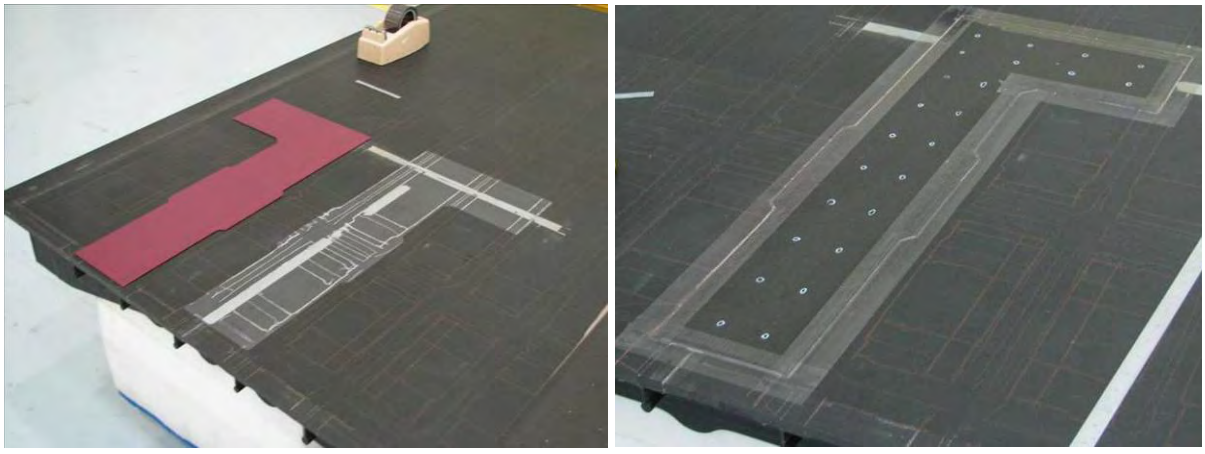

Figure B-12. Pre-cured Repair Patches Were Taped Before Applying the Vacuum Bag

Figure B-13. Bagged Crown Panel With IML Side Facing Up and Repair Patches Taped to the OML

To minimize thermal distortion and out-gassing during the bonding operation, the combination of an FM-209 adhesive and a 250ºF cure cycle was used. The processing parameters were identical to those used for the test coupons and no abnormal conditions were encountered. The post-bond inspection of the patch edges and bleed holes showed normal adhesive wet-out without any indications of voids or trapped air beneath the patches (Figure B-14).

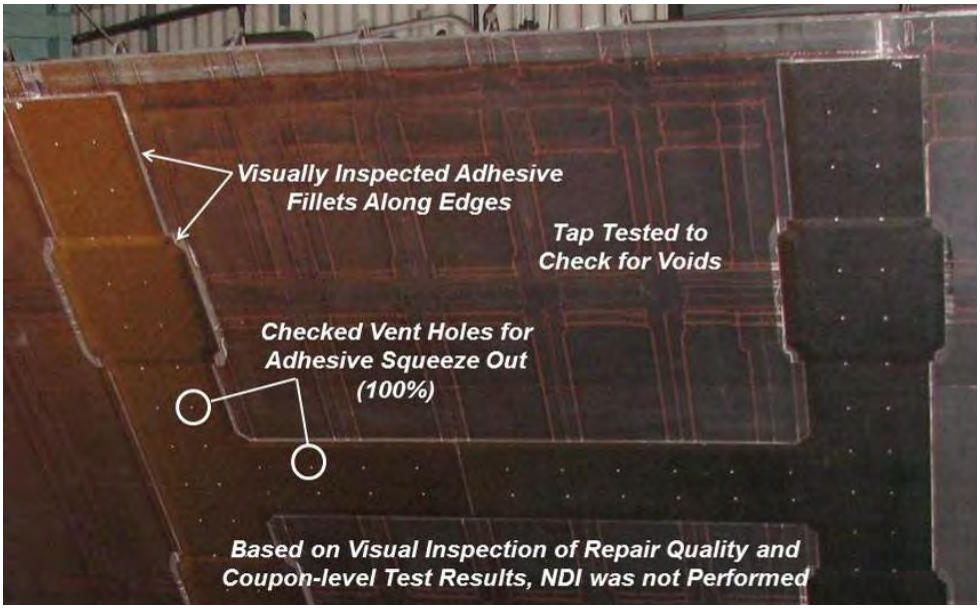

Figure B-14. Region of Bonded Repair Patches Shown on OML

Due to the large variation in geometric complexity of the internal structure covered by the patches, the use of common inspection techniques using pre-sampled reference standards was not practical; therefore, no ultrasonic nondestructive inspection was performed. The repair was approved based on using the same process-control standards as used for the test coupons (visual inspection of the adhesive wet-out and tap testing of the completed repair), which, ultimately, replicated the favorable results of the coupon test effort. The repaired panel was then delivered to the assembly site (Figure B-15).

Figure B-15. Completed Bonded Repair Patches on Crown Panel OML

REPORT DOCUMENTATION PAGE

Form Approved
OMB No. 0704-0188

1. REPORT DATE *(DD-MM-YYYY)*	2. REPORT TYPE	3. DATES COVERED *(From - To)*
01/09/2017	Contractor Report	

4. TITLE AND SUBTITLE

Hybrid Wing Body Multi-Bay Test Article Analysis and Assembly Final Report

5a. CONTRACT NUMBER
NNL10AA05B

5b. GRANT NUMBER

5c. PROGRAM ELEMENT NUMBER

6. AUTHOR(S)

Velicki, Alexander; Hoffman, Krishna; Linton, Kim A.; Baraja, Jaime; Wu, Hsi-Yung T.; Thrash, Patrick

5d. PROJECT NUMBER

5e. TASK NUMBER
NNL11AA68T

5f. WORK UNIT NUMBER
699959.02.22.07.04

7. PERFORMING ORGANIZATION NAME(S) AND ADDRESS(ES)

NASA Langley Research Center
Hampton, Virginia 23681-2199

8. PERFORMING ORGANIZATION REPORT NUMBER

9. SPONSORING/MONITORING AGENCY NAME(S) AND ADDRESS(ES)

National Aeronautics and Space Administration
Washington, DC 20546-0001

10. SPONSOR/MONITOR'S ACRONYM(S)
NASA

11. SPONSOR/MONITOR'S REPORT NUMBER(S)
NASA-CR-2017-219668

12. DISTRIBUTION/AVAILABILITY STATEMENT
Unclassified
Subject Category 05
Availability: NASA STI Program (757) 864-9658

13. SUPPLEMENTARY NOTES
Langley Technical Monitor: Dawn C. Jegley

14. ABSTRACT
This report summarizes work performed by The Boeing Company, through its Boeing Research & Technology organization located in Huntington Beach, California, under the Environmentally Responsible Aviation (ERA) project. The report documents work performed to structurally analyze and assemble a large-scale Multi-bay Box (MBB) Test Article capable of withstanding bending and internal pressure loadings representative of a Hybrid Wing Body (HWB) aircraft. The work included fabrication of tooling elements for use in the fabrication and assembly of the test article.

15. SUBJECT TERMS

Article; Bay; Body; Boeing; Hybrid; Multi; Test; Wing

16. SECURITY CLASSIFICATION OF:			17. LIMITATION OF ABSTRACT	18. NUMBER OF PAGES	19a. NAME OF RESPONSIBLE PERSON
a. REPORT	b. ABSTRACT	c. THIS PAGE			STI Help Desk(email help@sti.nasa.gov
					19b. TELEPHONE NUMBER *(Include area code)*
U	U	U	UU	472	(757) 864-9658